



Università degli Studi della Basilicata

PhD in
“Applied Biology and Environmental Safeguard”

**“DEFINITION OF AN ADVANCED PROCESS FOR THE
PRODUCTION OF LOW ENVIRONMENTAL IMPACT
CONTAINERS AS POTENTIAL ALTERNATIVE TO
PLASTICS”**

Scientific-Disciplinary Sector
“CHIM/01”

PhD Coordinator

Prof. Patrizia Falabella

PhD student

Dr. Acquavia Maria Assunta

Tutor

Prof. Giuliana Bianco

Co-tutor

Prof. Giuseppe Martelli

Dr. José Alejandro Heredia-Guerrero

Cycle XXXV

Summary

For decades, petroleum-based synthetic polymers, commonly known as plastics, have become one of the most appealing materials used for a wide variety of applications. Nevertheless, currently, conventional petroleum-based plastics represent a serious problem for global pollution because they remain for hundreds of years in the environment when discarded. In order to reduce dependence on fossil resources, bioplastic materials are being proposed as safer and more sustainable alternatives. Bioplastics are bio-based and/or biodegradable materials, typically derived from renewable sources. Among different resources, food waste is attracting more and more attention in the research field of bioplastics' production. The sources of food waste include household, commercial, industrial and agricultural residues. In fact, every year, around one-third of all food resources produced for human consumption are lost or wasted. Although European Union guidelines stated that food waste should preferentially be used as animal feed, in some cases, it became illegal because of disease control concerns and other times its nutritional value is very poor. On the other hand, the production of bioplastics from food waste is a renewable, sustainable process, in which materials are fabricated from carbon neutral resources, thus aligning itself with the principles of the circular bioeconomy. However, the conversion of fruit and vegetable by-products into eco-friendly materials with mechanical and hydrodynamic performances comparable to those of fossil-based plastics still remains a challenge. In this thesis, different approaches have been investigated for the valorization of fruit and vegetable wastes to produce low environmental impact materials, as a potential alternative to plastics with application in the field of food packaging. In the first section, apple waste and tomato peel by-products have been used as fillers to fabricate starch-based biocomposites. The mechanical characterization of the samples showed their suitability for covering purposes, since a ductile and soft behaviour was exhibited. In the second section, an avocado by-product extract has been incorporated to an ethyl cellulose matrix for the production of impregnated paper with enhanced durability. Since fruit wastes can contain potential pathogens and physical and chemical contaminants which can be released when used as additive for active packaging, a preliminary untargeted metabolomic characterization of the extract was conducted by LC-ESI(-)-Q Exactive-Orbitrap- MS/MS. The lipid components detected in the extract proved to be useful additives to improve paper hydrophobicity, preventing food browning and moisture loss. In general, the addition of all tested wastes (apple waste, tomato peel and avocado by-products) has proved to be useful to increase the biodegradability of the fabricated biomaterials. Hence, the environmental benefits associated with their recovery are proposed as a driving force to expand

their further use for these purposes. The upcycling of food waste through the production of value-added products is an ideal and practical end use, allowing to save huge economic and energy losses.

Index

1. Introduction.....	1
1.1 Bioplastics classification.....	3
1.1.1 Bio-based content and biodegradability.....	6
1.1.2 Bioplastics' physical properties.....	10
1.2 Food waste as a feedstock for bioplastic production.....	12
1.2.1 Processing methods.....	14
1.2.2 Biopolymers-based plastics.....	15
1.2.3 Food waste usage for bio-composites production.....	20
1.3 Environmental impacts of food waste-based bioplastics production.....	23
1.4 Bioplastics market.....	25
References.....	29
2. Methodologies.....	41
2.1 Tensile test.....	41
2.2 Contact angle.....	44
2.3 Biodegradability.....	46
References.....	48
3. Contribution 1.....	49
Apple waste and tomato peel by-products as fillers for starch-based bio-based composites.....	49
Abstract.....	49
3.1 Introduction.....	50
3.2 Experimental section.....	55
3.2.1 Materials.....	55
3.2.2 Biocomposites preparation.....	55
3.2.3 Chemical, mechanical and thermal characterization.....	56
3.2.4 Water uptake.....	57
3.2.5 Biodegradability.....	57
3.2.6 DPPH radical scavenging assay.....	57
3.2.7 ABTS free radical cation scavenging assay.....	58
3.2.8 Statistical analysis.....	58
3.3 Results and Discussion.....	59
3.3.1 Chemical, mechanical and thermal characterization.....	59
3.3.2 Water uptake.....	63
3.3.3 Biodegradability.....	64

3.3.4 Antioxidant properties	66
3.4 Conclusions.....	68
References.....	69
Supplementary Information	74
4. Contribution 2	75
Untargeted profiling of the avocado by-product extract for the fabrication of bio-based plastics	75
Abstract	75
4.1 Introduction.....	76
4.2 Experimental section	78
4.2.1 Reagents and solvents	78
4.2.2 Raw material and sample extraction	78
4.2.3 LC-MS/MS Analysis	78
4.3 Results and Discussion	79
4.3.1 LC-MS/MS Analysis	79
4.4 Conclusions.....	82
References.....	85
5. Contribution 3	88
Antioxidant, biodegradable, and hydrophobic food packaging materials fabricated by impregnation of paper with ethyl cellulose and avocado by-product extract.....	88
Abstract	88
5.1 Introduction.....	89
5.2 Experimental section	93
5.2.1 Materials	93
5.2.2 Optimization of bioactive compounds extraction by experimental design.....	93
5.2.3 Determination of extraction yield	94
5.2.4 Determination of total phenolic content (TPC)	95
5.2.5 Determination of total flavonoid content (TFC).....	95
5.2.6 LC-MS/MS Analysis	95
5.2.7 Preparation of impregnated papers.....	96
5.2.8 Morphological, chemical and mechanical characterization	97
5.2.9 Water uptake	97
5.2.10 Water contact angle	98
5.2.11 Water vapor permeability	98
5.2.12 Oil contact angle	99
5.2.13 Oil and Grease Resistance Testing.....	99

5.2.14 Biodegradability	99
5.2.15 DPPH radical scavenging assay	100
5.2.16 Overall Migration of Components in Tenax®	100
5.2.17 Evaluation of Moisture Preservation	101
5.2.18 Statistical analysis	101
5.3 Results and Discussion	101
5.3.1 EC-impregnated paper-based bioplastics.....	101
5.3.1.1 Morphological, chemical and mechanical characterization	101
5.3.1.2 Water uptake, wettability and water barrier properties	105
5.3.2 Avocado by-product extraction: optimization and chemical characterization....	107
5.3.2.1 Optimization of bioactive compounds extraction by experimental design.....	107
5.3.2.2 LC-MS/MS Analysis	110
5.3.3 Effect of the incorporation of the avocado by-product extract into the bioplastic formulation	111
5.3.3.1 Chemical and mechanical characterization	111
5.3.3.2 Wettability, water uptake and water barrier properties	112
5.3.3.3 Oil contact angle and oil and grease resistance testing	114
5.3.3.4 Biodegradability	114
5.3.3.5 Antioxidant properties	116
5.3.3.6 Migration test.....	117
5.3.3.7 Evaluation of Fruit Preservation	118
5.4 Conclusions.....	121
References.....	122
6. Concluding remarks and outlooks	128
Publications	130
Articles	130
Oral Communications	131
Attended Workshops and Schools.....	132
Workshops.....	132
Schools	132
Acknowledgements	133

1. Introduction

Conventional plastics include a wide number of polymers such as polypropylene, polyethylene, polyvinyl chloride, polystyrene, nylon, polycarbonate, etc., that derive from fossil resources. The global production of synthetic plastics accounts approximately for 4–8% of the total oil consumption. This value is expected to double by 2050 [1]. Since they can be readily manufactured to an expanding range of products thanks to their light-weight, flexibility and durability, the global oil-based plastics production has remarkably increased over the last 50 years from 15 million metric tons in 1964 to 359 million metric tons in 2018 [2]. Although plastics have greatly contributed to the ease of everyday life as a result of their large-scale utility, their ubiquity and the huge amount of plastic wastes are very important issues for both environmental and human health-related problems [3].

Each step of plastics production, from manufacturing to disposal, contributes to a different extent with persistent negative impacts on the environment. The extraction of oil and gas which are commonly used for plastics manufacturing, particularly hydraulic fracturing (viz. “fracking”) for natural gas, releases an array of toxic substances into the air and water, often in significant volumes [4–7]. In addition to the use of petroleum, plastic manufacturing requires the use of chemical additives that serve as plasticizers, flame retardants, heat and UV stabilizers, biocides, pigments and extenders. Most of them are classified as hazardous according to the European Union regulations, since they are carcinogenic, mutagenic, harmful for reproductive health or aquatic life [8]. Phthalates, bisphenol A, formaldehyde, acetaldehyde, 4-nonylphenol and other volatile organic compounds are good examples of toxic chemicals which are bioavailable for direct or indirect animal and human exposure, leading to reduced feeding or blocking the intestinal tract, when plastics are improperly disposed of [9,10]. At the end of their life-cycle, plastic products are wasted in landfills, burned in incinerators or littered. In the case of littering, plastic wastes fail to reach landfills or incinerators. This is an improper way of disposing plastics and it has been identified as the cause of manifold ecological problems, as at the end of the 20th century they were found to be largely non-biodegradable. In fact, dumped plastics can remain unaltered for a hundred to thousands of years. However, they can break down, creating micro and nano fragmented particles. These micro and nano-plastic particles accelerate the problems even further by affecting animal and human health. Additionally, since none of the material is recovered, the “management” system of the landfill waste is entirely linear and does not reduce virgin resource utilisation, stifling the vision of a circular economy. On the other side,

incineration of plastic wastes significantly reduces the volume of waste requiring disposal. The volume reduction brought by incineration ranges from 80 to 95%, but it should be considered that toxic heavy metals and noxious gases (for instance, dioxins and furans) are released by burning [11]. Moreover, plastics burning emits 2.9 kg of CO₂ every kg of plastic burned, thus contributing to the problem of the greenhouse effect. In order to fix this drawback about plastic and plastic production, recycling emerged as a solution. Nevertheless, although the cost and the greenhouse gas (GHG) emission can be reduced by implementing optimisation strategies [12], to date recycling has been relatively successful due to difficulties in identification and sorting of various other materials and additives which make the process really expensive when possible [13]. As a matter of fact, recycling now accounts for 30% of plastic waste treatment in the EU, with very large differences from country to country [2] and the International Energy Agency, in its Net Zero Emissions by 2050 scenario, assumes that 55% of the world's plastic waste will be recycled by 2050.

Therefore, the current strategies for plastic waste reduction show progress, although they are not the best suited (incineration) or do not reach the set targets (recycling). In this sense, international policies initiated the reduction of single-use plastics such as plates, cutlery, straws and cotton bud sticks (for example, they have been banned in EU by 2021). In this context, scientific investigations are looking for suitable materials to replace petroleum-based plastics. One of the potential substitutes of traditional plastics, which has been introduced so far into the market with high potentiality, is known as bio-based plastic or simply "bioplastic" [14]. Bioplastic materials are made of polymers from renewable resources (i.e. biomass) and can be biodegradable and/or compostable [15]. Bio-based and biodegradable plastics contribute to the reduction in CO₂ emissions during their production and offer new end-of-life management options, such as anaerobic digestion or composting, thus addressing the bioeconomy of the future [16]. Among the countless renewable biomass sources, food waste has received great attention as feedstock for bio-materials production, since it allows to overcome the problem of reducing both plastic and food waste at the same time, through the manufacturing of bio-based plastics with a reduced carbon footprint in accordance with the principles of circular economy and green chemistry.

1.1 Bioplastics classification

According to the European Bioplastics Organization (EBO), bioplastics refers to the family of plastic materials which are either bio-based or biodegradable or which show both the properties [17]. Bio-based means that the material is partly or completely derived from renewable sources, i.e. biomass which replaces the petrochemical resin typical of conventional plastics [14]. As regard to biodegradability, when a material shows this property, it could be converted by biological processes into natural substances such as water, CO₂ and biomass without leaving other distinguishable or toxic residue, within a certain time and at a particular location [18]. Therefore, the term “bio” before “plastic” refers to the carbon source and/or to the biodegradability of the material. Thus, some bio-based plastics can be non-biodegradable. In fact, almost half of the available bioplastics are non-biodegradable [14,19–21]. One of the main classification scheme groups bioplastics according to their biodegradability and bio-based content in (1) drop-ins, i.e. bio-based but non-biodegradable plastics, and (2) non drop-in bioplastics, i.e. biodegradable plastics based on renewable or fossil sources (**Figure 1.1**) [17].

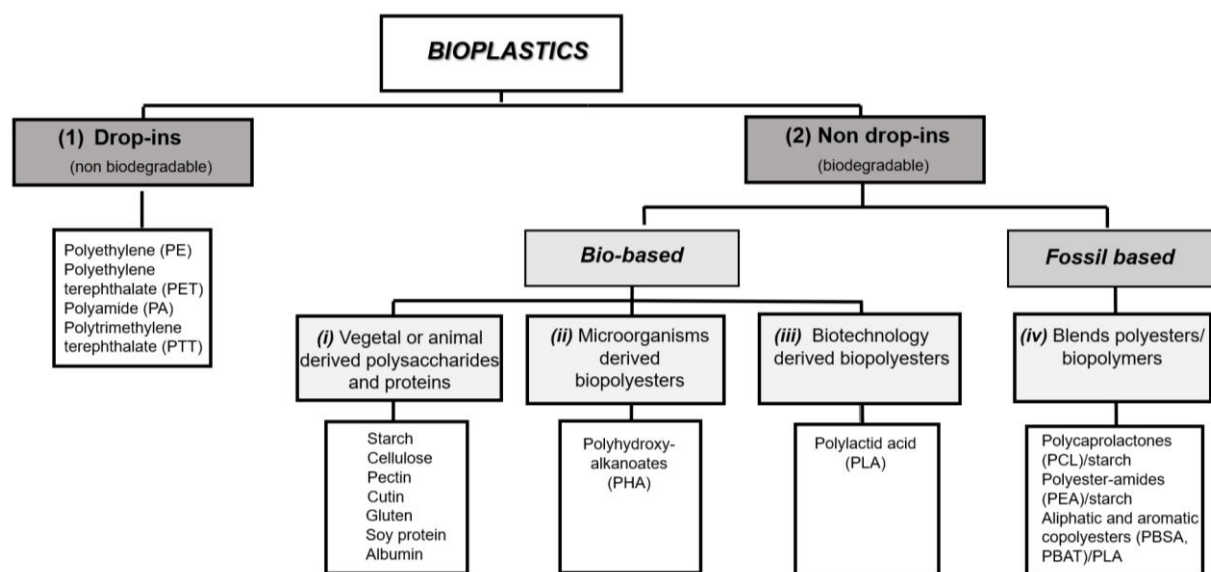


Figure 1.1 Bioplastics classification according to their biodegradability and bio-based content. (1) Drop-in bioplastics (i.e. bio-based or partly bio-based but non-biodegradable plastics), (2) non drop-in bioplastics (i.e. bio-based or fossil based biodegradable plastics). According to their origin, non-drop-ins are divided into (i) vegetal or animal derived polysaccharides and proteins, (ii) polymers from microorganisms, (iii) polymers from biotechnology, and (iv) blends of commercial polyesters and biopolymers [19].

Non-biodegradable bioplastics, obtained from renewable sources, are comparable to classical plastics for the time needed for their complete environmental degradation [22] and, nowadays, represent one of the largest sectors of the global bioplastics production. Bio-polyethylene terephthalate (bio-PET) represents a very common drop-in bioplastic example. For PET production, an esterification reaction between terephthalic acid (PTA) and ethylene glycol (EG), followed by a polymerization through a polycondensation reaction with water as a by-product, is used [23]. In the traditional production of PET, both PTA and EG are fossil refinery products: petroleum refiners first separate out *p*-xylene (PX) from BTX (benzene, toluene, xylene) mixtures by crystallization method and then oxidize it to PTA. Similarly, in order to obtain EG, ethylene derived from the alkene co-products of natural gas production is processed through hydration and oxidation [24]. For bio-PET, instead, EG or both monomers are obtained from renewable sources by a process identical to that used for petro-PET and also their technical properties are identical to those of their fossil counterparts [25]. Ethylene glycol is always available on large scale from biomass: cellulose recovered from lignocellulosic biomass is converted into xylitol and sorbitol, which are easily hydrolyzed to EG in presence of several mono- and bimetallic phosphide catalysts [26,27]. Moreover, also bio-ethanol derived from sugar cane or corn stover and glycerol, as a co-product of biodiesel, have been used as a feedstock to produce EG [28]. The production of terephthalic acid by green chemistry processes based on the use of chemical precursors extracted from corn, sugar beet or orange peel (isobutanol, 5-hydroxymethylfurfural and limonene, respectively) is used to a lesser extent [25].

While drop-ins are well known on the market, non-drop-in bioplastics, i.e. plastics that are biodegradable and bio-based or based on fossil sources, are alternative materials usually employed in specific fields, for example for food services, agriculture or biomedical applications. Therefore, their trade is emerging only in recent years [22,29,30]. These biodegradable polymers can be classified, according to their origin, into four major categories, namely (i) agro-polymers, (ii) polymers from microorganism, (iii) polymers from biotechnology and (iv) blends of commercial polyesters and biopolymers [14,31,32] (**Figure 1.1**).

Starch, cellulose, pectin, chitin, chitosan and cutin as well as animal and vegetable proteins such as casein and gluten are well known for being feedstock of agro-polymers based bioplastics [33–35]. Starch, cellulose and pectin are polysaccharides typically used to produce packaging materials and can be extracted from several vegetables and fruits (potato, corn, rice, tapioca, apple) [14]. As regard to chitin, it is the second most abundant natural polymer in the world after cellulose. The main sources exploited are two marine crustaceans: shrimps and crabs. The most important chitin derivative is chitosan. It is obtained by partial deacetylation under alkaline

conditions and it is extensively investigated for bioplastics production due to its insolubility in common solvents [36]. Also cutin has been investigated for this purpose. Cutin is the main component of plant cuticles. It is composed of esterified bi- and trifunctional fatty acids and shows full biodegradability in short times, relatively high thermal resistance, good hydrophobicity and low values of water adsorption and water vapor permeance [37]. Often, protein additives are used to fabricate materials with novel and improved technological properties. In fact, due to the difference between the elemental composition of proteins (covalent bonds between hundreds of amino acids) and polysaccharides (covalent bonds between monosaccharides with ramifications), their mixtures can evidence a wide variety of two- and three-dimensional structures with different physicochemical and rheological properties [38]. In addition, there are a lot of polymers which can be produced by many types of microorganisms, cultured under different nutrient and environmental conditions [39]. Polyhydroxyalkanoates (PHAs), for example, are linear thermoplastic polymers, with hydroxyalkanoic acid as a monomer unit, which can be synthesized intracellularly as insoluble cytoplasmic inclusions by heterotrophic bacteria such as *Cupriavidus necator* [40,41], recombinant *Escherichia coli* [42] and also by photoautotrophic microorganisms like microalgae [43]. Their synthesis occurs in the presence of an excess of carbon when other essential nutrients such as oxygen, phosphorus, or nitrogen are limited. After their extraction from cell cultures, they can be processed in an analogous way as polypropylene, including extrusion and injection molding, obtaining a material with similar properties to the petroleum-based plastics.

On the other hand, bacterial microorganisms can also be used to produce, in a biotechnological approach, biodegradable polymers through the fermentation of carbohydrates obtained from agricultural by-products such as starchy substances from corn and wheat. Polylactic acid or polylactide (PLA)-based bioplastics are prepared from a fermentative process that involves conversion of corn or other carbohydrate sources into dextrose, followed by fermentation/conversion into lactic acid [19]. Thus, lactic acid is isolated and polymerized to yield a low molecular weight, brittle polymer whose chain length could be increased by using external coupling agents [21].

The last group of biodegradable materials is represented by blends of biopolymers and polymers obtained by chemical synthesis from fossil resources [44–46]. Polymer blending is a technique that allows the modification of the properties of a material using a conventional technology at low cost. In this sense, biodegradable polyesters such as polycaprolactone (PCL), which is obtained by the condensation of 6-hydroxycaproic acid or through the ring opening polymerization of ϵ -caprolactone [47], can be easily used to improve mechanical properties of

natural polymers, conferring them a better water resistance due to its hydrophobicity [48]. Among the different polymeric blends currently available, the one involving PCL and starch has received the most attention since the 1980s. Novamont has been the first company that manufactured a PCL/starch composite under the trademark Mater-Bi[®]. The properties of this blend are interesting because the composite components have completely different characteristics. PCL is a synthetic, hydrophobic polymer with a low degradation rate. Instead, starch is a natural, hydrophilic polymer with a high degradation rate. Thus, PCL can adjust humidity sensitivity of starch as a biomaterial, while starch can enhance the low biodegradation rate of PCL [49]. Nowadays, although with different percentages, all bioplastics are used in a wide range of sectors: from packaging to textiles, including catering products, consumer electronics, automotive, agriculture/horticulture and toys, among others. The field of application of a given bioplastic is clearly dictated by its mechanical and hydrodynamic (water permeability, water uptake, water contact angle) properties as well as by its bio-based content or its biodegradability. These characteristics are evaluated before bioplastics are promoted on the market. Moreover, to produce functional materials with biological properties, in the case of bioplastics obtained from fruit and vegetable wastes, a metabolic characterization of the raw material is needed. Among the analytical techniques used to this aim both chromatography and mass spectrometry are critical, as they allow both targeted and untargeted characterization of the main classes of metabolites occurring in a given matrix [50,51,60,61,52–59].

1.1.1 Bio-based content and biodegradability

Both bio-based and biodegradable plastics have become the most widely used option among bioplastic materials as their production has a low-environmental impact compared to traditional petroleum-based plastics [62]. To promote the diffusion of these polymers, the Public Procurement Working Group of the European Commission's Expert Group for Bio-based Products published several recommendations in order to enable procurement policies to embrace eco-friendly materials. For instance, it is necessary a common labelling as well as the existence of standards and test methods to define and measure properties and characteristics such as bio-based content, biodegradability and other specific attributes of ready-to-market products.

The bio-based content of a material is the amount of the biomass-derived carbon, as compared to its total organic carbon content (TOC). The carbon content of bio-based materials is determined independently and unequivocally as reported in international standard methods of the American Society for Testing and Materials (ASTM) and of the International Organization

for Standardization (ISO). In particular, ASTM D6866-20 and ISO 16620-2 methods report radiocarbon analysis as the technique to determine the bio-based content of solid, liquid and gaseous samples. The employment of the radiocarbon dating method is based on the significant difference in ^{14}C isotopic signature between the fossil derived (^{14}C -free) and the biomass derived (^{14}C -including) materials. In detail, the presence of ^{14}C in the bio-based materials is due to the fact that ^{14}C containing carbon dioxide formed in the atmosphere participates in the photosynthetic processes from which the biomass derives. Thus, the ^{14}C content of biomass derived materials is the result, in a first approximation, of ^{14}C atmospheric levels [63,64]. ^{14}C measurements can be done by using Accelerator Mass Spectrometry (AMS) along with Isotope Ratio Mass Spectrometry (IRMS) or by using Liquid Scintillation Counting (LSC) techniques (ASTM International, 2020). In order to define a bioplastic as bio-based, a biomass-derived carbon content not less than 25% is required [65] (**Figure 1.2**).

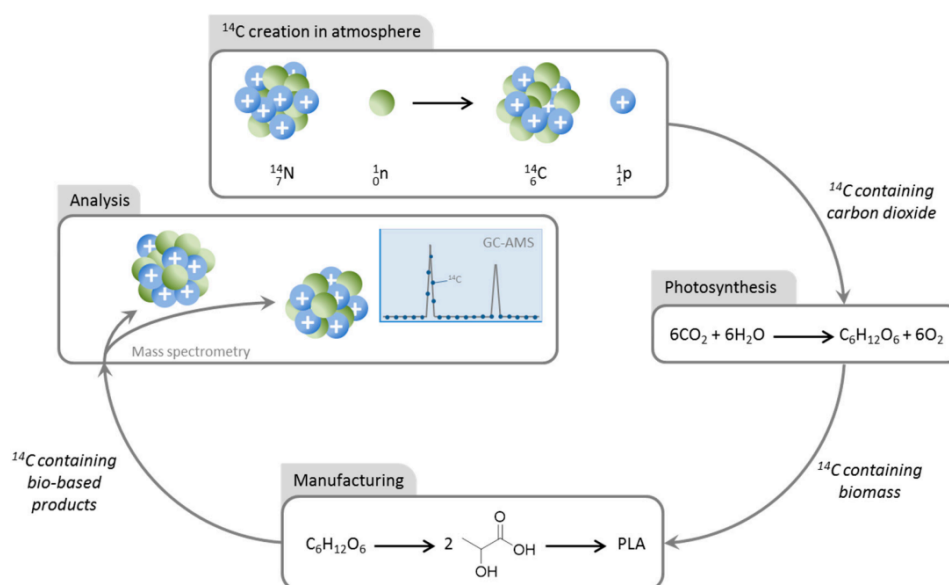


Figure 1.2 Radiocarbon dating method used for bio-based content analysis. Reproduced under the terms of the Creative Common CC BY license which permits reuse in any medium, provided the original open access work is properly cited [64].

Another key bioplastic property to be measured is the biodegradability, that refers to the ability of a material to decompose after interactions with biological elements [20]. The degradation of bioplastics occurs through the materials physical-chemical decomposition and/or materials breakdown by microorganisms. When the decomposition in the environment occurs through microbial action, it is called biodegradation. The biodegradation of polymers involves three steps: bio-deterioration, bio-fragmentation and assimilation (**Figure 1.3**) [66]. Bio-deterioration

is the modification of mechanical, chemical, and physical properties of the polymer due to the growth of microorganisms on or inside the surface of the polymers. In the bio-fragmentation step, microorganisms hydrolyze polymers in oligomers and monomers which, in the next assimilation step, are available as their carbon, energy and nutrient sources that finally derive in CO₂, water and biomass as by-products [20]. It should be pointed out that only specific microorganisms can degrade a given type of bioplastic. It has been reported that PCL can be degraded by bacteria isolated in deep sea sediments, which are incapable of degrading other types of bioplastics such as PLA, PHB and PBS. However, there are composting bacteria able to degrade the latter [20]. This specificity towards a given type of bioplastic is due to microorganisms' enzymes (cutinases, lipases) involved in the biodegradation. All these enzymes act on the polymer in a similar manner, causing the hydrolytic cleavage of the long carbon chains and then assimilating the smaller subunits into the microbial cell for further enzymatic degradation [67]. However, the active site of the enzyme is specific, as it is accessible and can accommodate more or less easily only specific polymers.

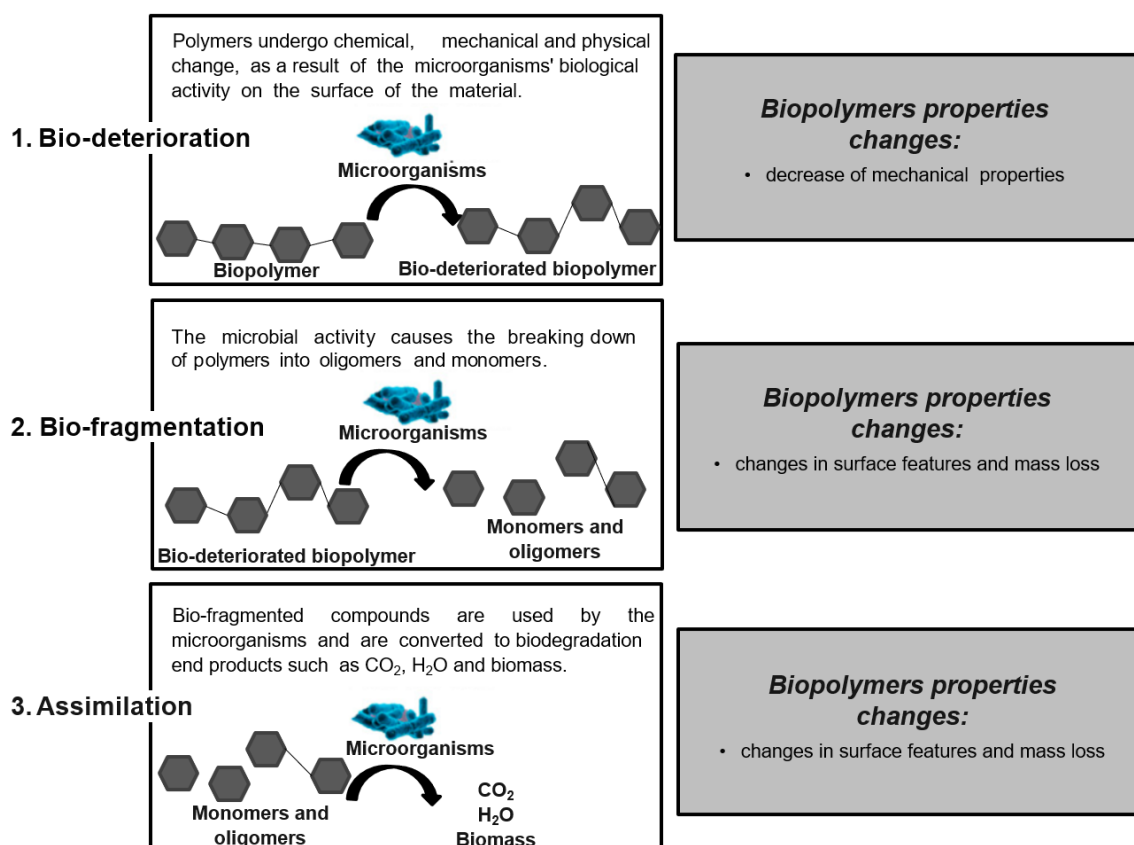


Figure 1.3 The main three steps through which the biodegradation of polymers occurs: (1) bio-deterioration, (2) bio-fragmentation and (3) assimilation.

The biodegradation of bio-plastic materials is highly dependent on their chemical structures. In general, polymers with a lower molecular weight and more amorphous domains are more susceptible to biodegradation by microorganisms [68]. The molecules in the amorphous region are loosely packed and, hence, more accessible thus making it more susceptible to degradation. As biodegradation generally occurs through hydrolytic cleavage of bonds, an important requisite for high biodegradation rate is the presence of hydrolyzable bonds such as O-C=O and -C-O-C-bonds. The presence of additives can also influence the biodegradability of a matrix. As an example, polypyrrole, the archetype of polymers used in devices for biomedical applications, has enhanced biodegradability when it is grafted onto cellulose chains, thus forming a biocomposite [69,70]. Moreover, also the pH, the temperature and the oxygen content of the environment in which the polymers are placed or disposed of are key factors for their biodegradation [71,72]. For example, oxidative-degradable or photodegradable polymers accelerate their decomposition under the effect of oxidation through heat and/or UV light. UV radiation can disrupt polymer chains, since the radiation can be absorbed by oxygen-containing components to initiate a primary degradation. During photodegradation, both molar mass and crystal structure are affected. The plastics that have the capacity to biodegrade by hydrolytic mechanisms such as biopolymers made of cellulose, starch, and polyesters such as PHA are known as hydro-biodegradable bioplastics [73].

To date, a wide variety of methods for measuring the biodegradability of polymeric bio-materials have been currently developed and most of them are in agreement with ASTM, ISO and European Standards (EN) standard methods in terms of environmental conditions, timings and scales of the tests. Overall, all methods are focused on an indirect measure of the degradation process such as oxygen consumption or biogas generation (CO₂), by measuring differences of pressure in the test flasks and carbon dioxide production [18]. A biodegradation level higher than 90% in comparison with cellulose (positive standard) in 180 days, under conditions of controlled composting measured through respirometric methods, has been established by the European Norm EN 13432 as level for a material/product to be defined as biodegradable and compostable. In addition, a disintegration level higher than 90% in 3 months and the respect of ecotoxicity and chemical safety criteria should be kept. Then, only when the products meet the EN 13432 standard criteria the wording “biodegradable” could be reported on the packaging label. The biodegradation of bioplastics has been extensively investigated in soil and compost environments where they mainly show high degradability [20]. In any case, the conditions of the experiments conducted to study the bioplastics’ biodegradability are highly variable and a fair comparison among them is difficult. The experiments carried out in compost or in anaerobic

digestion environments show a bioplastics' biodegradability over 50% in 65 and 68% of the cases, respectively. For those carried out in aquatic environments, this share is 44% and for experiments carried out in soil, it is 33% of the cases [73]. It should be pointed out that, in addition to increasing bio-based content and biodegradability, bioplastics' intrinsic properties often need to be improved to meet industrial expectations. The optimization is referred to, for example, mechanical and barrier properties (e.g. increased material flexibility, rigidity and resilience as well as lower water permeability and water uptake) [74–76].

1.1.2 Bioplastics' physical properties

In order to assess the suitability of a biomaterial for a given sector and establish the service life that can be expected, an evaluation of its physical (for instance, mechanical, thermal, optical and barrier) properties is mandatory. Among them, mechanical properties are the most important. The main mechanical properties which are typically tested after the production of a bioplastic are the ultimate tensile strength, the Young's modulus and the elongation at break. The ultimate tensile strength, or just tensile strength, indicates the maximum stress that a material can withstand before fracturing, while the Young's modulus, also known as elastic modulus, defines the stiffness of a material: the higher is its numerical value, the stiffer is the material [77]. As regard to the elongation at break values, they are a measure of material ductility. The elongation at break value is, generally, very small and close to zero for brittle materials. On the contrary, materials with a better capacity to handle an excessive load without failure show higher elongation than 100% [78]. Obviously, all these properties are affected by the chemical structure, e.g. the orientation degree of the polymers and the crystallinity of the material, as well as by the eventual presence of fibres, which act as reinforcement, or plasticizers [79,80]. Plasticizers are low volatile molecules that, when added to polymer matrices, ensure an increase of their extensibility, flexibility and elasticity [81]. Several theories to explain the mechanisms of plasticization action have been proposed [82]. The lubrication theory states that plasticizers, by interspersing themselves, act as internal lubricants by reducing frictional forces between polymer chains. The gel theory, instead, postulates that the rigidity of polymers comes from three-dimensional structures and plasticizers take effect by breaking polymer-polymer interactions (e.g. hydrogen bonds and van der Waals or ionic forces). The free volume theory states a plasticization as a study of ways to increase free volume and it is useful for explaining the lowering of the glass transition temperature (T_g) by a plasticizer. Ideal plasticizers are miscible

and compatible in all proportions with plastic components and may be added to polymers in solution (dispersion technique) or after solvents have been removed (absorption technique) [83,84]. Water, oligosaccharides, polyols and lipids are different types of plasticizers widely used for edible films and coatings [85].

For hydrophilic polymers, polyols have been proven to be very efficient as plasticizers [86,87]. In particular, for bio-based polymers obtained from fruits and vegetables waste, recent studies have focused on the usage of glycerol [88–92] and sorbitol [93]. Glycerol content has significant effects on the mechanical properties as well as on the dynamic rheological behaviour of thermo-molded bioplastics. Indeed, it was demonstrated that the increase of glycerol content decreases tensile strength and Young's modulus, but improves ductility at room temperature [94]. Several studies on plasticization of chitosan films revealed that polyethylene glycol (PEG) can improve the elastic properties of the chitosan biopolymer. For example, Caner et al. [95] observed that chitosan plasticization using PEG was stable until 9 weeks of storage (**Figure 1.4**).

In addition to the mechanical properties, plasticizers also affect other physical properties such as water vapor permeability (WVP), oxygen permeability (OP) and water contact angle (WCA) of bioplastics (**Figure 1.4**) [44]. These parameters are indicators of how easily water vapor or oxygen can penetrate into a biodegradable material. They are a function of its hydrophilicity and hydrophobicity ratio. The water contact angle, which is measured as the angle between the baseline of a drop deposited on the surface of the material and the tangent at the drop boundary, increases with higher surface hydrophobicity [87]. Furthermore, the evaluation of WVP and OP is also typically demanded. Recently, Aguilar et al. [96] found that different physical and mechanical properties can be achieved at room temperature for bioplastics based on a soy protein isolated as a by-product of the soy oil industry and added with different polyols, e.g. glycerol (GLY), ethylene glycol (EG), diethylene glycol (DEG) and triethylene glycol (TEG). In this sense, TEG-bioplastics were opaque, brittle and also with a higher water uptake capacity, while EG-bioplastics were more ductile and translucent, absorbing much less water when immersed. Only GLY and TEG remained in the bioplastic after 9 days of storage at 50°C, pointing out the volatility of EG and DEG causing a major ageing effect. On the other hand, sugars such as sucrose and trehalose can act as plasticizers in the presence of water. When water is included in the bioplastic formulation together with glycerol, sugars are solubilized within the aqueous fraction, and then play a plasticizer role in the bioplastics. In that case, lower viscoelastic properties and higher water absorptions are generally observed [97].

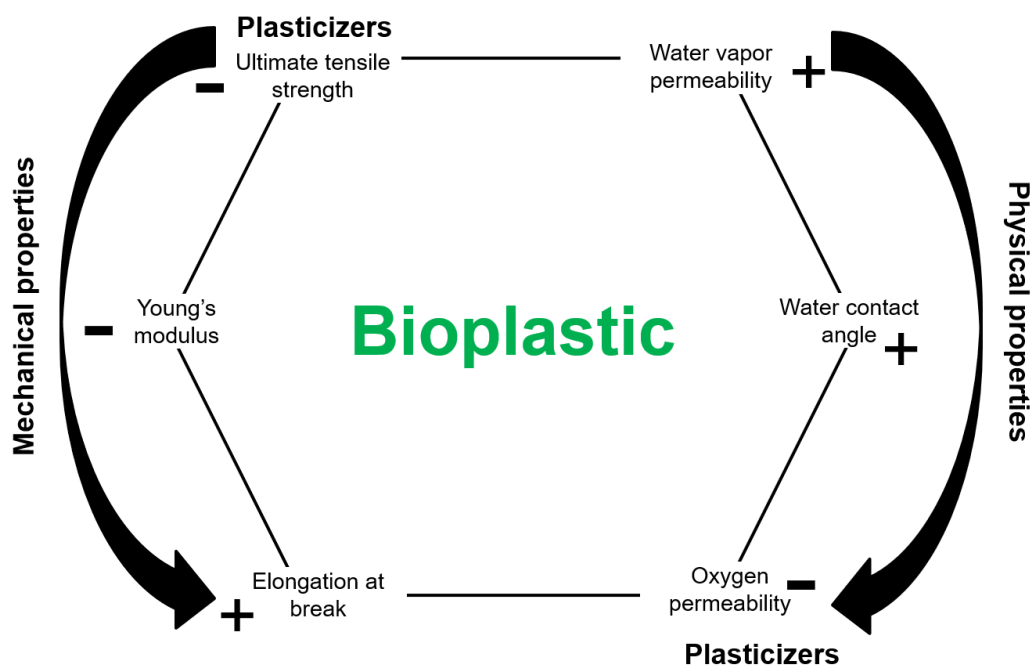


Figure 1.4 Effects of the plasticizers' addition on mechanical and other physical properties of bioplastic materials.

1.2 Food waste as a feedstock for bioplastic production

The most recent research concerning bioplastic production focuses on by-products and waste materials of food industries. According to the Food and Agriculture Organization (FAO) of the United Nations, every year an estimated 1.3 billion tons of food is wasted globally from all stages of the food supply chain including post-production, handling/storage, manufacturing, wholesale/retail and consumption. Since food waste landfilling yields undesirable results such as greenhouse gas (GHG) emissions and groundwater contamination, their valorization through bioplastics production offers the possibility to overcome their disposal problem by renewable sustainable processes [98]. In addition, the production of value-added products while reducing the volume of waste is expected to reduce the production costs of biodegradable plastics in comparison to conventional routes of production using overpriced pure substrates [98]. Food waste (FW) can be valorised in several ways in order to produce bioplastics (**Figure 1.5**).

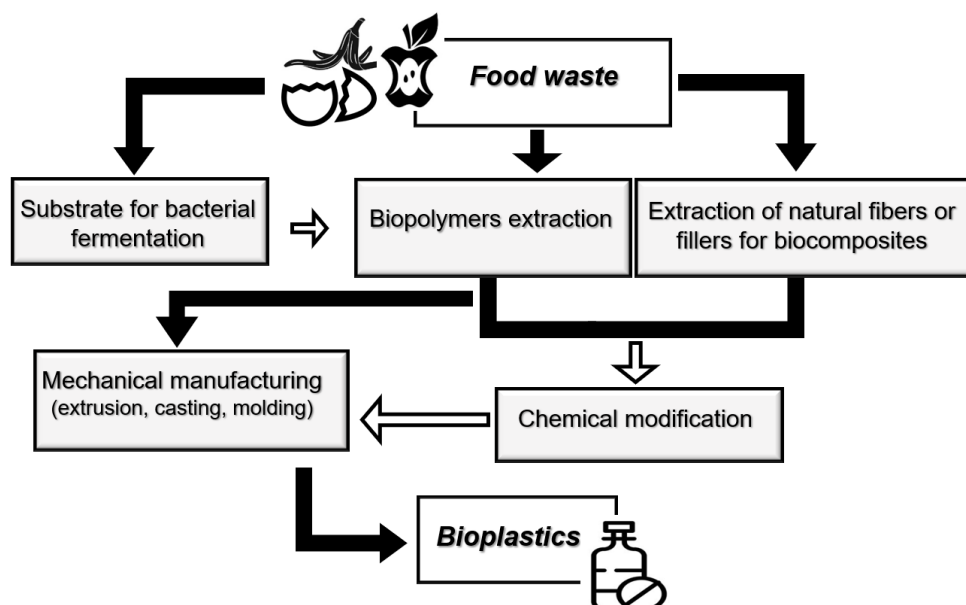


Figure 1.5 Conversion of food wastes into bioplastics occurs through biopolymers extraction and their mechanical manufacturing (extrusion, casting, molding or a combination of them). In more complex processes, food wastes are used as substrates for bacterial fermentation in order to produce biopolymers or as raw materials for the extraction of other natural components, such as fibers, which act as reinforcing agents and/or natural fillers of bio-composites. For some bioplastics, a chemical modification is also necessary.

Food waste is often used as a substrate for bacterial fermentation to obtain natural polyesters, namely PHA and PLA. When used to produce PHAs, food waste is a main candidate for an inexpensive carbon source, due to its widespread availability and the potential to solve significant waste problems. In this case, physical, thermo-chemical and biological pre-treatments of the FW are requested. Briefly, as reported by Tsang et al. [98], a preliminary liberation of monomers from the FW (e.g. lignocellulosic components) with increasing accessibility of proteins, lipids, and polysaccharides (mainly starch and cellulose), for subsequent enzymatic hydrolysis and fermentation, are essential. After the pre-treatment, the FW is ready for a fermentation step in presence of bacteria by using several cultivation strategies. Other simple technologies for the production of bioplastics involve the direct extraction of the biopolymeric components of interest from the food-waste-stream. More complex processes, on the other hand, require additional steps through which the biomass or the biopolymers extracted from it are used as reinforcement or fillers for the fabrication of bio-composites or even chemically modified [99].

In many cases, the different "bioplastic formulations" need to be blended with additives in order to fix some problems of the materials such as thermal instability, high water vapour permeability, brittleness and low melt strength. Plasticizers are often required to improve the processability

and the mechanical properties by interrupting hydrogen bonding and reducing the interactions between the biopolymers chains [81]. However, both formulations, biopolymeric and bio-composite are finally processed to obtain biofilms or three-dimensional objects by applying conventional mechanical techniques: extrusion, molding, casting or a combination of them [88,100,101]. All these processing methods selected for the manufacturing of food waste-based bioplastics play an important role in their final properties [102].

1.2.1 Processing methods

The mechanical technique chosen for the processing of the bioplastic formulation depends on the thermal stability of the natural sourced materials. As many of them show low thermal stability, the processing temperatures used are lower than 200 °C [103]. Extrusion is a highly efficient way for the continuous shaping of biomaterials that consists in pushing the bioplastic dough against an orifice with the desired geometry and dimensions. The mass of the dough inside the extrusion chamber is compacted and the semi-finished product that comes out is cut to give the wanted length. Casting is a common processing technique employed to produce biofilms, which consists in the preparation of a polymer solution subsequently poured into a mold and dried under ambient conditions or oven-dried at elevated temperatures. Instead, by using molding process, the dough is pressed against a rigid frame. Compression molding technique has been widely employed for the development of biofilm or 3D objects without the use of any solvent or binder [88,104]. With this technique, the waste of interest or its dried extract is finely powdered and subjected to high temperatures and pressures through a heated press. One of the most important advantages of this technique is the possibility to control fibers orientation: fibers can be selectively or randomly orientated to produce a composite with isotropic properties, as desired. Furthermore, the molding method is more suitable for industrial applications since it is characterized by lower energy demand and processing time compared to other techniques like solution casting [104].

In the last ten years, several food wastes have been used as a raw material for the production of bioplastics, including bio-composites, mostly fruit and vegetable wastes rich in polysaccharides (such as cellulose, starch, cutin and pectin) and in fibres [90,93,102,105–107]. In the next paragraphs, a focus on the main uses of fruits and vegetables wastes for the production of bioplastics is provided.

1.2.2 Biopolymers-based plastics

Biopolymers extracted from fruit and vegetable wastes show different characteristics and properties that make them more or less suitable for the production of eco-friendly materials (**Table 1.1**). The extraction of biopolymers from food waste is usually achieved by chemical or enzymatic procedures. Enzymatic processes are widely considered “clean” since they are organic solvent-free [108]. However, this technology is still hindered by economic and technical limits, i.e. expensive enzymes and long processing periods. Also the production of bioplastics through bacterial fermentation of sugars naturally occurring in food waste is disadvantageous, as it is expensive and time-consuming. Therefore, chemical extraction with solvents is considered as the best solution at the lowest amount of energy.

Table 1.1 Properties associated with the main biopolymers extracted from fruit and vegetable wastes for bioplastics production [37,109–111].

Biopolymer	Biopolymer type	Properties	Fruit and vegetable wastes used as biopolymer source
<i>Cellulose</i>	Polysaccharide	Highly structured intermolecular hydrogen bonding network; insoluble and infusible.	Banana peels, carrots waste, cauliflower waste, cocoa pod husks, orange peels, parsley stems, radicchio waste, rice hulls, spinach stems, tea leaves waste.
<i>Starch</i>	Polysaccharide	Strong inter- and intra-molecular hydrogen bonding; water sensitivity and poor flowability; brittleness.	Banana peels, cassava peels, potato peels.
<i>Pectin</i>	Polysaccharide	Gelling ability but poor tensile and barrier properties; water sensitivity.	Apple pomace, banana peels, citrus waste, orange peels
<i>Cutin</i>	Polyester of hydroxy fatty acids	Amorphous and flexible three-dimensional polymer; hydrophobic, low water sensitivity.	Tomato waste

One of the main macromolecules extracted from fruits and vegetables waste and used for the production of bioplastics is cellulose. The preparation of pure cellulose-based bioplastics from bioresources is not easy due to the highly structured intermolecular hydrogen bonding network of the polymer, which cannot be melted or dissolved by standard processes such as thermoforming [33,112]. Thus, cellulose is usually used in industrial applications in the form of derivatives, such as esters or ethers, from which cellulose is then regenerated [113]. Nevertheless, in recent years, several bioplastics have been manufactured through amorphous cellulose extracted from vegetables by using different solvents. Bayer et al. [33] prepared amorphous cellulose-based biomaterial by digesting microcrystalline cellulose (MCC), parsley

and spinach stems, rice hulls and cocoa pod husks wastes in trifluoroacetic acid (TFA), followed by casting and evaporation. TFA is a naturally occurring and biodegradable organic acid that can co-solubilize cellulose with the other contained organic matter. It partially trifluoroacetylates OH groups of cellulose, breaking the hydrogen bonds between neighbouring cellulose chains and. When the solution is casted, TFA quickly evaporates and the trifluoroacetates are hydrolyzed by the moisture, resulting in the formation of amorphous cellulose materials [114]. The mechanical properties of the produced cellulose-based biofilms were proved to be largely dependent on the starting agro-waste. Indeed, cocoa pod husk-based bioplastic displayed a tensile stress at break of approximately 30 MPa, whereas for rice hull, parsley and spinach stems-based derived films, the obtained values were, respectively, of 7 MPa, 5 MPa, and 1 MPa, i.e values close to elastomers and thermoplastic low density polyethylene [33] (**Figure 1.6a**). Moreover, these values were significantly lower compared to pure cellulose-based films, which showed a tensile stress at break of ~65 MPa.

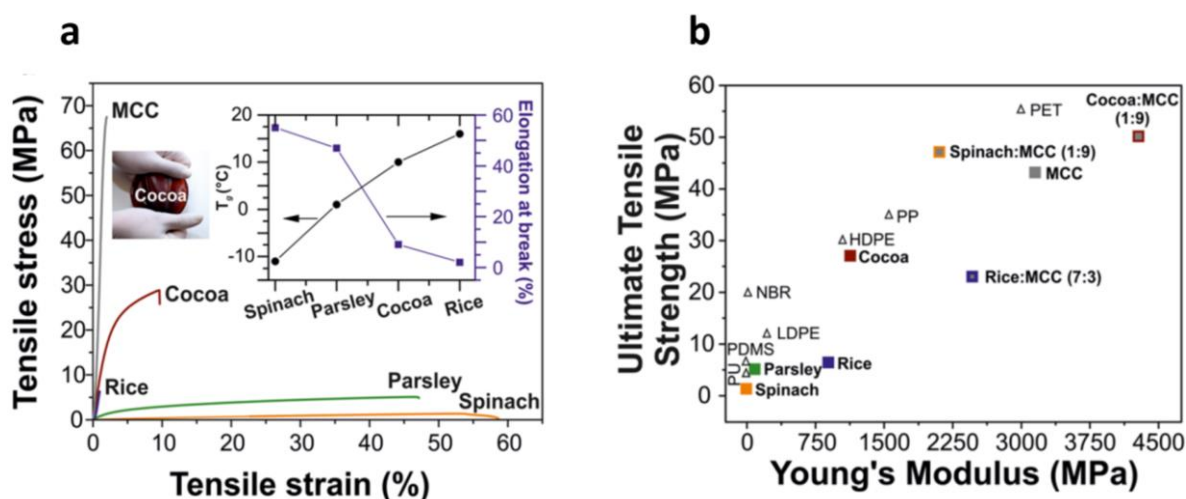


Figure 1.6 Stress-strain curves for pure cellulose (MCC), cocoa, rice, parsley, and spinach films (a). Ultimate tensile strength versus Young's modulus data (b). Adapted with permission from Bayer, I. S., Guzman-Puyol, S., Heredia-Guerrero, J. A., Ceseracciu, L., Pignatelli, F., Ruffilli, R., Cingolani, R. & Athanassiou, A. Direct transformation of edible vegetable waste into bioplastics. *Macromolecules*, 47(15), 5135-5143. Copyright 2014 American Chemical Society [33].

Such a higher stress and strain at break for cocoa pod husk-based bioplastic was due to its significant amount of triglycerides. Instead, residual silica in the rice hull derived material conferred a higher rigidity compared to parsley and spinach based-biomaterials. Ultimate tensile strength (UTS) at high Young's modulus of bioplastics from cocoa pod husk were comparable with petroleum-based thermoplastics such as high density polyethylene and polypropylene (**Figure 1.6b**). Rice straw was used also by Bilo et al. [115] to produce a new cellulose-based bioplastic material through a process which involved the digestion with TFA, preceded by an

extraction pre-treatment performed in a rapid dynamic solid-liquid extractor. With this process, a bioplastic with better mechanical properties than those evaluated by Bayer et al. [33] was obtained, as the extraction pre-treatment presumably allowed to partially remove silica. Indeed, the tensile test of dried and wet dumbbell specimens allowed to ascertain tensile strengths and elongations at break equal to 45 MPa and 6.1% and 10 MPa and 63%, respectively. The replacement of TFA with a diluted aqueous hydrochloric acid (HCl) solution has been found to be a more sustainable method to fabricate bioplastics with higher stiffness and lower ductility. Perotto et al. [116] used this water-based process to convert carrot, parsley, radicchio and cauliflower wastes into flexible bioplastic films, made by cellulose crystals fused together with some soluble components such as pectin and sugars acting as plasticizers. Compared to oil-based polymers, the Young's modulus (1.3 ± 0.2 GPa) and the UTS (38 ± 5 GPa) of the carrot bioplastics are similar to those of polypropylene, albeit with lower elongation. The mild conditions of the conversion process were demonstrated also to preserve the functional properties of the original vegetable like the antioxidant activity [116].

Although TFA and HCl are efficient acids for vegetable waste derived-cellulose dissolution, their utilization and waste production remain problematic if considering the principles of green chemistry. Recently, a less harmful acid, i.e. citric acid, has been used by Liu et al. [117] in a green, non-toxic, waste-free method of synthesizing hydrophobic bioplastic films from spent tea leaves. The resultant material exhibited an ultimate tensile strength of 6.2 MPa and an elongation at break of 13.3%, thus it had a lower stiffness compared to oil-derived polymers, such as PP. Since citric acid was found to not fully react with the tea waste matrix, the authors hypothesized that unreacted citric acid acted as a hygroscopic plasticizer in the bioplastic film.

In addition to cellulose, also starch (i.e. a polysaccharide consisting of a long chain of two glucose units joined together, namely branched polymerized amylopectin and amylose) can be considered as an effective eco-solution for the production of bioplastics, since it is inexpensive and easily available (**Table 1.1**). Starch can be isolated from different sources, mainly potatoes, banana and cassava peels [90,118–123]. Arikan et al. [119] investigated the production of bioplastics from potato peel wastes, obtaining satisfactory results in terms of biodegradability (the time for the complete biodegradation of the material was 28 days). However, native starch-based films are limited due to their high-water affinity and brittleness. To overcome this drawbacks, other natural biopolymers are often added as fillers to modify and improve starch-based films' properties. As an example, Dasumiati et al. [121] and Fathanah et al. [122] improved the mechanical properties of starch derived from cassava peels by introducing chitosan as filler. In another work by Muhammad et al., proteins derived from soybeans waste were mixed with

starch. Glycerol was used as plasticizer, since the structure of soybeans proteins consists of stable three-dimensional networks which do not ensure material with enough plasticity [124]. Instead, Sultan et al. [90] developed bioplastic films from a combination of starch derived from banana peels and different concentrations of corn starch (1% up to 5%) as co-biopolymer. Based on the obtained results, the film with 4% of corn starch gave the highest tensile strength (34.7 N/m^2) compared to other samples. Moreover, the authors stated that the films with 3% of corn starch were resistant to water uptake by absorbing water up to 60.7%. However, this value is considerably higher compared to conventional plastics such as PP, whose percentage of water absorption after 24 hours of immersion ranges between 0.01 and 0.03.

On the other hand, pectins are a family of covalently linked galacturonic acid-rich plant cell wall polysaccharides with functions in plant growth, morphology and development, serving also as gelling and stabilizing polymers in diverse foods [125]. The production of pectin-based films typically involves the introduction of cellulose and hemicellulose components, since films with pectin as the single component show poor tensile and barrier properties compared to those of petroleum-derived polymers. To this regard, Oliveira et al. [75] isolated pectin from banana peels in order to prepare a bioplastic whose tensile strength was increased through the addition of cellulose nanocrystals (CNCs) extracted from the same banana wastes (tensile strength values were about 7 MPa). The tensile strength increase was due to the favourable nanocrystal–pectin interactions as well as to the reinforcing effect through stress transfer at the nanocrystal–pectin interface [126].

Aside from the poor mechanical properties, the strong hydrophilic character of polysaccharidic films makes them soluble in contact with water, limiting their applications [75]. To overcome the high water permeability, citric acid can be added, as it crosslinks polysaccharidic films by forming covalent diester linkages between two of their carboxyl groups and hydroxyl groups of different polysaccharide chains [127]. However, in the previous mentioned work reported by Oliveira et al. [75], the presence of citric acid was ascertained to not significantly decrease the water vapor permeability, as WVP passed from 3.3 to $3.1 \text{ g mm kPa}^{-1} \text{ h}^{-1} \text{ m}^{-2}$ for samples obtained without and with citric acid, respectively. Citric acid was used also for the processing of orange and apple wastes (OW and AW) in order to prepare a biodegradable film through a casting method in which cellulose and hemicelluloses were suspended in the pectin solution and further dried [88,92]. On the other hand, Batori et al. [92] used a solution of citric acid and glycerol to form a bio-based film from OW, exploiting the gelling ability of pectin and the strength of its cellulosic fibres. The tensile strengths of the films were 31.7 ± 4.2 and 34.8 ± 2.6 MPa, respectively, for the oven-dried and incubator-dried films. These values were within the range

of different commodity plastics. In addition, anaerobic digestion was performed for testing the biodegradability of the material and a time of 15 day was requested to reach 90% of degradation. Instead, from a mixture of AW and glycerol, a fluffier and connected structure (tensile strength 3.3 ± 0.3 MPa without including a washing step) was obtained by Gustaffson et al. [88], but with significant flexibility, similar to those of PP (elongation at break of bioplastic: $55.4 \pm 5.4\%$).

The same authors [88] made an attempt to produce bioplastics by using solvent-free mechanical processing of AW. Compression molding technique has been widely employed for the development of pectin-based biofilm or 3D objects without the use of any solvent or binder [88,104]. Gurram et al. [104] applied a compression molding method for the production of bioplastic films with pectin derived from citrus peel. Moreover, free sugars and water-soluble nutrients were extracted from citrus waste and employed for cultivation of the filamentous fungus *Rhizopus oryzae*, whose biomass was incorporated into the pectin films. The addition of fungal biomass (up to 20%) enhanced the tensile strength (16.1–19.3 MPa) and reduced the water vapor permeability of the pectin films.

In addition to cellulose, starch and pectin, a sustainable solvent-free, melt polycondensation of unsaturated and polyhydroxylated fatty acids recovered from tomato pomace agro-wastes has been recently carried out in order to prepare an aliphatic polyester type of bioplastic [128]. Polyhydroxylated fatty acids are found in tomato pomace in the form of cutin, i.e. a biopolyester mainly composed of C₁₆ and C₁₈ fatty acids monomers linked together and forming an amorphous and flexible three-dimensional polymer matrix [129]. Since cutin isolation to produce bioplastics is a long multistep process and unsuitable for large-scale applications, a direct depolymerized of tomato pomace through alkaline hydrolysis (that allows the incorporation of unsaturated fatty acids from tomato seeds), followed by monomers polycondensation, has been proposed by Heredia-Guerrero et al. [128] as a simpler and cheaper alternative. To that purpose, the influence of different temperatures, reaction times and amounts of tin (II) 2-ethylhexanoate used as a catalyst, was evaluated. Synthesized tomato pomace-based bioplastics showed an amorphous molecular structure, whose mechanical properties were dependent on the degree of polymerization. Thus, an increase in hardness of the polyesters synthesized at higher reaction temperatures and amount of catalyst was detected (~1.8 MPa for biopolymers obtained at 125°C and 0 mmol of catalyst against ~26.3 MPa for biopolymers obtained at 175 °C and 0.1 mmol of catalyst), since in those conditions a higher degree of polymerization was achieved. The water-contact angles of more polymerized samples were around 109°, which are values comparable to traditional hydrophobic polymers such as PDMS and PTFE. Regarding water uptake, the obtained percentages were typical of low-absorbing plastics (from 2 to 61%).

1.2.3 Food waste usage for bio-composites production

Usually, biopolymers extracted from food waste whose mechanical and physical properties are not suitable to accomplish commercially acceptable products, are combined with fillers thus fabricating composite materials, known as bio-composites [101]. Biocomposite materials are usually made by a polymeric matrix coming from a renewable and available origin reinforced by fillers, which can be inorganic or natural particles or other polymers. Examples of natural fillers are layered silicates. They can be synthesized from silica naturally occurring in leaves, husks, blades, hulls, roots and stems of many terrestrial and marine plants, including wheat, rice, horsetails, oats, barley, grasses and algae. Among biological wastes, one of the most silica-rich sources is largely available rice husks, being typically 20–22 wt% of rice grains. They have been used by Deng et al. [130] for layered silicates synthesis. Layered silicates (LSs) have hydrophilic characteristics owing to the presence of inorganic cations (Na^+ and Ca^{2+}) in the interlayer spacing, hence being miscible with different hydrophilic polymers, including starch and pectin, able to compensate their rheological property differences [101]. Despite not being recovered from vegetable wastes, Cokaygil et al. [101] used LSs as a natural filler to prepare biocomposite films having corn starch and pectin extracted from orange peels as a polymeric matrix. Different pectin jelly-to-starch weight ratios (63/37, 60/40, 57/43, and 54/46 w/w) were considered when formulating the film ingredients. Furthermore, to enhance the compatibility and wettability among starch, LS and pectin, starch and LSs were chemically modified through reaction with propylene oxide and hexadecyltrimethylammonium chloride, respectively. Among all the films considered, pectin jelly/modified starch-based biocomposite film (54/46 w/w) containing 0.25 wt % of LSs was found to be the most promising in terms of texture structure and mechanical integrity.

In the most recent years, wastes of agro-food industries have attracted attention also as sources of natural fibres exploitable as reinforcing elements of biodegradable biocomposite materials. These biological fibres, which are natural polymers, can be obtained from a large variety of fruits and vegetables [131]. In 2013, Schettini et al. [107] developed a novel biocomposite by using hemp and tomato peels and seeds fibres as a natural reinforcement for sodium alginate polymer to produce biodegradable pots in agriculture. Three different biocomposites were prepared by varying the percentage of tomato and hemp fibres added to sodium alginate water solution. By soaking the doughs with a calcium chloride solution, a three-dimensional and stable crosslinked network of calcium alginate was obtained as well and it was subjected to investigation of its functionality, physico-chemical and mechanical behaviour. As reported by the authors, by

increasing the hemp fibres content, a general enhance of the mechanical parameters of both un-crosslinked and crosslinked samples was registered, since fibres from hemp strands are more rigid, stiff and long in comparison to the more flexible and short fibres from tomato peels and seeds [132]. Moreover, crosslinked biocomposites showed a lower rigidity and strength with respect to their corresponding non-crosslinked counterparts (Young's modulus for non-crosslinked 100% tomato fibres biocomposite was 63.6 MPa, while for crosslinked 100% tomato fibres biocomposite it was decreased to 48.1 MPa). Such a behaviour was due to the loss of adhesive properties which occurs when carboxylated and hydroxyl groups of alginate are strongly engaged in physical interaction with calcium ions during the crosslinking process, thus reducing the bonding strength between the matrix and the fibres [133]. However, these obtained values were all comparable to those of conventional plastics. Instead, Mathivanan et al. [134] used different percentages of pineapple leaf fibres to reinforce tapioca-based bioplastic resin through a method based on extrusion followed by hot compression moulding. The 30% composition showed the best average modulus value among other compositions, leading to the conclusion that the increase of pineapple leaf fibres increases the modulus strength of the composite.

Since passion fruit waste contains about 60% of fibres [135] it can be used as a reinforcement. In this sense, Moro et al. [136] developed an extruded starchy bioplastic, reinforced with different content of passion fruit peel (0, 4, 10, 16, and 20%), glycerol and starch mix, recovered from corn and cassava. In this manner, it was possible to obtain starch-based bioplastic with stronger and midterm elastic properties (tensile strength ranged between 1.6 MPa and 9.0 MPa, while the elongation at break values were between 24.7% and 54.5%). Despite this, the tensile strength values were lower than those of oil-derived polymers.

On the other hand, bio-based blends of poly-butylene succinate (PBS) and poly-butylene-adipate-*co*-terephthalate (PBAT) have been recently proved to be strengthened in terms of higher modulus (3.0 GPa) and lower water absorption (3.4%) with the addition of Miscanthus fibre and oat hull followed by reactive extrusion [137]. Indeed, PBS alone has a tensile strength of around 26.5 MPa, elongation at break of 21.5% and a Young's modulus of ~48 MPa. The incorporation of fibers or cellulose remarkably improves the Young's modulus of neat PBS.

For their rich content in lipids, lignin and fibrous polysaccharide components (cellulose, hemicellulose), also peanut hulls and cocoa shell waste (CW) and hazelnut skin (HS) extracts have been introduced into synthetic elastomers matrices as reinforcement fillers and plasticizers [76,138,139]. Battegazzore et al. [76] made selective and serial extractions from CW and HS to recover biocomponents for producing high-added value PLA and PP plastics. Briefly, a first

extraction with diethyl ether mainly separated lipids, phospholipids and triglycerides which acted as plasticizers. In the second extracted fraction, phenolic compounds and flavonoids such as gallic acid and catechin were distinguished by UV spectroscopy. This fraction served as antioxidant and photo-stabilizer for PP. In addition, it positively influenced the PP thermal stability in air. Indeed, the temperature of its maximum weight loss was increased from 319 to 330 °C and 345 °C by adding HS and CW extracts, respectively. Finally, the last fraction extracted, comprising both lipids and phenols was used as a reinforcement filler for PLA and PP. Their content linearly influenced the oxygen permeability of the prepared bioplastics. Instead, Tran et al. [139] introduced cocoa shell waste powder within an acetoxypoly(dimethylsiloxane) silicone network, through a process that involved a physical mixing with a nontoxic solvent and casting into a mold, with the advantage of direct utilization of CW without any extraction or purification steps. In this case, the antioxidant activity of the final cross-linked bioelastomers was investigated, demonstrating very effective radical scavenging activity against 2,2-diphenyl-1-picrylhydrazyl free radical and 2,2'-azinobis(3-ethylbenzothiazoline-6-sulfonic acid) radical cation.

As PLA reinforcement, also cellulose extracted from pumpkins peels, and subsequently acetylated, has been used [140]. In this case, the addition of 10% of acetylated cellulose enhanced the PLA mechanical properties with an increase of the storage modulus at 40 °C of around 40%. Overall, cellulose or cellulose nanocrystals have been obtained from various vegetable and fruit wastes such as banana peels, pine flowers waste, rice straw, palm empty fruit bunch, sago waste, mangosteen peels and successfully employed also as reinforcements of biopolymers, mainly starch [105,141–145]. Also banana pseudostem wastes have been recently used to isolate nanocellulose employed for the production of green composites enriched with nano-fillers such as graphene oxide and nanoclay and glycerol as plasticizer [91]. Regarding to rice straw, besides being considered as reinforcement, its fibres were proved to act as flame-retardant fillers in combination with PLA and lignin by Dahy et al. [146]. Typically, synthetic flame retardant used to reduce combustibility of the polymers are halogen-based additives which act in the vapour phase by a radical mechanism to interrupt the exothermic processes, interfering with the combustion process during heating, pyrolysis, ignition or flame spread. Instead, natural fillers such as rice straw-derived fibres act by releasing non-flammable gases or decomposing endothermically to cool the pyrolysis zone at the combustion surface [147].

1.3 Environmental impacts of food waste-based bioplastics production

The so-called bioeconomy, which comprises those parts of the economy that use renewable biological resources from land and sea such as crops, forest, fish, animals and microorganisms to produce food, materials and energy, is becoming of great interest in the modern world [148]. The European Commission strongly highlights the importance of bioeconomy as a way to stimulate the economic growth of developed economies, while reducing the dependence on natural resources, transforming manufacturing, promoting sustainable production of renewable resources from land and their conversion into food, feed, fiber, bio-based products [149]. The conversion via various routes of bioenergy or other value-added products can regard also the biomass waste, thus allowing a shift to a resource-circular bioeconomy [150].

Currently, most bioplastics are produced from agricultural crop-based feedstock (carbohydrates and other plant materials). These, however, are not yet ideally aligned with sustainable development goals (SDGs) due to their competition for arable land, fresh water, and food production [151]. On the contrary, food waste valorization through the production of green materials is becoming one of the main pillars of the circular economy. Its use to substitute fossil resources for the production of plastics is a widely accepted strategy towards sustainable development. In fact, the displacing of conventional plastics with food waste-based bioplastics can lead to considerable energy and GHGs emissions savings [98]. However, it should be noted that this is not always true. Further details about advantages and drawbacks related to the bioplastics use and production are provided in **Table 1.2**. Despite being promoted as a safer alternative to their oil-based counterparts, bioplastics production involves major drawbacks. Indeed, bioplastics are generally not cost-competitive compared to conventional plastics and their production is expensive and plagued by low yields. Moreover, some bioplastics have a shorter lifetime than oil-based plastics due to weaker mechanical properties, and higher water vapour permeability, being easy to tear or very brittle. Being compostable and biodegradable is positive, but many bioplastics must follow a specific disposal procedure and require industrial composting in order to avoid being incinerated or going to landfill. It should be noted that biodegradable polymers require a controlled fate in order to kickstart the expected biodegradation process and as a result, it is nearly impossible to control and ensure the complete degradation of even potentially degradable plastic materials. When they are disposed of in an uncontrolled fashion, they accumulate in the environment and fragment into microplastics (MPs). These bio-based MPs have proven to display diverse impacts over ingested organisms

and ecosystems similar to those of conventional MPs. Thus, as conventional plastics, also bioplastics can avoid the problem of MPs only if properly disposed of [152].

Table 1.2 Main advantages and drawbacks related to the production and the use of bioplastic materials.

	Advantages	Drawbacks
Production	Reduction of greenhouse gas emission; saving fossil fuels, possibility of using a local resource, less energy during the manufacturing cycle.	Use of croplands to produce items, not cost-competitive compared to conventional plastics
Use	No toxic, no release of chemicals into food if used as packaging	Often characterized by thermal instability, brittleness, low melt strength, high water vapor and oxygen permeability; when hydrophilic polymers are used they possess low water vapor barrier and vulnerability to degradation.
Disposal	Biodegradable; broken down by naturally-occurring bacteria; do not persist for many years in the environment.	Controlled fate in order to kickstart the expected biodegradation process; a specific disposal procedure must be followed to avoid they fragment into microplastics which accumulate in the environment.

As a matter of fact, the employment of fruit and vegetable wastes as reinforcement of non-biodegradable polymers in drop-ins significantly increases the energy demand and CO₂ emission compared to biodegradable bioplastics [153]. Therefore, when the aim is the production of new bioplastic materials from agro-food waste, the effective sustainability of the process should be evaluated. The sustainability of bio-based plastics production depends on several factors which are often summarized in the life cycle assessments (LCAs) of the products [154]. Among them, there are availability of commercially viable quantities of renewable feedstock and agricultural waste, scalable and green production routes, cost and competition with synthetic polymers and useful life and biodegradation/end of life treatment [155]. Many of these aspects are very often not sufficiently deepened, thus making it difficult to assess environmental impacts associated with the agro-food waste based bioplastics production.

The greenhouse gas emissions generated by food waste represent the third largest emitter in the world, thus any measure to reduce food waste, even to a small extent, may have a significant impact on overall environmental footprint [156]. However, even though the amount of fruits and vegetables wasted every year is estimated to be around 484 million metric tons, the volume of waste produced does not predict the availability of agricultural waste for conversion into bioplastics. Indeed, a large quantity is employed in other competing applications such as bio-

fertilizer and biogas production [157]. In addition, not all the routes proposed for obtaining bioplastics are applicable on a large scale, since sometimes they require extensive and advanced processing. This mainly concerns biocomposites production, which is often based on obtaining fillers and reinforcements through complex treatment of the agro-food waste [105,126]. On the contrary, more feasible and scalable processes allow bioplastics production after chemical extraction of agro-polymers from the food waste stream. A low environmental impact is associated with this step, as no harsh chemicals, like pyridine and diethyl ether used for the production of PHA, with potential occupational hazards covered.

Regarding the end of life of the agro-food waste based bioplastics, reuse and recycling are preferred solutions to energy recovery or disposal. However, to date, for materials other than bio-PE or bio-PET, there is no recycling stream established yet [17]. An alternative is their composting, i.e. their aerobic biodegradation under controlled conditions of temperature, humidity and aeration [72]. Compostability is a clear benefit of agro waste-based bioplastics compared to conventional plastics, resulting in the creation of more valuable compost.

1.4 Bioplastics market

Currently, the amount of bioplastics produced annually in the world represents only about one percent of the global plastic production. However, due to the growing sensitivity towards the adoption of a “green and circular economy” dependent policy, the global bioplastics production capacity is set to increase from around 2.11 million tonnes in 2019 to approximately 2.43 million tonnes in 2024 [17]. With a view to regional capacity development, Asia remains a major production hub with over 50 percent of bioplastics currently being produced there. Currently, only one fifth of the production capacity is located in Europe. This share is predicted to grow to up to 27 percent by 2023. The expected growth will be supported by recently adopted policies in several European Member States such as Italy, Spain and France. Innovative biopolymers such as bio-based PP, bio-based PET, bio-based polyamide (bio-PA) and PHAs continue to drive the growth in bioplastic production. To date, they make up for 40 percent (0.8 million tonnes) of the global bioplastics production capacities.

Bioplastics materials are currently used in an increasing number of markets. The global production capacities of bioplastics in 2021 by market segment are reported in **Figure 1.7**.

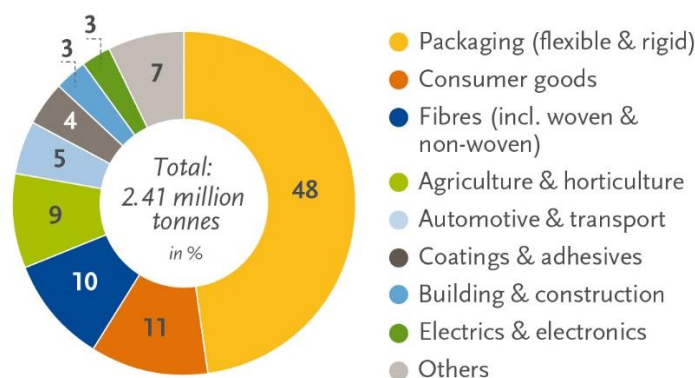


Figure 1.7 Global production capacities of bioplastics in 2021 by market segment. Source: European Bioplastics, nova-Institute (2021). www.european-bioplastics.org/market

Among these several market segments, electronics is the less developed (only about 3% of the global bioplastic production concerns this segment), while packaging remains the largest field of application for bioplastics since around 50% of the global bioplastic production is used for shopping bags producers and plastic bottles producers and food packaging industry [17]. Biodegradable shopping bags are made of polymers that decompose when exposed to air, water, sunlight, soil and microorganism. There are three main types of biodegradable bags, i.e. (1) biodegradable bags made from resins containing starches, polyethylene, (2) biodegradable bags made by using starches combined with biodegradable polymers such as PLA and (3) oxo-biodegradable bags, which use totally Degradable Plastics Additives (TDPAT) to stimulate the breakdown of polymers and thus speed up the biodegradation process of conventional plastics. As regard to food packaging, in the USA premarketing approval by the Food and Drug Administration is required to ensure that materials are innocuous, safe and effective [158]. On the other hand, in Europe food contact materials regulations set specific manufacturing goals to assure a good quality control system and specify the thresholds according to the form and composition of polymers which shall explicitly be authorized in order to preserve food safety (European Commission, 2006; European Commission 2011). In any case, biobased materials are mostly used to pack short and long shelf-life products that do not need very high oxygen and/or water barrier properties such as fresh fruits, vegetables, pasta and chips [159]. Actually, available bioplastics show such a wide range of properties, that they are also applicable as packaging materials for other food products, which request stricter conditions, like Modified Atmosphere Packaging (MAP).

Bioplastic materials offer several advantages also in the agriculture sector. 9% of the global production of bioplastics is covered by the agriculture and horticulture segment. Examples of bio-based products used in agriculture are mulching films and pots [107,160]. Soil mulching is

a practice used in cultivation, which allows weed suppression, reduces the loss of moisture from the soil, and may promote the increasing of soil temperature. Ploughing-in of bio-based and biodegradable mulching films after use instead of collecting them from the field and cleaning off the soil is a more practical and time saving solution. In the same way, bio-based pots are used.

For the automotive field, components made completely or partially from bioplastics can provide a safety standard that is of ultimate importance in the transportation sector [161]. The products include seat and airbag covers as well as steering wheels. Some of the bio-based plastics such as bio-based polyamides and bio-based polyesters are already successfully being used by leading automotive brands around the world today with the aim of reducing their products' environmental impact [162]. For example, Toyota typically uses bio-based polypropylene/polylactic acid (PP/PLA) composite derived from plant materials for the fabrication of up to 60% of the interior design of cars.

Biopolymers find applications in several housewares such as kitchen tools and utensils, washable storage containers and cups, bathroom accessories, toys, hangers, and hooks. For example, hangers from United Colors of Benetton are made of biodegradable polymers. Nontoxic biodegradable polymers such as PHA are being used also as sutures by surgeons in life-saving heart operations and other procedures. Easily sterilized, the sutures remain strong and intact until the surrounding tissues have healed. PHA sutures dissolve and are readily metabolized in the body leaving no trace [163]. Moreover, there has been a surge of bioplastic products which are being introduced in the fast-moving consumer electronics sector, such as touch screen computer casings, loud speakers, keyboard elements, mobile casings, vacuum cleaners, and a mouse for a laptop [164]. SUPLA, produced the first bioplastic touch screen computer by using PLA, in collaboration with a Taiwanese company (Kuender).

To date, a lot of companies, mainly located in Europe, have been identified as key players in the production of bioplastics and their distribution. Many of these companies produce sustainable bioplastics made from plant-based renewable resources such as corn, potatoes and wheat. Land used to grow the renewable feedstock for the production of bioplastics is estimated to be 0.7 million hectares in 2021 and continues to account for 0.015 percent of the global agricultural area of 4.7 billion hectares. Despite the market growth predicted in the next five years, the land use share for bioplastics will only slightly increase to 0.02 percent.

Novamont SpA (www.novamont.com) is one of the major starch bioplastics producers. The trade name of their starch-based bioplastic is “Mater-Bi” and it is provided for a wide range of manufacturers, which use it to make bags, mulching film, disposable tableware, and packaging.

Also Aynova Polymers GmbH (www.amynova.com) is engaged in the production of a starch-based substance named “CropCover”. CropCover is an innovative “adhesive” non-toxic, non-combustible and fully biodegradable applied together with pesticides and foliar fertilizers, in order to reduce their rinsing during heavy rainfall and to guarantee a longer stay time on the plant. Biotec Biologische Naturverpackungen GmbH & Co. KG (www.biotec.de) and Cardia Bioplastics (www.cardiabioplastics.com) produce and sell a new generation of customized thermoplastic materials too, with various functional properties fully biodegradable and compostable according to EN 13432. Moreover, there are companies that exploit waste as feedstock for bioplastics production. An example is NaturePlast (www.natureplast.eu) that, since 2015, has been producing and marketing a range of biocomposites consisting of by-products and plant fibres (such as hemp), sourced mostly from the French territory. The objective is to incorporate by-products or local waste material in different polymers to ensure a circular economy and the upcycle of waste material.

References

1. Narancic, T., Cerrone, F., Beagan, N., and O'Connor, K.E. (2020) Recent advances in bioplastics: Application and biodegradation. *Polymers (Basel)*, **12** (4).
2. Plastics Europe (2019) An Analysis of European Plastics Production, Demand and Waste Data. *Plast. - Facts 2019*.
3. Wright, S.L., and Kelly, F.J. (2017) Plastic and Human Health: A Micro Issue? *Environ. Sci. Technol.*, **51** (12), 6634–6647.
4. Caniani, D., Caivano, M., Pascale, R., Bianco, G., Mancini, I.M., Masi, S., Mazzone, G., Firouzian, M., and Rosso, D. (2019) CO₂ and N₂O from water resource recovery facilities: Evaluation of emissions from biological treatment, settling, disinfection, and receiving water body. *Sci. Total Environ.*, **648**, 1130–1140.
5. Caivano, M., Pascale, R., Mazzone, G., Buchicchio, A., Masi, S., Bianco, G., and Caniani, D. (2017) N₂O and CO₂ Emissions from secondary settlers in WWTPs: Experimental results on full and pilot scale plants, in *Frontiers in Wastewater Treatment and Modelling* (eds.Mannina, G.), Springer, Italy, pp. 412–418.
6. Caivano, M., Pascale, R., Mazzone, G., Masi, S., Panariello, S., and Caniani, D. (2017) Disinfection unit of water resource recovery facilities: Critical issue for N₂O Emission, in *Frontiers in Wastewater Treatment and Modelling* (eds.Mannina, G.), Springer, Italy, pp. 444–449.
7. Pascale, R., Caivano, M., Buchicchio, A., Mancini, I.M., Bianco, G., and Caniani, D. (2017) Validation of an analytical method for simultaneous high-precision measurements of greenhouse gas emissions from wastewater treatment plants using a gas chromatography-barrier discharge detector system. *J. Chromatogr. A*, **1480**, 62–69.
8. Lots, F.A.E., Behrens, P., Vijver, M.G., Horton, A.A., and Bosker, T. (2017) A large-scale investigation of microplastic contamination: Abundance and characteristics of microplastics in European beach sediment. *Mar. Pollut. Bull.*, **123** (1–2), 219–226.
9. Bradney, L., Wijesekara, H., Palansooriya, K.N., Obadamudalige, N., Bolan, N.S., Ok, Y.S., Rinklebe, J., Kim, K.H., and Kirkham, M.B. (2019) Particulate plastics as a vector for toxic trace-element uptake by aquatic and terrestrial organisms and human health risk. *Environ. Int.*, **131** (June), 104937.
10. Hahladakis, J.N., Velis, C.A., Weber, R., Iacovidou, E., and Purnell, P. (2018) An overview of chemical additives present in plastics: Migration, release, fate and environmental impact during their use, disposal and recycling. *J. Hazard. Mater.*, **344**, 179–199.
11. Okunola A, A., Kehinde I, O., Oluwaseun, A., and Olufiropo E, A. (2019) Public and Environmental Health Effects of Plastic Wastes Disposal: A Review. *J. Toxicol. Risk Assess.*, **5** (2).
12. Gu, F., Guo, J., Zhang, W., Summers, P.A., and Hall, P. (2017) From waste plastics to industrial raw materials: A life cycle assessment of mechanical plastic recycling practice based on a real-world case study. *Sci. Total Environ.*, **601–602**, 1192–1207.
13. Yates, M.R., and Barlow, C.Y. (2013) Resources , Conservation and Recycling Life cycle assessments of biodegradable , commercial biopolymers — A critical review. *Resour.*

- Conserv. Recycl.*, **78**, 54–66.
14. Kumar, S., and Thakur, K. (2017) Bioplastics - classification, production and their potential food applications. *J. Hill Agric.*, **8** (2), 118.
 15. Polman, E.M.N., Gruter, G.J.M., Parsons, J.R., and Tietema, A. (2021) Comparison of the aerobic biodegradation of biopolymers and the corresponding bioplastics: A review. *Sci. Total Environ.*, **753**, 141953.
 16. Brodin, M., Vallejos, M., Opedal, M.T., Area, M.C., and Chinga-Carrasco, G. (2017) Lignocellulosics as sustainable resources for production of bioplastics – A review. *J. Clean. Prod.*, **162**, 646–664.
 17. European Bioplastics (2019) Bioplastics Facts and Figures. *Eur. Bioplastics*, 1–16.
 18. Janssen, L.P.B.M., and Moscicki, L. (2009) *Termoplastic starch: A green material for Various Industries*, Wiley-VCH Verlag GmbH & Co. KGaA, Weinheim.
 19. Reddy, R.L., Reddy, V.S., and Gupta, G.A. (2013) Study of Bio-plastics As Green & Sustainable Alternative to Plastics. *Int. J. Emerg. Technol. Adv. Eng.*, **3** (5), 76–81.
 20. Emadian, S.M., Onay, T.T., and Demirel, B. (2017) Biodegradation of bioplastics in natural environments. *Waste Manag.*, **59**, 526–536.
 21. Ross, G., Ross, S., and Tighe, B.J. (2017) Bioplastics: New Routes, New Products, in *Brydson's Plastics Materials: Eighth Edition*, 8ed., Elsevier, Netherlands, pp. 631–652.
 22. De Almeida Oroski, F., Chaves Alves, F., and Bomtempo, V. (2014) Bioplastics Tipping Point: drop-in or non-drop-in? *J. Bus. Chem.*, **11** (1), 42–50.
 23. Xiao, B., Zheng, M., Pang, J., Jiang, Y., Wang, H., Sun, R., Wang, A., Wang, X., and Zhang, T. (2015) Synthesis and Characterization of Poly(ethylene terephthalate) from Biomass-Based Ethylene Glycol: Effects of Miscellaneous Diols. *Ind. Eng. Chem. Res.*, **54** (22), 5862–5869.
 24. Chen, L., Pelton, R.E.O., and Smith, T.M. (2016) Comparative life cycle assessment of fossil and bio-based polyethylene terephthalate (PET) bottles. *J. Clean. Prod.*, **137**, 667–676.
 25. Volanti, M., Cespi, D., Passarini, F., Neri, E., Cavani, F., Mizsey, P., and Fozer, D. (2019) Terephthalic acid from renewable sources: Early-stage sustainability analysis of a bio-PET precursor. *Green Chem.*, **21** (4), 885–896.
 26. Soták, T., Schmidt, T., and Hronec, M. (2013) Hydrogenolysis of polyalcohols in the presence of metal phosphide catalysts. *Appl. Catal. A Gen.*, **459**, 26–33.
 27. Yang, L., Yan, X., Wang, Q., Wang, Q., and Xia, H. (2015) One-pot catalytic conversion of cellulose into polyols with Pt/CNTs catalysts. *Carbohydr. Res.*, **404**, 87–92.
 28. Pang, J., Zheng, M., Sun, R., Wang, A., Wang, X., and Zhang, T. (2016) Synthesis of ethylene glycol and terephthalic acid from biomass for producing PET. *Green Chem.*, **18** (2), 342–359.
 29. Jain, R., Kosta, S., and Tiwari, A. (2010) Polyhydroxyalkanoates: a way to sustainable development of bioplastics. *Chronicles Young Sci.*, **1** (3), 10–15.
 30. Koller, M. (2014) Poly(hydroxyalkanoates) for Food Packaging: Application and

- Attempts towards Implementation. *Appl. Food Biotechnol.*, **1** (1), 3–15.
31. Averous, L., Fauconnier, N., Moro, L., and Fringant, C. (2000) Blends of Thermoplastic Starch and Polyesteramide: Processing and Properties. *J. Appl. Polym. Sci.*, **76** (7), 1117–1128.
 32. Pivsa-Art, W., Pavasupree, S., O-Charoen, N., Insuan, U., Jailak, P., and Pivsa-Art, S. (2011) Preparation of polymer blends between poly (L-lactic acid), poly (butylene succinate-co-adipate) and poly (butylene adipate-co-terephthalate) for blow film industrial application. *Energy Procedia*, **9**, 581–588.
 33. Bayer, I.S., Guzman-Puyol, S., Heredia-Guerrero, J.A., Ceseracciu, L., Pignatelli, F., Ruffilli, R., Cingolani, R., and Athanassiou, A. (2014) Direct transformation of edible vegetable waste into bioplastics. *Macromolecules*, **47** (15), 5135–5143.
 34. Sharma, S., and Luzinov, I. (2012) Water Aided Fabrication of Whey and Albumin Plastics. *J. Polym. Environ.*, **20** (3), 681–689.
 35. Jiménez-Rosado, M., Zarate-Ramírez, L.S., Romero, A., Bengoechea, C., Partal, P., and Guerrero, A. (2019) Bioplastics based on wheat gluten processed by extrusion. *J. Clean. Prod.*, **239**.
 36. Rinaudo, M. (2006) Chitin and chitosan: Properties and applications. *Prog. Polym. Sci.*, **31** (7), 603–632.
 37. Heredia-Guerrero, J.A., Heredia, A., Domínguez, E., Cingolani, R., Bayer, I.S., Athanassiou, A., and Benítez, J.J. (2017) Cutin from agro-waste as a raw material for the production of bioplastics. *J. Exp. Bot.*, **68** (19), 5401–5410.
 38. Zárata-Ramírez, L.S., Romero, A., Bengoechea, C., Partal, P., and Guerrero, A. (2014) Thermo-mechanical and hydrophilic properties of polysaccharide/gluten-based bioplastics. *Carbohydr. Polym.*, **112**, 16–23.
 39. Luengo, J.M., García, B., Sandoval, A., Naharro, G., and Olivera, E.R. (2003) Bioplastics from microorganisms. *Curr. Opin. Microbiol.*, **6** (3), 251–260.
 40. Ribeiro, P.L.L., da Silva, A.C.M.S., Filho, J.A.M., and Druzian, J.I. (2015) Impact of different by-products from the biodiesel industry and bacterial strains on the production, composition, and properties of novel polyhydroxyalkanoates containing achiral building blocks. *Ind. Crops Prod.*, **69**, 212–223.
 41. Campos, M.I., Figueiredo, T.V.B., Sousa, L.S., and Druzian, J.I. (2014) The influence of crude glycerin and nitrogen concentrations on the production of PHA by *Cupriavidus necator* using a response surface methodology and its characterizations. *Ind. Crops Prod.*, **52**, 338–346.
 42. Chen, G.Q. (2009) A microbial polyhydroxyalkanoates (PHA) based bio- and materials industry. *Chem. Soc. Rev.*, **38** (8), 2434–2446.
 43. Costa, S.S., Miranda, A.L., de Morais, M.G., Costa, J.A.V., and Druzian, J.I. (2019) Microalgae as source of polyhydroxyalkanoates (PHAs) — A review. *Int. J. Biol. Macromol.*, **131**, 536–547.
 44. Delgado, M., Felix, M., and Bengoechea, C. (2018) Development of bioplastic materials: From rapeseed oil industry by products to added-value biodegradable biocomposite materials. *Ind. Crops Prod.*, **125** (March), 401–407.

45. Muthuraj, R., Misra, M., Defersha, F., and Mohanty, A.K. (2016) Influence of processing parameters on the impact strength of biocomposites: A statistical approach. *Compos. Part A Appl. Sci. Manuf.*, **83**, 120–129.
46. Nguyen, H.T.H., Qi, P., Rostagno, M., Feteiha, A., and Mille, S.A. (2013) The quest for high glass transition temperature bioplastics. *J. Mater. Chem. A*, **1** (3), 1–38.
47. Labet, M., and Thielemans, W. (2009) Synthesis of polycaprolactone: A review. *Chem. Soc. Rev.*, **38** (12), 3484–3504.
48. Averous, L., Moro, L., Dole, P., and Fringant, C. (2000) Properties of thermoplastic blends: Starch-polycaprolactone. *Polymer (Guildf.)*, **41** (11), 4157–4167.
49. Ali Akbari Ghavimi, S., Ebrahimzadeh, M.H., Solati-Hashjin, M., and Abu Osman, N.A. (2015) Polycaprolactone/starch composite: Fabrication, structure, properties, and applications. *J. Biomed. Mater. Res.*, **103** (7), 2482–2498.
50. Bianco, G., Agerbirk, N., Losito, I., and Cataldi, T.R.I. (2014) Acylated glucosinolates with diverse acyl groups investigated by high resolution mass spectrometry and infrared multiphoton dissociation. *Phytochemistry*, **100**, 92–102.
51. Cataldi, T.R.I., Orlando, D., Nardiello, D., Rubino, A., Bianco, G., Abate, S., Ciriello, R., and Guerrieri, A. (2007) A three-factor Doehlert matrix design in optimising the determination of octadecyltrimethylammonium bromide by cation-exchange chromatography with suppressed conductivity detection. *Anal. Chim. Acta*, **597** (1), 129–136.
52. Zianni, R., Bianco, G., Lelario, F., Losito, I., Palmisano, F., and Cataldi, T.R.I. (2013) Fatty acid neutral losses observed in tandem mass spectrometry with collision-induced dissociation allows regiochemical assignment of sulfoquinovosyl-diacylglycerols. *J. Mass Spectrom.*, **48** (2), 205–215.
53. Bianco, G., Zianni, R., Anzillotta, G., Palma, A., Vitacco, V., Scrano, L., and Cataldi, T.R.I. (2013) Dibenzo-p-dioxins and dibenzofurans in human breast milk collected in the area of Taranto (Southern Italy): First case study. *Anal. Bioanal. Chem.*, **405** (7), 2405–2410.
54. Pascale, R., Onzo, A., Ciriello, R., Scrano, L., Bufo, S.A., and Bianco, G. (2020) *LC/MS Based Food Metabolomics*, Elsevier.
55. Cataldi, T.R.I., Bianco, G., Abate, S., and Losito, I. (2011) Identification of unsaturated N-acylhomoserine lactones in bacterial isolates of *Rhodobacter sphaeroides* by liquid chromatography coupled to electrospray ionization-hybrid linear ion trap-Fourier transform ion cyclotron resonance mass spectrometry. *Rapid Commun. Mass Spectrom.*, **25** (13), 1817–1826.
56. Pascale, R., Bianco, G., Cataldi, T.R.I., Kopplin, P.S., Bosco, F., Vignola, L., Uhl, J., Lucio, M., and Milella, L. (2018) Mass spectrometry-based phytochemical screening for hypoglycemic activity of Fagioli di Sarconi beans (*Phaseolus vulgaris* L.). *Food Chem.*, **242** (June 2017), 497–504.
57. Bianco, G., Pascale, R., Carbone, C.F., Acquavia, M.A., Cataldi, T.R.I., Schmitt-Kopplin, P., Buchicchio, A., Russo, D., and Milella, L. (2018) Determination of soyasaponins in Fagioli di Sarconi beans (*Phaseolus vulgaris* L.) by LC-ESI-FTICR-MS and evaluation of their hypoglycemic activity. *Anal. Bioanal. Chem.*, **410** (5), 1561–1569.

58. Pascale, R., Bianco, G., Cataldi, T.R.I., Buchicchio, A., Losito, I., Altieri, G., Genovese, F., Tauriello, A., Di Renzo, G.C., and Lafiosca, M.C. (2018) Investigation of the Effects of Virgin Olive Oil Cleaning Systems on the Secoiridoid Aglycone Content Using High Performance Liquid Chromatography–Mass Spectrometry. *JAOCS, J. Am. Oil Chem. Soc.*, **95** (6), 665–671.
59. Pascale, R., Acquavia, M.A., Cataldi, T.R.I., Onzo, A., Coviello, D., Bufo, S.A., Scrano, L., Ciriello, R., Guerrieri, A., and Bianco, G. (2020) Profiling of quercetin glycosides and acyl glycosides in sun-dried peperoni di Senise peppers (*Capsicum annum* L .) by a combination of LC-ESI (-) -MS / MS and polarity prediction in reversed-phase separations. *Anal. Bioanal. Chem.*, **412**, 3005–3015.
60. Pascale, R., Bianco, G., Coviello, D., Cristina Lafiosca, M., Masi, S., Mancini, I.M., Bufo, S.A., Scrano, L., and Caniani, D. (2020) Validation of a liquid chromatography coupled with tandem mass spectrometry method for the determination of drugs in wastewater using a three-phase solvent system. *J. Sep. Sci.*, **43** (5), 886–895.
61. Onzo, A., Acquavia, M.A., Cataldi, T.R.I., Ligonzo, M., Coviello, D., Pascale, R., Martelli, G., Bondoni, M., Scrano, L., and Bianco, G. (2020) Coceth sulfate characterization by electrospray ionization tandem mass spectrometry. *Rapid Commun. Mass Spectrom.*, **34** (20), 1–10.
62. Thakur, S., Chaudhary, J., Sharma, B., Tamulevicius, S., and Thakur, V.K. (2018) ScienceDirect Sustainability of bioplastics : Opportunities and challenges. *Curr. Opin. Green Sustain. Chem.*, **13**, 68–75.
63. Quarta, G. (2013) Determination of the Biobased Content in Plastics by Radiocarbon. *Radiocarbon*, **55** (3–4), 1834–1844.
64. Sherwood, J., Clark, J.H., Farmer, T.J., Herrero-Davila, L., and Moity, L. (2017) Recirculation: A new concept to drive innovation in sustainable product design for bio-based products. *Molecules*, **22** (1), 1–17.
65. Iwata, T. (2015) Biodegradable and bio-based polymers: Future prospects of eco-friendly plastics. *Angew. Chemie - Int. Ed.*, **54** (11), 3210–3215.
66. Lucas, N., Bienaime, C., Belloy, C., Queneudec, M., Silvestre, F., and Nava-saucedo, J. (2008) Polymer biodegradation : Mechanisms and estimation techniques. *Chemosphere*, **73**, 429–442.
67. Kaushal, J., Khatri, M., and Arya, S.K. (2021) Recent insight into enzymatic degradation of plastics prevalent in the environment: A mini - review. *Clean. Eng. Technol.*, **2** (March), 100083.
68. Ruggero, F., Gori, R., and Lubello, C. (2019) Methodologies to assess biodegradation of bioplastics during aerobic composting and anaerobic digestion: A review. *Waste Manag. Res.*, **37** (10), 959–975.
69. Ciriello, R., Lo Magro, S., and Guerrieri, A. (2018) Assay of serum cholinesterase activity by an amperometric biosensor based on a co-crosslinked choline oxidase/overoxidized polypyrrole bilayer. *Analyst*, **143** (4), 920–929.
70. Ciriello, R., De Gennaro, F., Frascaro, S., and Guerrieri, A. (2018) A novel approach for the selective analysis of L-lysine in untreated human serum by a co-crosslinked L-lysine– α -oxidase/overoxidized polypyrrole bilayer based amperometric biosensor.

- Bioelectrochemistry*, **124**, 47–56.
71. Massardier-Nageotte, V., Pestre, C., Cruard-Pradet, T., and Bayard, R. (2006) Aerobic and anaerobic biodegradability of polymer films and physico-chemical characterization. *Polym. Degrad. Stab.*, **91** (3), 620–627.
 72. Kale, G., Kijchavengkul, T., Auras, R., Rubino, M., Selke, S.E., and Singh, S.P. (2007) Compostability of bioplastic packaging materials: An overview. *Macromol. Biosci.*, **7** (3), 255–277.
 73. Folino, A., Karageorgiou, A., Calabrò, P.S., and Komilis, D. (2020) Biodegradation of wasted bioplastics in natural and industrial environments: A review. *Sustainability*, **12** (15), 1–37.
 74. Wang, K., Wang, W., Ye, R., Liu, A., Xiao, J., Liu, Y., and Zhao, Y. (2017) Mechanical properties and solubility in water of corn starch-collagen composite films: Effect of starch type and concentrations. *Food Chem.*, **216**, 209–216.
 75. Oliveira, T.Í.S., Rosa, M.F., Ridout, M.J., Cross, K., Brito, E.S., Silva, L.M.A., Mazzetto, S.E., Waldron, K.W., and Azeredo, H.M.C. (2017) Bionanocomposite films based on polysaccharides from banana peels. *Int. J. Biol. Macromol.*, **101**, 1–8.
 76. Battezzore, D., Bocchini, S., Alongi, J., and Frache, A. (2014) Plasticizers, antioxidants and reinforcement fillers from hazelnut skin and cocoa by-products: Extraction and use in PLA and PP. *Polym. Degrad. Stab.*, **108**, 297–306.
 77. Granda, L.A., Espinach, X., Méndez, J.A., Tresserras, J., Delgado-Aguilar, M., and Mutjé, P. (2016) Semichemical fibres of *Leucaena collinsii* reinforced polypropylene composites: Young's Modulus analysis and fibre diameter effect on the stiffness. *Compos. Part B Eng.*, **92**, 332–337.
 78. Palomba, D., Vazquez, G.E., and Díaz, M.F. (2014) Chemometrics and Intelligent Laboratory Systems Prediction of elongation at break for linear polymers. *Chemom. Intell. Lab. Syst.*, **139**, 121–131.
 79. Sanjay, M.R., Arpitha, G.R., and Yogesha, B. (2015) Study on Mechanical Properties of Natural - Glass Fibre Reinforced Polymer Hybrid Composites : A Review. *Mater. today Proc.*, **2** (4–5), 2959–2967.
 80. Suderman, N., Isa, M.I.N., and Sarbon, N.M. (2018) Food Bioscience The effect of plasticizers on the functional properties of biodegradable gelatin-based film : A review. *Food Biosci.*, **24**, 111–119.
 81. Vieira, G.M.A., da Silva, A.M., dos Santos, L.O., and Beppu, M.M. (2011) Natural-based plasticizers and biopolymer films : A review. *Eur. Polym. J.*, **47** (3), 254–263.
 82. Suyatma, N.E., Tighzert, L., Copinet, A., and Coma, V. (2005) Effects of hydrophilic plasticizers on mechanical, thermal, and surface properties of chitosan films. *J. Agric. Food Chem.*, **53** (10), 3950–3957.
 83. Di Gioia, L., and Guilbert, S. (1999) Corn protein-based thermoplastic resins: Effect of some polar and amphiphilic plasticizers. *J. Agric. Food Chem.*, **47** (3), 1254–1261.
 84. Santosa, F.X.B., and Padua, G.W. (1999) Tensile properties and water absorption of zein sheets plasticized with oleic and linoleic acids. *J. Agric. Food Chem.*, **47** (5), 2070–2074.

85. Saberi, B., Chockchaisawasdee, S., Golding, J.B., Scarlett, C.J., and Stathopoulos, C.E. (2017) Physical and mechanical properties of a new edible film made of pea starch and guar gum as affected by glycols, sugars and polyols. *Int. J. Biol. Macromol.*, **104**, 345–359.
86. Ghasemlou, M., Khodaiyan, F., and Oromiehie, A. (2011) Physical , mechanical , barrier , and thermal properties of polyol-plasticized biodegradable edible film made from kefiran. *Carbohydr. Polym.*, **84** (1), 477–483.
87. Tihminlioglu, F., Atik, I.D., and Ozen, B. (2010) Water vapor and oxygen-barrier performance of corn – zein coated polypropylene films. *J. Food Eng.*, **96**, 342–347.
88. Gustafsson, J., Landberg, M., Bátori, V., Åkesson, D., Taherzadeh, M.J., and Zamani, A. (2019) Development of bio-based films and 3D objects from apple pomace. *Polymers (Basel)*, **11** (2), 1–11.
89. Yaradoddi, J., Patil, V., Ganachari, S., Banapurmath, Nagaraj¹, 3, Hunashyal, Anand¹, 4, and Shettar, A. (2016) Biodegradable plastic production from fruit waste material and its sustainable use for green applications. *Int. J. Pharm. Res. Allied Sci.*, **5** (4), 56–65.
90. Sultan, N.F.K., and Johari, W.L.W. (2017) The Development of Banana Peel / Corn Starch Bioplastic Film : A Preliminary Study. *Bioremediation Sci. Technol. Res.*, **5** (1), 12–17.
91. Faradilla, R.H.F., Lee, G., Roberts, J., Martens, P., Stenzel, M., and Arcot, J. (2018) Effect of glycerol, nanoclay and graphene oxide on physicochemical properties of biodegradable nanocellulose plastic sourced from banana pseudo-stem. *Cellulose*, **25** (1), 399–416.
92. Bátori, V., Jabbari, M., Åkesson, D., Lennartsson, P.R., Taherzadeh, M.J., and Zamani, A. (2017) Production of Pectin-Cellulose Biofilms: A New Approach for Citrus Waste Recycling. *Int. J. Polym. Sci.*, **2017**, 1–10.
93. Lestari, R.A.S., Kasmiyatun, M., Dermawan, K., Aini, A.N., Riyati, N., and Putri, F.R. (2020) Bioplastic from Jackfruit Seeds and Rice. *IOP Conf. Ser. Mater. Sci. Eng.*, **835** (1), 1–10.
94. Sun, S., Song, Y., and Zheng, Q. (2008) Morphology and mechanical properties of thermo-molded bioplastics based on glycerol-plasticized wheat gliadins. *J. Cereal Sci.*, **48** (3), 613–618.
95. Caner, C., Vergano, P.J., and Wiles, J.L. (1998) Chitosan film mechanical and permeation properties as affected by acid, plasticizer, and storage. *J. Food Sci.*, **63** (6), 1049–1053.
96. Aguilar, J.M., Bengoechea, C., Pérez, E., and Guerrero, A. (2020) Effect of different polyols as plasticizers in soy based bioplastics. *Ind. Crops Prod.*, **153** (August 2019).
97. Alonso-González, M., Ramos, M., Bengoechea, C., Romero, A., and Guerrero, A. (2020) Evaluation of Composition on Processability and Water Absorption of Wheat Gluten-Based Bioplastics. *J. Polym. Environ.*, (0123456789).
98. Tsang, Y.F., Kumar, V., Samadar, P., Yang, Y., Lee, J., Ok, Y.S., Song, H., Kim, K.H., Kwon, E.E., and Jeon, Y.J. (2019) Production of bioplastic through food waste valorization. *Environ. Int.*, **127** (January), 625–644.
99. Bashir, A.S.M., and Manusamy, Y. (2015) Recent Developments in Biocomposites Reinforced with Natural Biofillers from Food Waste. *Polym. Plast. Technol. Eng.*, **54**, 87–

99.

100. Cinar, S.O., Chong, Z.K., Kucuker, M.A., Wieczorek, N., Cengiz, U., and Kuchta, K. (2020) Bioplastic Production from Microalgae : A Review. *Int. J. Environ. Res. public Heal.*, **17** (11), 1–21.
101. Çokaygil, Z., Banar, M., and Seyhan, A.T. (2014) Orange peel-derived pectin jelly and corn starch-based biocomposite film with layered silicates. *J. Appl. Polym. Sci.*, **131** (16), 1–12.
102. González-Gutiérrez, J., Partal, P., García-Morales, M., and Gallegos, C. (2011) Effect of processing on the viscoelastic, tensile and optical properties of albumen/starch-based bioplastics. *Carbohydr. Polym.*, **84** (1), 308–315.
103. Gowman, A.C., Picard, M.C., Lim, L.T., Misra, M., and Mohanty, A.K. (2019) Fruit waste valorization for biodegradable biocomposite applications: A review. *BioResources*, **14** (4), 10047–10092.
104. Gurram, R., Souza Filho, P.F., Taherzadeh, M.J., and Zamani, A. (2018) A Solvent-Free Approach for Production of Films from Pectin and Fungal Biomass. *J. Polym. Environ.*, **26** (11), 4282–4292.
105. Muhammad, A., Roslan, A., Sanusi, S.N.A., Shahimi, M.Q., and Nazari, N.Z. (2019) Mechanical properties of bioplastic form cellulose nanocrystal (CNC) mangosteen peel using glycerol as plasticizer. *J. Phys. Conf. Ser.*, **1349** (1), 1–8.
106. Oliveira, T.Í.S., Rosa, M.F., Cavalcante, F.L., Pereira, P.H.F., Moates, G.K., Wellner, N., Mazzetto, S.E., Waldron, K.W., and Azeredo, H.M.C. (2016) Optimization of pectin extraction from banana peels with citric acid by using response surface methodology. *Food Chem.*, **198**, 113–118.
107. Schettini, E., Santagata, G., Malinconico, M., Immirzi, B., Scarascia Mugnozza, G., and Vox, G. (2013) Recycled wastes of tomato and hemp fibres for biodegradable pots: Physico-chemical characterization and field performance. *Resour. Conserv. Recycl.*, **70**, 9–19.
108. Jha, A., and Kumar, A. (2019) Biobased technologies for the efficient extraction of biopolymers from waste biomass. *Bioprocess Biosyst. Eng.*, **42** (12), 1893–1901.
109. Corre, D. Le, Bras, J., and Dufresne, A. (2010) Starch Nanoparticles: A review. *Biomacromolecules*, **11**, 1139–1153.
110. Mellinas, C., Ramos, M., Jiménez, A., and Garrigós, M.C. (2020) Recent trends in the use of pectin from agro-waste residues as a natural-based biopolymer for food packaging applications. *Materials (Basel)*, **13** (3).
111. Bedane, A.H., Eić, M., Farmahini-Farahani, M., and Xiao, H. (2015) Water vapor transport properties of regenerated cellulose and nanofibrillated cellulose films. *J. Memb. Sci.*, **493**, 46–57.
112. Pingali, S.V., Urban, V.S., Heller, W.T., McGaughey, J., O'Neill, H., Foston, M.B., Li, H., Wyman, C.E., Myles, D.A., Langan, P., Ragauskas, A., Davison, B., and Evans, B.R. (2017) Understanding Multiscale Structural Changes during Dilute Acid Pretreatment of Switchgrass and Poplar. *ACS Sustain. Chem. Eng.*, **5** (1), 426–435.
113. Wang, S., Lu, A., and Zhang, L. (2016) Recent advances in regenerated cellulose

- materials. *Prog. Polym. Sci.*, **53**, 169–206.
114. Zhao, H., Holladay, J.E., Kwak, J.H., and Zhang, Z.C. (2007) Inverse Temperature-Dependent Pathway of Cellulose Decrystallization in Trifluoroacetic Acid. *J. Phys. Chem. B*, **111** (19), 5295–5300.
 115. Bilo, F., Pandini, S., Sartore, L., Depero, L.E., Gargiulo, G., Bonassi, A., Federici, S., and Bontempi, E. (2018) A sustainable bioplastic obtained from rice straw. *J. Clean. Prod.*, **200**, 357–368.
 116. Perotto, G., Ceseracciu, L., Simonutti, R., Paul, U.C., Guzman-Puyol, S., Tran, T.N., Bayer, I.S., and Athanassiou, A. (2018) Bioplastics from vegetable waste: Via an eco-friendly water-based process. *Green Chem.*, **20** (4), 894–902.
 117. Liu, M., Arshadi, M., Javi, F., Lawrence, P., Davachi, S.M., and Abbaspourrad, A. (2020) Green and facile preparation of hydrophobic bioplastics from tea waste. *J. Clean. Prod.*, **276**, 1–10.
 118. Rizwana Beevi, K., Sameera Fathima, A.R., Thahira Fathima, A.I., Thameemunisa, N., Noorjahan, C.M., and Deepika, T. (2020) Bioplastic Synthesis Using Banana Peels And Potato Starch And Characterization. *Int. J. Sci. Technol. Res.*, **9** (1), 1809–1814.
 119. Arikan, E.B., and Bilgen, H.D. (2019) Production of bioplastic from potato peel waste and investigation of its biodegradability. *Int. Adv. Res. Eng. J.*, **03** (02), 093–097.
 120. Masruri, M., Azhar, A.Z., Rosyada, I., and Febrianto, A. (2019) The effect of kaffir lime (*Citrus hystrix* DC) essential oil on bioplastic derived from cassava peel waste. *J. Phys. Conf. Ser.*, **1374**, 1–6.
 121. Dasumiati, Saridewi, N., and Malik, M. (2019) Food packaging development of bioplastic from basic waste of cassava peel (*manihot utilisima*) and shrimp shell. *IOP Conf. Ser. Mater. Sci. Eng.*, **602** (1), 1–9.
 122. Fathanah, U., Lubis, M.R., Nasution, F., and Masyawi, M.S. (2018) Characterization of bioplastic based from cassava crisp home industrial waste incorporated with chitosan and liquid smoke. *IOP Conf. Ser. Mater. Sci. Eng.*, **334** (1), 1–8.
 123. Samer, M., Khalefa, Z., Abdelall, T., Moawya, W., Farouk, A., Abdelaziz, S., Soliman, N., Salah, A., Gomaa, M., and Mohamed, M. (2019) Bioplastics production from agricultural crop residues. *Agric. Eng. Int. CIGR J.*, **21** (3), 190–194.
 124. Muhammad, A., Rashidi, A.R., Roslan, A., and Idris, S.A. (2017) Development of bio based plastic materials for packaging from soybeans waste. *AIP Conf. Proc.*, **1885** (020230), 1–8.
 125. Mohnen, D. (2008) Pectin structure and biosynthesis. *Curr. Opin. Plant Biol.*, **11** (3), 266–277.
 126. Khan, A., Khan, R.A., Salmieri, S., Le Tien, C., Riedl, B., Bouchard, J., Chauve, G., Tan, V., Kamal, M.R., and Lacroix, M. (2012) Mechanical and barrier properties of nanocrystalline cellulose reinforced chitosan based nanocomposite films. *Carbohydr. Polym.*, **90** (4), 1601–1608.
 127. Olsson, E., Hedenqvist, M.S., Johansson, C., and Järnström, L. (2013) Influence of citric acid and curing on moisture sorption, diffusion and permeability of starch films. *Carbohydr. Polym.*, **94** (2), 765–772.

128. Heredia-Guerrero, J.A., Caputo, G., Guzman-Puyol, S., Tedeschi, G., Heredia, A., Ceseracciu, L., Benitez, J.J., and Athanassiou, A. (2019) Sustainable polycondensation of multifunctional fatty acids from tomato pomace agro-waste catalyzed by tin (II) 2-ethylhexanoate. *Mater. Today Sustain.*, **3** (4), 1–10.
129. Domínguez, E., Heredia-Guerrero, J.A., and Heredia, A. (2015) Plant cutin genesis: Unanswered questions. *Trends Plant Sci.*, **20** (9), 551–558.
130. Deng, M., Zhang, G., Zeng, Y., Pei, X., Huang, R., and Lin, J. (2016) Simple process for synthesis of layered sodium silicates using rice husk ash as silica source. *J. Alloys Compd.*, **683**, 412–417.
131. Mohanty, A.K., Misra, M., and Hinrichsen, G. (2000) Biofibres, biodegradable polymers and biocomposites: An overview. *Macromol. Mater. Eng.*, **276–277**, 1–24.
132. Ashori, A., and Nourbakhsh, A. (2010) Bio-based composites from waste agricultural residues. *Waste Manag.*, **30** (4), 680–684.
133. Russo, R., Malinconico, M., and Santagata, G. (2007) Effect of cross-linking with calcium ions on the physical properties of alginate films. *Biomacromolecules*, **8** (10), 3193–3197.
134. Mathivanan, D., Norfazilah, H., Siregar, J.P., Rejab, M.R.M., Bachtiar, D., and Cionita, T. (2016) The study of mechanical properties of pineapple leaf fibre reinforced tapioca based bioplastic resin composite. *MATEC Web Conf.*, **74**, 1–4.
135. Yapo, B.M., and Koffi, K.L. (2008) Dietary fiber components in yellow passion fruit rind - A potential fiber source. *J. Agric. Food Chem.*, **56** (14), 5880–5883.
136. Moro, T.M.A., Ascheri, J.L.R., Ortiz, J.A.R., Carvalho, C.W.P., and Meléndez-Arévalo, A. (2017) Bioplastics of Native Starches Reinforced with Passion Fruit Peel. *Food Bioprocess Technol.*, **10** (10), 1798–1808.
137. Wu, F., Misra, M., and Mohanty, A.K. (2020) Sustainable green composites from biodegradable plastics blend and natural fibre with balanced performance : Synergy of nano-structured blend and reactive extrusion. *Compos. Sci. Technol.*, **200**, 1–8.
138. Troiano, M., Santulli, C., Roselli, G., Di Girolami, G., Cinaglia, P., and Gkrilla, A. (2018) DIY Bioplastics from Peanut Hulls Waste in a Starch-Milk Based Matrix. *FME Trans.*, **46** (4), 503–512.
139. Tran, T.N., Heredia-Guerrero, J.A., Mai, B.T., Ceseracciu, L., Marini, L., Athanassiou, A., and Bayer, I.S. (2017) Bioelastomers Based on Cocoa Shell Waste with Antioxidant Ability. *Adv. Sustain. Syst.*, **1** (7), 1700002.
140. Côto, T., Moura, I., de Sá, A., Vilarinho, C., and Machado, A. V. (2018) Sustainable materials based on cellulose from food sector agro-wastes. *J. Renew. Mater.*, **6** (7), 688–696.
141. Nasihin, Z.D., Masruri, M., Warsito, W., and Srihardyastutie, A. (2020) Preparation of Nanocellulose Bioplastic with a Gradation Color of Red and Yellow. *IOP Conf. Ser. Mater. Sci. Eng.*, **833**, 1–6.
142. Azieyanti, N.A., Amirul, A., Othman, S.Z., and Misran, H. (2020) Mechanical and Morphology Studies of Bioplastic-Based Banana Peels. *J. Phys. Conf. Ser.*, **1529**, 1–6.
143. Sharif Hossain, A.B.M., Ibrahim, N.A., and AlEissa, M.S. (2016) Nano-cellulose derived

- bioplastic biomaterial data for vehicle bio-bumper from banana peel waste biomass. *Data Br.*, **8**, 286–294.
144. Iriani, E.S., Permana, A.W., Yuliani, S., Kailaku, S.I., and Sulaiman, A.A. (2019) The effect of agricultural waste nanocellulose on the properties of bioplastic for fresh fruit packaging. *IOP Conf. Ser. Earth Environ. Sci.*, **309** (1), 1–7.
 145. Yacob, N., Yusof, M.R., Mohamed, A.Z., and Badri, K.H. (2019) Effect of cellulose fiber loading on the properties of starch-based films. *AIP Conf. Proc.*, **2111** (June), 1–7.
 146. Dahy, H. (2019) Efficient Fabrication of Sustainable Building Products from Annually Generated Non-wood Cellulosic Fibres and Bioplastics with Improved Flammability Resistance. *Waste and Biomass Valorization*, **10** (5), 1167–1175.
 147. Lu, S.-T., and Hamerton, I. (2002) Recent developments in the chemistry of halogen-free flame retardant polymers. *Prog. Polym. Sci.*, **27** (8), 1661–1712.
 148. McCormick, K., and Kautto, N. (2013) The Bioeconomy in Europe: An Overview. *Sustain.*, **5** (6), 2589–2608.
 149. Kardung, M., Cingiz, K., Costenoble, O., Delahaye, R., Heijman, W., Lovrić, M., van Leeuwen, M., M'barek, R., van Meijl, H., Piotrowski, S., Ronzon, T., Sauer, J., Verhoog, D., Verkerk, P.J., Vracholi, M., Wesseler, J.H.H., and Zhu, B.X. (2021) Development of the circular bioeconomy: Drivers and indicators. *Sustain.*, **13** (1), 1–24.
 150. Stegmann, P., Londo, M., and Junginger, M. (2020) The circular bioeconomy: Its elements and role in European bioeconomy clusters. *Resour. Conserv. Recycl. X*, **6** (July 2019), 100029.
 151. Karan, H., Funk, C., Grabert, M., Oey, M., and Hankamer, B. (2019) Green Bioplastics as Part of a Circular Bioeconomy. *Trends Plant Sci.*, **24** (3), 237–249.
 152. Shruti, V.C., and Kuttralam-Muniasamy, G. (2019) Bioplastics: Missing link in the era of Microplastics. *Sci. Total Environ.*, **697**, 134139.
 153. Bhagwat, G., Gray, K., Wilson, S.P., Muniyasamy, S., Vincent, S.G.T., Bush, R., and Palanisami, T. (2020) Benchmarking Bioplastics: A Natural Step Towards a Sustainable Future. *J. Polym. Environ.*, **28** (12), 3055–3075.
 154. Hottle, T.A., Bilec, M.M., and Landis, A.E. (2013) Sustainability assessments of bio-based polymers. *Polym. Degrad. Stab.*, **98** (9), 1898–1907.
 155. Maraveas, C. (2020) Production of sustainable and biodegradable polymers from agricultural waste. *Polymers (Basel)*, **12** (5), 1–22.
 156. Kakadellis, S., and Harris, Z.M. (2020) Don't scrap the waste: The need for broader system boundaries in bioplastic food packaging life-cycle assessment – A critical review. *J. Clean. Prod.*, **274**, 122831.
 157. Panuccio, M.R., Attinà, E., Basile, C., Mallamaci, C., and Muscolo, A. (2016) Use of Recalcitrant Agriculture Wastes to Produce Biogas and Feasible Biofertilizer. *Waste and Biomass Valorization*, **7** (2), 267–280.
 158. Heckman, J.H. (2005) Food packaging regulation in the United States and the European Union. *Regul. Toxicol. Pharmacol.*, **42** (1), 96–122.
 159. Peelman, N., Ragaert, P., De Meulenaer, B., Adons, D., Peeters, R., Cardon, L., Van Impe,

- F., and Devlieghere, F. (2013) Application of bioplastics for food packaging. *Trends Food Sci. Technol.*, **32** (2), 128–141.
160. Malinconico, M., Immirzi, B., Santagata, G., Schettini, E., Vox, G., and Mugnozza, G.S. (2008) An overview on innovative biodegradable materials for agricultural applications, in *Progress in Polymer Degradation and Stability Research* (eds. Moeller, H.W.), Nova Science Publishers, Inc., New York, pp. 69–114.
161. Bouzouita, A., Notta-Cuvier, D., Raquez, J.M., Lauro, F., and Dubois, P. (2018) Poly(lactic acid)-based materials for automotive applications. *Adv. Polym. Sci.*, **282**, 177–219.
162. Koronis, G., Silva, A., and Fontul, M. (2013) Green composites: A review of adequate materials for automotive applications. *Compos. Part B Eng.*, **44** (1), 120–127.
163. Mukheem, A., Hossain, M., Shahabuddin, S., and Muthoosamy, K. (2018) *Bioplastic Polyhydroxyalkanoate (PHA): Recent Advances in Modification and Medical Applications*.
164. Bozó, É., Ervasti, H., Halonen, N., Shokouh, S.H.H., Tolvanen, J., Pitkänen, O., Järvinen, T., Pálvölgyi, P.S., Szamosvölgyi, Á., Sápi, A., Konya, Z., Zaccone, M., Montalbano, L., De Brauwer, L., Nair, R., Martínez-Nogués, V., San Vicente Laurent, L., Dietrich, T., Fernández De Castro, L., and Kordas, K. (2021) Bioplastics and Carbon-Based Sustainable Materials, Components, and Devices: Toward Green Electronics. *ACS Appl. Mater. Interfaces*, **13** (41), 49301–49312.

2. Methodologies

Most natural materials are complex composites whose mechanical properties are often outstanding, considering the weak constituents from which they are assembled. These complex structures, which have risen from hundreds of million years of evolution, are inspiring Materials Scientists in the design of novel materials. Bio-based composites afford the unique possibility of designing the material, the manufacturing procedure and the structure in one unified and concurrent process. The entire process requires a reliable database of material properties, standardized structural analysis methods, modelling and simulation techniques, and models for materials processing. The numerous options available make the design and optimization process more involved and the analysis more complex. In this chapter, a description of the methodologies used to evaluate the main composites' properties is provided.

2.1 Tensile test

The tensile test is an important standard engineering procedure useful to evaluate the relevant elastic and plastic variables related to the mechanical behaviour of materials [1]. The strength of a material is often the primary parameter and can be measured in terms of either the stress necessary to cause appreciable plastic deformation or the maximum stress that the material can withstand. Beside material's strength, also its ductility is of great interest. Material's ductility is a measure of how much it can be deformed before it fractures. Rarely ductility is incorporated directly in design, but it is included in material specifications to ensure quality and toughness. Low ductility in a tensile test means low resistance to fracture under other forms of loading. For the evaluation of elastic properties, special techniques must be used during tensile testing, and more accurate measurements can be made by ultrasonic techniques. The typical tensile specimen for tensile testing is shown in **Figure 2.1**.

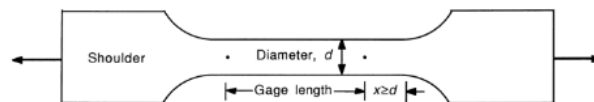


Figure 2.1 Typical tensile specimen, showing a reduced gage section and enlarged shoulders. To avoid end effects from the shoulders, the length of the transition region should be at least as great as the diameter and the total length of the reduced section should be at least four times the diameter.

The important part of the specimen is the gage section [2]. The cross-sectional area of the gage section is reduced relative to that of the remainder of the specimen so that deformation and failure will be localized in this region. The gage length is the region on which measurements are made and it is centered within the reduced section. The distance between the ends of the gage section and the shoulders should be great enough so that the larger ends do not constrain deformation within the gage section, and the length of the gage depends on its diameter. There are various ways of gripping the specimen. The end could be screwed into a threaded grip, or it could be pinned, but ends may be used, or the grip section may be held between wedges. The most important aspect that should be considered in the selection of a gripping method is that the specimen has to be held at the maximum load without slippage or failure in the grip section. Moreover, bending should be minimized.

As regard to testing machines, the most common are universal testers, which test materials in tension, compression or bending. Testing machines are either electromechanical or hydraulic. The principal difference is the method by which the load is applied. Electromechanical machines are based on a variable-speed electric motor, a great reduction system and one, two or four screws that move the crosshead up or down. This motion loads the specimen in tension or in compression. Crosshead speeds can be changed by changing the speed of the motor. To effectively control the speed of the crosshead, a microprocessor-based closed-loop servo system can be implemented [2]. Hydraulic testing machines (**Figure 2.2**) are based on either a single or dual-acting piston that moves the crosshead up or down. However, most static hydraulic testing machines have a single acting piston or ram. In a manually operated machine, the operator adjusts the orifice of a pressure-compensated needle valve to control the rate of loading.

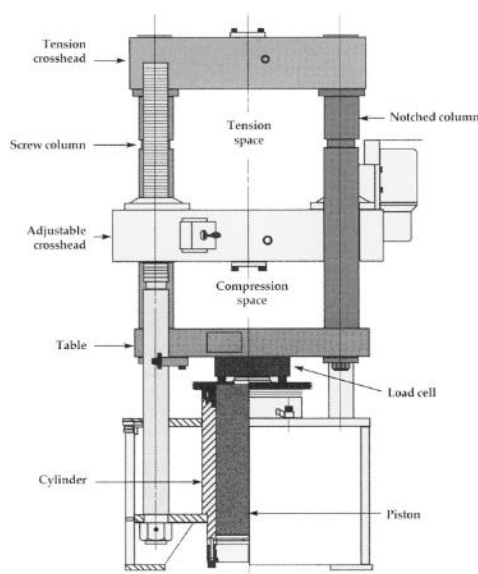


Figure 2.2 Components of a hydraulic universal testing machine.

Testing machines are used in order to obtain the stress-strain curve. Stress-strain curve is an extremely important graphical measure of a material's mechanical properties and is the plot of stress and strain of a material or metal on the graph [3]. In this graph, the stress is plotted on the y-axis and its corresponding strain on the x-axis.

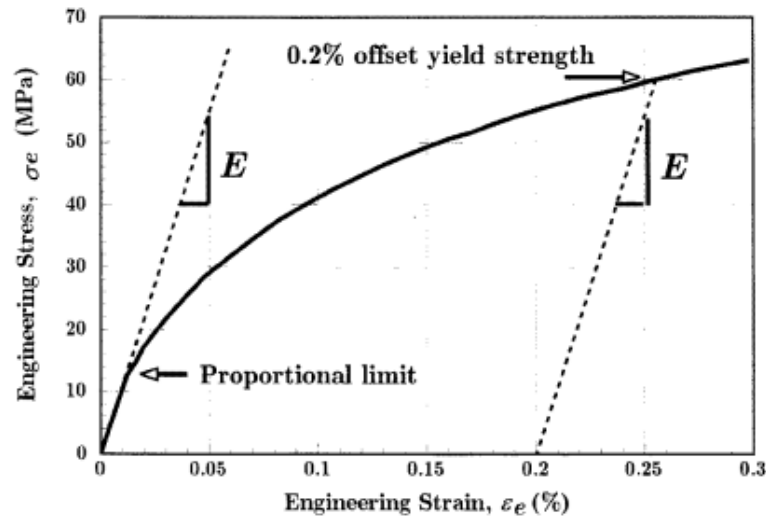


Figure 2.3 An example of stress-strain curve typical of many ductile metals.

In low strain portion of the stress-strain curve, many materials obey Hooke's law to a reasonable approximation: in this region the stress is proportional to strain with the constant of proportionality being the modulus of elasticity or Young's modulus, denoted E :

$$\sigma = E \cdot \varepsilon$$

As strain is increased, many materials eventually deviate from this linear proportionality and the point of departure is the proportional limit [4]. This non-linearity is usually associated with stress-induced "plastic" flow in the sample. The material is undergoing a rearrangement of its internal molecular or microscopic structure, with atoms being moved to new equilibrium positions. This plasticity requires a mechanism for molecular mobility, which in crystalline materials can arise from dislocation motion. Materials which lack this mobility, for example by having internal microstructures that block dislocation motion, are usually brittle rather than ductile. The stress-strain curve for brittle materials are typically linear over their full range of strain, eventually terminating in fracture without appreciable plastic flow [5].

2.2 Contact angle

The determination of solid–vapor (γ_{sv}) and solid–liquid (γ_{sl}) interfacial tensions is extremely important for bio-based materials, in order to determine their wettability. Contact angles θ measurement is easily done by measuring the tangent of a liquid drop with a solid surface at the base [6], suitably prepared. More in detail, the equilibrium contact angle (θ) is the angle of a liquid formed on a solid surface at the solid–liquid–vapor contact line, i.e. the three-phase contact line (**Figure 2.4**). The angle is governed by the interfacial tensions between those three phases, and is expressed by the Young's equation as [7]:

$$\cos \theta = \frac{\gamma_{sv} - \gamma_{sl}}{\gamma_{lv}}$$

where γ is the interfacial tension and subscripts s , v and l refer to the solid, vapor and liquid phases, respectively. The Young's equation shows that the contact angle is unique for every system and it depends only on the interfacial tensions of the three phases in that system. For these reasons, the contact angle can be used to quantitatively describe the wettability of a certain solid by a liquid in a particular system [6]. Generally, a large angle value suggests that the liquid of interest does not wet the surface well and beads up on the surface, whereas a low angle suggests that the liquid wets the surface.

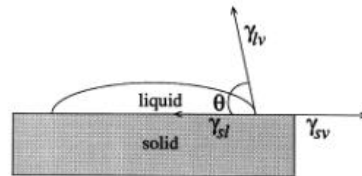


Figure 2.4 Schematic of a sessile-drop contact angle system.

Young's equation contains only two measurable quantities, i.e. the contact angle θ and the liquid–vapor surface tension, γ_{lv} . Anyway, this equation suggests that the observation of the equilibrium contact angles of liquids on solids may be a starting point for investigating the solid surface tensions, γ_{sv} and γ_{sl} . Many studies have been done to develop methodologies for determining solid surface tensions. Since γ_{lv} , γ_{sv} and γ_{sl} are thermodynamic properties of the liquid and solid, Young's equation implies a single, unique contact angle. Nevertheless, contact angle phenomena are complicated and it should be considered that the contact angle made by an

advancing liquid (θ_a) and that made by a receding liquid (θ_r) are not identical; nearly all solid surfaces exhibit contact angle hysteresis, H (the difference between θ_a and θ_r):

$$H = \theta_a - \theta_r$$

Contact angle hysteresis can be due to roughness and heterogeneity of a solid surface. If roughness is the most important cause, the measured contact angles are meaningless in terms of Young's equation. On very rough surfaces, contact angles are larger than measured on chemically identical, smooth surfaces.

One of the most extensively employed method for evaluating the contact angle is the direct measurement of the tangent angle at three-phase equilibrium interfacial point by using the sessile drop method. With this method, a telescope goniometer is capable to view the liquid drop profile placed over the smooth surface and measure angle formed between three interfacial tensions [8,9]. An image of the adhering bubble is projected onto a screen and the outlines traced, there after the angle is measured. The graphical representation of the sessile drop technique was presented in **Figure 2.5**.

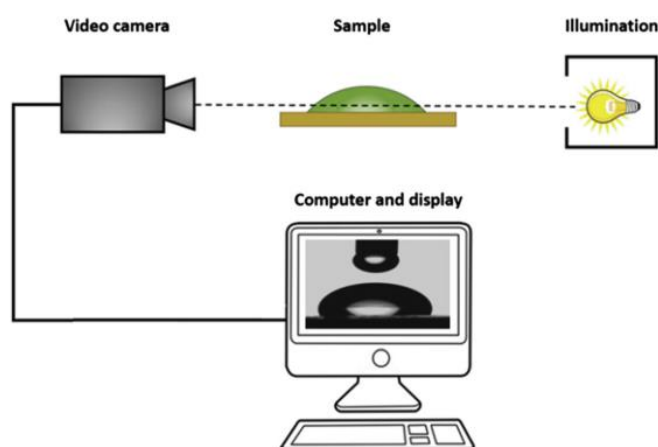


Figure 2.5 Graphical representation of sessile drop technique. Reproduced with the permission of Springer [10].

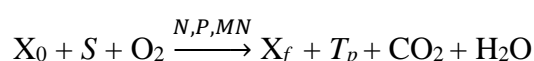
The advantages of the sessile drop technique are related to the simplicity of the operations and the small surface area of substrates and small amounts of liquid required. Nevertheless, it should be considered that this method is highly influenced by impurities due to the small size of the substrate and liquid. The reproducibility and accuracy of contact angle measurement mainly depend on the assignment of the tangent line and consistency of the operator [11].

The wetting characteristics of bioplastics surfaces play an important role in determining the end-use of the materials. Hydrophilicity and hydrophobicity are used to describe the relative affinity of the water molecules to spreading on the surface of these substrates. The affinity of water

molecules with the surface is due to unbalanced secondary force of interaction when drop profile comes in contact with the material. As explained before, the analysis of this interaction is done by measuring the contact angle θ and the obtained value is associated to surface energy of the materials. It is generally accepted that a value of θ lower than 90 degrees represents the surface having the affinity toward the liquid and water contact angle smaller than 90 degrees and is normally called as hydrophilic. Thus, the surface will show the tendency to wet or forming a thin hydration film over the surface. The value of θ higher than 90 degrees represents the nonwetting characteristic of the surface or showing less affinity toward the liquid. Such surfaces are called hydrophobic. Drops of water tend to form “beads” on hydrophobic solid surfaces due to the absence of any attraction with the water molecules, i.e., “water rejecting”. Surfaces on which the water contact angle is above 140 degrees are called superhydrophobic surfaces [11].

2.3 Biodegradability

Alongside with good mechanical performances and hydrophobicity, another important characteristic that bio-based materials should present is an improved biodegradability. Usually, bioplastics’ biodegradability is monitored by evaluating the Biochemical Oxygen Demand (BOD) during aerobic biodegradation. Aerobic biodegradation consists of oxidising organic matter biologically. During this process, the organic matter is converted by microorganisms into microbial biomass, eventual transformation products of biodegradation reaction, derived from the initial organic matter, CO_2 and H_2O , according to the following equation [12]:



where X_0 is the initial biomass, S is the organic carbon sources, N, P, MN are the nitrogen and phosphorous source and the mineral nutrients, respectively. Instead, X_f is the final biomass and T_p are the transformation products of biodegradation.

Traditionally, the BOD measurement is performed according to a standardised method, currently named the closed bottle test, described in the International Standards ISO 5815-1:2003. Briefly, the protocol consists of putting the samples potentially contaminated with organic matter, i.e. the bioplastics’ material, into specific bottles aerating them, and adding a microbial population. Then, the bottles are hermetically sealed and incubated at 20 °C in a dark room. The bottles are incubated for n days, during which the dissolved residual oxygen is measured for all analysed

samples to estimate the BOD. The oxygen could be determined either by the iodometric method (Winkler's method) or by an electrochemical probe method [13].

Recently, a semi-automated version has been commercialised. It consists of an electrochemical probe inserted into the sealed bottle to measure the dissolved oxygen concentration in real time, according the standardised method. This standardised method allows the measurement of the dissolved oxygen consumption in order to estimate the BOD value. However, it should be considered that some limitations are involved: a variability higher than 20 per cent in the results is usually observed, mainly due to the microbial population and a proper working area is required [14].

References

1. Hart, E.W. (1967) Theory of the tensile test. *Acta Metall.*, **15** (2), 351–355.
2. Lim, W., and Kim, H.K. (2013) Design and development of a miniaturised tensile testing machine. *Glob. J. Eng. Educ.*, **15** (1), 48–53.
3. Roylance, D. (2001) Stress-strain cruves. *Massachusetts Inst. Technol. study, Cambridge*, 1–14.
4. Zhao, Y.H., Guo, Y.Z., Wei, Q., Topping, T.D., Dangelewicz, A.M., Zhu, Y.T., Langdon, T.G., and Lavernia, E.J. (2009) Influence of specimen dimensions and strain measurement methods on tensile stress-strain curves. *Mater. Sci. Eng. A*, **525** (1–2), 68–77.
5. Chou, S.C., Robertson, K.D., and Rainey, J.H. (1973) The effect of strain rate and heat developed during deformation on the stress-strain curve of plastics. *Exp. Mech.*, **13** (10), 422–432.
6. Kwok, D.Y., and Neumann, A.W. (1999) *Contact angle measurement and contact angle interpretation*.
7. Alghunaim, A., Kirdponpattara, S., and Newby, B.M.Z. (2016) Techniques for determining contact angle and wettability of powders. *Powder Technol.*, **287**, 201–215.
8. Bigelow, W.C., Pickett, D.L., and Zisman, W.A. (1946) Oleophobic monolayers. Films adsorbed from solution in non-polar liquids. *J. Colloid Sci.*, **1** (6), 513–538.
9. Chau, T.T. (2009) A review of techniques for measurement of contact angles and their applicability on mineral surfaces. *Miner. Eng.*, **22** (3), 213–219.
10. Bracco, G., and Holst, B. (2013) *Surface science techniques*, Springer, Berlin, Heidelberg.
11. Hebbar, R.S., Isloor, A.M., and Ismail, A.F. (2017) *Contact Angle Measurements*, Elsevier B.V.
12. Reuschenbach, P., Pagga, U., and Strotmann, U. (2003) A critical comparison of respirometric biodegradation tests based on OECD 301 and related test methods. *Water Res.*, **37** (7), 1571–1582.
13. Tai, H., Yang, Y., Liu, S., and Li, D. (2012) A Review of Measurement Methods of Dissolved Oxygen in Water. *Int. Conf. Comput. Technol. Agric.*, **369**, 569–576.
14. Jouanneau, S., Recoules, L., Durand, M.J., Boukabache, A., Picot, V., Primault, Y., Lakel, A., Sengelin, M., Barillon, B., and Thouand, G. (2014) Methods for assessing biochemical oxygen demand (BOD): A review. *Water Res.*, **49** (1), 62–82.

3. Contribution 1

Apple waste and tomato peel by-products as fillers for starch-based bio-based composites

Abstract

Nowadays, bioplastics contribute towards a better global sustainability. The increased use of bioplastics is reducing landfill waste by upcycling of renewable feedstocks and limiting the use of finite resources (i.e. fossil resources) to fabricate products that perform as well as traditional plastics in many applications. One of the main natural polymers used for bioplastics' production is starch. Despite their large biodegradability, many of the features of starch-based edible films are still poor, if compared with those of the traditional plastics, as they are usually characterized by high hydrophilicity and low water vapor barrier and mechanical strength. One possible solution to enhance the properties of these materials can be the addition of natural fillers, in order to prepare bio-based composites. In this chapter, potassium silicate, apple waste (AW) and tomato peel by-products (TP) were used as fillers for starch-based bio-based composites. Different composites were fabricated by varying the ratio among AW and TP (from 100% AW to 0 % AW). A mechanical characterization of the samples, conducted by uniaxial tensile tests, showed a ductile and soft behaviour: Young's moduli ranged from 0.5 to 1.7 MPa. However, the introduction of food waste into the bioplastic formulations proved to be useful to increase biodegradability and to reduce water adsorption. A third lower water uptake was found for TP containing bioplastics, compared to a control without food waste. Moreover, the antioxidant properties of the samples were measured following the standard DPPH \cdot and ABTS $^{\cdot+}$ methods. The obtained results suggested their potential use as active coatings, in food-packaging applications.

3.1 Introduction

Starch is a polysaccharide produced by many plants. It is the second most abundant biomass material in nature after cellulose and represents the main storage polymer in plant cells. From a chemical point of view, it consists of molecules of amylopectin and amylose, i.e. a highly branched and a straight chain polymer of D-glucose, respectively [1]. Starch is made of about 70–80% amylopectin by weight, while amylose makes up approximately 20–30%. After its extraction from plants, starch occurs as a flour-like white powder insoluble in cold water and alcohol because of the hydrogen bonds which join together the amylose and amylopectin chains. The powder of starch consists of microscopic granules, with diameters from 2 to 100 μm and variable shapes, depending on its botanic origin, with a density of 1.5 g/mL [2]. These microscopic granules present pores on the surface and are organized into concentric growth rings with molecular domains, or blocklets, of amorphous and crystalline lamellae containing amylopectin and amylose chains (**Figure 3.1**).

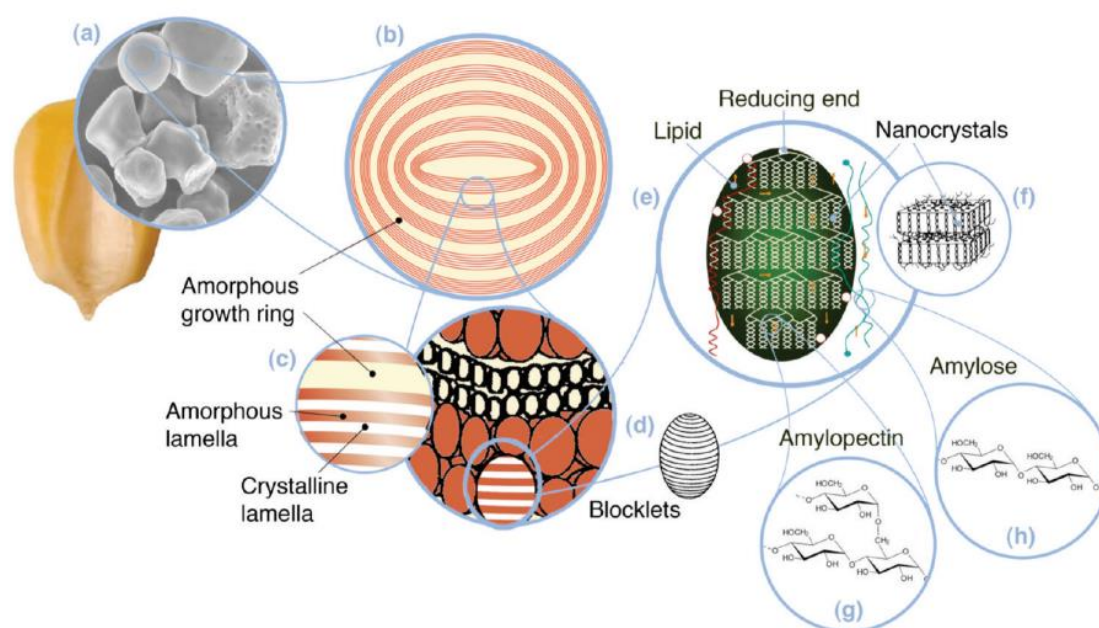


Figure 3.1 Starch microscopic granules' structure: (a) starch granules (30 μm), (b) amorphous and semicrystalline growth rings (120-500 nm), (c) amorphous and crystalline lamellae (9 nm), (d) blocklets (20-50 nm) constituting a unit of the growth rings, (e) amylopectin double helices forming the crystalline lamellae of the blocklets, (f) nanocrystals, (g) amylopectin's molecular structure, and (h) amylose's molecular structure (0.1-1 nm). Reproduced with the permission of American Chemical Society [2].

Native starches contain between 15 and 45% of crystalline material. Depending on their X-ray diffraction pattern (XRD), starches are categorized in different crystalline types, called A, B, and V. Both A and B structures are thought to be composed of left-handed, parallel-stranded double helices of amylopectin. The two polymorphs differ in the double helices packing and in the number of water molecules within the crystalline lattice. On the other hand, the V structure is typically observed when linear starch molecules form complexes with guest molecules such as iodine or fatty acids. This structure is usually made of a 6-fold left-handed single amylose helices packed in an antiparallel arrangement, with a hydrophilic outer surface and a hydrophobic inner. Crystals of such intrahelical inclusion complexes can be in the form of V-hydrate (V_h) or V-anhydrous (V_a). The V_a -type crystals contain two water molecules per unit cell. During storage at ambient humidity they can absorb water molecules and transform to the more hydrophilic V_h -type crystals, with three water molecules in their unit cell [3]. Starch can be found in all organs of most of higher plants, including pollen, leaves, stems, roots, tubers, bulbs, fruits and pericarp. Although in less amount, it can also be found in mosses, ferns and some algae [4,5]. The specific source of starch, the environmental conditions during starch maturation and the age of the plant affect its chemical composition, mainly the amylose and amylopectin ratio [6]. Almost as much variation for amylose percentage has been observed among cultivars of a single species. For example, amylose percentage ranges from 20 to 36% for maize starch, from 18 to 23% for potatoes, from 21 to 35% for sorghum, from 17 to 29% for wheat and from 8 to 37% for rice. Starches from cereal products contain lipids in the native granule which may allow the formation of amylose-lipid complexes, promoting changes in the starch chemical-physical properties such as the swelling capacity or the gelatinization temperature [1]. Structural studies of starch–lipid complexes indicated that the aliphatic chain of the lipid is inserted into the internal cavity of the amylose helix, while the carboxyl group of the fatty acid or the glyceride moiety of a monoacylglycerol remains exposed on the outside of the helix due to steric hindrance and electrostatic repulsions. In general, amylose complexation with lipid ligand requires eighteen to twenty-four monomer units that can create three turns, accommodating six to eight glucose units per pitch, i.e. the distance between identical points in sequential turns [7]. The lipid-containing helices can stack into crystalline lamellae which are packed into micron-sized spherulites with the interspersing amorphous regions (**Figure 3.2**) [8].

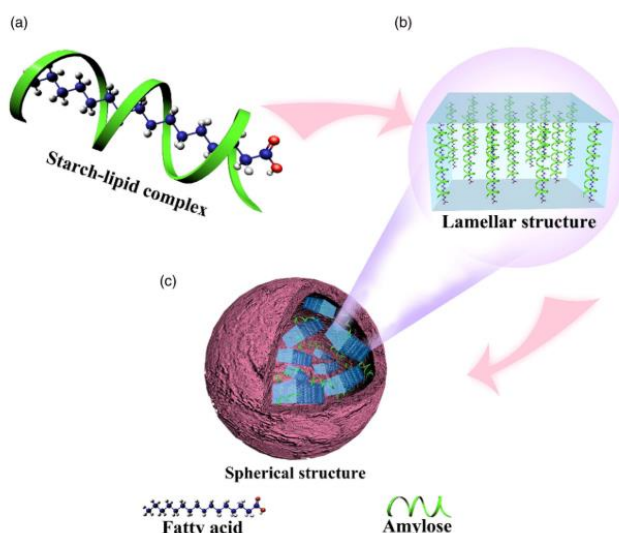


Figure 3.2 Structure of starch-lipid complexes from molecular (a) to nano- (b) and micro- (c) level. Reproduced with the permission of Wiley&Sons [8].

In any case, as cereal starches have about 1% lipid, only 15–55% of the amylose fraction is complexed. Lipid molecules prevent amylose slow recrystallization upon cooling or dehydration [9]. Their use to produce edible films is helpful to reduce thickness, opacity and water vapor permeability values [10,11]. The production of starch-based biofilms is usually based on a procedure of three main steps: (i) starch gelatinization, (ii) casting and (iii) starch retrogradation. The term “gelatinization” describes an irreversible structural change of starch polymer, which takes place when the polymer is exposed to temperatures ranging from 50–60 up to 90 °C, in presence of water [12]. At these temperatures, the breakdown of hydrogen bonds occurs, causing significant changes in the amylose and amylopectin structure. The semi-crystalline arrangement is lost and the minor amylose particles begin percolating out of the granule, forming a network that contributes to the increase of the solution viscosity. The structural loss in the double helix of starch is followed by interactions between added water and starch through free hydroxyls, starting from the amorphous regions [13]. Bioplastics production from starch is completed with the deposition of the gelatinized filmogenic solution on a non-adherent surface. This procedure is known as casting. The solution is cooled and dehydrated, thus facilitating the starch retrogradation due to the increase in intramolecular interactions between polymers, from the reduction of the volume in the polymeric matrix. Basically, the retrogradation is a process during which the cooled gelatinized solution undergoes an increase in the ordering degree of hydrogen bonds between the amylose molecules, which crystallize with the formation of a double helix and reducing the volume of the film [14].

Starch-based polymeric materials show several advantageous characteristics such as biodegradability, biocompatibility, odourless and tasteless, which make them suitable for coating and packaging (edible) applications. Moreover, the availability and the relatively simple extraction process allow a widespread use of this type of polymer [15–17]. However, starch-based bioplastics also show several drawbacks, e.g. high hydrophilicity, low water vapor barrier and poor mechanical properties during bioplastics formation. These drawbacks depend on the amylose content in the polymeric starch [18,19] and can be improved through physical, enzymatic or chemical processes which modify its native structure or by addition of plasticizers and other fillers. The incorporation of a plasticizing agent allows the conversion of native starch into a thermoplastic material [20]. The plasticizer effect consists of the induction of a higher flexibility due to an increase in the interstitial volume of the polymeric matrix and, hence, a lower interaction between polymer chains. Therefore, it reduces the glass transition temperature (T_g) [15] and increases the molecular mobility of the polymer [21]. The formulation of starch-based solutions with plasticizers increases the water uptake and the elongation at break and reduces the tensile strength. Examples of plasticizers used for the fabrication of starch-based bioplastics are gelatin, glycerol and sorbitol which, in general, are compatible with polysaccharides. The blending starch/gelatin is a useful way to increase the mechanical resistance [22]. Such an increase in the tensile strength of starch-based bioplastics blended with gelatin is attributed to the ability of this protein to interweave with starch. The conformation and arrangement of protein chains in the matrix led to strong interchain forces close to the collagen structure, enhancing the mechanical performance of the material [23,24]. Among glycerol and sorbitol, the first one has a greater plasticizer character than sorbitol due to its smaller size. As sorbitol has a relatively longer molecular length than glycerol, with more hydroxyl groups, it shows a greater chance of hydrogen bond formation with starch chains, causing a more stable microstructure. In other words, the starch chain movements are effectively restricted in sorbitol-plasticized starch, leading to a more rigid material, due to the formation of strong intermolecular hydrogen bonding. Moreover, XRD studies demonstrated that sorbitol favours the formation of V_a type crystals, which can decrease the hydrophilicity of thermoplastic starch and keep it resistant against the recrystallization that occurs due to water uptake [25]. However, the higher hydrophilic character of glycerol allows glycerol plasticized starch bioplastics to biodegrade faster than the ones prepared with sorbitol as plasticizer [26]. As regard to the barrier properties, they can be enhanced through the derivatization of starch through common reactions such as esterification (acetylation) or etherification (hydroxypropylation) that makes the polymer more hydrophobic [27]. Another option is blending with natural polymers such as pectin, cellulose,

and cutin, typically recovered from biomass (i.e. sugarcane bagasse, rice straw, flax, Kenaf, hemp, forest wood, and apple and tomato peels). They also represent a valid alternative to non-biodegradable synthetic fibers used as fillers for improving the mechanical properties of starch-based bio-composites [28], due to their excellent biodegradation characteristics and good reinforcement effect provided [29]. A recent filler used for starch-based bioplastics is silicate. Silicate can be extracted from many renewable sources such as rice, bamboo, wheat and sugarcane [30–33] and its addition provides good antifungal properties to bio-materials [34]. However, the mechanical properties still remained poor if compared with the conventional synthetic plastics (tensile strength of ~1 MPa).

In this chapter, new starch-based bioplastics have been fabricated by incorporation of apple waste and tomato peel by-products as polymeric matrix fillers, in addition to silicate, and glycerol used as a plasticizer. At global level, ~70 million tons of apples are yearly produced and millions of tons of apple waste are generated, mainly apple pomace, as a by-product of juice or cider production [35]. Although not suitable for landfilling or animal feedstock, due to its high sugar amount and low protein content, apple waste can be used as raw material for bioplastics fabrication, since it is rich in biodegradable natural polymers. Apple pomace is mainly composed of cellulose (7–44%), starch (14–17%), pectin (4–14%), and insoluble lignin (15–20%), in addition to a wide range of polyphenolics compounds such as cinnamic acid and its derivatives, epicatechin, epicatechin dimer trimer, tetramer and oligomer, and quercetin, which act as natural antioxidants [36,37]. As regard to tomato peels, one of the main advantages related to its use as feedstock for bioplastic production is the high content of cutin, an amorphous polymeric network of polyhydroxylated C₁₆ and C₁₈ fatty acids monomers cross-linked by ester bonds, which guarantees the fabrication of edible films with a low water adsorption, as it has a low interaction with water molecules [38,39]. When tomatoes are processed into products like ketchup, salsa and sauces, 10–30% of their weight becomes waste or pomace [40]. Its conversion into green materials, as well as the conversion of apple waste, is an ideal alternative in the context of environmental sustainability and circular bioeconomy.

3.2 Experimental section

3.2.1 Materials

Reagent grade acetic acid, potato starch, ethanol (96%), 1,1-diphenyl-2-picrylhydrazyl (DPPH) radical, 2,2'-azinobis(3-ethylbenzothiazoline-6-sulfonic acid) diammonium salt (ABTS) and potassium persulfate used in the antioxidant assay were purchased from Sigma-Aldrich (Milano, Italy) and used without further purification. Vegetable glycerol was obtained from Farmalabor srl (Barletta, Italia). Chitosan (CAS number: 9012-76-4) and commercial aqueous solution based on potassium silicate (10 % of potassium oxide soluble in water and 24% of silica) were obtained by Fertildea srl (Napoli, Italy), a local trader of products for bio-horticulture. Deionized water was obtained from a Milli-Q RG Ultrapure Water Purification device from Millipore (Bedford, MA, USA). Tomato peels were collected from local farmers and oven-dried before their use, while dehydrated apple waste, including cores and peels, was provided as by a local fruit industry.

3.2.2 Biocomposites preparation

The dehydrated apple waste (AW) and the oven-dried tomato peels (TP) were grounded to a fine powder by using a commercial coffee mill. Different composites were obtained by varying the combination of AW and TP. 1 g of food waste powder was mixed with 2 g of potato starch. The resultant combination was mixed in 15 mL of water by continuous stirring on a hot-plate at 70°C. Then, glycerol (8 mL), potassium silicate solution (5 mL) and chitosan solution (5 mL, 1% w/w prepared in 0.16 M acetic acid), were added to the mixture and stirred for 20 minutes until a viscous and homogeneous solution was obtained. The resultant solution was cast in polystyrene Petri dishes (diameter 90 mm) and air-dried in order to get a bio-based composite. A control without food waste was prepared by mixing 2 g of starch with water, glycerol, potassium silicate solution and chitosan solution. The composites were labelled as indicated in **Table 3.1** and are shown in **Figure 3.3**.

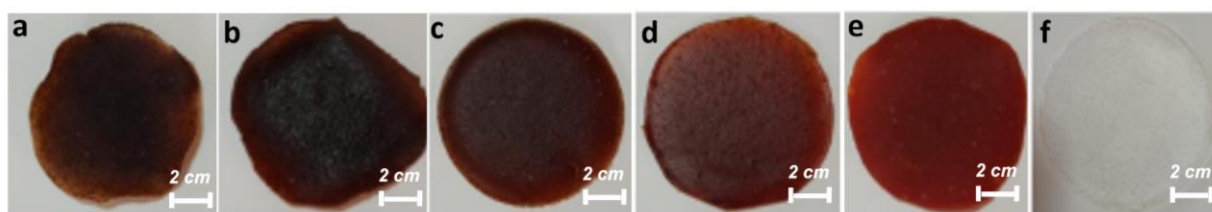


Figure 3.3 Dried composites prepared in this work: (a) AW100 sample; (b) AW75 sample; (c) AW50 sample; (d) AW25 sample; (e) AW0 sample, (f) C control.

Table 3.1 Sample label and composition*

Label	AW	TP	Starch	Water	Glycerol	Silicate	Chitosan
<i>AW100</i>	1 g (2.9%)	0 g	2 g (5.8%)	15 g (43.3%)	10 g (28.8%)	6.6 g (19.1%)	0.05 g (0.1%)
<i>AW75</i>	0.75 g (2.2%)	0.25 g (0.7%)	2 g (5.8%)	15 g (43.3%)	10 g (28.8%)	6.6 g (19.1%)	0.05 g (0.1%)
<i>AW50</i>	0.50 g (1.4%)	0.50 g (1.4%)	2 g (5.8%)	15 g (43.3%)	10 g (28.8%)	6.6 g (19.1%)	0.05 g (0.1%)
<i>AW25</i>	0.25 g (0.7%)	0.75 g (2.2%)	2 g (5.8%)	15 g (43.3%)	10 g (28.8%)	6.6 g (19.1%)	0.05 g (0.1%)
<i>AW0</i>	0 g	1 g (2.9%)	2 g (5.8%)	15 g (43.3%)	10 g (28.8%)	6.6 g (19.1%)	0.05 g (0.1%)
<i>C</i>	0 g	0 g	2 g (5.9%)	15 g (44.4%)	10 g (29.9%)	6.6 g (19.6%)	0.05 g (0.2%)

*abbreviations: AW: apple waste; TP: tomato peels.

3.2.3 Chemical, mechanical and thermal characterization

All composites were chemically characterized by Fourier-transform infrared spectroscopy (FTIR), using an Equinox 70 FT-IR (Bruker) spectrometer. All spectra were acquired in the range from 4000 to 600 cm^{-1} with a resolution of 4 cm^{-1} , accumulating 128 scans. Three acquisitions were made for each sample in three different areas in order to assess the homogeneity of chemical composition.

The mechanical properties of the composites were determined with a MTS Criterion 42 machine equipped with a 50 N load cell. All the measurements were done according to ASTM D 882 Standard Test Methods for Tensile Properties of Thin Plastic Sheeting. Thus, dog-bone shapes of 20 mm length and 5 mm width were cut for each sample and stretched at a rate of 5 mm/min. Stress-strain curves were acquired for each sample, thus allowing the calculation of Young's modulus, yield stress, elongation at break, and toughness. The values were expressed as average of at least seven independent measurements.

The thermal degradation behaviour of the composites was studied by thermogravimetric analysis (TGA). The measurements were made by using a Q500 analyzer from TA instruments, under an inert N_2 atmosphere on 3 mg samples in an aluminium pan at a heating rate of 10 $^{\circ}\text{C}/\text{min}$, from 30 $^{\circ}\text{C}$ to 600 $^{\circ}\text{C}$. For each sample, weight loss and its first derivative were recorded simultaneously as a function of time and temperature, in order to obtain TG curve and DTG curve, respectively.

3.2.4 Water uptake

To assess the water uptake, the composites were dried by conditioning in a desiccator until no change in sample weight was measured. Then, 80 mg of dry samples were weighed with a sensitive electronic balance (0.0001 g accuracy) and placed in different chambers under different humidity conditions (RH) at 25 °C. The following humidity conditions were set: 0%, 11%, 57%, 84% and 100% RH. After conditioning in the different humidity chambers until equilibrium conditions (1 day), each sample was weighed and the amount of adsorbed water was calculated, in percentage, as the difference with the initial dry weight according to the following equation:

$$\text{Water uptake (\%)} = \frac{m_f - m_0}{m_0} \times 100$$

Where m_f is the sample weight at specific RH condition of interest and m_0 is the sample weight at 0% RH. Three replicates were measured for each sample and the results were averaged to obtain a mean value.

3.2.5 Biodegradability

The biodegradability of the composites was evaluated by measuring the amount of oxygen consumed during a biodegradation reaction in water, through the standard biochemical oxygen demand (BOD) test. Briefly, 200 mg of each sample were finely minced and immersed in dark glass bottles containing 164 mL of seawater collected from the Malaga (Spain) area shoreline. The seawater, already containing microbial species and saline nutrients needed for their growth, allowed to mimic the real environmental conditions of biodegradation. Each bottle was sealed and maintained at 25°C. The O₂ consumed during the biodegradation process was recorded at different time intervals, for 30 days, by using sealed OxyTop caps on each bottle which can assess the oxygen levels. For each sample, three measurements were done and the results were averaged to obtain a mean value.

3.2.6 DPPH radical scavenging assay

The antioxidant capacity was calculated by measuring the free radical scavenging activity of the total released phenolic compounds on the DPPH[•] (2,2-diphenyl-1-picrylhydrazyl) radical. 5 × 5 mm² discs of each sample were added to 4 mL of 0.1 mM DPPH solution in ethanol. The decrease in the absorbance solution due to the antioxidant composites' action was determined at 515 nm with a Cary JEOL spectrophotometer at different times. Radical scavenging activity was

expressed as the inhibition percentage of free radical by the sample and calculated through the following equation:

$$\text{Radical Scavenging Activity (\%)} = \frac{A_0 - A_1}{A_0} \times 100$$

where A_0 is the absorbance value of the control (3 mL of 0.1 mM DPPH solution in ethanol) and A_1 is the absorbance value of the sample at different times. All measurements were performed in triplicate and the results were expressed as the mean \pm SD.

3.2.7 ABTS free radical cation scavenging assay

The 2,2'-azinobis-(3-ethylbenzothiazoline-6-sulphonate) radical cation ($\text{ABTS}^{\cdot+}$) was obtained by the reaction between ABTS aqueous solution (7 mM) with potassium persulfate aqueous solution (2.45 mM) in the dark at room temperature for 12–16 h [41,42]. The $\text{ABTS}^{\cdot+}$ solution was diluted with water to obtain an absorbance of 0.80 a.u. at 734 nm. After that, 5×5 mm² films were added to 3 mL of diluted radical solution. The decrease in absorbance was determined at 734 nm with a Cary JEOL spectrophotometer at different times. Radical scavenging activity was expressed as the inhibition percentage of free radical by the sample and calculated as follows:

$$\text{Radical Scavenging Activity (\%)} = \frac{A_0 - A_1}{A_0} \times 100$$

where A_0 is the absorbance value of the control radical cation solution and A_1 is the absorbance value of the sample at different times. All measurements were performed in triplicate and the results were expressed as the mean \pm SD.

3.2.8 Statistical analysis

Significant differences of the results among the variances were statistically analyzed by SPSS 19.0 software (IBM SPSS Statistics, Armonk, NY, USA). Statistical significance was accepted at a level of $p < 0.05$.

3.3 Results and Discussion

3.3.1 Chemical, mechanical and thermal characterization

The chemical influence of the potassium silicate, glycerol, chitosan and food waste, the possible bond formation or starch modification was evaluated by Fourier-transform infrared spectroscopy. **Figure 3.4a** shows the FTIR spectra of the polymeric matrix (starch) as well as of the additives used for bio-composites preparation in the 4000-600 cm^{-1} region. On the other hand, the FTIR spectra of AW100, AW75, AW50, AW25, AW0 and C bioplastics are reported in **Figure 3.4b**. The polymeric matrix showed typical absorption bands of starch: OH stretching mode at 3310 cm^{-1} and peaks in the 100-900 cm^{-1} region, due to the C–O stretching of the C–O–C group of the starch anhydro glucose ring. In addition to the band associated to the OH stretching mode, asymmetric and symmetric CH_2 stretching modes at 2932 cm^{-1} and 2879 cm^{-1} , respectively, were observed in the FTIR spectra of glycerol. Potassium silicate FTIR spectrum exhibited a single absorption band at 977 cm^{-1} related to the asymmetric stretching of the Si–O–Si bond [43], while the C=C stretching mode of conjugated alkene was noticed in the FTIR spectra of apple and tomato wastes at 1604 cm^{-1} . The results obtained by FTIR analysis of the control C showed that the use of additives to allow the plasticization of the material, i.e., glycerol, modifies the chemical properties of the starch, as the characteristic peak at ca. 3300 cm^{-1} , which corresponds to OH stretching mode, shifted to lower wavenumbers due to more stable and stronger hydrogen bond formation. Moreover, the addition of apple and tomato wastes caused a shift of the C=C stretching mode of alkene groups to higher wavenumbers. A band at 1645 cm^{-1} , corresponding to the $\delta(\text{O–H})$ flexion of adsorbed water [44] and a band at 1412 cm^{-1} , associated with the bending of CH_2 and C–OH groups whose the main contributors were starch and glycerol, were observed in all spectra. In addition, a band at 1028 cm^{-1} assigned to the C–O stretch vibration in C–O–H groups of starch, glycerol and chitosan, and two bands at 921 cm^{-1} and 852 cm^{-1} assigned to anhydro glucose ring stretching vibrations of the starch structure, were noticed [44].

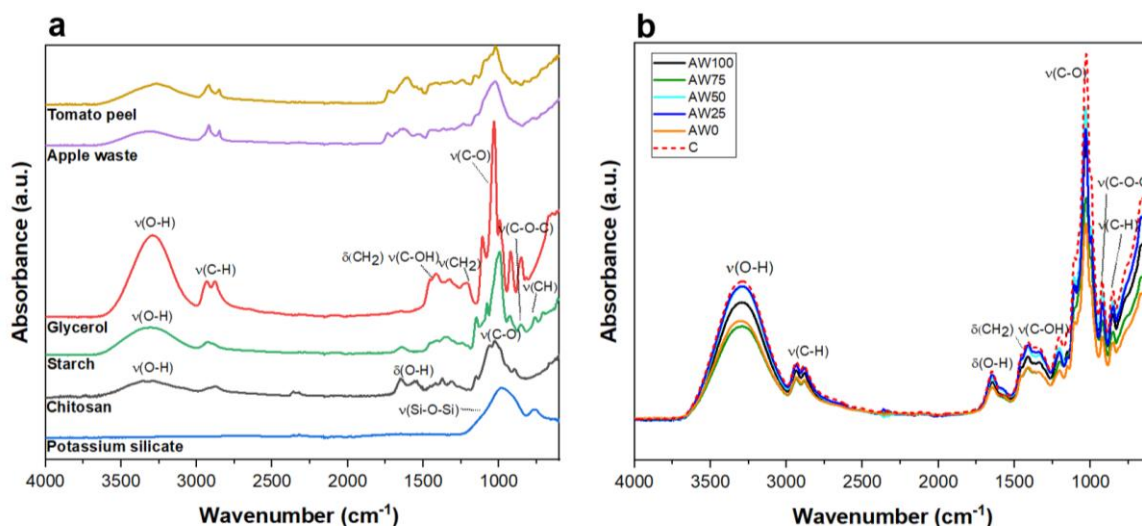


Figure 3.4 (a) FTIR spectra of tomato peel, apple waste, glycerol, starch, chitosan and potassium silicate in the 4000-600 cm⁻¹ region. (b) FTIR spectra of AW100, AW75, AW50, AW25, AW0 samples and of C control in the 4000-600 cm⁻¹ region.

The mechanical properties of the most representative samples prepared within this work, i.e. AW100, AW75, AW25, AW0 and C films, are presented in **Figure 3.3**. **Figure 3.3a** shows the typical tensile stress-strain curves, while the Young's modulus and elongation at break are displayed in **Figures 3.5b-c**. All bio-based composites prepared by addition of food waste exhibited a similar ductile, soft behaviour with slight increases of Young's modulus (from 0.5 MPa for AW0 to 1.7 MPa for AW100) and yield stress (from 0.09 MPa for AW0 to 0.025 MPa for AW100), while keeping the strain at break (~20% for all samples). Among all biocomposites, some differences were noted, as the Young's moduli were lower than control C (2.5 MPa) and increased by increasing the amount of apple waste, thus contributing to a more rigid behaviour of the materials. This change is associated with the effect of the apple waste and tomato peel particles, which separate and reduce the interactions between the polymeric chains of starch. In any case, all values were far from the values of the conventional petroleum-based plastics, which show Young's modulus in the order of GPa and elongations at break of several hundred percent. On the other hand, the inclusion of food waste into the bioplastic formulation did not affect the elongation at break as the obtained values for AW100-AW0 samples were not significantly different compared to the % of elongation at break registered for C control, **Figure 3.5c**. **Figure 3.5d** compares the values of the stress at break versus Young's modulus of the biocomposites prepared in this work with common plastics materials such as polyurethane (PU), polydimethylsiloxane (PDMS), low- and high-density polyethylene (LDPE and HDPE,

respectively), acrylonitrile-butadiene rubber (NBR), polypropylene (PP), and poly(ethylene terephthalate) (PET) [45]. AW0 was found in the lowest values range. The elongation at break of the samples was comparable with or even higher than that of rigid polymers such as polystyrene (PS) at 1–4%, styrene-acrylonitrile (SAN) at 2–5%, nylon 66 at 20%, poly(methyl methacrylate) (PMMA) at 3–5%, melamine-formaldehyde resin (MF) at 0.5–15%, or epoxy resin at 1–2% [45]. This suggests that the application as films is discarded, although these biocomposites can find application in other uses where soft materials are employed such as (edible) coatings. It is also suggested the incorporation of other fibres to improve the mechanical properties.

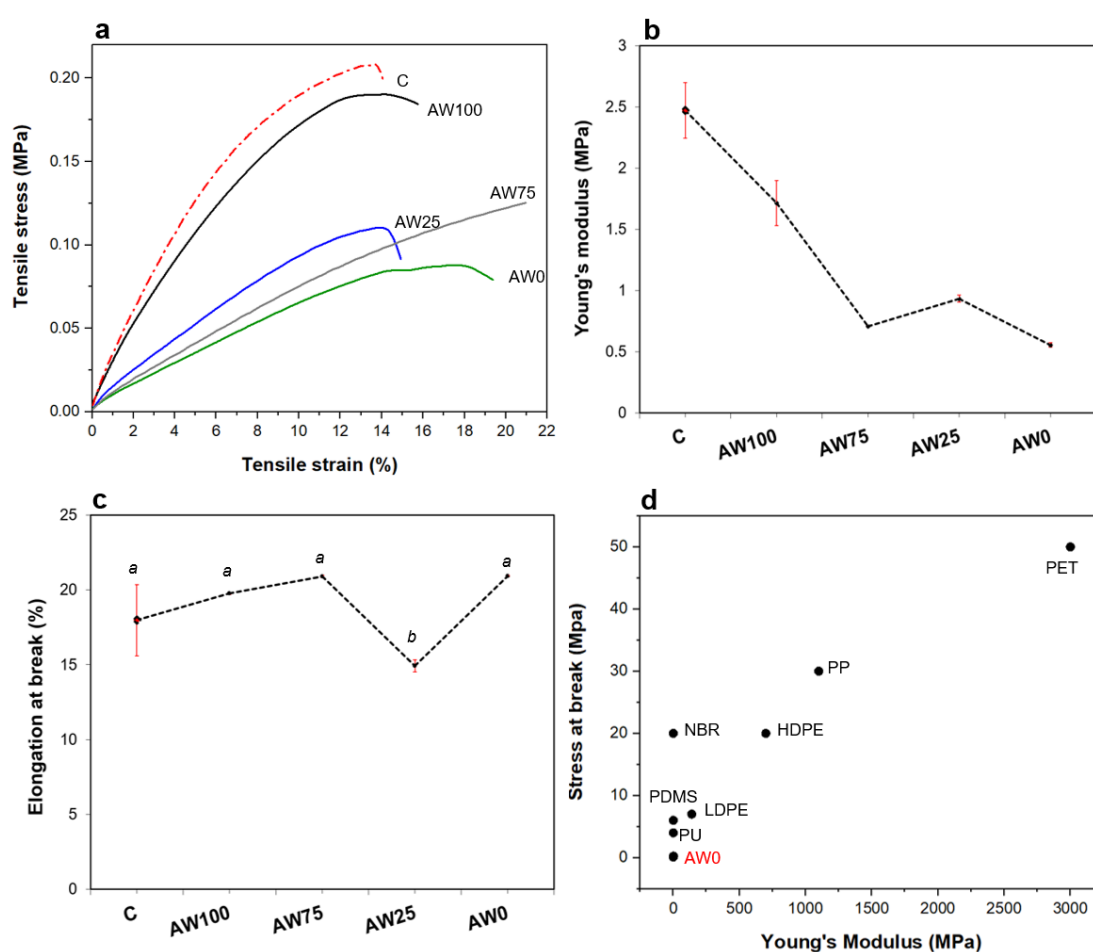


Figure 3.5 (a) Typical stress-strain curves for AW100, AW75, AW25, AW0 samples and control C. (b), (c) Young's modulus and elongation at break parameters, respectively, for AW100, AW75, AW25, AW0 samples and control C calculated from the stress-strain curves. Values marked by the same letter are not significantly different ($p < 0.05$). (d) Comparison of stress at break versus Young's modulus of AW0 sample with different man-made polymeric materials. Data from Mark [45]. AW0 was chosen as its value of stress at break represented the minimum obtained value among all the tested samples.

In order to evaluate the thermal stability of the biocomposites prepared in this work and to know the maximum temperature at which these materials can be used without degradation or loss of their characteristics, thermogravimetric analysis (TGA) was used. The thermograms (TG) and the corresponding derivative curves are reported in **Figure 3.6a-b** and **Figure 3.S1**. All samples exhibited four weight losses at $\sim 105^{\circ}\text{C}$, $\sim 210^{\circ}\text{C}$, $\sim 250^{\circ}\text{C}$ and $\sim 340^{\circ}\text{C}$. No significant differences were detected for thermally treated samples containing apple waste or tomato peels compared to the control, thus suggesting that the addition of food waste did not affect the thermal stability or the residual weight of the samples. The first weight loss of $\sim 10\%$ at $\sim 105^{\circ}\text{C}$ is attributed to evaporation of free water [46]. The second one of $\sim 20\%$ at $\sim 210^{\circ}\text{C}$ is related to glycerol degradation [25] and the dehydration of polysilicate silanol groups [47]. Glycerol degradation occurs to the breakage of the C–C, C–O, and O–H bonds to form carbonyl and alkene and then generation of water, formaldehyde and acetaldehyde. Moreover, glycerol undergoes an intramolecular dehydration reaction, producing 3-hydroxypropionaldehyde [48]. The third stage of mass loss, also of $\sim 20\%$, and the fourth weight loss step ($\sim 15\%$) at ~ 250 and $\sim 340^{\circ}\text{C}$, respectively, can be attributed to starch thermal degradation. In detail, thermal condensation between hydroxyl groups of starch chains to form ether segments and liberation of water molecules and other small molecular species occurs. Dehydration of neighboring hydroxyl groups in the glucose ring also happens, resulting in the formation of C–C bonds or breakdown of the glucose ring. Aldehyde groups can also be formed at the same time as end groups when the glucose ring is fractured [49]. Above 400°C no further weight loss occurred. The remaining mass at 400°C was of $\sim 23\%$ for all the samples.

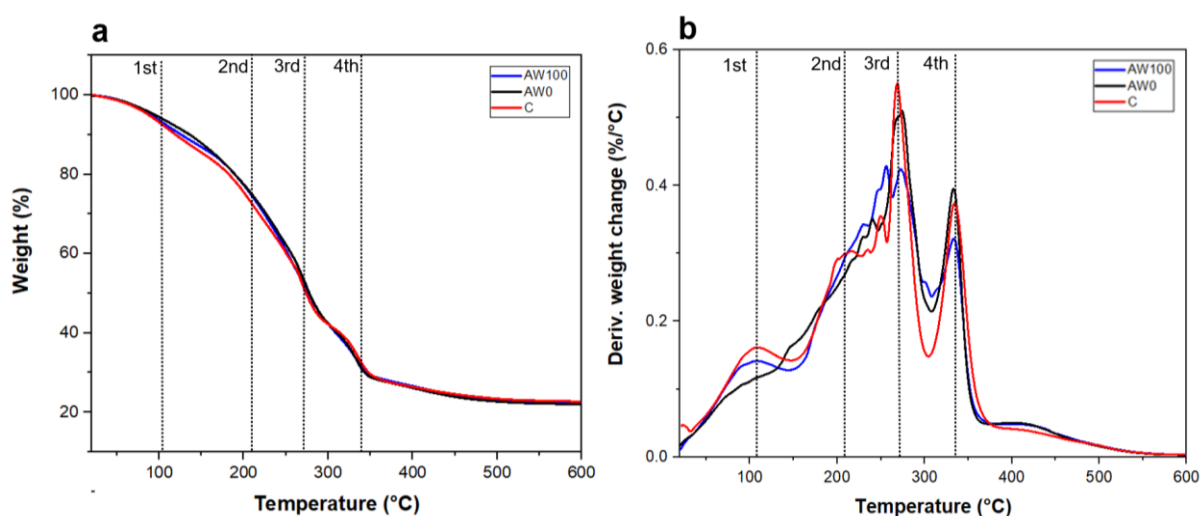


Figure 3.6 TGA thermograms (a) and derivative thermogravimetric curves (b) of the most representative biocomposites prepared in the present work, i.e. AW100, AW0 and C samples.

3.3.2 Water uptake

Water uptake properties of all fabricated biocomposites were analyzed by measuring water adsorption levels under different humidity conditions, i.e. RH 0%, 11%, 57%, 84% and 100% (**Figure 3.7**). The water adsorption isotherms presented similar shapes, which can be defined as type III isotherms as they were convex to RH% axis over their entire range and no knee points could be observed [50]. Adsorption isotherms describe the equilibrium performance of adsorbents when the temperature is constant. Thus, the most important information that they give is related to the surface porosity and the adsorbate-adsorbent equilibrium process. They depend on the adsorbed species, adsorbate, adsorbent and other properties of the solution including pH, ionic strength and temperature. In terms of edible films, the adsorption isotherm is used to predict the stability of the film towards the surrounding environment. Here, the obtained type III isotherms suggested adsorbate-adsorbate (i.e. water-water) interactions bigger compared to adsorbate-adsorbent interactions [51]. Moreover, the absence of a knee point suggested that no multilayer formation occurred over the biocomposites. This means that only a single layer of water molecules on the biocomposite surface are absorbed, biocomposite surface is homogeneous and adsorption energy is uniform for all sites and there is no transmigration of adsorbate in the plane of the surface [52]. As expected, water uptake values were relatively high at all humidity conditions, as the starch is a strongly hydrophilic biopolymer. The hydrophilic character of starch is due to the great number of free hydroxyl groups, which allow to keep numerous water molecules incorporated within the polymeric matrix, thanks to the establishment of strong hydrogen bonds. Moreover, the addition of hydrophilic plasticizers to starch-based formulations needed to produce bioplastics can increase the hydrophilicity. A water uptake of ~55% was found for a neat starch film plasticized with glycerol by Ban et al. [53] at RH 95%, as the hydrophilic character of glycerol facilitates both adsorption of water molecules [54]. In our study, a water absorption of around 90% under the highest RH was obtained for the control prepared without the addition of food waste, probably due to silicates filler which are hygroscopic. In general, also the samples containing apple waste and/or tomato peels were found to be very sensitive to relative humidity. In particular, after 80% R.H., water uptake levels of all films were almost ten times higher compared to the adsorption obtained under low humidity conditions (water uptake ~4% for all samples at RH 11%). The increase of apple waste content into the bioplastic formulation caused an increase of the water adsorption (**Figure 3.7b**). The water uptake, calculated as percentage of dry weight, passed from 64 % for AW0 sample to 83 % for AW100 sample. This tendency can be explained by the higher degree of hydrophobicity

of AW0 compared to AW100, ensured by the higher content of tomato peels that is a prominent source of the aliphatic biopolyester cutin [38,39]. Compared to tomato peels, cutin content is much lower in apple waste, being these fruits rich in other hydrophilic polysaccharides such as pectin [37]. Thus, the addition of AW into the bioplastic formulation significantly enhances the water uptake compared to the biocomposite containing only tomato peels, namely AW0. In any case, all samples obtained by the incorporation of food waste into the starch polymeric matrix showed a marked reduced water adsorption capacity with respect to sample C ($p > 0.05$), thus suggesting the utility of this biomass as modifying agent of the water uptake of bioplastics.

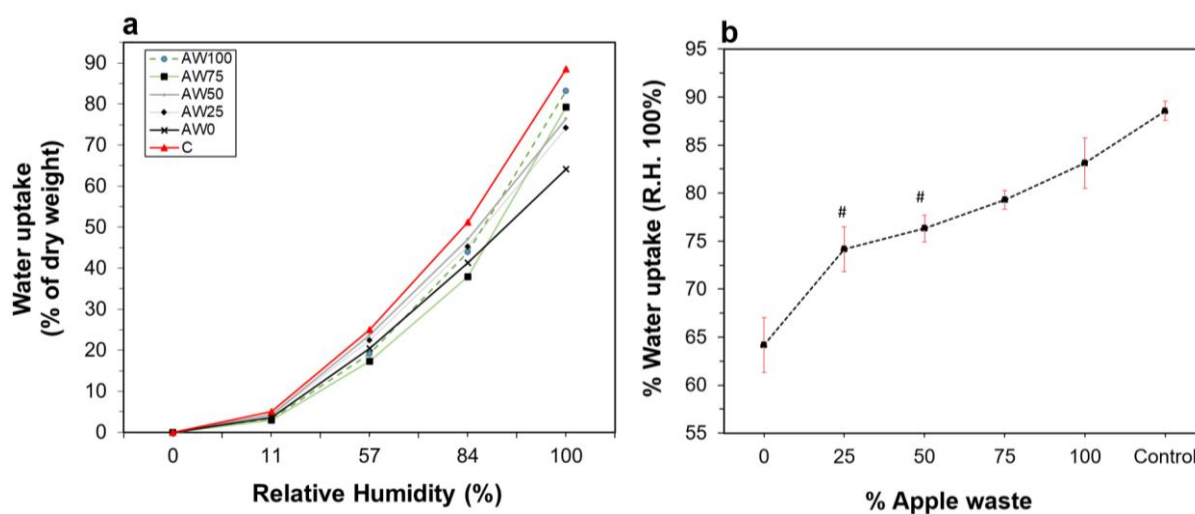


Figure 3.7 (a) Water adsorption (uptake) values under different humidity conditions (R.H. 0%, 11%, 57%, 84% and 100%) for AW100, AW75, AW50, AW25, AW0 samples and for control C. (b) Water uptake values at a relative humidity of 100% as a function of the apple waste content. Values marked by # symbol are not significantly different ($p < 0.05$).

3.3.3 Biodegradability

One of the main problems associated with the extensive use of petroleum-based plastics is their non-biodegradability, which results in the accumulation of millions of tons of plastic waste per year. Therefore, among the mandatory requirements in the field of new sustainable materials' production, there is the need to propose largely biodegradable alternatives. The biodegradability of the developed biocomposites was studied by monitoring the biochemical oxygen demand during 30 days in seawater. The results are shown in **Figure 3.8**.

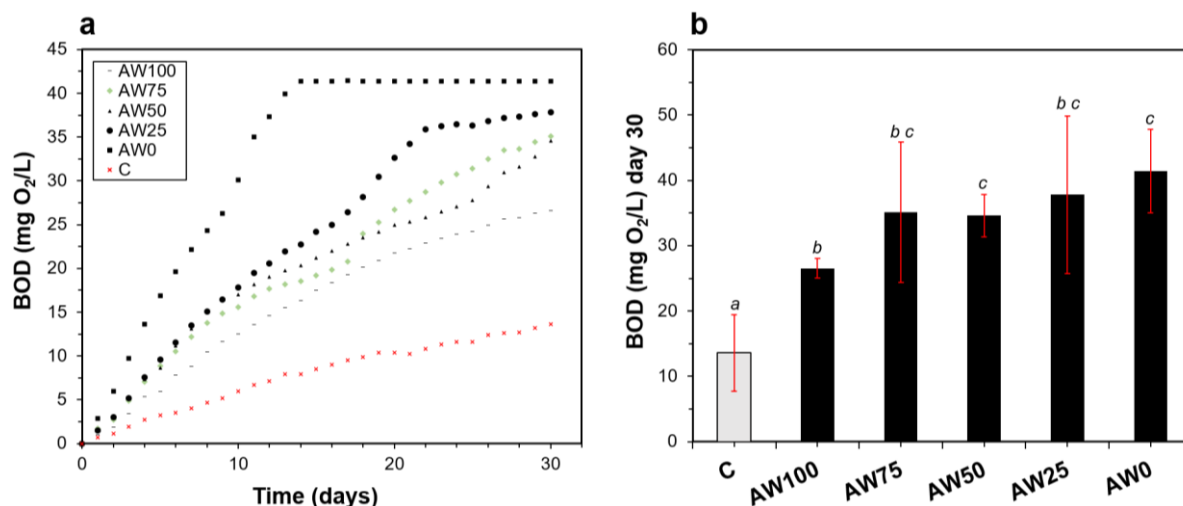


Figure 3.8 (a) Biochemical oxygen consumption (mgO₂/L) as a function of time (days) for AW100, AW75, AW50, AW25, AW0 samples and the control C. (b) Biochemical oxygen consumption (mgO₂/L) at day 30 for all the samples and the control. Values marked by the same letter are not significantly different ($p < 0.05$).

The obtained results showed that all composites prepared by addition of apple waste and tomato peels to the starch polymeric matrix exhibited a higher biodegradability compared to the control. Indeed, a maximum oxygen consumption of around 14 mg O₂/L was reached after 30 days by the sample not containing food waste (**Figure 3.8b**). This value was significantly lower than the one obtained for food waste-containing composite with the least biodegradability, i.e. AW100 sample (35 mg O₂/L of oxygen consumption after 30 days). Several studies report the biodegradability of starch films with natural additives [6,55,56]. Among the AW samples, some differences are noted in terms of biodegradability. In general, the biochemical oxygen consumption in seawater increased as the content of tomato peel increased, in the following order: AW0>AW25>AW50>AW75>AW100. This trend can be explained by the higher amount of proteins contained in tomatoes than apple fruits, which enhance the rate of degradation of the biomaterials. As reported by Emadian et al. [57] the addition of materials containing high protein content is a valid tool to improve the bioplastics biodegradability, since this parameter is positively affected by the content of soluble sugar. On the other hand, for the biocomposites containing up to 75% of tomato peels, i.e. AW100, AW75, AW50 and AW25, the plateau in the oxygen consumption was reached after 27 days on average, while for AW0 (no apple waste added), 15 days were enough to achieve the maximum oxygen consumption at 41.4 mg/L. A comparison of final BOD values of AW0 and AW100 biocomposites with other common polymers such as cotton, polyhydroxybutyrate (PHB), lignin and xylan as well as other bioplastics prepared from rice and seaweed was made (**Figure 3.9a**) [42,58–61]. In general,

AWx bioplastics exhibited good BOD values, better than cotton, PHB lignin and xylan. Both AW0 and AW100 showed a final BOD between xylan and other plant-based materials such as rice bioplastic. In order to get the % of biodegradation, once BOD test was completed the remaining material was collected from the bottles and weighted. The weight loss is presented in **Figure 3.9b**. In all the cases, very high values of weight loss close to 90% were obtained, indicating that these biocomposites are easily biodegraded in seawater.

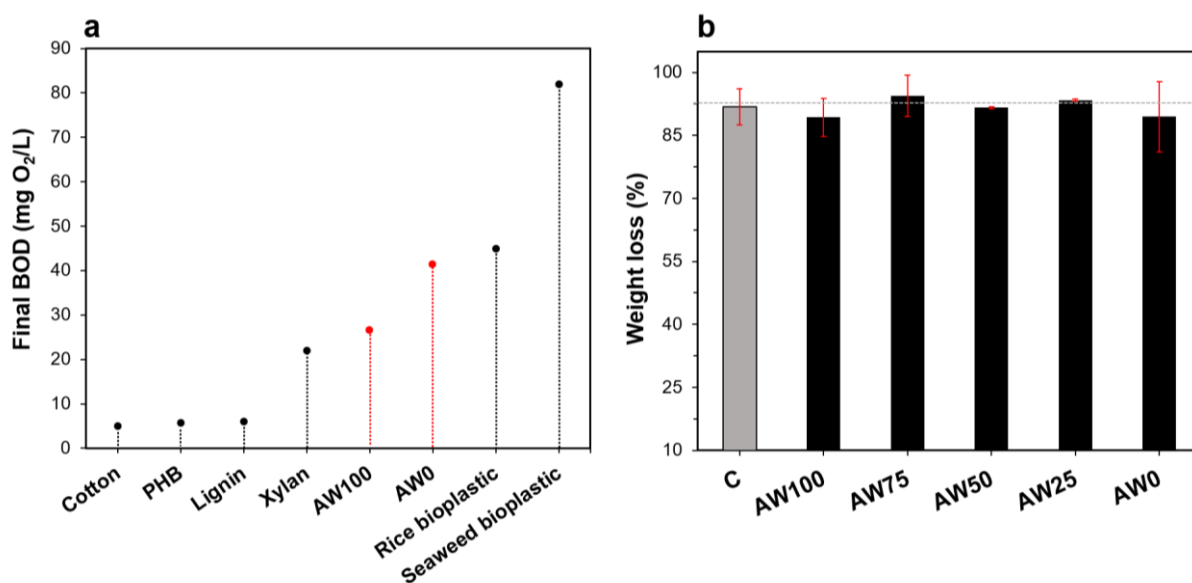


Figure 3.9 (a) Comparison of final BOD values of AW0 and AW100 samples with other common bio-based polymers. (b) Weight loss of AW100, AW75, AW50, AW25, AW0 samples and the control C after BOD test.

3.3.4 Antioxidant properties

The antioxidant properties of the samples were measured following the standard DPPH· and ABTS⁺ methods. **Figure 3.10a** shows the results both for the control C and the composite bioplastics obtained with the addition of apple waste and/or tomato peels by using DPPH· method. All biocomposite materials displayed final values of radical scavenging activity (RSA) between 20% and 30% after 6 hours of measurement. Results obtained for the bioplastics were much higher compared to the control (RSA=22.3±0.7%). The antioxidant capacity increased with the apple waste content: the RSA was 24.3±0.6% for AW0, 24.6±1.9% for AW25, 26.6±0.5% for AW50, 28.4±0.6% for AW75 and 31.0±1.0% for AW100. This trend is ascribed to the higher presence of antioxidant compounds in apple waste, mainly phenolics and flavonoids [37]. Such a trend was observed also in the case of ABTS⁺ method (**Figure 3.10b**), with RSA passing from 87.7±0.8% for AW0 to 93.1±0.5% for AW100 after 4 hours of measurement.

However, higher values for $\text{ABTS}^{\cdot+}$ method can be due to the participation of both the hydrophilic and lipophilic fraction, instead of just the lipophilic antioxidants as in the case of $\text{DPPH}\cdot$ method [41,62]. Moreover, the antioxidant compounds that react quickly with $\text{ROO}\cdot$ may react slowly or may even be inert in $\text{DPPH}\cdot$ assay. Since the $\text{ABTS}^{\cdot+}$ radical is more reactive than $\text{DPPH}\cdot$ radical, the $\text{ABTS}^{\cdot+}$ assay allowed to quickly reach the plateau: the highest radical scavenging activity values were recorded after only 1 hour. Indeed, while the reactions with (2,2-diphenyl-1-picrylhydrazyl) radical involve hydrogen atom transfer (HAT), the reactions with 2,2'-azinobis-(3-ethylbenzothiazoline-6-sulphonate) radical involve both HAT and single-electron transfer (SET). It should be noted that, unlike $\text{DPPH}\cdot$ method, with $\text{ABTS}^{\cdot+}$ assay the C sample, namely composite biomaterial obtained without the addition of food waste, showed the highest RSA% value, i.e., $94.5\pm 0.3\%$. It can be argued that the test medium used (water), dissolves the C biofilm easier than ethanol, which is the solvent of the $\text{DPPH}\cdot$ test, therefore favouring the release of strong antioxidant additives. Data obtained by antioxidant assays highlight how the presence of food waste contributes to a lesser extent to the radical scavenging activity of the biocomposites: an increase of 8% was recorded as maximum for AW100 sample compared to the control within the $\text{DPPH}\cdot$ test, thus suggesting the antioxidant potential of the other additives included in the polymeric matrix. In fact, after 4 hours, both silicate and chitosan showed around 50% of RSA tested by $\text{ABTS}^{\cdot+}$ assay (**Figure 3.10b inset**). Also glycerol exhibited a moderate radical scavenging activity ($\sim 20\%$), explaining the high antioxidant capacity of the control.

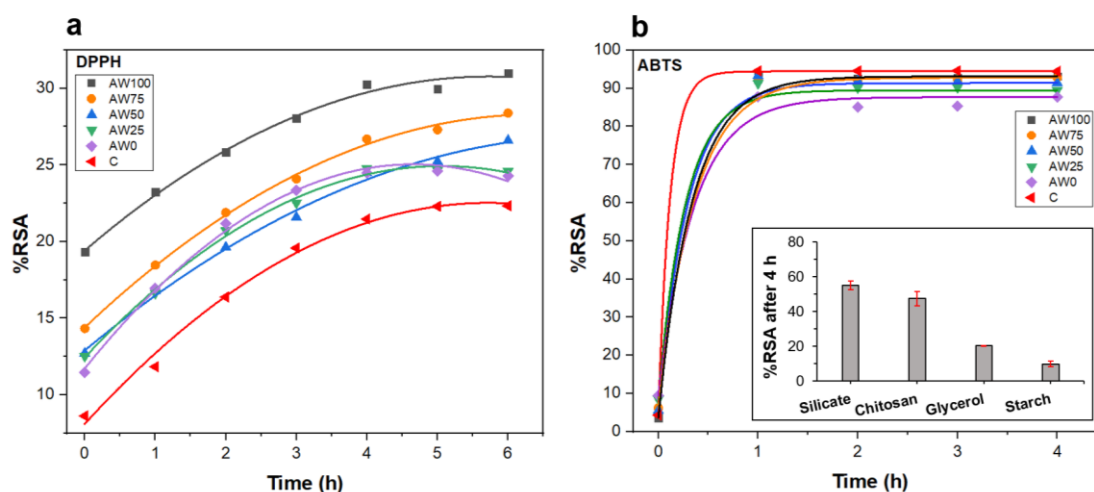


Figure 3.10 Antioxidant capacity as a function of time (hours) for AW100, AW75, AW50, AW25, AW0 samples and for control C, calculated by using two different methods: 2,2-diphenyl-1-picrylhydrazyl free radical ($\text{DPPH}\cdot$, **a**) and 2,2'-azinobis-(3-ethylbenzothiazoline-6-sulphonate) radical ($\text{ABTS}^{\cdot+}$, **b**). Inset: radical scavenging activity of silicate, chitosan, glycerol and starch, calculated after 4 hours by using the $\text{ABTS}^{\cdot+}$ assay.

3.4 Conclusions

The growing interest in the development of sustainable, biodegradable materials with a low toxicity as potential substitutes of petroleum-based plastics has driven the research towards the use of several raw materials as building blocks for bioplastics production. Since agri-food wastes are produced in very high quantities posing serious environmentally and economically problems, their use to produce eco-compatible materials is a good solution under the new circular economy and bioeconomy policies. Within this study, apple waste and tomato peels were used without further pre-treatments to fabricate different biocomposites. The incorporation of AW and TP in bioplastic formulations kept the thermal stability and the mechanical performances of the polymer matrix. The mechanical characterization showed a ductile and soft behaviour of the samples, making them suitable for covering applications. An improved biodegradability of food waste-containing materials was ascertained, alongside with a reduced water adsorption, above all for AW0 sample, due to the higher content of hydrophobic cutin present in TP. Moreover, the antioxidant properties shown by the samples, mainly due to the occurrence of the silicate filler used and to the apple waste phenolic compounds, suggested their potential use as active food-packaging.

References

1. Mira, I., Persson, K., and Villwock, V.K. (2007) On the effect of surface active agents and their structure on the temperature-induced changes of normal and waxy wheat starch in aqueous suspension. Part I. Pasting and calorimetric studies. *Carbohydr. Polym.*, 68 (4), 665–678.
2. Corre, D. Le, Bras, J., and Dufresne, A. (2010) Starch Nanoparticles: A review. *Biomacromolecules*, 11, 1139–1153.
3. Kong, L., Lee, C., Kim, S.H., and Ziegler, G.R. (2014) Characterization of starch polymorphic structures using vibrational sum frequency generation spectroscopy. *J. Phys. Chem. B*, 118 (7), 1775–1783.
4. Yu, S., Blennow, A., Bojko, M., Madsen, F., Olsen, C.E., and Engelsen, S.B. (2002) Physico-chemical characterization of floridean starch of red algae. *Starch/Staerke*, 54 (2), 66–74.
5. Carvalho, J.C.M., Matsudo, M.C., Bezerra, R.P., Ferreira-Camargo, L.S., and Sato, S. (2014) Algal Biorefineries: Cultivation of Cells and Products. *Microalgae bioreactors*, 1, 83-126.
6. Marichelvam, M.K., Jawaid, M., and Asim, M. (2019) Corn and rice starch-based bioplastics as alternative packaging materials. *Fibers*, 7 (4), 1–14.
7. Li, L., Liu, Z., Zhang, W., Xue, B., and Luo, Z. (2021) Production and Applications of Amylose-Lipid Complexes as Resistant Starch: Recent Approaches. *Starch/Staerke*, 73 (5–6), 1–13.
8. S, W., C, C., J, C., B, N., L, C., and S, W. (2020) Starch–lipid and starch–lipid–protein complexes: A comprehensive review. *Compr. Rev. food Sci. food Saf.*, 19 (3), 1056–1079.
9. Becker, A., Hill, S.E., and Mitchell, J.R. (2001) Relevance of amylose-lipid complexes to the behaviour of thermally processed starches. *Starch/Staerke*, 53 (3–4), 121–130.
10. Santacruz, S., Rivadeneira, C., and Castro, M. (2015) Edible films based on starch and chitosan. Effect of starch source and concentration, plasticizer, surfactant's hydrophobic tail and mechanical treatment. *Food Hydrocoll.*, 49, 89–94.
11. Thakur, R., Pristijono, P., Golding, J.B., Stathopoulos, C.E., Scarlett, C.J., Bowyer, M., Singh, S.P., and Vuong, Q. V. (2017) Amylose-lipid complex as a measure of variations in physical, mechanical and barrier attributes of rice starch- κ -carrageenan biodegradable edible film. *Food Packag. Shelf Life*, 14 (April), 108–115.
12. Ratnayake, W.S., and Jackson, D.S. (2008) *Starch Gelatinization*.
13. Halley, P.J., Truss, R.W., Markotsis, M.G., Chaleat, C., Russo, M., Sargent, A.L., Tan, I., and Sopade, P.A. (2007) A Review of Biodegradable Thermoplastic Starch Polymers. 287–300.
14. Wang, S., Li, C., Copeland, L., Niu, Q., and Wang, S. (2015) Starch Retrogradation: A Comprehensive Review. *Compr. Rev. Food Sci. Food Saf.*, 14 (5), 568–585.
15. Ghanbarzadeh, B., Almasi, H., and Entezami, A.A. (2011) Improving the barrier and mechanical properties of corn starch-based edible films: Effect of citric acid and

- carboxymethyl cellulose. *Ind. Crops Prod.*, 33 (1), 229–235.
16. Falguera, V., Quintero, J.P., Jiménez, A., Muñoz, J.A., and Ibarz, A. (2011) Edible films and coatings: Structures, active functions and trends in their use. *Trends Food Sci. Technol.*, 22 (6), 292–303.
 17. Souza, A.C., Benze, R., Ferrão, E.S., Ditchfield, C., Coelho, A.C.V., and Tadini, C.C. (2012) Cassava starch biodegradable films: Influence of glycerol and clay nanoparticles content on tensile and barrier properties and glass transition temperature. *LWT - Food Sci. Technol.*, 46 (1), 110–117.
 18. Shah, U., Naqash, F., Gani, A., and Masoodi, F.A. (2016) Art and Science behind Modified Starch Edible Films and Coatings: A Review. *Compr. Rev. Food Sci. Food Saf.*, 15 (3), 568–580.
 19. Liu, H., Xie, F., Yu, L., Chen, L., and Li, L. (2009) Thermal processing of starch-based polymers. *Prog. Polym. Sci.*, 34 (12), 1348–1368.
 20. Wang, N., Yu, J., Chang, P.R., and Ma, X. (2007) Influence of citric acid on the properties of glycerol-plasticized dry starch (DTPS) and DTPS/poly(lactic acid) blends. *Starch/Staerke*, 59 (9), 409–417.
 21. Wang, S., Ren, J., Li, W., Sun, R., and Liu, S. (2014) Properties of polyvinyl alcohol/xylan composite films with citric acid. *Carbohydr. Polym.*, 103 (1), 94–99.
 22. Fakhoury, F.M., Maria Martelli, S., Canhadas Bertan, L., Yamashita, F., Innocentini Mei, L.H., and Collares Queiroz, F.P. (2012) Edible films made from blends of manioc starch and gelatin - Influence of different types of plasticizer and different levels of macromolecules on their properties. *LWT - Food Sci. Technol.*, 49 (1), 149–154.
 23. Sobral P J a, Menegalli F C, Hubinger M D, and Roques M a (2001) Mechanical, water vapor barrier and thermal properties of gelatin based edible films. *Food Hydrocoll.*, 15 (4–6), 423–432.
 24. Vanin, F.M., Hirano, M.H., Carvalho, R.A., Moraes, I.C.F., Bittante, A.Mô.Q.B., and Sobral, P.J. do A. (2014) Development of active gelatin-based nanocomposite films produced in an automatic spreader. *Food Res. Int.*, 63, 16–24.
 25. Esmaeili, M., Pircheraghi, G., and Bagheri, R. (2017) Optimizing the mechanical and physical properties of thermoplastic starch via tuning the molecular microstructure through co-plasticization by sorbitol and glycerol. *Polym. Int.*, 66 (6), 809–819.
 26. Ryu, S.Y., Rhim, J.W., Roh, H.J., and Kim, S.S. (2002) Preparation and physical properties of zein-coated high-amylose corn starch film. *LWT - Food Sci. Technol.*, 35 (8), 680–686.
 27. Ashok, A., Mathew, M., and Rejeesh, C.R. (2016) Innovative Value Chain Development of Modified Starch for a Sustainable Environment: A Review. *Int. J. Polym. Sci. Eng.*, (May 2016).
 28. Stevens, E.S., Klamczynski, A., and Glenn, G.M. (2010) Starch-lignin foams. *Express Polym. Lett.*, 4 (5), 311–320.
 29. Yang, J., Ching, Y.C., and Chuah, C.H. (2019) Applications of lignocellulosic fibers and lignin in bioplastics: A review. *Polymers (Basel)*, 11 (5), 1–26.

30. Della, V.P., Kühn, I., and Hotza, D. (2002) Rice husk ash as an alternate source for active silica production. *Mater. Lett.*, 57 (4), 818–821.
31. Kow, K.W., Yusoff, R., Aziz, A.R.A., and Abdullah, E.C. (2014) From bamboo leaf to aerogel: Preparation of water glass as a precursor. *J. Non. Cryst. Solids*, 386, 76–84.
32. Liu, S.W., Wei, Q., Cui, S.P., Nie, Z.R., Du, M.H., and Li, Q.Y. (2016) Hydrophobic silica aerogel derived from wheat husk ash by ambient pressure drying. *J. Sol-Gel Sci. Technol.*, 78 (1), 60–67.
33. Alves, R.H., Reis, T.V.D.S., Rovani, S., and Fungaro, D.A. (2017) Green Synthesis and Characterization of Biosilica Produced from Sugarcane Waste Ash. *J. Chem.*, 2017.
34. de Azevedo, L.C., Rovani, S., Santos, J.J., Dias, D.B., Nascimento, S.S., Oliveira, F.F., Silva, L.G.A., and Fungaro, D.A. (2020) Biodegradable Films Derived from Corn and Potato Starch and Study of the Effect of Silicate Extracted from Sugarcane Waste Ash. *ACS Appl. Polym. Mater.*, 2 (6), 2160–2169.
35. Perussello, C.A., Zhang, Z., Marzocchella, A., and Tiwari, B.K. (2017) Valorization of Apple Pomace by Extraction of Valuable Compounds. *Compr. Rev. Food Sci. Food Saf.*, 16 (5), 776–796.
36. Bhushan, S., Kalia, K., Sharma, M., Singh, B., and Ahuja, P.S. (2008) Processing of apple pomace for bioactive molecules. *Crit. Rev. Biotechnol.*, 28 (4), 285–296.
37. Acquavia, M.A., Pascale, R., Foti, L., Carlucci, G., Scrano, L., Martelli, G., Brienza, M., Coviello, D., Bianco, G., and Lelario, F. (2021) Analytical methods for extraction and identification of primary and secondary metabolites of apple (*Malus domestica*) fruits: A review. *Separations*, 8 (7).
38. Heredia-Guerrero, J.A., Heredia, A., Domínguez, E., Cingolani, R., Bayer, I.S., Athanassiou, A., and Benítez, J.J. (2017) Cutin from agro-waste as a raw material for the production of bioplastics. *J. Exp. Bot.*, 68 (19), 5401–5410.
39. Heredia-Guerrero, J.A., Heredia, A., García-Segura, R., and Benítez, J.J. (2009) Synthesis and characterization of a plant cutin mimetic polymer. *Polymer (Guildf.)*, 50 (24), 5633–5637.
40. Benakmoum, A., Abbeddou, S., Ammouche, A., Kefalas, P., and Gerasopoulos, D. (2008) Valorisation of low quality edible oil with tomato peel waste. *Food Chem.*, 110 (3), 684–690.
41. Alam, M.N., Bristi, N.J., and Rafiquzzaman, M. (2013) Review on in vivo and in vitro methods evaluation of antioxidant activity. *Saudi Pharm. J.*, 21 (2), 143–152.
42. Guzman-Puyol, S., Russo, D., Penna, I., Ceseracciu, L., Palazon, F., Scarpellini, A., Cingolani, R., Bertorelli, R., Bayer, I.S., Heredia-Guerrero, J.A., and Athanassiou, A. (2017) Facile production of seaweed-based biomaterials with antioxidant and anti-inflammatory activities. *Algal Res.*, 27 (August), 1–11.
43. Yang, X., and Zhang, S. (2016) Characterizing and Modeling the Rheological Performances of Potassium Silicate Solutions. *J. Solution Chem.*, 45 (12), 1890–1901.
44. Pankaj, S.K., Bueno-Ferrer, C., Misra, N.N., O'Neill, L., Tiwari, B.K., Bourke, P., and Cullen, P.J. (2015) Dielectric barrier discharge atmospheric air plasma treatment of high amylose corn starch films. *Lwt*, 63 (2), 1076–1082.

45. Mark, J.E.. (2007) *Physical Properties of Polymers Handbook*.
46. Luchese, C.L., Benelli, P., Spada, J.C., and Tessaro, I.C. (2018) Impact of the starch source on the physicochemical properties and biodegradability of different starch-based films. *J. Appl. Polym. Sci.*, 135 (33), 1–11.
47. Petersen, R.R., Christensen, J.F.S., Jørgensen, N.T., Gustafson, S., Lindbjerg, L.A., and Yue, Y. (2021) Preparation and thermal properties of commercial vermiculite bonded with potassium silicate. *Thermochim. Acta*, 699 (December 2020).
48. Zhang, D., Cao, Y., Zhang, P., Liang, J., Xue, K., Xia, Y., and Qi, Z. (2021) Investigation of the thermal decomposition mechanism of glycerol: the combination of a theoretical study based on the Minnesota functional and experimental support. *Phys. Chem. Chem. Phys.*, 23 (36), 20466–20477.
49. Liu, X., Wang, Y., Yu, L., Tong, Z., Chen, L., Liu, H., and Li, X. (2013) Thermal degradation and stability of starch under different processing conditions. *Starch/Staerke*, 65 (1–2), 48–60.
50. Sing, K.S.W., Everett, D.H., Haul, R.A.W., Moscou, L., Pierotti, R.A., Rouquerol, J., and Siemieniewska, T. (1985) Reporting Physisorption Data for Gas/Solid Systems with Special Reference to the Determination of Surface Area and Porosity. *Pure Appl. Chem.*, 57 (4), 603–619.
51. Al-Ghouti, M.A., and Da'ana, D.A. (2020) Guidelines for the use and interpretation of adsorption isotherm models: A review. *J. Hazard. Mater.*, 393 (February), 122383.
52. Saadi, R., Saadi, Z., Fazaeli, R., and Fard, N.E. (2015) Monolayer and multilayer adsorption isotherm models for sorption from aqueous media. *Korean J. Chem. Eng.*, 32 (5), 787–799.
53. Ban, W., JianguoSong, Argyropoulos, D.S., and Lucia, L.A. (2006) Improving the physical and chemical functionality of starch-derived films with biopolymers. *J. Appl. Polym. Sci.*, 100 (3), 2542–2548.
54. Mali, S., Grossmann, M.V.E., García, M.A., Martino, M.N., and Zaritzky, N.E. (2004) Barrier, mechanical and optical properties of plasticized yam starch films. *Carbohydr. Polym.*, 56 (2), 129–135.
55. Xie, Q., Li, F., Li, J., Wang, L., Li, Y., Zhang, C., Xu, J., and Chen, S. (2018) A new biodegradable sisal fiber–starch packing composite with nest structure. *Carbohydr. Polym.*, 189 (January), 56–64.
56. Leon-Bejarano, M., Durmus, Y., Ovando-Martínez, M., and Simsek, S. (2020) Physical, barrier, mechanical, and biodegradability properties of modified starch films with nut by-products extracts. *Foods*, 9 (2), 1–17.
57. Emadian, S.M., Onay, T.T., and Demirel, B. (2017) Biodegradation of bioplastics in natural environments. *Waste Manag.*, 59, 526–536.
58. Maraveas, C. (2020) Production of sustainable and biodegradable polymers from agricultural waste. *Polymers (Basel)*, 12 (5), 1–22.
59. Guzmán-Puyol, S., Heredia, A., Heredia-Guerrero, J.A., and Benítez, J.J. (2021) Cutin-Inspired Polymers and Plant Cuticle-like Composites as Sustainable Food Packaging Materials. *Sustain. Food Packag. Technol.*, 161–198.

60. Jariyasakoolroj, P., Leelaphiwat, P., and Harnkarnsujarit, N. (2020) Advances in research and development of bioplastic for food packaging. *J. Sci. Food Agric.*, 100 (14), 5032–5045.
61. Bayer, I.S., Guzman-Puyol, S., Heredia-Guerrero, J.A., Ceseracciu, L., Pignatelli, F., Ruffilli, R., Cingolani, R., and Athanassiou, A. (2014) Direct transformation of edible vegetable waste into bioplastics. *Macromolecules*, 47 (15), 5135–5143.
62. Brand-Williams, W., Cuvelier, M.E., and Berset, C. (1995) Use of a free radical method to evaluate antioxidant activity. *LWT - Food Sci. Technol.*, 28 (1), 25–30.

Apple waste and tomato peel by-products as fillers for starch-based bio-based composites

Supplementary Information

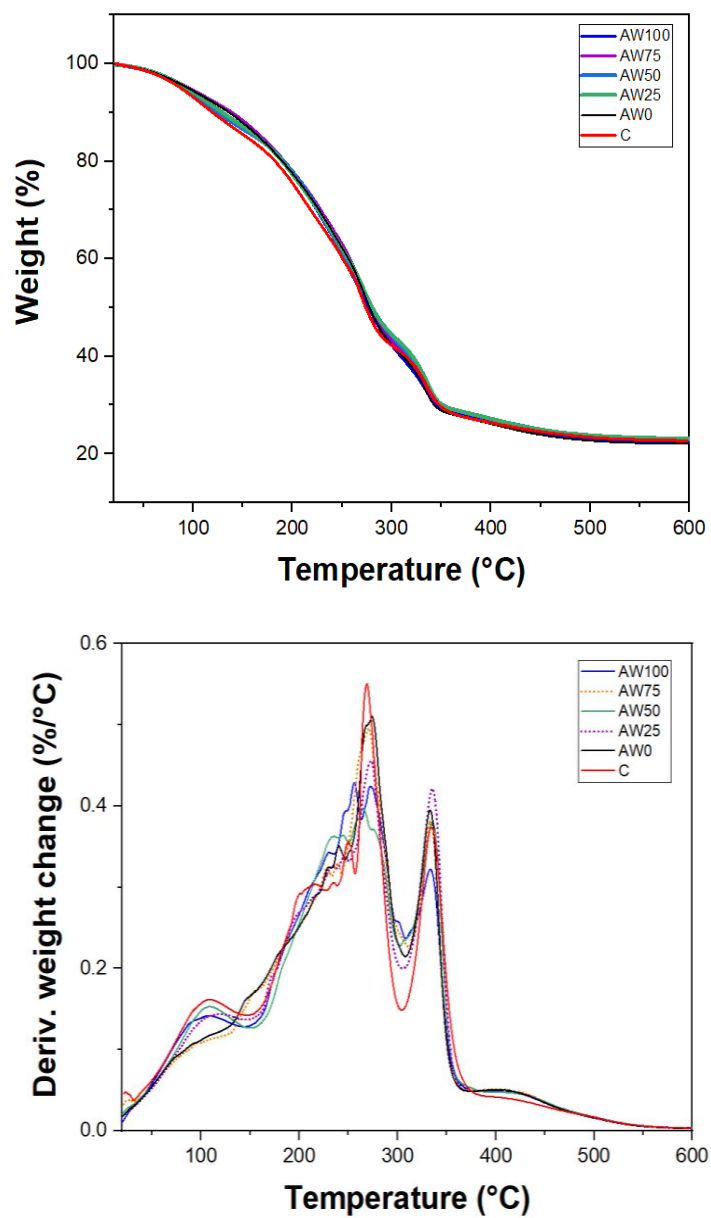


Figure 3.S1 TGA thermograms of AW100, AW75, AW50, AW25, AW0 and C samples (top) and the corresponding derivative curves (bottom).

4. Contribution 2

Untargeted profiling of the avocado by-product extract for the fabrication of bio-based plastics

Abstract

Avocado is a worldwide cultivated and consumed fruit which has been exploited as a source of many phytochemicals with beneficial health properties. Nowadays, the processing of avocado for food consumption as well as for food-related products such as guacamole, produces a significant amount of by-product, which can cause multiple environmental problems. Indeed, fruit and vegetal wastes are currently a source of pollution due to the excess of organic compounds that they release in the environment. To date, several solutions have been exploited in order to valorize avocado by-products, for example the production of bioplastics for active food-packaging. In these cases, the waste extract is usually directly added to a polymeric solution to be casted. Since fruit waste can contain potential pathogens, organic residues and physical and chemical contaminants which can potentially be released into the food when an active packaging is used, a comprehensive characterization of all chemical substances occurring in the extract is necessary. Here, an untargeted profiling of an ethyl acetate extract of the resulting avocado by-product after guacamole production was conducted by LC-ESI(-)-Q Exactive-Orbitrap-MS/MS. Accurate mass measurements and tandem mass spectrometric experiments, as well as a comparison with literature data and spectral databases, allowed the identification of 23 metabolites, mainly belonging to the class of fatty acids (monounsaturated, polyunsaturated and oxidized fatty acids). The results indicated that the oven-drying process used as preliminary treatment for the supplied avocado waste can modify the chemical structures of the molecules, as the oxidation of fatty acids typically occurs upon thermal treatment.

4.1 Introduction

Persea americana Mill., more commonly known as avocado, is a warm climate species originating in tropical America, including the eastern and central highlands of Mexico, Guatemala, Central America down to the northern parts of South America (Peru, Ecuador) [1]. Avocado is recently gaining popularity also among the countries of Europe, North America and the developed parts of Asia. Although according to data reported by FAOSTAT the total production of avocados in all countries overpasses 5.5 million tons per year, Mexico still remains the world's largest producer, representing over one-third of global production. As regard to Europe, the main producer and only exporting country is Spain, followed by France and Greece [2]. In detail, 91,000 tonnes of avocado are produced in Spain, i.e. 93% of the European production, mostly concentrated in the provinces of Malaga and Granada. Currently, avocado is intended for different types of consumption and commercial uses in many food products such as guacamole (a sauce made with mashed avocado pulp seasoned with various condiments), chips, ice cream, frozen products and avocado paste [3]. Moreover, due to the high levels of lipids compared to other fruits, avocado is also used for oil production. Oil content in commercially mature avocados can range between 10 and 32% on a flesh fresh weight basis, depending on the cultivar and the time of harvest. For avocados belonging to the Hass cultivar (the most common), this content can be as high as 30% on a flesh fresh weight basis, depending on the growing region [4,5]. The avocado processing line for food consumption and commercial uses generate every year a considerable amount of by-product (mainly peel and seeds), which account for ~30% of the fresh weight of the fruit [6]. If we consider one of the reference countries for guacamole production, i.e. Mexico, ~5% of the fruits used for sauce production results in a total amount of approximately 20,000 tons of generated residues. The production process of guacamole consists of the selection of ripe avocados, washing and removal of peel and seed to recover the pulp. Then, the pulp is mixed with onion, tomato and salt to finally obtain the sauce. Regardless of the type of production method, the peel and seed and/or exhausted pulp are discarded as a waste. The biomass material that is discarded remains very high: the solid residue wasted represent 21–76% of the fruit weight and also the wastewater [7]. In Europe, with particular reference to Spain, 2,000 tonnes of stone and skin are discarded, which can potentially be used as a source of bioactive compounds with an added value. The valorization of avocado waste deserves further attention due to its chemical composition, including the major constituents and also the minor ones which are not less relevant. Apart from lipids (4.4-9.1%), avocado peel contains carbohydrates (62-73.3%), proteins (4-8.3%), fibres (almost 50%) and other important vitamins, minerals and phytochemicals which confer to avocado fruits high flavour and overall quality as well

as beneficial health related properties (e.g. anti-cancer and anti-obesity properties, prevention of lipid oxidation and reduction of the risk of inflammatory diseases) [3,8–10]. In general, peel extracts show a higher antioxidant capacity compared to seed, due to the higher content of phenolic compounds [11]. In any case, the whole biomass obtained by avocado processing is a promising material for the production of functional foods and pharmaceutical products. Avocado by-products find several non-food applications as well. For example, seed oil has been used for the synthesis of biodiesel, charcoal, liquid fuels and fuel additives [12]. On the other hand, also avocado seed and peel extracts have been explored as additive for functional bio-based plastics usable as active food packaging [13]. Active packaging is a system by which an active agent is intentionally incorporated into a specially selected part of the packaging. With this interactive technology, active compounds can be freely released into the head space of packaging or food or they can act as antioxidants without direct contact with food [14]. In Europe, all packaging materials intended to come into contact with food are strictly regulated by the Commission Regulation No 10/2011 that lists all the substances and their specific limits with which they are allowed within plastics. Since fruit wastes can contain potential pathogens, organic residues and physical and chemical contaminants [15] which can be released when used as additive for active packaging, a comprehensive characterization of their extract is required. Nowadays, liquid chromatography (LC) is one the most used analytical technique for the separation of individual compounds in food or food waste extracts. Its coupling with mass spectrometry (MS) or tandem mass spectrometry (MS/MS) has increasingly been used for food analysis and quality control, due to the high performance reached in terms of sensitivity, selectivity, and flexibility [16–19].

In this chapter, liquid chromatography coupled to tandem mass spectrometry with electrospray ionization in negative ion mode (LC-ESI(-)-MS/MS) has been used to provide an untargeted characterization of the bioactive compounds occurring in an extract of avocado by-products, applicable as an additive for the development of bio-materials for active food-packaging. Avocado waste develops rotting characteristics during waste stream process, presenting changes in the colour and rancidity, due to phenols and fatty acids oxidation, respectively. Therefore, it is expected that the original composition of the fruit, in terms of phytochemicals, does not remain unaltered. Currently, LC-MS/MS investigations allowed to identify several chemical constituents of avocado waste (both seed and peel), mainly phenols, flavonoids and catechins and the extracting solvent used were based on ethanol or ethanol/water mixtures [20–22]. Here, ethyl acetate (EA) has been used as a solvent for the untargeted extraction. EA is a primary green solvent widely used for hydrophobic biopolymers dissolution (e.g. ethyl cellulose) [23], since it has a low degree of hydrophilicity ($\log P=0.71$) and minimizes the emissions of hazardous substances. The extraction

of bioactive compounds with EC allows the extract to be directly used in a one-pot process [24], as an additive for the biopolymer solution, without preconcentration and resolubilization steps, to obtain edible and active films.

4.2 Experimental section

4.2.1 Reagents and solvents

Ethyl acetate (99.5%) for avocado by-product extraction was purchased from Sigma-Aldrich (Milano, Italy). HPLC gradient grade methanol (MeOH) and acetonitrile (ACN) for extract purification, LC separation and MS detection were obtained from Sigma-Aldrich (Milano, Italy). Formic acid (98%), used as additive of the aqueous mobile phase, was purchased from Carlo Erba Srl (Milano, Italy). Deionized water was obtained from a Milli-Q RG Ultrapure Water Purification device from Millipore (Bedford, MA, USA).

4.2.2 Raw material and sample extraction

Avocado by-product was obtained from a local company (Avomix) located in Malaga (Spain). The waste was dried in the oven at 50°C for three days. After drying, it was grounded into a powder by using a Moulinex mill. 0.25 g of dried powder were extracted with 15 mL ethyl acetate, at 65°C for 45 minutes under continuous stirring on a hot-plate. Then, the supernatant was recovered and purified by solid-phase extraction (STRATA C18-E cartridges, 500mg/6mL, Phenomenex, Torrance, California, USA). Cartridges were conditioned with 6 mL of methanol and 6 mL of deionized water. The sample was loaded on the SPE cartridge, and then washed with 6 mL of MeOH/H₂O (20:80), followed by elution with 5 mL of MeOH/ACN (50:50). Finally, the elute was filtered through 0.2 µm PTFE membrane (Whatman, Maidstone, UK) and injected into the LC-MS/MS system.

4.2.3 LC-MS/MS Analysis

LC-MS/MS untargeted analyses were conducted to characterize the phytochemical compounds occurring in the ethyl acetate extract. Experiments were achieved using an UltiMate 3000 ultra-high-pressure liquid chromatography (UPLC) system (Thermo Fisher Scientific, Bremen, Germany) coupled to a Q-Exactive Orbitrap mass spectrometer (Thermo Fisher Scientific, Bremen, Germany). Analytes were chromatographically separated on a Kinetex C18 2.6 µm (Phenomenex Aschaffenburg, Germany) column. The mobile phase consisted of solvent A (water + 0.1% formic acid) and solvent B (acetonitrile + 0.1% formic acid). The elution gradient was conducted at a

constant flow rate of 0.250 mL/min as follows: 0 min, 95% A; 25 min, 50% A; 33 min, 0% A; 36 min, initial conditions until 40 min as a re-equilibration step. The sample volume injected was 5 μ L. The analyses were performed in negative ion mode. ESI source parameters were set as follows: spray voltage 2500 V; tube lens voltage 630 V; capillary temperature 300 °C; sheath and auxiliary gas flow (N_2), 50 and 15 (arbitrary units). MS spectra were acquired by full range acquisition covering m/z 180-2000. For fragmentation studies, a data dependent scan experiment was performed, selecting precursor ions corresponding to most intensive peaks in LC-MS analysis. Xcalibur software version 2.1 was used for instrument control, data acquisition and data analysis. The LC-MS data were imported, elaborated, and plotted by SigmaPlot 11.0 (Systat Software, London, UK).

4.3 Results and Discussion

4.3.1 LC-MS/MS Analysis

Avocado discarded wastes have proved to retain different natural compounds targeted by interesting studies which aim at reducing the food waste stream under the principles of the circular economy, such as the production of bio-based films for active food packaging. In this study an extract of avocado by-product supplied by a company interested in the production of guacamole was analyzed by an untargeted LC-ESI(-)-Q Exactive-Orbitrap MS/MS-based method. The Total Ion Current (TIC) profile obtained for the avocado by-product ethyl acetate extract is reported in **Figure 4.1**. The use of a common green solvent used for the processing of polymers during bioplastics production, i.e. ethyl acetate, allowed to mainly extract the lipophilic constituents of the biomass. This was expected as avocado fruit is rich in lipids compared to other fruits [25]. The accurate mass measurements (root mean square (RMS) error lower than 5 ppm) and the tandem mass spectrometric experiments, alongside with research in both literature data and spectral database for lipidic substances (LipidMaps database; www.lipidmaps.org) led to the identification of 23 metabolites. In general, they belonged to the subclasses of free fatty acids (saturated, monounsaturated, polyunsaturated and oxidized) (FAs) and oxylipins (**Table 4.1**). FAs were labelled according to their systematic name and also by using the conventional x:y nomenclature, where x represents the number of carbons occurring in the alkyl chain and y the number of double bonds which are present [26]. For oxylipins, a x:y-zO nomenclature was used, where z represent the number of oxygens occurring on the carbon chain apart those of the polar carboxylic head of the molecules [27].

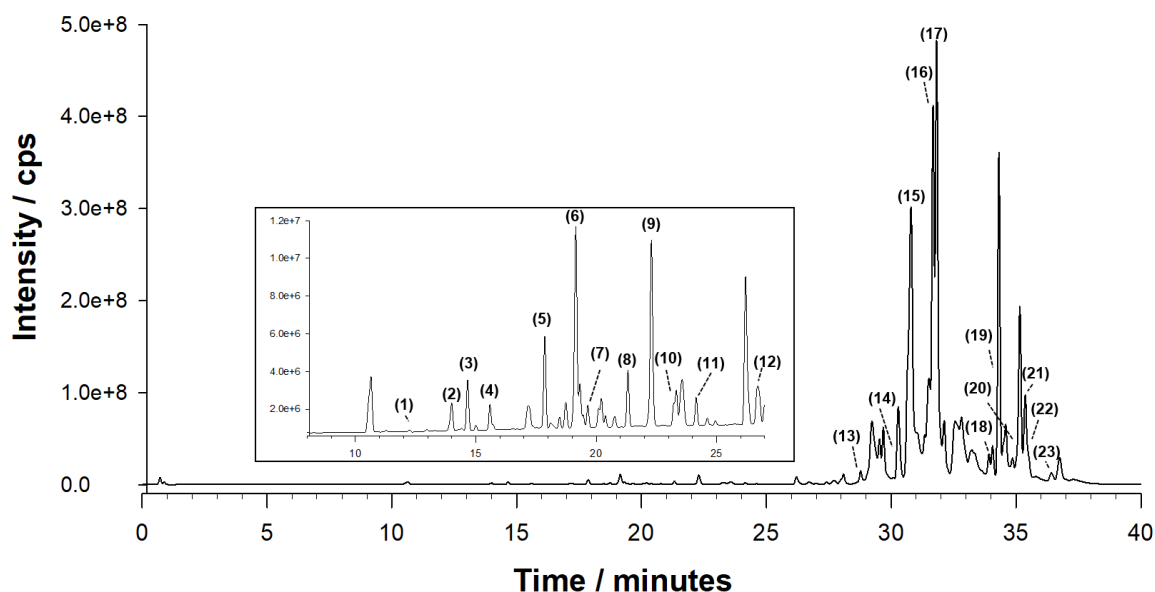


Figure 4.1 Total Ion Current (TIC) chromatogram obtained by LC-ESI-MS acquired in negative ion mode for an ethyl acetate extract of avocado by-product. **Inset:** enlargement of the TIC in the time window 8-27 minutes.

All the lipids were eluted within 40 minutes of chromatographic run. As negative polarity mode was used, all the compounds were detected as $[M-H]^-$ ions. Free fatty acids occurred in the extract as saturated and both monounsaturated and polyunsaturated FAs. In detail, as saturated fatty acid, palmitic acid (**20**) was detected. Instead, as monounsaturated and polyunsaturated FAs, palmitoleic (**18**) and oleic acid (**21**) and linolenic (**14**) and linoleic acid (**22**), were identified respectively. Palmitic acid (16:0) tandem mass spectrum exhibited a fragment ion at m/z 237.1870 ($[M-H_2O]^-$), due to the loss of water which probably occurs through an H^+ migration from one of the methylene carbons of the side chain towards the negatively charged oxygen atom of the carboxylate moiety [28]. Then, an acetal could be formed by a cyclization, followed by water loss, as proposed by Voinov et al. [28]. For palmitoleic acid (16:1), oleic acid (18:1), linoleic acid (18:2) and linolenic acid (18:3), the most prominent fragment originated from the loss of CO_2 (-44 Da) from the molecular ion, respectively at m/z 253.2171 ($[C_{16}H_{29}O_2]^-$, RMS error 3.53 ppm), 281.2483 ($[C_{18}H_{33}O_2]^-$, RMS error 2.82 ppm), 279.2326 ($[C_{18}H_{31}O_2]^-$, RMS error 2.66 ppm) and 277.2177 ($[C_{18}H_{29}O_2]^-$, RMS error 4.39 ppm) [29]. Unsaturated fatty acids are important nutrients involved in many body functions, including neuro-protective, antioxidant, anti-inflammatory effects and cardiovascular health. However, their development as nutritional supplements is limited by their high susceptibility to oxidative rancidity, which leads to the formation of off-flavors [30]. Unsaturated fatty acids (e.g. oleic acid) can be converted into hydroxy fatty acids by oxygenases or fatty acid double bond hydratases to obtain oxylipins. Compared with oleic acid (*cis*-octadec-9-

enoic acid), linoleic acid (*cis, cis*-octadeca-9,12-dienoic acid) reacts with oxygen 12 times faster and linolenic acid (*cis, cis, cis*-octadeca-9, 12, 15-trienoic acid) reacts 25 times faster.

As regard to oxidized FAs and oxylipins, 13 compounds belonging to these classes were identified and all were eluted in the first 32 minutes. Oxylipins are a class of oxidized lipophilic molecules derived mainly from the oxidation of the most abundant polyunsaturated fatty acids in plants [31]. Among the most abundant PUFAs occurring in vegetables, there are linoleic acid, i.e. a 18:2 fatty acid, α -linolenic acid, i.e. a 18:3 fatty acid, and roushanic acid, i.e. a 16:3 fatty acid [32]. In some case oxylipins can be obtained from the oxidation of monounsaturated fatty acids as well. Oxylipins obtained in plants include hydroperoxy-, hydroxy-, oxo- and epoxy-fatty acids, divinyl ethers, volatile aldehydes and the vegetal hormone, jasmonic acid. Moreover, the structural diversity of oxylipins could be further increased by their esterification in complex glycerolipids (glycolipids, phospholipids and neutral lipids) and their conjugation to amino acids and other metabolites, such as sulphate, glutathione, ethanolamine and carbohydrates [33]. Here, mainly hydroxy or oxo derivatives of oleic (18:1) and linoleic acid (18:2) were detected, although also hydroxylated derivatives of stearic acid (18:0) were identified, i.e. tri-hydroxystearate (**10**) and di-hydroxystearic acid (**13**). The oxylipins presence in the studied extract could be attributed to the oven-drying step to which avocado by-products were subjected before the extraction. Indeed, in a previous work, Degenhardt et al. [34] identified these compounds as key contributors of the bitter off-taste developed upon thermal processing of avocado. For tri-hydroxystearate (18:0-3O), a signal at m/z 331.2490 corresponding to $[M]^-$ ion was observed in the MS/MS spectrum. While, for di-hydroxystearic acid the signal related to molecular ion was observed at m/z 315.2535. It should be considered that hydroxy derivatives of fatty acids are important industrial materials because the hydroxyl group on fatty acid gives special properties such as higher viscosity and reactivity compared with other non-hydroxylated fatty acids [35]. As regard to oxidized FAs derived from oleic acid, 7 compounds were identified, i.e. ion at m/z 345.2278 (**3**) ($[C_{18}H_{33}O_6]^-$, RMS error 1.84 ppm), ion at m/z 327.2177 (**5**) ($[C_{18}H_{31}O_5]^-$, RMS error 2.75 ppm), ion at m/z 329.2333 (**6**) ($[C_{18}H_{33}O_5]^-$, RMS error 3.19 ppm), ion at m/z 327.2175 (**7**) ($[C_{18}H_{31}O_5]^-$, RMS error 2.75 ppm), ion at m/z 329.2333 (**8**) ($[C_{18}H_{33}O_5]^-$, RMS error 3.19 ppm), ion at m/z 313.2385 (**12**) ($[C_{18}H_{33}O_4]^-$, RMS error 3.72 ppm) and ion at m/z 311.1685 (**16**) ($[C_{18}H_{31}O_4]^-$, RMS error 4.00 ppm). Instead, ions at m/z 293.2118 (**15**) ($[C_{18}H_{29}O_3]^-$, RMS error 2.31 ppm) and m/z 295.2274 (**17**) ($[C_{18}H_{31}O_3]^-$, RMS error 2.81 ppm) respectively, were identified as linoleic acid (18:2) oxidized derivatives, i.e. keto-octadecadienoic acid and hydroxy-octadecadienoic acid. Keto-octadecadienoic acid was previously identified as one of the major metabolites in diethyl ether extracts of stored apples [36]. Instead, hydroxy-octadecadienoic acid has been already identified in avocado peel by Figueroa et al.

[21]. Hydroxy-octadecadienoic acids have been shown to be predominant regulators of inflammation on different cell systems. In detail, they induce beneficial effects by regulating inflammation in the vascular wall [37]. Except for tetrahydroxy octadecenoic acid (18:1-4O) and hydroxy-oxo-octadecenoic acid (18:1-2O), their MS/MS spectra exhibited a diagnostic fragment ion at m/z 171 corresponding to the $[-\text{OOC}(\text{CH}_2)_7\text{CH-OH}]^-$ species, containing a carboxyl and an OH-group which allowed to confirm their identification [32]. Based on their structural peculiarities, these compounds could be used in resins, waxes, nylons, plastics, lubricants, cosmetics, and additives in coatings and paintings. In addition, most of the compounds identified within this study proved to be potential antimicrobial agents [38,39]. For example, some studies about dihydroxy-octadecenoic acid and trihydroxy-octadecenoic acid reported that they have antimicrobial activities against plant pathogenic fungi [40]. On the other hand, a strong antibacterial activity against food-borne bacteria, such as *Bacillus subtilis* ATCC 6633, *Listeria monocytogenes* ATCC 19166, *Staphylococcus aureus* and *Pseudomonas aeruginosa* KCTC 2004, was shown by hydroxylated linoleic acid derivatives [41]. On this basis, the use of avocado by-product extracts to produce active materials for food packaging represent a valid solution for waste valorization.

4.4 Conclusions

Nowadays the interest in the production of avocado is growing in many European countries, mainly Spain, alongside with the high amount of by-product which is annually produced during the processing line. The valorization of avocado waste needs particular attention due to its chemical composition, including the major constituents and also the minor ones which are not less relevant. Here, LC-ESI(-)-Q Exactive-Orbitrap-MS/MS allowed to conduct an untargeted characterization of the bioactive compounds occurring in an ethyl acetate extract of avocado by-product. The LC-MS/MS analysis revealed that the extract was rich in lipid components, mainly fatty acids hydroxylated fatty acids and oxylipins, which make them suitable as additive to plasticize and increase the hydrophobic properties of edible bio-based films.

Table 4.1 Metabolites identified in avocado by-product ethyl acetate extract by LC-ESI(-)-MS/MS analysis. FAs were labelled according to their systematic name and also by using the conventional x:y nomenclature, where x represents the number of carbons occurring in the alkyl chain and y the number of double bonds which are present [26]. For oxylipins, a x:y-zO nomenclature was used, where z represent the number of oxygens occurring on the carbon chain apart those of the polar carboxylic head of the molecules [27].

Peak	RT (min)	Proposed compound	m/z	Molecular formula	RMS error ^a	Fragments
1	12.51	10-(1-Hydroxyhexoxy)-10-oxodecanoate	319.2117	C ₁₆ H ₃₁ O ₆ ⁻	0.58	301.2030
2	13.99	Unassigned	341.1394	C ₂₀ H ₂₁ O ₅ ⁻	1.05	326.1157 [M-CH ₃] ⁻ 311.0925 [M-C ₂ H ₆] ⁻
3	14.68	Tetrahydroxy octadecenoic acid (18:1-4O)	345.2278	C ₁₈ H ₃₃ O ₆ ⁻	1.84	99.0436
4	15.58	16:0-3O (tentatively)	303.2178	C ₁₆ H ₃₁ O ₅ ⁻	3.96	285.2072 [M -H ₂ O] ⁻ 270.8253
5	17.89	9-oxo-12,13-dihydroxy-10-octadecenoic acid (18:1-3O)	327.2177	C ₁₈ H ₃₁ O ₅ ⁻	2.75	309.2070 [M -H ₂ O] ⁻ ; 291.1968; 229.1443; 211.1333; 171.1017; 85.0282
6	19.16	9,12,13-Trihydroxy-10-octadecenoic acid (18:1-3O)	329.2333	C ₁₈ H ₃₃ O ₅ ⁻	3.19	229.1439; 211.1333; 171.1018; 139.1118
7	19.65	13-oxo-9,10-dihydroxy-11-octadecenoic acid (18:1-3O)	327.2175	C ₁₈ H ₃₁ O ₅ ⁻	2.74	201.1126; 171.1017; 137.0961; 119.0853
8	21.29	9,10,13-Trihydroxy-11-octadecenoic acid (18:1-3O)	329.2333	C ₁₈ H ₃₃ O ₅ ⁻	3.19	201.1126; 171.1019; 139.1118
9	22.28	Sucrose	387.1148	C ₁₃ H ₂₃ O ₁₃ ⁻	3.83	387.1148 [M + HCO ₂ H - H] ⁻ ; 341.1113; 179.8484; 160.9976; 102.0548; 89.0230
10	23.37	9,10,18-Trihydroxystearate (18:0-3O)	331.2490	C ₁₈ H ₃₅ O ₅ ⁻ [M] ⁻	2.11	313.2390; 295.2297; 185.1178; 59.0126
11	24.15	10,16-Dihydroxyhexadecanoic acid (16:0-2O)	287.2227	C ₁₆ H ₃₁ O ₄ ⁻	3.53	269.2123; 251.2019
12	26.71	Dihydroxyoctadecenoic acid (18:1-2O)	313.2385	C ₁₈ H ₃₃ O ₄ ⁻	3.72	295.2227; 277.2181; 201.1128; 185.1178; 171.1020; 155.1068
13	28.80	9,10-Dihydroxystearic acid (18:0-2O)	315.2535	C ₁₈ H ₃₅ O ₄ ⁻	1.63	297.2433
14	30.23	Linolenic acid (18:3)	277.2177	C ₁₈ H ₂₉ O ₂ ⁻	4.39	243.7457; 233.1552 [M-CO ₂] ⁻
15	30.70	9-Keto-octadecadienoic acid (18:2-O)	293.2118	C ₁₈ H ₂₉ O ₃ ⁻	2.32	249.2220; 185.1172; 113.0959
16	31.66	Hydroxy-oxo-octadecenoic acid (18:1-2O)	311.1685	C ₁₈ H ₃₁ O ₄ ⁻	4.00	183.0110; 249.2236; 293.2117
17	31.77	Hydroxyoctadecadienoic acid (18:2-O)	295.2274	C ₁₈ H ₃₁ O ₃ ⁻	2.81	277.2173; 251.2378; 195.1379
18	33.97	Palmitoleic acid (16:1)	253.2171	C ₁₆ H ₂₉ O ₂ ⁻	3.53	209.1548 [M-CO ₂] ⁻
19	34.37	Linoleate (18:2)	279.2326	C ₁₈ H ₃₁ O ₂ ⁻	2.66	171.1017
20	35.21	Palmitic acid (16:0)	255.2326	C ₁₆ H ₃₁ O ₂ ⁻	2.91	237.1870 [M-H ₂ O] ⁻

4. Contribution 2

21	35.40	Oleic acid (18:1)	281.2483	$C_{18}H_{33}O_2^-$	2.82	237.2219 [M-CO ₂] ⁻
22	35.40	Linoleic acid (18:2)	279.2326	$C_{18}H_{31}O_2^-$	2.66	235.2070 [M-CO ₂] ⁻
23	36.36	1-hexadecanoyl-2-(6Z,9Z,12Z-octadecatrienoyl)-glycero-3-phosphate	669.4496	$C_{37}H_{66}O_8P^-$	0.92	201.1125

^aMass accuracy expressed as root-mean-square (RMS) in part per million (ppm) of nine (n=9) *m/z* measurements

References

1. Silva, T.A., and Ledesma, N. (2014) Avocado History, Biodiversity and Production, in *Sustainable Horticultural Systems, Sustainable Development and Biodiversity*, vol. 2, © Springer International Publishing Switzerland 2014, pp. 301–313.
2. Sommaruga, R., and Eldridge, H.M. (2021) Avocado Production: Water Footprint and Socio-economic Implications. *EuroChoices*, **20** (2), 48–53.
3. Akan, S. (2021) Phytochemicals in avocado peel and their potential uses. *Food Heal.*, **7** (2), 138–149.
4. Woolf, A., Wong, M., Eyres, L., McGhie, T., Lund, C., Olsson, S., Wang, Y., Bulley, C., Wang, M., Friel, E., and Requejo-Jackman, C. (2009) *Avocado Oil*.
5. Pedreschi, R., Hollak, S., Harkema, H., Otma, E., Robledo, P., Westra, E., Somhorst, D., Ferreyra, R., and Defilippi, B.G. (2016) Impact of postharvest ripening strategies on “Hass” avocado fatty acid profiles. *South African J. Bot.*, **103**, 32–35.
6. Rodríguez-Carpena, J.G., Morcuende, D., Andrade, M.J., Kylli, P., and Estevez, M. (2011) Avocado (*Persea americana* Mill.) phenolics, in vitro antioxidant and antimicrobial activities, and inhibition of lipid and protein oxidation in porcine patties. *J. Agric. Food Chem.*, **59** (10), 5625–5635.
7. García-Vargas, M.C., Contreras, M.D.M., and Castro, E. (2020) Avocado-derived biomass as a source of bioenergy and bioproducts. *Appl. Sci.*, **10** (22), 1–29.
8. Dreher, M.L., and Davenport, A.J. (2013) Hass Avocado Composition and Potential Health Effects. *Crit. Rev. Food Sci. Nutr.*, **53** (7), 738–750.
9. Peou, S., Milliard-Hasting, B., and Shah, S.A. (2016) Impact of avocado-enriched diets on plasma lipoproteins: A meta-analysis. *J. Clin. Lipidol.*, **10** (1), 161–171.
10. Tramontin, N. dos S., Luciano, T.F., Marques, S. de O., de Souza, C.T., and Muller, A.P. (2020) Ginger and avocado as nutraceuticals for obesity and its comorbidities. *Phyther. Res.*, **34** (6), 1282–1290.
11. Tremocoldi, M.A., Rosalen, P.L., Franchin, M., Massarioli, A.P., Denny, C., Daiuto, É.R., Paschoal, J.A.R., Melo, P.S., and De Alencar, S.M. (2018) Exploration of avocado by-products as natural sources of bioactive compounds. *PLoS One*, **13** (2), 1–12.
12. Dagde, K.K. (2019) Extraction of vegetable oil from avocado seeds for production of biodiesel. *J. Appl. Sci. Environ. Manag.*, **23** (2), 215.
13. Merino, D., Bertolacci, L., Paul, U.C., Simonutti, R., and Athanassiou, A. (2021) Avocado Peels and Seeds: Processing Strategies for the Development of Highly Antioxidant Bioplastic Films. *ACS Appl. Mater. Interfaces*, **13** (32), 38688–38699.
14. Wrona, M., and Nerín, C. (2020) Analytical approaches for analysis of safety of modern food packaging: A review. *Molecules*, **25** (3).
15. Socas-Rodríguez, B., Álvarez-Rivera, G., Valdés, A., Ibáñez, E., and Cifuentes, A. (2021) Food by-products and food wastes: are they safe enough for their valorization? *Trends Food Sci. Technol.*, **114**, 133–147.
16. Pascale, R., Acquavia, M.A., Cataldi, T.R.I., Onzo, A., Coviello, D., Bufo, S.A., Scrano, L., Ciriello, R., Guerrieri, A., and Bianco, G. (2020) Profiling of quercetin glycosides and acyl

- glycosides in sun-dried peperoni di Senise peppers (*Capsicum annuum* L.) by a combination of LC-ESI (-) -MS / MS and polarity prediction in reversed-phase separations. *Anal. Bioanal. Chem.*, **412**, 3005–3015.
17. Acquavia, M.A., Pascale, R., Pappalardo, I., Santarsiero, A., Martelli, G., and Bianco, G. (2021) Characterization of quercetin derivatives in crossing combination of habanero white and capsicum annuum peppers and of anti-inflammatory and cytotoxic activity. *Separations*, **8** (7).
 18. Onzo, A., Acquavia, M.A., Pascale, R., Iannece, P., Gaeta, C., Nagornov, K.O., Tsybin, Y.O., and Bianco, G. (2021) Metabolic profiling of Peperoni di Senise PGI bell peppers with ultra-high resolution absorption mode Fourier transform ion cyclotron resonance mass spectrometry. *Int. J. Mass Spectrom.*, **470**, 116722.
 19. Bianco, G., Pascale, R., Carbone, C.F., Acquavia, M.A., Cataldi, T.R.I., Schmitt-Kopplin, P., Buchicchio, A., Russo, D., and Milella, L. (2018) Determination of soyasaponins in Fagioli di Sarconi beans (*Phaseolus vulgaris* L.) by LC-ESI-FTICR-MS and evaluation of their hypoglycemic activity. *Anal. Bioanal. Chem.*, **410** (5), 1561–1569.
 20. Gómez, F.S., Peirósánchez, S., Iradi, M.G.G., Azman, N.A.M., and Almajano, M.P. (2014) Avocado seeds: Extraction optimization and possible use as antioxidant in food. *Antioxidants*, **3** (2), 439–454.
 21. Figueroa, J.G., Borrás-Linares, I., Lozano-Sánchez, J., and Segura-Carretero, A. (2018) Comprehensive identification of bioactive compounds of avocado peel by liquid chromatography coupled to ultra-high-definition accurate-mass Q-TOF. *Food Chem.*, **245** (December 2017), 707–716.
 22. Figueroa, J.G., Borrás-Linares, I., Lozano-Sánchez, J., and Segura-Carretero, A. (2018) Comprehensive characterization of phenolic and other polar compounds in the seed and seed coat of avocado by HPLC-DAD-ESI-QTOF-MS. *Food Res. Int.*, **105** (December 2017), 752–763.
 23. Heredia-Guerrero, J.A., Ceseracciu, L., Guzman-Puyol, S., Paul, U.C., Alfaro-Pulido, A., Grande, C., Vezzulli, L., Bandiera, T., Bertorelli, R., Russo, D., Athanassiou, A., and Bayer, I.S. (2018) Antimicrobial, antioxidant, and waterproof RTV silicone-ethyl cellulose composites containing clove essential oil. *Carbohydr. Polym.*, **192** (December 2017), 150–158.
 24. Quilez-Molina, A.I., Heredia-Guerrero, J.A., Armirotti, A., Paul, U.C., Athanassiou, A., and Bayer, I.S. (2020) Comparison of physicochemical, mechanical and antioxidant properties of polyvinyl alcohol films containing green tealeaves waste extracts and discarded balsamic vinegar. *Food Packag. Shelf Life*, **23** (December 2019), 100445.
 25. Takenaga, F., Matsuyama, K., Abe, S., Torii, Y., and Itoh, S. (2008) Lipid and fatty acid composition of mesocarp and seed of avocado fruits harvested at northern range in Japan. *J. Oleo Sci.*, **57** (11), 591–597.
 26. Davidson, B., and Cantrill, R. (1985) Fatty acid nomenclature. *South African Med. J.*, **67** (May 1985), 633–634.
 27. Vu, H.S., Tamura, P., Galeva, N.A., Chaturvedi, R., Roth, M.R., Williams, T.D., Wang, X., Shah, J., and Welti, R. (2012) Direct infusion mass spectrometry of oxylipin-containing arabidopsis membrane lipids reveals varied patterns in different stress responses. *Plant Physiol.*, **158** (1), 324–339.

28. Voinov, V.G., Van Den Heuvel, H., and Claeys, M. (2002) Resonant electron capture mass spectrometry of free fatty acids: Examination of ion structures using deuterium-labeled fatty acids and collisional activation. *J. Mass Spectrom.*, **37** (3), 313–321.
29. Bollinger, J.G., Rohan, G., Sadilek, M., and Gelb, M.H. (2013) LC/ESI-MS/MS detection of FAs by charge reversal derivatization with more than four orders of magnitude improvement in sensitivity. *J. Lipid Res.*, **54** (12), 3523–3530.
30. Yeon, Y.J., and Park, J.B. (2018) *Regiospecific Conversion of Lipids and Fatty Acids through Enzymatic Cascade Reactions*, Elsevier Inc.
31. Grechkin, A. (1998) Recent developments in biochemistry of the plant lipoxygenase pathway. *Prog. Lipid Res.*, **37** (5), 317–352.
32. Rettner, J., Werner, M., Meyer, N., Werz, O., and Pohnert, G. (2018) Survey of the C20 and C22 oxylipin family in marine diatoms. *Tetrahedron Lett.*, **59** (9), 828–831.
33. Göbel, C., and Feussner, I. (2009) Methods for the analysis of oxylipins in plants. *Phytochemistry*, **70** (13–14), 1485–1503.
34. Degenhardt, A.G., and Hofmann, T. (2010) Bitter-tasting and kokumi-enhancing molecules in thermally processed avocado (*Persea americana* Mill.). *J. Agric. Food Chem.*, **58** (24), 12906–12915.
35. Kim, H., Kuo, T.M., and Hou, C.T. (2000) Intermediate in the conversion of ricinoleic acid to 7, 10, 12- trihydroxy-8 (E)-octadecenoic acid by *Pseudomonas aeruginosa*. *J. Ind. Microbiol. Biotechnol.*, **24**, 167–172.
36. Beuerle, T., and Schwab, W. (1999) Metabolic profile of linoleic acid in stored apples: Formation of 13(R)- hydroxy-9(Z),11(E)-octadecadienoic acid. *Lipids*, **34** (4), 375–380.
37. Vangaveti, V.N., Jansen, H., Kennedy, R.L., and Malabu, U.H. (2016) Hydroxyoctadecadienoic acids: Oxidised derivatives of linoleic acid and their role in inflammation associated with metabolic syndrome and cancer. *Eur. J. Pharmacol.*, **785**, 70–76.
38. Dilika, F., Bremner, P.D., and Meyer, J.J.M. (2000) Antibacterial activity of linoleic and oleic acids isolated from *Helichrysum pedunculatum*: A plant used during circumcision rites. *Fitoterapia*, **71** (4), 450–452.
39. Bajpai, V., Shin, S.Y., Kim, M.J., Kim, H.R., and Kang, S.C. (2004) Anti-fungal Activity of Bioconverted Oil Extract of Linoleic Acid and Fractionated Dilutions against Phytopathogens *Rhizoctonia solani* and *Botrytis cinerea*. *Agric. Chem. Biotechnol.*, **47** (4), 199–204.
40. Hou, C.T., and Forman, R.J. (2000) Growth inhibition of plant pathogenic fungi by hydroxy fatty acids. *J. Ind. Microbiol. Biotechnol.*, **24** (4), 275–276.
41. Shin, S.-Y., Kim, H.-R., and Kang, S.-C. (2004) Antibacterial Activity of Various Hydroxy Fatty Acids Bioconverted by *Pseudomonas aeruginosa* PR3. *J. Appl. Biol. Chem.*, **47** (4), 205–208.

5. Contribution 3

Antioxidant, biodegradable, and hydrophobic food packaging materials fabricated by impregnation of paper with ethyl cellulose and avocado by-product extract

Abstract

Paper and paperboards represent around 31% of the global packaging market segment due to their low cost, non-toxic and environmental-friendly characteristics. On the other hand, the hygroscopic properties and the water vapor barrier of these materials are not suitable for foodstuffs storage in environments with high relative humidity, since they are water-absorbing and porous. When paper absorbs H₂O from the environment or from the food, this causes the loss of its original mechanical strength. To minimize this problem, the impregnation of papers with non-hygroscopic and biodegradable polymers is presented as a functional and scalable technique. In this chapter, solutions of ethyl cellulose (EC) at different concentrations (0.025, 0.05 and 0.1 g/mL) were used to impregnate a commercially available paper. The presence of EC improved the mechanical properties, while the interaction with water was reduced by covering the free hydroxyl groups of cellulose from paper fibres with ethyl cellulose. Different amounts of avocado by-product (AW) extract were also added to the material with the best coverage, mechanical properties and waterproofing performances (prepared by using EC impregnating solution at 0.1 g/mL). As the avocado waste resulted rich in lipid components, a reduction in the water uptake was observed. Moreover, an increased oil and grease resistance was ascertained by TAPPI um 557 test. The papers prepared within this work prevented food browning and moisture loss by using pear pieces as a representative example, thus suggesting their utility as packaging materials with good performances in maintaining the shelf-life of packaged-food.

5.1 Introduction

Paper is one of the most used materials in everyday life. Beyond its use as the basic material for written and printed communication, it is used for hundreds of other purposes, including wrapping, insulating, towelling and packaging. Paper is mainly obtained by wood pulp of coniferous trees, which is composed of cellulose, hemicelluloses and lignin (**Figure 5.1**). The contents of these three biopolymers in a typical plant-based raw material are 38-50%, 17-32%, and 15-30%, respectively [1]. Cellulose ($C_6H_{10}O_5$)_n is a long-chain polymeric polysaccharide of 5000-10000 glucopyranoses repeating units linked together by β -1,4 glycosidic bonds. It has fibre-forming properties owing to the presence of the straight, long and parallel fibres. Multiple linear cellulose chains form an elementary fibril stabilized by hydrogen bonds. Multiple bundles of cellulose fibers aggregate and form macrofibrils [2]. Due to the regularity of chains, cellulose fibers are characterized by a relatively high degree of crystallinity. However, in general, the supra-molecular structure of cellulose microfibrils is characterized by alternations along the chain axis between ordered crystalline and amorphous regions. The degree of polymerization of cellulose chains and the degree of crystallinity of cellulose micro-fibrils depend on the nature and origin of the vegetable fibers. Regarding the hemicelluloses, they are responsible for the hydration of wood pulp and development of bonding during beating process. Hemicelluloses are a mixed group of both linear and branched heteropolymers mainly comprising five monomeric sugars, namely D-glucose, D-mannose, D-galactose, D-xylose, and L-arabinose [3]. They are linked together mostly by β -1,4-glycosidic bonds, but β -1,3-, β -1,6-, α -1,2-, α -1,3-, and α -1,6-glycosidic bonds can also be found. The degree of polymerization of hemicelluloses is 100-200, which is much lower than that of cellulose. Hemicelluloses and lignin are covalently bound together and this binding provides additional strength to paper [4,5]. Lignin is a natural binding constituent of wood cells with no fibre forming ability. Indeed, it is an amorphous, aromatic, water insoluble, heterogeneous, three-dimensional and cross-linked polymer. It can be considered as having been formed by random copolymers deriving from unsaturated alcohol derivatives of phenyl-propane [6]. In detail, it is made up of phenylpropanoid units, i.e. coniferyl, *p*-coumaryl and sinapyl alcohols, linked together by more than ten different types of aryl ether and carbon-carbon linkages. In addition to methoxyl groups, lignin has other functional groups, including phenyl hydroxyl, benzyl alcohol and carbonyl. The function of this network is to provide a mechanically strong composite material with cellulose fibers [7].

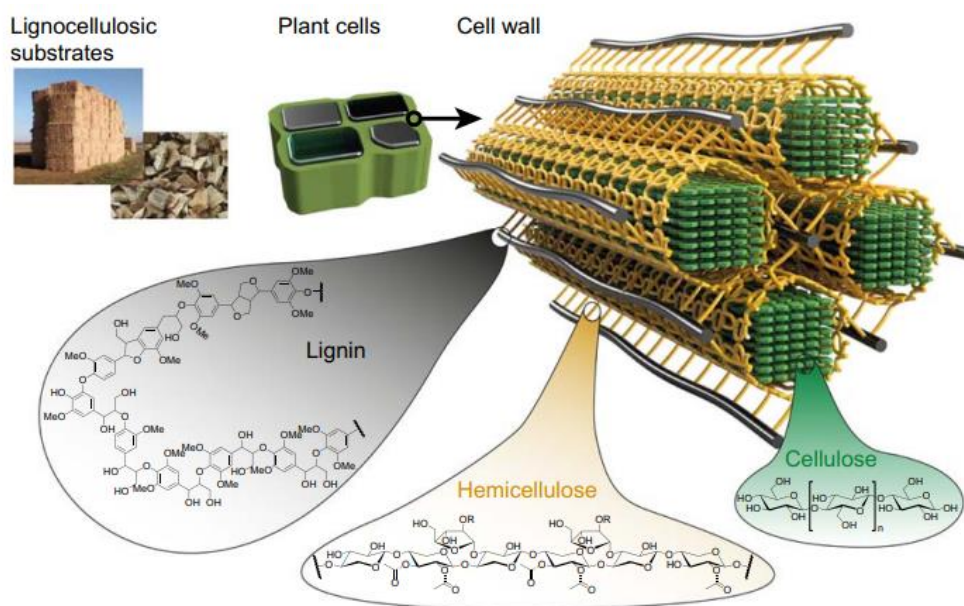


Figure 5.1 Simplified structure of lignocellulosic plant cell walls, mainly composed of cellulose, hemicelluloses and lignin. Reproduced under the terms of the Creative Commons CC BY license, which permits unrestricted use, distribution, and reproduction in any medium, provided the original work is properly cited [2].

The various stages of paper preparation involve: (i) pulping, i.e. the process during which wood fibres are separated through mechanical, chemical or thermal treatments, (ii) bleaching, i.e. the treatment applied to improve the whiteness of chemical and mechanical pulp and (iii) beating, i.e. the treatment used to produce shear, crushing, stretching, friction and other forces on the pulp fiber, changing their morphology and their average length. Then, fibrous material (containing approximately 99% of water) is passed through rollers or wire mesh to remove water and form the paper web [8]. The preparation process, as well as the raw material used for paper production, severely affect its quality and its overall behaviour, namely its mechanical properties, smoothness, pore size distribution, stiffness, stability and degradation, as they depend on interfiber bonding variation and pulp composition [9]. Although cellulose fibers contain nanostructures with promising properties including high reinforcing and barrier qualities, the potential properties of cellulose fibers are difficult to be achieved in cellulose-based products such as paper. This is mainly due to the lower specific surface area of microscale cellulose fibers ($1\text{--}3\text{ m}^2/\text{g}$) compared to that of nanoscale units ($100\text{--}500\text{ m}^2/\text{g}$). A correct beating of the pulp, which occurs through a properly choice of beater type and its specific edge load, allows to strengthen the fibrous material, as it increases the connectivity of cellulose nanostructures within paper network and the specific surface area [10]. Increasing the specific surface area allows to use this material in different membrane applications, e.g. liquid purification and filtering or tissue engineering [11–13]. On the contrary, paper strength

usually decreases when cellulose deterioration happens. Despite a properly beating, often the durability of paper still remains poor. Durability is the property of resisting deterioration by use or the degree to which a paper retains its original qualities under continue usage. Moreover, another drawback of paper is the pronounced hydrophilicity which limits various end-user applications such as in the food-packaging field. Its high hygroscopicity and poor barrier properties are not suitable for foodstuffs storage in environments with high relative humidity, since, in these conditions, paper can absorb water vapor from the environment or the food, thus losing its original mechanical properties. The intrinsic hydrophilicity of cellulose makes paper fibres very sensitive to water interactions, even though they are simultaneously insoluble in water [14]. The insolubility of cellulose in aqueous media is mostly related to strong intra- and intermolecular hydrogen bonding between cellulose molecules. Once a cellulose fibre is in contact with water or solvent, the molecules attach relatively fast to the outer polymer layer before they further penetrate into the surface, which leads to the instantaneous formation of a gel-like layer affecting further solvent interactions [15]. In any case, under humid conditions a permanent water uptake by cellulose fibres occurs. The adsorbed water is either included between the fibres and inside the fibre pores or bonded to the hydroxyl groups on the cellulose surface (**Figure 4.2**) [16].

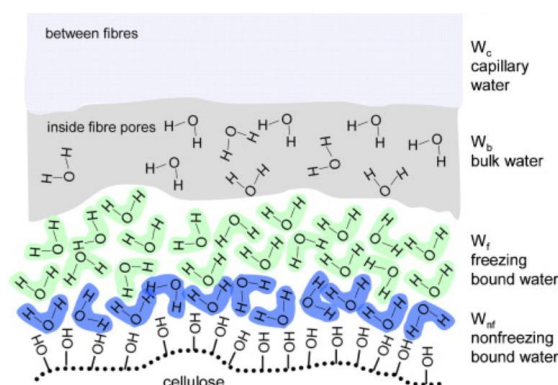


Figure 5.2 A schematic representation of the chemical situation in the region of phase transition between cellulose and surrounding environment. Reproduced with the permission of Elsevier [16].

In order to achieve the desired paper properties, such as higher durability and less hydrophilicity, several processes can be used, e.g. cellulose bulk modification through derivatization reactions or paper surface treatment. Many surface treatments include chemical vapor deposition of composites and polymers, surface coating using grafted polymers or metals, spraying with rapid expansion of supercritical CO_2 containing hydrophobic agents and ink-jet printing [17–19]. Recently also impregnation with a polymer solution has been proposed as way to impart durability to papers, while making them less sensitive to water. Compared to chemical vapor deposition or spraying with

supercritical CO₂, impregnation is a simpler and cost-effective process. Indeed, it is performed just by paper immersion in a covering solution. After the paper is accurately and uniformly saturated with the liquid, it is pulled out from the tray, the excess material is removed and paper is expected to dry. To date, different agents have been exploited as impregnating agents such as starch acetate, polyvinyl alcohol, epoxy resins, tetraethyl orthosilicate [20–23]. In general, the tensile strength of paper was proved to be positively affected by impregnation, while water sensitivity depends on the hydrophilic character of the used agent. For example, Guan et al. [22] noticed that tetraethyl orthosilicate improved the mechanical performances of paper and also paper transparency and thermal stability to some extent, but still remained the hydrophilicity. Thus, they furthered covered the impregnated material with PDMS to enhance water resistance.

In this chapter, ethyl cellulose (EC) has been used as an impregnating polymer in order to fabricate covered paper samples with enhanced mechanical strength. Ethyl cellulose is widely used as excipient in drug formulations, cosmetics and food technology, and also as matrix for the preparation of robust biofilms due to its interesting properties [24,25]. Indeed, EC is a non-toxic, odourless and thermoplastic polymer (melting point between 240 and 255°C), which is water-insoluble but soluble in common organic solvents [26]. Moreover, it is compatible with other synthetic polymers, fillers and plasticizers [27]. Due to such advantages, EC impregnation can be used for manufacturing special paper satisfying the consumer demands for good durability. To improve the antioxidant and hydro-repellent surface properties of the covered paper, avocado by-product extract has been added into the impregnating solution.

With a global production exceeding 4 million tons per year, avocado has recently become an important agro-industrial commodity [28]. Most of the avocado production and transformation industries are located in North and Central America, nevertheless recently it is extensively growing also in USA and European Union. In Europe, the largest percentage of the crop is concentrated in the province of Malaga (Spain), which has an annually production of ~ 46700 tons. The principal use of the avocado fruit is human consumption, as fresh fruit, in salads, or as processed fruit, in guacamole, i.e. a sauce made with mashed avocado pulp and other various condiments. Avocado industrial processing generates large quantities of agro-industrial by-products, ranging from 18% to 23% of fruit dry weight per year [29]. In Spain, the only country in Europe with a significant commercial production of avocados, guacamole production is an emerging activity. As a result, residues consisting of peels, seeds and pulp are increasing and, if not properly treated, can become a significant environmental concern [30]. Avocado by-products have been proposed for different applications. Seed oil has been explored for the synthesis of biodiesel, charcoal, liquid fuels and fuel additives [31], while peels have been investigated as carbonaceous adsorbent material for the

removal of contaminants in wastewater due to their relevant adsorption capacity [32]. Recent studies also showed the great potential of avocado waste for the production of active bioplastics, due to its richness in phytochemical substances [33]. As avocado by-products represent a fat-rich biomass [34,35], their use for the extraction of lipids and other bioactive compounds can be a valid alternative to recover waste while producing bio-based materials with potential utility as active food-packaging. Moreover, they can sensibly reduce the hydrophilic character of paper if used as additive of a suitable impregnating polymer.

5.2 Experimental section

5.2.1 Materials

Ethyl cellulose (48% ethoxyl, viscosity 22 cP for a solution 5% in toluene/ethanol 80:20), ethyl acetate (99.5%), ethanol (96%), gallic acid, quercetin, aluminium chloride, Folin and Ciocalteu phenol reagent, Tenax®, 1,1-diphenyl-2-picrylhydrazyl (DPPH) radical and Scienceware® filter paper were purchased from Sigma-Aldrich (Milano, Italy). HPLC gradient grade methanol (MeOH) and acetonitrile (ACN) for extract purification, LC separation and MS detection were obtained from Sigma-Aldrich (Milano, Italy). Formic acid (98%), used as an additive of the aqueous mobile phase, was purchased from Carlo Erba Srl (Milano, Italy). Deionized water was obtained from a Milli-Q RG Ultrapure Water Purification device from Millipore (Bedford, MA, USA). Avocado waste (AW) was obtained from a local company (Avomix) located in Malaga (Spain). The waste was dried in the oven at 50°C for three days and then grounded into a powder by using a Moulinex mill. The dried powder was stored at room temperature until the use.

5.2.2 Optimization of bioactive compounds extraction by experimental design

The bioactive compounds from avocado waste were extracted with ethyl acetate, after optimizing the extraction conditions through a face centered composite design. For a balanced extraction yield, the solid-liquid ratio was fixed at 1:60 according to a previous reported method [36]. Ethyl acetate was chosen as extraction solvent in order to directly add the extract in the solution prepared for paper impregnation. Two independent variables were selected for the experimental design, i.e. temperature (X_1 , °C) and time (X_2 , min), toward three responses, i.e. yield (weight %), total phenolic content (mg gallic acid equivalent (GAE)/g dried extract) and total flavonoid content (mg quercetin equivalent (QE)/g dried extract). Three variation levels were chosen for the selected

independent variables, as shown in **Table 5.1**. Low and high factor were coded as -1 and +1, respectively, while the central point was coded as 0.

Table 5.1. Variation levels chosen for the variables selected for the optimization of bioactive compounds extraction from avocado waste by experimental design, i.e. temperature (X_1) and time (X_2). The results obtained for the responses, i.e. yield (Y), total phenolic content (TPC) and total flavonoid content (TFC), are also reported.

Experiment	Variables		Responses		
	X_1 (°C)	X_2 (min)	Y (weight %)	TPC (mg GAE/g dried extract)	TFC (mg QE/g dried extract)
1	40 (-1)	15 (-1)	25.36	3.82	1.38
2	40 (-1)	30 (0)	26.96	3.32	2.07
3	40 (-1)	45 (+1)	23.00	5.31	4.85
4	65 (0)	15 (-1)	14.43	8.30	5.26
5	65 (0)	30 (0)	17.47	5.71	6.33
6	65 (0)	45 (+1)	15.33	7.53	6.95
7	90 (+1)	15 (-1)	26.35	4.79	1.28
8	90 (+1)	30 (0)	36.05	3.45	1.30
9	90 (+1)	45 (+1)	29.59	3.93	1.94

The statistical experimental design and optimization calculations were performed using the R software (v3.63, www.r-project.org). The responses and variables were correlated by response surface analysis to obtain the coefficients of the following equation:

$$Y = \beta_0 + \sum_{i=1}^k \beta_i x_i + \sum_{i=1, i < j}^{k-1} \sum_{j=2}^k \beta_{ij} x_j + \sum_{i=2}^k \beta_{ii} x_{ii}^2$$

where β_0 , β_i , β_{ii} , and β_{ij} are the regression coefficients, x_i and x_j are the coded levels of independent variables affecting the dependent response Y and k is the number of parameters. In order to validate the model, three replicates in the central point were performed to estimate the experimental error and to detect lack of fit.

5.2.3 Determination of extraction yield

In order to extract bioactive compounds, 0.25 g of avocado waste dried powder were weighted in a glass vial and 15 mL of ethyl acetate were added. The vial was heated under magnetic stirring on a hotplate according to the temperature and time conditions set by the experimental design. After that, the powder was removed by filtration and the supernatant was recovered and dried under hood. Extraction yield (Y %) was calculated from the following equation:

$$Y (\%) = \frac{m_0}{m} \times 100$$

where m_0 (g) is the weight of the dried extract and m (g) is the weight of the dried avocado waste powder.

5.2.4 Determination of total phenolic content (TPC)

The total phenolic content (TPC) of the extracts was measured using a modified Folin-Ciocalteu colorimetric method previously described by Villa-Rodriguez et al. [37]. Briefly, 15 μL of extract were mixed with 900 μL of H_2O and 75 μL of Folin and Ciocalteu phenol reagent. After 8 min of equilibrium time, 225 μL of Na_2CO_3 (20%) and 285 μL of H_2O were added to the extracts. Subsequently, microcuvettes containing the solution were incubated for 30 min at room temperature. Then, the absorbance was read at 765 nm using a UV–VIS Cary JEOL spectrophotometer. Total phenolic compounds were calculated using a standard curve of gallic acid and expressed as mg/g of dried extract.

5.2.5 Determination of total flavonoid content (TFC)

The total flavonoid content (TFC) of the extracts was determined using a previously colorimetric method with slight modifications [37]. 150 μL of extract were mixed with 600 μL of deionized H_2O and 45 μL NaNO_2 (5%). After an equilibration time of 5 min, 45 μL of AlCl_3 (10%) were added to the microcuvettes containing the solution. Then, they were reposed for 1 min and 300 μL of NaOH (1 M) were subsequently added. The volume was made up to 1.5 μL with deionized water, stirred, and the absorbance was determined at 415 nm, using a UV–VIS Cary JEOL spectrophotometer. Total flavonoids were determined using a standard curve of quercetin and expressed as mg of quercetin equivalents/g of dried extract.

5.2.6 LC-MS/MS Analysis

In order to characterize the phytochemical compounds occurring in the AW extract, LC-MS untargeted analyses were conducted. Before LC-MS analysis, the sample was purified by solid-phase extraction (STRATA C18-E cartridges, 500 mg/6 mL, Phenomenex, Torrance, California, USA). Cartridges were conditioned with 6 mL of methanol and 6 mL of deionized water. The sample was loaded on the SPE cartridge, and then washed with 6 mL of $\text{MeOH}/\text{H}_2\text{O}$ (20:80), followed by elution with 5 mL of MeOH/ACN (50:50). Finally, the elute was filtered through 0.2 μm PTFE membrane (Whatman, Maidstone, UK) before LC-MS/MS analysis. Experiments were achieved using an UltiMate 3000 ultra-high-pressure liquid chromatography (UPLC) system (Thermo Fisher Scientific, Bremen, Germany) coupled to a Q-Exactive Orbitrap mass spectrometer (Thermo Fisher Scientific, Bremen, Germany). Analytes were chromatographically separated on a Kinetex C18 2.6 μm (Phenomenex Aschaffenburg, Germany) column. The mobile phase consisted of solvent A (water + 0.1% formic acid) and solvent B (acetonitrile + 0.1% formic acid). The elution gradient was conducted at a constant flow rate of 0.250 mL/min as follows: 0 min, 95% A; 25 min,

50% A; 33 min, 0% A; 36 min, initial conditions until 40 min as a re-equilibration step. The sample volume injected was 5 μ L. The analyses were performed in negative ion mode. ESI source parameters were set as follows: spray voltage 2500 V; tube lens voltage 630 V; capillary temperature 300 °C; sheath and auxiliary gas flow (N_2), 50 and 15 (arbitrary units). MS spectra were acquired by full range acquisition covering m/z 180-2000. For fragmentation studies, a data dependent scan experiment was performed, selecting precursor ions corresponding to most intensive peaks in LC–MS analysis. Xcalibur software version 2.1 was used for instrument control, data acquisition and data analysis.

5.2.7 Preparation of impregnated papers

Ethyl cellulose impregnation solutions with concentrations of 0.025, 0.05 and 0.1 g/mL were prepared by dissolving ethyl cellulose powder in ethyl acetate under continuous stirring on a magnetic plate at room conditions. The complete dissolution occurred after 1.5 h. Concentrations higher than 0.1 g/mL were avoided as resulted in too viscous solutions, which are unsuitable for impregnation because they cause a reduction in the pickup weight of the impregnated paper [20]. Avocado waste extract was directly added to 0.1 g/mL ethyl cellulose impregnation solution at different percentages of the total amount of polymer (0, 2, 10, 15 and 30 wt %). Circular discs of filter paper with a diameter of 60 mm were immersed in the solutions for 30 s. The paper was removed from the immersion tray and dried under hood for 24 h. The pickup weight of each paper was calculated by the difference between its weight before and after impregnation. The percentage of ethyl cellulose and avocado waste incorporated by paper after impregnation as well as labels used to name the prepared samples are listed in **Table 5.2**.

Table 5.2 Sample label*, concentration of the EC solution used for paper impregnation and percentage of ethyl cellulose and avocado waste incorporated by paper after impregnation.

Label	Concentration of EC solution	Impregnated ethyl cellulose (wt%)	Incorporated avocado waste (wt%)
<i>PE10</i>	0.025 g/mL	10 %	-
<i>PE20</i>	0.05 g/mL	20%	-
<i>PE50</i>	0.1 g/mL	50%	-
<i>PE50A1</i>	0.1 g/mL	50%	1%
<i>PE50A5</i>	0.1 g/mL	50%	5%
<i>PE50A10</i>	0.1 g/mL	50%	10%
<i>PE50A20</i>	0.1 g/mL	50%	20%

*abbreviations: P: paper; E: ethyl cellulose; A: avocado waste.

5.2.8 Morphological, chemical and mechanical characterization

The morphology of the paper samples was characterized by scanning electron microscopy (SEM), using a JEOL JSM-6490LA microscope working in high vacuum mode, with an acceleration voltage of 15 kV. Samples were previously covered with a ~10 nm gold coating by using a JEOL ION SPUTTER JFC 1100.

All samples were chemically characterized by Attenuated Total Reflectance (ATR)-Fourier-transform infrared spectroscopy (FTIR), using a MIRacle ATR (PIKE Technologies) accessory coupled to an Equinox 70 FT-IR (Bruker) spectrometer. All spectra were acquired in the range from 4000 to 700 cm^{-1} with a resolution of 4 cm^{-1} , accumulating 128 scans. Three acquisitions were made for each sample in three different areas in order to assess the homogeneity of chemical composition.

The mechanical properties of the impregnated paper samples were determined with a MTS Criterion 42 machine equipped with a 50 N load cell. All the measurements were done according to ASTM D 882 Standard Test Methods for Tensile Properties of Thin Plastic Sheeting. Thus, dog-bone shapes of 20 mm length and 5 mm width were cut for each sample and stretched at a rate of 5 mm/min. Stress-strain curves were acquired for each sample, thus allowing the calculation of Young's modulus, yield stress and elongation at break. The values were expressed as average of at least seven independent measurements.

5.2.9 Water uptake

To assess the water uptake properties, the treated paper substrates were dried by conditioning in a desiccator until no change in sample weight was measured. Then, ~80 mg of dry samples were weighed with a sensitive electronic balance (0.0001 g accuracy) and placed in different chambers under different humidity conditions (RH) at 25°C. The following humidity conditions were set: 0%, 11%, 57%, 84% and 100% RH. After conditioning in the different humidity chambers until equilibrium conditions (1 day), each sample was weighed and the amount of adsorbed water was calculated, in percentage, as the difference with the initial dry weight according to the following equation:

$$\text{Water uptake (\%)} = \frac{m_f - m_0}{m_0} \times 100$$

Where m_f is the sample weight at RH (%) condition of interest and m_0 is the sample weight at 0% RH. Three replicates were measured for each sample and the results were averaged to obtain a mean value.

5.2.10 Water contact angle

In order to evaluate the surface wettability of the samples, water static contact angles (W-CA) were measured with the sessile drop method at room temperature at nine different locations on each surface using a contact angle goniometer (DataPhysics OCAH 200). Three μL droplets of milli-Q water were deposited on the surfaces and side view images of the drops were captured. W-CAs were automatically calculated by fitting the captured drop shape. W-CAs were measured after 30 seconds from drop deposition on the surface in order to consider values at equilibrium.

5.2.11 Water vapor permeability

The water vapor permeability (WVP) and transmission rate (WVTR) of the impregnated paper samples were determined at 25°C and under 100% relative humidity gradient (ΔRH %) according to the ASTM E96 standard method [38,39]. Briefly, 350 μL of deionized water (which generates 100% RH inside permeation cell) was placed in each test permeation cell with a 4 mm inner diameter and a 10 mm inner depth. Each biomaterial was cut into circles and mounted on the top of the permeation cells. The permeation cells were placed in 0% RH desiccator with anhydrous silica gel as a desiccant agent. The water transferred through the film was determined by the weight change of the permeation cell every hour during the first 7 h using an electronic balance (0.0001 g accuracy). The weight loss of the permeation cells was plotted as a function of time. The slope of each line was calculated by linear fitting. Then, the water vapor transmission rate and permeability were determined, respectively, according to the following equations [39]:

$$\text{WVTR (g/(m}^2 \cdot \text{s))} = \frac{\text{Slope}}{A}$$

$$\text{WVP (g/(m} \cdot \text{s} \cdot \text{Pa))} = \frac{\text{WVTR} \cdot l \cdot 100}{p_s \cdot \Delta\text{RH}}$$

where A and l are the area and the thickness (measured with a micrometer with 0.001 mm accuracy) of the film, respectively, ΔRH (%) is the relative humidity percentage gradient, and p_s (Pa) is the saturation water vapor pressure at 25°C (3168 Pa). WVTR and WVP measurements were replicated three times for each film.

5.2.12 Oil contact angle

Oil contact angle measurements were performed by using the sessile drop method in a DataPhysics OCAH 200 contact angle goniometer equipped with a CCD camera and image processing software operating under laboratory conditions (temperature 22–25 °C and relative humidity 50–60%). For the characterization, 5 μL droplets of extra-virgin olive oil were used. Up to 10 measurements were carried out on every sample at random locations and their average values and the corresponding standard deviations are reported.

5.2.13 Oil and Grease Resistance Testing

Oil and grease resistance of the coated papers was evaluated using a 3 M Scotchban visibility method, also known as the TAPPI Kit test for oil and grease resistance (TAPPI um 557). Briefly, different standard solutions of mixture of castor oil, toluene and heptane were prepared by changing the ratio among them. Each standard solution had a Kit number ranging from 1 to 12 according to its increasing degree of hydrophobicity. A drop of each solution was applied on the tested paper substrates and left for 15 seconds. Once the 15 seconds elapsed, the fluid was cleaned with a tissue and the wetted area was examined. If a pronounced dark spot was visible, the test was considered failed as the oil penetrated the sheet. A rating from 1-12 was assigned to the tested substrate depending on the highest kit test number of the solution which did not stain the sample surface. Three measurements were done for each sample and the results were expressed as mean \pm SD.

5.2.14 Biodegradability

The biodegradability of the samples was evaluated by measuring the amount of oxygen consumed during a biodegradation reaction in water through the standard biochemical oxygen demand (BOD) test. Briefly, ~200 mg of each sample were finely minced and immersed in dark glass bottles containing 164 mL of seawater collected from the Malaga (Spain) area shoreline. The seawater, already containing microbial species and saline nutrients needed for their growth, allowed to mimic the real environmental conditions of biodegradation. Each bottle was sealed and maintained at 20°C. The O₂ consumed during the biodegradation process was recorded at different time intervals, for 28 days, by using sealed OxyTop caps on each bottle which can assess the oxygen levels. For each sample, three measurements were done and the results were averaged to obtain a mean value.

5.2.15 DPPH radical scavenging assay

The antioxidant capacity was calculated by measuring the free radical scavenging activity of the total released phenolic compounds on the DPPH (2,2-diphenyl-1-picrylhydrazyl) radical. Discs of $5 \times 5 \text{ mm}^2$ of each sample were added to 4 mL of 0.1 mM DPPH solution in ethanol. The decrease in the absorbance solution due to the antioxidant composites' action was determined at 515 nm with a Cary JEOL spectrophotometer at different times. Radical scavenging activity was expressed as the inhibition percentage of free radical by the sample and calculated through the following equation:

$$\text{Radical Scavenging Activity (\%)} = \frac{A_0 - A_1}{A_0} \times 100$$

where A_0 is the absorbance value of the control (3 mL of 0.1 mM DPPH solution in ethanol) and A_1 is the absorbance value of the sample at different times. All measurements were performed in triplicate and the results were expressed as mean \pm SD.

5.2.16 Overall Migration of Components in Tenax®

The migration of components from the different impregnated papers into the food was evaluated by using Tenax® as a simulant for dry food, following the EU Technical guidelines for compliance testing in the framework of the plastic FCM Regulation (EU) No 10/2011. For this, a round sample with a 20 mm diameter was cut for each covered paper as well as for an uncovered paper and an ethyl cellulose film and put in a pre-cleaned glass vial with 80 mg of Tenax® (40 mg below and 40 mg above the sample). All vials were covered with cap and parafilm in order to avoid the evaporation of simulant during contact period and kept in a temperature-controlled chamber at $20 \pm 0.5 \text{ }^\circ\text{C}$ for 10 days. After this contact period, the glass vials containing the sample and Tenax® were removed from the chamber and the overall migration as milligrams per square decimeter of the surface of the sample, which is intended to come into contact with foodstuffs, was calculated according to the following equation:

$$M = (m_0 - m_f) / S$$

where M is the overall migration into the dry food simulant (mg dm^{-2}), m_0 is the original mass of the Tenax® in grams, m_f is the mass of Tenax® after migration in grams and S is the surface area of the test specimen intended to come into contact with foodstuff in dm^2 . For each sample, the final migration value was reported as mean \pm SD. Blank samples with only 80 mg of Tenax® were used as a control.

5.2.17 Evaluation of Moisture Preservation

In order to evaluate the ability of the produced covered papers to protect food from moisture loss, pear pieces were used as model. Mature pears were purchased from a local store (Potenza, Italy). The moisture preservation was studied according to a previous reported method [40]. Briefly, each pear was cut into pieces with a similar weight (~10 g). Each piece was put into a 50 mL centrifuge tube with a hole of a diameter of 1.5 cm being drilled into the cap of the tube. The hole was covered by PE50A20 paper affixed to the cap. Tubes in which the hole was covered with low-density polyethylene (LDPE) film, not-impregnated paper and tubes with uncovered hole were used for comparison. All tubes were kept at 4 ± 1 °C. The weight of the tube was measured every 48 hours. Each measurement was made in triplicate.

5.2.18 Statistical analysis

Significant differences of the results among the variances were statistically analyzed by SPSS 19.0 software (IBM SPSS Statistics, Armonk, NY, USA). Statistical significance was accepted at a level of $p < 0.05$.

5.3 Results and Discussion

5.3.1 EC-impregnated paper-based bioplastics

5.3.1.1 Morphological, chemical and mechanical characterization

The morphology of PE10, PE20 and PE50 paper samples, covered with ethyl cellulose impregnation solutions with concentration of 0.025, 0.05 and 0.1 g/mL, respectively, was characterized by SEM. SEM top view and cross-section images of EC impregnated and uncovered papers are reported in **Figure 5.3a-d**. Uncovered paper morphology showed a typical fibrous structure (**Figure 5.3a**), due to cellulose fibers, and a thin and quite homogeneous cross-section. Large numbers of interstitial voids with size of several ten micrometers were noticed in the paper top view. It can be observed, in **Figure 5.3b-d**, that when the ethyl cellulose concentration of the impregnating solution increased, the roughness of the cellulose fibers decreased and the junction points among fibers were gradually covered. EC was uniformly distributed at the surface of the paper and no obvious aggregation was distinguished, suggesting that with the used impregnation method the EC polymer was homogeneously loaded at the surface of paper. The introduction of EC made the paper become denser, as observed by comparing the SEM images in cross section.

Impregnating solution at 0.1 g/mL ensured a better coating. Indeed, cellulose fibers on the surface and in the inner side of the paper were coated with EC more uniformly, as can be noted in the cross-section image of the PE50 paper sample in **Figure 5.3d (right)**. In addition, no apparent interface was observed between cellulose fibers and the EC coating, indicating a strong adhesion between them.

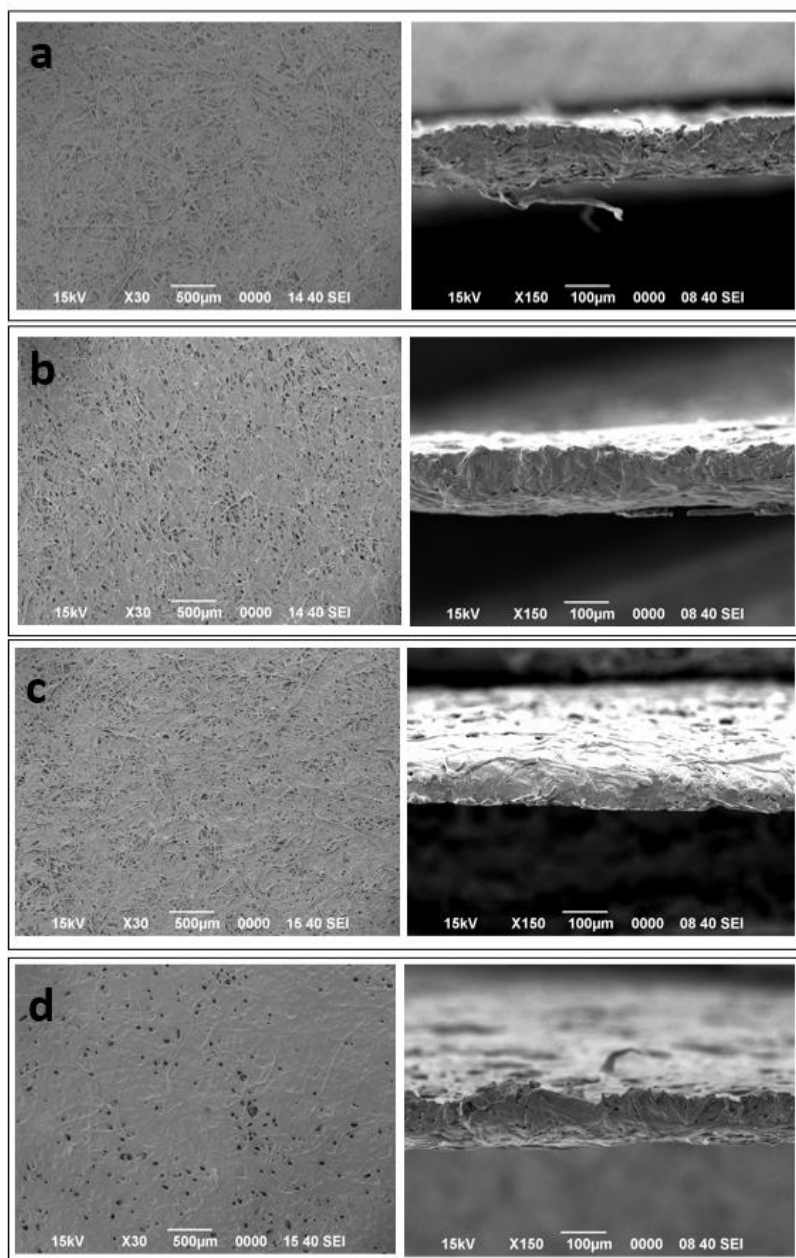


Figure 5.3 SEM top-view (left) and cross-section (right) images of uncovered paper (a), PE10 (b), PE20 (c) and PE50 (d) samples.

The chemical characterization of the EC impregnated samples was carried out by ATR-FTIR. **Figure 5.4** shows the infrared spectra of PE10, PE20 and PE50 samples, uncovered paper (P) and an ethyl cellulose (EC) film. Uncovered paper was characterized by the presence of different peaks in the region 1400-800 cm^{-1} due to typical cellulose bands such as C-H bending and C-O, C-O-C and C-O-H stretching modes. OH stretching mode at 3330 cm^{-1} , related to the occurrence H-bonded hydroxyl groups of cellulose, was also observed. The ATR-FTIR spectra of EC showed the absorption bands for C-O-C stretching vibrations of the ethoxy groups and the glycosidic bond at 1052 cm^{-1} , C-H bending at 1375 cm^{-1} , -CH₃ asymmetric and symmetric stretching modes at 2975 and 2872 cm^{-1} , respectively, and -OH stretching mode at 3471 cm^{-1} [24]. For PE samples, ATR-FTIR spectra was the sum of both P and EC. It should be noted that the band representative of free -OH decreased in relative intensity by increasing the ethyl cellulose concentration of the impregnating solution, thus confirming the better covering entity with the EC polymer.

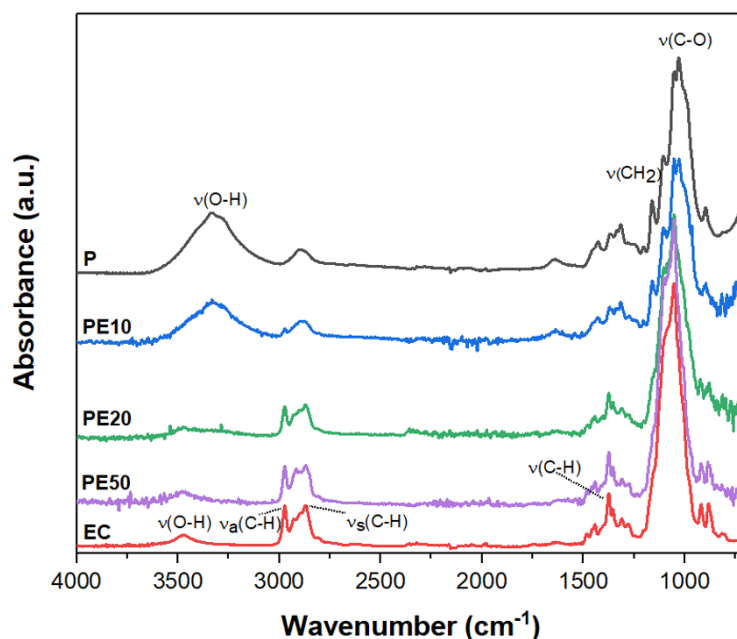


Figure 5.4 ATR-FTIR spectra of uncovered paper, PE10, PE20, and PE50 samples and ethyl cellulose in the 4000-700 cm^{-1} region.

The mechanical properties of the ethyl cellulose covered paper samples prepared within this work, i.e. PE10, PE20 and PE50, are presented in **Figure 5.5**. **Figure 5.5a** shows the typical tensile stress-strain curves, while the measured mechanical parameters (i.e. Young's modulus, yield stress and elongation at break) are displayed in **Figure 5.5b-d**. All covered papers exhibited a similar behaviour with slight increases of yield stress (from 33 MPa for PE10 to 39 MPa for PE50) and elongation at break (from 4% for PE10 to 7% for PE50), while keeping the Young's modulus ~1400 MPa for all of them. PE50 exhibited a higher strength and flexibility compared with the papers

impregnated by using less concentrated ethyl cellulose solutions. In any case, all of their values were mechanically better than uncovered paper (P), that presented a yield stress and a Young's modulus of 18 MPa and 1257 MPa, respectively, and an elongation at break of ~3.9%. These results suggested that the impregnation of paper with ethyl cellulose markedly improved the mechanical strength and the durability of paper. Indeed, durable papers should have high mechanical strength, as this prevents materials from being severely damaged with long term use [20].

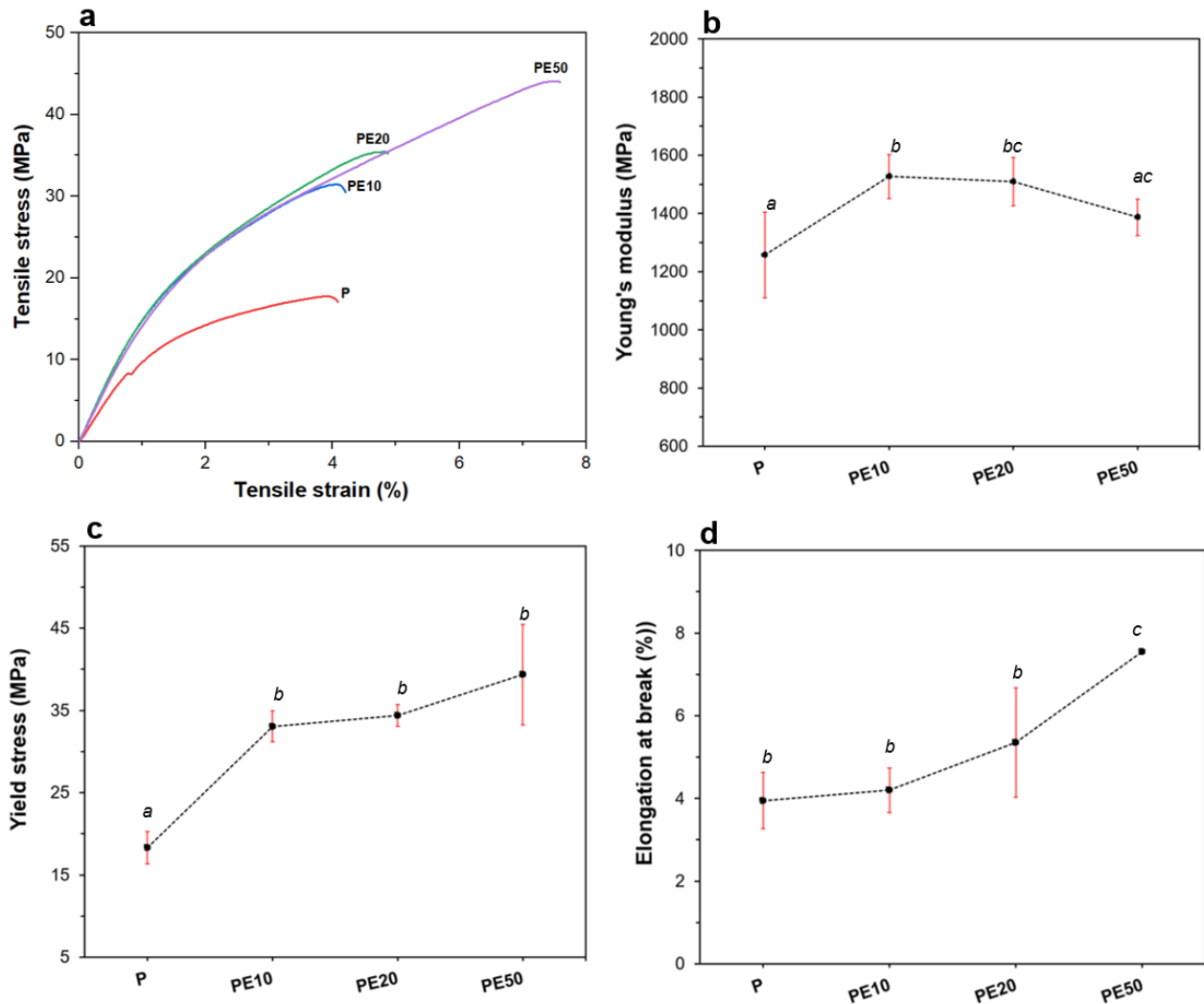


Figure 5.5 (a) Typical stress-strain curves for PE10, PE20 and PE50 samples and uncovered paper P. (b, c, d) Young's modulus, yield stress and elongation at break parameters, respectively, for PE10, PE20 and PE50 samples and for uncovered paper P, calculated from the stress-strain curves. Values marked by the same letter are not significantly different ($p < 0.05$).

5.3.1.2 Water uptake, wettability and water barrier properties

The water uptake, water contact angle (WCA) and water vapor permeability (WVP) of PE samples are presented in **Figure 5.6**. Water uptake of all covered paper samples was analyzed by measuring water adsorption levels under different humidity conditions, i.e. RH 0%, 11%, 57%, 84% and 100% (**Figure 5.6a**). The water adsorption isotherms for all samples presented similar shapes, which can be defined as type III isotherms as they were convex to RH% axis over their entire range [41]. This suggested that the adsorbate–adsorbate (i.e. water–water) interactions were higher compared to adsorbate–adsorbent interactions. In this situation, the adsorbate molecules build clusters around preferred sites of the adsorbent, covering only partially the surface [42]. A confirmation of the surfaces' homogeneity was achieved, since no knee points were observed [43]. In general, water uptake values were relatively high, due to the intrinsic hydrophilicity of cellulose, which makes paper fibres very sensitive to water. A water absorption of 30.3 ± 2.0 % under the highest RH was obtained for uncovered paper in our study. In general, also the samples covered with ethyl cellulose were found to be slightly sensitive to relative humidity. However, the water uptake decreased by increasing the percentage of the adsorbed ethyl cellulose after impregnation, according to the following linear trend: $PE50 < PE20 < PE10 < P$ (**Figure 5.6 b**). As ethyl cellulose is a partly *O*-ethylated hydrophobic cellulose ether derivative, this tendency confirmed the better covering ensured by using the impregnating solution at 0.1 g/mL. In fact, after 80% R.H., water uptake levels of PE50 sample were around half of those obtained for both PE10 and uncovered paper. The water uptake, calculated as percentage of dry weight, passed from $27.5 \pm 3.5\%$ for PE10 to $17.9 \pm 1.7\%$ for PE50. On the other hand, the difference in the water contact angles among samples with different percentage of ethyl cellulose covering were found to be not statistically significant ($p < 0.05$). Values on average around 93° were obtained in all the cases, thus allowing their classification as hydrophobic materials (**Figure 5.6a, inset**) [44,45]. Considered that water in contact with uncovered paper was rapidly absorbed (value of contact angle for paper is $\sim 30^\circ$ [46]), a hydro-repellent behaviour of PE10, PE20 and PE50 samples can be stated.

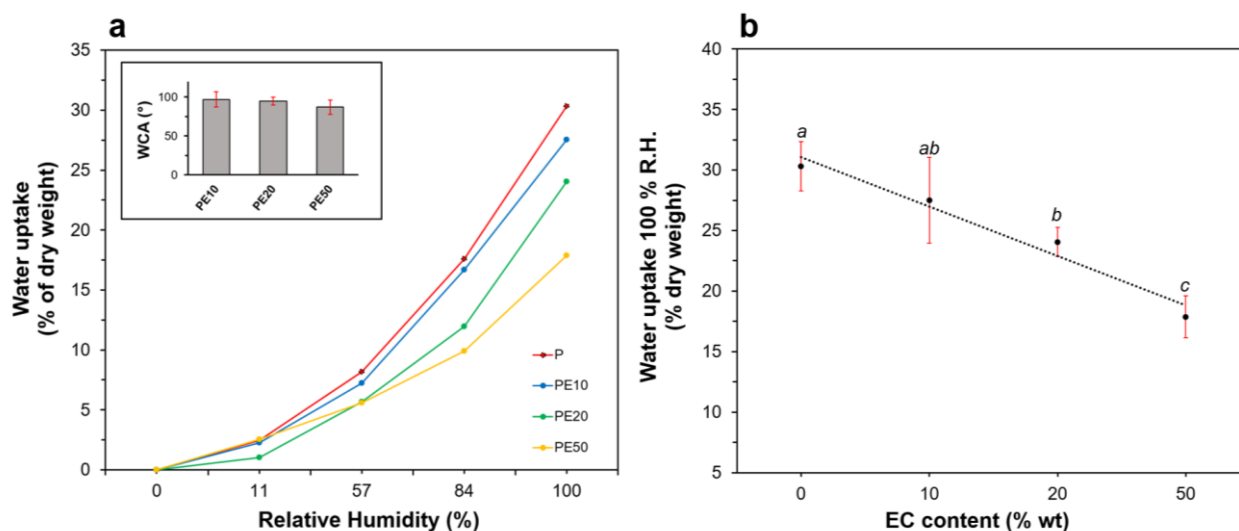


Figure 5.6 (a) Water adsorption (uptake) values under different humidity conditions (R.H. 0%, 11%, 57%, 84% and 100%) for PE10, PE20 and PE50 samples and for uncovered paper P. Inset: water contact angle for PE10, PE20 and PE50 samples. **(b)** Water uptake values at a relative humidity of 100% as a function of EC content (wt%). Values marked by the same letter are not significantly different ($p < 0.05$).

Similarly to water contact angles, also the WVP decrease with the percentage of ethyl cellulose covering was low, as it passed from $2.67 \cdot 10^{-9} \text{ g m}^{-1} \text{ s}^{-1} \text{ Pa}^{-1}$ for PE10 to $2.34 \cdot 10^{-9} \text{ g m}^{-1} \text{ s}^{-1} \text{ Pa}^{-1}$ for PEC50. In any case, these values were significantly lower ($p > 0.05$) compared to the one registered for uncovered paper ($3.27 \cdot 10^{-9} \text{ g m}^{-1} \text{ s}^{-1} \text{ Pa}^{-1}$) (**Figure 5.7**). The large WVP of paper might be partially attributed to its porous structure, enabling direct diffusion of water vapor through the air in the pores and even convection or capillary flow at high relative humidity [47]. As paper permeability was significantly reduced after impregnation, ethyl cellulose penetration into the internal paper pores can be ascertained.

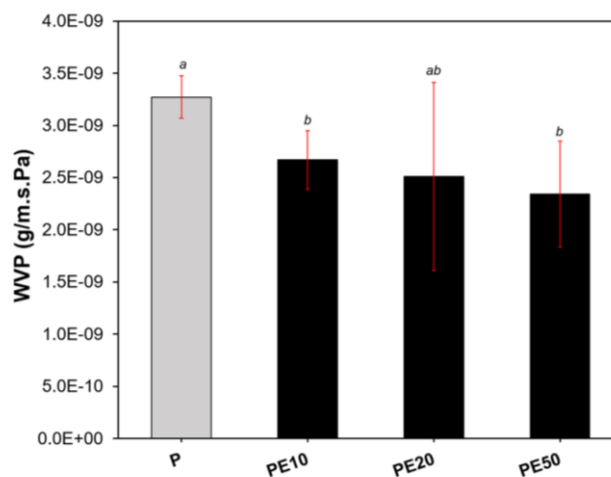


Figure 5.7 Water vapor permeability for PE10, PE20 and PE50 samples and for uncovered paper P. Values marked by the same letter are not significantly different ($p < 0.05$).

5.3.2 Avocado by-product extraction: optimization and chemical characterization

5.3.2.1 Optimization of bioactive compounds extraction by experimental design

Avocado by-products (seeds, pulp and peels) are an important source of bioactive compounds, mainly lipids and phenolic compounds with high antioxidant capacity [48]. The extraction of these bioactive compounds usually involves strategies based on systematic studies of one variable-at-a-time (OVAT) during which all variables affecting the extraction efficiency are held constant during test runs, except the one being studied. However, the classical univariate approach can result in wrong optimizations, since it does not consider the interactions between different factors, assuming that all variables are independent and the effect, at a given set condition, is the same also if the remaining variables are changed [49]. In order to avoid erroneous run tests, an optimization planned according to an experimental design is the best option. Indeed, with an experimental design (DoE) all variables are studied at the same time, enabling a reduction in the number of experiments with a complete exploration of the experimental domain [50,51]. In this study, the optimization of the main parameters affecting AW bioactive compounds extraction efficiency, i.e. extraction time and temperature, was conducted by applying a face centered composite design. In order to directly add the AW extract to the EC impregnating solution and produce durable and hydrophobic covered papers through a one-pot fabrication approach, ethyl acetate was chosen as extraction solvent of bioactive compounds. The applied DoE allowed to select the best conditions to obtain high extraction yields, with a high number of antioxidant compounds such as phenols and flavonoids and the lowest number of experiments. Yield % was chosen as the investigated response, since it is

related to the extraction efficiency, while the total phenolic content (TPC) and the total flavonoid content (TFC) were introduced in the model as a means to evaluate the potential of the extract as additive for active food-packaging. In particular, the extraction time was varied between 15 and 45 minutes and the temperature between 40 and 90°C [52]. Prolonged extraction time and higher temperatures were avoided since the degradation and the oxidation of the chemical compounds could occur. Moreover, at high extraction temperatures, the formation of toxic and mutagenic compounds, known as Maillard reaction products, can happen [53]. Regression analysis for the experimental data revealed that a second-order polynomial model was found to predict the best conditions for yield %, total phenols and flavonoids compounds extraction within the range of the experimental variables. The second-order polynomial models of the optimization of extraction to obtain better responses as a function of extraction temperature and extraction time are expressed in the equations reported in **Table 5.3**.

Table 5.3 Polynomial equations generated to evaluate the relationship between process variables, i.e. extraction temperature (X_1) and extraction time (X_2), and responses, i.e. extraction yield, total phenol content (TPC) and total flavonoid content (TFC). The explained variance by each model is reported.

Polynomial equations	Explained variance
$Y (\%) = 18.73 + 2.78 X_1 + 0.29 X_2 + 1.40 X_1 X_2 + 12.14 X_1^2 - 4.48 X_2^2$	91.38%
$TPC (\text{mg GAE/g dried extract}) = 6.21 - 0.045 X_1 - 0.024 X_2 - 0.59 X_1 X_2 - 3.08 X_1^2 + 1.45 X_2^2$	89.64%
$TFC (\text{mg QE/g dried extract}) = 5.93 - 0.63 X_1 + 0.97 X_2 - 0.70 X_1 X_2 - 4.04 X_1^2 + 0.37 X_2^2$	96.38%

All coefficients were found to be statistically significant and the yield, TPC and TFC values were properly fitted (explained variance by the models ~90%), indicating a good reliability for the experimental predictions. In order to investigate the effect of the extraction time and temperature on the response variables, the response surface plots were obtained (**Figure 5.8a-c**). In general, the surface plot illustrated that the highest yield (**Figure 5.8a**) was obtained for extractions performed at the highest temperature and at intermediate times. At high temperatures, less volatile and thermolabile compounds can be extracted, among them polyphenols are not included as they are heat-sensitive compounds [53]. Indeed, the results obtained here by the DoE showed that total phenolic and flavonoid content decreased at temperature higher than 60°C. The highest values for TPC and TFC were obtained at intermediate values of time and temperature, according to previous studies which reported that the polyphenolic yield decreases at temperatures above 80°C [54–56]. Since the aim of this study was the extraction of bioactive compounds useful as additive for food-packaging materials, further extracts for paper impregnation were carried out by setting the temperature and the time at 65°C and 45 minutes, respectively.

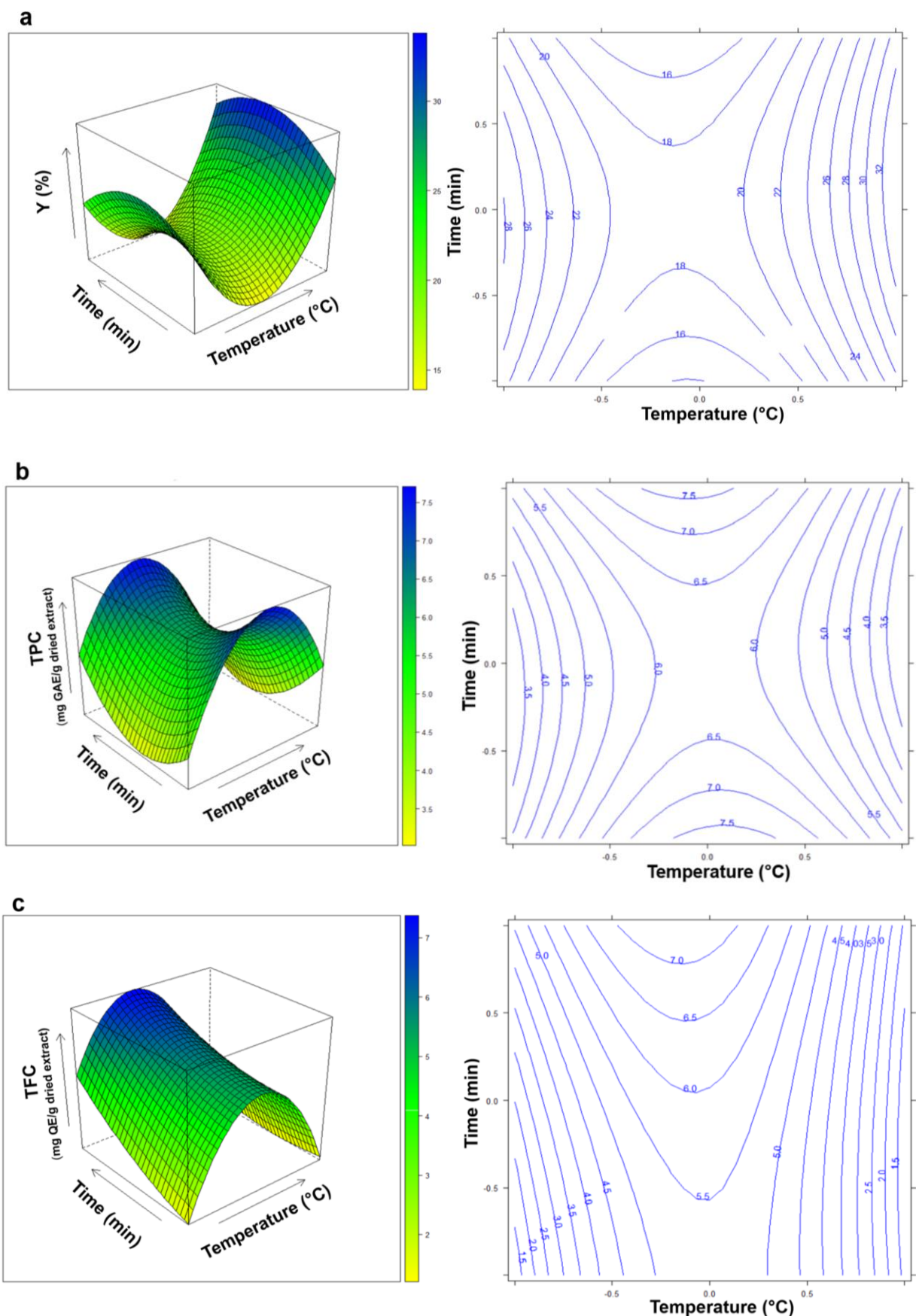


Figure 5.8 Response surface plot (left) and the corresponding contour plot (right) for (a) extraction yield (Y%), (b) total phenolic content (mg GAE/g dried extract) and (c) total flavonoid content (mg QE/ g dried extract) with time and temperature as main factors.

5.3.2.2 LC-MS/MS Analysis

Liquid chromatography coupled to tandem mass spectrometric detection was used for the chemical characterization of the AW extract (**Table 5.4**). Ethyl acetate mainly extracted lipid components from avocado waste (pulp, peel and seeds), as avocado fruit is also referred to as “butter fruit” due to its higher content of lipids compared to other fruits [34]. Here, the LC-MS/MS findings pointed out that different free fatty acids occurred in the extract (i.e. linolenic, palmitoleic, palmitic, oleic and linoleic acids). Other major compounds identified in the AW extract by LC-MS/MS were oxylipins, with hydroxy-octadecadienoic acid being the one with the higher amount expressed as percentage of the area of the chromatographic peak (**Table 5.4**). Oxylipins are the oxidation products of unsaturated fatty acids [57]. Many of the identified oxylipins were various oxidation products of linoleic (*cis*, *cis*-9,12-octadecadienoic) acid, characterized by the MS² fragment ion $-\text{OOC}(\text{CH}_2)_7\text{CH-OH}$ at $m/z = 171$ amu, containing a carboxyl and an OH-group. Although not commonly present in avocado, these chemical compounds are originated by thermal treatment or air-drying of the fruits and induce an unpleasant off-taste centering around a slightly pungent mouthfeel and a pronounced lingering bitter after-taste [58]. It is presumable to think that these compounds were obtained here after the air-exposing and oven drying of AW. Due to their great structural variety, also oxylipins have various biological roles as second messengers and antimicrobial as well as antifungal compounds.

Table 5.4 Identification of bioactive compounds in avocado waste ethyl acetate extract by LC-ESI-MS/MS.

Peak	t_r (min)	Proposed compound	m/z	Molecular formula	Area %
1	12.51	10-(1-Hydroxyhexoxy)-10-oxodecanoate	319.2117	$\text{C}_{16}\text{H}_{31}\text{O}_6^-$	0.0
3	14.68	Tetrahydroxy octadecenoic acid	345.2278	$\text{C}_{18}\text{H}_{33}\text{O}_6^-$	0.2
5	17.89	9-oxo-12,13-dihydroxy-10-octadecenoic acid	327.2177	$\text{C}_{18}\text{H}_{31}\text{O}_5^-$	0.4
6	19.16	9,12,13-Trihydroxy-10-octadecenoic acid	329.2333	$\text{C}_{18}\text{H}_{33}\text{O}_5^-$	1.0
7	19.65	13-oxo-9,10-dihydroxy-11-octadecenoic acid	327.2175	$\text{C}_{18}\text{H}_{31}\text{O}_5^-$	0.1
8	21.29	9,10,13-Trihydroxy-11-octadecenoic acid	329.2333	$\text{C}_{18}\text{H}_{33}\text{O}_5^-$	0.2
9	22.28	Sucrose	387.1148	$\text{C}_{13}\text{H}_{23}\text{O}_{13}^-$	0.8
10	23.37	9,10,18-Trihydroxystearate	331.2490	$\text{C}_{18}\text{H}_{35}\text{O}_5^-$	0.1
11	24.15	10,16-Dihydroxyhexadecanoic acid	287.2227	$\text{C}_{16}\text{H}_{31}\text{O}_4^-$	0.2
12	26.71	Dihydroxyoctadecenoic acid	313.2385	$\text{C}_{18}\text{H}_{33}\text{O}_4^-$	0.2
13	28.80	9,10-Dihydroxystearic acid	315.2535	$\text{C}_{18}\text{H}_{35}\text{O}_4^-$	0.9
14	30.23	Linolenic acid	277.2177	$\text{C}_{18}\text{H}_{29}\text{O}_2^-$	0.4
15	30.70	9-Keto-octadecadienoic acid	293.2118	$\text{C}_{18}\text{H}_{29}\text{O}_3^-$	27.3
16	31.66	Hydroxy-oxo-octadecenoic acid	311.1685	$\text{C}_{18}\text{H}_{31}\text{O}_4^-$	11.2
17	31.77	Hydroxyoctadecadienoic acid	295.2274	$\text{C}_{18}\text{H}_{31}\text{O}_3^-$	50.3
18	33.97	Palmitoleic acid	253.2171	$\text{C}_{16}\text{H}_{29}\text{O}_2^-$	0.2
19	34.37	Linoleate	279.2326	$\text{C}_{18}\text{H}_{31}\text{O}_2^-$	1.1
20	35.21	Palmitic acid	255.2326	$\text{C}_{16}\text{H}_{31}\text{O}_2^-$	0.1

21	35.40	Oleic acid	281.2483	$C_{18}H_{33}O_2^-$	4.0
22	35.40	Linoleic acid	279.2326	$C_{18}H_{31}O_2^-$	1.2
23	36.36	1-hexadecanoyl-2-(6Z,9Z,12Z-octadecatrienoyl)-glycero-3-phosphate	669.4496	$C_{37}H_{66}O_8P^-$	0.1

5.3.3 Effect of the incorporation of the avocado by-product extract into the bioplastic formulation

5.3.3.1 Chemical and mechanical characterization

The effect of the AW extract on the chemical and mechanical properties of PE50 sample, the treated paper substrate with the best coverage, mechanical and waterproofing properties, was studied. ATR-FTIR spectra of the most representative samples, i.e. PE50A1 (1% of incorporated AW) and PE50A20 (20% of incorporated AW), and the AW extract are reported in **Figure 5.9a**. ATR-FTIR spectra of avocado by-product extract showed typical adsorption bands related to the presence of sterols, triglycerides and fatty acids: the stretching vibration of -OH at 3438 cm^{-1} [59], asymmetrical and symmetrical stretching of $-\text{CH}_2$ at 2923 cm^{-1} and 2854 cm^{-1} , respectively, C=O stretching mode at 1737 cm^{-1} and $-\text{CH}_3$ bending at 1273 cm^{-1} were observed. These results were in accordance with those reported in other studies concerning the ATR-FTIR characterization of avocado oil [60]. All PE50Ax covered paper samples prepared within this work showed an intense peak at 1051 cm^{-1} related to C–O–C stretching vibrations of the ethoxy groups and the glycosidic bond of ethyl cellulose. Moreover, all infrared bands characteristic of AW extract were present, except for that related to $-\text{CH}_3$ bending which was masked by peaks in the region $1400\text{--}800\text{ cm}^{-1}$ due to C–H bending, and to C–O, C–O–C and C–O–H vibrations from paper cellulose and ethyl cellulose. The intensity of the bands related to AW extract increased with its content.

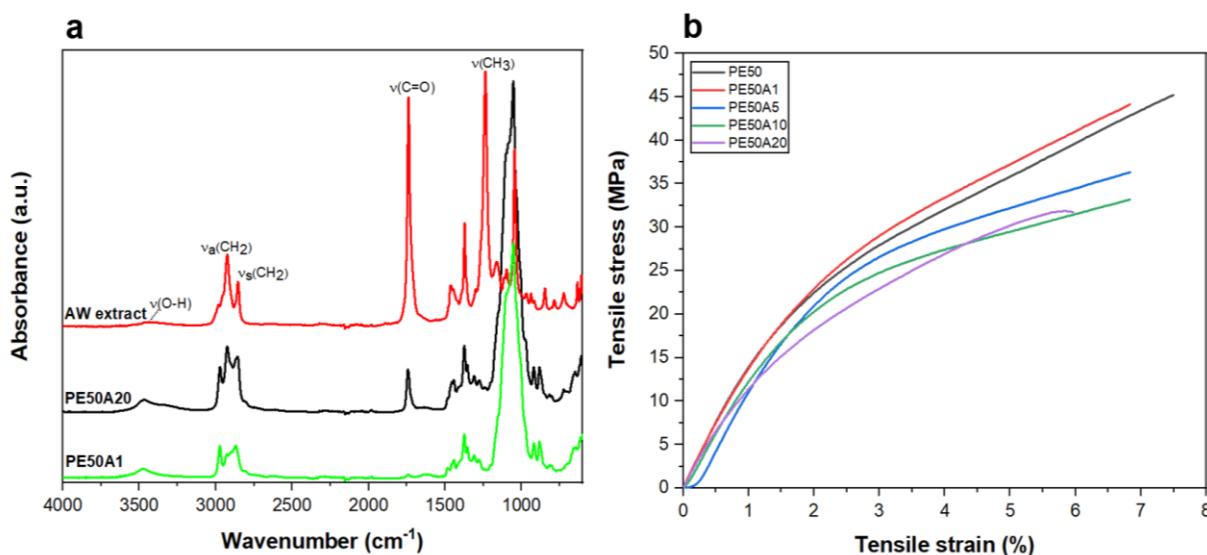


Figure 5.9 (a) ATR-FTIR spectra of PE50A1 and PE50A20 sample and avocado waste (AW) extract in the 4000–600 cm^{-1} region. (b) Typical stress-strain curves for PE50, PE50A1, PE50A5, PE50A10 and PE50A20 samples.

The tensile mechanical properties of the paper covered with ethyl cellulose were not significantly modified by the presence of the avocado waste extract, as displayed in **Figure 5.9b**. Both yield stress and elongation at break were kept at ~ 40 MPa and $\sim 7\%$, respectively, for all samples as for PE50. Young's modulus slightly increased with the addition of AW, as it passed from ~ 1387 MPa for PE50 to ~ 1449 MPa for PE50A20, thus slightly increasing material stiffness. Nevertheless, no significant differences were detected among the values of all the samples containing avocado waste ($p < 0.05$).

5.3.3.2 Wettability, water uptake and water barrier properties

Interestingly, the addition of avocado waste extract into the ethyl cellulose-based impregnation solution at 0.1 g/mL caused a reduction in the water uptake of the samples, as presented in **Figure 5.10a**. Such a reduction showed a linear relationship with the AW amount. PE50A20 sample absorbed around three times less water compared with PE50 sample. Water absorption values at 100% RH of around 7% and 18% were obtained for PE50A20 and PE50, respectively. Also water vapor permeability and transmission rate values showed a decrease due to the presence of avocado waste (**Figure 5.10b-c**). However, unlike water uptake, for both WVP and WVTR, the values were kept almost unchanged with increasing avocado waste in paper covering. In particular, WVP passed from $0.90 \cdot 10^{-9} \text{ g m}^{-1} \text{ s}^{-1} \text{ Pa}^{-1}$ for PE50A5 to $0.93 \cdot 10^{-9} \text{ g m}^{-1} \text{ s}^{-1} \text{ Pa}^{-1}$ for PE50A20. While WVTR passed from $0.028 \text{ g m}^{-2} \text{ s}^{-1}$ for PE50A5 to $0.024 \text{ g m}^{-2} \text{ s}^{-1}$ for PE50A20. These values were comparable with those obtained by Larotonda et al. for Kraft paper impregnated with cassava starch

acetate under vacuum. Indeed, a WVTR of $\sim 0.021 \text{ g m}^{-2} \text{ s}^{-1}$ was obtained by these authors [21], suggesting that the AW extract introduction into the impregnation solution allows to reach a barrier grade comparable to those guaranteed by conventional hydrophobic polymers thanks to the lipids present. **Figure 5.10d** compares the values of the water contact angle of the papers impregnated with ethyl cellulose and AW extract with common plastic materials such as poly-4-methyl-1-pentene (TPX), polyethylene terephthalate (PET), poly-2-vinylpyridine (PVP), polymethylmethacrylate (PMMA), polyethylene (PE), polyvinylbenzyl chloride (PVBC) and polytetrafluoroethylene (PTFE) [61]. Both PE50 and PE50A20 were found in the highest values range, between PE and PTFE. Thus, the bioplastics developed within this work are materials with excellent water repellency, as those of the common hydrophobic materials used in packaging applications.

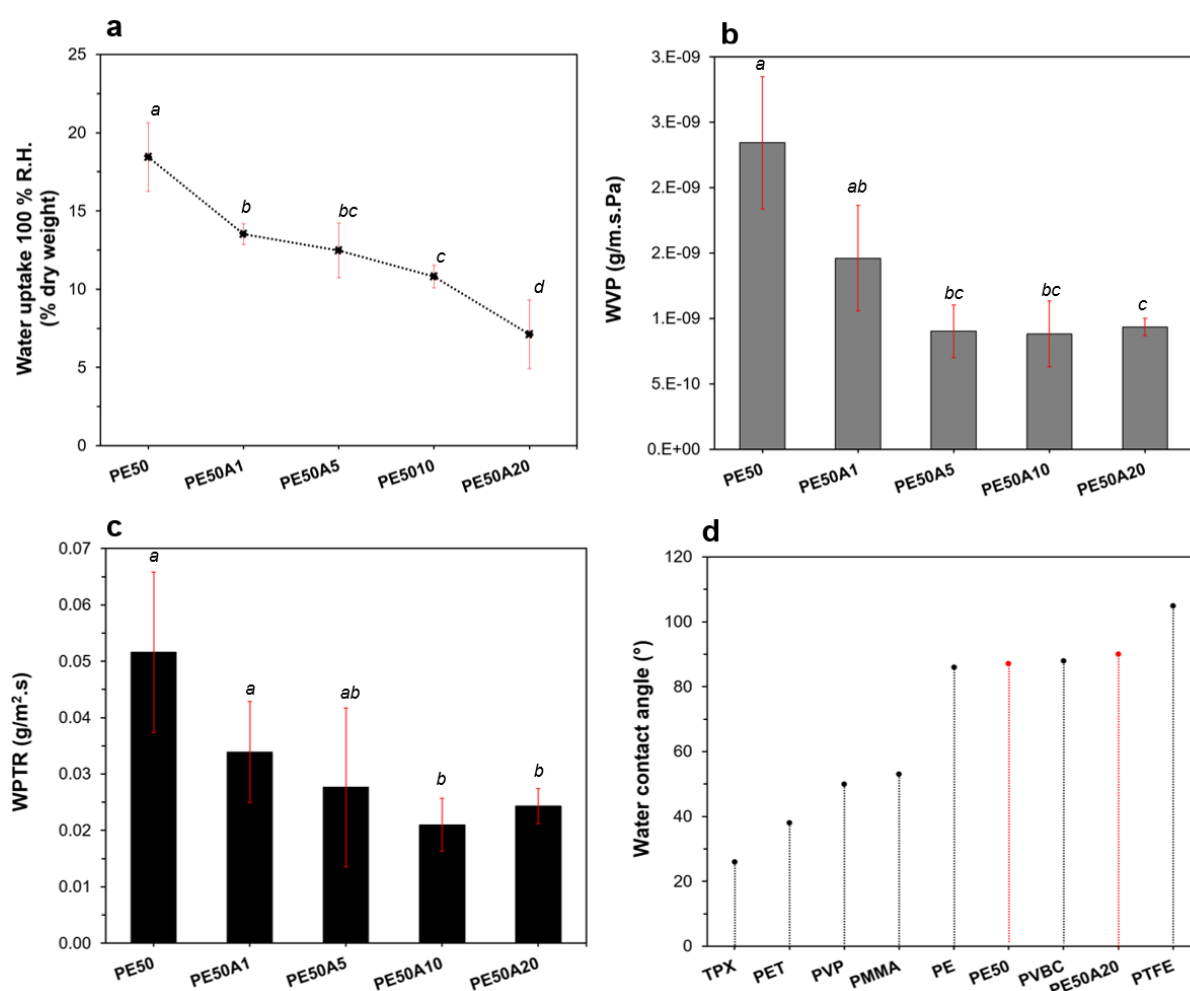


Figure 5.10 (a, b, c) Water uptake values at a relative humidity of 100%, water vapor permeability and water vapor transmission rate, respectively, for PE50, PE50A1, PE50A5, PE50A10 and PE50A20 samples. Values marked by the same letter are not significantly different ($p < 0.05$). (d) Comparison of water contact angles of PE50 and PE50A20 sample with different polymeric materials. Data from Myshkin et al. [61]. PE50 and PE50A20 were chosen as their WCA angles represented, respectively, the minimum and the maximum obtained value among all the tested samples.

5.3.3.3 Oil contact angle and oil and grease resistance testing

Since the main use of these bioplastics is as food packaging materials, the interaction with oils and greases is a key parameter to be evaluated. **Figure 5.11a** shows the extra-virgin oil contact angle (OCA) for PE50, PE50A1, PE50A5, PE50A10 and PE50A20 samples. All samples showed a lower oil wettability (OCA 40-50°) compared to untreated paper substrate (OCA ~3° for P sample). The addition of avocado waste did not affect the oil wettability of the covered paper. On the other hand, TAPPI um-557, also known as the Kit test, was used to measure the oil and grease resistance (OGR) of covered paper samples. **Figure 5.11b** displays the Kit rating reached by each sample. The Kit rating increased with the amount of avocado waste extract introduced in the impregnation solution. PE50A20 sample reached the highest level of OGR (9), while the lowest level was exhibited by paper un-treated with AW extract (Kit rate was 6.3 for PE50). The increase of the grease resistance is similar to those described for other systems for papers where aliphatic molecules are used [62–64].

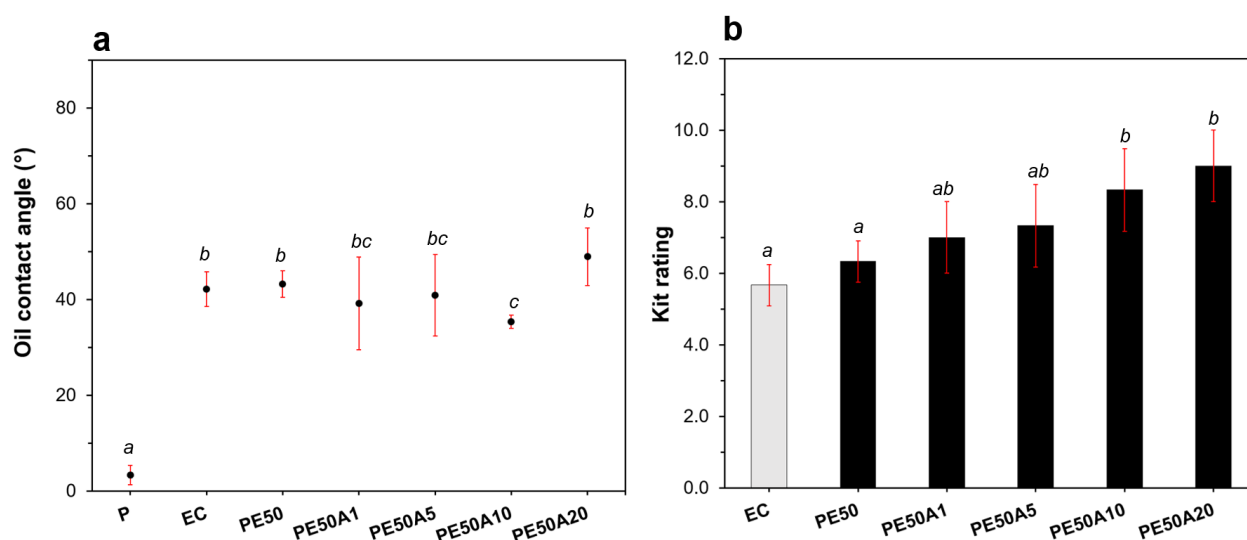


Figure 5.11 (a) Oil contact angle for PE50, PE50A1, PE50A5, PE50A10 and PE50A20 samples, paper (P) and ethyl cellulose (EC) film. Values marked by the same letter are not significantly different ($p < 0.05$). (b) Kit test results for PE50, PE50A1, PE50A5, PE50A10 and PE50A20 samples and ethyl cellulose (EC) film.

5.3.3.4 Biodegradability

Paper is made of cellulose, hemicellulose and lignin fibers linked through hydrogen bonds. The formation and quantity of such links greatly affect its physical and chemical properties as well as biodegradability. Different studies have investigated the paper-based products' biodegradability [65,66]. In general, the lignin content of these materials is responsible for the low biodegradability level achieved in controlled composting tests, which measure carbon dioxide evolution due to

microbial degradation [66]. However, the addition of biomass as covering can improve paper biodegradation. In our study, the biodegradability of PE50Ax paper samples, i.e. papers impregnated with ethyl cellulose and avocado waste extract, was studied by monitoring the biochemical oxygen demand during 28 days in seawater. The results are shown in **Figure 5.12a-b**.

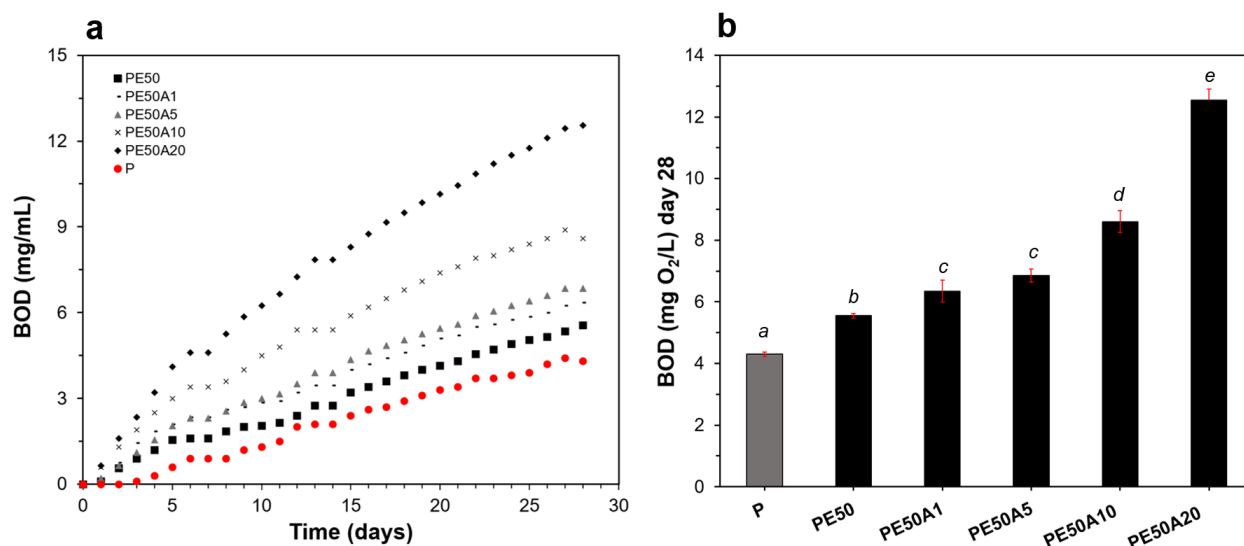


Figure 5.12 (a) Biochemical oxygen demand (mg O₂/L) as a function of time (days) for PE50, PE50A1, PE50A5, PE50A10, PE50A20 samples and uncovered paper (P). (b) Biochemical oxygen demand (mg O₂/L) at day 28 for all samples. Values marked by the same letter are not significantly different ($p < 0.05$).

The obtained results showed that all PE50Ax impregnated papers exhibited a higher biodegradability compared to uncovered paper. P sample reached a maximum oxygen consumption of around 4 mg O₂/L after 28 days (**Figure 5.12b**). This value was significantly lower than the one obtained for the EC-covered paper without AW extract (PE50, 5.6 ± 0.1 mg O₂/L of oxygen consumption after 28 days). It should be noted that the addition of avocado waste to the impregnation solution positively affected the biodegradability. It has been previously proved that the inclusion of the organic matter in polymeric materials enhances the biodegradability [67]. Therefore, although ethyl cellulose is a quite inert, non-ionic water-insoluble polymer [68], the addition of AW in the impregnating polymeric solution, can likely to improve the hydrolytic microorganisms' activity. Here, the biochemical oxygen consumption in seawater was higher as the content of AW increased, according to the following order: PE50A20 > PE50A10 > PE50A5 > PE50A1. This trend can be explained by the increasing content of lipids detected in the ethyl acetate AW extract. Although knowledge regarding microorganisms degrading plastic in the marine environment is still poor, many heterotrophic bacteria playing a predominant role in particulating and dissolving lipid-rich organic matter through hydrolytic reactions are known [69], thus

accounting for the highest biochemical oxygen consumption value observed for PE50A20 paper sample, i.e. 12.6 ± 0.4 mg O₂/L.

5.3.3.5 Antioxidant properties

Currently, the increasing consumer demand for safer and healthier foodstuff has encouraged research towards the development of novel preservation strategies, aiming at minimizing food oxidation by the addition of antioxidants directly to foodstuff or their incorporation into packaging materials [70]. Since the direct addition of natural antioxidants to foodstuff shows several drawbacks, mainly due to the fast degradation which occurs when they are chemically consumed, the use of active packaging seems to be the preferred way [71]. Here, the potential antioxidant properties of the covered PE50Ax paper samples were evaluated following the standard DPPH· method in order to establish their usefulness as active packaging materials. **Figure 5.13a** shows the results both for uncovered and impregnated papers as well as for the control paper and a pure ethyl cellulose film.

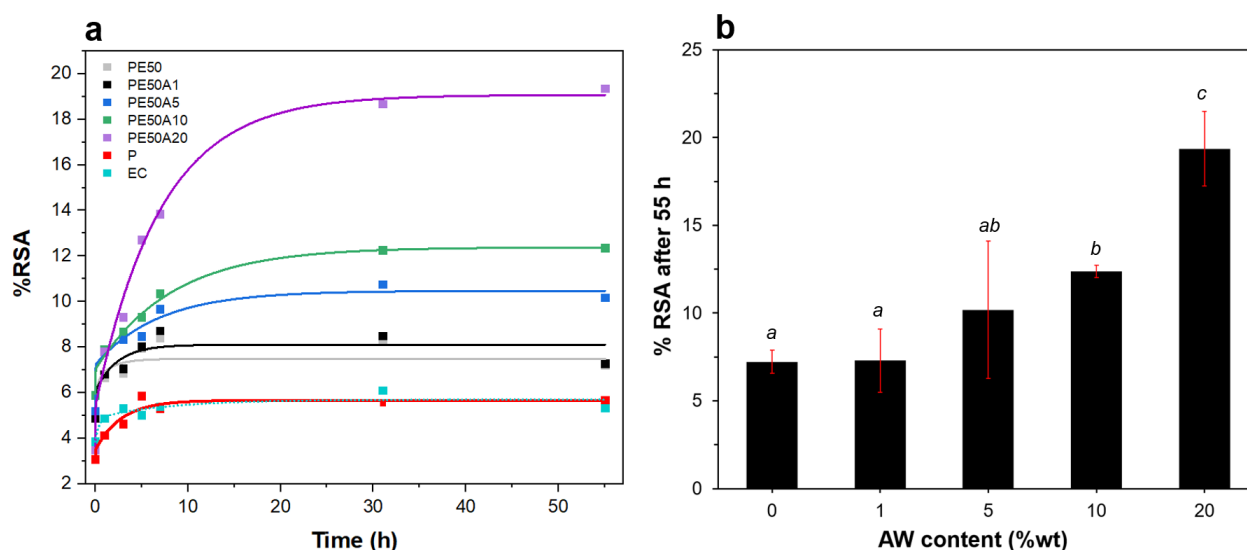


Figure 5.13 (a) Antioxidant capacity as a function of time (hours) for PE50, PE50A1, PE50A5, PE50A10, PE50A20 samples and for uncovered paper (P) and pure ethyl cellulose film (EC), calculated by 2,2-diphenyl-1-picrylhydrazyl free radical method (DPPH·). **(b)** Antioxidant capacity calculated after 55 hours by using the DPPH· assay, as a function of AW content (wt%). Values marked by the same letter are not significantly different ($p < 0.05$).

All PE50Ax covered paper samples displayed final values of radical scavenging activity (RSA) between 7% and 20% after 55 hours of measurement (**Figure 5.13b**), thus suggesting the potential of these materials in extend the shelf life of products (for a period of time higher than 48 hours), if used as an active packaging. It should be noted that, for all samples, a slow release of antioxidant compounds occurred, as the plateau was reached after around 15 hours. This can be due to the time required by the ethyl cellulose matrix to freely release in the solvent test, i.e. ethanol, the antioxidants that exhibit their action against DPPH· by hydrogen atom transfer. Results obtained for paper covered with ethyl cellulose and avocado waste extract were much higher compared to not-impregnated paper and pure ethyl cellulose biofilm (RSA was $5.9 \pm 0.6\%$ and $5.0 \pm 0.0\%$ for P and EC, respectively, after 55 h). In particular, the antioxidant capacity increased with the avocado waste amount after 55 h: the RSA was $7.2 \pm 0.7\%$ for PE50, $7.3 \pm 1.8\%$ for PE50A1, $10.2 \pm 3.9\%$ for PE50A5, $12.4 \pm 0.3\%$ for PE50A10 and $19.4 \pm 2.1\%$ for PE50A20. This trend was expected as it can be ascribed to the increasing content of unsaturated fatty acids characterized in the avocado waste extract by LC-MS/MS. The inclusion of AW extract into the paper coverage accounts for the antioxidant properties of the materials as several studies available in literature confirm an increased inhibitory activities of both saturated and unsaturated fatty acids against cyclooxygenase enzymes [72]. Edible oils with high level of saturations are considered with higher oxidative stability and can be used as a natural antioxidant in food stability [73].

5.3.3.6 Migration test

Packaging materials can represent a source of contamination through the migration of substances from the packaging into the foodstuff. Therefore, the food contact material should be checked for compliance using food simulants. Here, the adsorbent poly(2,6-diphenylphenylene oxide) or Tenax® has been used as simulant for dry foodstuffs in order to evaluate the overall migration of the impregnated paper samples. The results of overall migration are presented in **Table 5.5**. Except for PE50A20, all samples gave a migration lower than 10 mg/dm^2 , thus complying with the current legislation, since this is the limit established in the EU. Although the migration increased as the content of avocado waste increased, all values (except that of PE50A20) were significantly lower than uncovered paper ($p < 0.05$), thus proving that the coating is a good strategy to expand its field of applicability for food packaging.

Table 5.5 Overall migration values obtained for PE50, PE50A1, PE50A5, PE50A10, and PE50A20 samples and for uncovered paper (P) and ethyl cellulose film (EC). Values marked by the same letter are not significantly different ($p < 0.05$).

Sample	Overall migration (M , mg/dm ²)
<i>P</i>	14.3 ± 2.2^a
<i>EC</i>	3.18 ± 0.1^b
<i>PE50</i>	4.8 ± 2.2^b
<i>PE50A1</i>	6.8 ± 0.1^b
<i>PE50A5</i>	7.9 ± 0.2^c
<i>PE50A10</i>	9.55 ± 0.01^d
<i>PE50A20</i>	17.5 ± 2.2^{ae}

5.3.3.7 Evaluation of Fruit Preservation

As PE50A10 was the sample with the best antioxidant and hydro-repellent properties among those complying with the legislation for migration test, its ability to preserve food from moisture loss was evaluated by using pear pieces, as a food model. The results were compared with the ones obtained by using a low-density polyethylene (LDPE) film and not-impregnated paper. The setup in which the hole in the cap was uncovered was used as control. As expected, the control showed the highest weight loss (%) throughout the whole observation period (**Figure 5.14**). Indeed, moisture loss occurs through transpiration, when a gradient of water vapour pressure between the food and the surrounding air is present [74]. A high vapour pressure deficit usually occurs when no packaging materials are used, as the relative humidity around the product is not enough high. Thus, food packaging is a good strategy to improve RH and, hence, limiting at the same time the moisture loss. Here, moisture loss increased according to the following order: uncovered hole (control) > paper > PE50A20 > LDPE. This trend is due to the different barrier properties towards oxygen and water vapor of the used packaging materials. LDPE film exhibited the lowest percentage of weight loss, being a reference material for moisture preservation in food packaging [75]. PE50A10 film guaranteed a significantly better fruit preservation than paper. Indeed, weight loss for pear protected with PE50A10 was about 60% of the value registered for paper at day 6 ($2.9 \pm 0.3\%$ vs $5.0 \pm 0.2\%$). This can be due to the presence of lipid components in the avocado waste, which made the impregnated paper less sensitive to water vapor. Although statistically different, the weight loss obtained with PE50A10 was not so far from that obtained with LDPE, i.e. $1.6 \pm 0.3\%$.

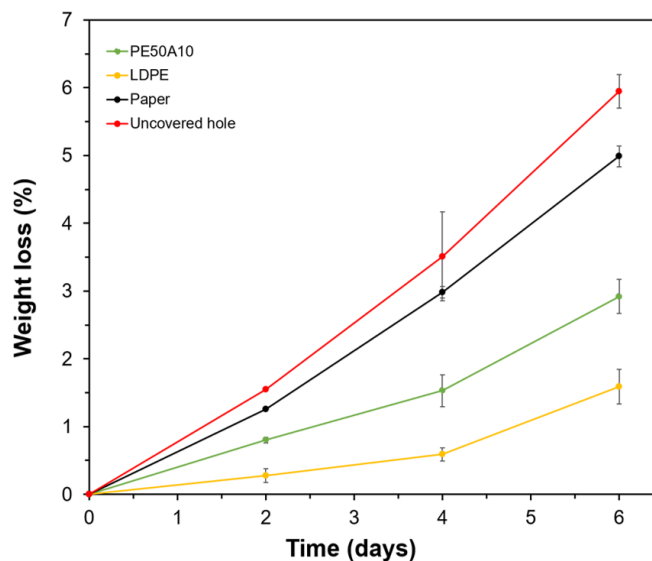


Figure 5.14 Weight loss (%) of pear pieces stored in a tube with the hole in the cap protected by PE50A10, LDPE film and paper. The setup in which the hole in the cap is uncovered is used as the control.

The results regarding moisture loss percentages were supported by the different signs of dehydration and enzymatic browning shown by pears stored in the different packaging materials (**Figure 5.15**). The enzymatic browning occurs through a reaction which involves the action of the polyphenol oxidase (PPO) enzyme. After a tissue damage, the fruits phenolic compounds and PPOs are exposed to oxygen, initiating the oxidation of phenols into quinones. Then, quinones and their derivatives are polymerized, forming a relatively insoluble brown pigment known as melanin [76]. Here, the pear pieces protected by PE50A10 film showed a lower degree of enzymatic browning compared to the control and to those protected by paper. Moreover, with PE50A10 film the extent of enzymatic browning and the degree of surface wrinkling was comparable to that obtained with LDPE, most likely due to its high antioxidant and moisture barrier properties. This suggests that paper impregnation can be adopted to obtain packaging materials with good performances in maintaining the shelf-life of packaged-food.

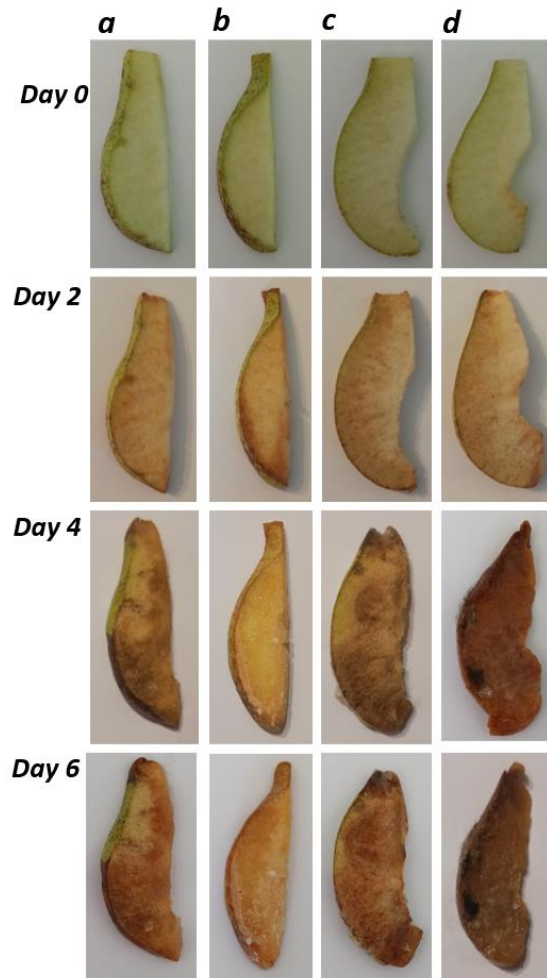


Figure 5.15 Pictures of pear pieces stored in a tube with a hole in the cap, either protected by PE50A10 paper (**a**), LDPE film (**b**), not-impregnated paper (**c**) or uncovered (**d**), at 4°C for 0, 2, 4 and 6 days.

5.4 Conclusions

Paper and paperboard are among the preferred packaging materials with good flexibility, biodegradability and low cost. However, for various end-user applications, papers require an enhanced durability and a broad range of properties with respect to liquid interactions, which could be achieved through surface treatment. In this study, an ethyl cellulose-based solution was used to impregnate paper. An improved mechanical strength was ascertained after impregnation, thus preventing material from being damaged with long term use. Avocado by-product extract was investigated as an additive into the EC impregnation solution to refine the hydrophobic properties of the treated paper substrates, as it was rich in lipid components. The recovery of AW to extract bioactive compounds was proposed and optimized as a good solution under the new circular economy and bioeconomy policies. Paper covering with EC and AW extract reduced the water uptake because of their hydrophobic and lipid nature. Besides, it allowed to increase the biodegradation rate and provided antioxidant properties as well. The capacity of paper in serving as an active food packaging was proved to extend and maintain the shelf-life of packaged pieces of pear.

References

1. Sankaran, R., Markandan, K., Khoo, K.S., Cheng, C.K., Ashokkumar, V., Deepanraj, B., and Show, P.L. (2021) The Expansion of Lignocellulose Biomass Conversion Into Bioenergy via Nanobiotechnology. *Front. Nanotechnol.*, **3** (December), 1–10.
2. Brethauer, S., Shahab, R.L., and Studer, M.H. (2020) Impacts of biofilms on the conversion of cellulose. *Appl. Microbiol. Biotechnol.*, **104** (12), 5201–5212.
3. Jacobs, A., and Dahlman, O. (2001) Characterization of the molar masses of hemicelluloses from wood and pulps employing size exclusion chromatography and matrix-assisted laser desorption ionization time-of-flight mass spectrometry. *Biomacromolecules*, **2** (3), 894–905.
4. Farhat, W., Venditti, R.A., Hubbe, M., Taha, M., Becquart, F., and Ayoub, A. (2017) A Review of Water-Resistant Hemicellulose-Based Materials: Processing and Applications. *ChemSusChem*, **10** (2), 305–323.
5. Zhang, X., Yang, W., and Blasiak, W. (2011) Modeling study of woody biomass: Interactions of cellulose, hemicellulose, and lignin. *Energy and Fuels*, **25** (10), 4786–4795.
6. Huang, Y., Wang, L., Chao, Y., Nawawi, D.S., Akiyama, T., Yokoyama, T., and Matsumoto, Y. (2016) Relationships between Hemicellulose Composition and Lignin Structure in Woods. *J. Wood Chem. Technol.*, **36** (1), 9–15.
7. Area, M.C., and Cheradame, H. (2011) Paper aging and degradation: Recent findings and research methods. *BioResources*, **6** (4), 5307–5337.
8. Deshwal, G.K., Panjagari, N.R., and Alam, T. (2019) An overview of paper and paper based food packaging materials: health safety and environmental concerns. *J. Food Sci. Technol.*, **56** (10), 4391–4403.
9. Bennis, H., Benslimane, R., Vicini, S., Mairani, A., and Princi, E. (2010) Fibre width measurement and quantification of filler size distribution in paper-based materials by SEM and image analysis. *J. Electron Microsc. (Tokyo)*, **59** (2), 91–102.
10. Afra, E., Yousefi, H., Hadilam, M.M., and Nishino, T. (2013) Comparative effect of mechanical beating and nanofibrillation of cellulose on paper properties made from bagasse and softwood pulps. *Carbohydr. Polym.*, **97** (2), 725–730.
11. Sehaqui, H., Zhou, Q., Ikkala, O., and Berglund, L.A. (2011) Strong and tough cellulose nanopaper with high specific surface area and porosity. *Biomacromolecules*, **12** (10), 3638–3644.
12. Ye, S.H., Watanabe, J., Iwasaki, Y., and Ishihara, K. (2003) Antifouling blood purification membrane composed of cellulose acetate and phospholipid polymer. *Biomaterials*, **24** (23), 4143–4152.
13. Johnson, J., Ghosh, A., and Lannutti, J. (2007) Microstructure-Property Relationships in a Tissue-Engineering Scaffold. *J. Appl. Polym. Sci.*, **104** (5), 2919–2927.
14. Samyn, P. (2013) Wetting and hydrophobic modification of cellulose surfaces for paper applications. *J. Mater. Sci.*, **48** (19), 6455–6498.

15. Mazeau, K., and Heux, L. (2003) Molecular dynamics simulations of bulk native crystalline and amorphous structures of cellulose. *J. Phys. Chem. B*, **107** (10), 2394–2403.
16. Bechtold, T., Manian, A.P., Öztürk, H.B., Paul, U., Široká, B., Široký, J., Soliman, H., Vo, L.T.T., and Vu-Manh, H. (2013) Ion-interactions as driving force in polysaccharide assembly. *Carbohydr. Polym.*, **93** (1), 316–323.
17. Yang, H., and Deng, Y. (2008) Preparation and physical properties of superhydrophobic papers. *J. Colloid Interface Sci.*, **325** (2), 588–593.
18. Malmström, E., and Carlmark, A. (2012) Controlled grafting of cellulose fibres - An outlook beyond paper and cardboard. *Polym. Chem.*, **3** (7), 1702–1713.
19. Barona, D., and Amirfazli, A. (2011) Producing a superhydrophobic paper and altering its repellency through ink-jet printing. *Lab Chip*, **11** (5), 936–940.
20. Park, H., Park, S.Y., Yook, S., Kim, T.Y., and Youn, H.J. (2020) Impregnation of paper with cellulose nanofibrils and polyvinyl alcohol to enhance durability. *Nord. Pulp Pap. Res. J.*, **35** (1), 106–114.
21. Larotonda, F.D.S., Matsui, K.S., Paes, S.S., and Laurindo, J.B. (2003) Impregnation of Kraft paper with cassava-starch acetate - Analysis of the tensile strength, water absorption and water vapor permeability. *Starch/Staerke*, **55** (11), 504–510.
22. Guan, F., Song, Z., Xin, F., Wang, H., Yu, D., Li, G., and Liu, W. (2020) Preparation of hydrophobic transparent paper via using polydimethylsiloxane as transparent agent. *J. Bioresour. Bioprod.*, **5** (1), 37–43.
23. Słonina, M., Dziurka, D., and Smardzewski, J. (2020) Experimental research and numerical analysis of the elastic properties of paper cell cores before and after impregnation. *Materials (Basel)*, **13** (9).
24. Heredia-Guerrero, J.A., Ceseracciu, L., Guzman-Puyol, S., Paul, U.C., Alfaro-Pulido, A., Grande, C., Vezzulli, L., Bandiera, T., Bertorelli, R., Russo, D., Athanassiou, A., and Bayer, I.S. (2018) Antimicrobial, antioxidant, and waterproof RTV silicone-ethyl cellulose composites containing clove essential oil. *Carbohydr. Polym.*, **192** (December 2017), 150–158.
25. Davidovich-Pinhas, M., Barbut, S., and Marangoni, A.G. (2014) Physical structure and thermal behavior of ethylcellulose. *Cellulose*, **21** (5), 3243–3255.
26. Cerqueira, M.A.P.R., Pereira, R.N.C., da Silva Ramos, O.L., and Teixeira, J. A. C., & V. (2016) *Edible Food Packaging: Materials and Processing Technologies*.
27. Murtaza, G. (2012) Ethylcellulose microparticles: A review. *Acta Pol. Pharm. - Drug Res.*, **69** (1), 11–22.
28. Lefebvre, G., Jiménez, E., and Cabañas, B. (2016) *Environment, Energy and Climate Change II - Energies from New Resources and the Climate Change*.
29. Wang, W., Bostic, T.R., and Gu, L. (2010) Antioxidant capacities, procyanidins and pigments in avocados of different strains and cultivars. *Food Chem.*, **122** (4), 1193–1198.

30. González-Fernández, J.J., Galea, Z., Álvarez, J.M., Hormaza, J.I., and López, R. (2015) Evaluation of composition and performance of composts derived from guacamole production residues. *J. Environ. Manage.*, **147**, 132–139.
31. Dagde, K.K. (2019) Extraction of vegetable oil from avocado seeds for production of biodiesel. *J. Appl. Sci. Environ. Manag.*, **23** (2), 215.
32. Palma, C., Lloret, L., Puen, A., Tobar, M., and Contreras, E. (2016) Production of carbonaceous material from avocado peel for its application as alternative adsorbent for dyes removal. *Chinese J. Chem. Eng.*, **24** (4), 521–528.
33. Merino, D., Bertolacci, L., Paul, U.C., Simonutti, R., and Athanassiou, A. (2021) Avocado Peels and Seeds: Processing Strategies for the Development of Highly Antioxidant Bioplastic Films. *ACS Appl. Mater. Interfaces*, **13** (32), 38688–38699.
34. Takenaga, F., Matsuyama, K., Abe, S., Torii, Y., and Itoh, S. (2008) Lipid and fatty acid composition of mesocarp and seed of avocado fruits harvested at northern range in Japan. *J. Oleo Sci.*, **57** (11), 591–597.
35. Figueroa, J.G., Borrás-Linares, I., Lozano-Sánchez, J., and Segura-Carretero, A. (2018) Comprehensive identification of bioactive compounds of avocado peel by liquid chromatography coupled to ultra-high-definition accurate-mass Q-TOF. *Food Chem.*, **245** (December 2017), 707–716.
36. Gómez, F.S., Peirósánchez, S., Iradi, M.G.G., Azman, N.A.M., and Almajano, M.P. (2014) Avocado seeds: Extraction optimization and possible use as antioxidant in food. *Antioxidants*, **3** (2), 439–454.
37. Villa-Rodríguez, J.A., Molina-Corral, F.J., Ayala-Zavala, J.F., Olivas, G.I., and González-Aguilar, G.A. (2011) Effect of maturity stage on the content of fatty acids and antioxidant activity of “Hass” avocado. *Food Res. Int.*, **44** (5), 1231–1237.
38. Bedane, A.H., Eić, M., Farmahini-Farahani, M., and Xiao, H. (2015) Water vapor transport properties of regenerated cellulose and nanofibrillated cellulose films. *J. Memb. Sci.*, **493**, 46–57.
39. Guzman-Puyol, S., Ceseracciu, L., Tedeschi, G., Marras, S., Scarpellini, A., Benítez, J.J., Athanassiou, A., and Heredia-Guerrero, J.A. (2019) Transparent and robust all-cellulose nanocomposite packaging materials prepared in a mixture of trifluoroacetic acid and trifluoroacetic anhydride. *Nanomaterials*, **9** (3), 1–14.
40. Lai, W.F., Yip, W., and Wong, W.T. (2021) UV-Shielding and Clusteroluminogenic Cellulose-Based Films with Tuneable Wettability and Permeability for Dually Self-Indicating Food Packaging. *Adv. Mater. Technol.*, **6** (8), 1–9.
41. Sing, K.S.W., Everett, D.H., Haul, R.A.W., Moscou, L., Pierotti, R.A., Rouquerol, J., and Siemieniewska, T. (1985) Reporting Physisorption Data for Gas/Solid Systems with Special Reference to the Determination of Surface Area and Porosity. *Pure Appl. Chem.*, **57** (4), 603–619.
42. Al-Ghouti, M.A., and Da'ana, D.A. (2020) Guidelines for the use and interpretation of adsorption isotherm models: A review. *J. Hazard. Mater.*, **393** (February), 122383.

43. Ban, W., Jianguo Song, Argyropoulos, D.S., and Lucia, L.A. (2006) Improving the physical and chemical functionality of starch-derived films with biopolymers. *J. Appl. Polym. Sci.*, **100** (3), 2542–2548.
44. Feng, L., Li, S., and Li, Y. (2002) Super-Hydrophobic Surfaces : From Natural to Artificial Super-Hydrophobic Surfaces : From Natural to Artificial. *Adv. Mater.*, **14** (24), 1857–1860.
45. Geissler, A., Loyal, F., Biesalski, M., and Zhang, K. (2014) Thermo-responsive superhydrophobic paper using nanostructured cellulose stearoyl ester. *Cellulose*, **21** (1), 357–366.
46. Liukkonen, A. (1997) Contact angle of water on paper components: Sessile drops versus environmental scanning electron microscope measurements. *Scanning*, **19** (6), 411–415.
47. Wang, J., Gardner, D.J., Stark, N.M., Bousfield, D.W., Tajvidi, M., and Cai, Z. (2018) Moisture and Oxygen Barrier Properties of Cellulose Nanomaterial-Based Films. *ACS Sustain. Chem. Eng.*, **6** (1), 49–70.
48. Vinha, A.F., Sousa, C., Soares, M.O., and Barreira, S.V.P. (2020) *Avocado and Its By-products: Natural Sources of Nutrients, Phytochemical Compounds and Functional Properties*.
49. Parameswaran, R., Box, G.E.P., Hunter, W.G., and Hunter, J.S. (1979) Statistics for Experimenters: An Introduction to Design, Data Analysis, and Model Building. *J. Mark. Res.*, **16** (2), 291.
50. Bouaid, A., Ramos, L., Gonzalez, M.J., Fernández, P., and Cámara, C. (2001) Solid-phase microextraction method for the determination of atrazine and four organophosphorus pesticides in soil samples by gas chromatography. *J. Chromatogr. A*, **939** (1–2), 13–21.
51. Varrone, C., Giussani, B., Izzo, G., Massini, G., Marone, A., Signorini, A., and Wang, A. (2012) Statistical optimization of biohydrogen and ethanol production from crude glycerol by microbial mixed culture. *Int. J. Hydrogen Energy*, **37** (21), 16479–16488.
52. Araújo, R.G., Rodriguez-Jasso, R.M., Ruiz, H.A., Govea-Salas, M., Pintado, M.E., and Aguilar, C.N. (2020) Process optimization of microwave-assisted extraction of bioactive molecules from avocado seeds. *Ind. Crops Prod.*, **154** (June), 112623.
53. Antony, A., and Farid, M. (2022) Effect of Temperatures on Polyphenols during Extraction. *Appl. Sci.*, **12** (4).
54. Lang, G.H., Lindemann, I. da S., Ferreira, C.D., Hoffmann, J.F., Vanier, N.L., and de Oliveira, M. (2019) Effects of drying temperature and long-term storage conditions on black rice phenolic compounds. *Food Chem.*, **287** (September 2018), 197–204.
55. Daniel, D.L., Huerta, B.E.B., Sosa, I.A., and Mendoza, M.G.V. (2012) Effect of fixed bed drying on the retention of phenolic compounds, anthocyanins and antioxidant activity of roselle (*Hibiscus sabdariffa* L.). *Ind. Crops Prod.*, **40** (1), 268–276.
56. Vega-Gálvez, A., Di Scala, K., Rodríguez, K., Lemus-Mondaca, R., Miranda, M., López, J., and Perez-Won, M. (2009) Effect of air-drying temperature on physico-chemical properties, antioxidant capacity, colour and total phenolic content of red pepper (*Capsicum annum*, L. var. Hungarian). *Food Chem.*, **117** (4), 647–653.

57. Püssa, T., Raudsepp, P., Toomik, P., Pällin, R., Mäeorg, U., Kuusik, S., Soidla, R., and Rei, M. (2009) A study of oxidation products of free polyunsaturated fatty acids in mechanically deboned meat. *J. Food Compos. Anal.*, **22** (4), 307–314.
58. Degenhardt, A.G., and Hofmann, T. (2010) Bitter-tasting and kokumi-enhancing molecules in thermally processed avocado (*Persea americana* Mill.). *J. Agric. Food Chem.*, **58** (24), 12906–12915.
59. Lumakso, F.A., Rohman, A., Handoy, M., Riyanto, S., and Yusuf, F.M. (2015) Detection and quantification of soybean and corn oils as adulterants in avocado oil using fourier transform mid infrared (FT-MIR) spectroscopy aided with multivariate calibration. *J. Teknol.*, **77** (1), 251–255.
60. Jiménez-Sotelo, P., Hernández-Martínez, M., Osorio-Revilla, G., Meza-Márquez, O.G., García-Ochoa, F., and Gallardo-Velázquez, T. (2016) Use of ATR-FTIR spectroscopy coupled with chemometrics for the authentication of avocado oil in ternary mixtures with sunflower and soybean oils. *Food Addit. Contam. - Part A*, **33** (7), 1105–1115.
61. Myshkin, N., and Kovalev, A. (2018) Adhesion and surface forces in polymer tribology—A review. *Friction*, **6** (2), 143–155.
62. Zhang, W., Xiao, H., and Qian, L. (2014) Enhanced water vapour barrier and grease resistance of paper bilayer-coated with chitosan and beeswax. *Carbohydr. Polym.*, **101** (1), 401–406.
63. Ren, K., Fei, T., Metzger, K., and Wang, T. (2019) Coating performance and rheological characteristics of novel soybean oil-based wax emulsions. *Ind. Crops Prod.*, **140** (July), 111654.
64. Liu, D., Duan, Y., Wang, S., Gong, M., and Dai, H. (2022) Improvement of Oil and Water Barrier Properties of Food Packaging Paper by Coating with Microcrystalline Wax Emulsion. *Polymers (Basel)*, **14** (9).
65. Alvarez, J.V.L., Larrucea, M.A., Bermúdez, P.A., and Chicote, B.L. (2009) Biodegradation of paper waste under controlled composting conditions. *Waste Manag.*, **29** (5), 1514–1519.
66. Venelampi, O., Weber, A., Rönkkö, T., and Itävaara, M. (2003) The biodegradation and disintegration of paper products in the composting environment. *Compost Sci. Util.*, **11** (3), 200–209.
67. Wu, C.S. (2012) Characterization and biodegradability of polyester bioplastic-based green renewable composites from agricultural residues. *Polym. Degrad. Stab.*, **97** (1), 64–71.
68. Ni, B., Liu, M., and Lü, S. (2009) Multifunctional slow-release urea fertilizer from ethylcellulose and superabsorbent coated formulations. *Chem. Eng. J.*, **155** (3), 892–898.
69. Duflos, M., Goutx, M., and Van Wambeke, F. (2009) Determination of lipid degradation by marine lipase-producing bacteria: Critical evaluation of lipase activity assays. *Lipids*, **44** (12), 1113–1124.
70. Asgher, M., Qamar, S.A., Bilal, M., and Iqbal, H.M.N. (2020) Bio-based active food packaging materials: Sustainable alternative to conventional petrochemical-based packaging materials. *Food Res. Int.*, **137** (July).

71. Navikaite-Snipaitiene, V., Ivanauskas, L., Jakstas, V., Rüegg, N., Rutkaite, R., Wolfram, E., and Yildirim, S. (2018) Development of antioxidant food packaging materials containing eugenol for extending display life of fresh beef. *Meat Sci.*, **145** (July 2017), 9–15.
72. Henry, G.E., Momin, R.A., Nair, M.G., and Dewitt, D.L. (2002) Antioxidant and cyclooxygenase activities of fatty acids found in food. *J. Agric. Food Chem.*, **50** (8), 2231–2234.
73. Wei, C.C., Yen, P.L., Chang, S.T., Cheng, P.L., Lo, Y.C., and Liao, V.H.C. (2016) Antioxidative activities of both oleic acid and *Camellia tenuifolia* seed oil are regulated by the transcription factor DAF-16/FOXO in *Caenorhabditis elegans*. *PLoS One*, **11** (6), 1–15.
74. Aindongo, W. V., Caleb, O.J., Mahajan, P. V., Manley, M., and Opara, U.L. (2014) Effects of storage conditions on transpiration rate of pomegranate aril-sacs and arils. *South African J. Plant Soil*, **31** (1), 7–11.
75. Bastarrachea, L., Dhawan, S., and Sablani, S.S. (2011) Engineering Properties of Polymeric-Based Antimicrobial Films for Food Packaging. *Food Eng. Rev.*, **3** (2), 79–93.
76. Moon, K.M., Kwon, E. Bin, Lee, B., and Kim, C.Y. (2020) Recent Trends in Controlling the Enzymatic Browning of Fruit and Vegetable Products. *Molecules*, **25** (12).

6. Concluding remarks and outlooks

Nowadays, bioplastics are becoming more prominent due to the depletion of oil resources, the increase in the cost of conventional fuel-based commodities and growing environmental concerns with the dumping of non-biodegradable plastics in landfills. The upcycling of food waste can create several opportunities to produce new valuable bioplastics, as an alternative to conventional petroleum-based plastics. Bioplastics produced from fruit and vegetable wastes are compatible with the “circular economy”, therefore achieving the “zero waste” objectives of this strategy. Moreover, they create positive synergies between industry and the agro-food sector, with considerable advantages for the environmental pollution. Currently, the fabrication of new eco-friendly materials from waste and not from specially grown crops, whose production comes at an environmental cost in terms of water and soil, is a real challenge since the attention must be placed on numerous variables, including the pre-treatment and the processing of the waste.

This thesis deals with the study of the use of food waste as a raw material for the fabrication of novel biomaterials with potential applications in the field of food packaging. In particular, wastes from different origins have been used, i.e. apple waste, tomato peels and avocado by-products, for two different purposes: the production of bio-composites and impregnated papers. The result was the preparation of materials with many properties complementary to those of common plastics. The inclusion of food waste, either without pre-treatment or with a preliminary extraction, enhanced the materials' hydrophobicity, that is a feature often difficult to satisfy for biomass-derived plastics. Moreover, it conferred antioxidant properties to the materials, making them suitable for active food packaging. Nowadays, oxidative degradation is the main reason of food spoilage after microbial growth, since oxidative reactions are responsible for decreasing the nutritional value of food caused by the degradation of essential fatty acids, proteins and lipid soluble vitamins, and producing off-flavours and odours. Furthermore, it also causes a colour change due to pigment degradation. Thus, a lot of interest has been placed on the development of bio-based plastics with antioxidant properties due to their ability to improve the stability of oxidation-sensitive food products, since it has proved that the advantage of enclosing antioxidants within the packaging material surpasses the beneficial of their direct inclusion in food formulations.

Some considerations need to be made on the mechanical properties of the fabricated materials. The lack of a pre-treatment step for apple waste and tomato peels resulted in a ductile and soft behaviour of the starch-polymeric matrix used for the production of bio-based composites, making them more suitable for covering applications than conventional containers or edible films. From this point, several ways are envisaged in order to optimize the protocols and methodologies used in this thesis.

For instance, a study of the effect of a preliminary dissolution of the biomass is advisable, since it could guarantee the formation of a better network of bonds between the matrix and the fillers. On the other hand, even the inclusion of an extract such as the one obtained from avocado by-products did not particularly affect the mechanical performances of the paper. In fact, the best yield stress and elongation at break values were given by the impregnation with ethyl cellulose. The impregnation turned out to be an excellent process to enhance paper durability, thus ensuring a long-term use. Together with ethyl cellulose, the avocado by-product extract improved the capacity of paper in serving as a barrier to water vapor, hence extending and maintaining the shelf-life of the packaged food. Starting from these results, a detailed economic analysis about the use of the impregnation process for the large-scale fabrication of antioxidant, biodegradable and hydrophobic materials is mandatory to evaluate its potential industrial application.

Publications

Articles

1. Onzo, A., Acquavia, M.A., Pascale, R., Iannece, P., Gaeta, C., Lelario, F., Ciriello, R., Tesoro, C., Bianco, G., Di Capua, A. (2022). Untargeted metabolomic analysis by ultra-high-resolution mass spectrometry for the profiling of new Italian wine varieties. *Analytical and Bioanalytical Chemistry*.
2. Tesoro, C., Lelario, F., Ciriello, R., Bianco, G., Di Capua, A., & Acquavia, M. A. (2022). An Overview of Methods for L-Dopa Extraction and Analytical Determination in Plant Matrices. *Separations*, 9(8), 224.
3. Onzo, A., Acquavia, M. A., Pascale, R., Iannece, P., Gaeta, C., Nagornov, K. O., & Bianco, G. (2021). Metabolic profiling of Peperoni di Senise PGI bell peppers with ultra-high resolution absorption mode Fourier transform ion cyclotron resonance mass spectrometry. *International Journal of Mass Spectrometry*, 470, 116722.
4. Pappalardo, I., Santarsiero, A., De Luca, M., Acquavia, M. A., Todisco, S., Caddeo, C., & Vassallo, A. (2021). Exploiting the Anti-Inflammatory Potential of White Capsicum Extract by the Nanoformulation in Phospholipid Vesicles. *Antioxidants*, 10(11), 1683.
5. Acquavia, M. A., Pascale, R., Pappalardo, I., Santarsiero, A., Martelli, G., & Bianco, G. (2021). Characterization of quercetin derivatives in crossing combination of habanero white and *Capsicum annum* peppers and of anti-inflammatory and cytotoxic activity. *Separations*, 8(7), 90.
6. Acquavia, M. A., Pascale, R., Foti, L., Carlucci, G., Scrano, L., Martelli, G., & Lelario, F. (2021). Analytical methods for extraction and identification of primary and secondary metabolites of apple (*Malus domestica*) fruits: A review. *Separations*, 8(7), 91.
7. Pascale, R., Acquavia, M. A., Onzo, A., Cataldi, T. R., Calvano, C. D., & Bianco, G. (2021). Analysis of surfactants by mass spectrometry: Coming to grips with their diversity. *Mass spectrometry reviews*.
8. Acquavia, M. A., Pascale, R., Martelli, G., Bondoni, M., & Bianco, G. (2021). Natural polymeric materials: A solution to plastic pollution from the agro-food sector. *Polymers*, 13(1), 158.
9. Onzo, A., Pascale, R., Acquavia, M. A., Cosma, P., Gubitosa, J., Gaeta, C., & Bianco, G. (2021). Untargeted analysis of pure snail slime and snail slime-induced Au nanoparticles metabolome with MALDI FT-ICR MS. *Journal of Mass Spectrometry*, 56(5), e4722.
10. Acquavia, M. A., Foti, L., Pascale, R., Nicolò, A., Brancaleone, V., Cataldi, T. R., Martelli, G., Scrano, L., & Bianco, G. (2020). Detection and quantification of Covid-19 antiviral drugs in biological fluids and tissues. *Talanta*, 121862.
11. Santarsiero, A., Onzo, A., Pascale, R., Acquavia, M. A., Coviello, M., Convertini, P., Todisco, S., Marsico, M., Pifano, C., Iannece, C., Gaeta, C., D'Angelo, S., Bianco, G., & Infantino, (2020). Pistacia lentiscus Hydrosol: Untargeted Metabolomic Analysis and Anti-Inflammatory Activity Mediated by NF- κ B and the Citrate Pathway. *Oxidative medicine and cellular longevity*, 2020.
12. Onzo, A., Acquavia, M. A., Cataldi, T. R., Ligonzo, M., Coviello, D., Pascale, R., Martelli, G., Bondoni, M., Scrano, L. & Bianco, G. (2020). Coceth sulfate characterization by electrospray ionization tandem mass spectrometry. *Rapid Communications in Mass*

Spectrometry, 34(20), e8884.

13. Pascale, R., Acquavia, M. A., Cataldi, T. R., Onzo, A., Coviello, D., Bufo, S. A., Scrano L., Ciriello R., Guerrieri A., & Bianco, G. (2020). Profiling of quercetin glycosides and acyl glycosides in sun-dried peperoni di Senise peppers (*Capsicum annum* L.) by a combination of LC-ESI (-)-MS/MS and polarity prediction in reversed-phase separations. *Analytical and Bioanalytical Chemistry*, 1-11.

Oral Communications

1. C. Tesoro, M. A. Acquavia, G. Bianco, R. Ciriello, F. Lelario, A. Di Capua “Liquid Chromatography/Electrospray Ionization with Multistage Mass Spectrometry for L-Dopa determination in food matrices” 7th Food Day, 5-7th, October 2022, Florence.
2. M.A. Acquavia, R. Pascale, A. Onzo, C. Gaeta, P. Iannece, R. Ciriello, F. Lelario, C. Tesoro, R. Rubino, G. Bianco “Raw materials in food manufacturing: a complexity ascertained by high-resolution mass spectrometry” Massa 2022, 20-22nd, June 2022 Carlentini (Sicily).
3. A. Onzo, M.A. Acquavia, R. Pascale, C. Tesoro, C. Gaeta, P. Iannece, R. Ciriello, F. Lelario, G. Bianco “HRMS-based metabolomic characterization of new Italian wine varieties” 4th MS Day 22-24th, June 2022 Carlentini (Sicily).
4. M.A. Acquavia, C. Tesoro, A. Capece, R. Pietrafesa, G. Alberico, B. Giussani, G. Mauriello, D. Maresca, G. Bianco “Influence of mixed starter cultures of *Hanseniaspora Osmophila* and *Saccharomyces cerevisiae* on wine flavor profile explored through HS-SPME/GC-MS” Congresso Nazionale della Società Chimica Italiana 14-23rd, September 2021.
5. R. Pascale, M. A. Acquavia, A. Onzo, P. Iannece, C. Gaeta, K. O. Nagornove, Y. O. Tsybin, G. Bianco “An interplay between FT-ICR MS and LC-LTQ MS/MS for Metabolic Profiling of Peperoni di Senise PGI Bell Peppers” Congresso Nazionale della Società Chimica Italiana 14-23rd, September 2021.
6. M.A. Acquavia, R. Pascale, C. Caddeo, A. Zizzamia, G. Martelli, G. Bianco, A. Vassallo “Characterization of quercetin derivatives in a crossing combination of Habanero white and *Capsicum annum* peppers and evaluation of the encapsulation efficiency of peppers extract in liposomes by LC-MS/MS” 9th MS J-day, I giovani e la spettrometria di Massa”, 2ND ONLINE EDITION – 24th, June 2021.
7. M. A. Acquavia, A. Onzo, T.R.I Cataldi, M. Ligonzo, D. Coviello, R. Pascale, G. Martelli, M. Bondoni, L. Scrano, G. Bianco. “Structural investigations on “green” alkyl ether sulfates by direct injection mass spectrometry”. MASSA 2020- VIP (Virtual International Pre-Congress). 13rd, September 2020.
8. M. A. Acquavia, R. Pascale, T. R. I. Cataldi, A. Onzo, D. Coviello, S. A. Bufo, L. Scrano, R. Ciriello, A. Guerrieri, G. Bianco. “QUEdb: a new comprehensive database of quercetin glycosides and acyl-glycosides derivatives”. Banche Dati tools informatici in Spettrometria di massa. 11th, December 2019, Roma.

Attended Workshops and Schools

Workshops

- *Massa 2022*, 20-22nd, June 2022 Carlentini (Sicily, Italy).
- *4th MS Day*, 22-24th, June 2022 Carlentini (Sicily, Italy).
- *Storie di spettrometria di massa*, online, 18th, May 2018.
- *L'accreditamento: competenza tecnica e assicurazione qualità del dato*, Potenza (Italy), 11th, May 2022.
- *Le indagini forensi ed il contributo della spettrometria di massa*, online, 25th, March 2022.
- *Congresso Nazionale della Società Chimica Italiana*, online, 14-23rd, September 2021.
- Member of the organizing committee for the *9th MS J-day, I giovani e la spettrometria di Massa*, Teramo (Italy), 24th, June 2021.
- *MASSA 2020- VIP (Virtual International Pre-Congress)*, online, 13rd, September 2020.
- *50 anni dalle prime banche dati: Banche dati e tools informatici in spettrometria di massa*, Roma (Italy), 11th, December 2019.

Schools

- *25° CORSO DI SPETTROMETRIA DI MASSA*, Pontignano (Italy), 27th September-1st October 2021.
- *Bioeconomy: wood and food value chain partnerships, Ticass srl and Univesity of Genoa under the European Project FORCE Cities cooperating for circular economy*. 16-20th November 2020.
- *Green Jobs-Gestire i rifiuti tra legge e tecnica*, CONAI (Italy), 22nd June-17th July 2020.

Acknowledgements

I would like to express my sincere gratitude to my supervisor Prof. Giuliana Bianco for giving me the opportunity to work within her research group, and for all the invaluable advices and suggestions provided during my PhD research. I would also like to thank my co-tutor Prof. Giuseppe Martelli for all the time spent supporting my research activity.

A deep and sincere thanks is for my co-tutor Dr. Alejandro Heredia-Guerrero, for his immense knowledge and plentiful experience that he made available to me and for offering me the opportunity to work with his research group at the IHSM-CSIC in Malaga.

A special thanks is for Dr. Susana Guzman Puyol, for her kind help and professional support during my staying abroad.

Thanks to Dr. Bruno Torresan and Dr. Marcella Bondoni, who funded this PhD scholarship. Moreover, I would like to thank the Mass Spectrometry Lab at the Pharmacy Department of University of Salerno, where the LC-MS/MS analysis were conducted, under the supervision of Prof. Paola Montoro, and the Institute of Materials Science of Seville and the Department of Inorganic Chemistry of the University of Malaga where the mechanical tests and the TGA analysis were carried out.

Finally, I would like to thank all the professors, researchers, technicians and colleagues I had the pleasure of working with and collaborating with during these three years.



Profiling of quercetin glycosides and acyl glycosides in sun-dried peperoni di Senise peppers (*Capsicum annuum* L.) by a combination of LC-ESI(-)-MS/MS and polarity prediction in reversed-phase separations

Raffaella Pascale¹ · Maria A. Acquavia^{1,2} · Tommaso R. I. Cataldi³ · Alberto Onzo¹ · Donatella Coviello¹ · Sabino A. Bufo^{1,4} · Laura Scrano⁵ · Rosanna Ciriello¹ · Antonio Guerrieri¹ · Giuliana Bianco¹

Received: 28 January 2020 / Revised: 19 February 2020 / Accepted: 25 February 2020 / Published online: 25 March 2020
© Springer-Verlag GmbH Germany, part of Springer Nature 2020

Abstract

Interest in targeted profiling of quercetin glycoconjugates occurring in edible foodstuffs continues to expand because of their recognized beneficial health effects. Quercetin derivatives encompass several thousands of chemically distinguishable compounds, among which there are several compounds with different glycosylations and acylations. Since reference standards and dedicated databases are not available, the mass spectrometric identification of quercetin glycoconjugates is challenging. A targeted liquid chromatography (LC) coupled with tandem mass spectrometry (MS/MS) was applied for screening quercetin glycoconjugates in edible peperoni di Senise peppers (*Capsicum annuum* L.), protected by the European Union with the mark PGI (i.e., Protected Geographical Indication), and cultivated in Basilicata (Southern Italy). Chromatographic separation was accomplished by reversed-phase liquid chromatography (RPLC) using water/acetonitrile as the mobile phase and detection was performed on a linear ion trap mass spectrometer fitted with an electrospray ionization (ESI) source operating in negative ion mode. A correlation between experimental RP chromatographic retention time and those predicted by partition coefficients ($\log P$) along with MS/MS data and an in-house developed database (named QUEdb) provided deep coverage for sixteen quercetin glycoconjugates. Among them, eleven quercetin glycoconjugates were already described in the literature and five were reported for the first time. These last acyl glycosidic quercetin derivatives were tentatively identified as quercetin-(galloyl-rhamnoside)-hexoside, $[C_{34}H_{33}O_{20}]^-$ at m/z 761.1; quercetin-(sinapoyl-hexoside)-rhamnoside, $[C_{38}H_{39}O_{20}]^-$ at m/z 815.4; quercetin-(galloyl-caffeoyl-hexoside)-rhamnoside, $[C_{43}H_{39}O_{23}]^-$ at m/z 923.0; quercetin-(feruloyl-hexoside)-rhamnoside, $[C_{37}H_{37}O_{19}]^-$ at m/z 785.1; and quercetin-(succinyl-rhamnoside)-rhamnoside, $[C_{31}H_{33}O_{18}]^-$ at m/z 693.1.

Keywords Quercetin derivatives · Database · Peperoni di Senise · Mass spectrometry · RP polarity prediction

Raffaella Pascale and Maria A. Acquavia contributed equally to this work.

Electronic supplementary material The online version of this article (<https://doi.org/10.1007/s00216-020-02547-2>) contains supplementary material, which is available to authorized users.

✉ Giuliana Bianco
giuliana.bianco@unibas.it

¹ Dipartimento di Scienze, Università degli Studi della Basilicata, Via dell'Ateneo Lucano, 10, 85100 Potenza, Italy

² ALMAGISI s.r.l., via Al Boschetto 4B, 39100 Bolzano, Italy

³ Dipartimento di Chimica, Università degli Studi di Bari Aldo Moro, via E. Orabona 4, 70126 Bari, Italy

⁴ Department of Geography, Environmental Management & Energy Studies, University of Johannesburg, Johannesburg, South Africa

⁵ Dipartimento delle Culture Europee e del Mediterraneo: Arch., Ambiente, Patrimoni Culturali, Università degli Studi della Basilicata, Via del Castello, 75100 Matera, Italy

Introduction

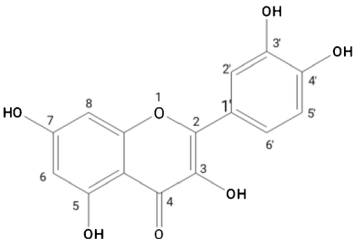
Quercetin ($C_{15}H_{10}O_7$, 3,3',4',5,7-pentahydroxyl-flavone) is a flavonol belonging to a class of plant secondary metabolites known as flavonoids. It is recognized for its potent antioxidant activity due to the ability to remove highly reactive oxygen species and to modulate cell apoptosis along with migration and growth via various signaling pathways [1]. Recently, its anti-cancer activity has been extensively explored, revealing its anti-proliferative effect on different cancer cell lines, both in vitro and in vivo [2]. In plants and plant-derived foods, quercetin mostly occurs in the forms of glycoconjugates, meaning that the –OH groups of the flavonoid aglycone at 3, 3', 4', 5, and 7 positions could be substituted by glucose, galactose, rhamnose, arabinose, xylose, or apiose [3]. Moreover, glycosylation may occur at multiple sites along with monosaccharide acylation with aliphatic acids (e.g., acetic, malonic, succinic, and 2-hydroxypropionic acids), and/or aromatic acids (e.g., benzoic, gallic, caffeic, and ferulic acids) [3]. Thus, the acyl glyconjugation of quercetin gives rise to a great number of chemically distinguishable compounds (Table 1) with different biological functions and substrate specificity of an endogenous acyl transferase [8].

Quercetin derivatives after ingestion are transported into the gastrointestinal tract, where they are hydrolyzed to their aglycone, which is absorbed and metabolized [9]. Typically, glycosylation and acyl glycosylation increase the polarity of quercetin derivatives and their biological activity. The content and form of all quercetin derivatives in edible foodstuffs strongly affect their bioavailability as well and there is the need to characterize the molecular structure of these compounds. Although several techniques have been used in the field of food and vegetables [10], nuclear magnetic resonance spectroscopy (NMR), liquid chromatography coupled with mass spectrometry (LC-MS), or tandem mass spectrometry (LC-MS/MS) and combination of them have been the most common techniques

used in natural products research [11–15]. Despite NMR spectroscopy has allowed the unambiguous identification of glycosylation and acylation positions of isomeric compounds, it is more time consuming and much less sensitive compared with LC-MS/MS, which is playing an important role in the research and identification of different classes of metabolites [16, 17] among which are polyphenols [18]. Tandem mass spectrometry allows not only the determination of this family of compounds but also the molecular characterization of new polyphenols [18], especially for relatively complex samples, such as plant-derived foodstuffs. To date, only about 130 quercetin glycosides have been identified by NMR and LC-MS/MS [19]. In addition, the structure modification of flavonoids can occur in soil and during food fermentation processes, leading to a high degree of variety of derivate compounds and the need of a dedicated database containing all chemical structures. Although there is a remarkable number of freely available software for protein identification [20, 21], the same is not true in metabolomics and especially in the field of polyphenols and flavonoids. Indeed, all freely available spectral libraries such as USDA Database for the Flavonoid Content of Selected Foods [22], PhytoHub [23], MassBank [24], Phenol-Explorer [25], FlavonoidSearch [26], and FooDB [19] allow identification of a large number of molecules from MS/MS data, but lack information on closely related quercetin compounds. Recently, Cerrato et al. [27] implemented a spectral database of flavonoid derivatives, considering the combination with two or three sugar moieties and one acid moiety. However, for quercetin derivatives, a higher number of substituents should be considered.

To allow a targeted profiling of quercetin derivatives in plant and plant-derived food matrices, a database of putative quercetin glycosides with their monoisotopic mass (M) for a wider use in MS (i.e., high- and low-resolution MS instruments) was created based on flavonoid biosynthetic pathways and substituents on the aglycone –OH moieties, including for the first time four possible sugar substituents and two acyl ones. Reversed-

Table 1 Monoisotopic mass (M) of quercetin aglycone and typical substituents as reported in literature [4–7]

Quercetin aglycone	Glycosylation		O-acylations			
	Name	$M-H_2O$	Name	$M-H_2O$	Name	$M-H_2O$
 $C_{15}H_{10}O_7$ M 302.04265	Glucose/galactose	$C_6H_{10}O_5$ 162.05282	Acetyl	C_2H_2O 42.01056	Galloyl	$C_7H_4O_4$ 152.01096
	Rhamnose	$C_6H_{10}O_4$ 146.05791	Malonyl	$C_3H_2O_3$ 86.00039	Caffeoyl	$C_9H_6O_3$ 162.03169
	Xylose/arabinose/apiose	$C_5H_8O_4$ 132.04226	Succinyl	$C_4H_4O_3$ 100.01604	Feruloyl	$C_{10}H_8O_3$ 176.04734
			2-hydroxy-propionyl	$C_3H_4O_2$ 72.02113	Coumaroyl	$C_9H_6O_2$ 146.03678
	Glucuronic acid	$C_6H_8O_6$ 176.03209	Benzoyl	$C_7H_4O_1$ 104.02621	Sinapoyl	$C_{11}H_{10}O_4$ 206.05791

phase liquid chromatography (RPLC) coupled with online tandem mass spectrometry by collision-induced dissociation (CID) (HPLC-MS/MS) and electrospray ionization (ESI) source, operated in negative mode, was used to examine quercetin glycosides and acyl glycosides naturally occurring in methanolic extracts of red *peperoni di Senise* pepper fruits (*Capsicum annuum* L.). These sun-dried peppers are cultivated in Basilicata (Southern Italy) and protected by the European Union (Commission Regulation (EC) No. 1263/96) with the mark PGI (for “Protected Geographical Indication”), for their traditional manufacturing process. The search for targeted quercetin derivatives was based on the chromatographic profile of the sample extract by using the home-made database of m/z values, followed by MS/MS data confirmation and RP retention time correlation predicted by $\log P$ values (octanol-water partition coefficients) of putative structures [28].

Materials and methods

Reagents and chemicals

Acetonitrile and methanol (LC-MS grade) were purchased from Sigma-Aldrich (Schnellendorf, Germany). Analytical standards ($\geq 95\%$) of quercetin, quercetin 7-glucoside, and quercetin 7-rhamnoside were obtained from Sigma-Aldrich (Milano, Italy). Analytical standards ($\geq 98\%$) of isorhamnetin 3-O- β -D-glucoside and quercetin 3-O-rutinoside were purchased from ChemFaces (China). Ultra-pure water was produced using a Milli-Q RG system from Millipore (Bedford, MA, USA). Pure nitrogen (99.996%) was delivered to the LC-MS system as sheath gas. The ion trap pressure was maintained with helium 99.999%, which was used for trapping and collisional activation of the trapped ions.

Plant material and sample preparation

Sun-dried peppers (*Capsicum annuum* L.) were cultivated in small farms located in Senise village in Basilicata (Southern Italy). They were sun-dried, according to the IGP production specification. All samples were provided, as spans of 1.5–2 m length, by the Agency for Development and Innovation in Agriculture (ALSIA, Agenzia Lucana di Sviluppo e di Innovazione in Agricoltura). The extraction procedure of quercetin derivatives from peppers was adapted from Wahyuni et al. [29] with slight modifications. Briefly, the freeze-dried sample (0.5 g) was extracted with 1.5 ml of MeOH and sonicated for 15 min at room temperature (Sonorex Super RK 100/H sonicator; Bandelin electronic, Berlin, Germany) with a 35-kHz automatic frequency control and a high-frequency power of 80 W. Then, the supernatant was filtered through 0.20- μ m nylon filters (Whatman, Maidstone, UK) and injected into the LC-MS system.

LC-ESI(-)-MS and MS/MS analysis

A volume of 25 μ L of the methanolic pepper extract was analyzed using an HPLC system coupled to a linear trap quadrupole (LTQ) mass spectrometer (Thermo Fisher Scientific, Bremen, Germany). The separation was achieved on a 150 \times 4.6 mm i.d., 3.0 μ m, 100 Å reversed-phase Luna C18 (2) (Phenomenex, Torrance, CA, USA) with water (A) and acetonitrile (B), as the mobile phases. The linear gradient started with A 100% reaching 70% in 15 min, 65% in 25 min, hold for 5 min, 60% at 40 min, and 15% after 50 min. Finally, the column was reconditioned for 10 min. The flow rate of 0.8 mL/min was post-column splitted 4:1 to allow 200 μ L/min to enter the ESI source. Negative ion ESI-MS was chosen for the detection of quercetin derivatives, since it resulted more sensitive for analysis of flavonoids [30]. The source voltage was set to 4.5 kV, the temperature of the heated capillary was set to 350 °C, the capillary voltage was set to -45 V, and the tube lens' voltage was set to -75 V. The sheath gas (N_2) flow rate was 5 arbitrary units (a.u). Full-scan MS experiments were performed in the LTQ in the range m/z 100–1500. For all masses listed in in-house database, mass spectra were displayed as eXtracted ion currents (XICs) and ions found in pepper extract were selected for MS² experiments by collision-induced dissociation (CID). Collision energy was optimized for each precursor ion, between 18% and 23% of the normalized collision energy (NCE). The fragmentation nomenclatures of Ma et al. [31] and Domon and Costello [32] were employed for quercetin aglycone and quercetin glycoconjugates; ions k^lX_j , Y_{nj} , and Z_{nj} represent those fragments still containing the flavonoid aglycone, where “j” is the number of the interglycosidic bond broken, counted from the aglycone, “n” represents the position of the phenolic hydroxyl, where the oligosaccharide is attached, and “k” and “l” denote the cleavage within the carbohydrate rings. While “X” is used to designate sugar fragmentations, “Y” and “Z” are used for fragment ions obtained, respectively, after the cleavage of the glycosidic bond without or with the concurrent loss of a H₂O molecule. All MS and MS/MS experiments were achieved under automatic gain control (AGC) conditions, using helium as damping and collision gas as well, and were performed in five replicates. The data were acquired and analyzed using the Xcalibur software package (version 2.0 SR1 Thermo Electron). The chromatographic raw data were imported, elaborated, and plotted by SigmaPlot 11.0 (Systat Software, London, UK).

Database construction and statistics

The dedicated database, named QUEdb, was built on excel sheet (Excel 2013, Microsoft Office) and exported to word document (Word 2013, Microsoft Office). $\log P$ calculations were performed by ChemDraw Pro 8.0 (CambridgeSoft

Corporation). Model computation was performed using R software (<https://www.r-project.org/>).

Results and discussion

Construction of a QUercetin DataBase

Although there are several database containing LC-ESI-MS/MS data about flavonoids, there is a lack of information about the most of the quercetin derivatives, making difficult their identification in complex matrices [4]. In addition, among available database [19, 22–26], information concerning all supposed quercetin derivative compounds that might be hypothetically biosynthesized is still missing. To enable the study of quercetin derivatives, a rationale database gathering all molecular structure information would be useful. To achieve this goal, we developed a home-made database, named QUercetin DataBase (QUEdb), which contains all the putative quercetin glycosidic and acyl glycosidic derivatives (vide infra) with their corresponding monoisotopic mass (M) values, by using most common pentoses and hexoses, also including acyl substituents as described in literature [4] (Table 1).

QUEdb is an Excel datasheet built on by combining the quercetin aglycone (M 302.04265) with glucose/galactose (Hex, [M-H₂O] 162.05282), rhamnose (Rha, [M-H₂O] 146.05791), arabinose/xylose (Pent, [M-H₂O] 132.04266) or apiose (Api, [M-H₂O] 132.04266), and glucuronic acid (Glc, [M-H₂O] 176.03209) up to four glycosylation bonds [4, 5]. Then, the acyl glycosidic derivatives were obtained by combining each of 70 glycosylated derivatives with the acyl substituents known in literature, viz. acetyl (Ac, [M-H₂O] 42.01056), malonyl (Mal, [M-H₂O] 86.00039), succinyl (Succ, [M-H₂O] 100.01604), 2-hydroxy-propionyl (2-Idrp, [M-H₂O] 72.02113), benzoyl (Benz, [M-H₂O] 104.02621), galloyl (Gall, [M-H₂O] 152.01096), caffeoyl (Caff, [M-H₂O] 162.03169), feruloyl (Fer, [M-H₂O] 176.04734), coumaroyl (Cum, [M-H₂O] 146.03678), and sinapoyl (Sin, [M-H₂O] 206.05791) up to two acylations [5–7]. Up to 5016 putative quercetin derivatives were systematically annotated; an electronic form of QUEdb is provided as Electronic Supplementary Material (ESM) for use in mass spectrometry (ESM Tables S1–S12).

The identification strategy of quercetin derivatives in sample extracts of sun-dried peppers

In this work, the characterization of naturally occurring quercetin glycosides and acyl glycosides in methanolic extracts of sun-dried *peperoni di Senise* peppers is described. To our purpose, reversed-phase liquid chromatography coupled to ESI-MS and tandem mass spectrometry (MS/MS), performed by

CID, was used. Identification of quercetin glycosides and acyl glycosides in foodstuffs is often a difficult task because of the lack of both standard compounds and dedicated databases. To address this issue, a quercetin database, as mentioned earlier, was developed (Fig. 1).

The first step of identification was based on the generation of a list of candidates by extracted ion currents (XICs) with a mass-to-charge ratio window of ± 0.1 units around each targeted deprotonated molecule (i.e., [M-H]⁻ ± 0.1 Da) using the home-made database. Since several derivatives (up to 22 candidates) could correspond to a given nominal mass value listed in the QUEdb, and the mass accuracy of a linear trap quadrupole is not enough to unequivocally determine the elemental composition belonging to a *m/z* signal, MS/MS experiments were of crucial importance. CID tandem mass spectra were used to discriminate between candidates, allowing to reduce the numbers of potential candidates up to a maximum of seven. Due to the use of a low-resolution mass analyzer (LTQ), there was no way to distinguish between candidates having substituents with the same nominal mass values (i.e., rhamnosyl and coumaroyl or hexosyl and caffeoyl, Table 1). For this reason, a correlation between reversed-phase (RP) retention times and *log P* values was introduced. As previously reported [33], retention times (RT) are related to *log P* values of each analyte and a polarity prediction is possible starting from experimental retention times. Notice that within the same polyphenol class, the chemical feature and number of glycosylations affect the reversed-phase chromatographic behavior by decreasing the retention time compared with the

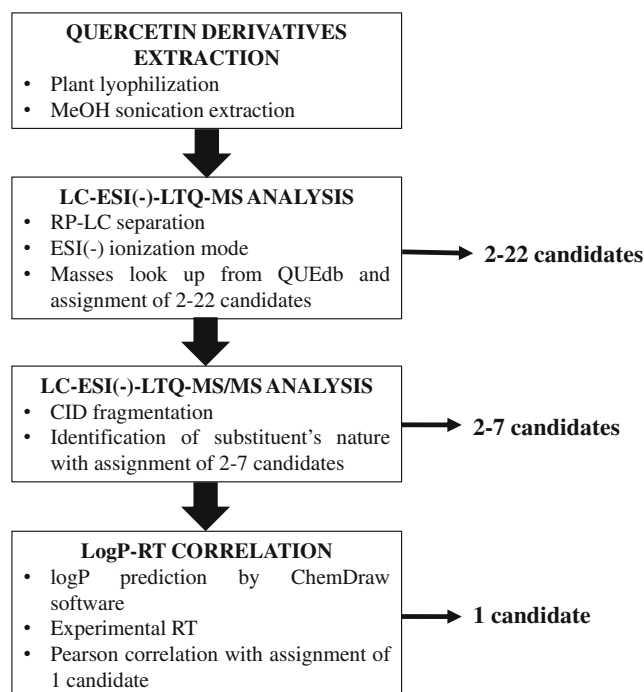


Fig. 1 Identification strategy of quercetin derivatives in sample extracts of sun-dried peppers

Table 2 Glycosylated quercetins occurring in extract of *peperoni di Senise* peppers (*Capsicum annuum* L.) identified by LC-ESI-MS/MS also exploiting the correlation between observed retention times and calculated $\log P$ values

Peak no.	RT (min)	Compound ^a	Substituents ^b	$\log P^c$	Molecular formula	m/z [M-H] ⁻	CID (% NCE)	MS/MS fragment ions ^d m/z [M-H] ⁻
Q1	10.6	Quercetin-6-C-hexoside-8-C-pentoside/apioside	Hex Pent/Api	-2.84	C ₂₆ H ₃₈ O ₁₆	595.1	18%	577.1 ([M-H ₂ O] ⁻), 505.0 ([M- ^{0,2} X _{Pent/Api}] ⁻), 487.1 ([M- ^{0,2} X _{Pent/Api} -H ₂ O] ⁻), 475.0 ([M- ^{0,1} X _{Pent/Api}] ⁻), 457.1 ([M- ^{0,1} X _{Pent/Api} -H ₂ O] ⁻), 415.0 ([M- ^{0,1} X _{Api} - ^{0,2} X _{Pent/Api}] ⁻), 385.0 ([M- ^{0,1} X _{Api} - ^{0,3} X _{Hex}] ⁻), 355.0 ([M- ^{0,1} X _{Pent/Api} - ^{0,2} X _{Hex}] ⁻), 300.9 ([M- ^{0,1} X _{Pent/Api} - ^{0,2} X _{Hex}] ⁻), 519.0 ([M- ^{0,3} X _{Hex}] ⁻), 489.0 ([M- ^{0,2} X _{Hex}] ⁻), 463.0 ([M-Rha] ⁻), 447.1 ([M-Hex] ⁻), 301.0 ([M-Rha] ⁻), 463.0 ([M-Rha-Pent/Api] ⁻), 300.9
Q2	11.6	Quercetin-4'-rhamnoside-7-hexoside	Rha	-2.47	C ₂₇ H ₃₀ O ₁₆	609.1	18%	
Q3	11.7	Quercetin-3-O-pentosyl/apiosyl rhamnosyl-hexoside	Hex Rha Pent/Api	-3.48	C ₃₂ H ₃₈ O ₂₀	741.2	19%	
Q4	12.3	Quercetin 7-O-pentoside/apioside	Pent/Api	-1.00	C ₂₀ H ₁₈ O ₁₁	433.1	18%	301.0 ([M-Pent/Api] ⁻)
Q5	13.0	Isorhamnetin-3-O-glucoside	Me	-1.13	C ₂₂ H ₂₂ O ₁₂	477.2	18%	459.1 ([M-H ₂ O] ⁻), 357.0 ([M- ^{0,2} X _{Hex}] ⁻), 315.0 ([M-Hex] ⁻), 301.0
Q6	14.4	Quercetin-3-O-rhamnoside-7-O-hexoside	Rha	-2.38	C ₂₇ H ₃₀ O ₁₆	609.0	18%	519.0 ([M- ^{0,3} X _{Hex}] ⁻), 489.0 ([M- ^{0,2} X _{Hex}] ⁻), 463.0 ([M-Rha] ⁻), 447.1 ([M-Hex] ⁻), 301.0
Q7	14.5	Quercetin-7-O-(acetyl-hexoside)-3-O-rhamnoside	Hex-Ac Rha	-2.05	C ₂₉ H ₃₂ O ₁₇	651.1	18%	505.0 ([M-Rha] ⁻), 447.0 ([M-Hex-Ac] ⁻), 300.9
Q8	14.9	Quercetin (galloyl-rhamnoside)-hexoside	Rha-Gall Hex	-1.47	C ₃₄ H ₃₄ O ₂₀	761.1	20%	743.1 ([M-H ₂ O] ⁻), 729.1 ([M-CH ₃ OH] ⁻), 717.3 ([M-CO ₂] ⁻), 681.1 ([M- ^{0,4} X _{Rha} -2H ₂ O] ⁻), 614.9 ([M- ^{0,4} X _{Rha} - ^{2,3} X _{Hex} -4H ₂ O] ⁻), 599.1 ([M-Hex] ⁻), 447.1 ([M-Hex-Gall] ⁻), 300.9
Q9	15.5	Quercetin 7-O-glucoside	Hex	-1.44	C ₂₁ H ₂₀ O ₁₂	463.0	18%	301.0 ([M-Hex] ⁻)
Q10	15.8	Quercetin-3-O-rutinose	Hex Rha	-2.28	C ₂₇ H ₃₀ O ₁₆	609.0	18%	447.0 ([M-Hex] ⁻), 301.0 ([M-Hex-Rha] ⁻)
Q11	16.5	Quercetin 7-O-rhamnoside	Rha	-0.59	C ₃₁ H ₃₀ O ₁₁	447.1	18%	300.9 ([M-Rha] ⁻)
Q12	16.7	Quercetin rhamnoside (sinapoyl-hexoside)	Rha	-0.60	C ₃₈ H ₄₀ O ₂₀	815.4	20%	669.0 ([M-Rha] ⁻), 447.0 ([M-Hex-Sin] ⁻), 300.9
Q13	17.1	Quercetin rhamnoside-(galloyl-caffeoyl-hexoside)	Hex-Sin Rha Caff-Hex-Gall	-0.58	C ₄₃ H ₄₀ O ₂₃	923.0	21%	843.1 ([M- ^{0,4} X _{Rha}] ⁻), 777.0 ([M-Rha] ⁻), 447.0, 300.9
Q14	17.1	Quercetin rhamnoside-(feruloyl-hexoside)	Rha	-0.47	C ₃₇ H ₃₈ O ₁₉	785.1	20%	639.0 ([M- ^{2,3} X _{Hex} - ^{0,4} X _{Rha} -4H ₂ O] ⁻), 447.0 ([M-Hex-Fer] ⁻), 323.0, 314.9, 300.9
Q15	17.6	Dimethylquercetin-3-O-dihexoside	Hex-Fer Me	-0.67	C ₂₉ H ₃₄ O ₁₇	653.2	18%	635.1 ([M-H ₂ O] ⁻), 507.1, 491.1 ([M-Hex] ⁻), 449.0, 403.0, 359.0, 345.0, 329.0 ([M-Hex] ⁻), 315.0, 301.0
Q16	17.7	Quercetin rhamnoside-(succinyl-rhamnoside)	Hex Rha	+0.23	C ₃₁ H ₃₄ O ₁₈	693.1	18%	547.0 ([M-Rha] ⁻), 447.0 ([M-Rha-Succ] ⁻), 300.9
Qsid	25.7	Quercetin	Rha-Succ /	+0.35	C ₁₅ H ₁₀ O ₇	301.0	30%	272.9 ([M-CO] ⁻), 256.9 ([M-CO ₂] ⁻), 228.9 ([M-CO-CO ₂] ⁻), 192.8, 178.8 (^{1,2} A), 150.8 (^{1,2} A-CO), 120.8 (^{1,2} B), 106.7 (^{1,2} A-CO-CO ₂)

^a Nomenclature according to IUPAC Recommendations 2017 for flavonoids [41]

^b Hex, hexose (glucose or galactose); Pent, pentose (xylose or arabinose); Api, apiose; Rha, rhamnose; Me, methyl; Ac, acetyl; Succ, succinyl; Gall, galloyl; Sin, sinapoyl; Caff, caffeoyl; Fer, feruloyl

^c $\log P$ values calculated by ChemDraw Pro 8.0 (CambridgeSoft Corporation)

^d The ions obtained after sugar moiety fragmentation or aglycone fragmentation are designed according the nomenclature proposed, respectively, by Domon and Costello [32] and Ma et al. [31]

corresponding aglycone molecule. Conversely, the acyl glycosylation leads to an increase of the retention times compared with those with non-acylated sugars. Theoretical $\log P$ values were calculated as preferred to experimental ones because of the lack of reliable data [33].

Thus, a discrimination between putative quercetin derivatives differing only for the nature of their substituents, but having the same nominal mass values, was made by using a model in which $\log P$ values of standard compounds have been correlated to their experimental retention times (see ESM Fig. S4). Such a model was useful to predict retention time values of possible candidates and thus select the correct ones. Experimental RTs and $\log P$ values of standard quercetin derivatives were found to follow a cubic relationship, as expected since it is known that lipophilicity is not linearly related to retention time [34]. According to the obtained model, RTs seem to increase dramatically after $\log P = -1.00$ (see ESM Fig. S4). Seen that, in this work, each putative quercetin derivative shows a lower experimental RT than quercetin standard ($\log P = +0.35$, RT = 25.7 min), this observation is sufficient to exclude all candidates with a $\log P$ value higher than +0.35. However, the obtained model was unsuccessful to identify positional isomers since no significant difference between predicted retention time values was observed. Therefore, when possible, glycosylation positions were tentatively proposed by ion product intensities of MS/MS spectra since, as reported in literature, the glycosylation position significantly affects the fragmentation behavior of flavonoid O-glycosides, including the relative abundances of radical aglycone ions $[Y_0-H]^-$, which are most pronounced for flavonol 3-O-glycosides [35].

With regard C-glycosides, 6-C-glycosides usually undergo a more extended fragmentation compared with 8-C-glycosides, and the former are typically associated with an abundant $^{0,3}X^-$ ion, while for the latter, no typical product ions have been ascertained with a low abundance of the $^{0,3}X^-$ ion [5].

An unprecedented insight into the nature of quercetin derivatives of the sun-dried pepper samples was gained by this combination of data.

RPLC-ESI(-)-MS and MS/MS analysis and $\log P$ -RT correlation

Poor profiles of polyphenols in peppers have usually been reported in literature [36–38], no one focusing on quercetin derivatives. Here, all quercetin derivatives identified were eluted within 25 min of chromatographic run without mobile phase additives because ion suppression was the most relevant effect when attempts to improve the chromatographic peak shape by addition of organic acids, salts, ion-pairing agents, and buffers were made [39]. Identification of quercetin derivatives was accomplished by CID fragmentation using a linear ion trap MS instrument. Besides, the application of a

regression model which correlates experimental retention times of standard quercetin derivatives with their $\log P$ values provided a possible approach useful for the identification of putative quercetin glycosides and acyl glycosides with the same nominal mass. In the sample extract of red peppers, twenty-three flavonoid derivatives were identified. Among them, MS/MS analysis of 16 chromatographic peaks showed a product ion at m/z 301, corresponding to aglycone fragment, $Y_0^- = [C_{15}H_9O_7]^-$, thus suggesting the presence of the quercetin core, in agreement with data reported by Fabre et al. [30].

Among 16 quercetin derivatives, eleven compounds (Table 2, Q1, Q2, Q3, Q4, Q5, Q6, Q7, Q9, Q10, Q11, and Q15) were already described in literature. The corresponding MS/MS spectra (see ESM Fig. S1) allowed to identify the glycan moiety. In detail, three quercetin monosaccharides

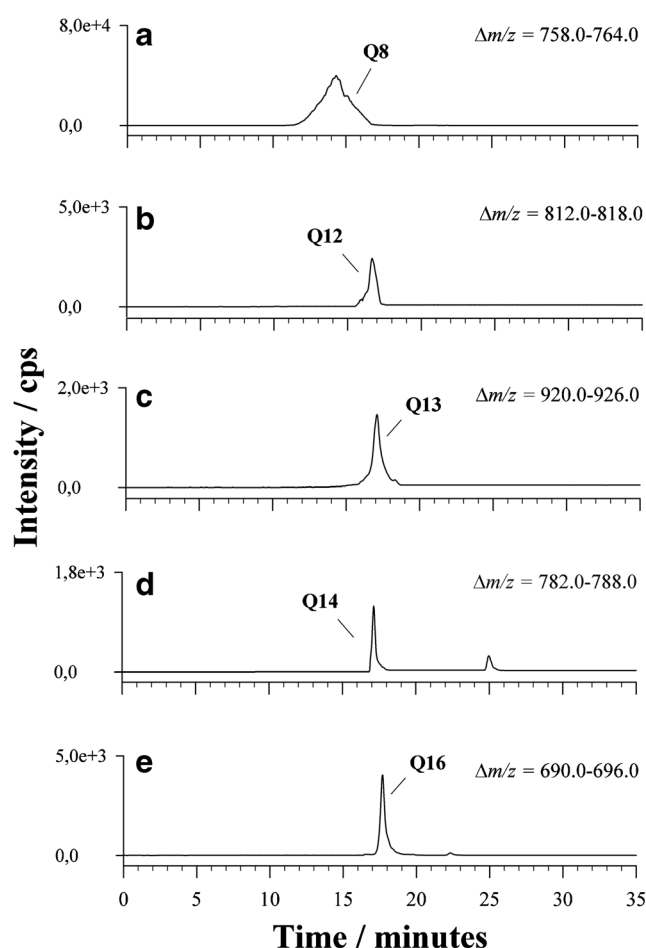


Fig. 2 Extracted ion current (XIC) chromatograms by LC-ESI-MS acquired in negative ion mode of five new quercetin glycosidic derivatives found in a methanolic extract of *peperoni di Senise* peppers (*Capsicum annuum* L.). The monitored ions are displayed in each plot a–e and correspond to the most deprotonated molecules $[M-H]^-$ using a window of ± 6.0 m/z unit centered around each selected value. Peak numbers correspond to **a** quercetin-(galloyl-rhamnoside)-hexoside, **b** quercetin-rhamnoside-(sinapoyl-hexoside), **c** quercetin-rhamnoside-(galloyl-caffeoyl-hexoside), **d** quercetin-rhamnoside-(feruloyl-hexoside), and **e** quercetin-rhamnoside-(succinyl-rhamnoside)

(Table 2, Q4, Q9, and Q11) were identified, as quercetin 7-O-pentoside/apioside at m/z 433.1 (Q4, $[C_{20}H_{17}O_{11}]^-$), quercetin 7-O-glucoside at m/z 463.0 (Q9, $[C_{21}H_{19}O_{12}]^-$), and quercetin 7-O-rhamnoside at m/z 447.1 (Q11, $[C_{21}H_{19}O_{11}]^-$) by Y_0 neutral losses of the apiose/pentose (-132), glucose (-162), and rhamnose (-146) units (see Table 1), respectively. The 7-glycosylation position was determined by the most abundant Y_0^- ion (m/z 301.0) compared with the radical aglycone ion $[Y_0-H]^-$ (m/z 300.0, see ESM Fig. S3), as typical MS² fragmentation behavior of flavonoid 7-O-glycosides, instead of 3-O-glycosides [35]. Then, the aglycone features as quercetin were confirmed by MS³ experiments. In addition, for derivatives Q9 and Q11, their identification was confirmed respectively through LC-MS analysis of quercetin 7-O-glucoside standard and quercetin 7-O-rhamnoside standard (see ESM Fig. S2). It is worth mentioning that Q1, Q2, Q6, and Q10 were quercetin diglycosides with two sugars attached to the flavonoid aglycone either at two different positions (di-O-glycosides, di-C,O-glycosides) or at the same position (O-diglycosides, C,O-diglycosides) making a disaccharide. The quercetin derivate Q1 at m/z 595.1 ($[M-H]^-$, $[C_{26}H_{27}O_{16}]^-$) exhibited the typical fragmentation pattern of intraglycosidic cleavages (ⁱjX) and water losses (-18 Da): ions at m/z 505.0 ($[M-H-90]^-$), m/z 487.1 ($[M-H-108]^-$), and m/z 475.0 ($[M-H-120]^-$) corresponded respectively to ^{0,2}X, ^{0,2}X-H₂O, and ^{0,1}X fragmentations of a pentose (xylose or arabinose) or apiose, while the additional product ions ^{0,4}X (-60), ^{0,3}X (-90), and ^{0,2}X (-120) were most likely generated by a hexose moiety at m/z 415.0 ($[M-H-120-60]^-$), m/z 385.0 ($[M-H-120-90]^-$), and m/z 355.0 ($[M-H-120-120]^-$), respectively. Since the ⁱjX fragments are characteristic of C-glycosylation and ^{0,3}X⁻ ion is favored for the 6-C-isomer, instead of 8-C-isomer [5], the compound Q1 was tentatively identified as quercetin-6-C-hexoside-8-C-pentoside/apioside. Q2, Q6, and Q10 compounds at m/z

609.1 showed the neutral loss of 146 Da, 162 Da, and their mass combination of 308 Da (m/z 609 \rightarrow m/z 301). Unfortunately, both rhamnosyl ($C_6H_{10}O_4$, 146.05791 Da) and coumaroyl ($C_9H_6O_2$, 146.03678 Da), as well as hexosyl ($C_6H_{10}O_5$, 162.05282 Da) and caffeoyl ($C_9H_6O_3$, 162.03169 Da), exhibit a mass difference with monoisotopic m/z values of only 21 mDa (Table 1), which cannot be resolved with a low-resolution mass analyzer. In addition, these substitutions are characterized by the same CID fragmentation: $[M-H-146]^-$ for coumaroyl and rhamnosyl, and $[M-H-162]^-$ for hexosyl and caffeoyl substituents. However, the retention times observed for Q2, Q6, and Q10 (11.62 min, 14.42 min, and 15.85 min) were shorter than that of the more hydrophobic quercetin standard (25.71 min), thus suggesting the presence of rhamnose-hexose unit, instead of acylated combination (coumaroyl-hexose unit or caffeoyl-rhamnose unit), reported in QUESdb. As reported by Ablajan et al. [35], Y_i fragments are generated by heterolytic cleavage of hemiacetal O-C bond of the O-glycosides. Therefore, Q2 and Q6 corresponded to two di-O-glycosyl isomer forms because the Y_1^- ion was the base peak (100% relative abundance), and the Y_0^- of medium intensity (about 50% relative abundance). The O-glycosylation position was tentatively inferred by comparing the two observed RTs and theoretical $\log P$ values as quercetin-4'-rhamnoside-7-hexoside (Q2, RT 11.62 min, $\log P$ -2.47) and quercetin-3-O-rhamnoside-7-O-hexoside [34] (Q6, RT 14.42 min, $\log P$ -2.38). Concerning the Q10 species that eluted at 15.85 min, it was assigned to quercetin-3-O-hexosylrhamnoside ($\log P$ -2.28), because Y_0^- ion exhibited the highest abundance [30]. This identification was supported by the analysis of a standard solution of quercetin 3-O-rutinose, i.e., quercetin-3-O-hexosylrhamnoside (see ESM Fig. S2).

The quercetin derivate Q3 at m/z 741.2 ($[M-H]^-$, $C_{32}H_{37}O_{20}^-$) was a quercetin triglycoside as the MS/MS

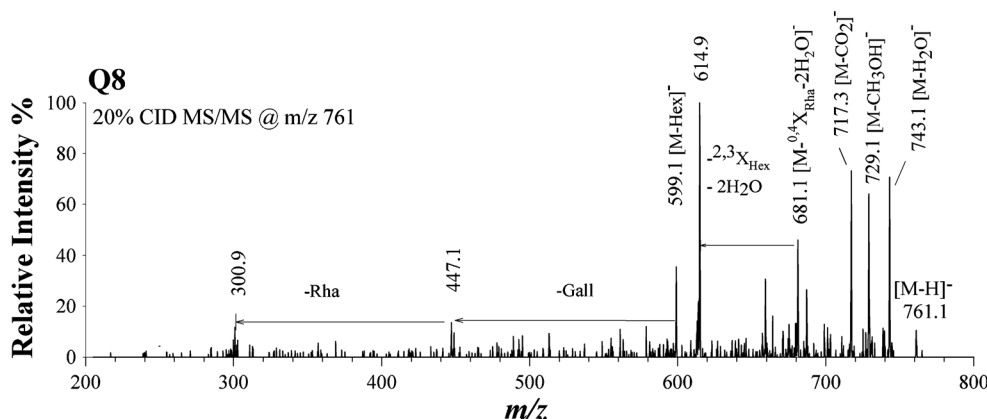


Fig. 3 Tandem mass spectra of quercetin-(galloyl-rhamnoside)-hexoside (Q8), $[C_{34}H_{33}O_{20}]^-$ (m/z 761.1), identified in *peperoni di Senise* peppers (*Capsicum annuum* L.) and never reported in other foodstuffs. Ion fragment at m/z 447.1, corresponding to quercetin rhamnoside, was a result of the loss of a galloyl-hexose moiety (-314 Da); in addition, ion fragments at

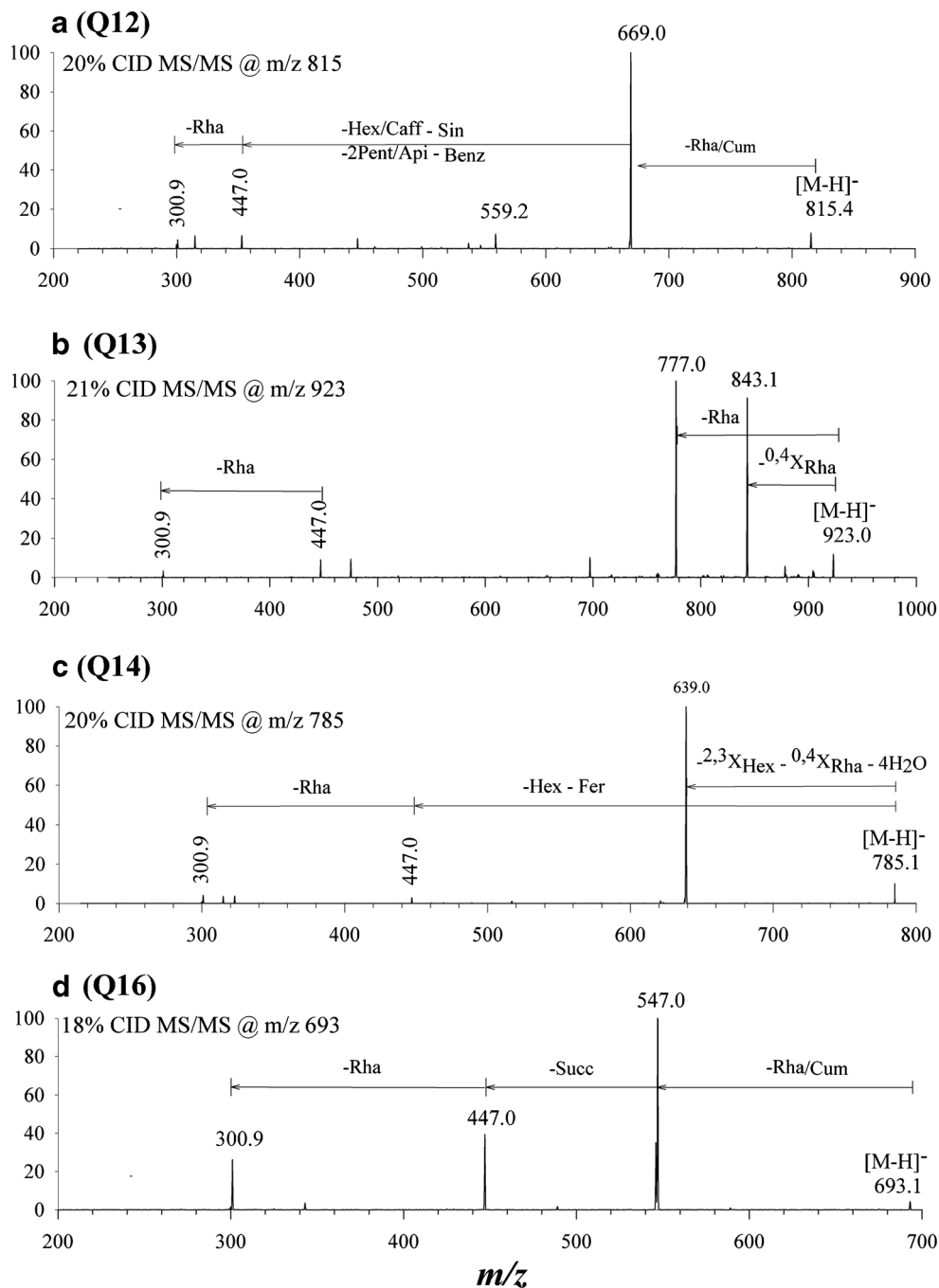
m/z 681.1 and 599.1 confirmed the nature of sugar substituents since they were obtained by ^{0,4}X_{Rha}-2H₂O (-80 Da) and ^{2,3}X_{Hex}-2H₂O (-66 Da) fragmentations. Hex, hexose (glucose or galactose); Rha, rhamnose; Gall, galloyl. The ions obtained after sugar moiety fragmentation are designed according the nomenclature proposed by Domon and Costello [32]

spectrum showed sequential losses of rhamnosyl (m/z 595.1, $[M-H-146]^-$), pentosyl/apiosyl (m/z 463.0, $[M-H-146-132]^-$), and hexosyl (m/z 300.9, $[M-H-146-132-162]^-$) residues from the precursor ion. In low-resolution MS, neutral losses of 146 Da and 162 Da could also correspond to coumaroyl and caffeoyl groups, respectively, but these acylations were discarded as the observed retention time of 11.63 min was relatively low; Q3 was assigned as quercetin-3-O-pentosyl/apiosyl rhamnosyl-hexoside, already found in cereal products [19]. Moreover, the reliability of assignment was confirmed by the cubic regression model, which

predicts too high retention times for the other candidates, thus suggesting their exclusion.

Peperoni di Senise peppers also contain two well-known methylated glycosyl-quercetin compounds, i.e., methylquercetin-3-O-hexoside, also called isorhamnetin-3-glucoside, at m/z 477.2 (Table 2, Q5) and dimethylquercetin-3-O-dihexoside (rhamnazin 3-sophoroside) at m/z 653.2 (Table 2, Q15), recognized from their characteristic rearranged methylated quercetin ions at nominal values m/z 315 ($C_{16}H_{11}O_7^-$) and 329 ($C_{17}H_{13}O_7^-$), as the base peaks in MS/MS spectra [19]. The retention time of Q5 was also in good

Fig. 4 Tandem mass spectra of four new quercetin glycosidic derivatives found in *peperoni di Senise* peppers (*Capsicum annuum* L.) and never reported in other foodstuffs. a (Q12) quercetin-rhamnoside-(sinapoyl-hexoside) [$C_{38}H_{39}O_{20}$] (m/z 815.4). b (Q13) quercetin-rhamnoside-(galloyl-caffeoyl-hexoside) [$C_{43}H_{39}O_{23}$] (m/z 923.0). c (Q14) quercetin-rhamnoside-(feruloyl-hexoside) [$C_{37}H_{37}O_{19}$] (m/z 785.1). d (Q16) quercetin-rhamnoside-(succinyl-rhamnoside) [$C_{31}H_{33}O_{18}$] (m/z 693.1). Hex, hexose (glucose or galactose); Pent, pentose (xylose or arabinose); Api, apiose; Rha, rhamnose; Succ, succinyl; Sin, sinapoyl; Cum, coumaroyl; Fer, feruloyl. The ions obtained after sugar moiety fragmentation are designed according the nomenclature proposed by Domon and Costello [32]



agreement with that obtained with a standard solution of isorhamnetin (see ESM Fig. S2). The peak signal named Q7 at m/z 651.1 is an analogue of Q6 identified as the quercetin-7-O-(acetyl-hexoside)-3-O-rhamnoside; the presence of an acetyl substituent (Table 2) was confirmed by the ion at m/z 447.0 ($[M-H-162-42]^-$) generated from the loss of an acetylated hexose moiety, while the product ion at m/z 505.0 is most likely due to a loss of rhamnose moiety ($[M-H-146]^-$), instead of the hydrophobic coumaroyl group. Furthermore, the assignment was confirmed by the cubic model in this case too. To our knowledge, compounds Q1, Q3, Q4, Q5, Q7, and Q15 (Table 2) are reported for the first time in *peperoni di Senise* peppers.

Among the quercetin derivatives, five acylated glycosylquercetin compounds (Fig. 2, Q8, Q12, Q13, Q14, and Q16) were characterized for the first time by their mass fragmentation patterns, and by the observed RTs compared with quercetin one, although the first searching for the corresponding m/z values in the home-made database resulted in a number of candidates between 6 and 22 (Table 2). Indeed, the deprotonated molecules Q8 at m/z 761.1 ($[C_{34}H_{33}O_{20}]^-$), Q12 at m/z 815.4 ($[C_{38}H_{39}O_{20}]^-$), Q13 at m/z 923.0 ($[C_{43}H_{39}O_{23}]^-$), and Q14 at m/z 785.1 ($[C_{37}H_{37}O_{19}]^-$) were tentatively identified as the mono- and diacylated derivatives of quercetin-hexoside-rhamnoside, and Q16 (m/z 693.1, $[C_{31}H_{33}O_{18}]^-$) as an acylated derivative of quercetin rhamnoside-rhamnoside.

The tandem MS spectra of all acylated derivatives always showed the fragment ions due to the neutral loss of the acylated sugar moieties. Despite having a little abundance, the peak signal of the aglycone anion at m/z 301 was always observed [40]. Compound Q8 was identified as quercetin-(galloyl-rhamnoside)-hexoside since its MS/MS analysis (Fig. 3) produced a fragment ion at m/z 447.1, corresponding to quercetin rhamnoside obtained by the neutral loss of a galloyl-hexose unit (-314 Da). This also occurred with the simultaneous fragmentation of sugar substituents, i.e., $^{0,4}X_{Rha}-2H_2O$ (-80 Da), $^{2,3}X_{Hex}-2H_2O$ (-66 Da), thus confirming their presence.

For all the other new acylated derivatives, in a similar way, the MS/MS spectra (Fig. 4a–d) showed the deprotonated quercetin rhamnoside at m/z 447 as a result of the loss of acylated sugar moieties, i.e., 368 Da (Hex+Sin) for Q12 (Fig. 4a), 476 Da (Hex+Caff+Gall) for Q13 (Fig. 4b), 338 Da (Hex+Fer) for Q14 (Fig. 4c), and 246 Da (Rha+Succ) for Q16 (Fig. 4d).

However, for Q12, Q13, and Q14, tandem MS spectra did not allow us to discriminate among the several putative candidates listed in QUEdb (ESM Tables S1–S12). Therefore, in this case, the information provided by the cubic model was crucial to tentatively identify compound Q12 as quercetin-rhamnoside-(sinapoyl-hexoside), Q13 as quercetin-rhamnoside-(galloyl-caffeoyl-hexoside), and Q14 as quercetin

rhamnoside-(feruloyl-hexoside). The elution order in RPLC of the acylated derivatives Q8, Q12, and Q14 (monoacylated derivatives of Q6) resulted in agreement with hydrophobicity of acyl substituents, galloyl ($\log P + 0.61$), sinapoyl ($\log P + 1.02$), and feruloyl ($\log P + 1.15$) groups. Also, the diacylated compound Q13 showed a retention time higher than that of the corresponding monoacylated compound Q8, because of the presence of an additional apolar substituent as the caffeoyl group ($\log P + 0.89$).

It is interesting to note that, except Q16, all putative selected candidates fit well the cubic relationship of RT and $\log P$ (see ESM Fig. S5). The apparent irregular chromatographic behavior of Q16 could be explained taking into account the hydrophobicity of rhamnose moieties that is comparatively greater than that of the hexose-rhamnose unit and other acylated derivatives as well (Q8, Q12, Q13, and Q14).

Conclusions

When paired with software tools, LC retention data and tandem MS spectra are very useful for unknown metabolite identification. The construction of an in-house database containing a consistent number of quercetin derivatives allowed to tentatively establish the occurrence of sixteen glycosidic and acyl glycosidic quercetin derivatives in methanolic extract of *peperoni di Senise* peppers (*C. annuum* L.). A database of 5016 putative quercetin derivatives was generated, being very useful to enable a tentative identification of five quercetin acyl glycosides in sun-dried peppers for the first time. As more information about unknown quercetin derivatives becomes available, the database will be expanded and improved accordingly.

Acknowledgments The authors wish to thank ALSIA for providing the analyzed sun-dried peppers (*Capsicum annuum* L.).

Compliance with ethical standards

Conflict of interest The authors declare that they have no conflicts of interest.

References

1. Lesjak M, Beara I, Simin N, Pintač D, Majkić T, Bekvalac K, et al. Antioxidant and anti-inflammatory activities of quercetin and its derivatives. *J Funct Foods*. 2018;40:68–75.
2. Rauf A, Imran M, Khan IA, ur-Rehman M, Gilani SA, Mehmood Z, Mubarak MS. Anticancer potential of quercetin: a comprehensive review. *Phyther Res* 2018;32.11: 2109–2130.
3. Materska M. Quercetin and its derivatives: chemical structure and bioactivity—a review. *Polish J Food Nutr Sci*. 2008;58(4).
4. Cai T, Guo ZQ, Xu XY, Wu ZJ. Recent (2000–2015) developments in the analysis of minor unknown natural products based on characteristic fragment information using LC-MS. *Mass Spectrom Rev*. 2018;37(2):202–16.

5. Pinheiro P, Justino G. Structural analysis of flavonoids and related compounds - a review of spectroscopic applications. *Phytochem A Glob Perspect Their Role Nutr Health*. 2012;33–56.
6. Abad-García B, Berrueta LA, Garmón-Lobato S, Gallo B, Vicente F. A general analytical strategy for the characterization of phenolic compounds in fruit juices by high-performance liquid chromatography with diode array detection coupled to electrospray ionization and triple quadrupole mass spectrometry. *J Chromatogr A*. 2009;1216(28):5398–415.
7. Cuyckens F, Claeys M. Mass spectrometry in the structural analysis of flavonoids. *J Mass Spectrom*. 2004;39(1):1–15.
8. Bianco G, Agerbirk N, Losito I, Cataldi TR. Acylated glucosinolates with diverse acyl groups investigated by high resolution mass spectrometry and infrared multiphoton dissociation. *Phytochemistry*. 2014;100:92–102.
9. Murota K, Terao J. Antioxidative flavonoid quercetin: implication of its intestinal absorption and metabolism. *Arch Biochem Biophys*. 2003;417(1):12–7.
10. Cataldi TR, Bianco G. Capillary electrophoresis of tropane alkaloids and glycoalkaloids occurring in Solanaceae plants. *Capillary Electrophor*. 2008:171–203.
11. Patel KN, Patel JK, Patel MP, Rajput GC, Patel HA. Introduction to hyphenated techniques and their applications in pharmacy. *Pharm Methods*. 2010;1(1):2–13.
12. Blunder M, Orthaber A, Bauer R, Bucar F, Kunert O. Efficient identification of flavones, flavanones and their glycosides in routine analysis via off-line combination of sensitive NMR and HPLC experiments. *Food Chem*. 2017;218:600–9.
13. Prashanth SN, Bianco G, Cataldi TR, Iacobellis NS. Acylhomoserine lactone production by bacteria associated with cultivated mushrooms. *J Agric Food Chem*. 2011;59(21):11461–72.
14. Cataldi TR, Bianco G, Abate S, Losito I. Identification of unsaturated N-acylhomoserine lactones in bacterial isolates of *Rhodobacter sphaeroides* by liquid chromatography coupled to electrospray ionization-hybrid linear ion trap-Fourier transform ion cyclotron resonance mass spectrometry. *Rapid Commun Mass Spectrom*. 2011;25(13):1817–26.
15. Pascale R, Bianco G, Cataldi TR, Kopplin PS, Bosco F, Vignola L, et al. Mass spectrometry-based phytochemical screening for hypoglycemic activity of Fagioli di Sarconi beans (*Phaseolus vulgaris* L.). *Food Chem*. 2018;242:497–504.
16. Bianco G, Buchicchio A, Cataldi TR. Structural characterization of major soyasaponins in traditional cultivars of Fagioli di Sarconi beans investigated by high-resolution tandem mass spectrometry. *Anal Bioanal Chem*. 2015;407(21):6381–9.
17. Bianco G, Pascale R, Carbone CF, Acquavia MA, Cataldi TR, Schmitt-Kopplin P, et al. Determination of soyasaponins in Fagioli di Sarconi beans (*Phaseolus vulgaris* L.) by LC-ESI-FTICR-MS and evaluation of their hypoglycemic activity. *Anal Bioanal Chem*. 2018;410(5):1561–9.
18. Lucci P, Saurina J, Núñez O. Trends in LC-MS and LC-HRMS analysis and characterization of polyphenols in food. *Trends Anal Chem*. 2017;88:1–24.
19. Wishart DS. FooDB: the food database. 2018; <http://foodb.ca/>. Accessed 2 Mar 2019.
20. Laurino S, Grossi G, Pucci P, Flagiello A, Bufo SA, Bianco G, et al. Identification of major *Toxoneuron nigriceps* venom proteins using an integrated transcriptomic/proteomic approach. *Insect Biochem Mol Biol*. 2016;76:49–61.
21. Pascale R, Grossi G, Cruciani G, Mecca G, Santoro D, Calace RS, et al. Sequence protein identification by randomized sequence database and transcriptome mass spectrometry (SPIDER-TMS): from manual to automatic application of a ‘de novo sequencing’ approach. *Eur J Mass Spectrom*. 2016;22(4):193–8.
22. Bhagwat S, Haytowitz DB, Holden JM. USDA database for the flavonoid content of selected foods: U.S. Dep. Agriculture; 2014.
23. Giacomoni F, Fillatre Y, Rothwell J, Eisner R, Cesaire D, Pujos-Guillot E, Manach C. PhytoHub version 1.0: a food metabolome database dedicated to dietary phytochemicals. 2014; <http://phytohub.eu/>. Accessed 2 March 2019.
24. Horai H, Arita M, Kanaya S, Nihei Y, Ikeda T, Suwa K, et al. MassBank: a public repository for sharing mass spectral data for life sciences. *J Mass Spectrom*. 2010;45(7):703–14.
25. Neveu V, Perez-Jiménez J, Vos F, Crespy V, Du Chaffaut L, Mennen L, Knox C, Eisner R, Cruz J, Wishart D, Scalbert A. Phenol-Explorer: an online comprehensive database on polyphenol contents in foods. Database 2010; <http://phenol-explorer.eu/>. Accessed 2 Mar 2019.
26. Akimoto N, Ara T, Nakajima D, Suda K, Ikeda C, Takahashi S, et al. FlavonoidSearch: a system for comprehensive flavonoid annotation by mass spectrometry. *Sci Rep*. 2017;7(1):1243.
27. Cerrato A, Cannazza G, Capriotti AL, Citti C, La Barbera G, Laganà A, et al. A new software-assisted analytical workflow based on high-resolution mass spectrometry for the systematic study of phenolic compounds in complex matrices. *Talanta*. 2020;209:120573.
28. Fekete A, Frommberger M, Rothballer M, Li X, Englmann M, Fekete J, et al. Identification of bacterial N-acylhomoserine lactones (AHLs) with a combination of ultra-performance liquid chromatography (UPLC), ultra-high-resolution mass spectrometry, and in-situ biosensors. *Anal Bioanal Chem*. 2007;387(2):455–67.
29. Wahyuni Y, Ballester AR, Tikunov Y, de Vos RCH, Pelgrom KTB, Maharijaya A, et al. Metabolomics and molecular marker analysis to explore pepper (*Capsicum* sp.) biodiversity. *Metabolomics*. 2013;9(1):130–44.
30. Fabre N, Rustan I, De Hoffmann E, Quetin-Leclercq J. Determination of flavone, flavonol, and flavanone aglycones by negative ion liquid chromatography electrospray ion trap mass spectrometry. *J Am Soc Mass Spectrom*. 2001;12(6):707–15.
31. Ma YL, Li QM, Van Den Heuvel H, Claeys M. Characterization of flavone and flavonol aglycones by collision-induced dissociation tandem mass spectrometry. *Rapid Commun Mass Spectrom*. 1997;11(12):1357–64.
32. Domon B, Costello CE. A systematic nomenclature for carbohydrate fragmentations in FAB-MS/MS spectra of glycoconjugates. *Glycoconj J*. 1988;5(4):397–409.
33. Eugster PJ, Boccard J, Debrus B, Bréant L, Wolfender JL, Martel S, et al. Retention time prediction for dereplication of natural products (CxHyOz) in LC-MS metabolite profiling. *Phytochemistry*. 2014;108:196–207.
34. Podunavac-Kuzmanović SO, Jevrić LR, Tepić AN, Šumić Z. Reversed-phase HPLC retention data in correlation studies with lipophilicity molecular descriptors of carotenoids. *Hemijaska Indust*. 2013;67(6):933–40.
35. Ablajan K, Abliz Z, Shang XY, He JM, Zhang RP, Shi JG. Structural characterization of flavonol 3,7-di-O-glycosides and determination of the glycosylation position by using negative ion electrospray ionization tandem mass spectrometry. *J Mass Spectrom*. 2006;41(3):352–60.
36. Jeong WY, Jin JS, Cho YA, Lee JH, Park S, Jeong SW, et al. Determination of polyphenols in three *Capsicum annuum* L. (bell pepper) varieties using high-performance liquid chromatography-tandem mass spectrometry: their contribution to overall antioxidant and anticancer activity. *J Sep Sci*. 2011;34(21):2967–74.
37. Marín A, Ferreres F, Tomás-Barberán FA, Gil MI. Characterization and quantitation of antioxidant constituents of sweet pepper (*Capsicum annuum* L.). *J Agric Food Chem*. 2004;52(12):3861–9.
38. Morales-Soto A, Gómez-Caravaca AM, García-Salas P, Segura-Carretero A, Fernández-Gutiérrez A. High-performance liquid chromatography coupled to diode array and electrospray time-of-

- flight mass spectrometry detectors for a comprehensive characterization of phenolic and other polar compounds in three pepper (*Capsicum annuum* L.) samples. *Food Res Int.* 2013;51.2:977–84.
39. Gosetti F, Mazzucco E, Zampieri D, Gennaro MC. Signal suppression/enhancement in high-performance liquid chromatography tandem mass spectrometry. *J Chromatogr A.* 2010;1217(25): 3929–37.
 40. Vallejo F, Tomás-Barberán FA, Ferreres F. Characterisation of flavonols in broccoli (*Brassica oleracea* L. var. *italica*) by liquid chromatography-UV diode-array detection-electrospray ionisation mass spectrometry. *J Chromatogr A.* 2004;1054.1–2:181–93.
 41. Rauter AP, Ennis M, Hellwich KH, Herold BJ, Horton D, Moss GP, et al. Nomenclature of flavonoids (IUPAC recommendations 2017). *Pure Appl Chem.* 2018;90(9):1429–86.

Publisher's note Springer Nature remains neutral with regard to jurisdictional claims in published maps and institutional affiliations.

RESEARCH ARTICLE

Coceth sulfate characterization by electrospray ionization tandem mass spectrometry

Alberto Onzo¹ | Maria A. Acquavia^{1,2} | Tommaso R. I. Cataldi³ | Mattia Ligonzo¹ |
 Donatella Coviello¹ | Raffaella Pascale¹ | Giuseppe Martelli¹ | Marcella Bondoni² |
 Laura Scrano⁴ | Giuliana Bianco¹ 

¹Dipartimento di Scienze, Università degli Studi della Basilicata, Via dell'Ateneo Lucano 10, Potenza, 85100, Italy

²ALMAGISI s.r.l, Corso Italia, 27, Bolzano, 39100, Italy

³Dipartimento di Chimica, Università degli Studi di Bari Aldo Moro, via E. Orabona 4, Bari, 70126, Italy

⁴Dipartimento delle Culture Europee e del Mediterraneo: Arch, Università degli Studi della Basilicata, Ambiente, Patrimoni Culturali, Via Lanera, 20, Matera, 75100, Italy

Correspondence

G. Bianco, Università degli Studi della Basilicata, Dipartimento di Scienze, Via dell'Ateneo Lucano 10, 85100 Potenza, Italy.
 Email: giuliana.bianco@unibas.it

Rationale: The anionic surfactants, among which are alkyl ether sulfates (AESs), are the most used class of surfactants in cleansing applications. The negatively charged head group of AESs is a sulfate moiety linked with a variable number of ethylene oxide units, i.e. a polyethylene glycol chain. The hydrophobic part of an AES is constituted by a linear alkyl chain of carbon atoms, generally obtained from natural fatty acids. Coconut oil fatty acids, including the sodium salts of coceth sulfate (CES) with chemical formula $C_xH_y(OCH_2CH_2)_nOSO_3Na$, are widely used as feedstock for AESs synthesis. CES is added to many cleaning products and detergents defined as non-aggressive. Currently, no detailed structural information concerning the alkyl chain length x and, more importantly, the degree of ethoxylation n has been reported.

Methods: A commercial standard solution of CES was characterized by tandem mass spectrometry, employing direct injection into the electrospray ionization (ESI) source of a linear quadrupole ion trap mass spectrometer.

Results: Two series of oligomeric species, characterized by a C12 and C14 alkyl chains, i.e. $[C_{12}H_{25}(OCH_2CH_2)_nOSO_3]^-$ and $[C_{14}H_{29}(OCH_2CH_2)_nOSO_3]^-$ with n ranging from 0 to 7, were successfully identified. The interpretation of these data was very useful for CES identification in three commercial dishwasher cleaning products.

Conclusions: Direct injection MS/MS analysis of CES revealed a well-defined molecular weight distribution and allowed the alkyl chain composition and the number of ethylene oxide units to be identified.

1 | INTRODUCTION

Surfactants, or “surface active agents”, are organic compounds employed in a wide range of applications such as detergents, emulsifiers, wetting or dispersing agents, household and personal-care products.^{1–3} Each surfactant exhibits both a hydrophilic moiety, i.e. the so-called surfactant head, and a hydrophobic surfactant tail.⁴ Due to the competitive interplay of head–head, head–tail and tail–tail interactions, surfactants are able to self-assemble, leading to the

formation of micelles,^{4–7} which are able to capture hydrophobic species by trapping them inside the apolar core, thus improving their solubility in aqueous media.

Among the different types of surfactants, the anionic ones are the most important in terms of volume and range of applications.³ Alkyl ether sulfates (AESs), belonging to this group of tensioactive agents, can be used in hard waters and are capable of maintaining foaming at low temperatures. These features make them suitable for use in most cleaning formulations.^{1,2,8}

From the chemical structural point of view, AESs are formed of a linear alkyl chain of carbon atoms, which represents the hydrophobic tail, with a hydrophilic head composed of a variable number n of ethylene oxide groups (EOs) with a terminal sulfate group.^{8,9} AESs are prepared by reacting ethoxylated alcohols with a sulfating agent, normally sulfur trioxide; feedstocks for ethoxylated alcohols are made from synthetic or natural fatty acids, with carbon chain lengths between C6 and C18 depending on the required applications.⁹ Typically, ethoxylation is carried out in batches or occasionally in a continuous process, and feedstocks for AESs show degrees of ethoxylation n up to 3, but it should be noted that the composition of the feedstock (and the resulting surfactant) is complex, with the ethoxylation number representing an average, rather than an absolute, value. Most ethoxylates for detergents contain significant quantities of both un-ethoxylated alcohol and higher ethoxylates; the absolute composition of an ethoxylate, as well as the average degree of ethoxylation, can affect surfactant performance.⁹

To obtain substantial yields of hydrophobic surfactants, fatty acids derived from coconut, palm, and palm kernel oils are used. Coconut oil is commercially a major source of lauric acid, a C12 fatty acid which represents approximately 50% of the coconut oil fatty acid composition, but it also contains myristic acid (C14) and palmitic acid (C16), as well as small amounts of both shorter and longer fatty acids.¹⁰ Coconut oil is the base ingredient of the surfactant, sodium coceth sulfate (CES); CES is obtained as the sodium salt of the sulfate esters of the polyethylene glycol ether of coconut alcohols and it is employed in bath and fragrance preparations, soaps, shampoo, and household detergents. Its chemical formula is $C_xH_y(OCH_2CH_2)_nOSO_3Na$, where the number of hydrogens “ y ” depends on the degree of unsaturation occurring in the alkyl chain.⁷ Despite the increasing use of these products in industry and the adverse effects of their degradation products in the environment,^{8,10–12} no detailed structural investigation of CES has been reported.

Currently, highly selective analytical methods are required for the identification and evaluation of surfactants in industrial raw materials, manufactured products, and environmental samples. Because of the existence of many alkyl homologues, lack of chromophores, high polarity, and thermal instability, it is difficult to analyse non-aromatic surfactants in commercial products. Despite this, several techniques for their determination have been reported, including titration,^{13,14} Fourier-transform infrared spectroscopy (FT-IR), nuclear magnetic resonance (NMR) spectroscopy,^{15–20} attenuated total reflectance (ATR) combined with FTIR,²¹ ion chromatography with suppressed or non-suppressed conductivity detection (IC-CCD),^{22,23} gas chromatography coupled to mass spectrometry (GC/MS),^{24,25} capillary electrophoresis (CE) with UV detection,^{26–28} high-performance liquid chromatography coupled with mass spectrometry (HPLC/MS) or evaporative light scattering detector (HPLC-ELSD),^{29–31} and supercritical fluid chromatography coupled with mass spectrometry (SFC/MS).³² Among the above-mentioned techniques, the chromatographic ones have many advantages for analysing surfactant mixtures. Good resolution can be expected by using IC-

CCD; however, this technique can only be applied to ionic surfactants. In the case of GC/MS, direct resolution for ionic surfactants is not easy, since derivatization or pyrolysis is necessary before their analysis.³³ HPLC, on the other hand, is applicable for the analysis of surfactant mixtures without any concern regarding their charge.^{34,35} HPLC coupled with different detectors, such as mass spectrometers and UV-Vis diode array, has been widely used for AES analysis, allowing the concentration of single homologues and isomers to be determined, without any derivatization steps. However, low polymer solubility and increased solution viscosity, with the ensuing issues of sample injection and elution, as well as relatively low chromatographic resolution of individual oligomers, make its use challenging.^{11,12,36} In addition, HPLC/MS- or HPLC-UV-based methods have some disadvantages, such as being solvent-consuming, and requiring complicated analytical instrumentation and long analysis times. As an alternative, stand-alone mass spectrometry has been widely used for surfactant analysis, and mass spectrometry provides a wide range of advantages, such as supplying key structural information with a simple direct-injection analysis, carried out in few minutes. Moreover, a huge number of molecules can be identified at the same time, thus making this technique useful generally for the analysis of complex mixtures.^{37–42} Matrix-assisted laser desorption/ionization time-of-flight mass spectrometry (MALDI-TOF-MS)⁴³ has been used to analyse non-ionic surfactants in previous studies. Although it is a convenient and powerful technique, it can be difficult to identify some oligomers. Ion mobility mass spectrometry (IM-MS), which has a short analysis time and minimal solvent usage, has also been used to analyse oligomers.^{44,45} Soft ionization techniques such as field desorption (FD), fast atom bombardment (FAB), atmospheric pressure chemical ionization (APCI) and electrospray ionization (ESI) have been used for the qualitative characterization of surfactant mixtures in environmental samples.^{46–49} Depending on the physicochemical properties of the surfactant (mainly polarity and acidity), operation in positive or negative ion mode can be chosen.⁵⁰ To our knowledge, although many applications have been reported for the detection of anionic surfactants, no structural information is available for CES. In the present study, direct-injection analysis coupled to negative electrospray ionization mass spectrometry (ESI(-)-MS) and dual-stage MS (tandem MS) analysis was employed for the first time, to obtain a mass spectrometry fingerprint for the detection of methanolic solutions of CES in a raw material standard and three common commercial cleaning products, without any further pre-treatment.^{51–55}

2 | MATERIALS AND METHODS

2.1 | Chemicals and sample preparation

Methanol (LC-MS grade) was purchased from Sigma-Aldrich (Milano, Italy). A commercial solution of a sodium salt of coceth sulfate and three common commercial dishwasher cleaning products (sample A - Lot #901120, sample B - Lot #805483, and sample C

– Lot #904417) were provided by Almacabio S.r.l. (Bolzano, Italy). The samples were concentrated under reduced pressure (80 mbar) and controlled temperature (40°C) with a rotary evaporator (LABOROTA 4000eco, Heidolph, Schwebach, Germany) for 7 h, at 90 rpm. Then, 1-mL aliquots of the concentrated samples were diluted in MeOH in a 1:2 (v/v) ratio, filtered through 0.22- μ m PTFE filters (Whatman, Maidstone, UK) and injected directly into the ESI-LTQ mass spectrometer.

2.2 | Mass spectrometric analysis

Analysis of samples was performed using an LTQ XL linear ion trap mass spectrometer (Thermo Fisher Scientific, Bremen, Germany) equipped with an ESI source. Negative ion ESI-MS was used for the detection of the CES.^{2,56,57} The source voltage was set at 4.5 kV, the temperature of the heated capillary to 350°C, the capillary voltage to –45 V, and the tube lens voltage to –75 V. Pure nitrogen (99.996%, SIAD, Bergamo, Italy) was delivered to the MS system as the sheath gas. The ion trap pressure was maintained with pure helium (99.999%, SIAD), which was used for trapping and collisional activation of the trapped ions. The sheath gas (N₂) flow rate was 5 arbitrary units (a.u.). Full-scan MS experiments were performed in the LTQ in the range m/z 100–1500. The sodium coceth sulfate samples yielded [M][–] molecular anions, exhibiting repeating units of 44 and 28 Da. In order to confirm the structures of these anions, tandem mass spectrometry (MS/MS) experiments were carried out. The collision energy was optimized for each precursor ion, at between 0.9 and 1.5 eV in the centre-of-mass frame. All MS and MS/MS analyses were performed

under automatic gain control (AGC) conditions using helium as the damping as well as the collision gas for MS/MS experiments. The samples were injected at a flow rate of 10 μ L/min by using a 500- μ L syringe (Hamilton, Reno, NV, USA) connected directly to the ESI source by a polyethylene tube (ID 5 mm, length 50 cm), and controlled electronically by an integrated syringe pump. The data were acquired and analysed using the Xcalibur software package (version 2.0 SR1; Thermo Fisher Scientific, Milano, Italy). The raw data were imported, processed, and plotted by SigmaPlot 11.0 (Systat Software, London, UK) and RStudio software (<https://www.r-project.org/>).

3 | RESULTS AND DISCUSSION

Coceth sulfate [C_xH_y(OCH₂CH₂)_nOSO₃][–] is a AES surfactant commonly used in several cleaning formulations, which is obtained from coconut oil fatty acids. Since the fatty acid composition of coconut oils covers a wide range and thus affects the performance of the product, structural investigation of the alkyl chain backbone and the degree of ethoxylation “*n*” is necessary. In the present study, direct-injection ESI(–)-MS and MS/MS analyses were used to characterize a solution of CES and its occurrence in three commercial dishwasher cleaning products.

It is well known that surfactants are responsible for ion suppression in the ESI source.⁵⁸ However, this effect was alleviated by adding organic solvents such as methanol, thus allowing the qualitative ESI-MS detection of anionic surfactants.

Single-stage ESI-MS analysis was used to provide molecular weight information. Figure 1 shows a typical full-scan mass spectrum

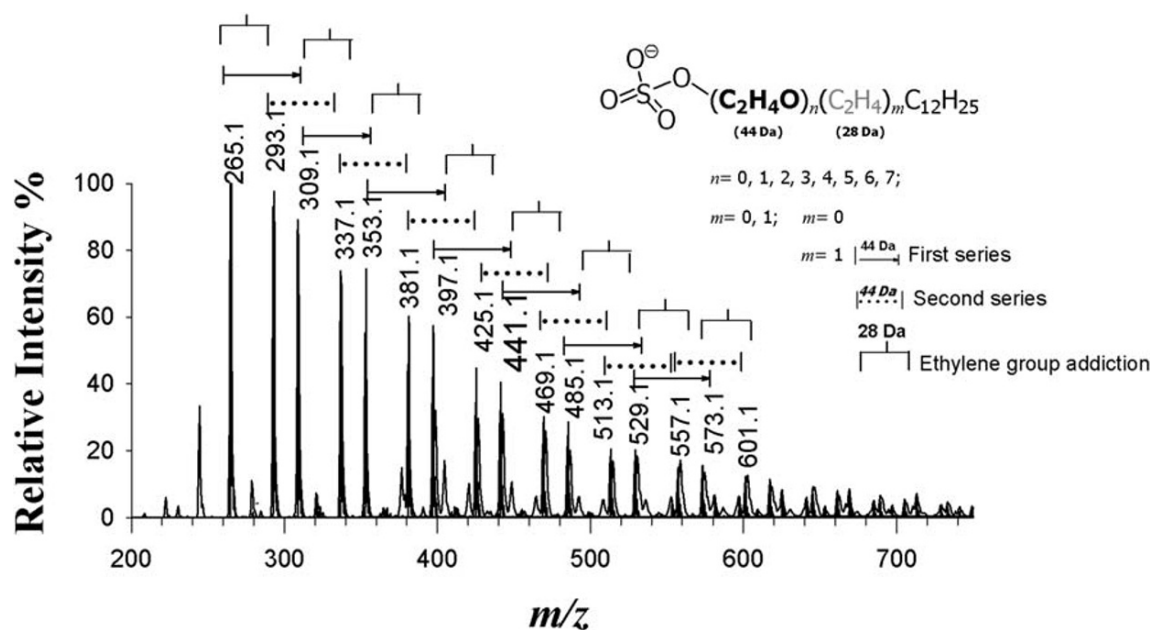


FIGURE 1 ESI(–)-MS spectrum by direct injection of a methanolic solution of coceth sulfate (CES). Inset: the general structure of alkyl ether sulfates (AESs) constituting CES: *n* indicates the number of ethylene oxide (CH₂CH₂O, 44 Da) units, between 0 and 7, and *m* (0 or 1) refers to the number of ethylene groups (CH₂CH₂, 28 Da) occurring in the alkyl chain of the two series of oligomeric species, i.e. [C₁₂H₂₅(OCH₂CH₂)_nOSO₃][–] and [C₁₄H₂₉(OCH₂CH₂)_nOSO₃][–]. No presence of unsaturation was found in the examined samples

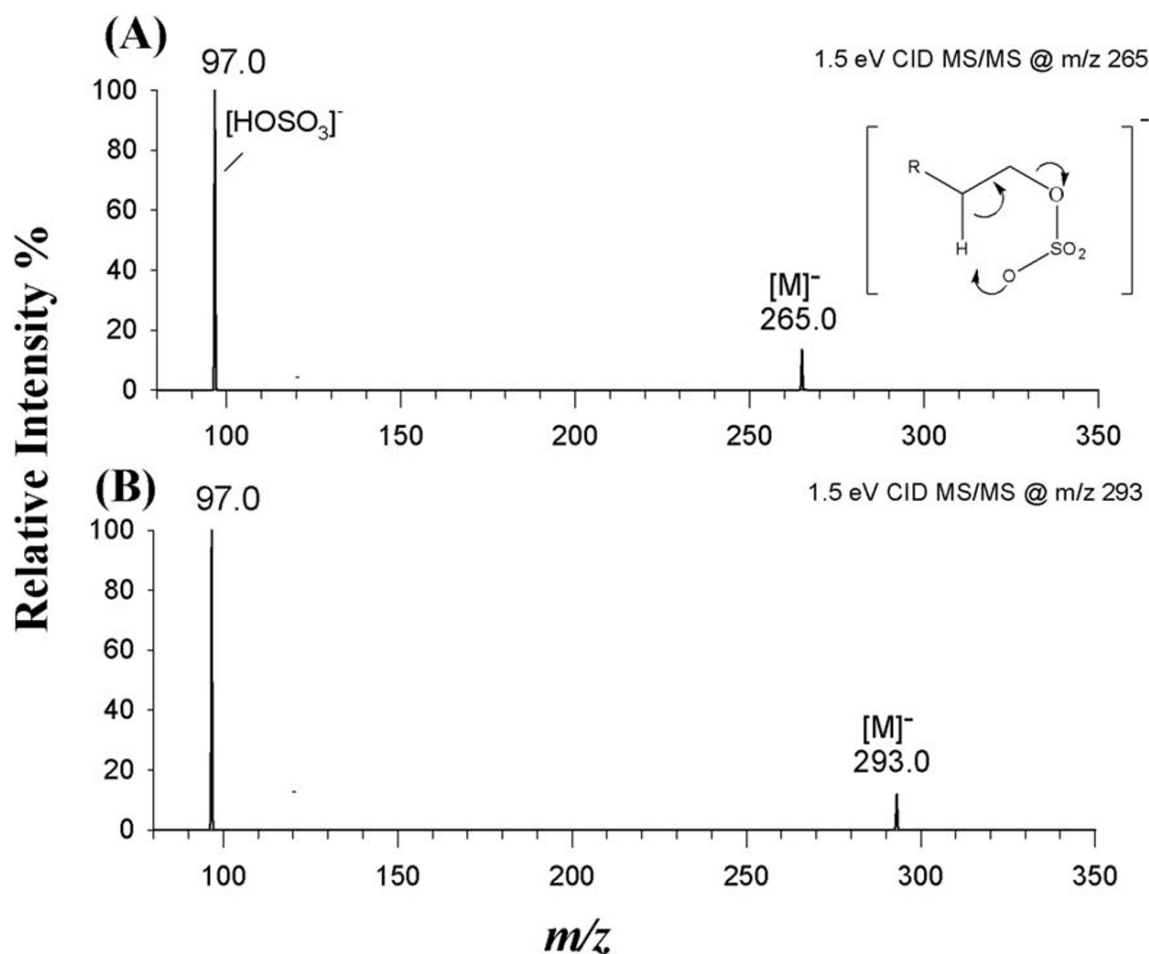
TABLE 1 Putative formulae of two anionic surfactants listed in the in-house dedicated database for ions at m/z 265.1 and 293.1

m/z	Anion formula	Number of carbons in the alkyl chain	Ethoxylate units	RDBE
m/z 265.1	$[\text{C}_{12}\text{H}_{25}\text{OSO}_3]^-$	12	0	0
	$[\text{C}_9\text{H}_{17}(\text{OCH}_2\text{CH}_2)\text{OSO}_3]^-$	9	1	1
	$[\text{C}_6\text{H}_9(\text{OCH}_2\text{CH}_2)_2\text{OSO}_3]^-$	6	2	2
	$[\text{C}_3\text{H}(\text{OCH}_2\text{CH}_2)_3\text{OSO}_3]^-$	3	3	3
m/z 293.1	$[\text{C}_{14}\text{H}_{29}\text{OSO}_3]^-$	14	0	0
	$[\text{C}_{11}\text{H}_{21}(\text{OCH}_2\text{CH}_2)\text{OSO}_3]^-$	11	1	1
	$[\text{C}_8\text{H}_{13}(\text{OCH}_2\text{CH}_2)_2\text{OSO}_3]^-$	8	2	2
	$[\text{C}_5\text{H}_5(\text{OCH}_2\text{CH}_2)_3\text{OSO}_3]^-$	5	3	3

of a methanolic solution of CES, which exhibits an asymmetric molecular weight distribution,¹ probably because lower molecular weight homologues (i.e. low number of ethoxylate units) are preferentially ionized, as already reported by Levine et al.⁵⁶ Nevertheless, it was possible to distinguish two different series whose members differed in molecular mass by 28 Da, i.e. the mass of the ethylene (C_2H_4) unit, thus suggesting the presence of C_x and $\text{C}_{(x+2)}$ alkyl homologues. For both series, a difference in the molecular mass of 44 Da, i.e. the mass of the monomeric ($-\text{CH}_2\text{CH}_2\text{O}-$) unit, was

ascertained. As CES is a polyethylene glycol derivative, i.e. a polymeric species with a variable number of ethylene oxide units, such behaviour was predictable.

Starting from the MS spectrum and from existing literature,^{1,2,8} a structural analysis of the species corresponding to each m/z signal was carried out to shed some light on the number of monomeric units "n" per oligomeric species. To this purpose, putative anionic formulae were assigned to m/z signals by using an in-house script, written in RStudio software, providing thus a series of advantages, such as

**FIGURE 2** MS/MS spectra of precursor ions at A, m/z 265.0 and B, m/z 293.0 obtained with 1.5 eV collision energy, with related fragmentation mechanisms

saving time, improving laboratory efficiency, and assuring the consideration of all possible combinations. The in-house script worked by adding methylene ($-\text{CH}_2-$) and ethylene oxide ($-\text{CH}_2\text{CH}_2\text{O}-$) groups to the basic CES formula $[\text{CH}_3\text{OSO}_3]^-$ containing only one carbon atom in the alkyl chain ($x = 1$) and no monomeric units ($n = 0$). Such an approach was followed because Karsa et al⁹ found that AES-based detergents could contain significant quantities of un-ethoxylated alcohols. In addition, chemical formulae with higher ring double-bond equivalent (RDBE) values of the alkyl chain were included and the maximum value of RDBE was set to 3 (Table S1, supporting information).⁵⁷ The obtained database reported the exact masses of each putative compound to enable its wider use in MS, both low- and high-resolution mode. However, we used nominal masses to find all possible candidates corresponding to a given m/z signal of the CES spectrum, along with MS/MS experiments for the final assignments.

In detail, the dedicated database was used to suggest a putative formula for ions whose signals in the MS spectrum of CES were the first of the two series, i.e. ions at m/z 265.1 and 293.1. The resulting potential database formulae for the mentioned signals are summarized in Table 1. Briefly, four possible chemical formulae were obtained for

each ion of interest, differing in the number of EO units n , the number of carbon atoms of the alkyl chain x , and the degree of unsaturation of the alkyl chain, i.e. the RDBE. In order to make the correct assignment, unfeasible chemical formulae for CES were ruled out. As an example, as the formula $[\text{C}_3\text{H}(\text{OCH}_2\text{CH}_2)_3\text{OSO}_3]^-$ for the ion at m/z 265.1 would correspond to a compound whose RDBE value is too high (RDBE = 3) compared with the length of the alkyl chain ($x = 3$), it was ignored. In addition, since the formula $[\text{C}_5\text{H}_5(\text{OCH}_2\text{CH}_2)_3\text{OSO}_3]^-$ of the ion at m/z 293.1 referred to its $\text{C}_{(x+2)}$ alkyl homologue, it was also rejected. Moreover, fatty acids with an odd number of carbon atoms are uncommon⁸; therefore, the formulae $[\text{C}_9\text{H}_{17}(\text{OCH}_2\text{CH}_2)\text{OSO}_3]^-$ and $[\text{C}_{11}\text{H}_{21}(\text{OCH}_2\text{CH}_2)\text{OSO}_3]^-$ were also ruled out. As laureth sulfate, C12 alkyl ether sulfate, and myreth sulfate, C14 alkyl ether sulfate, showed the same MS spectrum as that obtained for CES (Figure 1),⁵⁶ it was possible to assign the formulae $[\text{C}_{12}\text{H}_{25}\text{OSO}_3]^-$ and $[\text{C}_{14}\text{H}_{29}\text{OSO}_3]^-$ to the ions at m/z 265.1 and 293.1, respectively. Indeed, coconut oil, from which coceth sulfate is obtained, consists mainly of lauric acid, i.e. a C12 fatty acid, and myristic acid, i.e. a C14 fatty acid.¹⁰

In order to confirm the number of monomeric units n , MS/MS analyses were performed on single members of both series

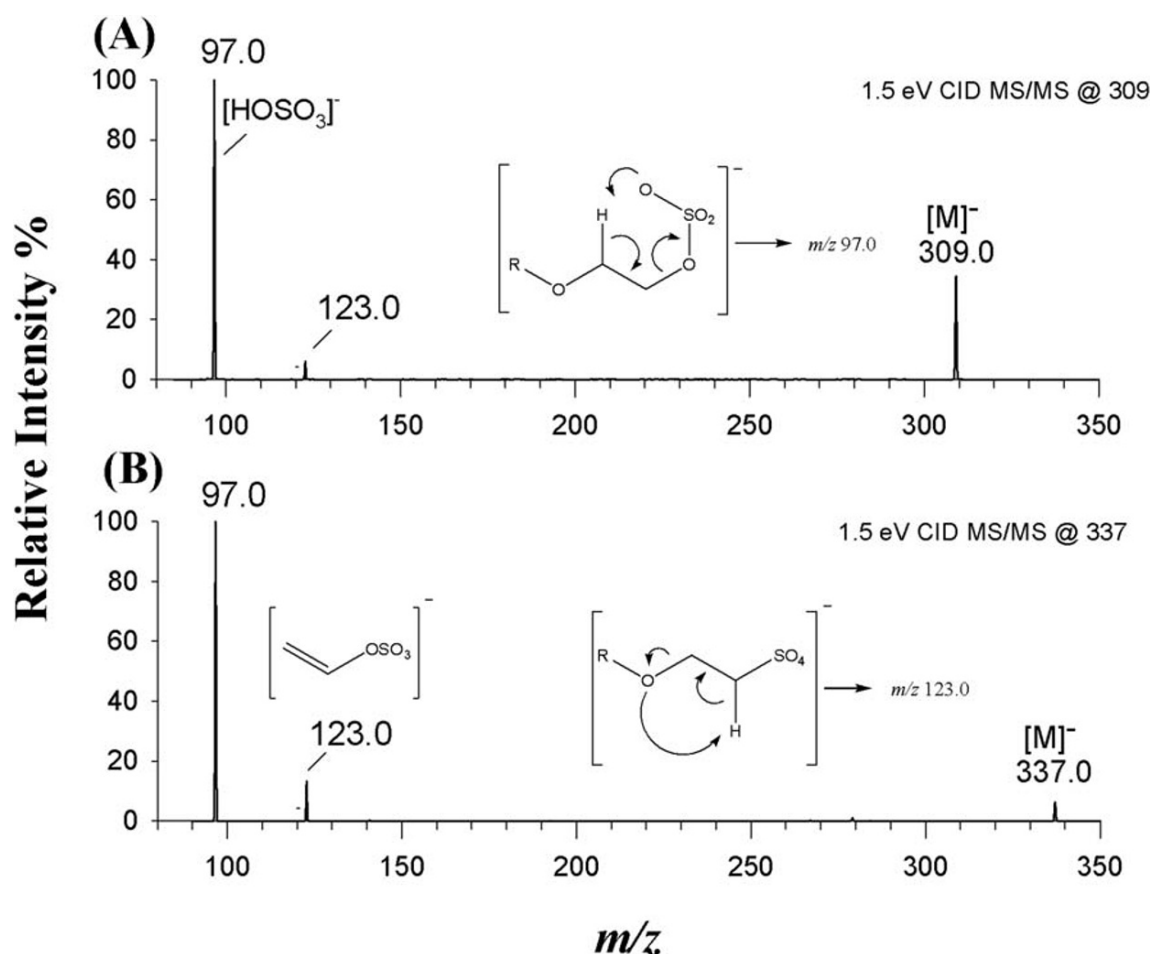


FIGURE 3 MS/MS spectra of precursor ions at A, m/z 309.0 and B, m/z 337.0 obtained with 1.5 eV collision energy, with related fragmentation mechanisms

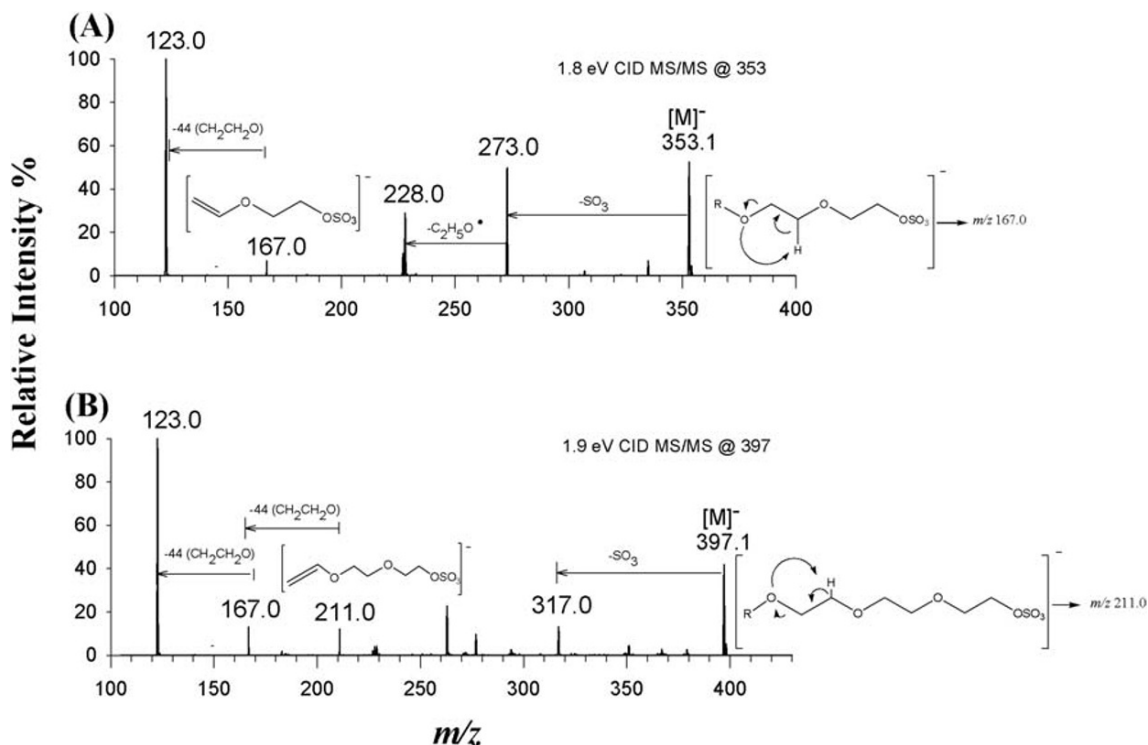


FIGURE 4 MS/MS spectra of precursor ions at A, m/z 353.1 and B, m/z 397.1 obtained with 1.8 and 1.9 eV collision energy, respectively, with related fragmentation mechanisms

(Figures 2 and 3). Since we are dealing with a long alkyl chain, different homologous product ions would be expected in the MS/MS spectrum. However, no charge-remote fragmentations were observed, as already reported for fatty acids,⁵⁹ where the fragmentation was only evidenced on unsaturated molecules with more than two double bonds. Extensive hydride migration is expected during the ESI-MS/MS of compounds with three or more double bonds. In the ESI(-)-MS/MS spectra of the ions at m/z 265.1 (Figure 2A) and 293.1 (Figure 2B), i.e. the first members of the two series of signals, a prominent product ion peak clearly attributable to $[\text{HOSO}_3]^-$ was observed at m/z 97.0.⁸ The formation of this anion requires the transfer of a proton to oxygen, in addition to the cleavage of a C–O bond. The origin of this transferred proton, however, has not been established, although the hydrogen atom geminal to the sulfate group has been suggested as its source.⁶⁰ In addition, for the precursor ions at m/z 309.1 and 337.1 (Figures 3A and 3B), whose signals in the MS spectrum of CES (Figure 1) were the second of both series, the most abundant product ion was the bisulfate anion (HSO_4^- , m/z 97.0). An additional product ion at m/z 123.0 was observed and it was rationalized as $[\text{CH}_2\text{CHOSO}_3]^-$, probably generated after the cleavage of the ether linkage with the alkyl chain.⁶¹ Since there was no evidence of the presence of this ion in the ESI(-)-MS/MS spectra of the ions at m/z 265.1 and 293.1, it was possible to ascertain that this species had a degree of ethoxylation of 0 ($n = 0$). Furthermore, fragmentation of ions at higher m/z values allowed us to confirm their higher degree of ethoxylation due to

TABLE 2 Summary of final assignments for m/z signals occurring in the MS spectrum of a methanolic solution of sodium coceth sulfate, with general chemical formula $[\text{C}_{12}\text{H}_{25}(\text{C}_2\text{H}_4)_m(\text{OC}_2\text{H}_4)_n\text{OSO}_3]^-$

m/z	$[\text{M}]^-$	m (28 Da)	n (44 Da)
265.1	$[\text{C}_{12}\text{H}_{25}\text{OSO}_3]^-$	0	0
293.1	$[\text{C}_{12}\text{H}_{25}\text{OSO}_3 + (\text{C}_2\text{H}_4)]^-$	1	0
309.1	$[\text{C}_{12}\text{H}_{25}\text{OSO}_3 + (\text{C}_2\text{H}_4\text{O})]^-$	0	1
337.1	$[\text{C}_{12}\text{H}_{25}\text{OSO}_3 + (\text{C}_2\text{H}_4) + (\text{C}_2\text{H}_4\text{O})]^-$	1	1
353.1	$[\text{C}_{12}\text{H}_{25}\text{OSO}_3 + (\text{C}_2\text{H}_4\text{O})_2]^-$	0	2
381.1	$[\text{C}_{12}\text{H}_{25}\text{OSO}_3 + (\text{C}_2\text{H}_4) + (\text{C}_2\text{H}_4\text{O})_2]^-$	1	2
397.1	$[\text{C}_{12}\text{H}_{25}\text{OSO}_3 + (\text{C}_2\text{H}_4\text{O})_3]^-$	0	3
425.1	$[\text{C}_{12}\text{H}_{25}\text{OSO}_3 + (\text{C}_2\text{H}_4) + (\text{C}_2\text{H}_4\text{O})_3]^-$	1	3
441.1	$[\text{C}_{12}\text{H}_{25}\text{OSO}_3 + (\text{C}_2\text{H}_4\text{O})_4]^-$	0	4
469.1	$[\text{C}_{12}\text{H}_{25}\text{OSO}_3 + (\text{C}_2\text{H}_4) + (\text{C}_2\text{H}_4\text{O})_4]^-$	1	4
485.1	$[\text{C}_{12}\text{H}_{25}\text{OSO}_3 + (\text{C}_2\text{H}_4\text{O})_5]^-$	0	5
513.1	$[\text{C}_{12}\text{H}_{25}\text{OSO}_3 + (\text{C}_2\text{H}_4) + (\text{C}_2\text{H}_4\text{O})_5]^-$	1	5
529.1	$[\text{C}_{12}\text{H}_{25}\text{OSO}_3 + (\text{C}_2\text{H}_4\text{O})_6]^-$	0	6
557.1	$[\text{C}_{12}\text{H}_{25}\text{OSO}_3 + (\text{C}_2\text{H}_4) + (\text{C}_2\text{H}_4\text{O})_6]^-$	1	6
573.1	$[\text{C}_{12}\text{H}_{25}\text{OSO}_3 + (\text{C}_2\text{H}_4\text{O})_7]^-$	0	7
601.1	$[\text{C}_{12}\text{H}_{25}\text{OSO}_3 + (\text{C}_2\text{H}_4) + (\text{C}_2\text{H}_4\text{O})_7]^-$	1	7

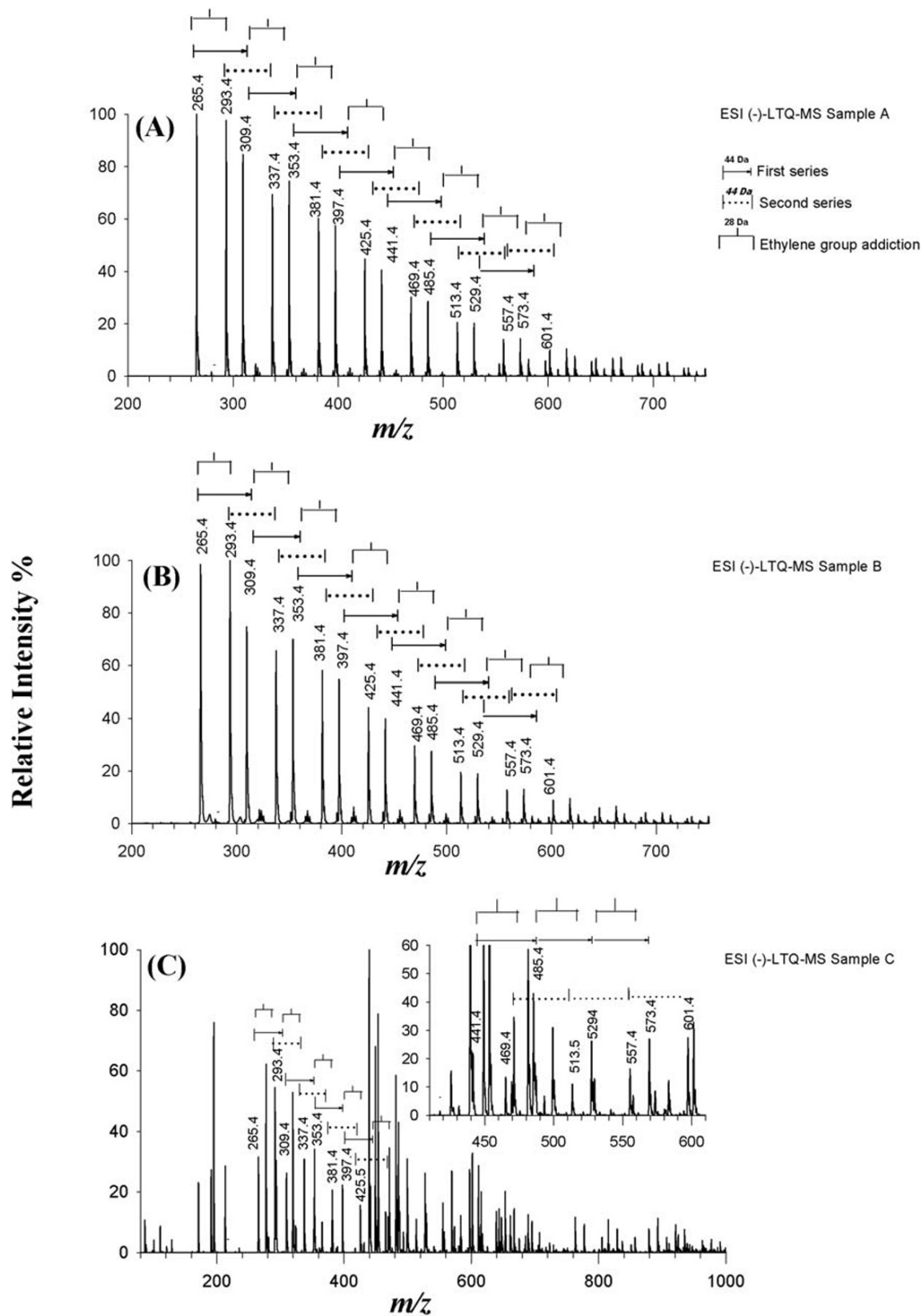


FIGURE 5 ESI(-)-MS spectra by direct injection of three cleaning products: A, Sample A; B, sample B; and C, sample C

the presence in the MS/MS spectra of products ions separated by 44 m/z units, i.e. the mass of the EO unit ($\text{CH}_2\text{CH}_2\text{O}$) (Figures 4A and 4B). As an example, the MS/MS spectrum of the ion at m/z 353.1 (Figure 4A), i.e. the third member of the first series with $n = 2$, showed an ion at m/z 167.0, corresponding to the $[\text{CH}_2\text{CHOCH}_2\text{CH}_2\text{OSO}_3]^-$ anion; the consecutive loss of the second monomeric EO unit resulted in the formation of the ion at m/z 123.0. For the precursor ion at m/z 397.1, i.e. the fourth member of the first series, an additional product ion at m/z 211.0 confirmed a degree of ethoxylation equal to 3 ($n = 3$) (Figure 4B).

Therefore, the commercial solution of CES is a mixture of two series of oligomeric species characterized by a C12 and C14 alkyl chain, i.e. $[\text{C}_{12}\text{H}_{25}(\text{C}_2\text{H}_4)_m(\text{OC}_2\text{H}_4)_n\text{OSO}_3]^-$ with $m = 0$ for the first series and $m = 1$ for the second series, and a degree of ethoxylation between 0 and 7 (i.e. $0 \leq n \leq 7$; see Table 2). Generally, CES performances are affected by the number of EO units; when the number of EO units is relatively small, bilayer aggregates (lamellae) are favoured. On increasing the same number, cylindrical micelles become possible and solubilization capacity increases.⁶² The MS analysis of the commercial CES raw material allowed us to define the corresponding fingerprint signals, useful for assessing its qualitative presence in commercial products.

Three commercial cleaning products containing CES, named sample A, sample B and sample C, were examined by direct-injection ESI(-)-MS analysis. Although with different content, the presence of CES in all the analysed samples was established. Two series differing by 28 Da, belonging to C12 and C14 alkyl homologues, respectively, were identified in the mass spectra of all three samples (see Figures 5A, 5B and 5C); in addition, a difference of 44 Da among the signals of the same series, corresponding to the mass of the monomeric unit ($-\text{CH}_2\text{CH}_2\text{O}-$), was confirmed, thus ascertaining a degree of ethoxylation between 0 and 7. The ESI(-)-MS full-scan mass spectrum obtained from the analysis of sample C (Figure 5C) showed a high number of signals, turning out to be more complex in composition. However, it was possible to identify the occurrence of the signals typical of CES in this sample. A further confirmation of the presence of CES in the cleaning products under study was given by CID-MS analyses performed on single signals of each examined sample, showing the same MS profile as reported in Figures 2, 3 and 4.

4 | CONCLUSIONS

Demand for reliable qualitative and rapid analysis is growing in various fields, including anionic surfactants. Direct-injection tandem mass spectrometric analysis of CES allowed us to gain more insights into the nature of the alkyl chain and the average degree of ethoxylation of the molecule, not reported previously. Moreover, the obtained structural information was used to obtain a mass spectrometric fingerprinting of CES in three commercial biodegradable detergents, thus supporting the utility of our results for future quantitative and/or traceability analyses. In addition, such a simple and low-cost approach could be used as a routine analysis method to detect potential frauds.

PEER REVIEW

The peer review history for this article is available at <https://publons.com/publon/10.1002/rcm.8884>.

ORCID

Giuliana Bianco  <https://orcid.org/0000-0001-9427-2274>

REFERENCES

1. Robinson VC, Bergfeld WF, Belsito DV, et al. Final report of the amended safety assessment of sodium laureth sulfate and related salts of sulfated ethoxylated alcohols. *Int J Toxicol*. 2010;29(4 Suppl): 151S-161S. <https://doi.org/10.1177/1091581810373151>
2. Nishikawa M, Katagi M, Miki A, Tsuchihashi H. Forensic toxicological determination of surfactant by liquid chromatography/electrospray ionization mass spectrometry and liquid chromatography/electrospray ionization tandem mass spectrometry. *J Heal Sci*. 2003;49(2):138-148. <https://doi.org/10.1248/jhs.49.138>
3. Broze G. *Handbook of Detergents, Part A: Properties*. Boca Raton: CRC Press; 1999.
4. Turro NJ, Grätzel M, Braun AM. Photophysical and photochemical processes in micellar systems. *Angew Chem Int Ed*. 1980;19(9): 675-696. <https://doi.org/10.1002/anie.198006751>
5. Lichtenberg D, Robson RJ, Dennis EA. Solubilization of phospholipids by detergents structural and kinetic aspects. *Biochim Biophys Acta - Rev Biomembr*. 1983;737(2):285-304. [https://doi.org/10.1016/0304-4157\(83\)90004-7](https://doi.org/10.1016/0304-4157(83)90004-7)
6. Seddon AM, Curnow P, Booth PJ. Membrane proteins, lipids and detergents: Not just a soap opera. *Biochim Biophys Acta - Biomembr*. 2004;1666(1-2):105-117. <https://doi.org/10.1016/j.bbamem.2004.04.011>
7. Paria S, Khilar KC. A review on experimental studies of surfactant adsorption at the hydrophilic solid-water interface. *Adv Colloid Interface Sci*. 2004;110(3):75-95. <https://doi.org/10.1016/j.cis.2004.03.001>
8. Bernabé-Zafón V, Ortega-Gadea S, Simó-Alfonso EF, Ramis-Ramos G. Characterization and quantitation of mixtures of alkyl ether sulfates and carboxylic acids by capillary electrophoresis with indirect photometric detection. *Electrophoresis*. 2003;24(16):2805-2813. <https://doi.org/10.1002/elps.200305544>
9. Karsa DR, Houston J. What are surfactants? In: *Chemistry and Technology of Surfactants*. Oxford, UK: Blackwell Publishing Ltd; 2007:1-23.
10. Gervajio GC. *Fatty acids and derivatives from coconut oil*. In: *Kirk-Othmer Encyclopedia of Chemical Technology*. Hoboken, NJ, USA: John Wiley & Sons, Inc.; 2012:1-38.
11. Morrall SW, Dunphy JC, Cano ML, et al. Removal and environmental exposure of alcohol ethoxylates in US sewage treatment. *Ecotoxicol Environ Saf*. 2006;64(1):3-13. <https://doi.org/10.1016/j.ecoenv.2005.07.014>
12. Rai SK, Mukherjee AK. Statistical optimization of production, purification and industrial application of a laundry detergent and organic solvent-stable subtilisin-like serine protease (Alzwpiprase) from *Bacillus subtilis* DM-04. *Biochem Eng J*. 2010;48(2):173-180. <https://doi.org/10.1016/j.bej.2009.09.007>
13. International Organization for Standardization. 1973. Surface active agents - Detergents - Determination of cationic-active matter - Direct two-phase titration procedure (ISO 2871:1973). <https://www.iso.org/standard/7885.html>
14. Fielden ML, Claesson PM. A comparison of three methods for the convenient determination of sodium dodecyl sulfate in aqueous solutions. *J Colloid Interface Sci*. 1998;198(2):261-265. <https://doi.org/10.1006/jcis.1997.5241>

15. Marcomini A, Giger W. Simultaneous determination of linear alkylbenzenesulfonates, alkylphenol polyethoxylates, and nonylphenol by high-performance liquid chromatography. *Anal Chem.* 1987;59(13):1709-1715.
16. Lee SM, Lee JY, Yu HP, Lim JC. Synthesis of environment friendly nonionic surfactants from sugar base and characterization of interfacial properties for detergent application. *J Ind Eng Chem.* 2016;38:157-166. <https://doi.org/10.1016/j.jiec.2016.04.019>
17. Jain RM, Mody K, Mishra A, Jha B. Physicochemical characterization of biosurfactant and its potential to remove oil from soil and cotton cloth. *Carbohydr Polym.* 2012;89(4):1110-1116. <https://doi.org/10.1016/j.carbpol.2012.03.077>
18. Muga A, Arrondo JLR, Bellon T, Sancho J, Bernabeu C. Structural and functional studies on the interaction of sodium dodecyl sulfate with β -galactosidase. *Arch Biochem Biophys.* 1993;300(1):451-457. <https://doi.org/10.1006/abbi.1993.1061>
19. Matar-Merheb R, Rhimi M, Leydier A, et al. Structuring detergents for extracting and stabilizing functional membrane proteins. *PLoS One.* 2011;6(3):1-10, e18036. <https://doi.org/10.1371/journal.pone.0018036>
20. Ferrage F, Zoonens M, Warschawski DE, Popot JL, Bodenhausen G. Slow diffusion of macromolecular assemblies by a new pulsed field gradient NMR method. *J Am Chem Soc.* 2003;125(9):2541-2545. <https://doi.org/10.1021/ja0211407>
21. Carolei L, Gutz IGR. Simultaneous determination of three surfactants and water in shampoo and liquid soap by ATR-FTIR. *Talanta.* 2005;66(1):118-124. <https://doi.org/10.1016/j.talanta.2004.10.005>
22. Levine LH, Judkins JE, Garland JL. Determination of anionic surfactants during wastewater recycling process by ion pair chromatography with suppressed conductivity detection. *J Chromatogr A.* 2000;874(2):207-215. [https://doi.org/10.1016/S0021-9673\(00\)00155-2](https://doi.org/10.1016/S0021-9673(00)00155-2)
23. Stemp A, Boriraj VA, Walling P, Neill P. Ion-chromatographic characterization of ethoxylated anionic surfactants. *J Am Oil Chem Soc.* 1995;72(1):17-21. <https://doi.org/10.1007/BF02635773>
24. Ding WH, Liao YH. Determination of alkylbenzyltrimethylammonium chlorides in river water and sewage effluent by solid-phase extraction and gas chromatography/mass spectrometry. *Anal Chem.* 2001;73(1):36-40. <https://doi.org/10.1021/ac000655i>
25. Ding WH, Tsai PC. Determination of alkyltrimethylammonium chlorides in river water by gas chromatography/ion trap mass spectrometry with electron impact and chemical ionization. *Anal Chem.* 2003;75(8):1792-1797. <https://doi.org/10.1021/ac020536y>
26. Piera E, Erra P, Infante MR. Analysis of cationic surfactants by capillary electrophoresis. *J Chromatogr A.* 1997;757(1-2):275-280. [https://doi.org/10.1016/S0021-9673\(96\)00663-2](https://doi.org/10.1016/S0021-9673(96)00663-2)
27. Liu HY, Ding WH. Determination of homologues of quaternary ammonium surfactants by capillary electrophoresis using indirect UV detection. *J Chromatogr A.* 2004;1025(2):303-312. <https://doi.org/10.1016/j.chroma.2003.10.108>
28. Sebastiano R, Citterio A, Righetti PG, Simó-Alfonso E, Ramis-Ramos G. Separation of fatty alcohol polyethoxylates by capillary electrophoresis through easy electroosmotic flow control with a quaternary ammonium salt. *J Chromatogr A.* 2004;1053(1-2):235-239. <https://doi.org/10.1016/j.chroma.2004.06.119>
29. Im SH, Jeong YH, Ryoo JJ. Simultaneous analysis of anionic, amphoteric, nonionic and cationic surfactant mixtures in shampoo and hair conditioner by RP-HPLC/ELSD and LC/MS. *Anal Chim Acta.* 2008;619(1):129-136. <https://doi.org/10.1016/j.aca.2008.03.058>
30. Pascale R, Bianco G, Coviello D, et al. Validation of a liquid chromatography coupled with tandem mass spectrometry method for the determination of drugs in wastewater using a three-phase solvent system. *J Sep Sci.* 2020;43(5):886-895. <https://doi.org/10.1002/jssc.201900509>
31. Ventura G, Calvano CD, Losito I, et al. Effect of pH and mobile phase additives on the chromatographic behaviour of an amide-embedded stationary phase: Cyanocobalamin and its diaminemonochloroplatinum(II) conjugate as a case study. *J Sep Sci.* 2019;42(6):1155-1162. <https://doi.org/10.1002/jssc.201801060>
32. Pan J, Tang Y, Shen Z, Du Z. Development of supercritical fluid chromatography coupled with mass spectrometry method for characterization of a nonionic surfactant and comparison with liquid chromatography coupled with mass spectrometry method. *J Mass Spectrom.* 2020;55(5):1-8, e4499. <https://doi.org/10.1002/jms.4499>
33. Schmitt TM. *Analysis of Surfactants*, 2nd ed., Revised and Expanded. New York, Basel: Marcel Dekker, Inc.; 2001.
34. Morelli JJ, Szajer G. Analysis of surfactants: Part I. *J Surfactant Deterg.* 2000;3(4):539-552. <https://doi.org/10.1007/s11743-000-0154-8>
35. Morelli JJ, Szajer G. Analysis of surfactants: Part II. *J Surfactant Deterg.* 2001;4(1):75-83. <https://doi.org/10.1007/s11743-001-0163-7>
36. Heinig K, Vogt C, Werner G. Separation of ionic and neutral surfactants by capillary electrophoresis and high-performance liquid chromatography. *J Chromatogr A.* 1996;745(1-2):281-292. [https://doi.org/10.1016/0021-9673\(96\)00399-8](https://doi.org/10.1016/0021-9673(96)00399-8)
37. Bianco G, Zianni R, Anzillotta G, et al. Dibenzo-p-dioxins and dibenzofurans in human breast milk collected in the area of Taranto (southern Italy): First case study. *Anal Bioanal Chem.* 2013;405(7):2405-2410. <https://doi.org/10.1007/s00216-013-6706-7>
38. Bianco G, Novario G, Anzillotta G, Palma A, Mangano A, Cataldi TRI. Polybrominated diphenyl ethers (PBDEs) in Mediterranean mussels (*Mytilus galloprovincialis*) from selected Apulia coastal sites evaluated by GC-HRMS. *J Mass Spectrom.* 2010;45(9):1046-1055. <https://doi.org/10.1002/jms.1799>
39. Zianni R, Bianco G, Lelario F, Losito I, Palmisano F, Cataldi TRI. Fatty acid neutral losses observed in tandem mass spectrometry with collision-induced dissociation allows regiochemical assignment of sulfoquinovosyl-diacylglycerols. *J Mass Spectrom.* 2013;48(2):205-215. <https://doi.org/10.1002/jms.3149>
40. Cataldi TRI, Orlando D, Nardiello D, et al. A three-factor Doehlert matrix design in optimising the determination of octadecyltrimethylammonium bromide by cation-exchange chromatography with suppressed conductivity detection. *Anal Chim Acta.* 2007;597(1):129-136. <https://doi.org/10.1016/j.aca.2007.06.038>
41. Bianco G, Agerbirk N, Losito I, Cataldi TRI. Acylated glucosinolates with diverse acyl groups investigated by high resolution mass spectrometry and infrared multiphoton dissociation. *Phytochemistry.* 2014;100:92-102. <https://doi.org/10.1016/j.phytochem.2014.01.010>
42. Pascale R, Bianco G, Cataldi TRI, et al. Mass spectrometry-based phytochemical screening for hypoglycemic activity of Fagioli di Sarconi beans (*Phaseolus vulgaris* L.). *Food Chem.* 2018;242:497-504. <https://doi.org/10.1016/j.foodchem.2017.09.091>
43. Ayorinde FO, Gelain SV, Johnson JH, Wan LW. Analysis of some commercial polysorbate formulations using matrix-assisted laser desorption/ionization time-of-flight mass spectrometry. *Rapid Commun Mass Spectrom.* 2000;14(22):2116-2124. [https://doi.org/10.1002/1097-0231\(20001130\)14:22<2116::AID-RCM142>3.0.CO;2-1](https://doi.org/10.1002/1097-0231(20001130)14:22<2116::AID-RCM142>3.0.CO;2-1)
44. Solak Erdem N, Alawani N, Wesdemiotis C. Characterization of polysorbate 85, a nonionic surfactant, by liquid chromatography vs. ion mobility separation coupled with tandem mass spectrometry. *Anal Chim Acta.* 2014;808:83-93. <https://doi.org/10.1016/j.aca.2013.07.026>
45. Katzenmeyer BC, Hague SF, Wesdemiotis C. Multidimensional mass spectrometry coupled with separation by polarity or shape for the characterization of sugar-based nonionic surfactants. *Anal Chem.* 2016;88(1):851-857. <https://doi.org/10.1021/acs.analchem.5b03400>

46. Barco M, Planas C, Palacios O, Ventura F, Rivera J, Caixach J. Simultaneous quantitative analysis of anionic, cationic, and nonionic surfactants in water by electrospray ionization mass spectrometry with flow injection analysis. *Anal Chem.* 2003;75(19):5129-5136. <https://doi.org/10.1021/ac020708r>
47. Caivano M, Pascale R, Mazzone G, Masi S, Panariello S, Caniani D. Disinfection unit of water resource recovery facilities: Critical issue for N₂O emission. *Frontiers in Wastewater Treatment and Modelling, FICWTM Springer.* 2017;444-450. https://doi.org/10.1007/978-3-319-58421-8_70
48. Caivano M, Pascale R, Mazzone G, et al. N₂O and CO₂ emissions from secondary settlers in WWTPs: Experimental results on full and pilot scale plants. *Frontiers in Wastewater Treatment and Modelling, FICWTM. Springer.* 2017;412-418. https://doi.org/10.1007/978-3-319-58421-8_65
49. Lyon PA, Stebbings WL, Crow FW, Tomer KB, Lippstreu DL, Gross ML. Analysis of anionic surfactants by mass spectrometry/mass spectrometry with fast atom bombardment. *Anal Chem.* 1984;56(1):8-13. <https://doi.org/10.1021/ac00265a004>
50. González S, Barceló D, Petrovic M. Advanced liquid chromatography-mass spectrometry (LC-MS) methods applied to wastewater removal and the fate of surfactants in the environment. *TrAC - Trends Anal Chem.* 2007;26(2):116-124. <https://doi.org/10.1016/j.trac.2006.12.003>
51. Hester TH, Castillo DE, Goebbert DJ. Fragmentation of deprotonated polyethylene glycols, [PEG - H]. *Rapid Commun Mass Spectrom.* 2013; 27(14):1643-1648. <https://doi.org/10.1002/rcm.6615>
52. Fonseca-Corona C, Vera-Avila LE, Gallegos-Pérez JL. Use of mass spectrometry for identification and quantitation of tensoactive agents in synthetic latex samples. *J Mex Chem Soc.* 2014;58(4):444-451. <https://doi.org/10.29356/jmcs.v58i4.54>
53. Ceraulo L, Giorgi G, Liveri VT, et al. Mass spectrometry of surfactant aggregates. *Eur J Mass Spectrom.* 2011;17(6):525-541. <https://doi.org/10.1255/ejms.1158>
54. Lyon PA, Crow FW, Tomer KB, Gross ML. Analysis of cationic surfactants by mass spectrometry/mass spectrometry with fast atom bombardment. *Anal Chem.* 1984;56(13):2278-2284. <https://doi.org/10.1021/ac00277a004>
55. Farsang E, Gaál V, Horváth O, Bárdos E, Horváth K. Analysis of non-ionic surfactant triton X-100 using hydrophilic interaction liquid chromatography and mass spectrometry. *Molecules.* 2019;24(7):1-13. <https://doi.org/10.3390/molecules24071223>
56. Levine LH, Garland JL, Johnson JV. Simultaneous quantification of poly-dispersed anionic, amphoteric and nonionic surfactants in simulated wastewater samples using C18 high-performance liquid chromatography-quadrupole ion-trap mass spectrometry. *J Chromatogr A.* 2005;1062(2):217-225. <https://doi.org/10.1016/j.chroma.2004.11.038>
57. Marina AM, Che Man YB, Nazimah SAH, Amin I. Chemical properties of virgin coconut oil. *J Am Oil Chem Soc.* 2009;86(4):301-307. <https://doi.org/10.1007/s11746-009-1351-1>
58. Rundlett KL, Armstrong DW. Mechanism of signal suppression by anionic surfactants in capillary electrophoresis-electrospray ionization mass spectrometry. *Anal Chem.* 1996;68(19):3493-3497. <https://doi.org/10.1021/ac960472p>
59. Kerwin JL, Wiens AM, Ericsson LH. Identification of fatty acids by electrospray mass spectrometry and tandem mass spectrometry. *J Mass Spectrom.* 1996;31(2):184-192. [https://doi.org/10.1002/\(SICI\)1096-9888\(199602\)31:2<184::AID-JMS283>3.0.CO;2-2](https://doi.org/10.1002/(SICI)1096-9888(199602)31:2<184::AID-JMS283>3.0.CO;2-2)
60. Attygalle AB, Garcia-Rubio S, Ta J, Meinwald J. Collisionally-induced dissociation mass spectra of organic sulfate anions. *J Chem Soc Perkin Trans.* 2001;2(4):498-506. <https://doi.org/10.1039/b009019k>
61. Jewett BN, Ramaley L, Kwak JCT. Atmospheric pressure ionization mass spectrometry techniques for the analysis of alkyl ethoxysulfate mixtures. *J Am Soc Mass Spectrom.* 1999;10(6):529-536. [https://doi.org/10.1016/S1044-0305\(99\)00017-3](https://doi.org/10.1016/S1044-0305(99)00017-3)
62. Aoudia M, Al-Haddabi B, Al-Harhi Z, Al-Rubkhi A. Sodium lauryl ether sulfate micellization and water solubility enhancement towards naphthalene and pyrene: Effect of the degree of ethoxylation. *J Surfactant Deterg.* 2010;13(1):103-111. <https://doi.org/10.1007/s11743-009-1131-9>

SUPPORTING INFORMATION

Additional supporting information may be found online in the Supporting Information section at the end of this article.

How to cite this article: Onzo A, Acquavia MA, Cataldi TRI, et al. Coceth sulfate characterization by electrospray ionization tandem mass spectrometry. *Rapid Commun Mass Spectrom.* 2020;34:e8884. <https://doi.org/10.1002/rcm.8884>

Research Article

***Pistacia lentiscus* Hydrosol: Untargeted Metabolomic Analysis and Anti-Inflammatory Activity Mediated by NF- κ B and the Citrate Pathway**

Anna Santarsiero ¹, Alberto Onzo ¹, Raffaella Pascale ¹, Maria Assunta Acquavia ¹, Marianna Coviello,¹ Paolo Convertini ¹, Simona Todisco ¹, Michela Marsico,¹ Corrado Pifano,² Patrizia Iannece,³ Carmine Gaeta ³, Salvatore D'Angelo,⁴ Maria Carmela Padula,⁴ Giuliana Bianco ¹, Vittoria Infantino ¹ and Giuseppe Martelli¹

¹Department of Science, University of Basilicata, Viale dell'Ateneo Lucano, 10, 85100 Potenza, Italy

²Bioinnova srls, Via Ponte Nove Luci, 22, 85100 Potenza, Italy

³Dipartimento di Chimica e Biologia, Università degli Studi di Salerno, Via Giovanni Paolo II, 132-84084 Fisciano, Italy

⁴Rheumatology Department of Lucania, Rheumatology Institute of Lucania (IREL), San Carlo Hospital of Potenza and Madonna delle Grazie Hospital of Matera, Potenza, Italy

Correspondence should be addressed to Giuliana Bianco; giuliana.bianco@unibas.it and Vittoria Infantino; vittoria.infantino@unibas.it

Received 24 June 2020; Revised 1 October 2020; Accepted 20 October 2020; Published 2 November 2020

Academic Editor: Marcos R. de Oliveira

Copyright © 2020 Anna Santarsiero et al. This is an open access article distributed under the Creative Commons Attribution License, which permits unrestricted use, distribution, and reproduction in any medium, provided the original work is properly cited.

Pistacia lentiscus shows a long range of biological activities, and it has been used in traditional medicine for treatment of various kinds of diseases. Moreover, related essential oil keeps important health-promoting properties. However, less is known about *P. lentiscus* hydrosol, a main by-product of essential oil production, usually used for steam distillation itself or discarded. In this work, by using ultra-high-resolution ESI(+)-FT-ICR mass spectrometry, a direct identification of four main classes of metabolites of *P. lentiscus* hydrosol (i.e., terpenes, amino acids, peptides, and condensed heterocycles) was obtained. Remarkably, *P. lentiscus* hydrosol exhibited an anti-inflammatory activity by suppressing the secretion of IL-1 β , IL-6, and TNF- α proinflammatory cytokines in lipopolysaccharide- (LPS-) activated primary human monocytes. In LPS-triggered U937 cells, it inhibited NF- κ B, a key transcription factor in inflammatory cascade, regulating the expression of both the mitochondrial citrate carrier and the ATP citrate lyase genes. These two main components of the citrate pathway were downregulated by *P. lentiscus* hydrosol. Therefore, the levels of ROS, NO, and PGE₂, the inflammatory mediators downstream the citrate pathway, were reduced. Results shed light on metabolic profile and anti-inflammatory properties of *P. lentiscus* hydrosol, suggesting its potential as a therapeutic agent.

1. Introduction

Pistacia lentiscus (*P. lentiscus*) belongs to the *Anacardiaceae* family, consisting of 70 genera and more than 600 species. The genus *Pistacia* includes deciduous resin-bearing shrubs and trees. They are xerophytic trees growing 8–10 m tall. *P. lentiscus*, commonly called mastic tree since its resin is known as mastic, is widely distributed in the Mediterranean

basin [1–3]. It is employed in food industry, as a food colorant; in cosmetics, usually sold as essential oil; and for medical purposes, because of its biological activities. Indeed, it is used in the treatment of inflammation, burns, and gastrointestinal complaints [4–8]. Many studies were carried out to uncover the chemical composition of *P. lentiscus* leaves and fruit extracts, by which many constituents were identified and quantified [9–12]. Observed metabolic profile allowed

explaining marked antioxidant activity of *P. lentiscus* and several pharmacological activities [11, 13, 14]. Moreover, *P. lentiscus* resin was analyzed by GC-MS, which demonstrated the presence of α -pinene, β -pinene, limonene, terpene-4-ol, and terpineol [15]. Meanwhile, essential oil obtained from leaves turned out to contain β -caryophyllene (31.38%), germaerene (12.05%), and γ -cadinene (6.48%). Volatile oil obtained from fruits was analyzed by GC-MS too, thanks to which the presence of α -pinene, myrcene and limonene, sesquiterpene, ketones and aliphatic esters, and phenolic compounds (thymol, carvacrol) was appreciated, whereas dimyrcene (0.5-4.4%) was found in all types of oil [16]. Furthermore, many efforts were dedicated to the chemical characterization of *P. lentiscus* essential oil, where the major constituents were terpinen-4-ol, α -terpineol, and germacrene D [17–20].

However, by now, less was done for the analysis and characterization of metabolome and biological properties of *P. lentiscus* hydrosol. During distillation for essential oil extraction, a small hydrophilic fraction escapes into the distillation water steam: the result is known as hydrosol. Although several hydrosols are marketed in the Western countries for aromatherapy and other applications, they are mostly considered by-products of steam distillation and, thus, redistilled to obtain more essential oil or discarded thereby losing an economically important coproduct. In the global market, essential oils valued USD 17.2 billion in 2019 and they could reach USD 33.26 billion in the next 8 years [21]. The economic value of the lost oil fraction was estimated to be USD 50-100 million in India [22]. Currently, it would be helpful to understand the potentiality of this low-cost by-product in terms of source of metabolites and therapeutic issues to demonstrate that *P. lentiscus* hydrosol could have potential as a global economic product of commerce.

To elucidate the phytochemical composition of complex matrices, a specific analytical technique is needed such as mass spectrometry, a valuable and mature tool for the assessment of metabolites in different matrices [23–26]. Above all, Fourier transform ion cyclotron resonance mass spectrometry (FT-ICR MS) has been shown to be a powerful technique for obtaining high-resolution accurate-mass spectra with outstanding levels of sensitivity, useful for a correct identification of thousands of unknown substances [27–33]. Thus, in this work, the analysis of *P. lentiscus* hydrosol was performed by using positive electrospray-Fourier transform ion cyclotron resonance mass spectrometry (ESI(+)-FT-ICR MS) together with a specific visualization tool of HRMS data, i.e., the Van Krevelen diagram, to shed some light on its phytochemical composition.

Moreover, since an anti-inflammatory activity of *P. lentiscus* leaf extracts is well-known [34], the influence of *P. lentiscus* hydrosol on proinflammatory cytokines IL-1 β , IL-6, and TNF- α and transcription factor NF- κ B was assessed in lipopolysaccharide-triggered macrophages. Then, the focus was set on the citrate pathway, a newly identified target of the immunometabolism under NF- κ B control and essential to produce ROS, NO, and PGE₂ inflammatory mediators [35]. To this end, the effect of *P. lentiscus* hydrosol was eval-

uated in LPS-triggered U937 cells by quantification of the two main components of the citrate pathway, which are the mitochondrial citrate carrier (CIC) and ATP citrate lyase (ACLY), and the levels of ROS, NO, and PGE₂ [36, 37].

2. Materials and Methods

2.1. Plant Material and Extraction. A selected genotype of *P. lentiscus* was applied to perform the different research actions. The genotype used was selected by Bioinnova (Potenza, Italy), starting from an endemism developed in Basilicata region. Young leaves and stems were utilized to obtain the hydrosol. In detail, 500 g of material was submitted to steam distillation for 90 min (with 1.5 L water) using a Clevenger-type apparatus. For each load, fresh material was placed into the distillation vessel. The first load was conducted to set up and establish the procedure and determine the processing parameters, and replications were conducted as the main study. Steam was supplied through a manifold pipe into the bottom of the vessel from a high-pressure boiler. The steam is routed upward through a false-bottom perforated plate to the plant material being extracted. The steam removes the essential oil, and both leave the vessel near the top via a flexible pipe and are carried to a water-cooled, parallel-piped multitubular glass condenser that is mounted vertically. The essential oil (lighter than water) and the water condensate (hydrosol) were then separated in a Pyrex florentine flask that was cleaned prior to and after each use. The yield of the hydrosol fraction obtained considering the initial load of 500 g of material was 0.3 L. Three replications of hydrosol were used to perform all the following experiments. Samples were stored into the fridge at 4°C prior to the analysis.

2.2. Mass Spectrometry Analysis. The FT-ICR mass spectrometer used was a Bruker solariX XR Fourier transform ion cyclotron resonance mass spectrometer (FT-ICR-MS) (Bruker Daltonik GmbH, Bremen, Germany) equipped with a 7 T superconducting magnet and an electrospray ionization (ESI) source. The external ESI source was set in positive ionization mode (ESI(+)) and was operated with a grounded capillary sprayer needle mounted 45° off-axis with nitrogen nebulizing gas at a pressure of 1.0 bar, a nitrogen drying gas temperature of 200°C, and a flow rate of 4.0 L/min. The ESI capillary voltage was set to 4.5 KV, while the spray shield voltage was set to -0.5 V. Samples were injected by using a 500 μ L syringe (Hamilton, Nevada, USA), setting a syringe flow rate of 120.0 μ L/h. Spectra were acquired with a time domain size of 16 megaword, an accumulation time of 0.1 s, and a mass range of 100-2000 m/z , with an average number of scans of 50. Calibration was performed by using a solution of sodium trifluoroacetic acid (NaTFA) clusters. At least 0.1 ppm mass accuracy FT-ICR MS was achieved. The *P. lentiscus* hydrosol solution filtered by means of a PTFE 0.22 μ m filter has been injected directly in the ESI source. An estimation of the noise level was performed by assuming the *N*-sigma methodology [38–40]. A noise level was first estimated by fitting low relative intensity distribution to a Gaussian one, according to the *N*-sigma methodology, in order to

calculate its mean. Once obtained, the noise level related to the mass spectrum of *P. lentiscus* hydrosol was set at a relative intensity of 0.5%, i.e., three times the extrapolated mean, in order to eliminate noise peaks, together with artifacts that resulted from Fourier transform execution on obtained free induction decays (FIDs). Moreover, mass spectra were smoothed to further eliminate wiggles and a m/z list was extracted. Analyses were done in triplicate, and common signals were considered for further data treatment. Then, possible elemental formulae were calculated for each m/z signal. To obtain unequivocal formulae, several constraints were applied, such as atom number limitations, i.e., $C \leq 100$, $H \leq 200$, $O \leq 80$, $N \leq 20$, $S \leq 8$, $P \leq 6$, $Na \leq 1$, and $K \leq 1$; restrictions on atoms to carbon number ratios, i.e., $0.2 \leq H/C \leq 3.1$, $O/C \leq 2$, $N/C \leq 1.3$, $S/C \leq 0.8$, and $P/C \leq 0.3$; $RDBE > 0$; nitrogen rule; and isotopic pattern filtering [41]. Moreover, a Kendrick mass defect analysis was performed to identify homologous series and to help formula assignment by solving redundancies [42–47]. In detail, only m/z peaks belonging to homologous series with a number of members higher or equal to 2 [45] were taken into account for assignment. The analysis was performed for every selected building block, i.e., CH_2 , CO , H_2O , H_2 , and O , and results were combined. HRMS data were processed by using Data Analysis (v4.2, Bruker Daltonik GmbH, Bremen, Germany) and R software (v. 3.6.0, <https://www.r-project.org/>).

2.3. Isolation of Human Monocytes from Whole Blood. Primary human monocytes were isolated from blood of healthy donors. The study was made in agreement with the Declaration of Helsinki and in accordance with the Committee on Human Research approved procedure no. 20170030156. All volunteers provided written informed consent approving and authorizing the use of their material for research purposes. Venous blood was collected directly into K2 EDTA-coated BD vacutainer tubes (Becton, Dickinson and Company, Franklin Lakes, NJ, USA). Peripheral blood mononuclear cells (PBMCs) were separated by Histopaque-1077 (Sigma-Aldrich, St. Louis, MO) density gradient centrifugation. In brief, whole blood was mixed with Hanks' Balanced Salt Solution (HBSS, Sigma-Aldrich) at a ratio of 1:2 (v/v), layered on the top of Histopaque-1077 (Sigma-Aldrich) and centrifuged at $1000 \times g$ for 15 minutes. The mononuclear cells at the interphase were recovered, washed twice in HBSS, and counted. PBMCs were incubated with CD14 antibody conjugated to magnetic beads (MACS[®], Miltenyi Biotec GmbH, Bergisch Gladbach, Germany) for 15 minutes at 4°C. After washing, cells were loaded onto a MACS[®] column (Miltenyi Biotec) placed in a magnetic field and CD14-positive ($CD14^+$) and CD14-negative ($CD14^-$) populations were separated. The $CD14^+$ monocytes were cultured in Roswell Park Memorial Institute (RPMI) 1640 medium supplemented with 10% fetal bovine serum, 2 mM L-glutamine, 100 U/mL penicillin, and 100 $\mu g/mL$ streptomycin at 37°C in 5% CO_2 .

2.4. Cell Culture and Treatments. Human monoblastic leukemia U937 cells (ICLC HTL94002-Interlab Cell Line Collection) were grown in suspension in RPMI 1640 medium

supplemented with 10% fetal bovine serum, 2 mM L-glutamine, 100 U/mL penicillin, and 100 $\mu g/mL$ streptomycin in a humidified chamber with 5% CO_2 at 37°C. Promonocytic U937 cells were differentiated to macrophages by using 10 ng/mL phorbol 12-myristate 13-acetate (PMA, Sigma-Aldrich) and further stimulated with lipopolysaccharide from *Salmonella enterica* serotype typhimurium (LPS, Sigma-Aldrich).

2.5. Cytotoxicity Assays. The effect of *P. lentiscus* hydrosol (*P.l*) on cell viability was determined by MTT assay and by cell counting. $CD14^+$ monocytes and U937 cells were seeded into a 96-well plate (1×10^4 cells/well) and treated with *P.l* at two different dilutions, 1:10 (*P.l* 1:10) and 1:100 (*P.l* 1:100), for 72 hours. MTT assay (*CellTiter 96[®] Non-Radioactive Cell Proliferation Assay*, Promega, Madison, WI, USA) was performed according to the manufacturer's instructions. In brief, a premixed dye solution was added. During 4-hour incubation, living cells converted a MTT tetrazolium component into formazan. Then, by adding Solubilization/Stop Solution, formazan crystals were solubilized and the absorbance at 570 nm was revealed by a microplate reader (GloMax, Promega). Cell counting was carried out by using the automated handheld *Scepter 2.0 Cell Counter* (Merck Millipore, Switzerland).

2.6. Quantification of Cytokines. The $CD14^+$ monocytes were treated with *P.l* 1:10 and *P.l* 1:100 for one hour, and then LPS was added to trigger the inflammatory cascade. Twenty-four hours later, the cell culture supernatants were collected and assayed for the concentration of IL-1 β (DLB50), IL-6 (D6050), and TNF- α (DTA00D) by using ELISA kits (R&D Systems, Inc., Minneapolis, MN, USA) following the manufacturer's recommendations.

2.7. SDS-PAGE and Western Blotting. For immunoblot analysis, cells were lysed in Laemmli buffer and boiled at 100°C for 5 minutes. Thirty micrograms of proteins was subjected to SDS/PAGE electrophoresis on 7–12% SDS polyacrylamide gels and then electroblotted onto nitrocellulose membranes. The membranes were blocked for 1 hour in a Tris-buffered saline (TBS) solution containing 5% nonfat dry milk and 0.5% Tween 20 and then incubated at 4°C overnight with anti-NF- $\kappa B/p65$ (ab7970, Abcam, Cambridge, MA), anti-CIC [35, 36], anti-ATP citrate lyase (ab157098, Abcam), or anti- β -actin (ab8227, Abcam) antibodies. Following 1-hour incubation with HRP goat anti-rabbit IgG antibody (Santa Cruz Biotechnology, Santa Cruz, CA, USA), the immunoreactions were detected by using the horseradish peroxidase substrate *WesternBright[™] ECL* (Advansta, Menlo Park, CA, USA).

2.8. Transient Transfection. To measure *ACLY* gene promoter activity, U937/PMA cells were transiently transfected as described previously [48] using 0.5 μg of pGL3 basic-LUC vector (Promega) containing the -3116/-20 bp region of the *ACLY* gene promoter or a deletion fragment of this region. Cells were transfected also with 10 ng of pRL-CMV (Promega) to normalize the extent of transfection. Twenty-four hours after transfection, U937/PMA cells were triggered

with LPS in the presence or absence of *P.l* 1 : 10 or *P.l* 1 : 100. The day after, cells were lysed and assayed for LUC activity using the *Dual-Luciferase® Reporter Assay System* (Promega), according to the manufacturer's protocol. Luminescence was measured as relative light units (RLU), taking the reading of luciferase assay substrate alone and then with cell lysate in a GloMax plate reader (Promega).

2.9. ACLY Activity. U937/PMA cells were treated for 3 hours with LPS in the presence or absence of *P.l* 1 : 10 or *P.l* 1 : 100; then, cells were washed twice in ice-cold PBS. The cell pellet was resuspended in ice-cold 0.1% NP40 in PBS, and three freeze-melt cycles (-80°C for 8 minutes/40°C for 4 minutes) were performed. After centrifugation, the supernatant was collected and protein concentration was determined by Bradford assay [49]. ACLY activity was assessed by the coupled malic dehydrogenase method [50–52]. In a cuvette, 150 µg of the cell lysate was added to the mixture, made of 50 mM Tris-HCl (pH 8.0), 10 mM MgCl₂, 1.9 mM DTT, 0.15 mM NADH, 0.07 mM CoA, 1 mM ATP, 2 mM potassium citrate, and 3.3 units/mL malic dehydrogenase. The reaction was started by adding ATP, and the NADH oxidation was measured at 340 nm at 25°C with a spectrophotometer. The specific ACLY activity was determined by normalization to the protein concentration and expressed as a percentage of the control.

2.10. ROS, NO, and PGE₂ Detection. To evaluate reactive oxygen species (ROS) and nitric oxide (NO) levels, U937 cells were differentiated to macrophages with PMA (U937/PMA) and triggered by LPS in the presence or not of *P.l* 1 : 10 or *P.l* 1 : 100. Following 24 hours, ROS and NO concentrations were measured by using 6-carboxy-2',7'-dichlorodihydrofluorescein diacetate (DCF-DA, Thermo Fisher Scientific, San Jose, CA, USA) and 4-amino-5-methylamino-2',7'-difluorofluorescein diacetate (DAF-FM Diacetate, Thermo Fisher Scientific), respectively. Cells were incubated with DCF-DA or DAF-FM diacetate for 30 minutes in the dark, and the fluorescence was recorded using a 96-well plate reader (GloMax, Promega). The levels of prostaglandin E₂ (PGE₂) were quantified in the cell culture supernatant after 48 hours of exposure to LPS by using *DetectX® Prostaglandin E2 High Sensitivity Immunoassay Kit* (Arbor Assays, Ann Arbor, MI, USA) according to the manufacturer's protocol.

2.11. Statistical Analysis. Results are shown as means ± S.D. of, at least three independent experiments. Statistical significance of differences was determined by using one-way ANOVA followed by Tukey's *post hoc* test for multiple comparisons. Differences were considered significant ($p < 0.05$), very significant ($p < 0.01$), and highly significant ($p < 0.001$).

3. Results

3.1. ESI(+)-FT-ICR MS Analysis. The ultra-high-resolution ESI(+)-FT-ICR mass spectrum of a sample of *P. lentiscus* hydrosol was obtained (Figure 1(a)), which immediately reveals its high complexity in terms of metabolomic profile.

Unfortunately, due to this, it is really hard to unbox to obtain important information related to its chemical composition. For this reason, utilization of specific visualization tools is compulsory. However, several pretreatment steps must be followed in order to eliminate noise peaks and artifacts [38–40]. 141 unequivocal formulae were assigned to leftover signals by considering several constraints and by assuming the Kendrick mass defect approach (see Materials and Methods), and these were used to build a Van Krevelen diagram, a well-known visualization tool over which molecular formulae are spread depending on their H/C (*Y*-axis) and O/C (*X*-axis) ratios (Figure 1(b)) [41]. This plot is extremely useful to shed some light on the metabolic profile of *P. lentiscus* hydrosol. Indeed, metabolites can be classified according to their position on the plot. In this way, the presence of four main classes of compounds could be appreciated, i.e., terpenes, amino acids, peptides, and condensed heterocycles. To be more specific, *CHO*-type formulae located in the upper part of the Van Krevelen diagram suggest the presence of terpenoid compounds in our sample. In detail, obtained formulae could correspond to molecules like verbenone and pinocarvone (C₁₀H₁₄O), linalool and borneol (C₁₀H₁₈O), β-phellandrenol and myrthenol (C₁₀H₁₆O), and sobrerol and p-menth-2-ene-1,8-diol (C₁₀H₁₈O₂), already found in hydro- and hydroalcoholic extracts of *P. lentiscus* in high quantities [5, 53]. Moreover, additional higher RDBE *CHO*-type formulae are present into the molecular map, which support the presence of higher RDBE lipid derivatives, like phenolic lipids. All these kinds of compounds are well-known for their affirmed biological activity [54].

By the way, it is interesting to note that there is a higher density of points in other regions of the *Van Krevelen* plot, thus revealing the presence of other types of metabolites never reported for *P. lentiscus*. In detail, the percentage of *CHON* and *CHONS* formulae (Figure 1(b)) is higher, thus suggesting a higher frequency of nitrogen- and sulphur-bearing compounds. From the position of points related to nitrogen-bearing class of formulae into the molecular map, it can be noticed that these species belong to two specific classes, i.e., peptides and condensed heterocycles, like purine and indole derivatives. Among these, amino acids and peptides deserve a special attention; in fact, most of them showed marked health-promoting properties [55–60]. Thus, analysis of high-resolution mass spectrometry data, together with the utilization of specific visualization tools, shed light on the wider complexity of *P. lentiscus* hydrosol metabolic profile, a characteristic that could turn out in a marked biological activity of our sample [61, 62].

3.2. *P. lentiscus* Hydrosol Affects the Secretion of the Proinflammatory Cytokines IL-1β, IL-6, and TNF-α. Since the leaf extracts of *P. lentiscus* have shown strong ability to reduce the levels of IL-6 and TNF-α in LPS-triggered polymorphonuclear cells [34], we decided to evaluate the anti-inflammatory activity of *P. lentiscus* hydrosol beginning from the analysis of its effect on proinflammatory cytokines. To this end, human CD14⁺ monocytes were treated with lipopolysaccharide, a structural component of the outer membrane of Gram-negative bacteria able to induce a strong

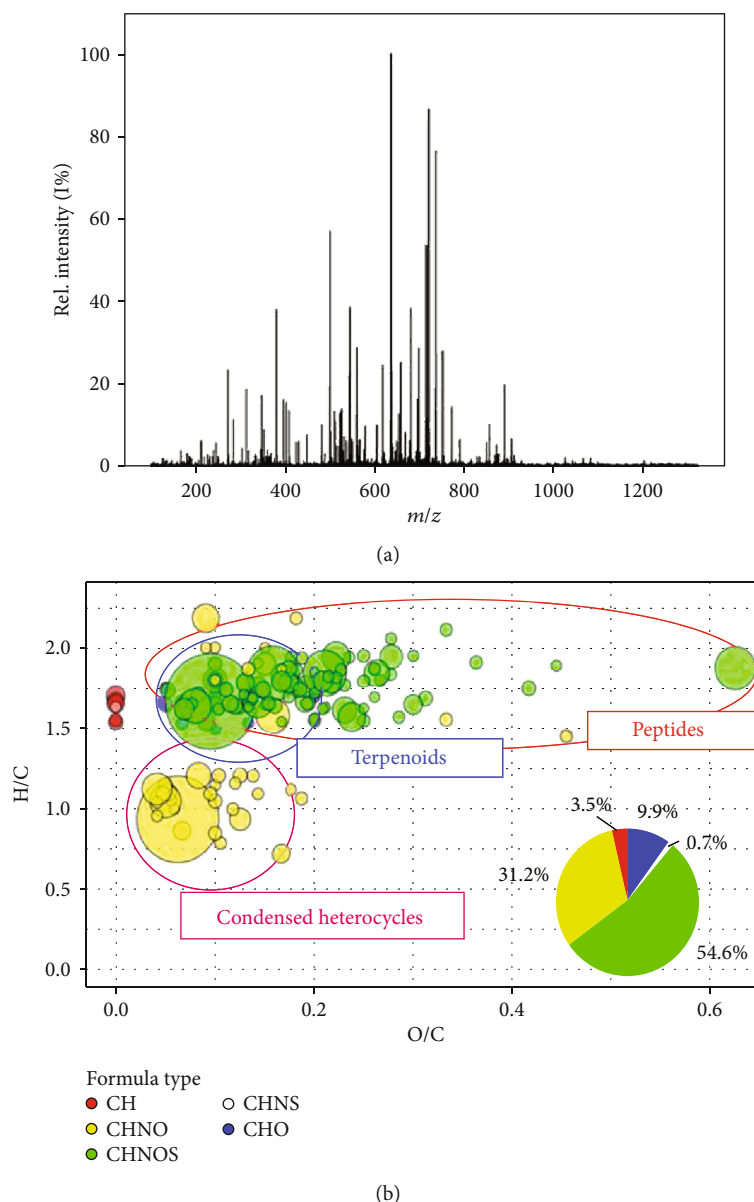


FIGURE 1: Untargeted metabolomic analysis of *P. lentiscus* hydrosol: (a) ultra-high-resolution ESI(+)-FT-ICR mass spectrum of a sample of *P. lentiscus* hydrosol; (b) Van Krevelen diagram of a sample of *P. lentiscus* hydrosol. Formula types are distinguished by colors, i.e., blue for CHO, yellow for CHON, green for CHONS, pink for CHNS, and red for CH. Moreover, a pie chart shows percentages of formulae per type.

inflammatory response, mediated by the toll-like receptor 4 (TLR4) [63]. LPS induces a wide range of responses in monocytes, including the rapid synthesis of the proinflammatory cytokines TNF- α , IL-1 β , and IL-6 [64].

Firstly, we evaluated the cytotoxicity of *P. lentiscus* hydrosol. To this end, human CD14⁺ monocytes, isolated from peripheral blood, were treated with this hydrosol at two different dilutions, 1:10 (*P.l* 1:10) and 1:100 (*P.l* 1:100). After 72 hours, cell counting and MTT assay were performed. As shown in Figure 2(a), at tested concentrations, the hydrosol had no obvious effect on the number of viable cells (one-way ANOVA). Similar results were obtained by using MTT assay (Figure S1). Therefore, for all subsequent experiments aimed at evaluating the anti-

inflammatory activity, *P. lentiscus* hydrosol was used at 1:10 and 1:100 dilutions.

In primary human monocytes, IL-1 β , IL-6, and TNF- α secretion after stimulation with LPS was assessed with and without coincubation with *P.l* 1:10 or *P.l* 1:100. More in detail, human CD14⁺ monocytes were treated for 1 hour with *P. lentiscus* hydrosol; then, LPS was added; 24 hours later, the concentration of IL-1 β , IL-6, and TNF- α was quantified in the cell culture supernatant. We observed a marked increase in the levels of all the proinflammatory cytokines analyzed after induction with LPS (Figures 2(b)–2(d): LPS vs. C, $p < 0.001$, Tukey's test). *P. lentiscus* hydrosol lowered IL-6 and TNF- α secretion in a dose-dependent manner, while *P.l* 1:100 brought the concentration of IL-1 β down

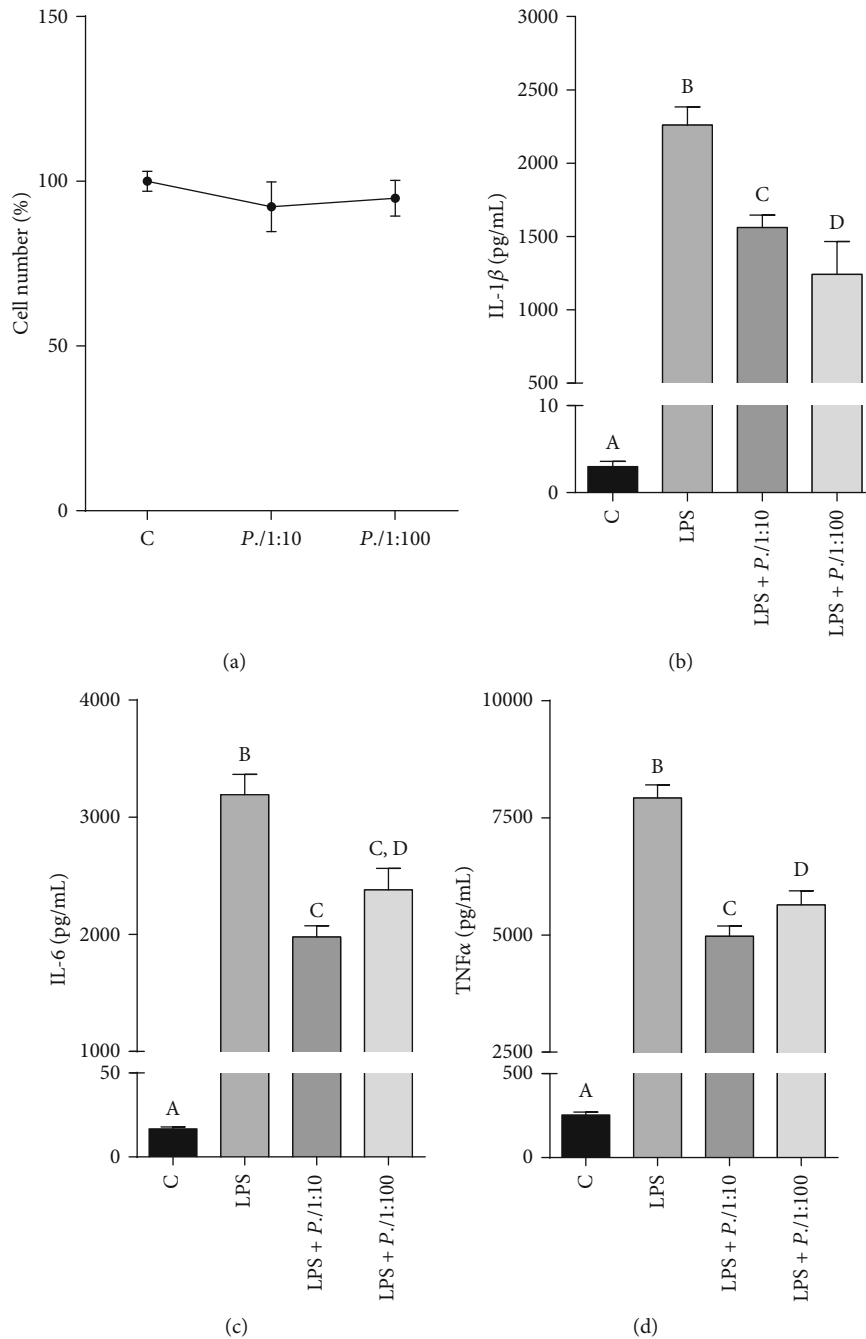


FIGURE 2: *P. lentiscus* hydrosol affects the release of the proinflammatory cytokines IL-1 β , IL-6, and TNF- α . (a) Primary human CD14⁺ monocytes were treated with *P.l* 1:10 and *P.l* 1:100 to evaluate the cytotoxic effect of *P. lentiscus* hydrosol. Cell viability was assessed by cell count after 72-hour exposure. Means \pm S.D. of three replicate independent experiments are shown. Differences between treated and untreated cells (C, set at 100%) were not significant (one-way ANOVA). (b–d) CD14⁺ monocytes were incubated for 1 hour with *P.l* 1:10 and *P.l* 1:100 and then activated with LPS. Twenty-four hours later, the concentration of the proinflammatory cytokines IL-1 β (b), IL-6 (c), and TNF- α (d) in cell culture supernatants was measured by ELISA. The values are presented as the mean \pm S.D. of three independent experiments. According to one-way ANOVA, differences in IL-1 β (b), IL-6 (c), and TNF- α (d) levels were significant ($p < 0.001$). Therefore, Tukey's post hoc test was performed and different letters indicate significant differences between treatments at $p < 0.05$.

more than *P.l* 1:10 (Figures 2(b)–2(d)). In particular, *P.l* 1:100 reduced almost half the levels of IL-1 β released after stimulation with LPS (Figure 2(b): LPS+*P.l* 1:100 vs. LPS, $p < 0.001$, Tukey's test), whereas the decrease caused by *P.l* 1:10 was about 35% (Figure 2(b): LPS+*P.l* 1:10 vs. LPS, $p < 0.001$, Tukey's test). On the other hand, *P.l* 1:10

led a 4-fold reduction in either IL-6 and TNF- α levels (Figures 2(c) and 2(d): LPS+*P.l* 1:10 vs. LPS, $p < 0.001$, Tukey's test); meanwhile, *P.l* 1:100 lowered the latter two cytokines by only 25% with respect to cells triggered only with LPS (Figures 2(c) and 2(d): LPS+*P.l* 1:100 vs. LPS, $p < 0.01$, Tukey's test).

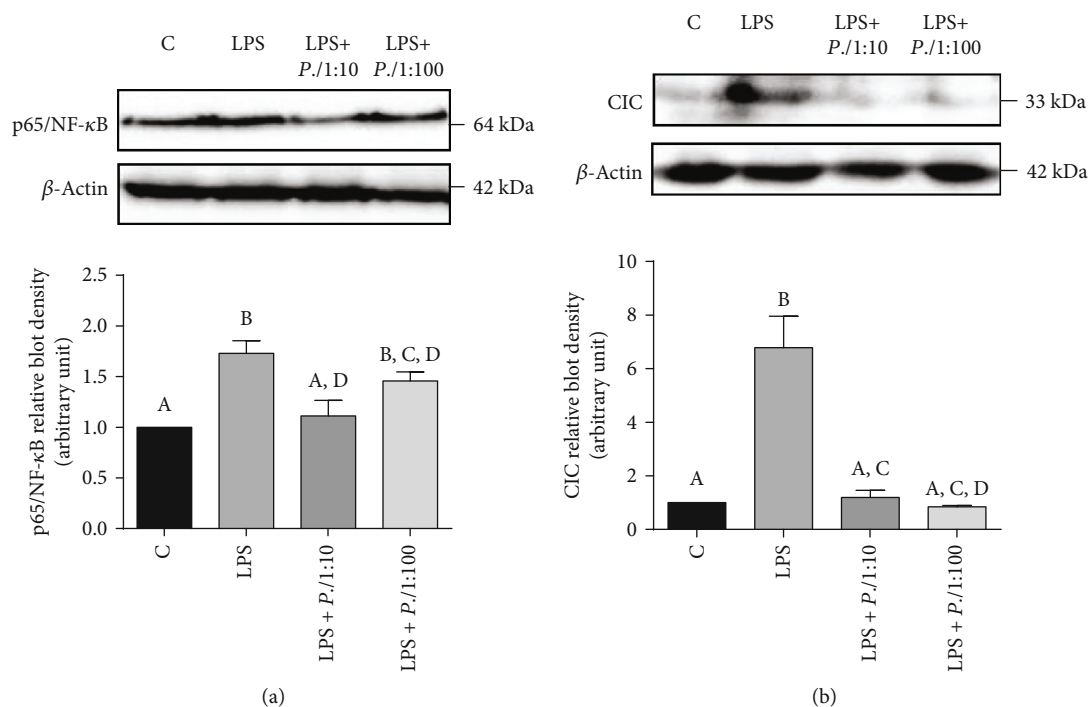


FIGURE 3: *P. lentiscus* hydrosol reduces p65/NF- κ B and CIC expression. U937 cells were treated with *P.l* 1:10 or *P.l* 1:100 for 1 hour and then activated with LPS. Cell lysates, obtained also from untreated cells (C) and cells triggered only with LPS (LPS), were used to evaluate the expression levels of p65/NF- κ B (a) and CIC (b). p65/NF- κ B, CIC, and β -actin were detected by specific antibodies, and Western blotting images (upper panel (a, b)) are representative of two independent experiments with similar results. The intensities of immunolabeled protein bands were measured by a quantitative software and normalized to β -actin (lower panel (a, b)). Bar charts reported means \pm S.D. of p65/NF- κ B (a) and CIC (b) protein levels obtained from the abovementioned two independent experiments. Different letters indicate significant differences between treatments at $p < 0.05$ (Tukey's test).

3.3. *P. lentiscus* Hydrosol Reduces NF- κ B and Mitochondrial Citrate Carrier Expression. The following experiments were performed on differentiated U937 cells (U937/PMA), which exert a myriad of macrophage functions and mimic the inflammatory response of activated macrophages when stimulated with LPS [65]. First of all, we checked that *P. lentiscus* hydrosol was not toxic also for U937 cells by cell counting (Figure S2a) and MTT assay (Figure S2b). Cell viability was not significantly altered after 72 hours of treatment with *P.l* 1:10 or *P.l* 1:100 (Figure S2). Therefore, *P. lentiscus* hydrosol was used at those two dilutions for all subsequent experiments on U937 cells.

The primary focus was on NF- κ B, which has a key role in the transcriptional activation of proinflammatory genes in LPS-triggered inflammation [66]. Interestingly, *P. lentiscus* hydrosol was able to resolve LPS-induced inflammation by reducing the levels of NF- κ B. In detail, U937 cells differentiated to macrophages with PMA were preincubated for 1 hour with *P.l* 1:10 or *P.l* 1:100. After that, U937/PMA cells were triggered with LPS. Following 6-hour incubation at 37°C, LPS induced a marked activation of NF- κ B p65 subunit (Figure 3(a)). Of note, *P. lentiscus* hydrosol reduced NF- κ B p65 subunit expression levels with respect to LPS-triggered cells (LPS) when used as 1:100 and at even lower values if employed at the highest concentration (1:10) (Figure 3(a)).

As shown above [67], among the proinflammatory genes activated by NF- κ B, there is *SLC25A1*, encoding the mitochondrial citrate carrier (CIC). CIC is a member of the mito-

chondrial carrier family (SLC25) localized in the inner membrane of mitochondria. SLC25s encode membrane proteins that transport many solutes across the inner mitochondrial membrane linking mitochondrial and cytosolic processes thus representing a wide integrated system interplaying with pathologies, such as inflammation or cancer [48, 68, 69]. For this reason, SLC25 gene expression is tightly regulated in physiological and pathological conditions as well as in different tissues and development [70–77]. Moving citrate from mitochondria to the cytosol, CIC is a newly identified target of the immunometabolism and its function is essential to produce inflammatory mediators. Indeed, a great *SLC25A1* upregulation occurs in M1 macrophages [36, 67].

Our analysis confirmed this change in gene expression since 7-fold increase in CIC protein levels was observed after 6 hours of exposure to LPS in U937/PMA cells (Figure 3(b)). *P. lentiscus* hydrosol totally abolished the CIC increased activation induced by LPS whether used as 1:10 or 1:100 (Figure 3(b)).

3.4. Effect of *P. lentiscus* Hydrosol on ATP Citrate Lyase. Since *P. lentiscus* hydrosol inhibited *SLC25A1* gene expression, we wondered if *ACLY*—the gene encoding the enzyme immediately downstream to CIC—could be a target too. *ACLY* is early upregulated in macrophages activated by LPS or proinflammatory cytokines TNF- α or IFN γ as well as in inflammatory conditions [37, 78, 79]. It is known that NF- κ B transcription

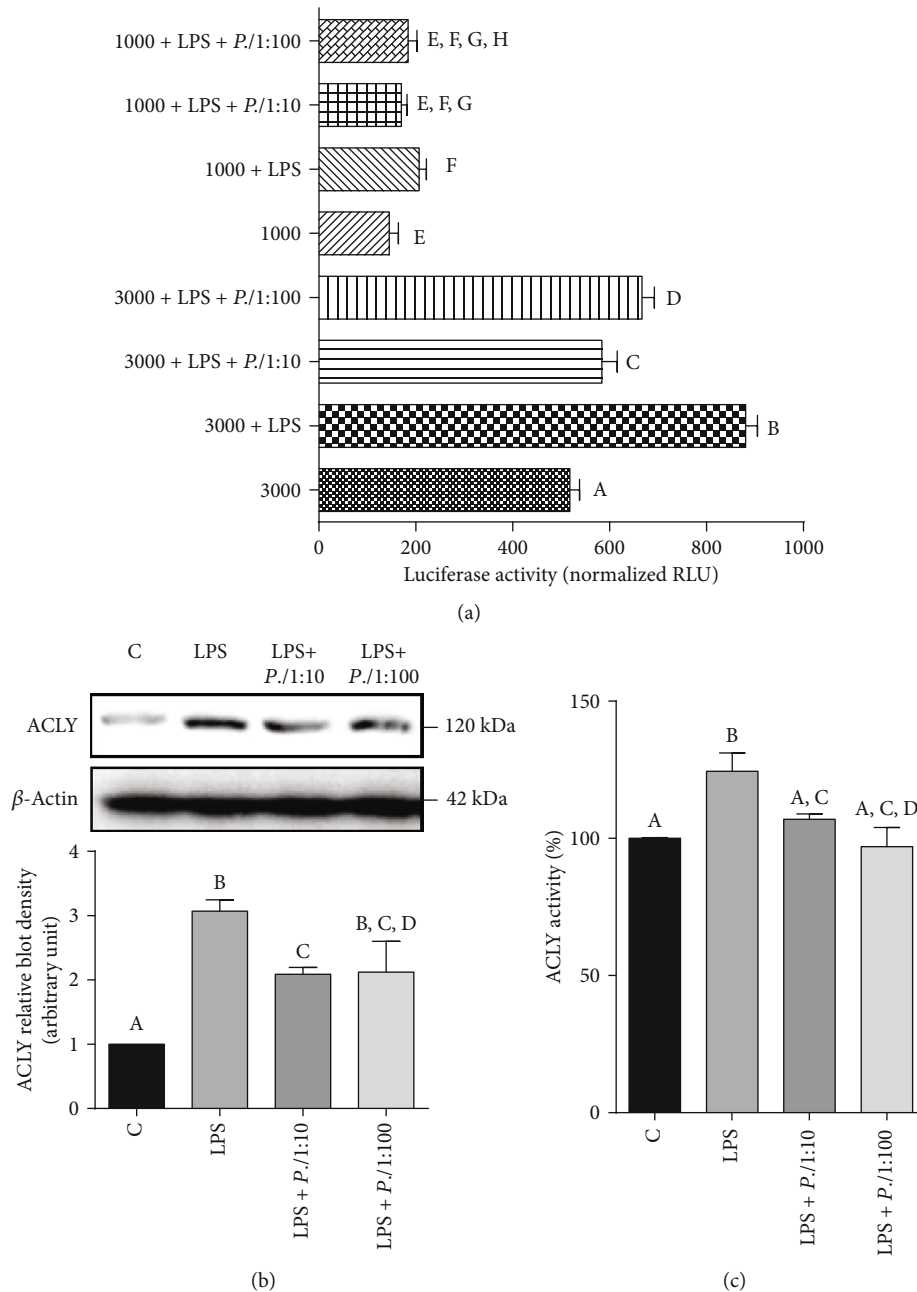


FIGURE 4: Effect of *P. lentiscus* hydrosol on ATP citrate lyase. (a) U937 cells were transiently transfected with pGL3 basic-LUC vector containing the full-length $-3116/-20$ bp region of the *ACLY* gene promoter (3000) or a truncated version of this region (1000). Then, cells were triggered with LPS in the absence (LPS) or in the presence of *P.l* 1 : 10 or *P.l* 1 : 100. Unstimulated cells were used as negative control. Twenty-four hours later, the luciferase gene reporter activity was assessed. (b, c) U937 cells, preincubated for 1 hour with *P.l* 1 : 10 or *P.l* 1 : 100, were activated with LPS, and *ACLY* protein levels (b) and enzymatic activity (c) were evaluated. In (b), *ACLY* and β -actin proteins were immunodecorated with specific antibodies. The Western blotting image (upper panel (b)) is representative of two independent experiments with similar results. The intensities of immunolabeled protein bands were measured by using a quantitative software and normalized to β -actin (lower panel (b)). The bar chart reported means \pm S.D. of *ACLY* (b) protein levels obtained from the abovementioned two independent experiments. In (a) and (c), activities are shown as the mean \pm S.D. of three experiments. Statistical significance of differences was evaluated by one-way ANOVA followed by Tukey's test for multiple comparisons. Different letters indicate significant differences between treatments at $p < 0.05$.

factor regulates the expression of *ACLY* in LPS-triggered macrophages [37]. Because the human *ACLY* gene promoter contains an active NF- κ B responsive element ($-2048/-2038$ bp), U937/PMA cells were transiently transfected with pGL3

basic-LUC vector containing the full-length $-3116/-20$ bp region of the *ACLY* gene promoter (3000, Figure 4(a)) or a truncated version of this region (1000, Figure 4(a)). First of all, lower *ACLY* gene promoter activity was observed in cells

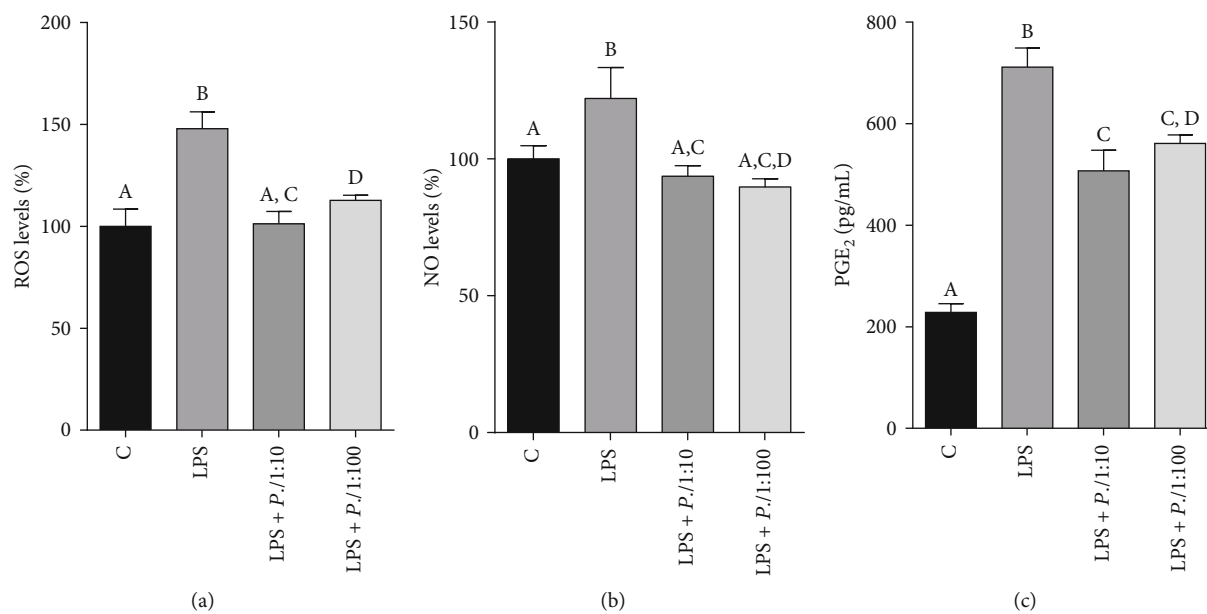


FIGURE 5: *P. lentiscus* hydrosol lowers ROS, NO, and PGE₂ levels. U937/PMA cells were untreated (C) or activated with LPS alone (LPS) or in the presence of *P.l* 1:10 or *P.l* 1:100. (a, b) Following 24 hours, ROS and NO levels were evaluated and expressed as percentage of C (set at 100%). (c) The concentration of PGE₂ secreted into cell culture supernatants was measured after 48 hours of treatment. Means \pm S.D. of four replicate independent experiments are shown. According to one-way ANOVA, differences in ROS (a), NO (b), and PGE₂ (c) levels were significant ($p < 0.001$). Therefore, Tukey's post hoc test was performed and different letters indicate significant differences between treatments at $p < 0.05$.

transfected with 1000 than 3000, which contains the binding site for NF- κ B, confirming that *ACLY* is under the transcriptional control of NF- κ B (Figure 4(a)). Following 24 hours of LPS treatment, the strongest promoter activity was registered in 3000 transfected U937 cells (3000+LPS, Figure 4(a)). The luciferase gene reporter activity was significantly reduced by 30% in cells treated with *P.l* 1:10 or *P.l* 1:100 (3000+LPS +*P.l* 1:10/1:100 vs. 3000+LPS, $p < 0.001$, Tukey's test, Figure 4(a)). *P. lentiscus* hydrosol was able to induce a parallel decrease in *ACLY* protein levels and enzymatic activity in LPS-triggered U937 (Figures 4(b) and 4(c)). More in detail, LPS induced a threefold increase in *ACLY* expression levels (Figure 4(b)) and a 30% rise in *ACLY* activity (Figure 4(c)). *P. lentiscus* hydrosol led to a reduction in *ACLY* protein levels in a dose-dependent manner (Figure 4(b)) while no significant differences were observed between *P.l* 1:10 and *P.l* 1:100 in bringing *ACLY* activity down (Figure 4(c)). All these results demonstrate that the inhibition of *ACLY* by *P. lentiscus* hydrosol in LPS-activated U937 cells is mediated by NF- κ B.

3.5. *P. lentiscus* Hydrosol Reduces ROS, NO, and PGE₂ Levels Acting through the Citrate Pathway. To shed more light on the role of *P. lentiscus* hydrosol in regulating the citrate pathway in LPS-activated macrophages, we took into consideration that CIC and *ACLY* supply intermediaries for the biosynthesis of inflammatory mediators such as ROS, NO, and prostaglandin E₂ [35]. Therefore, an enhanced release of ROS, NO, and PGE₂ was observed when U937/PMA cells were treated with LPS (Figures 5(a)–5(c)). *P. lentiscus* hydrosol was able to restore normal levels of reactive oxygen species and nitric oxide at both tested concentrations (Figures 5(a) and

5(b)). Instead, a dose-dependent reduction in PGE₂ levels occurred: *P.l* 1:10 induced a threefold decrease while *P.l* 1:100 lowered PGE₂ concentration only twice with respect to U937/PMA cells triggered with LPS (LPS+*P.l* 1:10/1:100 vs. LPS, $p < 0.001$, Tukey's test, Figure 5(c)).

4. Discussion

This study improves the knowledge on metabolites occurring in *P. lentiscus* hydrosol, thus revealing the wide diversity of its metabolic profile. The results of the present study also highlight the health-promoting value of *P. lentiscus* hydrosol. Of note, the sample showed a marked anti-inflammatory activity, most probably due to the presence of specific classes of metabolites, appreciated by the untargeted high-resolution mass spectrometric analysis. More specifically, the Van Krevelen diagram supported the presence of three main classes of metabolites, whose members are already known to show a marked anti-inflammatory activity. In detail, the presence of a considerable amount of anti-inflammatory peptides in different plant species was already demonstrated [55–57]. Moreover, most of the observed peptides are sulphur-bearing ones, thus suggesting the presence of cysteine and methionine units in their structures. It is well-known that the presence of cysteine units in some peptide structures, such as the glutathione (GSH) system, is compulsory to conduct an antioxidant activity against reactive oxygen species and nitric oxide [58–60]. Indeed, these species act synergically through oxidation and formation of disulphide bonds to reduce these harmful reactive species.

The sample tested was safe because of its null toxicity likewise all hydrosols. *P. lentiscus* hydrosol reduced the secretion of the proinflammatory cytokines IL-1 β , IL-6, and TNF- α , which have a key role in the immune response regulation. Notably, preliminary results of an ongoing investigation focused on Behçet's syndrome (BS), a multi-systemic inflammatory disorder [80, 81], shows a similar effect on cytokine IL-1 β .

Moreover, the ability of *P. lentiscus* hydrosol to modulate the activation of NF- κ B should be emphasized since NF- κ B is a nuclear transcription factor, which regulates the expression of most genes crucial in driving the inflammatory response. Among the NF- κ B target genes, we have chosen to focus on *SLC25A1* and *ACLY* immunometabolic genes encoding the mitochondrial citrate carrier and ATP citrate lyase, respectively. Indeed, *SLC25A1* and *ACLY* expression—transcriptionally regulated by NF- κ B—strongly decreased following the treatment with *P. lentiscus* hydrosol of LPS-triggered macrophages. Both CIC and *ACLY* proteins play a crucial role in M1 macrophages by exporting the accumulated citrate from mitochondria to the cytosol and converting it into oxaloacetate (OAA) and acetyl-CoA. OAA produces NADPH through the downstream reactions catalyzed by the cytosolic malate dehydrogenase (MDH1) and the malic enzyme 1 (ME1) [82]. This citrate-derived NADPH represents a critical source of reducing equivalents required for ROS and NO synthesis, as *ACLY/SLC25A1* gene silencing as well as their activity inhibition strongly reduces ROS and NO production in LPS-activated macrophages [35–37, 67, 83]. Moreover, NADPH or malate addition reverts *ACLY* inhibition phenotype leading to a huge increase of both inflammatory mediators in lymphoblasts [78]. Therefore, the effect of *P. lentiscus* hydrosol on ROS and NO levels could occur through the citrate pathway suppression together with a direct inhibition of NF- κ B which controls the expression of *SLC25A1* and *ACLY* but also of NADPH oxidase and inducible NO synthase genes involved in ROS and NO synthesis, respectively [84, 85].

Acetyl-CoA—the second citrate-derived metabolite—is a substrate for lipid biosynthesis including arachidonic acid, essential for the production of prostaglandins. Among them, prostaglandin E₂ is a key modulator of inflammation and innate immunity and plays a crucial role in inflammatory diseases [86]. Notably, treatment with exogenous acetate nearly entirely reverts the reduction of PGE₂ levels induced by citrate export pathway inhibition in M1 macrophages [67]. Thus, the lowering PGE₂ secretion observed in the presence of *P. lentiscus* hydrosol may be the effect of CIC and *ACLY* decreased expression and activity. Therefore, *P. lentiscus* hydrosol, in addition to diminishing the known IL-1 β , IL-6, and TNF- α proinflammatory cytokines, affects immunometabolism by suppressing the citrate export pathway through NF- κ B.

NF- κ B inhibition exploited by *P. lentiscus* hydrosol could be explained in terms of the metabolic profile of the sample. Indeed, ultra-high-resolution mass spectrometry data supported the presence of compounds that are known already to inhibit the activation of NF- κ B, such as linalool and α -terpineol [87, 88]. Moreover, sulphur-containing compounds could play a role into the inhibition process too, as already

seen for cysteine-containing peptides and derivatives. For example, N-acetyl cysteine was seen to suppress the activation of inhibitory protein I κ B kinases, thus inhibiting NF- κ B activation indirectly, and cysteine and glutathione levels turned out to be strictly correlated to the TNF-induced NF- κ B activity in cultured mouse hepatocytes [58, 89].

The achieved results are consistent and encouraging since they show for the first time the anti-inflammatory potential and envisage a therapeutic use of *P. lentiscus* hydrosol that until now has been discarded as it was considered a by-product. The exploitation of *P. lentiscus* hydrosol could represent a sustainable approach, according to the circular economy principles, to face the environmental issues derived by the generation of massive amount of these wastes. In fact, hydrosols are easy and inexpensive to produce since they are obtained at the same time of essential oil. Furthermore, in compliance with the circular economy concept, *P. lentiscus* hydrosol must be more investigated and valorized. Hydrosols find great application in aromatherapy for several reasons (e.g., antibacterial, antifungal, antiseptic, analgesic, antioxidant, anti-inflammatory, digestive, healing, and calming properties) [90–93]. Therefore, the study and the discovery of other *P. lentiscus* hydrosol activities could be helpful to drive toward an intensive use of this by-product. Moreover, further studies are needed to isolate, characterize, and elucidate the structure of the bioactive compounds of this sample, to understand which one of them is more correlated to its biological activity, and to be able to develop promising nutraceutical formulations.

5. Conclusions

For the first time, this study pointed out on the complex metabolic profile of *P. lentiscus* hydrosol, considered until now a by-product and, so, discarded. Its anti-inflammatory properties were highlighted. *P. lentiscus* hydrosol was able to reduce the secretion of IL-1 β , IL-6, and TNF- α proinflammatory cytokines and the expression of NF- κ B transcription factor as well as CIC and *ACLY*—key players of metabolic reprogramming occurring in inflammation—and in turn ROS, NO, and PGE₂ levels in lipopolysaccharide-triggered macrophages.

Data Availability

The data used to support the findings of this study are available from the corresponding authors upon request.

Conflicts of Interest

The authors declare no conflict of interest.

Authors' Contributions

The research was conceived and designed by Vittoria Infantino, Giuliana Bianco, and Giuseppe Martelli. The experiments were performed by Anna Santarsiero, Alberto Onzo, Raffaella Pascale, Maria Assunta Acquavia, Marianna Covello, Paolo Convertini, Michela Marsico, Corrado Pifano,

Patrizia Iannece, Carmine Gaeta, Salvatore D'Angelo, and Maria Carmela Padula. Experimental data were collected and analyzed by Anna Santarsiero, Alberto Onzo, Paolo Convertini, and Simona Todisco. Vittoria Infantino, Giuliana Bianco, Simona Todisco, and Giuseppe Martelli contributed reagents and materials. The manuscript was written by Vittoria Infantino, Giuliana Bianco, Anna Santarsiero, Alberto Onzo, Simona Todisco, and Giuseppe Martelli. All the authors have read and approved the final manuscript.

Acknowledgments

This research was supported by Funding for Basic Research (FFABR) from the Italian Ministry of Education, University and Research (MIUR) (grant number 102050101).

Supplementary Materials

Figure S1: effect of *P. lentiscus* hydrosol on primary human monocyte cell viability. Figure S2: effect of *P. lentiscus* hydrosol on U937 cell viability. (*Supplementary Materials*)

References

- [1] V. Mozaffarian, *Trees and Shrubs of Iran*, Farhang Moaser Publ, Tehran, 2005.
- [2] G. Bonnier and R. Douin, *La Grande flore en couleurs*, Belin, Paris, 1990.
- [3] F. Di Castri, D. W. Goodall, and R. L. Specht, *Mediterranean-type shrublands*, Elsevier, Amsterdam, 1981.
- [4] A. Dellai, H. Souissi, W. Borgi, A. Bouraoui, and N. Chouchane, "Antiinflammatory and antiulcerogenic activities of *Pistacia lentiscus* L. leaves extracts," *Industrial Crops and Products*, vol. 49, pp. 879–882, 2013.
- [5] D. Vlastos, D. Mademtoglou, E. Drosopoulou et al., "Evaluation of the genotoxic and antigenotoxic effects of Chios mastic water by the in vitro micronucleus test on human lymphocytes and the in vivo wing somatic test on *Drosophila*," *PLoS One*, vol. 8, no. 7, article e69494, 2013.
- [6] L. Iauk, S. Ragusa, A. Rapisarda, S. Franco, and V. M. Nicolosi, "In Vitro Antimicrobial activity of *Pistacia lentiscus*L. extracts: preliminary report," *Journal of Chemotherapy*, vol. 8, no. 3, pp. 207–209, 2013.
- [7] P. Magiatis, E. Melliou, A. L. Skaltsounis, I. B. Chinou, and S. Mitaku, "Chemical composition and antimicrobial activity of the essential oils of *Pistacia lentiscus*var.*chia*," *Planta Medica*, vol. 65, no. 8, pp. 749–752, 1999.
- [8] C. Koutsoudaki, M. Krsek, and A. Rodger, "Chemical composition and antibacterial activity of the essential oil and the gum of *Pistacia lentiscus* var. *chia*," *Journal of Agricultural and Food Chemistry*, vol. 53, no. 20, pp. 7681–7685, 2005.
- [9] L. Longo, A. Scardino, and G. Vasapollo, "Identification and quantification of anthocyanins in the berries of *Pistacia lentiscus* L., *Phillyrea latifolia* L. and *Rubia peregrina* L.," *Innovative Food Science & Emerging Technologies*, vol. 8, no. 3, pp. 360–364, 2007.
- [10] W. Bhouri, S. Derbel, I. Skandrani et al., "Study of genotoxic, antigenotoxic and antioxidant activities of the digallic acid isolated from *Pistacia lentiscus* fruits," *Toxicology In Vitro*, vol. 24, no. 2, pp. 509–515, 2010.
- [11] H. Azaizeh, F. Halahleh, N. Abbas et al., "Polyphenols from *Pistacia lentiscus* and *Phillyrea latifolia* impair the exsheathment of gastro-intestinal nematode larvae," *Veterinary Parasitology*, vol. 191, no. 1-2, pp. 44–50, 2013.
- [12] G. V. Dedoussis, A. C. Kaliora, S. Psarras et al., "Antiatherogenic effect of *Pistacia lentiscus* via GSH restoration and downregulation of CD36 mRNA expression," *Atherosclerosis*, vol. 174, no. 2, pp. 293–303, 2004.
- [13] D. Atmani, N. Chaher, M. Berboucha et al., "Antioxidant capacity and phenol content of selected Algerian medicinal plants," *Food Chemistry*, vol. 112, no. 2, pp. 303–309, 2009.
- [14] S. Remila, D. Atmani-Kilani, S. Delemasure et al., "Antioxidant, cytoprotective, anti-inflammatory and anticancer activities of *Pistacia lentiscus* (Anacardiaceae) leaf and fruit extracts," *European Journal of Integrative Medicine*, vol. 7, no. 3, pp. 274–286, 2015.
- [15] R. Congiu, D. Falconieri, B. Marongiu, A. Piras, and S. Porcedda, "Extraction and isolation of *Pistacia lentiscus* L. essential oil by supercritical CO₂," *Flavour and Fragrance Journal*, vol. 17, no. 4, pp. 239–244, 2002.
- [16] F. B. Douissa, N. Hayder, L. Chekir-Ghedira et al., "New study of the essential oil from leaves of *Pistacia lentiscus* L. (Anacardiaceae) from Tunisia," *Flavour and Fragrance Journal*, vol. 20, no. 4, pp. 410–414, 2005.
- [17] A. Barra, V. Coroneo, S. Dessi, P. Cabras, and A. Angioni, "Characterization of the volatile constituents in the essential oil of *Pistacia lentiscus* L. from different origins and its antifungal and antioxidant activity," *Journal of Agricultural and Food Chemistry*, vol. 55, no. 17, pp. 7093–7098, 2007.
- [18] E. H. Benyoussef, S. Charchari, N. Nacer-Bey, N. Yahiaoui, A. Chakou, and M. Bellatreche, "The essential oil of *Pistacia lentiscus*L. from Algeria," *Journal of Essential Oil Research*, vol. 17, no. 6, pp. 642–644, 2005.
- [19] A. Maxia, C. Sanna, M. A. Frau, A. Piras, M. S. Karchuli, and V. Kasture, "Anti-inflammatory Activity of *Pistacia lentiscus* Essential Oil: Involvement of IL-6 and TNF- α ," *Natural Product Communications*, vol. 6, no. 10, pp. 1543–1544, 2011.
- [20] F. Z. Mharti, B. Lyoussi, and A. Abdellaoui, "Antibacterial activity of the essential oils of *Pistacia lentiscus* used in Moroccan folkloric medicine," *Natural Product Communications*, vol. 6, no. 10, pp. 1505–1506, 2011.
- [21] *Essential Oils Market Size, Share & Trends Report Essential Oils Market Size, Share & Trends Analysis Report By Application (Food & Beverages, Spa & Relaxation), By Product (Orange, Peppermint), By Sales Channel, And Segment Forecasts, 2020 - 2027* June 2020 <https://www.grandviewresearch.com/industry-analysis/essential-oils-market>.
- [22] B. R. Rajeswara Rao, "Hydrosols and water-soluble essential oils of aromatic plants: future economic products," *Indian Perfumer*, vol. 56, pp. 29–33, 2012.
- [23] L. W. Sumner, P. Mendes, and R. A. Dixon, "Plant metabolomics: large-scale phytochemistry in the functional genomics era," *Phytochemistry*, vol. 62, no. 6, pp. 817–836, 2003.
- [24] G. Ventura, C. D. Calvano, I. Losito et al., "Effect of pH and mobile phase additives on the chromatographic behaviour of an amide-embedded stationary phase: cyanocobalamin and its diaminechloro-platinum(II) conjugate as a case study," *Journal of Separation Science*, vol. 42, no. 6, pp. 1155–1162, 2019.
- [25] R. Pascale, M. A. Acquavia, T. R. I. Cataldi et al., "Profiling of quercetin glycosides and acyl glycosides in sun-dried peperoni

- di Senise peppers (*Capsicum annum* L.) by a combination of LC-ESI(-)-MS/MS and polarity prediction in reversed-phase separations," *Analytical and Bioanalytical Chemistry*, vol. 412, no. 12, pp. 3005–3015, 2020.
- [26] G. Bianco, R. Zianni, G. Anzillotta et al., "Dibenzo-p-dioxins and dibenzofurans in human breast milk collected in the area of Taranto (Southern Italy): first case study," *Analytical and Bioanalytical Chemistry*, vol. 405, no. 7, pp. 2405–2410, 2013.
- [27] G. Bianco, N. Agerbirk, I. Losito, and T. R. Cataldi, "Acylated glucosinolates with diverse acyl groups investigated by high resolution mass spectrometry and infrared multiphoton dissociation," *Phytochemistry*, vol. 100, pp. 92–102, 2014.
- [28] G. Bianco, C. Labella, A. Pepe, and T. R. Cataldi, "Scrambling of autoinducing precursor peptides investigated by infrared multiphoton dissociation with electrospray ionization and Fourier transform ion cyclotron resonance mass spectrometry," *Analytical and Bioanalytical Chemistry*, vol. 405, no. 5, pp. 1721–1732, 2013.
- [29] T. R. Cataldi, D. Orlando, D. Nardiello et al., "A three-factor Doehlert matrix design in optimising the determination of octadecyltrimethylammonium bromide by cation-exchange chromatography with suppressed conductivity detection," *Analytica Chimica Acta*, vol. 597, no. 1, pp. 129–136, 2007.
- [30] R. Pascale, G. Bianco, T. R. I. Cataldi et al., "Investigation of the effects of virgin olive oil cleaning systems on the secoiridoid aglycone content using high performance liquid chromatography–mass spectrometry," *Journal of the American Oil Chemists' Society*, vol. 95, no. 6, pp. 665–671, 2018.
- [31] T. R. Cataldi, G. Bianco, S. Abate, and I. Losito, "Identification of unsaturated N-acylhomo-serine lactones in bacterial isolates of *Rhodobacter sphaeroides* by liquid chromatography coupled to electrospray ionization-hybrid linear ion trap-Fourier transform ion cyclotron resonance mass spectrometry," *Rapid Communications in Mass Spectrometry*, vol. 25, no. 13, pp. 1817–1826, 2011.
- [32] D. Caniani, G. Esposito, R. Gori et al., "Toward a new plant-wide experimental and modeling approach for reduction of greenhouse gas emission from wastewater treatment plants," *Journal of Environmental Engineering*, vol. 145, no. 8, article 04019043, 2019.
- [33] C. A. Hughey, R. P. Rodgers, and A. G. Marshall, "Resolution of 11,000 compositionally distinct components in a single electrospray ionization Fourier transform ion cyclotron resonance mass spectrum of crude oil," *Analytical Chemistry*, vol. 74, no. 16, pp. 4145–4149, 2002.
- [34] K. Qabaha, S. A. Ras, J. Abbadi, and F. Al-Rimawi, "Anti-inflammatory of both *Eucalyptus* spp. and *Pistascia lentiscus* were investigated along with their phenolic compounds analysis using HPLC with UV detection," *African Journal of Traditional, Complementary and Alternative Medicines*, vol. 13, no. 5, pp. 1–6, 2016.
- [35] V. Infantino, C. L. Pierri, and V. Iacobazzi, "Metabolic routes in inflammation: the citrate pathway and its potential as therapeutic target," *Current Medicinal Chemistry*, vol. 26, no. 40, pp. 7104–7116, 2020.
- [36] V. Infantino, P. Convertini, L. Cucci et al., "The mitochondrial citrate carrier: a new player in inflammation," *The Biochemical Journal*, vol. 438, no. 3, pp. 433–436, 2011.
- [37] V. Infantino, V. Iacobazzi, F. Palmieri, and A. Menga, "ATP-citrate lyase is essential for macrophage inflammatory response," *Biochemical and Biophysical Research Communications*, vol. 440, no. 1, pp. 105–111, 2013.
- [38] C. C. Wong, D. Cociorva, J. D. Venable, T. Xu, and J. R. Yates 3rd., "Comparison of different signal thresholds on data dependent sampling in Orbitrap and LTQ mass spectrometry for the identification of peptides and proteins in complex mixtures," *Journal of the American Society for Mass Spectrometry*, vol. 20, no. 8, pp. 1405–1414, 2009.
- [39] K. O. Zhurov, A. N. Kozhinov, L. Fornelli, and Y. O. Tsybin, "Distinguishing analyte from noise components in mass spectra of complex samples: where to cut the noise?," *Analytical Chemistry*, vol. 86, no. 7, pp. 3308–3316, 2014.
- [40] A. T. Zielinski, I. Kourtchev, C. Bortolini et al., "A new processing scheme for ultra-high resolution direct infusion mass spectrometry data," *Atmospheric Environment*, vol. 178, pp. 129–139, 2018.
- [41] R. Pascale, G. Bianco, T. R. I. Cataldi et al., "Mass spectrometry-based phytochemical screening for hypoglycemic activity of Fagioli di Sarconi beans (*Phaseolus vulgaris* L.)," *Food Chemistry*, vol. 242, pp. 497–504, 2018.
- [42] C. S. Hsu, K. Qian, and Y. C. Chen, "An innovative approach to data analysis in hydrocarbon characterization by on-line liquid chromatography-mass spectrometry," *Analytica Chimica Acta*, vol. 264, no. 1, pp. 79–89, 1992.
- [43] C. A. Hughey, C. L. Hendrickson, R. P. Rodgers, A. G. Marshall, and K. Qian, "Kendrick mass defect spectrum: a compact visual analysis for ultrahigh-resolution broadband mass spectra," *Analytical Chemistry*, vol. 73, no. 19, pp. 4676–4681, 2001.
- [44] E. Kendrick, "A mass scale based on $CH_2 = 14.0000$ for high resolution mass spectrometry of organic compounds," *Analytical Chemistry*, vol. 35, no. 13, pp. 2146–2154, 1963.
- [45] L. A. Lerno Jr., J. B. German, and C. B. Lebrilla, "Method for the identification of lipid classes based on referenced Kendrick mass analysis," *Analytical Chemistry*, vol. 82, no. 10, pp. 4236–4245, 2010.
- [46] Y. Qi, R. Hempelmann, and D. A. Volmer, "Two-dimensional mass defect matrix plots for mapping genealogical links in mixtures of lignin depolymerisation products," *Analytical and Bioanalytical Chemistry*, vol. 408, no. 18, pp. 4835–4843, 2016.
- [47] H. Sato, S. Nakamura, K. Teramoto, and T. Sato, "Structural characterization of polymers by MALDI spiral-TOF mass spectrometry combined with Kendrick mass defect analysis," *Journal of the American Society for Mass Spectrometry*, vol. 25, no. 8, pp. 1346–1355, 2014.
- [48] V. Infantino, F. Dituri, P. Convertini et al., "Epigenetic upregulation and functional role of the mitochondrial aspartate/glutamate carrier isoform 1 in hepatocellular carcinoma," *Biochimica et Biophysica Acta - Molecular Basis of Disease*, vol. 1865, no. 1, pp. 38–47, 2019.
- [49] M. M. Bradford, "A rapid and sensitive method for the quantitation of microgram quantities of protein utilizing the principle of protein-dye binding," *Analytical Biochemistry*, vol. 72, no. 1-2, pp. 1513–1523, 1976.
- [50] T. C. Linn and P. A. Srere, "Identification of ATP citrate lyase as a phosphoprotein," *The Journal of Biological Chemistry*, vol. 254, no. 5, pp. 1691–1698, 1979.
- [51] T. Migita, T. Narita, K. Nomura et al., "ATP citrate lyase: activation and therapeutic implications in non-small cell lung cancer," *Cancer Research*, vol. 68, no. 20, pp. 8547–8554, 2008.
- [52] Y. Takeda, F. Suzuki, and H. Inoue, "[27] ATP citrate lyase (citrate-cleavage enzyme)," *Methods in Enzymology*, vol. 13, pp. 153–160, 1969.

- [53] S. Paraschos, P. Magiatis, P. Gousia et al., "Chemical investigation and antimicrobial properties of mastic water and its major constituents," *Food Chemistry*, vol. 129, no. 3, pp. 907–911, 2011.
- [54] M. Stasiuk and A. Kozubek, "Biological activity of phenolic lipids," *Cellular and Molecular Life Sciences*, vol. 67, no. 6, pp. 841–860, 2010.
- [55] J. W. Hwang, S. J. Lee, Y. S. Kim et al., "Purification and characterization of a novel peptide with inhibitory effects on colitis induced mice by dextran sulfate sodium from enzymatic hydrolysates of *Crassostrea gigas*," *Fish & Shellfish Immunology*, vol. 33, no. 4, pp. 993–999, 2012.
- [56] M. C. Millán-Linares, F. Millán, J. Pedroche, and M. d. M. Yust, "GPETAFLR: a new anti-inflammatory peptide from *Lupinus angustifolius* L. protein hydrolysate," *Journal of Functional Foods*, vol. 18, pp. 358–367, 2015.
- [57] G. M. Qian, G. F. Pan, and J. Y. Guo, "Anti-inflammatory and antinociceptive effects of cordymin, a peptide purified from the medicinal mushroom *Cordyceps sinensis*," *Natural Product Research*, vol. 26, no. 24, pp. 2358–2362, 2012.
- [58] G. Aldini, A. Altomare, G. Baron et al., "N-Acetylcysteine as an antioxidant and disulphide breaking agent: the reasons why," *Free Radical Research*, vol. 52, no. 7, pp. 751–762, 2018.
- [59] I. Dini, G. C. Tenore, and A. Dini, "S-Alkenyl cysteine sulfoxide and its antioxidant properties from *Allium cepa* var. *tropeana* (red onion) seeds," *Journal of Natural Products*, vol. 71, no. 12, pp. 2036–2037, 2008.
- [60] E. Mukwehwo, Z. Ferreira, and A. Ayeleso, "Potential role of sulfur-containing antioxidant systems in highly oxidative environments," *Molecules*, vol. 19, no. 12, pp. 19376–19389, 2014.
- [61] G. Bianco, A. Buchicchio, and T. R. Cataldi, "Structural characterization of major soyasaponins in traditional cultivars of Fagioli di Sarconi beans investigated by high-resolution tandem mass spectrometry," *Analytical and Bioanalytical Chemistry*, vol. 407, no. 21, pp. 6381–6389, 2015.
- [62] G. Bianco, R. Pascale, C. F. Carbone et al., "Determination of soyasaponins in Fagioli di Sarconi beans (*Phaseolus vulgaris* L.) by LC-ESI-FTICR-MS and evaluation of their hypoglycemic activity," *Analytical and Bioanalytical Chemistry*, vol. 410, no. 5, pp. 1561–1569, 2018.
- [63] R. Medzhitov, "Inflammation 2010: new adventures of an old flame," *Cell*, vol. 140, no. 6, pp. 771–776, 2010.
- [64] R. Medzhitov, "Origin and physiological roles of inflammation," *Nature*, vol. 454, no. 7203, pp. 428–435, 2008.
- [65] Y. S. Baek, S. Haas, H. Hackstein et al., "Identification of novel transcriptional regulators involved in macrophage differentiation and activation in U937 cells," *BMC Immunology*, vol. 10, no. 1, 2009.
- [66] S. Ghosh and M. S. Hayden, "New regulators of NF- κ B in inflammation," *Nature Reviews Immunology*, vol. 8, no. 11, pp. 837–848, 2008.
- [67] V. Infantino, V. Iacobazzi, A. Menga, M. L. Avantiaggiati, and F. Palmieri, "A key role of the mitochondrial citrate carrier (SLC25A1) in TNF α - and IFN γ -triggered inflammation," *Biochimica et Biophysica Acta (BBA) - Gene Regulatory Mechanisms*, vol. 1839, no. 11, pp. 1217–1225, 2014.
- [68] V. Iacobazzi, V. Infantino, A. Castegna et al., "Mitochondrial carriers in inflammation induced by bacterial endotoxin and cytokines," *Biological Chemistry*, vol. 398, no. 3, pp. 303–317, 2017.
- [69] C. Indiveri, V. Iacobazzi, A. Tonazzi et al., "The mitochondrial carnitine/acylcarnitine carrier: function, structure and pathophysiology," *Molecular Aspects of Medicine*, vol. 32, no. 4–6, pp. 223–233, 2011.
- [70] V. Iacobazzi, V. Infantino, and F. Palmieri, "Epigenetic mechanisms and Sp1 regulate mitochondrial citrate carrier gene expression," *Biochemical and Biophysical Research Communications*, vol. 376, no. 1, pp. 15–20, 2008.
- [71] V. Infantino, V. Iacobazzi, F. De Santis, M. Mastrapasqua, and F. Palmieri, "Transcription of the mitochondrial citrate carrier gene: role of SREBP-1, upregulation by insulin and downregulation by PUFA," *Biochemical and Biophysical Research Communications*, vol. 356, no. 1, pp. 249–254, 2007.
- [72] V. Iacobazzi, P. Convertini, V. Infantino, P. Scarcia, S. Todisco, and F. Palmieri, "Statins, fibrates and retinoic acid upregulate mitochondrial acylcarnitine carrier gene expression," *Biochemical and Biophysical Research Communications*, vol. 388, no. 4, pp. 643–647, 2009.
- [73] V. Iacobazzi, V. Infantino, F. Bisaccia, A. Castegna, and F. Palmieri, "Role of FOXA in mitochondrial citrate carrier gene expression and insulin secretion," *Biochemical and Biophysical Research Communications*, vol. 385, no. 2, pp. 220–224, 2009.
- [74] V. Infantino, A. Castegna, F. Iacobazzi et al., "Impairment of methyl cycle affects mitochondrial methyl availability and glutathione level in Down's syndrome," *Molecular Genetics and Metabolism*, vol. 102, no. 3, pp. 378–382, 2011.
- [75] P. Convertini, S. Todisco, F. De Santis et al., "Transcriptional regulation factors of the human mitochondrial aspartate/glutamate carrier gene, isoform 2 (SLC25A13): USF1 as basal factor and FOXA2 as activator in liver cells," *International Journal of Molecular Sciences*, vol. 20, no. 8, p. 1888, 2019.
- [76] A. del Arco, J. Morcillo, J. R. Martinez-Morales et al., "Expression of the aspartate/glutamate mitochondrial carriers aralar1 and citrin during development and in adult rat tissues," *European Journal of Biochemistry*, vol. 269, no. 13, pp. 3313–3320, 2002.
- [77] V. Iacobazzi, V. Infantino, P. Costanzo, P. Izzo, and F. Palmieri, "Functional analysis of the promoter of the mitochondrial phosphate carrier human gene: identification of activator and repressor elements and their transcription factors," *The Biochemical Journal*, vol. 391, no. 3, pp. 613–621, 2005.
- [78] P. Convertini, A. Menga, G. Andria et al., "The contribution of the citrate pathway to oxidative stress in Down syndrome," *Immunology*, vol. 149, no. 4, pp. 423–431, 2016.
- [79] A. Santarsiero, P. Leccese, P. Convertini et al., "New insights into Behçet's syndrome metabolic reprogramming: citrate pathway dysregulation," *Mediators of Inflammation*, vol. 2018, Article ID 1419352, 8 pages, 2018.
- [80] A. Gul, "Pathogenesis of Behçet's disease: autoinflammatory features and beyond," *Seminars in Immunopathology*, vol. 37, no. 4, pp. 413–418, 2015.
- [81] M. C. Padula, P. Leccese, N. Lascaro et al., "From structure to function for the characterization of ERAP1 active site in Behçet syndrome. A novel polymorphism associated with known gene variations," *Molecular Immunology*, vol. 117, pp. 155–159, 2020.
- [82] S. Todisco, P. Convertini, V. Iacobazzi, and V. Infantino, "TCA cycle rewiring as emerging metabolic signature of hepatocellular carcinoma," *Cancers*, vol. 12, no. 1, p. 68, 2020.

- [83] V. Iacobazzi and V. Infantino, "Citrate—new functions for an old metabolite," *Biological Chemistry*, vol. 395, no. 4, pp. 387–399, 2014.
- [84] F. Aktan, "iNOS-mediated nitric oxide production and its regulation," *Life Sciences*, vol. 75, no. 6, pp. 639–653, 2004.
- [85] J. Anrather, G. Racchumi, and C. Iadecola, "NF- κ B Regulates Phagocytic NADPH Oxidase by Inducing the Expression of gp91phox," *Journal of Biological Chemistry*, vol. 281, no. 9, pp. 5657–5667, 2006.
- [86] J. Y. Park, M. H. Pillinger, and S. B. Abramson, "Prostaglandin E2 synthesis and secretion: the role of PGE2 synthases," *Clinical Immunology*, vol. 119, no. 3, pp. 229–240, 2006.
- [87] S. B. Hassan, H. Gali-Muhtasib, H. Goransson, and R. Larsson, "Alpha Terpineol: A Potential Anticancer Agent which Acts through Suppressing NF- κ B Signalling," *Anticancer Research*, vol. 30, no. 6, pp. 1911–1919, 2010.
- [88] X.-H. Zheng, C.-P. Liu, Z.-G. Hao, Y.-F. Wang, and X.-L. Li, "Protective effect and mechanistic evaluation of linalool against acute myocardial ischemia and reperfusion injury in rats," *RSC Advances*, vol. 7, no. 55, pp. 34473–34481, 2017.
- [89] H. Lou and N. Kaplowitz, "Glutathione depletion down-regulates tumor necrosis factor alpha-induced NF-kappaB activity via IkappaB kinase-dependent and -independent mechanisms," *The Journal of Biological Chemistry*, vol. 282, no. 40, pp. 29470–29481, 2007.
- [90] J. Rose, *375 Essential Oils and Hydrosols*, Frog, Berkeley, California, 2001.
- [91] S. Catty, *Hydrosols: The Next Aromatherapy*, Healing Arts Press, Rochester, Vermont, 2001.
- [92] L. Price and S. Price, "Understanding Hydrolats : The Specific Hydrosols for Aromatherapy," in *A Guide for Health Professionals*, Churchill Livingstone, Edinburgh, 2004.
- [93] J. Paolini, C. Leandri, J. M. Desjobert, T. Barboni, and J. Costa, "Comparison of liquid-liquid extraction with head-space methods for the characterization of volatile fractions of commercial hydrolats from typically Mediterranean species," *Journal of Chromatography A*, vol. 1193, no. 1-2, pp. 37–49, 2008.



Review

Detection and quantification of Covid-19 antiviral drugs in biological fluids and tissues

Maria A. Acquavia^{a,b}, Luca Foti^a, Raffaella Pascale^a, Antonia Nicolò^a, Vincenzo Brancaleone^a, Tommaso R.I. Cataldi^c, Giuseppe Martelli^a, Laura Scrano^d, Giuliana Bianco^{a,*}

^a Università Degli Studi Della Basilicata, Dipartimento di Scienze, Via Dell'Ateneo Lucano, 10-85100, Potenza, Italy

^b ALMAGISI S.r.l Corso Italia, 27-39100, Bolzano, Italy

^c Università Degli Studi di Bari Aldo Moro, Dipartimento di Chimica, Via E. Orabona, 4-70126, Bari, Italy

^d Università Degli Studi Della Basilicata, Dipartimento Delle Culture Europee e Del Mediterraneo: Arch., Ambiente, Patrimoni Culturali, Via Lanera, 20-75100, Matera, Italy



ARTICLE INFO

Keywords:

SARS-CoV-2

Antivirals

Analytical methods

Biological matrices

Mass spectrometry

Liquid chromatography

ABSTRACT

Since coronavirus disease 2019 (COVID-19) started as a fast-spreading pandemic, causing a huge number of deaths worldwide, several therapeutic options have been tested to counteract or reduce the clinical symptoms of patients infected with the severe acute respiratory syndrome coronavirus 2 (SARS-CoV-2). Currently, no specific drugs for COVID-19 are available, but many antiviral agents have been authorised by several national agencies. Most of them are under investigation in both preclinical and clinical trials; however, pharmacokinetic and metabolism studies are needed to identify the most suitable dose to achieve the desired effect on SARS-CoV-2. Therefore, the efforts of the scientific community have focused on the screening of therapies able to counteract the most severe effects of the infection, as well as on the search of sensitive and selective analytical methods for drug detection in biological matrices, both fluids and tissues. In the last decade, many analytical methods have been proposed for the detection and quantification of antiviral compounds currently being tested for COVID-19 treatment. In this review, a critical discussion on the overall analytical procedure is provided, i.e. (a) *sample pre-treatment and extraction methods* such as protein precipitation (PP), solid-phase extraction (SPE), liquid-liquid extraction (LLE), ultrasound-assisted extraction (UAE) and QuEChERS (quick, easy, cheap, effective, rugged and safe), (b) *detection and quantification methods* such as potentiometry, spectrofluorimetry and mass spectrometry (MS) as well as (c) *methods including a preliminary separation step*, such as high performance liquid chromatography (HPLC) and capillary electrophoresis (CE) coupled to UV-Vis or MS detection. Further current trends, advantages and disadvantages and prospects of these methods have been discussed, to help the analytical advances in reducing the harm caused by the SARS-CoV-2 virus.

Abbreviations: ACN, acetonitrile; AD, absolute deviation; ADME, adsorption, distribution, metabolism, and elimination; BeWos, human placental choriocarcinoma trophoblast cells; CE, capillary electrophoresis; CHCA, α -cyano-4-hydroxycinnamic acid; CRMs, certified reference materials; CSF, cerebrospinal fluid; CV, coefficient of variation; DEV, deviation from nominal concentration value; DHB, 2,5-dihydroxybenzoic acid; d-SPE, dispersive-solid-phase extraction; EMA, European Medicines Agency; Err, absolute value of the relative error; ESI, electrospray ionization; FDA, Food and Drug Administration; FL, fluorescence; HILIC, hydrophilic interaction liquid chromatography; HLB, hydrophilic-lipophilic balance; ICH, International Conference on Harmonization; LC, liquid chromatography; LLE, liquid-liquid extraction; LOD, limit of detection; LLOQ, lower limit of quantification; LOQ, limit of quantification; MALDI, matrix-assisted laser desorption/ionization; MCX, mixed-mode cationic exchange; MLC, micellar liquid chromatography; MRM, Multiple Reaction Monitoring; MSI, MALDI-MS Imaging; MTBE, methyltertbutyl ether; MS, mass spectrometry; NRTIs, nucleoside reverse transcriptase inhibitors; OSP, oseltamivir phosphate; PBA, phenylboronic acid; PBMCs, peripheral blood mononuclear cells; Ph. Eur, European Pharmacopoeia; PIs, protease inhibitors; PMA, phosphomolybdic acid; PP, protein precipitation; PSA, primary-secondary amine; Q, QuEChERS; QC, quality control; Q-MSI, quantitative MALDI-MS Imaging; RdRps, RNA polymerase inhibitors; RE, relative error; RSD, relative standard deviation; SDS, sodium dodecyl sulfate; SPE, solid-phase extraction; SRM, Selected Reaction Monitoring; TDM, therapeutic drug monitoring; TCA, trichloroacetic acid; UAE, ultrasound assisted extraction; UHPLC, ultra-high performance liquid chromatography.

* Corresponding author.

E-mail addresses: maria.acquavia@unibas.it (M.A. Acquavia), luca.foti@unibas.it (L. Foti), raff.pascale@gmail.com (R. Pascale), antonia.nicolo@studenti.unibas.it (A. Nicolò), vincenzo.brancaleone@unibas.it (V. Brancaleone), tommaso.cataldi@uniba.it (T.R.I. Cataldi), giuseppe.martelli@unibas.it (G. Martelli), laura.scrano@unibas.it (L. Scrano), giuliana.bianco@unibas.it (G. Bianco).

<https://doi.org/10.1016/j.talanta.2020.121862>

Received 22 August 2020; Received in revised form 30 October 2020; Accepted 2 November 2020

Available online 5 November 2020

0039-9140/© 2020 Elsevier B.V. All rights reserved.

1. Introduction

A new coronavirus infection, designated as COVID-19 by the World Health Organization (WHO), emerged in December 2019 in Wuhan (Central China) [1], and then it rapidly spread worldwide, thus becoming a pandemic emergency, which forced most of the countries to take drastic actions of containment. As in the case of the severe acute respiratory syndrome (SARS) and the middle east respiratory syndrome (MERS), the virus of COVID-19 pandemic is formally associated with SARS coronavirus 2 (SARS-CoV-2), which affects the lower respiratory tract, manifesting as pneumonia in humans [2]. Even though neither a vaccine nor an effective antiviral treatment is available for humans, several drugs are currently undergoing clinical studies to test their efficacy and safety to treat the clinical symptoms of patients infected with SARS-CoV-2. The infected subjects have received off-label therapies such as chloroquine, hydroxychloroquine, azithromycin, interferon, steroids, monoclonal antibodies, anti-IL-6 inhibitors and other drugs approved for different infections, including Ebola, malaria, influenza, myelofibrosis, hypertension, rheumatoid arthritis, and acquired immune deficiency syndrome (AIDS) [3–5]. A huge number of antivirals have been tested both in in vitro studies and in authorised clinical trials. From a biochemical standpoint, most of them are protease inhibitors

(PIs), i.e. darunavir, indinavir, lopinavir, ritonavir and saquinavir (Fig. 1) [6–10], thus preventing viral replication by selectively binding to viral proteases and blocking proteolytic cleavage of protein precursors that are necessary to produce infectious viral particles. Some others, like favipiravir, remdesivir and galidesivir [11–13] are RNA-dependent RNA polymerase inhibitors (RdRpis), as they avoid RNA replication from an RNA template catalysed by RNA polymerase (Fig. 2A). Favipiravir (6-fluoro-3-hydroxy-2-pyrazincarboxamide) is a carboxyamide derivative of pyrazine approved in Japan for treating influenza, but it is also active against various flu viruses, including the avian virus A (H7N9) and a paramyxovirus, respiratory syncytial virus [11]. Remdesivir, a monophosphoramidate prodrug, is an adenine nucleotide analogue, has been tested in 2015 in healthy volunteers to treat the Ebola virus disease [14]. Besides the families of PIs and RdRpis as antivirals, other drugs used in therapy that belong to reverse transcriptase inhibitors (i.e., emtricitabine and tenofovir, Fig. 2B), neuraminidase enzyme inhibitors (i.e. oseltamivir, Fig. 3A), RNA synthesis inhibitors (i.e. ribavirin, Fig. 3B), CAP-dependent endonuclease inhibitors (i.e. baloxavir-marboxil, Fig. 3C), and a membrane fusion inhibitors (umifenovir, Fig. 3D) [11,13,15–18].

A literature screening of these drugs showed that many analytical techniques are used for their detection and quantification in biological

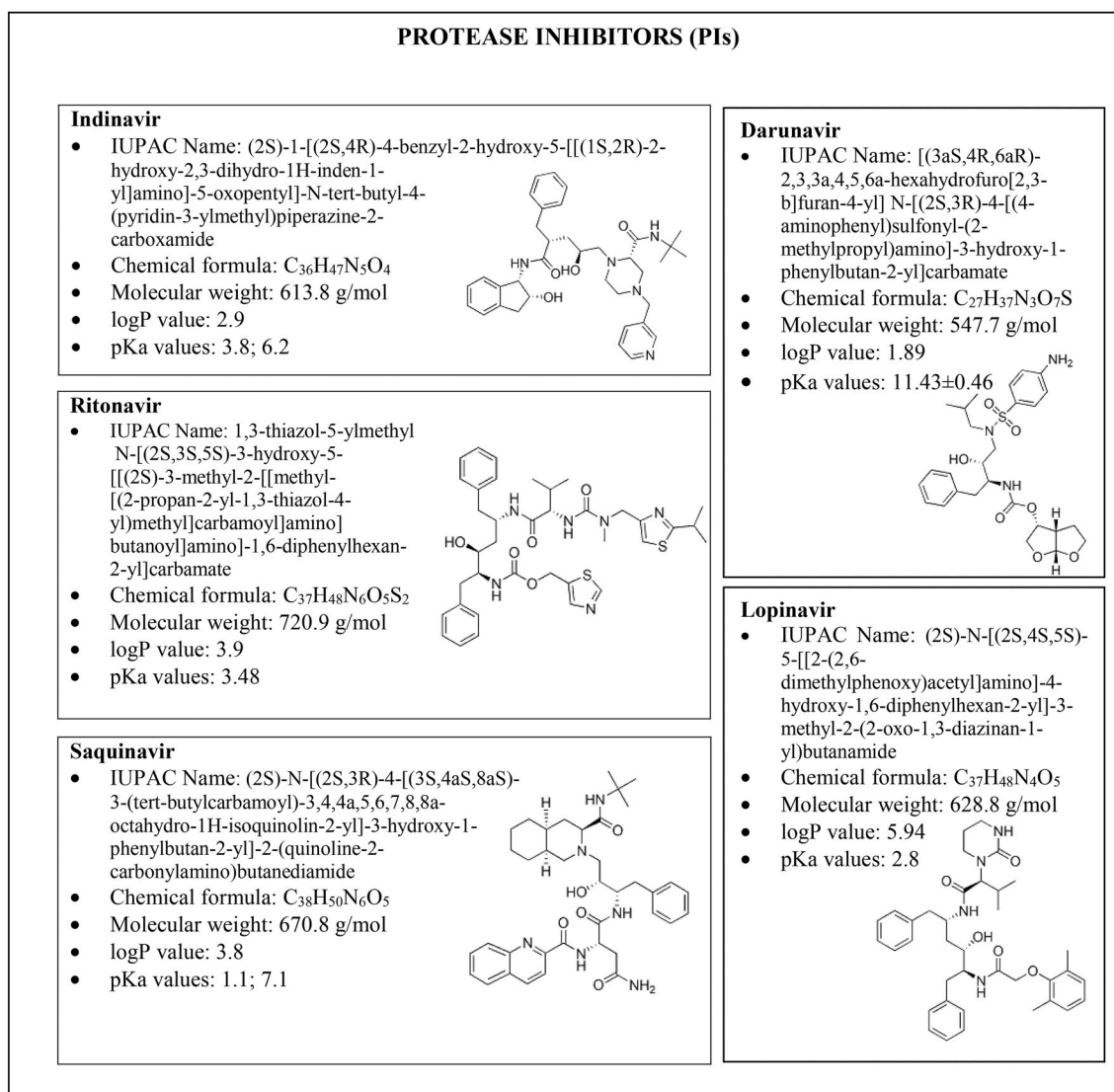


Fig. 1. Structures, chemical formula and chemical properties (octanol-water partition coefficients, i.e. logP, and acid dissociation constants, i.e. pKa) of antivirals belonging to the class of protease inhibitors (PIs) tested for COVID-19 treatment, i.e. indinavir, ritonavir, saquinavir, darunavir and lopinavir.

samples of both human and animal origin. Most studies concerning quantification in animal tissues were aimed at detecting trace residues of antivirals used in livestock farming for the fast increase in animal growing [19,20]. The huge administration to animals of antiviral drugs leads to severe issues, including poisoning and immunosuppression [20]. To minimise these risks, in 2006 the Food and Drug Administration (FDA) prohibited on the extra-label use of antiviral agents such as oseltamivir in poultry. Instead, the research work in human biological fluids is strongly required to support the pharmacokinetic and metabolic studies. In detail, suitable analytical methodologies are needed for the sensitive quantification of these drugs and their metabolites in bio-fluids and tissues, to follow their adsorption, distribution, metabolism, and elimination (ADME) [21]. Moreover, the determination in biological matrices is also helpful in the development of new drugs, bioequivalence studies, toxicological analysis and therapeutic drug monitoring (TDM) [22]. TDM is defined as the continuous clinical laboratory monitoring of drug concentrations in various biological fluids during pharmaceutical administration to select the best therapeutic dose and duration of treatment for optimal patient benefit [23], thus avoiding therapeutic failure. In this context, a review focusing on the analytical methods developed for COVID-19 antiviral drugs detection in biological matrices

is helpful to best know their ADME behavior. Due to the complexity of the biological samples and the low concentration of molecules of interest, sensitive and selective methods are demanded [24].

Here, we discuss the most recent and relevant literature, published in the period between 2010 and 2020, dealing with the analytical determination of antiviral drugs, currently tested for SARS-CoV-2 treatment, in human and animal biological samples. A special focus was addressed to method validation parameters, sample pre-treatment to remove endogenous interferences, drug extraction, chromatographic separation, and UV-Vis or MS detection. Such an overview would help the scientific community engaged on novel coronavirus studies for pharmacokinetics and drug monitoring scopes.

2. Method validation in pharmaceutical analysis of COVID-19 antiviral drugs in biological fluids and tissues

Analytical method validation is defined as the systematic process of establishing that an analytical method is acceptable for its intended purpose [25]. It demonstrates that a defined method protocol applies to a specified analyte with a defined concentration level and to a specified complex matrix and it represents the first level of quality control in the

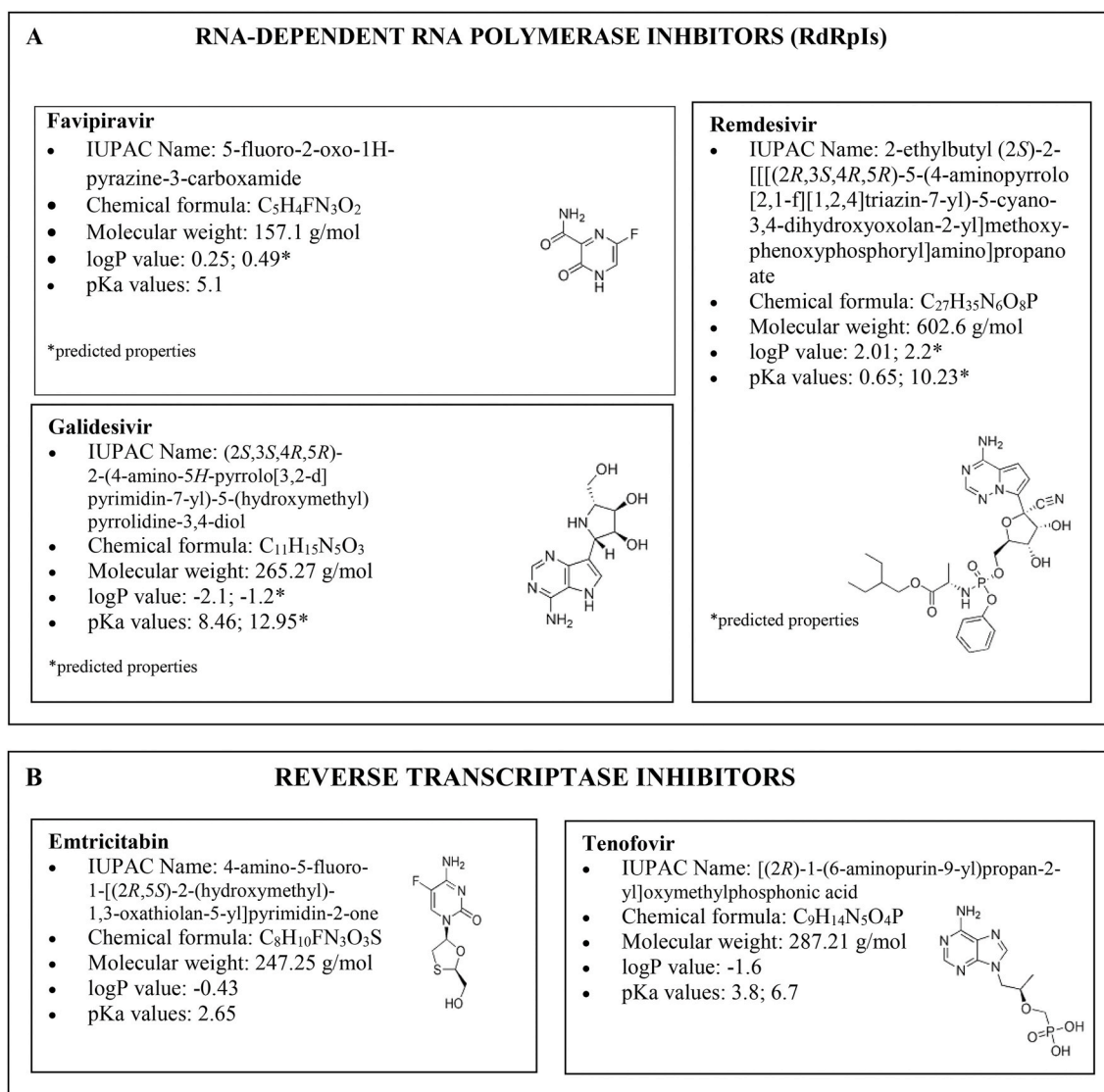


Fig. 2. Structures, chemical formula and chemical properties (octanol-water partition coefficients, i.e. logP, and acid dissociation constants, i.e. pKa) of antivirals belonging to the class of RNA-dependend RNA-polymerase inhibitors (A), i.e. favipiravir, remdesivir and galidesivir, and to the class of reverse transcriptase inhibitors (B), i.e. emtricitabin and tenofovir, tested for COVID-19 treatment.

laboratories [26]. Quality control is an essential operation for pharmaceutical analysis. The demonstration of the suitability of an analytical method for the quantification of drug compounds is of great importance to ensure their occurrence in biological matrices. Besides, the validation of bioanalytical methods employed for the quantitative determination of drugs and their metabolites in biological matrices plays a key role in the evaluation of bioavailability, bioequivalence, pharmacokinetic and toxicokinetic studies [27].

Several guidelines can be used to validate a bio-analytical method for drug quantification in biological matrices: the Food and Drug Administration (FDA) guidelines, the European Medicines Agency (EMA) guidelines, the International Conference on Harmonization (ICH) guidelines and the European Pharmacopoeia (Ph. Eur.) are the most important reference for the quality control of medicines. In addition, the European Commission Decision 2002/657/EC provides a useful framework for xenobiotic residue detection in animal tissues as well in their products. All the mentioned validation guidelines list the analytical parameters and the established acceptance criteria which should be taken into account to define the method of interest as sensitive, accurate and selective.

The analytical parameters commonly investigated for validation are linearity, limit of detection (LOD) and limit of quantification (LOQ), sensitivity, accuracy, precision, recovery and matrix effect [28]. Linearity evaluates the ability of the bioanalytical procedure to obtain test

results directly proportional to the concentration of analyte in the sample within the range of the standard curve [29]. As reported in the FDA guidelines [28], the linear range of the method, i.e. the calibration curve, should contain at least five standard points matrix-based, using single or replicate aliquots. The LOD and LOQ are defined, respectively, as the lowest amount of analyte that can be detected but not quantified and the lowest amount of analyte which can be quantitatively determined with suitable precision and accuracy [30]; LOQ defines the method sensitivity. The accuracy of a bioanalytical method is the closeness between the observed and the nominal or known true value and can be calculated for one day and between days [30,31]. It is expressed either as percent absolute bias or relative error (% RE) [29]. Instead, the precision is the ability to produce reproducible results between series of measurements from homogeneous samples. Precision is described as intra-day precision (i.e. repeatability) and inter-day precision (i.e. reproducibility) [30]. The precision is expressed as percent coefficient of variation (% CV) or percentage relative standard deviation (% RSD). Both accuracy and precision of a bioanalytical method need to be determined using quality control (QC) samples prepared at concentration levels covering the dynamic range of the method. Typically, QC samples are prepared at four levels: at the lower limit of quantification (LLOQC), low (LQC), middle (MQC) and high (HQC) limits of quantification [32]. The extraction efficiency of an analytical process, reported as a percentage of the known amount of an analyte carried through the

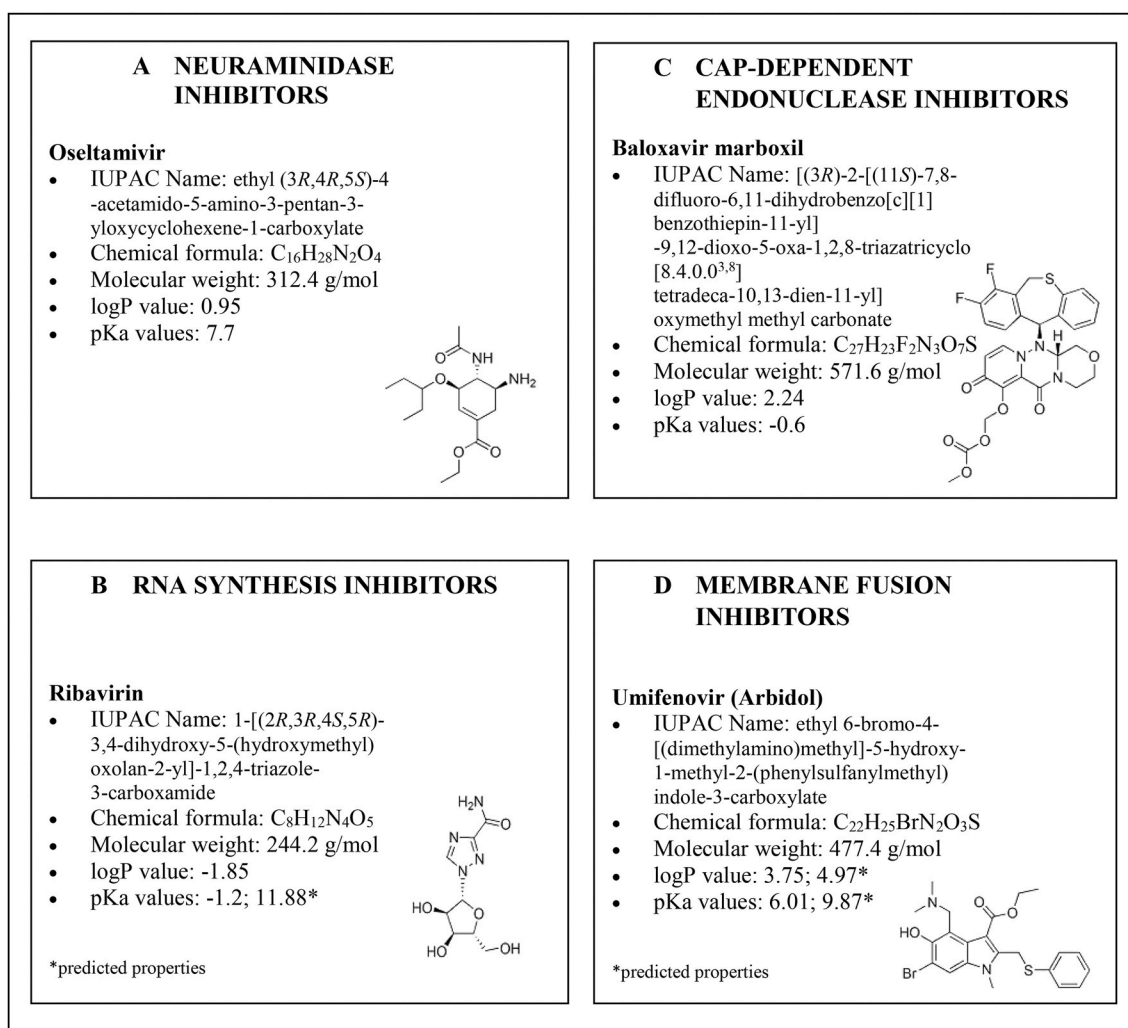


Fig. 3. Structures, chemical formula and chemical properties (octanol-water partition coefficients, i.e. logP, and acid dissociation constants, i.e. pKa) of antivirals belonging to the class of: inhibitors of the neuraminidase enzyme (A), i.e. oseltamivir, RNA synthesis inhibitors (B), i.e. ribavirin, cap-dependent endonuclease inhibitors (C), i.e. baloxavir marboxil and membrane fusion inhibitors (D), i.e. umifenovir, tested for COVID-19 treatment.

Table 1
Comparison of methods used to evaluate the main analytical validation parameters (linearity, sensitivity, accuracy, precision, recovery and matrix effect) as well as the corresponding acceptance criteria reported in the guidelines typically followed for bioanalytical methods validation developed for drugs quantitation in biological fluids and tissues.

Guideline	Linearity	Sensitivity	Accuracy	Precision	Recovery	Matrix effect
FDA	Analyse a blank (no analyte, no IS), a zero calibrator (blank plus IS), and at least six, non-zero calibrator levels covering the quantitation range, including LLOQ in every run.	The lowest non-zero standard on the calibration curve defines the sensitivity (LLOQ).	Accuracy should be established by analysis of replicate concentrations with at least three independent runs, four QC levels per run (LLOQ, L, M, H QC), and \geq five replicates per QC level.	Precision should be established with at least three independent runs, four QC levels per run (LLOQ, L, M, H QC), and \geq five replicates per QC level.	Extracted samples at L, M, and H QC concentrations versus extracts of blanks spiked with the analyte post extraction (at L, M, and H)	Compare calibration curves in multiple sources of the biological matrix against a calibration curve in the matrix for parallelism (serial dilution of incurred samples) and nonspecific binding.
	Non-zero calibrators should be $\pm 15\%$ of nominal (theoretical) concentrations, except at LLOQ where the calibrator should be $\pm 20\%$ of the nominal concentrations in each run.	The analyte response at the LLOQ should be \geq five times the analyte response of the zero calibrator.	$\pm 15\%$ of nominal concentrations; except $\pm 20\%$ at LLOQ.	$\pm 15\%$ CV, except $\pm 20\%$ CV at LLOQ	Recovery of analyte and IS need not be 100%, but it should be consistent, precise and reproducible	/
EMA	A minimum of six calibration concentration levels should be used, in addition to the blank sample (processed matrix sample without analyte and without IS) and a zero sample (processed matrix with IS). Each calibration standard can be analysed in replicate.	Not described	Accuracy should be assessed on samples spiked with known amounts of the analyte (a minimum of 4 QC levels). The QC samples are analysed against the calibration curve, and the obtained concentrations are compared with the nominal value.	Precision should be assessed on minimum of five samples per concentration level at LLOQ, L, M and H QC samples in a single run (within-run precision) or in at least three runs analysed on at least two different days should be evaluated (between-run precision).	Not described	For each analyte and the IS, the matrix factor (MF) should be calculated for 6 lots of blank matrix, by the ratio of the peak area in the presence of matrix (measured by analysing blank matrix spiked after extraction with analyte), to the peak area in absence of matrix (pure solution of the analyte). The CV of the IS-normalized MF calculated from the 6 lots of matrix should not be greater than 15%.
	The back calculated concentrations of the calibration standards should be within $\pm 15\%$ of the nominal value, except for the LLOQ for which it should be within $\pm 20\%$	/	The mean concentration should be within 15% of the nominal values for the QC samples, except for the LLOQ which should be within 20% of the nominal value.	The within-run and between-run CV value should not exceed 15% for the QC samples, except for the LLOQ which should not exceed 20%.	/	The matrix effect should be evaluated by analysing at least 3 replicates of L and H QCs, each prepared using matrix from at least 6 different sources/lots.
ICH	A calibration curve should be generated with a blank sample, a zero sample (blank sample spiked with IS), and at least 6 concentration levels of calibration standards, including the LLOQ and the ULOQ.	Not described	Within-run accuracy should be evaluated by analysing at least 5 replicates at 4 QC concentration level in each analytical run. Between-run accuracy should be evaluated by analysing each QC concentration level in at least 3 analytical runs over at least two days.	Within-run precision should be evaluated by analysing at least 5 replicates at 4 QC concentration level in each analytical run. Between-run precision should be evaluated by analysing each QC concentration level in at least 3 analytical runs over at least two days.	Recovery is determined by comparing the analyte response in a biological sample that is spiked with the analyte and processed, with the response in a biological blank sample that is processed and then spiked with the analyte (L, M and H QC levels).	

(continued on next page)

Table 1 (continued)

Guideline	Acceptance criteria	Linearity	Sensitivity	Accuracy	Precision	Recovery	Matrix effect
European Commission Decision 2002/657/EC	Method	The accuracy of the back-calculated concentrations of each calibration standard should be within $\pm 20\%$ of the nominal concentration at the LLOQ and within $\pm 15\%$ at all the other levels.	Not described	The overall accuracy at each concentration level should be within $\pm 15\%$ of the nominal concentration, except at the LLOQ, where it should be within $\pm 20\%$.	The precision (%CV) of the concentrations determined at each level should not exceed 15%, except at the LLOQ, where it should not exceed 20%.	Recovery of the analyte does not need to be 100%, but the extent of recovery of an analyte and of the IS (if used) should be consistent.	The accuracy should be within $\pm 15\%$ of the nominal concentration and the precision (%CV) should not be greater than 15% in all individual matrix sources/lots.
		At least five levels (including zero) should be used in the construction of the curve		Accuracy is determined by evaluating the trueness and the precision of the method. Trueness is evaluated by analysing six replicates of the CRM. Then, divide the detected mean concentration by the certified value (measured as concentration) and multiply by 100, to express the trueness as a percentage. If no CRM is available, instead of trueness, the recovery can be determined.	Fortify matrix with the analyte (to calculate repeatability) or CRM (for reproducibility) to yield concentrations equivalent to 1, 1.5 and 2 times the minimum required performance limit or 0.5, 1 and 1.5 times the permitted limit. Then, analyze the samples and calculate the concentration present in each sample to determine recovery as: % Recovery = $100 \times$ measured content/fortification level.	Select 18 aliquots of a blank material and fortify six aliquots at each of 1, 1.5 and 2 times the minimum required performance limit or 0.5, 1 and 1.5 times the permitted limit. Then, analyze the samples and calculate the concentration present in each sample to determine recovery as: % Recovery = $100 \times$ measured content/fortification level.	Not described
	Acceptance criteria	/	/	/	The CV under reproducibility conditions, shall not exceed the level calculated by the Horwitz Equation, or one half and two thirds (repeatability)	/	/

sample extraction and processing steps of the method, is known as recovery [33]. Higher values of recovery indicate high efficiency of extraction procedure, higher sensitivity and accuracy of the bio-analytical method. Extraction efficiencies up to 100% can be achieved by the optimisation of the overall extraction protocol, including the pH and polarity of the extraction solvents, as well as the sample quantity. However, the recovery of the analyte from the biological matrix should not be 100%, but it should be consistent over the dynamic range of the method [32]. A biological matrix contains many interfering components such as salts, phospholipids, proteins and other substances that affect the results of the analyte quantification, for example, causing ion suppression or ion enhancement in LC-MS bioanalysis; therefore, the matrix effect should be evaluated during method validation. Moreover, certified reference materials (CRMs) and internal standards are needed in a laboratory's quality control programme to develop and validate accurate methods, thus ensuring traceable measurement results at a specified working level.

To date, several methods have been developed and validated for the analysis of antiviral drugs in biological fluids (e.g., urine, saliva, breast milk, cerebrospinal fluid, seminal plasma), feces, cell lysates and tissues according to the previously described guidelines. Furthermore, many studies have been devoted to the dried samples (i.e. blood, plasma, breast milk) spots [34–41]. However, a lack of standard validation guidelines for drug quantification in dried samples spots is ascertained [34]. Therefore, accepted bio-analytical methodology validation practices are typically followed in those cases. One of the major challenges when developing a method for the quantification of pharmaceutical compounds in bio-fluids and tissues is the practical issues related to acquiring large volumes of sample for the preparation of calibration standards and quality controls [42]. Although the calibration standards should be prepared in the same biological matrix as the one that is going to be analysed, by adding an internal standard as well [28], many methods for antiviral drugs' quantification have been validated in aqueous solutions [20,43–49].

The methods used in the last decade for darunavir, indinavir, lopinavir, ritonavir, saquinavir, favipiravir, remdesivir, emtricitabine, ribavirin, tenofovir, oseltamivir and umifenovir detection in biological matrices are deepened in the next paragraphs. They were specific for a single drug or, more commonly, for the simultaneous analysis of several compounds, especially when they are used in the same therapy to improve long-term efficacy and tolerability. However, the validation parameters and the corresponding acceptance criteria are common to all of them and they are listed in Table 1, which provides a comparison of the guidelines [28,50–52] commonly used for the validation of methods in the pharmaceutical analysis of COVID-19 antiviral drugs, in biological fluids and tissues.

A method suitable for detecting and quantifying the drugs of interest in a relatively short time is essential for an efficient monitoring programme in biological matrices [53]. Irrespective of the type of method, at least three steps are required, among them sample pre-treatment and extraction, detection and quantification. In most cases a preliminary separation step is ensured before detection. Nevertheless, a description of each step of antiviral drugs analysis will be provided below. Note that for galidesevir and baloxavir-marboxil no studies are reported up to now.

3. Sample pre-treatment and extraction of COVID-19 antiviral drugs

An efficient sample preparation for detecting drugs in biological matrices should ensure recoveries as high as possible, remove potentially interfering with endogenous compounds, be quick, easy and cost-wise [54]. Typically it involves analytes extraction, clean-up and concentration before chromatographic separation [55].

Biological fluids, such as serum and plasma, as well as tissues are complex mixtures because they contain proteins, lipids, salts and

Table 2

Techniques used for the extraction of antiviral drugs from biological matrices with their main advantages and drawbacks.

Extraction technique	Matrices	Advantages	Drawbacks
<i>Protein precipitation (PP)</i>	Plasma samples, seminal plasma, cell lysates, cerebrospinal fluid, mice vaginal lavage, saliva, urine and breast milk.	Fastest and simplest extraction technique. It can be used also as sample pre-treatment before applying other extraction techniques.	Low selectivity; it could induce analytes co-precipitation. It does not sufficiently remove endogenous compounds such as lipids, phospholipids and fatty acids.
<i>Solid-phase extraction (SPE)</i>	Plasma, cell lysates, cerebrospinal fluid, chicken tissue, poultry muscle.	It combines extraction, clean-up and concentration procedures in a single step. It ensures analytes extraction with high selectivity.	Slightly tedious and time-consuming extraction technique. In some cases, it could result in less intense chromatographic peaks if compared to liquid-liquid extraction.
<i>Liquid-liquid extraction (LLE)</i>	Plasma, urine, faeces, hairs, mice vaginal tissues, liver tissues, poultry muscles, peripheral blood mononuclear cells, and human placental choriocarcinoma trophoblast cells.	Faster and easier than SPE. It desalts samples very well, lessening the problem of source fouling in mass spectrometry analyses.	Time-consuming technique and a rather hazardous one, due to the use of large amounts of toxic organic solvents. It is less selective than solid-phase extraction; moreover, the possibility of emulsion formation prevents automation of this technique.
<i>Ultrasound-assisted extraction (UAE)</i>	Urine, chicken tissue, dried sample spots.	Ultrasound increases the rate of mass transfer of analytes from matrix in the solvent compared to the classic liquid-liquid extraction.	Technique not widespread for the extraction from biological matrices.
<i>QuEChERS (Q)</i>	Plasma, chicken muscle.	More suitable for the extraction of drugs from biological tissues compared to liquid-liquid extraction or solid-phase extraction. It is a quick, easy, cheap, effective, rugged and safe method, ensuring an high selectivity of the extraction.	The QuEChERS method yields final extracts less concentrated compared to the traditional extraction techniques.

metabolites with properties similar to the analytes of interest. Therefore, their direct injection into conventional chromatographic support is not suitable, due to the rapid worsening of column frits and stationary phases whereby clogging cannot be avoided [56]. To overcome this problem, several pre-treatment and extraction methods can be used, according to the matrix complexity (Table 2). To date, the analysis of antiviral drugs, which are tested for COVID-19 treatment, was performed in several biological matrices; most TDM studies were conducted on human plasma, but interest in measuring drug levels in urine, saliva, breast milk, cerebrospinal fluid, seminal plasma, faeces, poultry muscles and cell lysates (PBMCs, i.e. peripheral blood mononuclear cells, and BeWos, i.e. human placental choriocarcinoma trophoblast cells) was manifested as well.

Typically, the preparation of plasma samples includes protein precipitation (PP), solid-phase extraction (SPE), liquid-liquid extraction (LLE) or a combination of two or more of them. PP protocols involve the addition of organic solvents to plasma, causing the precipitation of proteins by changing their solvation in water. Then, the resultant protein precipitates are separated from the analytes through centrifugation. This technique is one of the most commonly used for plasma samples, due to its low cost and minimal method development requirements [57]. As precipitating agents of antiviral drugs, acetonitrile/methanol mixtures have been widely preferred in different ratios [58–62]. Moreover, in some cases, acetonitrile [45,63,64] acidified with 0.01% HCl [65] or water adjusted with 8% (v/v) trichloroacetic acid (TCA) [66] and methanol alone [67] have been used

Table 3

Analytical methods employed in the last ten years for the detection of antivirals currently tested for COVID-19 treatment, with their main advantages and drawbacks.

		Advantages	Drawbacks
Methods for direct detection and quantification	<i>Potentiometry</i>	Fast and economical possibility to monitor the drug of interest thanks to ion-selective electrodes, whose the electric potential created over membrane depends on its the activity and allows its quantification.	Still limited since many common ions occurring in biofluids and tissues could interfere with the measurement of the target analyte.
	<i>Spectrofluorimetry (FL)</i>	Easy, less expensive and less time consuming methods; they offer better sensitivity compared to potentiometric methods.	Sometimes require derivatization steps before the detection to form fluorescent adducts, since not all the antivirals are characterized by native fluorescence. Endogenous compounds could interfere with the results of the analysis.
	<i>Matrix Assisted Laser Desorption Ionization mass spectrometry (MALDI-MS)</i>	Short analysis times and low ion suppression.	Quantification remains a major challenge due to problems associated with analyte recovery from the tissue and ionization matrix effects.
Methods including a preliminary separation step	<i>High performance liquid chromatography coupled to UV-Vis (HPLC-UV)</i>	Better sensitivity compared to CE-UV. Possibility to carry out multiresidue analysis.	Sensitivity and selectivity are rather limited because LC-UV requires a huge volume of sample and complex sample preparation to detect drugs at a low concentration.
	<i>High performance liquid chromatography coupled to spectrofluorometric detection (LC-FL)</i>	More sensitive and selective than LC-UV, since fluorescence is a characteristic of well-defined compounds.	Since not all the antivirals are characterized by native fluorescence, sometimes are required derivatization steps before the analysis.
	<i>Capillary electrophoresis coupled to UV-Vis (CE-UV)</i>	Faster analysis with higher efficiency than LC-UV, thanks to the drugs separation through a small capillary under the influence of an electric field.	Low concentration sensitivity
	<i>High performance liquid chromatography coupled to mass spectrometry (LC-MS)</i> <i>Ultra-high performance liquid chromatography coupled to mass spectrometry (UHPLC-MS)</i>	Higher selectivity and sensibility compared to LC-UV methods. Shorter analysis time. Possibility to carry out multiresidue analysis. Improved chromatographic efficiency compared to high performance liquid chromatography (HPLC) columns. Less susceptible to matrix effect.	Susceptibility to matrix effects, due to the outcome of co-eluting interfering compounds on the analyte ionization. Due to the smaller particles in the column, a more tedious pre-treatment of the sample in order to avoid its clogging is needed.

too. In addition to plasma samples, PP has been applied to other matrices, such as seminal plasma [42], cell lysates [68], cerebrospinal fluid [67], mice vaginal lavage [69], saliva [64], urine [46] and breast milk [70]. Yamada et al. [64] used protein precipitation for extracting darunavir, tenofovir and other antiviral drugs from saliva samples, through a three-step protocol, including the addition of ACN, drying of the supernatant and its regeneration with the mobile phase. Moreover, ACN was used also for the extraction from urine samples assisted by sonication in an ultrasonic bath, in a method developed by Gumustas et al. [46] for the quantification of emtricitabine, rilpivirine and tenofovir. For mice vaginal lavage, the addition of ACN is used to precipitate mucins and dilute salts [69], while in the case of breast milk, PP is conducted after lipid removal through hexane treatment [70]. When applied to samples different from plasma, protein precipitation gave satisfactory results; it should be noted however that, in some cases, to prevent carryover effects during liquid chromatography, but keeping the same LLOQ as in plasma, an extra dilution of the residue obtained after evaporation was needed [42].

In spite of quick and easy extraction, traditional protein precipitation is characterized by low selectivity, because of the analytes co-precipitation [56,71]. Moreover, it fails to sufficiently remove endogenous compounds such as lipids, phospholipids, fatty acids whose co-elution with the compounds of interest affects the ESI droplet desolvation process [72]. Therefore, PP is used as a pre-treatment of plasma samples in other extraction techniques. Accordingly, Charbe et al. [73] developed a method for the extraction from human plasma of nine antiretroviral agents, including darunavir and lopinavir, based on protein precipitation with acetate buffer at pH 4.5, followed by solid phase extraction (SPE). SPE uses the affinity of solutes dissolved or suspended in a liquid (known as the mobile phase) for a solid through which the sample is passed (known as the stationary phase) to separate a mixture into desired and undesired components. The analytes are recovered either by elution using a proper solvent or thermal desorption into the gas phase [74]. This technique has been used in many works, as an attractive alternative to PP, to quantify antiviral drugs in plasma and cell lysates [75] because it combines extraction and clean-up procedures in a single step. The extractions were performed by C18 [76] and hydrophilic-lipophilic balance (HLB) cartridges [77,78]. HLB cartridges ensure a less tedious process compared to conventional C18 based SPE, due to the ability to remain wetted and simultaneously to adsorb analytes with various polarities and pH values. Besides, they allow the simultaneous analysis of a higher number of samples [79,80]. Nevertheless, their versatility makes them less selective. Mixed-mode cationic exchange (MCX) cartridges, which are built upon HLB copolymer with additional presence of sulphonic groups to make them a strong cation-exchanger, can overcome the shortcomings of HLB [81]. They have been exploited for COVID-19 antiviral drugs tested extraction by some authors [82–84]. Ocque et al. [83] developed a method based on MCX-SPE cartridges for extracting tenofovir from both plasma and cerebrospinal fluid, upon sample pre-treatment with 4% phosphoric acid in water. MCX-based SPE was also used by Liu et al. [84] to purify and concentrate chicken tissue sample, after ultrasound-assisted extraction (UAE) and protein precipitation. This sample preparation method gave the highest recoveries for oseltamivir, ranging between 80% and 100%, by using a trichloroacetic acid solution (20 g/L)/acetonitrile (9:1, v/v) as extracting solvent. To further reduce the matrix effects and facilitate the detection of antiviral drugs in poultry muscle, a tandem solid-phase extraction procedure was used by Berendsen et al. [85] in 2012. This method was suggested to ensure the simultaneous analysis of compounds with a broad range of physical and chemical properties, including umifenovir, oseltamivir and ribavirin. All compounds, except ribavirin, were separated from the matrix constituents by retaining them on a Strata-XC cartridge. Then this cartridge, containing ribavirin, was made basic, centrifuged, and applied onto a phenylboronic acid (PBA) cartridge to retain ribavirin to separate this drug from matrix constituents.

Regardless of providing clean extracts, which can be directly analysed by LC, Gupta et al. [86] found that SPE when applied for extracting darunavir from plasma resulted in less intense chromatographic peaks if compared to liquid-liquid extraction (LLE). LLE is a popular alternative to SPE in the bioanalytical field because it can be applied more quickly and easier, desalting samples very well and lessening the problem of source fouling in mass spectrometry analyses [87]. The solvents, useful to extract antiviral drugs from plasma, are ethyl acetate [43,88], diethyl ether [89] and methylene chloride [49], but the most widely employed remains methyltertbutyl ether (MTBE) [86,90] because it ensures better reproducibility and recovery [86]. MTBE was used for samples of urine and faeces as well [91]. Wu et al. [92] proposed a method based on LLE with methanol for the quantification of tenofovir in the hair samples. Hair analysis overcomes some limitations associated with drug detection in plasma, saliva, and other bio-fluids, such as the lack of drug long-term stability. Indeed, the drug concentration in hair strands can retrospectively reflect the drug usage over one month [93,94]. LLE for simultaneous measurements of antiviral drugs in mice vaginal tissues [69], liver tissue [95,96], poultry muscles [19], PBMCs [49] and BeWo [97] cells have been reported as well. Regarding poultry tissues, the LLE is often followed by a SPE clean-up procedure [19], whereas a preliminary treatment aimed at destroying the cell and nuclear membranes of PBMCs is necessary [98]. Along with the LLE, a treatment of PBMCs with more complex preparation protocols has been reported, including a dephosphorylation step conducted by adding phosphatase enzymes and an acid buffer solution (i.e. Tris-HCl buffer 30 mM pH 8.0, pure water and acetate buffer 1 M pH 4, 3:1:0.25, v:v:v, respectively) to the sample, followed by protein precipitation [99].

In addition to the above-mentioned protocols, also a method named QuEChERS (quick, easy, cheap, effective, rugged and safe) was used to extract antiviral drugs from bio-fluids and biological tissues [20,92,100], for which liquid-liquid extraction or solid-phase extraction is less suitable [20]. The QuEChERS (Q) is a fast and easy multi-residue method that involves an acetonitrile salting-out extraction followed by dispersive solid-phase extraction (d-SPE) to remove most remaining matrix interferences [101]. d-SPE is based on the same SPE methodology, but the sorbent is directly added to the extract without conditioning the clean-up, being easily conducted by shaking and centrifugation. As sorbent, a primary-secondary amine (PSA) is used and it's mixed alongside with anhydrous $MgSO_4$ with the sample extract. QuEChERS was specifically developed in 2003 for pesticide determination [102] but it is currently used for drugs too, and many modifications have been proposed adapting to the nature and fat content of the sample [103]. Wu et al. [92] used a modified Q method for extracting ribavirin from chicken muscles, using 1% acetic acid methanol extraction followed by a dispersive solid-phase extraction clean-up procedure, with PSA and C18 sorbent. ACN salt-out, which is typical of Q methods, was avoided due to the low solubility of ribavirin in water and responsible of low drug extraction recoveries. Sichilongo et al. [100] used a Q method for extracting tenofovir, emtricitabine, lopinavir, ritonavir and efavirenz from plasma samples. In the same work, the efficiencies of combined extraction techniques, i.e. Q-PP, Q-LLE and LLE-PP were also evaluated. The obtained results showed that the mixed extraction modes gave lower recoveries and poor accuracies, when compared to Q, PP or LLE alone. However, LOD values for all sample preparation techniques fell below the clinically relevant therapeutic range (3–8 ppm), thus being suitable for TDM routine analysis.

A separate discussion is needed for the preparation of dried sample spots [34–41]. This low-cost technology has recently received a great deal of attention because of their distinct advantages of sample collection, less invasive sampling, simpler transfer, storage and shipping [104,105]. Dried sample spots are typically prepared by spotting low volumes (less than 50 μ L) of the biofluids of interest on suitable cards. Before the analysis, they are placed in clean tubes, where the extraction solution is added. The extraction can be assisted by sonication [34,38] and, after centrifugation, the supernatant is collected for chromatographic analysis.

4. Separation and detection of COVID-19 antiviral drugs

Several analytical methods have been developed to accurately quantify antiviral drugs, currently tested against SARS-COV-2. As interfering compounds are normally occurring in biological samples, the use of analytical techniques that provide high selectivity and sensitivity is of crucial importance. A summary of methods published in the last decade, with their main advantages and drawbacks, is reported in Table 3. Some methods based on potentiometry [44], spectrofluorimetry [45] or matrix-assisted laser desorption/ionization (MALDI) [106–108] were employed. However, as expected, the most widely used methods were based on hyphenated techniques, typically liquid chromatography but also capillary electrophoresis [46] (CE), coupled to UV–Vis detection or electrospray ionization (ESI) with mass spectrometry (MS). Indeed, besides their higher sensitivity, they offer the possibility to carry out multiresidue analyzes, i.e. analyzes in which more than one drug are detected and quantified simultaneously.

4.1. Potentiometric methods

Recently, there has been a growing need for constructing chemical sensors for the fast and economical monitoring of drug compounds through potentiometric methods in pharmaceutical analysis. The potentiometric sensors are also known as ion-selective electrodes, where the electric potential created over the ion-selective membrane depends on the activity of the analyte and allows its quantification [109]. However, potentiometric methods to determinate antiviral drugs in biological matrices remain still limited because many common ions occurring in biofluids and tissues interfere with the measurement of the target analyte.

Hassan et al. [44] proposed a potentiometric sensor for monitoring oseltamivir phosphate (OSP). The sensor consisted of an ion association complex between the drug and phosphomolybdic acid (OSP-PMA) dispersed in polyvinyl chloride. The method was applied to OSP detection in spiked samples of urine and plasma without preliminary sample pre-treatments. Despite it offered a low cost of analysis and short

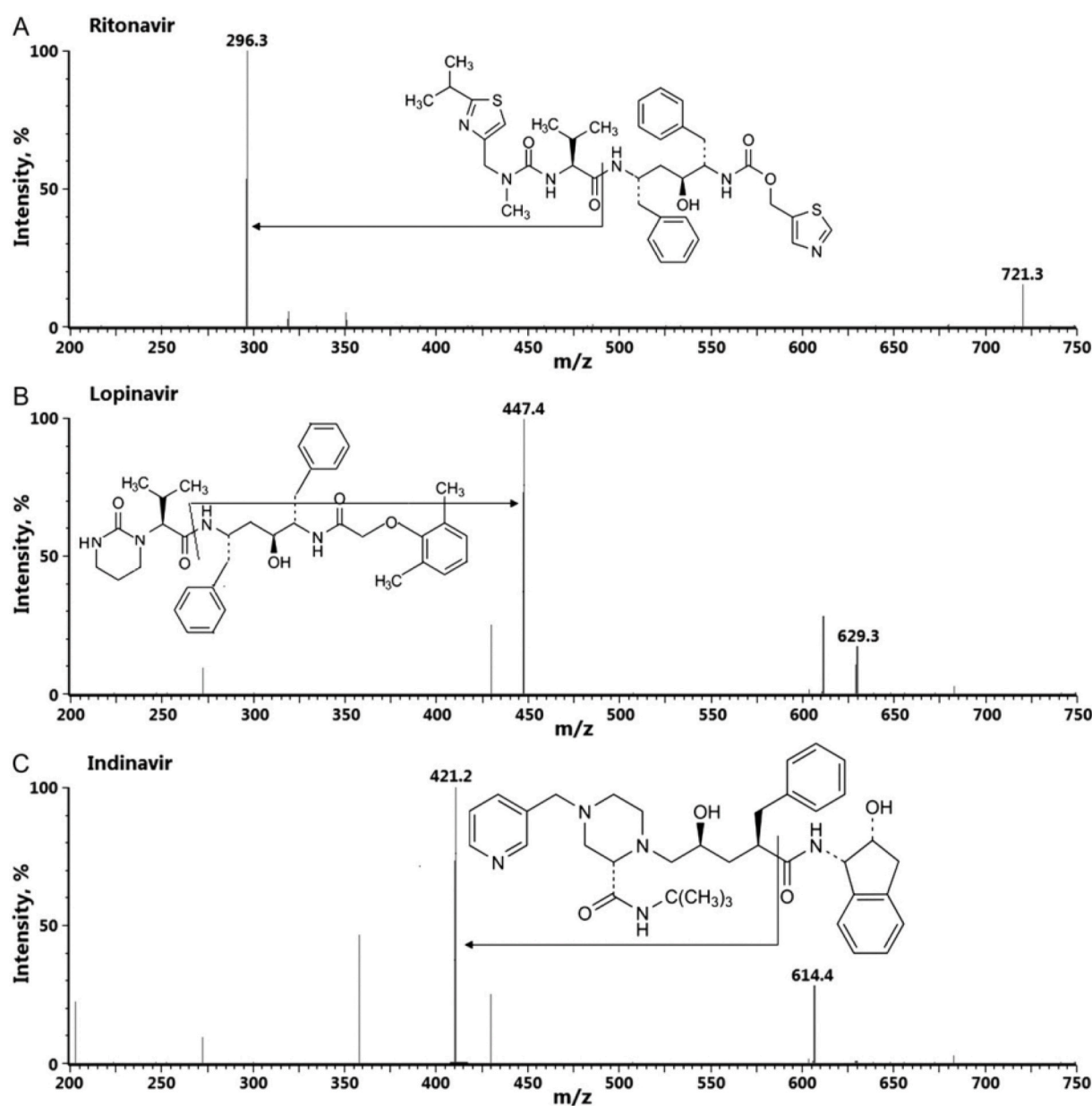


Fig. 4. Product ion mass spectra of some protease inhibitors, i.e. ritonavir, lopinavir and indinavir. Reproduced with the permission of Mishra et al., 2012 [138].

response times [110], the developed ion-selective electrode exhibited relatively high limits of detection (LODs), approximately in the micromolar range [111], if compared to the other analytical techniques.

4.2. Spectrofluorimetric and spectrophotometric methods

Spectrophotometric and spectrofluorometric methods are often used for the determination of drugs, thanks to their versatility and cost-effectiveness. They can be successfully applied for pharmaceutical analysis, consisting of quality control of commercialized products and pharmacodynamic studies [112]. Since antiviral compounds show several unsaturations and aromatic rings in their structure (see Figs. 1, Figs. 2 and 3), one of the main advantages of their determination through spectrophotometric methods is the possibility to analyse without preliminary derivatization steps. The detection requires absorbance measurements typically carried out between 207 nm and 280 nm, with differences in $\lambda_{\text{max absorption}}$ depending on the specific target drug.

Conversely, spectrofluorimetric methods require derivatization steps before the detection of the antivirals to form fluorescent adducts, since not all of them are characterized by native fluorescence. Slightly high $\lambda_{\text{excitation}}$ and $\lambda_{\text{emission}}$ are needed. As example, values of 408 nm and 475 nm were used, respectively, as $\lambda_{\text{excitation}}$ and $\lambda_{\text{emission}}$ by Omar et al. [45] in a spectrofluorimetric method developed and validated in distilled water to quantify oseltamivir phosphate in plasma spiked samples. OSP was derivatized through the Hantzsch reaction of its primary amino group with acetylacetone and formaldehyde [45]. The calculated LOQ and LOD values were respectively 0.08 $\mu\text{g/mL}$ and 0.24 $\mu\text{g/mL}$: these values were considerably lower than LLOQ (7.4 $\mu\text{g/mL}$) and LOD (3.73 $\mu\text{g/mL}$), obtained with the potentiometric method proposed by Hassan et al. [44].

Despite providing several advantages such as being easy, inexpensive and less time consuming, spectrophotometric and spectrofluorometric techniques alone for the quantification of drugs in biological matrices do not ensure high selectivity and suffer from the interference of many endogenous compounds, which can compromise the results of the analysis. Accordingly, a previous separation step by liquid chromatography (LC) or capillary electrophoresis (CE) is typically used before the detection of antiviral compounds.

CE is based on the separation of charged analytes through a small capillary under the influence of an electric field; thus, it represents a good alternative to conduct faster analysis with higher efficiency than LC [113]. However, the main disadvantage of CE is its low concentration sensitivity. In this regard, Gumustas et al. [46] compared LC-UV and CE-UV methods for the simultaneous determination of emtricitabine, rilpivirine and tenofovir. LC-UV sensitivity, calculated as the limit of detection (LOD) and limit of quantification (LOQ), was better than CE.

Moreover, the LC-UV was found to be more precise than the CE method. The RSD values varied between 0.3 and 0.9% for LC-UV and between 2.5 and 4.2% for CE-UV.

Liquid chromatography coupled with UV-Vis detectors has been used in many works in order to quantify antiviral drugs in biological fluids, i.e. blood and plasma [43,73,89,90,114–119]. Currently, reversed-phase liquid chromatography is the method of first choice for this task. The separation is carried out on C18 columns, with or without a guard-column system, and different mobile phase compositions (acidic or basic) are used. For ionizable species which are the drugs tested for the COVID-19 treatment, the simplest and fastest way to implement the selectivity and the specificity of the LC-UV method is to adjust the pH of the mobile phase [120], which is known also for affecting the quantification limit of the method [121]. Studies reported in literature showed that the retention times of weak acids decrease with increasing pH values, while those of weak bases increase with increasing pH [122]. The chromatographic separation through the LC-UV methods employed in last ten years for antivirals has been achieved with mobile phases whose pH ranged from 3.23 to 8.10, since their pKa values are strongly different ($-1.2 \leq \text{pKa} \leq 11.88$, see Figs. 1, Figs. 2 and 3). As organic modifiers, acetonitrile and methanol have been used and mixed with water, phosphate buffer or acetate buffer in different proportions. The chromatographic run time is usually comprised between 4 and 25 min. The fastest run times of 4 and 5 min, respectively, occurred in isocratic methods for the determination of a single analyte, i.e. ritonavir and darunavir [89,90]. The longer run time for the determination of more than two drugs can be explained by the use of gradient elution mode in order to achieve good separation of drugs also from their own metabolites [123].

Recently, LC-UV methods have been also developed for drug enantiomers detection in dried blood spots, by using chiral columns, namely (\pm) darunavir and (\pm) emtricitabine [37,38]. In this case, a Chiralpak IA column (250 mm \times 4.6 mm, 5 μm) has been employed and the chromatographic separation has been carried out isocratically with n-hexane-ethanol-diethyl amine (75:25:0.1) or with n-hexane-ethanol (65:35) as mobile phases. Run times of 13 and 15 min were needed, respectively, for the complete separations of the two enantiomers of darunavir and emtricitabine.

In addition, Peris-Vicente et al. [124] reported a method based on micellar liquid chromatography (MLC) combined with diode array detector for the simultaneous quantification of four antiretrovirals (darunavir, ritonavir, emtricitabine and tenofovir) in plasma. MLC, based on sodium dodecyl sulfate (SDS) as mobile phase, allows the direct injection of untreated plasma onto the chromatographic column for the rapid monitoring of drug contents. Apart from dilution and filtration, no sample pre-treatment is needed because SDS solubilizes plasma by

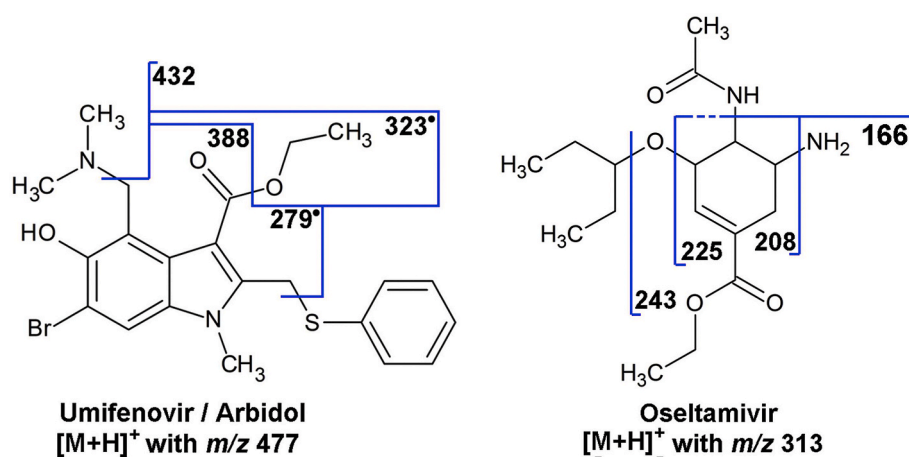


Fig. 5. Fragmentation pathways proposed for umifenovir and oseltamivir. Reproduced with the permission of Niessen et al., 2020 [139].

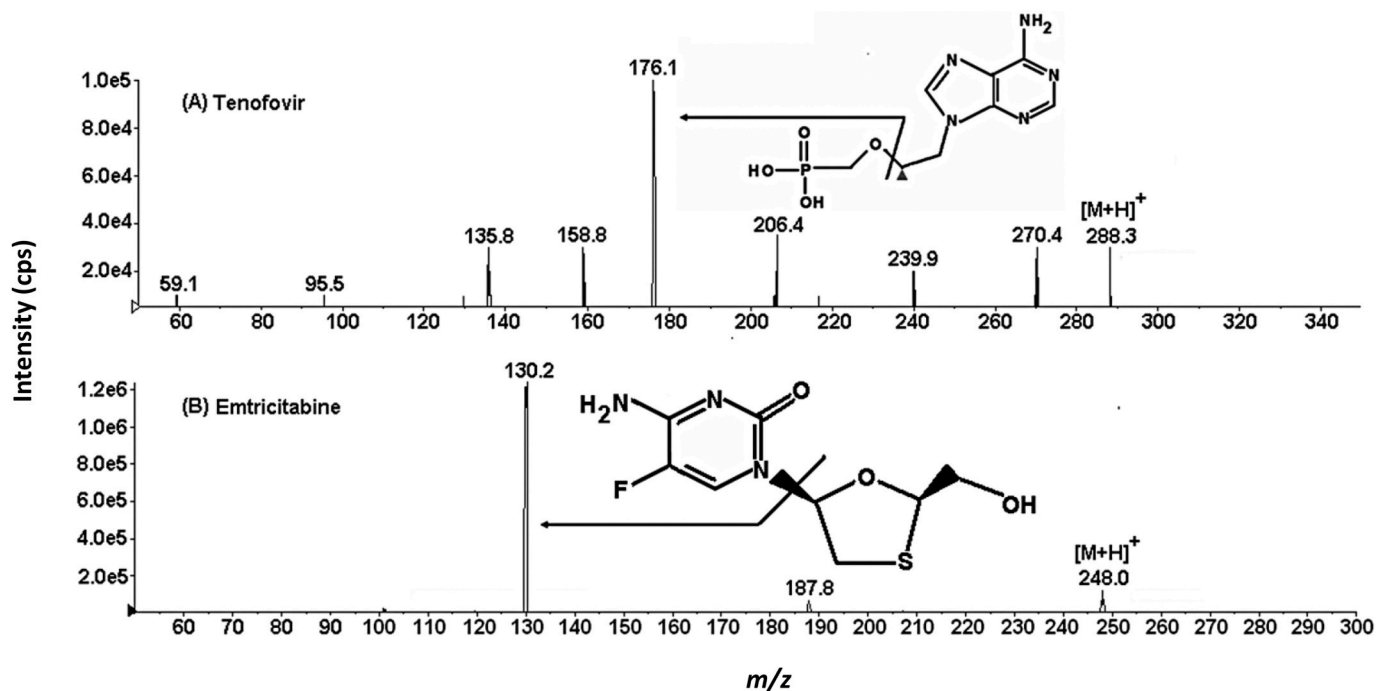


Fig. 6. Product ion mass spectra of tenofovir and emtricitabine. Reproduced with the permission of Yadav et al. [140].

denaturing proteins and avoiding their precipitation, by displacing the analytes from its components and by making them interact with the stationary phase [125]. A mobile phase consisting of 0.06 M SDS/2.5% 1-pentanol (pH 7) and running under isocratic mode through a C18 column, was chosen. The method, fully validated according to the ICH guideline, was linear between 0.25 and 25 $\mu\text{g/mL}$ ($r^2 > 0.995$); it showed an accuracy ranging from 89.3% to 103.2% and a precision lower than 8.2% for all the four analysed antivirals. The limit of detection was comprised between 0.080 and 0.110 $\mu\text{g/mL}$, while the limit of quantification ranged between 0.240 and 0.270 $\mu\text{g/mL}$.

Gralak-Dabrowska et al. [90] employed a LC-UV method to measure the level of darunavir in plasma. Although the proposed approach was advantageous for its run time of 5 min, considerably lower than the typical 10–30 min of the other reported methods, sensitivity and selectivity were rather limited because LC-UV requires a huge volume of sample and complex sample preparation to detect drugs at a low concentration [98,122]. Conversely, methods based on HPLC with fluorescence (FL) detection are inherently more sensitive than LC-UV. In addition, fluorescence is a characteristic of well-defined compounds, so that the FL detection is also more selective than UV, thus allowing to obtain a baseline without peaks associated to foreign substances [98, 118,126]. A method for the determination of darunavir in PBMCs by LC-FL detection was presented by Nagano et al. [98] in 2014. The method took advantage of the compound native fluorescence, not requiring derivatization. Chromatographic separation was achieved on a C18 column with a mobile phase consisting of 20 mmol/L potassium phosphate buffer (pH 4.3)/acetonitrile (57/43, v/v), and spectrofluorometric detection at $\lambda_{\text{excitation}} = 235 \text{ nm}$ and $\lambda_{\text{emission}} = 337 \text{ nm}$. Voriconazole was used as internal standard and linear calibration curves were in the range 5–100 $\text{ng}/10^6 \text{ cells}$. Intra-day precision and accuracy were lower than 8.77% and 12.0%, respectively.

4.3. Mass spectrometric methods

Mass spectrometry (MS) is a powerful analytical tool with many applications in several fields, such as in the environmental field [127] or in the foodomic [128]. Besides, it's useful also for both qualitative and quantitative application in the pharmaceutical field [136,137]. In detail,

soft ionization techniques such as matrix-assisted laser desorption ionization (MALDI) and, more importantly, electrospray ionization (ESI) are used to effectively ionize the drugs of interest [21,129–131]. Clearly, the polarity chosen for ionization, i.e. the positive or the negative one, depends on the relative acidity (pKa) of the functional groups occurring on the molecules [132]. For example, the detection of phenols is carried out in negative mode, since the deprotonation of phenolic OH groups is considered as the most likely ionization process under ESI conditions [133]. As regard to antiviral compounds, positive polarity is typically used because they have several secondary amino groups which can be readily protonated.

The main difference between MALDI and ESI ionization techniques is the physical state in which the sample is introduced to the ion source: ESI uses solvated samples that are infused into the instrument, whereas MALDI uses the solid state, as the sample is co-crystallized with an adequate matrix [134]. Anyway, both ESI-MS and MALDI-MS are very sensitive, as they allow the detection of analytes whose concentrations are as low as picomolar [134]. In addition, ESI-MS can efficiently be interfaced with analytical separation techniques, i.e. the chromatographic ones, enhancing its quantitative applications [135]. Regardless of the ionization source, the sensitivity of a mass spectrometer is related to its mass analyzer. Quadrupole (Q) and time of flight (ToF) mass analyzers are commonly used and they can be configured together as QqToF or QqQ tandem mass spectrometric instruments [138,139]. Tandem mass spectrometry (MS/MS) represents the most efficient and reliable analytical techniques for specific isolation, unequivocal identification and accurate quantification of drug compounds in biological samples.

The fragmentation pattern of COVID-19 tested antiviral drugs is well known for most of them. Due to the great variability and complexity in their structures, it is not possible to define a common behavior, but the breakdown of the same kinds of chemical bonds can be ascertained. In the product ion mass spectra of protease inhibitors, i.e. ritonavir ($[\text{M}+\text{H}]^+$ at m/z 721), lopinavir ($[\text{M}+\text{H}]^+$ at m/z 629) and darunavir ($[\text{M}+\text{H}]^+$ at m/z 548), fragment ions at m/z 296, m/z 447 and m/z 392, respectively, are obtained after breaking of amide linkage. As regards indinavir ($[\text{M}+\text{H}]^+$ at m/z 614) and saquinavir ($[\text{M}+\text{H}]^+$ at m/z 671), the signals at m/z 421 and m/z 570 are obtained by the cleavage of the

linkage between amide carbon and the carbon in alpha to the amide group (see Fig. 4 as example) [138].

Instead, MS/MS fragmentation of umifenovir ($[M+H]^+$ at m/z 477) involves the formation of product ions at m/z 432 and m/z 387 due to the loss of dimethylamine ($(H_3C)_2NH$) and to the subsequent loss of ethanal (C_2H_4O). The loss of dimethylamine and a phenylsulfanyl radical (C_6H_5S) produces a fragment ion at m/z 323 from which, after a subsequent elimination of an ethyl radical (C_2H_5) or ethanal, ions at m/z 294 and m/z 279 are obtained (Fig. 5) [139]. Oseltamivir ($[M+H]^+$ at m/z 313) fragmentation occurs through the formation of ions at m/z 296, due to the loss of ammonia (NH_3), at m/z 243, due to the loss of pentene (C_5H_{10}), and ions at m/z 225, m/z 208 and m/z 166 due, respectively, to the loss of 3-pentanol ($C_5H_{12}O$), ammonia or acetamide (C_2H_5NO) (Fig. 5) [139].

As for product ion mass spectra of tenofovir ($[M+H]^+$ at m/z 288) and emtricitabine ($[M+H]^+$ at m/z 248), fragment ions at m/z 176 and m/z 130 are obtained, respectively, after the cleavage of the phosphoester bond (tenofovir) and after the cleavage of the link with the nitrogen ring (emtricitabine) (Fig. 6) [140]. Instead, for ribavirin ($[M+H]^+$ at m/z 245), the loss of the pentofuranose unit from the molecular ion gives the fragment ion at m/z 113 [141].

MS/MS analyses are typically performed in Selected Reaction Monitoring (SRM) and Multiple Reaction Monitoring (MRM) mode, when one or more product ions are monitored, respectively [142]. Therefore, the monitoring of specific precursor-product ion transitions increases the sensibility in quantitative bioanalysis and the selectivity, by decreasing the probability of false positive identification [143]. For the antiviral drugs under study, the monitored transitions are the same for either MALDI-MS and ESI-MS analysis.

4.3.1. MALDI-MS

Nowadays, MALDI-MS and MALDI-MS imaging (MSI), are considered as a useful approach for the direct screening and mapping of xenobiotic compounds in complex biological samples, particularly tissues. MALDI-MS is characterized by short analysis times and low ion suppression, compared to ESI sources. However, the application of MSI for quantification (Q-MSI) of antiviral drugs extracted from biological samples remains a major challenge [129]. Q-MSI, in fact, has to deal with several fundamental aspects that are difficult to control for absolute quantification, such as analyte recovery from the tissue and ionization matrix effects. Thus, the use of internal standards and specific preparation of calibration standards is crucial [144]. In addition, the selection of an appropriate matrix is critical to ensure a successful Q-MSI experiment. A suitable matrix for the MALDI-MS analysis of small molecules, such as drug compounds, should reduce the background signal in order to facilitate the identification of target analytes [145]. In this regard, 2, 5-dihydroxybenzoic acid (DHB) and α -cyano-4-hydroxycinnamic acid (CHCA) are the preferred matrices [145].

Due to these limitations, few studies were proposed for the quantification of COVID-19 tested antiviral drugs in biological matrices, in the last ten years. In detail, the reported methods regarded tenofovir [107], indinavir, lopinavir, ritonavir and saquinavir [106] quantification in plasma and PBMCs samples. In order to overcome the problems associated with background signals, derived from the biological sample and the MALDI matrix, SRM and MRM scan modes were used to detect the target drugs. Tenofovir was quantified in plasma, through the application of a MALDI-QqQ-MS technology in combination with an isotope dilution method, by Meesters et al. [107]. These authors used CHCA as MALDI matrix and the laser power was set to 60%. The developed method was validated according to the FDA guidelines and values of 0.04 $\mu\text{mol/L}$ and 0.1 $\mu\text{mol/L}$ were obtained, respectively, for LOD and LLOQ. Besides, values of LLOQ ranging from 3.2 to 167 nM were obtained with a MALDI-QqQ-MS method developed and validated by Van Kampen et al. [106] for quantification of indinavir, lopinavir, ritonavir and saquinavir. It should be noted that, for lopinavir and ritonavir, SRMs were performed on the sodium adducts of the drugs. For those analyses,

sodium iodide (NaI) was added to the matrix solution, i.e. CHCA, to increase the intensity of the sodium adducts of the drugs, respectively, at m/z 651 and m/z 743.

In 2014, a quantitative mass spectrometry imaging method based on infrared matrix-assisted laser desorption electrospray ionization (IR-MALDESI) was developed for emtricitabine quantification [108]. IR-MALDESI combines advantages of both ESI and MALDI, such as the production of multiply charged ions, high salt tolerance, ambient nature and amenability to imaging. With this technique, the ablation occurs by using an IR laser in combination with ESI [146]. Bokhart et al. [108] set the IR laser wavelength to 2.94 μm in order to cause emtricitabine desorption. After applying the method to incubated human cervical tissues, the concentration level found in the analysed samples ($17.2 \pm 1.8 \mu\text{g/g}_{\text{tissue}}$) was compared to that resulting from LC-MS/MS analyses ($28.4 \pm 2.8 \mu\text{g/g}_{\text{tissue}}$) within a cross-validation study (see Supplementary Material, Table S1).

4.3.2. ESI-MS and MS/MS

Electrospray ionization has been the most used ionization technique for the analysis of COVID-19 tested antiviral drugs. Electrospray ionization mass spectrometric or tandem mass spectrometric (ESI-MS or ESI-MS/MS) analyses of antiviral compounds are always preceded by a chromatographic separation step. LC-MS is often preferred to ultraviolet or fluorescence detection in the bioanalytical field, because it offer a better selectivity and sensibility [143,154–168].

As for LC-UV methods, also with LC-MS methods the chromatographic separation of antiviral compounds is typically carried out on C18 columns, but some methods based on the use of C8 columns [147, 148], as well as one based on the use of a C30 column were also proposed [39]. As mobile phases, MeOH, ACN and ultrapure water added with formic acid have been mainly employed. Mobile phases additives, such as formic acid, are often used in the bioanalytical field to increase ionization with ESI (+). As previously described, positive polarity is typically used for ESI ionization of COVID-19 tested antiviral drugs. However, Valluru et al. [82] compared both negative (ESI-) and positive (ESI+) ion modes, finding that negative one showed better selectivity and sensitivity for tenofovir. Its quantification in plasma samples was carried out by using the peak signals at m/z 286.1 as precursor ion and at m/z 134.0 as product ion. The ionization efficiency of analytes undergoing quantification, can modulate well the selectivity of the LC-MS methods [149] and it can further be increased by promoting the ionization by proper desolvation temperature, gas flows and source settings [150]. When these strategies are not sufficient, the second easiest method to improve the selectivity of the method may be the replacement of the C18 phase with a different sort of stationary phase. As example, Chan et al. [19] analysed amantadine, rimantadine, oseltamivir (and its active metabolite oseltamivir carboxylate) and zanamivir in poultry muscle, on a zwitterionic hydrophilic interaction liquid chromatography (HILIC) column coupled to a triple quadrupole mass spectrometer. HILIC offers an alternative retention and separation mechanism to reversed phase, whereby polar compounds, such as oseltamivir or zanamivir, are more strongly retained, increasing the selectivity of the method.

Isocratic elution programs are generally used for the chromatographic separations of antivirals, also when more than one drugs have to be detected. Indeed, Yamada et al. [64] well separated, in 6 min, two drugs, namely abacavir and tenofovir, in human plasma and saliva samples through a chromatographic method performed on a C18 reverse phase column (1.5 \times 50 mm, 5 μm) isocratically, at a flow rate of 0.2 mL/min, using 5 mM formic acid-3% (v/v) acetonitrile as the mobile phase. It should be noted that the run times of the proposed LC-MS methods for the detection and quantification of antiviral compounds tested for the COVID-19 treatment are, on average, shorter if compared to those of the LC-UV methods. Indeed they range from 1 to a maximum of 11 min. Only Berendsen et al. [85] reported a method based on a run time of 20 min for the simultaneous analysis of seven antiviral drugs, i.e. zanamivir, ribavirin, oseltamivir, oseltamivir carboxylate, amantadine,

rimantadine and arbidol, in poultry muscle. The proposed method was based on a column-switch liquid chromatography system combining a C18 column with a Hypercarb column. In detail, zanamivir and ribavirin were eluted from the C18 column, within 5 min, and subsequently retained on the Hypercarb column. After that, on the Hypercarb column, zanamivir and ribavirin were separated from the matrix constituents using a gradient and then directly detected by MS. After their elution, the other antiviral drugs were eluted from the C18 column by increasing the organic content of the mobile phase, passing by the Hypercarb column and entering the MS directly. In general, LC-MS/MS allows to obtain LOD and LOQ values in the order of ng/mL within antivirals analysis. Kanneti et al. [77] developed and validated a high-throughput LC-MS/MS method for simultaneous quantitation of oseltamivir phosphate and its oseltamivir carboxylate metabolite in human plasma, obtaining the best values of LLOQ (lower limit of quantification), i.e. 0.92 ng/mL for OSP and 5.22 ng/mL for its metabolite. However, one limitation associated with LC-MS analysis is its susceptibility to matrix effects [151,152]. Matrix effect is defined as the outcome of co-eluting interfering compounds on the analyte ionization. Typically, suppression or enhancement of analyte response affect precision and accuracy of corresponding results [149,150]. This issue could be resolved by improving chromatographic efficiency, by using ultra high-performance liquid chromatography (UHPLC) columns. UHPLC has been used by numerous authors for the analysis of antivirals in biological matrices [58,59,67,70,83,86,95,96,99]. Since its commercial introduction in 2004, there has been a considerable interest in ultra-high-performance (pressure) liquid chromatography (UHPLC), which dramatically increases the throughput of regular HPLC methods [153]. One of the most recent UHPLC-MS/MS method for the antiviral compounds analysis was developed and fully validated by Courlet et al. [67] in 2018 for the quantification of five nucleoside reverse transcriptase inhibitors (NRTIs), among which emtricitabine and tenofovir, in plasma and cerebrospinal fluids. For the chromatographic separation, the mobile phase consisted of ultrapure water with 0.1% formic acid (component A) and MeOH with 0.1% formic acid (component B). The mobile phase was delivered at a flow rate of 0.5 mL/min using a 2-step gradient elution program; the total run time was of 5 min. With this method, the matrix effects were quantitatively estimated at three concentration levels, i.e. low (L, 10 ng/mL), medium (M, 300 ng/mL for plasma and 100 ng/mL for cerebrospinal fluid- CSF) and high (H, 3000 ng/mL) QC concentrations, through the standard line slope approach, and normalized to the internal standard. Briefly, the RSD of slopes from linear regressions estimated through L, M, H concentrations for spiked samples with both analytes and corresponding internal standard, after extraction were evaluated. The lack of significant matrix effects was confirmed by RSD values that did not exceed 3.4% for plasma or 2.5% for CSF. In addition, Avataneo et al. [62] calculated matrix effect by comparing the signal from the analysis of post-extraction spiked samples at high, medium, low QC levels and at LLOQ with those from direct injection of the same concentration of analytes without matrix, in the first UHPLC-MS/MS method, validated for remdesivir and its metabolite GS-441524 determination in plasma. In this case, the chromatographic conditions adopted, envisaged the use of an Acquity HSS T3 column, and a gradient elution program with ultrapure water with 0.05% formic acid (component A) and ACN with 0.1% formic acid (component B), as mobile phase. The mean matrix effect factor obtained were 6% (RSD 4%) for remdesivir and -2% (RSD 12%) for GS-441524; while mean internal standard-normalized matrix effect (IS-nME) were -5% (RSD 4%) and -6% (RSD 8%), respectively (see Supplementary Material, Table S1).

5. Conclusions

Currently, indinavir, ritonavir, saquinavir, darunavir, lopinavir, favipiravir, remdesivir, galidesivir, emtricitabine, tenofovir, oseltamivir, ribavirin, baloxavir-marboxil and umifenovir are tested for COVID-19 infection. In this review, the literature screening has revealed that

more than 80 analytical methods, most of them LC-MS/MS, have been developed and/or validated for the identification and detection of these antiviral drugs in biological samples. The absence of methods dedicated to baloxavir-marboxil and galidesivir was ascertained. The present article provides some degree of foundation for readers to successfully identify and/or establish the most suitable method to accurately quantify these compounds in biological fluids. It is desirable that with state-of-the-art analytical techniques, the selective identification and accurate quantification of antiviral drugs will lead us to a comprehensive understanding of their therapeutic effects.

Author contributions

Maria A. Acquavia: Writing - Original Draft, Visualization. **Luca Foti:** Data Curation, Investigation. **Raffaella Pascale:** Writing - Review & Editing. **Antonina Nicolò:** Investigation. **Vincenzo Brancaleone:** Validation. **Tommaso R. I. Cataldi:** Validation. **Giuseppe Martelli:** Supervision. **Laura Scranò:** Supervision. **Giuliana Bianco:** Supervision, Project administration.

Declaration of competing interest

The authors declare that they have no known competing financial interests or personal relationships that could have appeared to influence the work reported in this paper.

Appendix A. Supplementary data

Supplementary data to this article can be found online at <https://doi.org/10.1016/j.talanta.2020.121862>.

References

- [1] C.A. Devaux, J.M. Rolain, P. Colson, D. Raoult, New insights on the antiviral effects of chloroquine against coronavirus: what to expect for COVID-19? *Int. J. Antimicrob. Agents* 55 (2020) 1–6, <https://doi.org/10.1016/j.ijantimicag.2020.105938>.
- [2] C. Sohrabi, Z. Alsafi, N. O'Neill, M. Khan, A. Kerwan, A. Al-Jabir, C. Iosifidis, R. Agha, World Health Organization declares global emergency, A review of the 2019 novel coronavirus (COVID-19), *Int. J. Surg.* 76 (2020) 71–76, <https://doi.org/10.1016/j.ijsu.2020.02.034>.
- [3] P.B. Madrid, R.G. Panchal, T.K. Warren, A.C. Shurtleff, A.N. Endsley, C.E. Green, A. Kolokoltsov, R. Davey, I.D. Manger, L. Gilfillan, S. Bavari, M.J. Tanga, Evaluation of Ebola virus inhibitors for drug repurposing, *ACS Infect. Dis.* 1 (2016) 317–326, <https://doi.org/10.1021/acsinfecdis.5b00030>.
- [4] L. Tanenbaum, D.L. Tuffanelli, Antimalarial agents: chloroquine, hydroxychloroquine, and quinaquine, *Arch. Dermatol.* 116 (1980) 587–591, https://doi.org/10.1007/978-1-61779-213-7_16.
- [5] A. Markham, Baricitinib : first global approval, *Drugs* 77 (2017) 697–704, <https://doi.org/10.1007/s40265-017-0723-3>.
- [6] B. Cao, Y. Wang, D. Wen, W. Liu, J. Wang, G. Fan, L. Ruan, B. Song, Y. Cai, M. Wei, X. Li, J. Xia, N. Chen, J. Xiang, T. Yu, T. Bai, X. Xie, L. Zhang, C. Li, Y. Yuan, H. Chen, H. Li, H. Huang, S. Tu, F. Gong, Y. Liu, Y. Wei, C. Dong, F. Zhou, X. Gu, J. Xu, Z. Liu, Y. Zhang, H. Li, L. Shang, K. Wang, K. Li, X. Zhou, X. Dong, Z. Qu, S. Lu, X. Hu, S. Ruan, S. Luo, J. Wu, L. Peng, F. Cheng, L. Pan, J. Zou, C. Jia, J. Wang, X. Liu, S. Wang, X. Wu, Q. Ge, J. He, H. Zhan, F. Qiu, L. Guo, C. Huang, T. Jaki, F.G. Hayden, P.W. Horby, D. Zhang, C. Wang, A trial of lopinavir-ritonavir in adults hospitalized with severe covid-19, *N. Engl. J. Med.* 382 (2020) 1787–1799, <https://doi.org/10.1056/NEJMoa2001282>.
- [7] N. Ford, M. Vitoria, A. Rangaraj, S.L. Norris, A. Calmy, M. Doherty, Systematic review of the efficacy and safety of antiretroviral drugs against SARS, MERS or COVID-19: initial assessment, *J. Int. AIDS Soc.* 23 (2020) 1–9, <https://doi.org/10.1002/jia2.25489>.
- [8] M. Costanzo, M.A.R. De Giglio, G.N. Roviello, SARS CoV-2: recent reports on antiviral therapies based on lopinavir/ritonavir, darunavir/umifenovir, hydroxychloroquine, remdesivir, favipiravir and other drugs for the treatment of the new coronavirus, *Curr. Med. Chem.* 27 (2020) 1–6, <https://doi.org/10.2174/0929867327666200416131117>.
- [9] S. Agrawal, A.D. Goel, N. Gupta, Emerging prophylaxis strategies against COVID-19, *Monaldi Arch. Chest Dis.* 90 (2020) 169–172, <https://doi.org/10.4081/monaldi.2020.1289>.
- [10] A. Farag, P. Wang, M. Ahmed, S. Haaham, Identification of FDA approved drugs targeting COVID-19 virus by structure- based drug repositioning, *JAMA, J. Am. Med. Assoc.* 323 (2020) 1061–1069, <https://doi.org/10.7551/mitpress/3215.003.0017>.

- [11] Y.X. Du, X.P. Chen, Favipiravir: pharmacokinetics and concerns about clinical trials for 2019-nCoV infection, *Clin. Pharmacol. Ther.* (2020) 1–6, <https://doi.org/10.1002/cpt.1844>, 0.
- [12] S.G.V. Rosa, W.C. Santos, Clinical trials on drug repositioning for COVID-19 treatment, *Rev. Panam. Salud Pública* 44 (2020) 1, <https://doi.org/10.26633/rpsp.2020.40>.
- [13] A.A. Elfiky, Ribavirin, remdesivir, sofosbuvir, galidesivir, and tenofovir against SARS-CoV-2 RNA dependent RNA polymerase (RdRp): a molecular docking study, *Life Sci.* 253 (2020), <https://doi.org/10.1016/j.lfs.2020.117592>.
- [14] S.L. Bixler, A.J. Duplantier, S. Bavari, Discovering drugs for the treatment of Ebola virus, *Curr. Treat. Options Infect. Dis.* 9 (2017) 299–317, <https://doi.org/10.1007/s40506-017-0130-z>.
- [15] J.S. Khalili, H. Zhu, N.S.A. Mak, Y. Yan, Y. Zhu, Novel coronavirus treatment with ribavirin: groundwork for an evaluation concerning COVID-19, *J. Med. Virol.* (2020) 1–7, <https://doi.org/10.1002/jmv.25798>.
- [16] M.P. Lythgoe, P. Middleton, Ongoing clinical trials for the management of the COVID-19 pandemic, *Trends Pharmacol. Sci.* 41 (2020) 363–382, <https://doi.org/10.1016/j.tips.2020.03.006>.
- [17] Y. Lou, L. Liu, Y. Qiu, Clinical outcomes and plasma concentrations of baloxavir marboxil and favipiravir in COVID-19 patients: an exploratory randomized, controlled trial, *MedRxiv* (2020) 2020, <https://doi.org/10.1101/2020.04.29.20085761>, 04.29.20085761.
- [18] D. Wang, B. Hu, C. Hu, F. Zhu, X. Liu, J. Zhang, B. Wang, H. Xiang, Z. Cheng, Y. Xiong, Y. Zhao, Y. Li, X. Wang, Z. Peng, Clinical characteristics of 138 hospitalized patients with 2019 novel coronavirus-infected pneumonia in wuhan, China, *JAMA, J. Am. Med. Assoc.* 323 (2020) 1061–1069, <https://doi.org/10.1001/jama.2020.1585>.
- [19] D. Chan, J. Tarbin, M. Sharman, M. Carson, M. Smith, S. Smith, Screening method for the analysis of antiviral drugs in poultry tissues using zwitterionic hydrophilic interaction liquid chromatography/tandem mass spectrometry, *Anal. Chim. Acta* 700 (2011) 194–200, <https://doi.org/10.1016/j.aca.2010.11.015>.
- [20] P. Mu, N. Xu, T. Chai, Q. Jia, Z. Yin, S. Yang, Y. Qian, J. Qiu, Simultaneous determination of 14 antiviral drugs and relevant metabolites in chicken muscle by UPLC-MS/MS after QuEChERS preparation, *J. Chromatogr. B Anal. Technol. Biomed. Life Sci.* 1023 (2016) 17–23, <https://doi.org/10.1016/j.jchromb.2016.04.036>.
- [21] G. Hopfgartner, E. Bourgonne, Quantitative high-throughput analysis of drugs in biological matrices by mass spectrometry, *Mass Spectrom. Rev.* 22 (2003) 195–214, <https://doi.org/10.1002/mas.10050>.
- [22] I. Vasconcelos, C. Fernandes, Magnetic solid phase extraction for determination of drugs in biological matrices, *TrAC Trends Anal. Chem. (Reference Ed.)* 89 (2017) 41–52, <https://doi.org/10.1016/j.trac.2016.11.011>.
- [23] J.S. Kang, M.H. Lee, Overview of therapeutic drug monitoring, *Korean J. Intern. Med. (Korean Ed.)* 24 (2009) 1–10, <https://doi.org/10.3904/kjim.2009.24.1.1>.
- [24] N.M. Cassiano, V.V. Lima, R.V. Oliveira, A.C. De Pietro, Q.B. Cass, Development of restricted-access media supports and their application to the direct analysis of biological fluid samples via high-performance liquid chromatography, *Anal. Bioanal. Chem.* 384 (2006) 1462–1469, <https://doi.org/10.1007/s00216-005-0253-9>.
- [25] S. Chandran, P.R.S. Singh, Comparison of various international guidelines for analytical method validation, *Die Pharm. Int. J. Pharm. Sci.* 62 (2007) 4–14, <https://doi.org/10.1691/ph.2007.1.5064>.
- [26] I. Taverniers, M. De Loose, E. Van Bockstaele, laboratory II, Analytical method validation and quality assurance, *Trends Anal. Chem.* 23 (2004) 1–48, <https://doi.org/10.1016/j.trac.2004.04.001>.
- [27] V.P. Shah, The history of bioanalytical method validation and Regulation : evolution of a guidance document on bioanalytical methods validation, *AAPS J.* 9 (2007) E43–E47.
- [28] Food and Drug Administration, Bioanalytical method validation guidance, *Food Drug Adm* (2018) 1–41.
- [29] L. V. Sonawane, B.N. Poul, S. V. Usnale, P. V. Waghmare, L.H. Surwase, Bioanalytical method validation and its pharmaceutical application- A review, *Pharm. Anal. Acta* 5 (2014) 1–7, <https://doi.org/10.4172/2153-2435.1000288>.
- [30] M.M. Moein, A. El Beqqali, M. Abdel-Rehim, Bioanalytical method development and validation: critical concepts and strategies, *J. Chromatogr. B Anal. Technol. Biomed. Life Sci.* 1043 (2017) 3–11, <https://doi.org/10.1016/j.jchromb.2016.09.028>.
- [31] V.P. Shah, K.K. Midha, J.W.A. Findlay, H.M. Hill, H. James D, M. Iain J, G. McKay, K.J. Miller, R.N. Patnaik, M.L. Powell, A.V. Tonelli, A. Yacobi, Bioanalytical method validation—a revisit with a decade of progress, *Pharm. Res. (N. Y.)* 17 (2000) 1551–1557, <https://doi.org/10.1023/A>.
- [32] S. Kollipara, G. Bende, N. Agarwal, B. Varshney, J. Paliwal, International guidelines for bioanalytical method validation: a comparison and discussion on current scenario, *Chromatographia* 73 (2011) 201–217, <https://doi.org/10.1007/s10337-010-1869-2>.
- [33] S. Bansal, D. Stefano, Anthony, Key elements of bioanalytical method validation for macromolecules, *AAPS J.* 9 (2007) 109–114, <https://doi.org/10.1208/aapsj0902017>.
- [34] P.K. Prathipati, S. Mandal, C.J. Destache, LC-MS/MS method for the simultaneous determination of tenofovir, emtricitabine, elvitegravir and rilpivirine in dried blood spots, *Biomed. Chromatogr.* 32 (2018) 1–7, <https://doi.org/10.1002/bmc.4270>.
- [35] U. Duthaler, B. Berger, S. Erb, M. Battegay, E. Letang, S. Gaugler, S. Krähenbühl, M. Haschke, Automated high throughput analysis of antiretroviral drugs in dried blood spots, *J. Mass Spectrom.* 52 (2017) 534–542, <https://doi.org/10.1002/jms.3952>.
- [36] C. Waitt, S. Dilli Penchala, A. Olagunju, A. Amara, L. Else, M. Lamorde, S. Khoo, Development, validation and clinical application of a method for the simultaneous quantification of lamivudine, emtricitabine and tenofovir in dried blood and dried breast milk spots using LC-MS/MS, *J. Chromatogr. B Anal. Technol. Biomed. Life Sci.* 1060 (2017) 300–307, <https://doi.org/10.1016/j.jchromb.2017.06.012>.
- [37] R. Nageswara Rao, M.S. Arnipalli, N.V. Nimmu, Dried blood spot analysis of (+) and (-) darunavir enantiomers on immobilized amylose tris-(3, 5-dimethylphenylcarbamate) LC and its application to pharmacokinetics, *Biomed. Chromatogr.* 29 (2015) 1878–1884, <https://doi.org/10.1002/bmc.3510>.
- [38] R.N. Rao, K. Santhakumar, C.G. Naidu, Rat dried blood spot analysis of (R,S)-(-) and (S,R)-(+)- enantiomers of emtricitabine on immobilized tris-(3,5-dimethylphenyl carbamate) amylose silica as a chiral stationary phase, *J. Chromatogr. B Anal. Technol. Biomed. Life Sci.* 1002 (2015) 160–168, <https://doi.org/10.1016/j.jchromb.2015.08.016>.
- [39] L.C. Jimmerson, J.H. Zheng, L.R. Bushman, C.E. MacBrayne, P.L. Anderson, J. J. Kiser, Development and validation of a dried blood spot assay for the quantification of ribavirin using liquid chromatography coupled to mass spectrometry, *J. Chromatogr. B Anal. Technol. Biomed. Life Sci.* 944 (2014) 18–24, <https://doi.org/10.1016/j.jchromb.2013.10.035>.
- [40] K. Watanabe, E. Varesio, G. Hopfgartner, Parallel ultra high pressure liquid chromatography-mass spectrometry for the quantification of HIV protease inhibitors using dried spot sample collection format, *J. Chromatogr. B Anal. Technol. Biomed. Life Sci.* 965 (2014) 244–253, <https://doi.org/10.1016/j.jchromb.2014.05.008>.
- [41] G.P. Hooff, R.J.W. Meesters, J.J.A. Van Kampen, N.A. Van Huizen, B. Koch, A.F. Y. Al Hadithy, T. Van Gelder, A.D.M.E. Osterhaus, R.A. Gruters, T.M. Luider, Dried blood spot UHPLC-MS/MS analysis of oseltamivir and oseltamivircarboxylate-a validated assay for the clinic, *Anal. Bioanal. Chem.* 400 (2011) 3473–3479, <https://doi.org/10.1007/s00216-011-5050-z>.
- [42] S.M. Illamola, E. Valade, D. Hirt, E. Dulioust, Y. Zheng, J.P. Wolf, J.M. Tréluyer, Development and validation of a LC-MS/MS method for the quantification of tenofovir and emtricitabine in seminal plasma, *J. Chromatogr. B Anal. Technol. Biomed. Life Sci.* 1033–1034 (2016) 234–241, <https://doi.org/10.1016/j.jchromb.2016.08.011>.
- [43] M. Vanaja, J. Sreeramulu, Stability indicating determination of darunavir with hplc in blood plasma samples, *Rasayan J. Chem.* 12 (2019) 839–848, <https://doi.org/10.31788/RJC.2019.1225118>.
- [44] S.S.M. Hassan, R.M. El-Nashar, A.S.M. El-Tantawy, A new validated potentiometric method for batch and continuous quality control monitoring of oseltamivir phosphate (Taminil) in drug Formulations and biological fluids, *Electroanalysis* 25 (2013) 408–416, <https://doi.org/10.1002/elan.201200437>.
- [45] M.A. Omar, S.M. Derayea, I.M. Mostafa, Development and validation of stability-indicating spectrofluorometric method for determination of H1N1 antiviral drug (Oseltamivir phosphate) in human plasma through Hantzsch reaction, *R. Soc. Chem. Adv.* 5 (2015) 27735–27742.
- [46] M. Gumustas, M.G. Caglayan, F. Onur, S.A. Ozkan, Simultaneous determination and validation of emtricitabine, rilpivirine and tenofovir from biological samples using LC and CE methods, *Biomed. Chromatogr.* 32 (2018) 1–8, <https://doi.org/10.1002/bmc.4158>.
- [47] N. Wiriyakosol, A. Puangpetch, W. Manosuthi, S. Tomongkon, C. Sukasem, D. Pinthong, A LC/MS/MS method for determination of tenofovir in human plasma and its application to toxicity monitoring, *J. Chromatogr. B Anal. Technol. Biomed. Life Sci.* 1085 (2018) 89–95, <https://doi.org/10.1016/j.jchromb.2018.03.045>.
- [48] L. Belkhir, M. De Laveleye, B. Vandercam, F. Zech, K.A. Delongie, A. Capron, J. Yombi, A. Vincent, L. Elens, V. Haufroid, Quantification of darunavir and etravirine in human peripheral blood mononuclear cells using high performance liquid chromatography tandem mass spectrometry (LC-MS/MS), clinical application in a cohort of 110 HIV-1 infected patients and evidence of a pote, *Clin. Biochem.* 49 (2016) 580–586, <https://doi.org/10.1016/j.clinbiochem.2015.12.011>.
- [49] J. Koehn, Y. Ding, J. Freeling, J. Duan, R.J.Y. Ho, A simple, efficient, and sensitive method for simultaneous detection of anti-HIV drugs atazanavir, ritonavir, and tenofovir by use of liquid chromatography-tandem mass spectrometry, *Antimicrob. Agents Chemother.* 59 (2015) 6682–6688, <https://doi.org/10.1128/AAC.00869-15>.
- [50] European Parliament and the Council of the European Union, 96/23/EC COMMISSION DECISION of 12 August 2002 implementing Council Directive 96/23/EC concerning the performance of analytical methods and the interpretation of results (notified under document number C(2002) 3044)(Text with EEA relevance) (2002/657/EC), *Off. J. Eur. Communities* (2002) 8–36, <https://doi.org/10.1017/CBO9781107415324.004>.
- [51] G. Smith, European medicines agency guideline on bioanalytical method validation: what more is there to say? *Bioanalysis* 4 (2012) 865–868, <https://doi.org/10.4155/bio.12.44>.
- [52] European Medicines Agency, ICH Guideline M10 on Bioanalytical Method Validation, 2019, pp. 1–57.
- [53] W.M. Mullett, Determination of drugs in biological fluids by direct injection of samples for liquid-chromatographic analysis, *J. Biochem. Biophys. Methods* 70 (2007) 263–273, <https://doi.org/10.1016/j.jbbm.2006.10.001>.
- [54] H. Kataoka, New trends in sample preparation for clinical and pharmaceutical analysis, *Trends Anal. Chem.* 22 (2003) 232–244, [https://doi.org/10.1016/S0165-9936\(03\)00402-3](https://doi.org/10.1016/S0165-9936(03)00402-3).
- [55] R.D. McDowall, E. Doyle, G.S. Murkitt, V.S. Picot, Sample preparation for the HPLC analysis of drugs in biological fluids, *J. Pharm. Anal.* 7 (1989) 1087–1096.

- [56] S. Souverain, S. Rudaz, J. Veuthey, Restricted access materials and large particle supports for on-line sample preparation : an attractive approach for biological fluids analysis, *J. Chromatogr. B* 801 (2004) 141–156, <https://doi.org/10.1016/j.jchromb.2003.11.043>.
- [57] J. Ma, J. Shi, H. Le, R. Cho, J.C. Huang, S. Miao, B.K. Wong, A fully automated plasma protein precipitation sample preparation method for LC – MS/MS bioanalysis, *J. Chromatogr. B* 862 (2008) 219–226, <https://doi.org/10.1016/j.jchromb.2007.12.012>.
- [58] M. Simiele, A. Ariauo, A. De Nicolò, F. Favata, M. Ferrante, C. Carciari, S. Bonora, G. Di Perri, A. D'Avolio, UPLC–MS/MS method for the simultaneous quantification of three new antiretroviral drugs, dolutegravir, elvitegravir and rilpivirine, and other thirteen antiretroviral agents plus cobicistat and ritonavir boosters in human plasma, *J. Pharmaceut. Biomed. Anal.* 138 (2017) 223–230, <https://doi.org/10.1016/j.jpba.2017.02.002>.
- [59] Z. Djerada, C. Feliu, C. Tournois, D. Vautier, L. Binet, A. Robinet, H. Marty, C. Gozalo, D. Lamiable, H. Millart, Validation of a fast method for quantitative analysis of elvitegravir, raltegravir, maraviroc, etravirine, tenofovir, boceprevir and 10 other antiretroviral agents in human plasma samples with a new UPLC–MS/MS technology, *J. Pharmaceut. Biomed. Anal.* 86 (2013) 100–111, <https://doi.org/10.1016/j.jpba.2013.08.002>.
- [60] S. Pajares García, D. Guillén Tunica, M. Brunet Serra, Desarrollo y validación de un método para la determinación de darunavir en plasma mediante LC-MS/MS, *Rev. Del Lab. Clin.* 4 (2011) 127–133, <https://doi.org/10.1016/j.labcli.2010.12.002>.
- [61] R. Ter Heine, *Bioanalysis, Metabolism & Clinical Pharmacology of Antiretroviral Drugs*, Slotervaart Hospital/The Netherlands Cancer Institute, Amsterdam, The Netherlands, 2009. Publication.
- [62] V. Avataneo, A. de Nicolò, J. Cusato, M. Antonucci, A. Manca, A. Palermi, C. Waitt, S. Walimbwa, M. Lamorde, G. di Perri, A. D'Avolio, Development and validation of a UHPLC-MS/MS method for quantification of the prodrug remdesivir and its metabolite GS-441524: a tool for clinical pharmacokinetics of SARS-CoV-2/COVID-19 and Ebola virus disease, *J. Antimicrob. Chemother.* (2020) 1–6, <https://doi.org/10.1093/jac/dkaa152>.
- [63] L. Else, V. Watson, J. Tjia, A. Hughes, M. Siccardi, S. Khoo, D. Back, Validation of a rapid and sensitive high-performance liquid chromatography-tandem mass spectrometry (HPLC-MS/MS) assay for the simultaneous determination of existing and new antiretroviral compounds, *J. Chromatogr. B Anal. Technol. Biomed. Life Sci.* 878 (2010) 1455–1465, <https://doi.org/10.1016/j.jchromb.2010.03.036>.
- [64] E. Yamada, R. Takagi, K. Sudo, S. Kato, Determination of abacavir, tenofovir, darunavir, and raltegravir in human plasma and saliva using liquid chromatography coupled with tandem mass spectrometry, *J. Pharmaceut. Biomed. Anal.* 114 (2015) 390–397, <https://doi.org/10.1016/j.jpba.2015.06.005>.
- [65] A. Grigoriev, I. Borisova, I. Yaroshenko, A. Sidorova, In vitro and in vivo stability of oseltamivir within a bioequivalence trial, *Anal. Bioanal. Chem.* (2016) 3891–3897, <https://doi.org/10.1007/s00216-016-9483-2>.
- [66] W. Kromdijk, H. Rosing, M.P.H. van den Broek, J.H. Beijnen, A.D.R. Huitema, Quantitative determination of oseltamivir and oseltamivir carboxylate in human fluoride EDTA plasma including the ex vivo stability using high-performance liquid chromatography coupled with electrospray ionization tandem mass spectrometry, *J. Chromatogr. B Anal. Technol. Biomed. Life Sci.* 891–892 (2012) 57–63, <https://doi.org/10.1016/j.jchromb.2012.02.026>.
- [67] P. Courlet, D. Spaggiari, M. Cavassini, R. Du Pasquier, S. Alves Saldanha, T. Buclin, C. Marzolini, C. Csajka, L. Decosterd, Determination of nucleosidic/tidic reverse transcriptase inhibitors in plasma and cerebrospinal fluid by ultra-high-pressure liquid chromatography coupled with tandem mass spectrometry, *Clin. Mass Spectrom.* 8 (2018) 8–20, <https://doi.org/10.1016/j.clinms.2018.04.001>.
- [68] B. Ouyang, F. Zhou, L. Zhen, Y. Peng, J. Sun, Q. Chen, X. Jin, G. Wang, J. Zhang, Simultaneous determination of tenofovir alafenamide and its active metabolites tenofovir and tenofovir diphosphate in HBV-infected hepatocyte with a sensitive LC–MS/MS method, *J. Pharmaceut. Biomed. Anal.* 146 (2017) 147–153, <https://doi.org/10.1016/j.jpba.2017.08.028>.
- [69] L. Barreiros, C. Cunha-Reis, E.M.P. Silva, J.R.B. Carvalho, J. das Neves, B. Sarmiento, M.A. Segundo, Development and validation of a liquid chromatography-MS/MS method for simultaneous quantification of tenofovir and efavirenz in biological tissues and fluids, *J. Pharmaceut. Biomed. Anal.* 136 (2017) 120–125, <https://doi.org/10.1016/j.jpba.2016.12.028>.
- [70] A. Ramírez-Ramírez, E. Sánchez-Serrano, G. Loaiza-Flores, N. Plazola-Camacho, R.G. Rodríguez-Delgado, R. Figueroa-Damián, M. Domínguez-Castro, M. López-Martínez, Z. Flores-García, J. Hernández-Pineda, Simultaneous quantification of four antiretroviral drugs in breast milk samples from HIV-positive women by an ultra-high performance liquid chromatography tandem mass spectrometry (UPLC-MS/MS) method, *PLoS One* 13 (2018) 1–15, <https://doi.org/10.1371/journal.pone.0191236>.
- [71] S. Souverain, S. Rudaz, J. Veuthey, Protein precipitation for the analysis of a drug cocktail in plasma by LC – ESI –, *MS* 35 (2004) 913–920, <https://doi.org/10.1016/j.jpba.2004.03.005>.
- [72] A. Van Eeckhout, K. Lanckmans, S. Sarre, I. Smolders, Y. Michotte, Validation of bioanalytical LC-MS/MS assays: evaluation of matrix effects, *J. Chromatogr. B Anal. Technol. Biomed. Life Sci.* 877 (2009) 2198–2207, <https://doi.org/10.1016/j.jchromb.2009.01.003>.
- [73] N. Charbe, S. Baldelli, V. Cozzi, S. Castoldi, D. Cattaneo, E. Clementi, Development of an HPLC–UV assay method for the simultaneous quantification of nine antiretroviral agents in the plasma of HIV-infected patients, *J. Pharm. Anal.* 6 (2016) 396–403, <https://doi.org/10.1016/j.jpba.2016.05.008>.
- [74] C.F. Poole, New trends in solid-phase extraction, *Trends Anal. Chem.* 22 (2003) 362–373, [https://doi.org/10.1016/S0165-9936\(03\)00605-8](https://doi.org/10.1016/S0165-9936(03)00605-8).
- [75] L.R. Bushman, J.J. Kiser, J.E. Rower, B. Klein, J.H. Zheng, M.L. Ray, P. L. Anderson, Determination of nucleoside analog mono-, di-, and tri-phosphates in cellular matrix by solid phase extraction and ultra-sensitive LC-MS/MS detection, *J. Pharmaceut. Biomed. Anal.* 56 (2011) 390–401, <https://doi.org/10.1016/j.jpba.2011.05.039>.
- [76] E.M. Jr, A. Massele, E. Sepako, K. Sichelongo, A method employing SPE, MRM LC-MS/MS and a THF–water solvent system for the simultaneous determination of five antiretroviral drugs in human blood plasma, *Anal. Methods* 9 (2017) 450–458, <https://doi.org/10.1039/C6AY02442D>.
- [77] R. Kanneti, D. Bhavesh, D. Paramar, S. R. P.A. Bhatt, Development and validation of a high-throughput and robust LC-MS/MS with electrospray ionization method for simultaneous quantification of oseltamivir phosphate and its oseltamivir carboxylate metabolite in human plasma for pharmacokinetic studies, *Biomed. Chromatogr.* 25 (2011) 727–733, <https://doi.org/10.1002/bmc.1509>.
- [78] R. Kanneti, K.I. Jaswanth, K.R. Neeraja, P.A. Bhatt, Development and validation of LC-MS/MS method for determination of Darunavir in human plasma for application of clinical pharmacokinetics, *Int. J. Pharm. Pharmaceut. Sci.* 3 (2011) 491–496.
- [79] S. Aburuz, J. Millership, L. Heaney, J. McElnay, Simple liquid chromatography method for the rapid simultaneous determination of prednisolone and cortisol in plasma and urine using hydrophilic lipophilic balanced solid phase extraction cartridges, *J. Chromatogr. B* 798 (2003) 193–201, <https://doi.org/10.1016/j.jchromb.2003.09.044>.
- [80] M. Fernandez, J. Sepulveda, T. Aranguiz, C. Von Plessing, T technique validation by liquid chromatography for the determination of acyclovir in plasma, *J. Chromatogr. B* 791 (2003) 357–363.
- [81] H.C. Zhang, X. jun Yu, W. chao Yang, J. feng Peng, T. Xu, D.Q. Yin, X. lin Hu, MCX based solid phase extraction combined with liquid chromatography tandem mass spectrometry for the simultaneous determination of 31 endocrine-disrupting compounds in surface water of Shanghai, *J. Chromatogr. B Anal. Technol. Biomed. Life Sci.* 879 (2011) 2998–3004, <https://doi.org/10.1016/j.jchromb.2011.08.036>.
- [82] R.K. Valluru, P.B.R. B. K.S. S, P.K. V, N.B. Kilaru, High throughput LC-MS/MS method for simultaneous determination of tenofovir, lamivudine and nevirapine in human plasma, *J. Chromatogr. B Anal. Technol. Biomed. Life Sci.* 931 (2013) 117–126, <https://doi.org/10.1016/j.jchromb.2013.05.008>.
- [83] A.J. Ocque, C.E. Hagler, G.D. Morse, S.L. Letendre, Q. Ma, Development and validation of an LC–MS/MS assay for tenofovir and tenofovir alafenamide in human plasma and cerebrospinal fluid, *J. Pharmaceut. Biomed. Anal.* 156 (2018) 163–169, <https://doi.org/10.1016/j.jpba.2018.04.035>.
- [84] Z.C. Liu, F. Yang, M. Yao, Y.H. Lin, Z.J. Su, Simultaneous determination of antiviral drugs in chicken tissues by ultra high performance liquid chromatography with tandem mass spectrometry, *J. Separ. Sci.* 38 (2015) 1784–1793, <https://doi.org/10.1002/jssc.201401461>.
- [85] B.J.A. Berendsen, R.S. Wegh, M.L. Essers, A.A.M. Stolker, S. Weigel, Quantitative trace analysis of a broad range of antiviral drugs in poultry muscle using column-switch liquid chromatography coupled to tandem mass spectrometry, *Anal. Bioanal. Chem.* 402 (2012) 1611–1623, <https://doi.org/10.1007/s00216-011-5581-3>.
- [86] A. Gupta, P. Singhal, P.S. Shrivastav, M. Sanyal, Application of a validated ultra performance liquid chromatography-tandem mass spectrometry method for the quantification of darunavir in human plasma for a bioequivalence study in Indian subjects, *J. Chromatogr. B Anal. Technol. Biomed. Life Sci.* 879 (2011) 2443–2453, <https://doi.org/10.1016/j.jchromb.2011.07.008>.
- [87] N. Zhang, K.L. Hoffman, W. Li, D.T. Rossi, Semi-automated 96-well liquid-liquid extraction for quantitation of drugs in biological fluids, *J. Pharmaceut. Biomed. Anal.* 22 (2000) 131–138, [https://doi.org/10.1016/S0731-7085\(99\)00247-2](https://doi.org/10.1016/S0731-7085(99)00247-2).
- [88] L. Wang, J. Zhao, R. Zhang, L. Mi, X. Shen, N. Zhou, T. Feng, J. Jing, X. Liu, S. Zhang, Drug-drug interactions between PA-824 and darunavir based on pharmacokinetics in rats by LC-MS-MS, *J. Chromatogr. Sci.* 56 (2018) 327–335, <https://doi.org/10.1093/chromsci/bmy002>.
- [89] M. Louisa, V. Soetikno, Nafrialdi, R. Setiabudy, F.D. Suyatna, Primaquine decreased plasma concentration of ritonavir: single- and repeated-dose study in sprague dawley rats, *Med. J. Indones.* 20 (2011) 190–194, <https://doi.org/10.13181/mji.v20i3.449>.
- [90] B. Gralak-Dabrowska, T. Pawinski, P. Pulik, A. Horban, Interpatient variability of darunavir concentrations in plasma during long-term antiretroviral monotherapy, *HIV AIDS Rev* 13 (2014) 10–13, <https://doi.org/10.1016/j.hivar.2013.10.002>.
- [91] J.J.M.A. Hendrikx, H. Rosing, A.H. Schinkel, J.H.M. Schellens, J.H. Beijnen, Combined quantification of paclitaxel, docetaxel and ritonavir in human feces and urine using LC-MS/MS, *Biomed. Chromatogr.* 28 (2014) 302–310, <https://doi.org/10.1002/bmc.3021>.
- [92] Y.L. Wu, R.X. Chen, L. Zhu, Y. Lv, Y. Zhu, J. Zhao, Determination of ribavirin in chicken muscle by quick, easy, cheap, effective, rugged and safe method and liquid chromatography-tandem mass spectrometry, *J. Chromatogr. B Anal. Technol. Biomed. Life Sci.* 1012 (2016) 55–60, <https://doi.org/10.1016/j.jchromb.2016.01.016>.
- [93] N. Deshmukh, I. Hussain, J. Barker, A. Petroczi, D.P. Naughton, Analysis of anabolic steroids in human hair using LC-MS/MS, *Steroids* 75 (2010) 710–714, <https://doi.org/10.1016/j.steroids.2010.04.007>.

- [94] F. Pragst, M.A. Balikova, State of the art in hair analysis for detection of drug and alcohol abuse, *Clin. Chim. Acta* 370 (2006) 17–49, <https://doi.org/10.1016/j.cca.2006.02.019>.
- [95] A.J. Ocque, C.E. Hagler, R. DiFrancesco, Y. Woolwine-Cunningham, C.J. Bednasz, G.D. Morse, A.H. Talal, Development and validation of a UPLC-MS/MS method for the simultaneous determination of paritaprevir and ritonavir in rat liver, *Bioanalysis* 8 (2016) 1353–1363, <https://doi.org/10.4155/bio-2016-0040>.
- [96] A.J. Ocque, C.E. Hagler, R. DiFrancesco, G.D. Morse, A.H. Talal, Ultra-performance liquid chromatography tandem mass spectrometry for determination of Direct Acting Antiviral drugs in human liver fine needle aspirates, *J. Chromatogr. B Anal. Technol. Biomed. Life Sci.* 1052 (2017) 103–109, <https://doi.org/10.1016/j.jchromb.2017.03.020>.
- [97] M. Wang, M.S. Halquist, Y. Zhang, P.M. Gerk, Simultaneous determination of lopinavir and three ester prodrugs by LC-MS/MS in lysates of BeWo cells, *J. Chromatogr. B Anal. Technol. Biomed. Life Sci.* 975 (2015) 84–90, <https://doi.org/10.1016/j.jchromb.2014.10.032>.
- [98] D. Nagano, T. Araki, T. Nakamura, K. Yamamoto, Determination of intracellular darunavir by liquid chromatography coupled with fluorescence detection, *J. Chromatogr. Sci.* 52 (2014) 1021–1025, <https://doi.org/10.1093/chromsci/bmt147>.
- [99] D. Agnesod, A. De Nicolò, M. Simiele, A. Mohamed Abdi, L. Bognione, G. Di Perri, A. D'Avolio, Development and validation of a useful UPLC-MS/MS method for quantification of total and phosphorylated-ribavirin in peripheral blood mononuclear cells of HCV+ patients, *J. Pharmaceut. Biomed. Anal.* 90 (2014) 119–126, <https://doi.org/10.1016/j.jpba.2013.11.027>.
- [100] K. Sichilongo, E. Mwando, E. Sepako, A. Massele, Comparison of efficiencies of selected sample extraction techniques for the analysis of selected antiretroviral drugs in human plasma using LC-MS, *J. Pharmacol. Toxicol. Methods* 89 (2018) 1–8, <https://doi.org/10.1016/j.vascn.2017.10.001>.
- [101] T. Rejczak, T. Tuzimski, A review of recent developments and trends in the QuEChERS sample preparation approach, *Open Chem* 13 (2015) 980–1010, <https://doi.org/10.1515/chem-2015-0109>.
- [102] L.S.J. Anastasiades Michelangelo, Fast and easy multiresidue method employing acetonitrile extraction/partitioning and “dispersive solid-phase extraction” for the determination of pesticide residues in produce, *J. AOAC Int.* 86 (2003) 412–431.
- [103] R. Pascale, A. Onzo, R. Ciriello, L. Scrano, S.A. Bufo, G. Bianco, LC/MS Based Food Metabolomics, Elsevier, 2020, <https://doi.org/10.1016/b978-0-08-100596-5.22774-1>.
- [104] O.M.S. Minzi, A.Y. Massele, L.L. Gustafsson, Ö. Ericsson, Simple and cost-effective liquid chromatographic method for determination of pyrimethamine in whole blood samples dried on filter paper, *J. Chromatogr. B Anal. Technol. Biomed. Life Sci.* 814 (2005) 179–183, <https://doi.org/10.1016/j.jchromb.2004.10.049>.
- [105] J. V. Mei, J.R. Alexander, B.W. Adam, W.H. Hannon, Innovative non- or minimally-invasive technologies for monitoring Health and nutritional status in mothers and young children use of filter paper for the collection and analysis of human whole blood specimens 1, *J. Nutr.* 131 (2001) 1631–1636.
- [106] J.J.A. van Kampen, M.L. Reedijk, P.C. Burgers, L.J.M. Dekker, N.G. Hartwig, I. E. van der Ende, R. de Groot, A.D.M.E. Osterhaus, D.M. Burger, T.M. Luijder, R. A. Gruters, Ultra-fast analysis of plasma and intracellular levels of HIV protease inhibitors in children: a clinical application of MALDI mass spectrometry, *PLoS One* 5 (2010) 1–9, <https://doi.org/10.1371/journal.pone.0011409>.
- [107] R.J.W. Meesters, J.J.A. Van Kampen, R.D. Scheuer, M.E. Van Der Ende, R. A. Gruters, T.M. Luijder, Determination of the antiretroviral drug tenofovir in plasma from HIV-infected adults by ultrafast isotope dilution MALDI-triple quadrupole tandem mass spectrometry, *J. Mass Spectrom.* 46 (2011) 282–289, <https://doi.org/10.1002/jms.1897>.
- [108] M.T. Bokhart, E. Rosen, C. Thompson, C. Sykes, A.D.M. Kashuba, D.C. Muddiman, Quantitative mass spectrometry imaging of emtricitabine in cervical tissue model using infrared matrix-assisted laser desorption electrospray ionization, *Anal. Bioanal. Chem.* 407 (2015) 2073–2084, <https://doi.org/10.1007/s00216-014-8220-y>.
- [109] T. Tran, A. Chakraborty, X. Xi, H. Bohets, C. Cornett, K. Tsinman, T. Rades, A. Müllertz, Using potentiometric free drug sensors to determine the free concentration of ionizable drugs in colloidal systems, *J. Pharmacol. Sci.* 107 (2018) 103–112, <https://doi.org/10.1016/j.xphs.2017.05.016>.
- [110] A.H. Kamel, S.A.A. Almeida, M.G.F. Sales, F.T.C. Moreira, Sulfadiazine-potentiometric sensors for flow and batch determinations of sulfadiazine in drugs and biological fluids, *Anal. Sci.* 25 (2009) 365–371, <https://doi.org/10.2116/analsci.25.365>.
- [111] E. Bakker, E. Pretsch, Potentiometric sensors for trace-level analysis, *TrAC Trends Anal. Chem. (Reference Ed.)* 24 (2005) 199–207, <https://doi.org/10.1016/j.trac.2005.01.003>.
- [112] A.A. Gouda, M.I. Kotb El-Sayed, A.S. Amin, R. El Sheikh, Spectrophotometric and spectrofluorometric methods for the determination of non-steroidal anti-inflammatory drugs: a review, *Arab. J. Chem.* 6 (2013) 145–163, <https://doi.org/10.1016/j.arabj.2010.12.006>.
- [113] C.M. Boone, J.C.M. Waterval, H. Lingeman, K. Ensing, W.J.M. Underberg, Capillary electrophoresis as a versatile tool for the bioanalysis of drugs - a review, *J. Pharmaceut. Biomed. Anal.* 20 (1999) 831–863, [https://doi.org/10.1016/S0731-7085\(99\)00088-6](https://doi.org/10.1016/S0731-7085(99)00088-6).
- [114] A.A. Youssef, N. Magdy, L.A. Hussein, A.M. El-Kosasy, Validated RP-HPLC method for simultaneous determination of ribavirin, sofosbuvir and daclatasvir in human plasma: a treatment protocol administered to HCV patients in Egypt, *J. Chromatogr. Sci.* 57 (2019) 636–643, <https://doi.org/10.1093/chromsci/bmz038>.
- [115] R.S.C.H. Phani, K.R.S. Prasad, U.R. Mallu, New analytical HPLC method development and validation for the simultaneous quantification of paritaprevir ombitasvir and ritonavir spiked human plasma, *Orient. J. Chem.* 33 (2017) 2363–2369, <https://doi.org/10.13005/ojc/330528>.
- [116] P.R. Ravi, S. Joseph, U.S.R. Avula, S. Anthireddy, A simple liquid chromatographic method for the determination of tenofovir in rat plasma and its application to pharmacokinetic studies, *Acta Chromatogr.* 27 (2015) 597–612, <https://doi.org/10.1556/AChrom.27.2015.4.2>.
- [117] A. D'Avolio, A. De Nicolò, M. Simiele, S. Turini, D. Agnesod, L. Bognione, J. Cusato, L. Baietto, G. Cariti, A. Calcagno, M. Sciandra, G. Di Perri, S. Bonora, Development and validation of a useful HPLC-UV method for quantification of total and phosphorylated-ribavirin in blood and erythrocytes of HCV+ patients, *J. Pharmaceut. Biomed. Anal.* 66 (2012) 376–380, <https://doi.org/10.1016/j.jpba.2012.03.030>.
- [118] S.V. Sutar, H.N. More, S.A. Pishawkar, S.A. Bandgar, I.D. Raut, Validated RP-HPLC method development for estimation of Tenofovir Disoproxil Fumarate from plasma, *Res. J. Pharm. Technol.* 4 (2011) 1626–1629.
- [119] K.W. Crawford, J. Spritzler, R.C. Kalayjian, T. Parsons, A. Landay, R. Pollard, V. Stocker, M.M. Lederman, C. Flexner, Age-related changes in plasma concentrations of the HIV protease inhibitor lopinavir, *AIDS Res. Hum. Retrovir.* 26 (2010) 635–643, <https://doi.org/10.1089/aid.2009.0154>.
- [120] E. Lemasson, S. Bertin, P. Hennig, E. Lesellier, C. West, Impurity profiling of drug candidates: analytical strategies using reversed-phase and mixed-mode high-performance liquid chromatography methods, *J. Chromatogr. A* 1535 (2018) 101–113, <https://doi.org/10.1016/j.chroma.2018.01.014>.
- [121] A. Loregian, R. Gatti, G. Palu, D.P.E. F. Separation methods for acyclovir and related antiviral compounds, *J. Chromatogr. B* 764 (2001) 289–311, [https://doi.org/10.1016/S0378-4347\(01\)00319-X](https://doi.org/10.1016/S0378-4347(01)00319-X).
- [122] V. Das Gupta, M. Mathew, P. Division, Effect of mobile phase pH on the separation of drugs using high-performance liquid chromatography, *Drug Dev. Ind. Pharm.* 21 (1995) 833–837.
- [123] A.L.A. Wong, X. Xiang, P.S. Ong, E.Q.Y. Mitchell, N. Syn, I. Wee, A.P. Kumar, W. P. Yong, G. Sethi, B.C. Goh, P.C.L. Ho, L. Wang, A review on liquid chromatography-tandem mass spectrometry methods for rapid quantification of oncology drugs, *Pharmaceutics* 10 (2018) 1–20, <https://doi.org/10.3390/pharmaceutics10040221>.
- [124] J. Peris-vicente, I. Casas-breva, S. Carda-broch, J. Esteve-romero, Use of micellar liquid chromatography to analyze darunavir, ritonavir, emtricitabine, and tenofovir in plasma, *J. Separ. Sci.* (2014) 2825–2832, <https://doi.org/10.1002/jssc.201400574>.
- [125] F.J. DeLuccia, M. Arunyanart, L.J.C. Love, Direct serum injection with micellar liquid chromatography for therapeutic drug monitoring, *Anal. Chem.* 57 (1985) 1564–1568, <https://doi.org/10.1021/ac00285a015>.
- [126] B.S. Shin, S.H. Hong, H.J. Kim, H.S. Yoon, D.J. Kim, S.W. Hwang, J.B. Lee, S. D. Yoo, Development of a sensitive LC assay with fluorescence detection for the determination of zearalenone in rat serum, *Chromatographia* 69 (2009) 295–299, <https://doi.org/10.1365/s10337-008-0871-4>.
- [127] G. Bianco, G. Novario, G. Anzilotta, A. Palma, A. Mangone, T.R.I. Cataldi, Polybrominated diphenyl ethers (PBDEs) in Mediterranean mussels (*Mytilus galloprovincialis*) from selected Apulia coastal sites evaluated by GC-HRMS, *J. Mass Spectrom.* 45 (2010) 1046–1055, <https://doi.org/10.1002/jms.1799>.
- [128] G. Bianco, R. Pascale, C.F. Carbone, M.A. Acquavia, T.R.I. Cataldi, P. Schmitt-Kopplin, A. Buchicchio, D. Russo, L. Milella, Determination of soyasaponins in Fagioli di Sarconi beans (*Phaseolus vulgaris* L.) by LC-ESI-FTICR-MS and evaluation of their hypoglycemic activity, *Anal. Bioanal. Chem.* 410 (2018) 1561–1569, <https://doi.org/10.1007/s00216-017-0806-8>.
- [129] L.H. Cohen, A.I. Gusev, Small molecule analysis by MALDI mass spectrometry, *Anal. Bioanal. Chem.* (2002) 571–586, <https://doi.org/10.1007/s00216-002-1321-z>.
- [130] R. Pascale, G. Bianco, D. Coviello, M. Cristina Lafiosca, S. Masi, I.M. Mancini, S. A. Bufo, L. Scrano, D. Caniani, Validation of a liquid chromatography coupled with tandem mass spectrometry method for the determination of drugs in wastewater using a three-phase solvent system, *J. Separ. Sci.* 43 (2020) 886–895, <https://doi.org/10.1002/jssc.201900509>.
- [131] D.M. Drexler, T.J. Garrett, J.L. Cantone, R.W. Deters, J.G. Mitroka, M.C. Prieto Conaway, S.P. Adams, R.A. Yost, M. Sanders, Utility of imaging mass spectrometry (IMS) by matrix-assisted laser desorption ionization (MALDI) on an ion trap mass spectrometer in the analysis of drugs and metabolites in biological tissues, *J. Pharmacol. Toxicol. Methods* 55 (2007) 279–288, <https://doi.org/10.1016/j.vascn.2006.11.004>.
- [132] P. Liigand, K. Kaupmees, K. Haav, J. Liigand, I. Leito, M. Girod, R. Antoine, A. Kruve, Think negative: finding the best electrospray ionization/MS mode for your analyte, *Anal. Chem.* 89 (2017) 5665–5668, <https://doi.org/10.1021/acs.analchem.7b00096>.
- [133] R. Pascale, G. Bianco, T.R.I. Cataldi, A. Buchicchio, I. Losito, G. Altieri, F. Genovese, A. Tauriello, G.C. Di Renzo, M.C. Lafiosca, Investigation of the effects of virgin olive oil cleaning systems on the seicoridoid aglycone content using high performance liquid chromatography–mass spectrometry, *JAOCs, J. Am. Oil Chem. Soc.* 95 (2018) 665–671, <https://doi.org/10.1002/aocs.12072>.
- [134] A. El-Anead, A. Cohen, J. Banoub, Mass spectrometry, review of the basics: electrospray, MALDI, and commonly used mass analyzers, *Appl. Spectrosc. Rev.* 44 (2009) 210–230, <https://doi.org/10.1080/05704920902717872>.
- [135] J.J. Pitt, Principles and applications of liquid chromatography–mass spectrometry in clinical biochemistry, *Clin. Biochem. Rev.* 30 (2009) 19–34.
- [136] X. Ding, H. Ghobarah, X. Zhang, A. Jaochico, X. Liu, G. Deshmukh, B.M. Liederer, C.E.C.A. Hop, B. Dean, High-throughput liquid chromatography/mass

- spectrometry method for the quantitation of small molecules using accurate mass technologies in supporting discovery drug screening, *Rapid Commun. Mass Spectrom.* 27 (2013) 401–408, <https://doi.org/10.1002/rcm.6461>.
- [137] I.V. Chernushevich, A.V. Loboda, B.A. Thomson, An introduction to quadrupole-time-of-flight mass spectrometry, *J. Mass Spectrom.* 36 (2001) 849–865, <https://doi.org/10.1002/jms.207>.
- [138] T. Das Mishra, H. Kuran, P. Singhal, P.S. Shrivastav, Simultaneous quantitation of HIV-protease inhibitors ritonavir, lopinavir and indinavir in human plasma by UPLC-ESI-MS-MS, *J. Chromatogr. Sci.* 50 (2012) 625–635, <https://doi.org/10.1093/chromsci/bms048>.
- [139] W.M.A. Niessen, Tandem mass spectrometry of small-molecule antiviral drugs: 3. antiviral agents against herpes, influenza and other viral infections, *Int. J. Mass Spectrom.* 455 (2020) 1–12.
- [140] M. Yadav, P. Singhal, S. Goswami, U.C. Pande, M. Sanyal, P.S. Shrivastav, Selective determination of antiretroviral agents tenofovir, emtricitabine, and lamivudine in human plasma by a LC-MS-MS method for a bioequivalence study in healthy Indian subjects, *J. Chromatogr. Sci.* 48 (2010) 704–713, <https://doi.org/10.1093/chromsci/48.9.704>.
- [141] C.C. Lin, L.T. Yeh, J.Y.N. Lau, Specific, sensitive and accurate liquid chromatographic-tandem mass spectrometric method for the measurement of ribavirin in rat and monkey plasma, *J. Chromatogr. B Anal. Technol. Biomed. Life Sci.* 779 (2002) 241–248, [https://doi.org/10.1016/S1570-0232\(02\)00379-3](https://doi.org/10.1016/S1570-0232(02)00379-3).
- [142] K.K. Murray, R.K. Boyd, M.N. Eberlin, G.J. Langley, L. Li, Y. Naito, Standard definitions of terms related to mass spectrometry, *Chem. Int. – Newsmag. IUPAC.* 26 (2014) 1515–1609, <https://doi.org/10.1515/ci.2004.26.3.23a>.
- [143] A. Krueve, R. Rebane, K. Kipper, M.L. Oldekop, H. Evard, K. Herodes, P. Ravi, I. Leito, Tutorial review on validation of liquid chromatography-mass spectrometry methods: Part I, *Anal. Chim. Acta* 870 (2015) 29–44, <https://doi.org/10.1016/j.aca.2015.02.017>.
- [144] T. Porta, A. Lesur, E. Varesio, G. Hopfgartner, Quantification in MALDI-MS imaging: what can we learn from MALDI-selected reaction monitoring and what can we expect for imaging? *Anal. Bioanal. Chem.* 407 (2015) 2177–2187, <https://doi.org/10.1007/s00216-014-8315-5>.
- [145] S.R. Shanta, T.Y. Kim, J.H. Hong, J.H. Lee, C.Y. Shin, K.H. Kim, Y.H. Kim, S. K. Kim, K.P. Kim, A new combination MALDI matrix for small molecule analysis: application to imaging mass spectrometry for drugs and metabolites, *Analyst* 137 (2012) 5757–5762, <https://doi.org/10.1039/c2an35782h>.
- [146] G. Robichaud, J.A. Barry, D.C. Muddiman, IR-MALDESI mass spectrometry imaging of biological tissue sections using ice as a matrix, *J. Am. Soc. Mass Spectrom.* 25 (2014) 319–328, <https://doi.org/10.1007/s13361-013-0787-6>.
- [147] P.R.N. Bhuket, P. Teerawonganan, E. Yoosakul, W. Supasena, C. Watananikorn, B. Chuasuwan, P. Narakorn, I. Techatanawat, P. Pitisuttithum, Validation of liquid chromatography-tandem mass spectrometric method for simultaneous determination of lopinavir and ritonavir in human plasma, and its application in a bioequivalence study in Thai volunteers, *J. Heal. Res.* 29 (2015) 417–424, <https://doi.org/10.14456/jhr.2015.34>.
- [148] N. Ferreiros, S. Labocha, J. El-Duweik, C. Schleckler, J. Lotsch, G. Geisslinger, Quantitation of ribavirin in human plasma and red blood cells using LC – MS/MS, *J. Separ. Sci.* (2014) 476–483, <https://doi.org/10.1002/jssc.201301173>.
- [149] G. Ventura, C.D. Calvano, I. Losito, G. Bianco, R. Pascale, F. Palmisano, T.R. I. Cataldi, Effect of pH and mobile phase additives on the chromatographic behaviour of an amide-embedded stationary phase: cyanocobalamin and its diaminechloro-platinum(II) conjugate as a case study, *J. Separ. Sci.* 42 (2019) 1155–1162, <https://doi.org/10.1002/jssc.201801060>.
- [150] P.D. Rainville, N.W. Smith, D. Cowan, R.S. Plumb, Comprehensive investigation of the influence of acidic, basic, and organic mobile phase compositions on bioanalytical assay sensitivity in positive ESI mode LC/MS/MS, *J. Pharmaceut. Biomed. Anal.* 59 (2012) 138–150, <https://doi.org/10.1016/j.jpba.2011.10.021>.
- [151] R. Dams, M.A. Huestis, W.E. Lambert, C.M. Murphy, Matrix effect in bio-analysis of illicit drugs with LC-MS/MS: influence of ionization type, sample preparation, and biofluid, *J. Am. Soc. Mass Spectrom.* 14 (2003) 1290–1294, [https://doi.org/10.1016/S1044-0305\(03\)00574-9](https://doi.org/10.1016/S1044-0305(03)00574-9).
- [152] H. Mei, Y. Hsieh, C. Nardo, X. Xu, S. Wang, K. Ng, W.A. Korfmacher, Investigation of matrix effects in bioanalytical high-performance liquid chromatography/tandem mass spectrometric assays: application to drug discovery, *Rapid Commun. Mass Spectrom.* 17 (2003) 97–103, <https://doi.org/10.1002/rcm.876>.
- [153] S. Fekete, J. Schappler, J.L. Veuthey, D. Guillarme, Current and future trends in UHPLC, *TrAC Trends Anal. Chem. (Reference Ed.)* 63 (2014) 2–13, <https://doi.org/10.1016/j.trac.2014.08.007>.
- [154] F. Farouk, D. Wahba, S. Mogawer, S. Elkholy, A. Elmeligui, R. Abdelghani, S. Ibahim, Development and validation of a new LC-MS/MS analytical method for direct-acting antivirals and its application in end-stage renal disease patients, *Eur. J. Drug Metab. Pharmacokinet.* 45 (2020) 89–99, <https://doi.org/10.1007/s13318-019-00584-6>.
- [155] P. Hummert, T.L. Parsons, L.M. Ensign, T. Hoang, M.A. Marzinke, Validation and implementation of liquid chromatographic-mass spectrometric (LC-MS) methods for the quantification of tenofovir prodrugs, *J. Pharmaceut. Biomed. Anal.* 152 (2018) 248–256, <https://doi.org/10.1016/j.jpba.2018.02.011>.
- [156] Y. Wu, J. Yang, C. Duan, L. Chu, S. Chen, S. Qiao, X. Li, H. Deng, Simultaneous determination of antiretroviral drugs in human hair with liquid chromatography-electrospray ionization-tandem mass spectrometry, *J. Chromatogr. B Anal. Technol. Biomed. Life Sci.* 1083 (2018) 209–221, <https://doi.org/10.1016/j.jchromb.2018.03.021>.
- [157] P.K. Prathipati, S. Mandal, C.J. Destache, Simultaneous quantification of tenofovir, emtricitabine, rilpivirine, elvitegravir and dolutegravir in mouse biological matrices by LC-MS/MS and its application to a pharmacokinetic study, *J. Pharmaceut. Biomed. Anal.* 129 (2016) 473–481, <https://doi.org/10.1016/j.jpba.2016.07.040>.
- [158] Q. Xiao, D. Wang, W. Yang, L. Chen, Y. Ding, J. Yang, Simultaneous determination of pradefovir, PMEA and tenofovir in HBV patient serum using liquid chromatography-tandem mass spectrometry and application to phase 2 clinical trial, *J. Chromatogr. B Anal. Technol. Biomed. Life Sci.* 1022 (2016) 133–140, <https://doi.org/10.1016/j.jchromb.2016.04.019>.
- [159] A.V.B. Reddy, J. Jaafar, A. Bin Aris, Z.A. Majid, K. Umar, J. Talib, G. Madhavi, Development and validation of a rapid ultra high performance liquid chromatography with tandem mass spectrometry method for the simultaneous determination of darunavir, ritonavir, and tenofovir in human plasma: application to human pharmacokinetics, *J. Separ. Sci.* 38 (2015) 2580–2587, <https://doi.org/10.1002/jssc.201500250>.
- [160] X. Shi, D. Zhu, J. Lou, B. Zhu, A. rong Hu, D. Gan, Evaluation of a rapid method for the simultaneous quantification of ribavirin, sofosbuvir and its metabolite in rat plasma by UPLC-MS/MS, *J. Chromatogr. B Anal. Technol. Biomed. Life Sci.* 1002 (2015) 353–357, <https://doi.org/10.1016/j.jchromb.2015.08.038>.
- [161] T. Mishra, P.S. Shrivastav, Validation of simultaneous quantitative method of HIV protease inhibitors atazanavir, darunavir and ritonavir in human plasma by UPLC-MS/MS, *Sci. World J.* 2014 (2014) 1–12, <https://doi.org/10.1155/2014/482693>.
- [162] M.K. Matta, L. Burugula, N.R. Pilli, J.K. Inamadugu, S.R. Jvln, A novel LC-MS/MS method for simultaneous quantification of tenofovir and lamivudine in human plasma and its application to a pharmacokinetic study, *Biomed. Chromatogr.* 26 (2012) 1202–1209, <https://doi.org/10.1002/bmc.2679>.
- [163] D. Danso, L.J. Langman, C.L.H. Snozek, LC-MS/MS quantitation of ribavirin in serum and identification of endogenous isobaric interferences, *Clin. Chim. Acta* 412 (2011) 2332–2335, <https://doi.org/10.1016/j.cca.2011.07.016>.
- [164] J.G. Uo, F.M. Eng, L.I. Li, B.Z. Hong, Y.Z. Hao, Development and validation of an LC/MS/MS method for the determination of tenofovir in monkey, *Plasma* 34 (2011) 877–882.
- [165] R. Vats, A.N. Murthy, P.R. Ravi, Simple, rapid and validated LC determination of lopinavir in rat plasma and its application in pharmacokinetic studies, *Sci. Pharm.* 79 (2011) 849–863, <https://doi.org/10.3797/scipharm.1107-24>.
- [166] S.O. Choi, N. Rezk, J.S. Kim, A.D.M. Kashuba, Development of an LC-MS method for measuring TNF in human vaginal tissue, *J. Chromatogr. Sci.* 48 (2010) 219–223, <https://doi.org/10.1093/chromsci/48.3.219>.
- [167] R. Damaramadugu, J. Inamadugu, R. Kanneti, S. Polagani, V. Ponneri, Simultaneous determination of ritonavir and lopinavir in human plasma after protein precipitation and LC-MS-MS, *Chromatographia* 71 (2010) 815–824, <https://doi.org/10.1365/s10337-010-1550-9>.
- [168] R.S. Jansen, H. Rosing, W. Kromdijk, R. ter Heine, J.H. Schellens, J.H. Beijnen, Simultaneous quantification of emtricitabine and tenofovir nucleotides in peripheral blood mononuclear cells using weak anion-exchange liquid chromatography coupled with tandem mass spectrometry, *J. Chromatogr. B Anal. Technol. Biomed. Life Sci.* 878 (2010) 621–627, <https://doi.org/10.1016/j.jchromb.2010.01.002>.

RESEARCH ARTICLE

Untargeted analysis of pure snail slime and snail slime-induced Au nanoparticles metabolome with MALDI FT-ICR MS

Alberto Onzo¹ | Raffaella Pascale²  | Maria Assunta Acquavia^{1,3}  |
Pinalysa Cosma⁴  | Jennifer Gubitosa⁴ | Carmine Gaeta⁵  | Patrizia Iannece⁵ |
Yury Tsybin⁶ | Vito Rizzi⁴  | Antonio Guerrieri¹  | Rosanna Ciriello¹ |
Giuliana Bianco¹ 

¹Dipartimento di Scienze, Università degli Studi della Basilicata, Potenza, Italy

²Gnosis by Lesaffre, Matera, Italy

³ALMAGISI, Bolzano, Italy

⁴Dipartimento di Chimica, Università degli Studi "Aldo Moro" di Bari, Bari, Italy

⁵Dipartimento di Chimica e Biologia, Università degli Studi di Salerno, Fisciano, Italy

⁶Spectroswiss Sarl, Lausanne, Switzerland

Correspondence

Raffaella Pascale, Gnosis by Lesaffre, Pisticci, 75015 Matera, Italy.

Email: raff.pascale@gmail.com

[This article was published online on 25 March 2021. Subsequently, the eighth author's name was corrected, and the revision was published on 5 May 2021.]

Abstract

Chronic wounds result from the failure of the normal wound healing process. Any delay during the tissue repair process could be defined as chronic wound healing, potentially having a highly detrimental impact on human health. To face this problem, in the last years, the use of different technologies alternative to therapeutic agents is gaining more attention. The *Helix aspersa* snail slime-based products are increasingly being used for skin injury, thanks to their ability to make tissue repair processes faster. To date, a comprehensive overview of pure snail slime metabolome is not available. Besides, Au nanoparticles (AuNPs) technology is spreading rapidly in the medical environment, and the search for AuNPs "green" synthetic routes that involve natural products as precursor agents is demanded, alongside with a deep comprehension of the kind of species that actively take part in synthesis and product stabilization. The aim of this work is to characterize the metabolic profile of a pure snail slime sample, by an untargeted high-resolution mass spectrometry-based analysis. In addition, insights on AuNPs synthesis and stabilization by the main components of pure snail slime used to induce the synthesis were obtained. The untargeted analysis provided a large list of important classes of metabolites, that is, fatty acid derivatives, amino acids and peptides, carbohydrates and polyphenolic compounds that could be appreciated in both samples of slime, with and without AuNPs. Moreover, a direct comparison of the obtained results suggests that mostly nitrogen and sulfur-bearing metabolites take part in the synthesis and stabilization of AuNPs.

KEYWORDS

Au nanoparticles, MALDI FT-ICR MS, metabolomics, snail slime, untargeted high-resolution mass spectrometry

1 | INTRODUCTION

Snails are members of the *Mollusca phylum*, like slugs, oysters, squids and cuttlefish. They live widely spread across freshwater, seas and land, the latter of which preferring moist areas. In particular, *Helix aspersa* species, most commonly known as garden snails, are prevalent

in the European countries, especially in the north Mediterranean region.^{1–5} From ancient times, garden snails have been used frequently in food and medicine. Nowadays, garden snails are employed in a wide range of applications, principally in food and cosmetics, for its wound healing and antiaging properties.^{6–8} This is due to snail tissue-rich metabolic content. In detail, many targeted

analyses underlined the presence of many beneficial natural compounds in snail mucus, such as glycoproteins and vitamins, which can stimulate the formation of collagen, elastin, and dermal components that repair the signs of photoaging and minimize the damage generated by free radicals.^{9,10} Metabolites contained in snail secretion make it useful for chronic disease treatment too. Indeed, many studies evidenced its great inhibition activity against several bacteria, such as *Bacillus subtilis* and *Staphylococcus aureus*, and its ability to induce necrosis in breast cancer cells.^{11–13} However, to the best of our knowledge, a complete overview of the metabolic profile of snail mucus is missing, thus preventing an evaluation of the diversity of its components. Several analytical techniques have been applied to shed light on snail mucus composition, including high-performance liquid chromatography and UV detection (HPLC-UV),^{14–17} nuclear magnetic resonance (NMR),^{18,19} and liquid chromatography coupled to mass spectrometry (LC-MS), which is the most frequently used approach in targeted small molecules determination.^{20–26} However, these approaches have not provided as high levels of specificity and sensitivity, as high-resolution mass spectrometry (HRMS). Fourier transform ion cyclotron resonance mass spectrometry (FT-ICR MS) is a powerful HRMS technique, that is able to reach mass resolution performance higher than 1,000,000 and mass accuracy better than 1 ppm. The high mass resolution is beneficial in molecular formula calculations and compound identification. FT-ICR MS measurements lead to the identification of many metabolites, providing a comprehensive metabolome overview.^{27–29} This peculiar information leads directly to the knowledge of the classes of metabolites present in analyzed matrices, helping to understand the macroscopic health-promoting activity of the metabolites and to make hypotheses on their possible uses.

It is in light of the presence of a wide diversity of biocomponents that the use of natural products in the optimization of new therapeutic technologies is increasing during the last years, especially for the synthesis and stabilization of metallic nanoparticles. More specifically, many works focused on beneficial properties of gold nanoparticles (AuNPs) in many types of applications, such as tumor cell necrosis,³⁰ cancer cell imaging,³¹ analysis of trace amounts of substances in various biological samples and, especially, wound healing.³² Several features make AuNPs suitable for these applications, such as a marked selectivity for specific compounds and other important physical and chemical properties, that is, an excellent UV absorption profile and a high melting point.³³ AuNPs have been proved to be an excellent substrate for the detection of several types of biomolecules, as neutral steroids (testosterone, progesterone and cortisol), carbohydrates (ribose, glucose and maltose), indoleamines (5-hydroxyindole acetic acid and tryptophan), endogenous (palmitic acid, oleic acid and stearic acid), and exogenous (verampil) chemicals.^{33,34} Modified AuNPs were also used as a probe for the detection of the activity of thrombin.³⁵ In this case, the intensity of the produced Au cluster ions was correlated to the thrombin concentration. As a result, the probe could specifically detect thrombin with a limit of detection of 2.5 pM in human plasma samples. This kind of application was found to be suitable for the detection of different proteins. However, even if there is a wide range

of advantages in using this technology, there are huge problems related to AuNPs, the most important of which are related to their synthesis, such as the use of harsh chemical conditions of work, organic solvents, and the production of toxic by-products.³⁶ For this purpose, during the last years, many studies have been focused on finding greener alternative approaches to obtain AuNPs. The employment of pure snail slime (SS) for the synthesis of AuNPs via HAuCl_4 reduction could be a possible solution. Indeed, a recent study has been carried out to demonstrate the suitability of the SS as reducing agent, a fact supported by the many shreds of evidence related to reductant activity shown by several biocomponents, like peptides and glycoproteins, abundantly present in SS.³⁷ So SS is useful to improve the AuNPs stabilization, one of the main issues related to AuNPs application^{38–41} and size characterization,⁴² thus leading to better biological and wound healing activities of the final product.⁴³

Thus, in this work, matrix-assisted laser desorption ionization (MALDI) FT-ICR MS analysis was carried out on a sample of pure *H. aspersa* garden SS to obtain insights on its metabolites. This analysis led to the identification of SS important metabolite classes and supported the idea of the sample as a rich source of biocomponents, seeing the huge diversity of metabolites that could be appreciated. Moreover, MALDI FT-ICR MS analysis was performed on a pure SS sample in which synthesized AuNPs were stabilized. The latter provided information on product formation and on possible active species responsible for their synthesis and stabilization.

2 | MATERIALS AND METHODS

2.1 | Chemicals

The SS was received from the Società Agricola Dap, Francesco Paolo Perrotta & C. S.a.s (via Diego Rapolla, 85029, Venosa, Potenza, Basilicata, Italy). 2,5-Dihydroxybenzoic acid (DHBA, 98%) and tetrachloroauric acid (HAuCl_4) were purchased from Sigma Aldrich (Milan, Italy). Ultrapure water was produced using a Milli-Q RG system from Millipore (Bedford, MA, USA).

2.2 | Sample preparation

SS was produced by gas stimulation with ozone and, then, was collected. AuNPs–SS sample was obtained by reduction of HAuCl_4 , carried out by adding 1.5 ml of a 1-mM stock solution of this reactant to 2 ml of water and 500 μl of the received SS and by stirring the mixture at room temperature. The SS excess and unreacted HAuCl_4 were removed by washing in ultrapure water and centrifuging at 7,000g, for 10 min at room temperature (Kontron A8.24 rotor centrifuge). For the HRMS analyses, SS sample was mixed with DHBA in a 1:1 ratio and then employed without any further pretreatment. Similar sample preparation was done for AuNPs–SS sample analysis. SS and AuNPs–SS samples were stored at 4°C prior to the analysis.

2.3 | HRMS apparatus and data analysis

High-resolution mass spectra were acquired on a solarix XR 7 T FT ICR-MS equipped with a MALDI ion source (Bruker Daltonik GmbH, Bremen, Germany). Mass spectra were acquired in positive ion mode with a time-domain signal (transient) size of 16 mega-words, an accumulation time of 0.1 s and a mass range of 100–2,000 m/z . The positive ion mode was chosen because more compounds are expected to ionize in this mode and it ensured a better signal-to-noise ratio compared with a negative one. The number of scans to average was set to 50. For the analysis, a laser power of 32% and a number of laser shots of 28 were assumed. The size and intensities of peaks in MALDI experiments depend on the matrix chosen; DHBA was used because it is an optimal matrix for detecting lower-mass ions, with a detection of up to 10 kDa.⁴⁴ Then, the samples (pure SS and AuNPs-SS), were mixed with DHBA in a 1:1 ratio and were analyzed. The accuracy reached values of less than 0.1 ppm. FT-ICR mass spectra with m/z from 100 to 2,000 were smoothed by using the Savitzky–Golay algorithm (by setting a mass range of 0.001 Da and performing 30 cycles) and exported to peak lists by considering a relative intensity threshold of 0.1% for noise filtering.^{45,46} From these lists, possible elemental formulas were calculated for each peak. To obtain unequivocal formulas, several constraints were applied, such as atoms number limitations, that is, $C \leq 100$, $H \leq 200$, $O \leq 80$, $N \leq 10$, $S \leq 1$, $P \leq 1$, $Na \leq 1$, and $K \leq 1$,⁴⁶ restrictions on atoms to carbon number ratios, that is, $0.2 \leq H/C \leq 3.1$, $O/C \leq 2$, $N/C \leq 1.3$, $S/C \leq 0.8$ and $P/C \leq 0.3$, $RDBE > 0$, nitrogen rule, and isotopic pattern filtering. Moreover, a Kendrick mass defect (KMD) analysis was performed to identify homologous series, thus helping formulae assignment.^{47,48} HRMS data were processed by using Data Analysis (v4.2, Bruker Daltonik GmbH, Bremen, Germany) and the R software (www.r-project.org, v3.6.3).

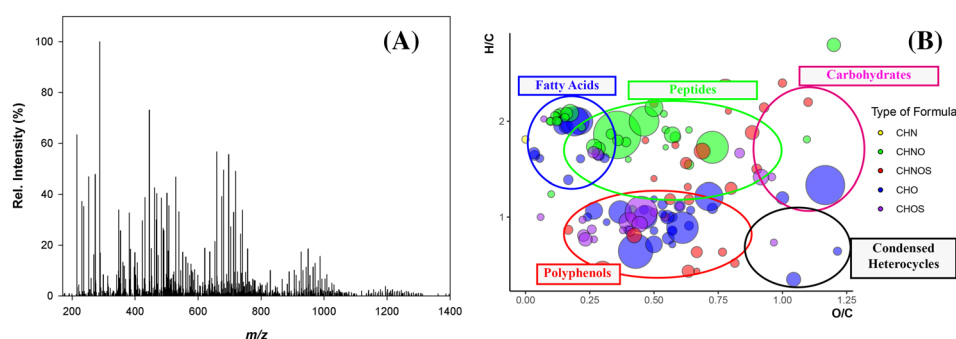
3 | RESULTS AND DISCUSSION

3.1 | MALDI (+) FT-ICR MS analysis

HRMS is often the technique of choice to generate high-throughput metabolomics data due to high sensitivity, relatively short analysis time, wide dynamic range, high reproducibility, and most importantly,

its ability to analyze samples with extreme molecular complexity.^{27,46} Fourier transform ion cyclotron resonance mass spectrometer (FT-ICR-MS) is the most advanced mass analyzer in terms of high accuracy and resolving power with sub-parts-per-million mass accuracy. In the present work, MALDI (+) FT-ICR MS has been used in the detection of small molecular metabolites to obtain the *fingerprint* of SS samples. MALDI (+) FT-ICR MS analysis resulted in a huge amount of data to be analyzed, thus revealing the high complexity of the SS sample. The mass spectrum showed an enormous number of signals (Figure 1A), hampering the easy extrapolation of desired information from the mass spectrum alone. Indeed, there is a need of a rapid, efficient and fully automated method for converting m/z ratios in the molecular formula. Accurate mass assignments were performed using KMD analysis, which is among the most widely used ones for the complex mass spectra,^{47,48} allowing the identification of homologous series and obtaining molecular formulae at high m/z ratios. Furthermore, by choosing $H_{-1}Na$ and $H_{-1}K$ as building blocks, it was possible through the KMD analysis to identify, respectively, Na and K adducts of simpler molecules, which turned out to be related to most of the detected MS signals. These signals were not considered for further molecular formula assignment, in order to focus the attention on the different compounds that are part of the metabolic profile of the sample. Moreover, redundancies were classified, and the assignment was performed based on the chemistry of SS sample.²⁹ A total of 122 formulae were determined, thanks to high accuracy too and by considering several constraints (see Section 2.3). To best interpret MS data, a well-known visualization method was assumed, that is, Van Krevelen diagram, in which elemental compositions are plotted depending on their O/C and H/C ratios.^{28,46,49} Thanks to this plot, it was possible to identify which kind of metabolite species are present in SS samples, simply by looking at the positions of the spots (Figure 1B). In this way, the presence of fatty acids, amino acids and peptides, carbohydrates, polyphenols and condensed heterocycles was assessed by means of a simple and fast direct HRMS analysis. It is worth noting that observed results agree with the literature. In detail, *H. aspersa* mucus is a well-known source of different amino acids, like proline and glycine found in different snail species, and sulfur-bearing peptides.⁵⁰ Among these, glutathione (GSH) derivatives deserve a special attention, because their sulfhydryl group (–SH) belonging to cysteine units is involved in reduction and conjugation reactions for the removal of peroxides and many xenobiotic compounds, making

FIGURE 1 MALDI (+) FT-ICR mass spectrum (A) and Van Krevelen diagram (B) obtained by the analysis of a sample of pure snail slime (SS). In plot B, types of formulae are distinguished by colors, that is, blue for CHO, green for CHON, red for CHONS, purple for CHOS, and yellow for CHN type



them the major endogenous intracellular antioxidants.⁵¹ The presence of organic acids, like acetic acid, citric acid, lactic acid and tartaric acid, is supported by the Van Krevelen plot too. Among these, lactic acid is widely used to inhibit the growth of important microbial pathogens, a biological activity probably caused by physiological and morphological changes in bacterial cells.⁵² Nevertheless, it is interesting to see how Van Krevelen plot supports the presence of a wide diversity of polyphenolic species in SS. These compounds were never found into this matrix, and they could contribute to antioxidant and wound-healing activity of SS.⁵³

On the other hand, the analysis of AuNPs-SS samples could shed some light on which kind of identified metabolites were necessary to induce their formation. As expected, the high-resolution mass spectrum of AuNPs-SS sample showed a lower content of MS signals in comparison with the pure SS one (Figure 2A). This reflects the selectivity of a restricted pool of metabolites for the AuNPs synthesis.^{32,54–57} Moreover, no more peaks were observed in the spectral range 1,000–2,000 m/z , suggesting the absence of compounds with a number of Au atoms higher than 4.⁵⁷ In this case, 205 unequivocal formulae were assigned: a higher number in comparison with the pure SS sample because of the increased number of identified long homologous series into the MS spectrum during the KMD analysis step. By using the Van Krevelen visualization strategy, it was possible to observe the presence of polar lipids, polyphenols, peptides and higher RDBE compounds, like condensed heterocycles and nucleotides (Figure 2B). Amino acids and peptides could coordinate with AuNPs through the formation of Au–N or

Au–O covalent bonds. The coordination can take place on different sites of the molecules: amidic nitrogen atoms and carboxylic groups could take part in the reaction, by donating a lone pair to Au (III) atoms.⁵⁸ Several side groups could work as ligands, and Au–S covalent bonds could be formed in the presence of cysteine units. For these reasons, amino acid derivatives are able to form gold complexes too, thus broadening the range of metabolites that can coordinate with AuNPs.⁵⁸ Moreover, free fatty acids could act as ligands too by coordinating through their carboxylic end. The presence of these species, as evidenced by the Van Krevelen plot, supports the fact that they could take an active part during the synthesis of AuNPs. However, the presence of species corresponding to high RDBE portions of the Van Krevelen plot suggests that other types of nitrogen and sulfur-bearing metabolites could be responsible for AuNPs synthesis and stabilization, compounds that seem to belong to the polyphenols and condensed heterocyclic class. By focusing on the Au atom content, it is possible to note that high levels of free organic compounds are observed (Figure 3), probably due to the dissociation of coordinated ones induced by MALDI HRMS conditions.⁵⁷ Higher values of the number of CHON and CHONS formulae are observed for organogold complexes (Figure 4), most probably due to the increasing number of available coordination sites, whereas the number of such formulae decreased exponentially for higher Au atom contents (Figure 5), thus reflecting the lower ionization efficiency related to higher organogold clusters and/or an higher tendency to dissociation, supported by the absence of peaks in the spectral range 1,000–2,000 m/z .

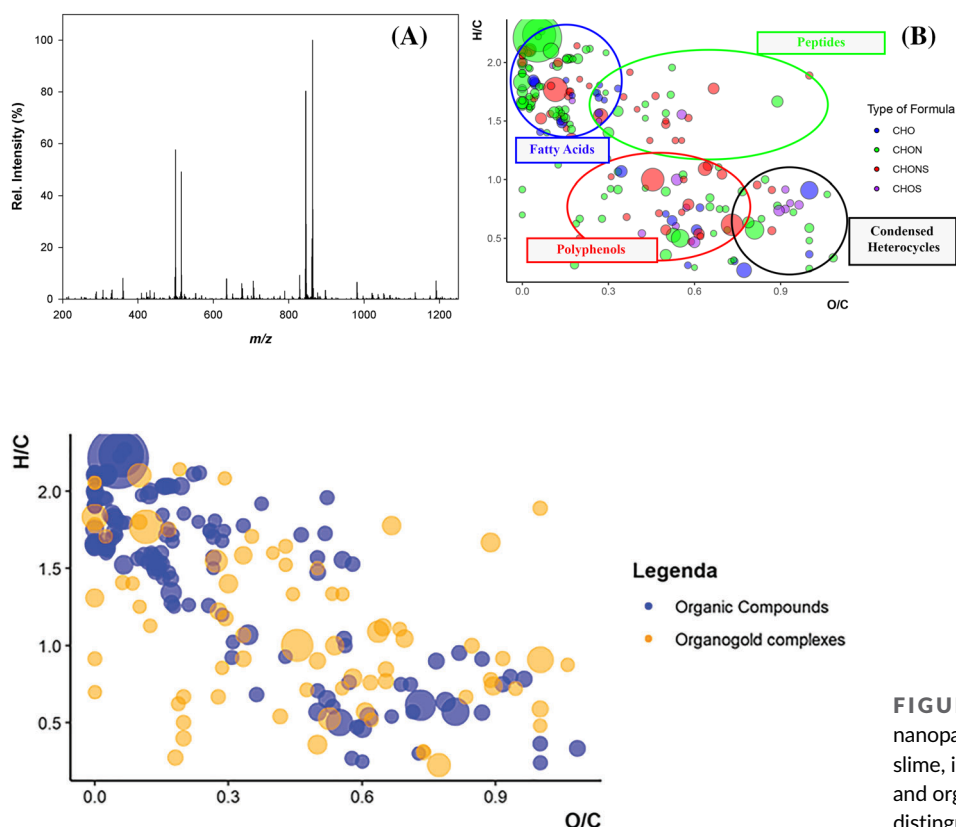


FIGURE 2 MALDI (+) FT-ICR mass spectrum (A) and Van Krevelen diagram (B) obtained by the analysis of a sample of Au nanoparticles (AuNPs) synthesized with snail slime. In plot B, types of formulae are distinguished by colors, that is, blue for CHO, green for CHON, red for CHONS, and yellow for CHOS type

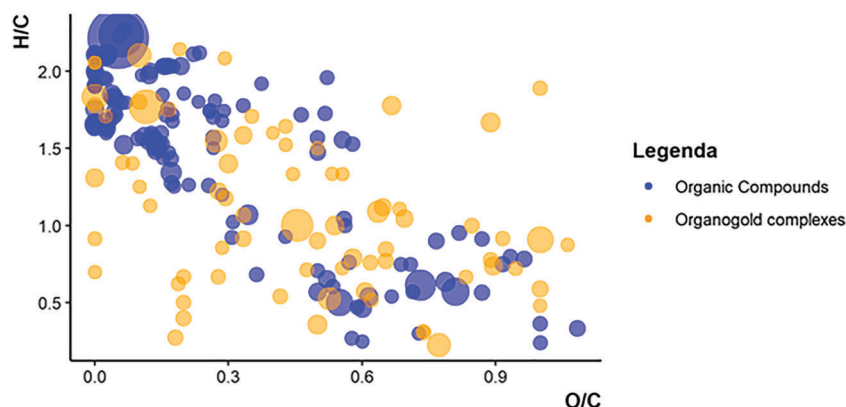
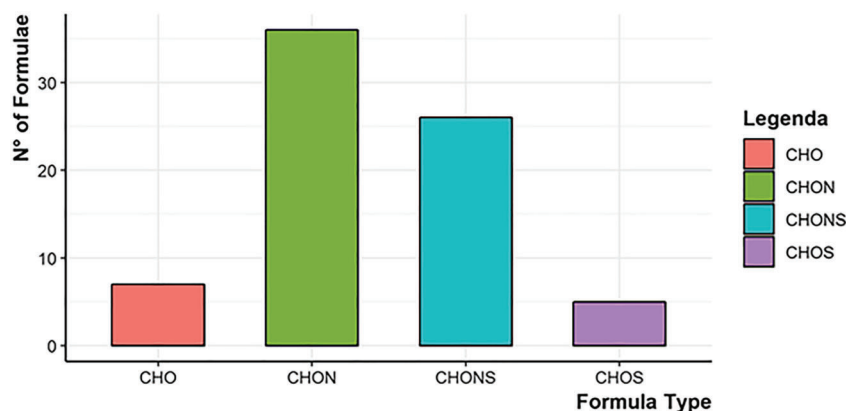
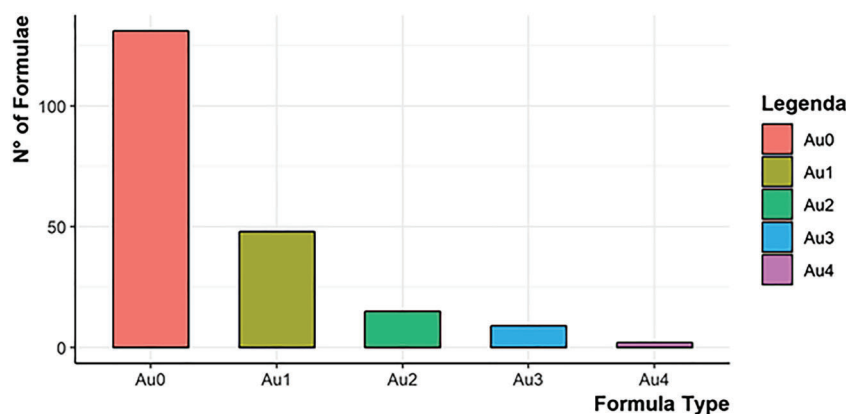


FIGURE 3 Van Krevelen diagram of Au nanoparticles (AuNPs) synthesized with snail slime, in which organic compounds (blue points) and organogold complexes (yellow points) are distinguished

FIGURE 4 Number of formulae per type for organogold complexes**FIGURE 5** Number of formulae per number of Au atoms

4 | CONCLUSIONS

For the first time, an untargeted HRMS analysis, together with dedicated visualization MS data tools, was performed on SS and AuNPs-SS samples. In detail, Van Krevelen plot obtained for pure SS sample, which can be considered as its *metabolomic fingerprint*, evidenced a marked diversity of types of metabolites and revealed which kind of classes they belong to. SS samples turned out to be a rich source of different compounds, most of which could be responsible for well-known related health-promoting properties. Moreover, direct HRMS analysis of AuNPs-SS allowed us to monitor AuNPs synthesis, and related Van Krevelen plots gave us hints on which metabolites could take part in their synthesis and stabilization. Thus, the new proposed HRMS approach resulted useful for evaluating metabolite profiling of SS and for providing insights on AuNPs synthesis and stabilization by SS.

ORCID

Raffaella Pascale <https://orcid.org/0000-0002-7650-653X>

Maria Assunta Acquavia <https://orcid.org/0000-0001-6103-8860>

Pinalysa Cosma <https://orcid.org/0000-0003-3018-4069>

Carmine Gaeta <https://orcid.org/0000-0002-2160-8977>

Vito Rizzi <https://orcid.org/0000-0002-7092-9689>

Antonio Guerrieri <https://orcid.org/0000-0002-1662-5203>

Giuliana Bianco <https://orcid.org/0000-0001-9427-2274>

REFERENCES

- De Vaufleury A, Landsnail for ecotoxicological assessment of chemicals and soil contamination—ecotoxicological assessment of chemicals and contaminated soils using the terrestrial snail, *Helix aspersa*, at various stage of its life cycle: a review, in: *Environmental Indicators*, Springer/Netherlands, 2015: pp. 365-391. https://doi.org/10.1007/978-94-017-9499-2_23
- Dunstan DJ, Hodgson DJ. Snails home. *Phys Scr*. 2014;89(6):1-10. <https://doi.org/10.1088/0031-8949/89/06/068002>
- Walker RJ, Chen ML, Pedder S, Holden-Dye L, White AR, Sharma R. Neuropharmacological studies on identified central neurones of the snail, *Helix aspersa*. *Zh Vyssh Nerv Deiat Im I P Pavlova*. 1993;43(1): 109-120.
- Attia J. Behavioural rhythms of land snails in the field. *Biol Rhythm Res*. 2004;35(1-2):35-41. <https://doi.org/10.1080/09291010412331313223>
- Bonnet J-C, Aupinel P, Vrillon J-L, Quae. *L'escargot Helix aspersa: biologie-élevage*; 1, 1st ed., Quae, Versailles, 1990.
- Kim BJ, No YA, Lee Y, et al. Use of cream containing mucus secreted by snails has an anti-aging effect on skin. *Korean J Dermatology*. 2015; 53:430-436. <https://doi.org/10.0000/kjd.2015.53.6.430>
- Li X, Li YC, Chen M, Shi Q, Sun R, Wang X. Chitosan/rectorite nanocomposite with injectable functionality for skin hemostasis. *J Mater Chem B*. 2018;6(41):6544-6549. <https://doi.org/10.1039/c8tb01085d>

8. Michailides TJ, Morgan DP. Effect of snail (*Helix aspersa*) damage on *Botrytis* gray mold caused by *Botrytis cinerea* in kiwifruit. *Plant Dis*. 1996;80(10):1141-1146. <https://doi.org/10.1094/pd-80-1141>
9. Sallam AAA, El-Massry SA, Nasr IN. Chemical analysis of mucus from certain land snails under Egyptian conditions. *Arch Phytopathol Plant Prot*. 2009;42(9):874-881. <https://doi.org/10.1080/03235400701494448>
10. Brieva A, Philips N, Tejedor R, et al. Molecular basis for the regenerative properties of a secretion of the mollusk *Cryptomphalus aspersa*. *Skin Pharmacol Physiol*. 2008;21(1):15-22. <https://doi.org/10.1159/000109084>
11. Iguchi SMM, Aikawa T, Matsumoto JJ. Antibacterial activity of snail mucus mucin. *Comp Biochem Physiol -- Part A Physiol*. 1982;72(3):571-574. <https://doi.org/10.1016/0300-9629>
12. Cilia G, Fratini F. Antimicrobial properties of terrestrial snail and slug mucus. *J Complement Integr Med*. 2018;15(3):1-10. <https://doi.org/10.1515/jcim-2017-0168>
13. El Ouar I, Braicu C, Naimi D, Irimie A, Berindan-Neagoe I. Effect of *Helix aspersa* extract on TNF α , NF- κ B and some tumor suppressor genes in breast cancer cell line Hs578T. *Pharmacogn Mag*. 2017;13(50):281-285. <https://doi.org/10.4103/0973-1296.204618>
14. Velkova L, Nissimova A, Dolashki A, Daskalova E, Topalova PDY. Glycine-rich peptides from *Cornu aspersum* snail with antibacterial activity. *Bulg Chem Commun*. 2018;50:169-175.
15. El Mubarak MAS, Lamari FN, Kontoyannis C. Simultaneous determination of allantoin and glycolic acid in snail mucus and cosmetic creams with high performance liquid chromatography and ultraviolet detection. *J Chromatogr A*. 2013;1322:49-53. <https://doi.org/10.1016/j.chroma.2013.10.086>
16. Mckenzie JD, Counce M, Hetherington MS, Winlow W. Serotonergic innervation of the foot of the pond snail *Lymnaea stagnalis* (L.). *J Neurocytol*. 1998;27(6):459-470. <https://doi.org/10.1023/A:1006944829563>
17. Trapella C, Rizzo R, Gallo S, et al. HelixComplex snail mucus exhibits pro-survival, proliferative and pro-migration effects on mammalian fibroblasts. *Sci Rep*. 2018;8(1):1-10. <https://doi.org/10.1038/s41598-018-35816-3>
18. Kobayashi A, Yamamoto I, Aoyama T. Tribology of a snail (terrestrial gastropod). *Tribol Ser*. 2003;41:429-436. <https://doi.org/10.1016/s0167-8922>
19. Chichibu S, Chiba A. Changes of 31P metabolism during mucus secretion in the slug (*Inclilaria bilineata*). *Comp Biochem Physiol Part C, Comp*. 1993;105:179-183. <https://doi.org/10.1016/0742-8413>
20. E-Kobon T, Thongaram P, Roytrakul S, Meesuk L, Chumnanpuen P. Prediction of anticancer peptides against MCF-7 breast cancer cells from the peptidomes of *Achatina fulica* mucus fractions. *Comput Struct Biotechnol J*. 2016;14:49-57. <https://doi.org/10.1016/j.csbj.2015.11.005>
21. Stewart MJ, Wang T, Harding BI, et al. Characterisation of reproduction-associated genes and peptides in the pest land snail, *Theba pisana*. *PLoS One*. 2016;11:1-16. <https://doi.org/10.1371/journal.pone.0162355>
22. Pascale R, Acquavia MA, Cataldi TRI, et al. Profiling of quercetin glycosides and acyl glycosides in sun-dried peperoni di Senise peppers (*Capsicum annum* L.) by a combination of LC-ESI (-) -MS/MS and polarity prediction in reversed-phase separations. *Anal Bioanal Chem*. 2020;412(12):3005-3015. <https://doi.org/10.1007/s00216-020-02547-2>
23. Pascale R, Bianco G, Coviello D, et al. Validation of a liquid chromatography coupled with tandem mass spectrometry method for the determination of drugs in wastewater using a three-phase solvent system. *J Sep Sci*. 2020;43(5):886-895. <https://doi.org/10.1002/jssc.201900509>
24. Caivano M, Pascale R, Mazzone G, Buchicchio A, Masi S, Bianco G, Caniani D, N₂O and CO₂ Emissions from secondary settlers in WWTPs: experimental results on full and pilot scale plants, in: Mannina G (Ed.), *Frontiers in Wastewater Treatment and Modelling*, Springer, Italy, 2017: pp. 412-418. https://doi.org/10.1007/978-3-319-58421-8_65
25. Caivano M, Pascale R, Mazzone G, Masi S, Panariello S, Caniani D, Disinfection unit of water resource recovery facilities: critical issue for N₂O Emission, in: Mannina G (Ed.), *Frontiers in Wastewater Treatment and Modelling*, Springer, Italy, 2017: pp. 444-449. https://doi.org/10.1007/978-3-319-58421-8_70
26. Onzo A, Acquavia MA, Cataldi TRI, et al. Coceth sulfate characterization by electrospray ionization tandem mass spectrometry. *Rapid Commun Mass Spectrom*. 2020;34(20):1-10. <https://doi.org/10.1002/rcm.8884>
27. Ghasse M, Mistrik R, Shulaev V. Applications of fourier transform ion cyclotron resonance (FT-ICR) and orbitrap based high resolution mass spectrometry in metabolomics and lipidomics. *Int J Mol Sci*. 2016;17(816):1-22. <https://doi.org/10.3390/ijms17060816>
28. Santarsiero A, Onzo A, Pascale R, et al. *Pistacia lentiscus* hydrosol: untargeted metabolomic analysis and anti-inflammatory activity mediated by NF- κ B and the citrate pathway. *Oxid Med Cell Longev*. 2020;2020:1-14. <https://doi.org/10.1155/2020/4264815>
29. Herzsprung P, Hertkorn N, von Tümping W, Harir M, Friese K, Schmitt-Kopplin P. Understanding molecular formula assignment of Fourier transform ion cyclotron resonance mass spectrometry data of natural organic matter from a chemical point of view. *Anal Bioanal Chem*. 2014;406(30):7977-7987. <https://doi.org/10.1007/s00216-014-8249-y>
30. Yamada M, Foote M, Prow TW. Therapeutic gold, silver, and platinum nanoparticles. *Wiley Interdiscip Rev Nanomed Nanobiotechnol*. 2015;7(3):428-445. <https://doi.org/10.1002/wnan.1322>
31. Tang HW, Lu W, Che CM, Ng KM. Gold nanoparticles and imaging mass spectrometry: double imaging of latent fingerprints. *Anal Chem*. 2010;82(5):1589-1593. <https://doi.org/10.1021/ac9026077>
32. Chen SA, Chen HM, der Yao Y, Hung CF, Tu CS, Liang YJ. Topical treatment with anti-oxidants and Au nanoparticles promote healing of diabetic wound through receptor for advance glycation end-products. *Eur J Pharm Sci*. 2012;47(5):875-883. <https://doi.org/10.1016/j.ejps.2012.08.018>
33. Picca RA, Calvano CD, Cioffi N, Palmisano F. Mechanisms of nanophase-induced desorption in LDI-MS. A short review. *Nanomater (Basel, Switzerland)*. 2017;7(4):1-20. <https://doi.org/10.3390/nano7040075>
34. Wu HP, Yu CJ, Lin CY, Lin YH, Tseng WL. Gold nanoparticles as assisted matrices for the detection of biomolecules in a high-salt solution through laser desorption/ionization mass spectrometry. *J Am Soc Mass Spectrom*. 2009;20(5):875-882. <https://doi.org/10.1016/j.jasms.2009.01.002>
35. Chang CY, Chu HW, Unnikrishnan B, et al. Pulse laser-induced generation of cluster codes from metal nanoparticles for immunoassay applications. *APL Mater*. 2017;5(053403):1-7. <https://doi.org/10.1063/1.4976020>
36. Guo S, Wang E. Synthesis and electrochemical applications of gold nanoparticles. *Anal Chim Acta*. 2007;598(2):181-192. <https://doi.org/10.1016/j.aca.2007.07.054>
37. Gubitosa J, Rizzi V, Fini P, et al. Biomolecules from snail mucus (*Helix aspersa*) conjugate Gold nanoparticles, exhibiting potential wound healing and anti-inflammatory activity. *Soft Matter*. 2020;16:10876-10888. <https://doi.org/10.1039/D0SM01638A>
38. Huang J, Li Q, Sun D, et al. Biosynthesis of silver and gold nanoparticles by novel sundried *Cinnamomum camphora* leaf. *Nanotechnology*. 2007;18(10):1-11. <https://doi.org/10.1088/0957-4484/18/10/105104>
39. Kalishwaralal K, Deepak V, Ram Kumar Pandian S, et al. Biosynthesis of silver and gold nanoparticles using *Brevibacterium casei*. *Colloids Surf B Biointerfaces*. 2010;77(2):257-262. <https://doi.org/10.1016/j.colsurfb.2010.02.007>

40. Philip D. Biosynthesis of Au, Ag and Au-Ag nanoparticles using edible mushroom extract. *Spectrochim Acta - Part A Mol Biomol Spectrosc.* 2009;73(2):374-381. <https://doi.org/10.1016/j.saa.2009.02.037>
41. Sylvestre JP, Kabashin AV, Sacher E, Meunier M, Luong JHT. Stabilization and size control of gold nanoparticles during laser ablation in aqueous cyclodextrins. *J Am Chem Soc.* 2004;126(23):7176-7177. <https://doi.org/10.1021/ja048678s>
42. Ciriello R, Iallore PT, Laurita A, Guerrieri A. Improved separation and size characterization of gold nanoparticles through a novel capillary zone electrophoresis method using poly (sodium4-styrenesulfonate) as stabiliser and a stepwise field strength gradient. *Electrophoresis.* 2017;38(6):922-929. <https://doi.org/10.1002/elps.201600478>
43. MubarakAli D, Thajuddin N, Jeganathan K, Gunasekaran M. Plant extract mediated synthesis of silver and gold nanoparticles and its antibacterial activity against clinically isolated pathogens. *Colloids Surf B Biointerfaces.* 2011;85(2):360-365. <https://doi.org/10.1016/j.colsurfb.2011.03.009>
44. Lavollay M, Rostane H, Compain F, Carbonnelle E. Identification methods: identification of clinical microorganisms with MALDI-TOF-MS in a microbiology laboratory, in: *Encyclopedia of Food Microbiology Second Edition*, 2nd ed., Elsevier Ltd, Amsterdam, The Netherlands, 2014. <https://doi.org/10.1016/B978-0-12-384730-0.00419-5>
45. Herzsprung P, Hertkorn N, Von Tümppling W, Harir M, Friese K, Schmitt-Kopplin P. Molecular formula assignment for dissolved organic matter (DOM) using high-field FT-ICR-MS: chemical perspective and validation of sulphur-rich organic components (CHOS) in pit lake samples. *Anal Bioanal Chem.* 2016;408(10):2461-2469. <https://doi.org/10.1007/s00216-016-9341-2>
46. Pascale R, Bianco G, Cataldi TRI, et al. Mass spectrometry-based phytochemical screening for hypoglycemic activity of Fagioli di Sarconi beans (*Phaseolus vulgaris* L.). *Food Chem.* 2018;242:497-504. <https://doi.org/10.1016/j.foodchem.2017.09.091>
47. Hughey CA, Hendrickson CL, Rodgers RP, Marshall AG, Qian K. Kendrick mass defect spectrum: a compact visual analysis for ultrahigh-resolution broadband mass spectra. *Anal Chem.* 2001;73(19):4676-4681. <https://doi.org/10.1021/ac010560w>
48. Tziotis D, Hertkorn N, Schmitt-Kopplin P. Kendrick-analogous network visualisation of ion cyclotron resonance Fourier transform mass spectra: improved options for the assignment of elemental compositions and the classification of organic molecular complexity. *Eur J Mass Spectrom.* 2011;17(4):415-421. <https://doi.org/10.1255/ejms.1135>
49. Kuhnert N, Dairpoosh F, Yassin G, Golon A, Jaiswal R. What is under the hump? Mass spectrometry based analysis of complex mixtures in processed food—lessons from the characterisation of black tea thearubigins, coffee melanoidines and caramel. *Food Funct.* 2013;4(8):1130-1147. <https://doi.org/10.1039/c3fo30385c>
50. Vassilev NG, Simova SD, Dangalov M, et al. An ¹H NMR- and MS-based study of metabolites profiling of garden snail *Helix aspersa* mucus. *Metabolites.* 2020;10(9):1-15. <https://doi.org/10.3390/metabo10090360>
51. Meister A. Biosynthesis and functions of glutathione: an essential bio-factor. *J Nutr Sci Vitaminol (Tokyo).* 1992;1-6.
52. Wang C, Chang T, Yang H, Cui M. Antibacterial mechanism of lactic acid on physiological and morphological properties of *Salmonella enteritidis*, *Escherichia coli* and *Listeria monocytogenes*. *Food Control.* 2015;47:231-236. <https://doi.org/10.1016/j.foodcont.2014.06.034>
53. De Mello Andrade JM, Fasolo D. Polyphenol antioxidants from natural sources and contribution to health promotion, in: *Polyphenols in Human Health and Disease*, 2014: pp. 253-265. <https://doi.org/10.1016/B978-0-12-398456-2.00020-7>
54. Chen WY, Chang HY, Lu JK, et al. Self-assembly of antimicrobial peptides on gold nanodots: against multidrug-resistant bacteria and wound-healing application. *Adv Funct Mater.* 2015;25(46):7189-7199. <https://doi.org/10.1002/adfm.201503248>
55. Kojima C, Hirano Y, Yuba E, Harada A, Kono K. Preparation and characterization of complexes of liposomes with gold nanoparticles. *Colloids Surf B Biointerfaces.* 2008;66(2):246-252. <https://doi.org/10.1016/j.colsurfb.2008.06.022>
56. Leu JG, Chen SA, Chen HM, et al. The effects of gold nanoparticles in wound healing with antioxidant epigallocatechin gallate and α -lipoic acid. *Nanomed Nanotechnol Biol Med.* 2012;8(5):767-775. <https://doi.org/10.1016/j.nano.2011.08.013>
57. Glišić BĐ, Rychlewska U, Djuran MI. Reactions and structural characterization of gold (III) complexes with amino acids, peptides and proteins. *Dalton Trans.* 2012;41(23):6887-6901. <https://doi.org/10.1039/c2dt30169e>
58. Harkness KM, Fenn LS, Cliffler DE, McLean JA. Surface fragmentation of complexes from thiolate protected gold nanoparticles by ion mobility-mass spectrometry. *Anal Chem.* 2010;82(7):3061-3066. <https://doi.org/10.1021/ac100251d>

How to cite this article: Onzo A, Pascale R, Acquavia MA, et al. Untargeted analysis of pure snail slime and snail slime-induced Au nanoparticles metabolome with MALDI FT-ICR MS. *J Mass Spectrom.* 2021;56(5):e4722. <https://doi.org/10.1002/jms.4722>

Review

Natural Polymeric Materials: A Solution to Plastic Pollution from the Agro-Food Sector

Maria Assunta Acquavia ^{1,2}, Raffaella Pascale ³ , Giuseppe Martelli ¹, Marcella Bondoni ² and Giuliana Bianco ^{1,*} 

¹ Dipartimento di Scienze, Università degli Studi della Basilicata, Via dell'Ateneo Lucano, 10-85100 Potenza, Italy; maria.acquavia@unibas.it (M.A.A.); giuseppe.martelli@unibas.it (G.M.)

² ALMAGISI s.r.l Corso Italia, 27-39100 Bolzano, Italy; m.bondoni@almacabio.com

³ Gnosis by Lesaffre, Pisticci, 75015 Matera, Italy; raff.pascale@gmail.com

* Correspondence: giuliana.bianco@unibas.it; Tel.: +39-0971205451

Abstract: Conventional petroleum-derived plastics represent a serious problem for global pollution because, when discarded in the environment, are believed to remain for hundreds of years. In order to reduce dependence on fossil resources, bioplastic materials are being proposed as safer alternatives. Bioplastics are bio-based and/or biodegradable materials, typically derived from renewable sources. Food waste as feedstock represents one of the recent applications in the research field of bioplastics production. To date, several food wastes have been used as raw materials for the production of bioplastics, including mostly fruit and vegetable wastes. The conversion of fruit and vegetable wastes into biomaterials could occur through simple or more complex processes. In some cases, biopolymers extracted from raw biomass are directly manufactured; on the other hand, the extracted biopolymers could be reinforced or used as reinforcing agents and/or natural fillers in order to obtain biocomposites. The present review covers available results on the application of methods used in the last 10 years for the design of biomaterials obtained from formulations made up with both fruits and vegetables by-products. Particular attention will be addressed to the waste pre-treatment, to the bioplastic formulation and to its processing, as well as to the mechanical and physical properties of the obtained materials.

Keywords: plastic pollution; bioplastics; biocomposites; fruits and vegetables waste



Citation: Acquavia, M.A.; Pascale, R.; Martelli, G.; Bondoni, M.; Bianco, G. Natural Polymeric Materials: A Solution to Plastic Pollution from the Agro-Food Sector. *Polymers* **2021**, *13*, 158. <https://doi.org/10.3390/polym13010158>

Received: 16 December 2020

Accepted: 30 December 2020

Published: 4 January 2021

Publisher's Note: MDPI stays neutral with regard to jurisdictional claims in published maps and institutional affiliations.



Copyright: © 2021 by the authors. Licensee MDPI, Basel, Switzerland. This article is an open access article distributed under the terms and conditions of the Creative Commons Attribution (CC BY) license (<https://creativecommons.org/licenses/by/4.0/>).

1. Introduction

Over the last 50 years, the global production of synthetic plastics, which are carbon-based polymers such as polypropylene, polyethylene, polyvinyl chloride, polystyrene, nylon, and polycarbonate, has continuously increased and it is expected to double in the next 20 years. Approximately 360 million tons of plastics were produced in 2018 and 17% of it has been produced in Europe [1]. Conventional plastics play a pivotal role in modern society, since they can be readily manufactured to an expanding range of products used in civil and industrial applications thanks to their light weight, flexibility, and durability [2]. However, the huge amount of plastic waste production is one of the most-faced issues over the world both for environmental problems and human health threat [3].

Traditional plastics are almost completely derived from petrochemicals, meaning that fossil feedstocks are used in their production [4,5]. Around 80% of nonfuel chemicals produced by the petrochemical industry are sold for the manufacturing of plastics, thus contributing to environmental pollution as the extraction of oil and gas, particularly hydraulic fracturing for natural gas, releases an array of toxic substances into the air and water, often in significant volumes [5–8]. Furthermore, at the end of the 20th century, plastics were found to be persistent pollutants in many environmental niches, since they are largely non-biodegradable; therefore, once they reach the environment in the form of macro or microplastics, contamination and accumulation in food chains through agricultural land,

terrestrial, and aquatic food chains and water supply could happen. Plastics spread in the environment could easily leach toxic additives or hazardous substances, for example, phthalates, brominated flame retardants, bisphenol A, formaldehyde, acetaldehyde, 4-nonylphenol, and many volatile organic compounds, making them bioavailable again for direct or indirect human exposure [9,10]. Toxic chemicals that enter the human body through microplastics ingestion can lead to several health impacts, including reduced feeding, blocking of the intestinal tract responsible for starvation and impaired bodily functioning, and translocation to the circulatory system [11].

At the end of their life-cycle, plastics product are disposed of by dumping in landfills, by burning in incinerators, or by littering. In the case of littering, plastic wastes fail to reach landfills or incinerators. This is an improper way of disposing plastics and is identified as the cause of manifold ecological problems. Incineration of plastic wastes significantly reduces the volume of waste requiring disposal. It is believed that the volume reduction brought about by incineration ranges from 80 to 95%. However, their burning releases toxic heavy metals and emits noxious gasses like dioxins and furans [12].

Recycling could be thought of as a good way to reduce plastic pollution, as the cost and the GHG emission can be further reduced by implementing optimization strategies [13], however to date it has been less successful due to difficulties in identification and sorting and the presence of various other materials and additives such as fillers and plasticizers which make the process really expensive [14]. As a result, of all the plastic waste generated, the European average of that collected for recycling is only 30%, with very large differences from country to country [1].

In order to deal with the negative effects of plastic pollution, the European Parliament has developed measures aiming at reducing the quantities of plastic waste, approving a new law banning in EU single-use plastic items such as plates, cutlery, straws, and cotton bud sticks, by 2021. As a consequence, many efforts are being made in the scientific world to found bio-based alternatives which could potentially replace them. This has led to the development of a rich and diversified field of research in bioplastic production [15]. Bioplastic materials are obtained from renewable resources and could be biodegradable and/or compostable. The bioplastic aim is to emulate the life cycle of biomass, which includes conservation of fossil resources, CO₂ production, and water [16]. Bio-based resources are expected to play a key role in the production of novel and bio-based materials, contributing to a reduction of the negative environmental impacts of fossil-based products and thus addressing the bioeconomy of the future [17]. The molecular complexity of plant and bacterial biomass provides a wealth of natural bio-based polymers as well as monomeric feedstocks for bioplastic production. Currently, most bioplastics are produced from agricultural crop-based feedstocks (carbohydrates and plant materials). These, however, are not yet ideally aligned with sustainable development goals (SDGs), due to their competition for arable land, fresh water, and food production [18]. Among the countless renewable biomass sources, food waste (FW) has also received particular attention for biodegradable materials production. The possibility to overcome the problems associated to FW disposal, through its reuse for the manufacturing of bio-based plastics with a reduced carbon footprint, is considered as an attractive proposition in the field of green chemistry.

Recently, several reviews have been published relating to the production of bioplastics starting from food waste [19–22]. A discussion on economic viability of FW valorization has been offered by Tsang et al. [19], which also reviewed the technologies commonly employed for the production of polyhydroxyalkanoates. Instead, Maraveas et al. [21] gathered on the general aspects of the synthesis of bio-based polymers from agricultural wastes, as well as on their applications. The main steps in the process of biodegradable films elaboration starting from fruit puree were investigated by Matheus et al. [22], especially lingering on the evaluation of the functional properties of the obtained materials, i.e., the antimicrobial and antioxidant properties.

The search for green formulations that can be suitably manufactured for the production of eco-friendly materials is mandatory in the field of green chemistry and environmental

sciences. In this review, we will highlight the developments in the application of the methods used over the past decade for the design of biomaterials. Although several reviews discuss on the same topic, here particular emphasis will be given to those obtained from formulations based on fruit and vegetable by-products. In detail, this review represents a comprehensive basis for scientists to direct their research towards natural sources of biopolymers that could be used appropriately for the production of bio-based materials, including cellulose, starch, pectin, cutin-based materials, and biocomposites. A first part will be dedicated to a complete description of the classification systems of bioplastics and to the methods that are commonly used to define their bio-content and biodegradability, as well as their main physical and mechanical properties. Then, a critical discussion on the latest research results concerning bioplastic production from by-products and waste materials of the fruit and vegetable industries made in the last 10 years will be conducted. A summary table (Table A1), containing all the information relating to the pre-processing of the waste, the definition of the green plastic formulation, and the type of manufacturing, as well as the properties of the final material, will be provided.

2. Bioplastics: Definition and Classification

According to the European Bioplastics Organization (EBO), a material could be defined as a bioplastic if it is either bio-based, biodegradable, or features both properties [23]. The term bio-based refers to materials or products that are completely or partly derived from renewable resources (biomass); thus the petrochemical resin typical of common plastics is replaced by vegetable or animal polymers and the compounds like glass or carbon fiber or talc are replaced by natural fibers (wood fibers, hemp, flax, sisal, jute) [15]. For those concerning biodegradability, a material could be defined as biodegradable if it undergoes degradation by biological processes during composting to yield carbon dioxide, water, inorganic compounds, and biomass at a rate consistent with those of other known, compostable materials and leaves no other distinguishable or toxic residue [24].

To date, several classification systems based on different criteria have been proposed to distinguish bioplastic materials, as they can show a wide variation in biodegradability percentage and can be derived from a large number of renewable or non-renewable sources [15,25–27].

Bioplastics could be grouped according to their biodegradability and bio-based content in: bio-based (or partly bio-based) but non-biodegradable plastics (or drop-in bioplastics); biodegradable and bio-based plastics and biodegradable plastics based on fossil sources (Figure 1) [23].

Non-biodegradable bioplastics are obtained from renewable sources and they are comparable to classical plastics for the time needed for their complete environmental degradation. This group of plastics are named “drop-in” bioplastics [28] and nowadays represent one of the largest sectors of the global bioplastics production. Bio-PET (bio-polyethylene terephthalate) represents a very common drop-in bioplastic example. For PET production, an esterification reaction between terephthalic acid (PTA) and ethylene glycol (EG) followed by a polymerization through a polycondensation reaction with water as by-product is used [29]. In the traditional production of PET, both PTA and EG are fossil refinery products: petroleum refiners first separate out *para*-xylene (PX) from BTX (Benzene, Toluene, Xylene) mixtures by crystallization method and then oxidize it to PTA. Similarly, in order to obtain EG, ethylene derived from the alkene co-products of natural gas production are processed through hydration and oxidation [30]. For bio-PET, instead, EG or both monomers are obtained from renewable sources by a process identical to that used for petro-PET and also their technical properties are identical to those of their fossil counterparts [31]. Ethylene glycol is always available on a large scale from biomass: at the beginning cellulose recovered from lignocellulosic biomass is converted into xylitol and sorbitol, which are easily hydrolyzed to EG in the presence of several mono- and bimetallic phosphide catalysts [32,33]. Moreover, bio-ethanol derived from sugar cane or corn stover and glycerol, as a co-product of biodiesel, have been used as a feedstock to

produce EG [34]. The production of terephthalic acid by green chemistry processes based on the use of chemical precursors extracted from corn, sugar beet, or orange peel, i.e., isobutanol, 5-hydroxymethylfurfural, and limonene, respectively, is used to a smaller extent [31].

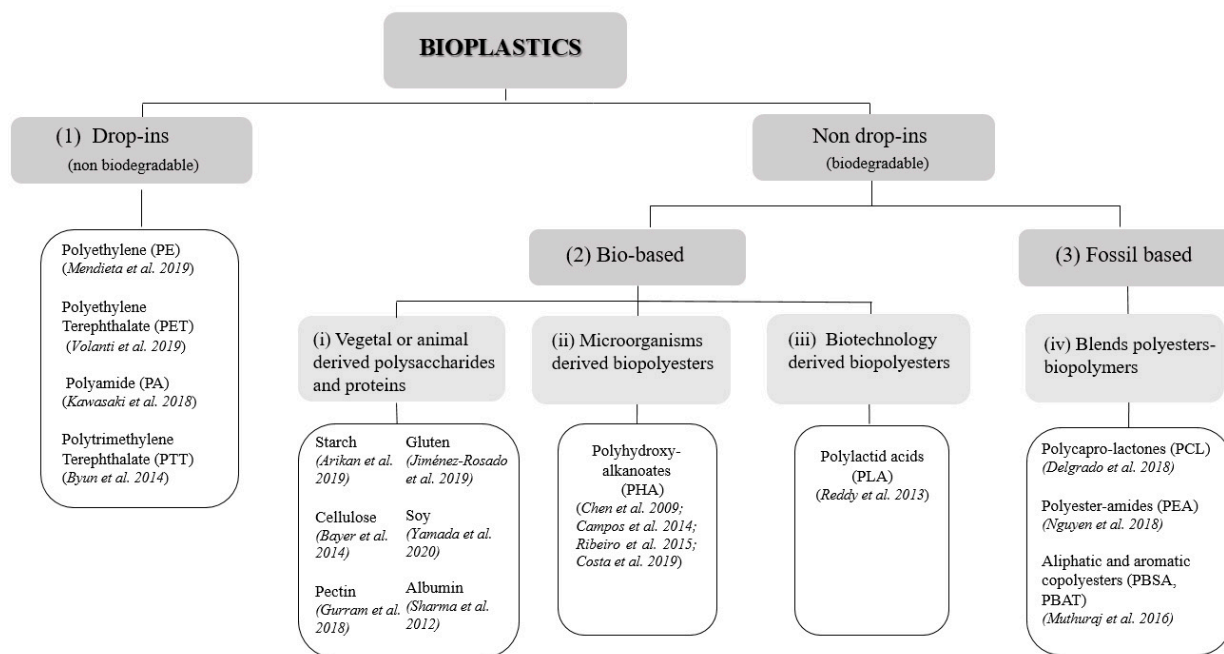


Figure 1. Scheme of bioplastics classification: (1) Drop-in bioplastics (i.e., bio-based or partly bio-based but non-biodegradable plastics), (2) bio-based non drop-in bioplastics, and (3) fossil based non drop-in bioplastics. According to their origin, non-drop-ins (i.e., biodegradable plastics) are divided into (i) vegetal or animal derived polysaccharides and proteins, (ii) polymers from microorganism, (iii) polymers from biotechnology, and (iv) blends of biopolymers and commercial polyesters [25].

While drop-ins are well known on the market, non-drop-in bioplastics, i.e., plastics that are biodegradable bio-based or based on fossil sources, are alternative materials usually used in niche fields, for example for food services, agriculture, or biomedical applications; therefore, their trade has been emerging only in recent years [28,35,36]. These biodegradable polymers can be classified, according to their origin, into four major categories, namely (i) agro-polymers, (ii) polymers from microorganism, (iii) polymers from biotechnology, and (iv) blend of biopolymer and commercial polyesters [15] (Figure 1).

Starch, cellulose, pectin as well as animal and vegetable proteins, such as casein and gluten, are well known for being feedstock of agro-polymers based bioplastics [37–39]. Starch, cellulose, and pectin are polysaccharides that can be extracted from several vegetables and fruits (potato, corn, rice, tapioca, apple) and they are used mainly to produce packaging materials [15]. Often, protein additives are used in order to fabricate materials with novel or improved technological properties. In fact, due to the difference between the elemental composition of proteins (covalent bonds between hundreds of amino acids) and polysaccharides (covalent bonds between monosaccharides with ramifications), their mixtures can evidence a wide variety of two- and three-dimensional structures with different physicochemical and rheological properties [40].

In addition, there are a lot of polymers that could be produced by a range of microorganisms, cultured under different nutrient and environmental conditions [41]. Polyhydroxyalkanoates (PHAs), for example, are linear thermoplastic polymers, with hydroxyalkanoic acid as a monomer unit, which can be synthesized intracellularly as insoluble cytoplasmic inclusions by heterotrophic bacteria, such as *Cupriavidus necator* [42,43], recombinant *Escherichia coli* [44], and also by photoautotrophic microorganisms like microalgae [45]. Their

synthesis occurs in the presence of an excess of carbon, when other essential nutrients such as oxygen, phosphorus, or nitrogen are limited; after their extraction from cell cultures, they can be processed in a similar way to that of polypropylene, including extrusion and injection molding, obtaining a material with similar properties as well.

On the other hand, bacterial microorganisms can also be used to produce, in a biotechnological approach, biodegradable polymers through the fermentation of carbohydrates obtained from agricultural by-products such as starchy substances as corn, wheat, or sugar and corn starch. Poly Lactic Acid (PLA)-based bioplastics are obtained from a fermentative process that involves conversion of corn, or other carbohydrate sources into dextrose, followed by fermentation/conversion into lactic acid [25]. Thus, lactic acid is isolated and polymerized to yield a low molecular weight, brittle polymer whose chain length could be increased by using external coupling agents [27].

The last group of biodegradable materials is represented by blends of biopolymers and polymers obtained by chemical synthesis from fossil resources [46–48]. Polymers blending is a technique that allows to modify the properties of a material using a conventional technology at low cost. In this way, biodegradable polyesters such as Poly CaproLactone (PCL), which is obtained by the condensation of 6-hydroxycaproic acid or through the ring opening polymerization of ϵ -caprolactone [49], could be easily used to improve mechanical properties of natural polymers as starch, conferring them a better water resistance due to its hydrophobicity [50].

Nowadays, although with different percentages, all bioplastics are used in a wide range of sectors: from packaging, catering products, consumer electronics, automotive, agriculture/horticulture, and toys to textile fields. The field of application of a given bioplastic material is clearly dictated by its mechanical properties as well as by its bio-based content or its biodegradability. These characteristics are evaluated before bioplastics are promoted on the market.

Moreover, to produce functional materials with biological properties, in the case of bioplastics obtained from fruits and vegetable wastes, a metabolic characterization of the raw material is needed. Among the analytical techniques used to this aim, both chromatography and the mass spectrometry are critical as they allow both targeted and untargeted characterization of the main classes of metabolites occurring in a given matrix [51–62].

2.1. Bioplastics Bio-Based Content and Biodegradability

Both bio-based and either biodegradable plastic materials have become the world's most widely choice among bioplastic materials as their production has a low environmental cost compared to traditional plastic ones [63]. To promote the diffusion of either bio-based or biodegradable plastic materials, the Public Procurement Working Group of the European Commission's Expert Group for Bio-based Products published 15 recommendations in order to enable procurement policies to embrace eco-friendly materials. Due to emerging trade of this type of materials, it is necessary to establish a labelling harmonization, as well as the existence of standards and test methods to define and measure properties and characteristics like bio-based content, biodegradability, and other attributes unique to ready-to-market products.

The bio-based content of a material is the amount of the biomass-derived carbon, as compared to its total organic carbon content (TOC). The carbon content of bio-based materials is determined independently and unequivocally as reported in international standard methods of the American Society for Testing and Materials (ASTM) and of the International Organization for Standardization (ISO). In detail, ASTM D6866-20 and ISO 16620-2 methods report radiocarbon analysis as the technique to determine the bio-based content of solid, liquid, and gaseous samples. The employment of the radiocarbon dating method is based on the significative difference in ^{14}C isotopic signature between the fossil derived (^{14}C -free) and the biomass derived (^{14}C -including) materials. In detail, the presence of ^{14}C in the bio-based materials is due to the fact that ^{14}C containing carbon dioxide formed in the atmosphere, participates in the photosynthetic processes from which

the biomass derives. Thus, the ¹⁴C content of biomass derived materials is the result, in a first approximation, of ¹⁴C atmospheric levels [64,65]. ¹⁴C measurements could be done by using Accelerator Mass Spectrometry (AMS) along with Isotope Ratio Mass Spectrometry (IRMS) or by using Liquid Scintillation Counting (LSC) techniques (ASTM International, 2020). In order to define a bioplastic as bio-based, a biomass-derived carbon content not less than 25% is required [66].

Another key bioplastic property to be measured is the biodegradability [26], which refers to the ability of a material to decompose after interactions with biological elements. The biodegradation of polymers involves three steps: bio-deterioration, bio-fragmentation, and assimilation (Figure 2) [67]. Bio-deterioration is the modification of mechanical, chemical, and physical properties of the polymer due to the growth of microorganisms on or inside the surface of the polymers. In the bio-fragmentation step, microorganisms fragment polymers in oligomers and monomers, which, in the next assimilation step, are available as their carbon, energy, and nutrient sources finally with CO₂, water, and biomass as by-products [26]. It should be pointed out that only specific microorganisms could degrade a given type of bioplastic. It has been reported that PCL can be degraded by bacteria isolates that exist in deep sea sediments, but these isolates are incapable of degrading other types of bioplastics, such as PLA, PHB, and PBS; however, there exist composting bacteria capable of degrading the latter [26].

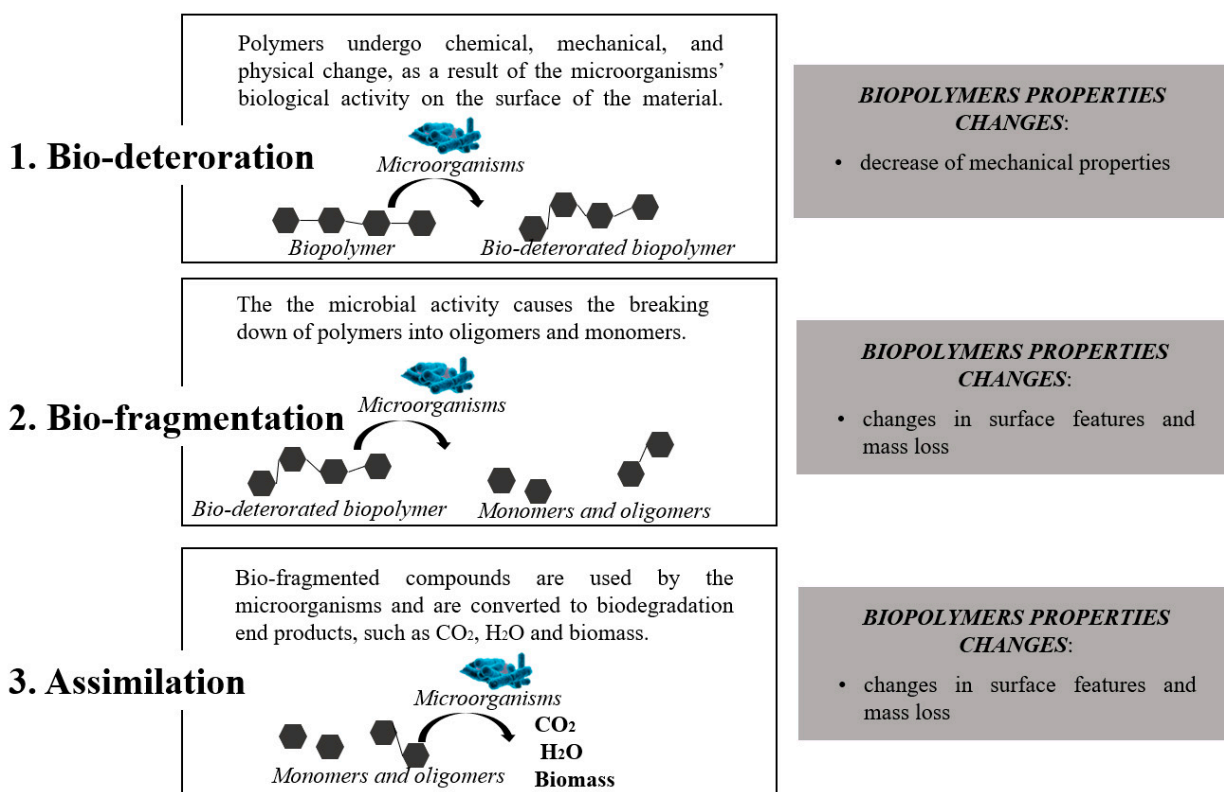


Figure 2. The main three steps through which the biodegradation of polymers occurs: (1) bio-deterioration, (2) bio-fragmentation, and (3) assimilation.

The biodegradation of bio-plastic materials is highly dependent on their chemical structures. Generally, polymers with a shorter chain, more amorphous parts, and less complex formula are more susceptible to biodegradation by microorganisms [68]. The presence of additives could influence the biodegradability of a matrix. As an example, polypyrrole, the archetype of polymers integrated in biosensing devices for biomedical applications, can acquire enhanced biodegradability if grafted onto cellulose chains, thus forming biocomposite [69,70]. Moreover, the pH, temperature, and the oxygen content of

the environment in which the polymers are placed or disposed of, could be key factors for their biodegradation [71,72]. For example, oxidative-degradable polymers accelerate their decomposition under the effect of oxidation through heat and/or UV light. UV radiation can disrupt polymer chains, since the radiation can be absorbed by oxygen-containing components to initiate a primary degradation; these polymers are known as photodegradable polymers. During photodegradation, both molar mass and crystal structure are affected. The plastics that have the capacity to biodegrade by hydrolytic mechanisms such as biopolymers made of cellulose, starch, and polyesters such as PHA are known as hydro-biodegradable bioplastics [73].

To date, a wide variety of methods for measuring the biodegradability of polymeric biomaterials have been currently developed and most of them are in agreement with ASTM, ISO, and European Standards (EN) standard methods in terms of environmental conditions, timings, and scales of the tests. Overall, all methods are focused on an indirect measure of degradation process, such as oxygen consumption or biogas generation (CO₂) by measuring differences of pressure in the test flasks and carbon dioxide production [24]. A biodegradation level higher than 90% in comparison with cellulose (positive standard) in 180 days, under conditions of controlled composting measured through respirometric methods has been established by the European Norm EN 13,432 as the level for a material/product to be defined as biodegradable and compostable. In addition, a disintegration level higher than 90% in three months and the respective ecotoxicity and chemical safety criteria should be kept. Then, only when the products meet the EN 13,432 standard criteria can the wording “biodegradable” be reported on the packaging label.

The biodegradation of bioplastics has been extensively investigated in soil and compost environments, where they mainly showed high degradability [26]. Anyway, the conditions of the experiments conducted to study the bioplastics biodegradability are highly variable, and to make a clear comparison among them is difficult. The experiments carried out in compost or in anaerobic digestion environments show a biodegradability over 50% in 65 and 68%, respectively. For those carried out in aquatic environments, this share is 44%, and for experiments carried out in soil, it is 33% of the cases [73].

It should be pointed out that, in addition to increasing bio-based content and biodegradability, bioplastics intrinsic properties often need to be improved to meet industrial expectations. The optimization can concern, for example, mechanical properties, increased material flexibility, increased rigidity, increased resilience, and improvement of water absorption capacity [74–76].

2.2. Bioplastics Mechanical and Physical Properties

In order to assess the suitability of a biomaterial for a given sector and to establish the service life that can be expected, an evaluation of its mechanical-physical properties is mandatory. The main mechanical properties that are typically tested after the production of a bioplastic are the ultimate tensile strength, the Young's Modulus, and the elongation at break. The ultimate tensile strength, or just tensile strength, indicates the maximum stress that a material can withstand before fracturing, while the Young's Modulus, also known as elastic modulus, defines the stiffness of a material: the bigger is its value, the stiffer the material [77]. As regard to the elongation at break values, they are a measure of material ductility and depend on the rate (crosshead speed) and the temperature. The elongation at break value is, generally, very small and close to zero for brittle materials. On the contrary, materials with a better capacity to handle an excessive load without failure show higher elongation than 100% [78]. Clearly, all these properties are affected by the chemical structure, the orientation degree of the polymers, and the crystallinity of the material, as well as by the eventual presence of fibers that act as reinforcement, or plasticizers [79,80]. Plasticizers are low volatile molecules, added to bio-polymeric materials to ensure an increasing of their extensibility, dispensability, flexibility, and elasticity [81]. Several theories to explain the mechanisms of plasticization action have been proposed [82]. The lubrication theory states that plasticizers, by interspersing themselves, act as internal lubricants by

reducing frictional forces between polymer chains. The gel theory, instead, postulates that the rigidity of polymers comes from three-dimensional structures, and plasticizers take effect by breaking polymer-polymer interactions (e.g., hydrogen bonds and van der Waals or ionic forces). The free volume theory states a plasticization as a study of ways to increase free volume and is useful in explaining the lowering of the glass transition temperature (T_g) by a plasticizer. Ideal plasticizers should be miscible and compatible in all proportions with plastic components, and they may be added to polymers in solution (dispersion technique) or after solvents have been removed (absorption technique) [83,84]. Water, oligosaccharides, polyols, and lipids are different types of plasticizers widely used for edible films and coatings [85].

For hydrophilic polymers, polyols have been proven to be very efficient as plasticizers [86,87]. In detail, for bio-based polymers obtained from fruits and vegetables waste, the recent researchers have focused on the usage of glycerol [88–92] and sorbitol [93]. Glycerol content has significant effects on the mechanical properties as well as on the dynamic rheological behavior of thermo-molded bioplastics. Indeed, it was demonstrated that the increasing of glycerol content decreases tensile strength and Young's modulus but improves ductility at room temperature [94]. Several studies on plasticization of chitosan films revealed that poly(ethylene glycol) (PEG) could improve the elastic properties of the chitosan biopolymer. Caner et al. [95] observed that chitosan plasticization using PEG was stable until nine weeks of storage (Figure 3).

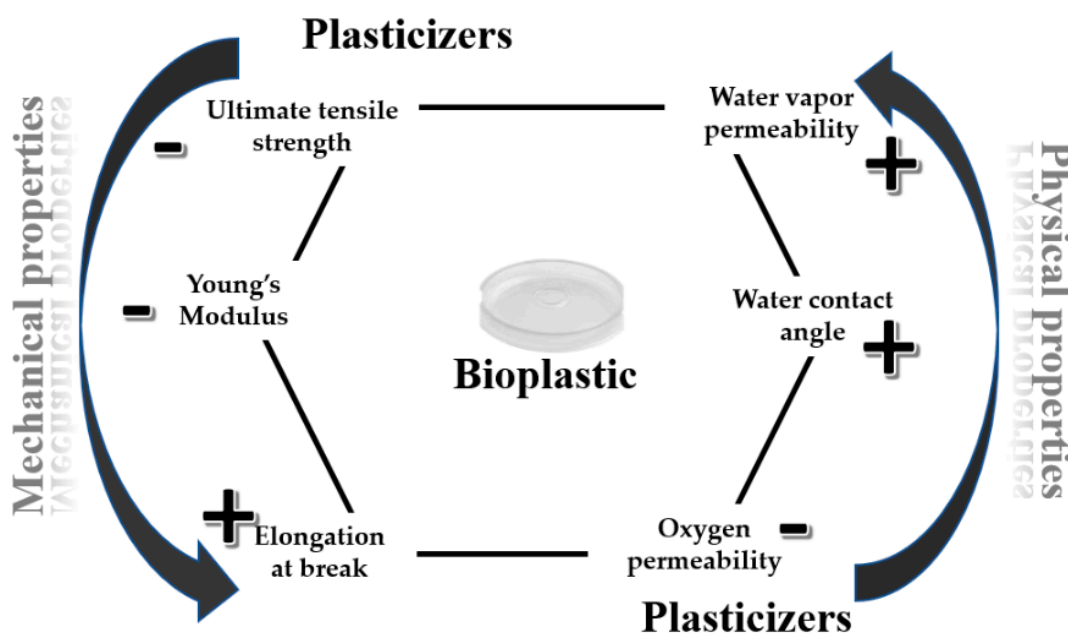


Figure 3. Effects of the plasticizers' addition on mechanical and physical properties of bioplastic materials.

In addition to the mechanical properties, plasticizers also affect the physical properties of the biomaterials, which means water vapor permeability (WVP), oxygen permeability (OP), and water contact angle (WCA) (Figure 3) [46]. These parameters serve as indicators of how easily water vapor or oxygen can penetrate a biodegradable material and they are a function of the hydrophilicity and hydrophobicity ratio of the main components by which the biomaterial is made. As to water contact angle, which is measured as the angle between the baseline of a drop deposited on the surface of the material and the tangent at the drop boundary, it increases with increasing surface hydrophobicity [87]. Since the surfaces degree of hydrophobicity is important to ensure good barrier properties, the evaluation of WVP, OP, and WCA is demanded. Recently, Aguilar et al. [96] found that different physical and mechanical properties could be achieved at room temperature for bioplastics based on a soy protein isolated as a byproduct of the soy oil industry and

added with different polyols, i.e., s (glycerol (GLY), ethylene glycol (EG), diethylene glycol (DEG) and triethylene glycol (TEG). In this sense, TEG-bioplastics were opaque, brittle, and also had a higher water uptake capacity, while EG-bioplastics were more ductile and translucent, absorbing much less water when immersed. Only GLY and TEG remained in the bioplastic after 9 days of storage at 50 °C, pointing out the volatility of EG and DEG causing a major ageing effect. On the other hand, it was also observed that sugars like sucrose and trehalose could act as plasticizers in presence of water. In detail, when water is included in the bioplastic formulation together with glycerol, sugars are solubilized within the aqueous fraction, and then play a plasticizer role in the bioplastics. In that case, lower viscoelastic properties and greater water absorption ability are generally detected [97].

3. Food Waste as Feedstock for Bioplastic Production

The most recent research concerning bioplastic production focuses on by-products and waste materials of food industries. According to the Food and Agriculture Organization (FAO) of the United Nations, every year an estimated 1.3 billion tons of food is wasted globally from all stages of the food supply chain including post-production, handling/storage, manufacturing, wholesale/retail, and consumption. Since food waste landfilling yields undesirable results, such as greenhouse gas (GHG) emissions and groundwater contamination, their valorization through bioplastics production could offer the possibility to overcome their disposal problem by renewable sustainable processes [19]. In addition, the production of value-added products while reducing the volume of waste is expected to reduce the production cost of biodegradable plastics, e.g. compared to conventional routes of production using overpriced pure substrates [19].

Food waste (FW) can be valorized in several ways in order to produce bioplastics (Figure 4).

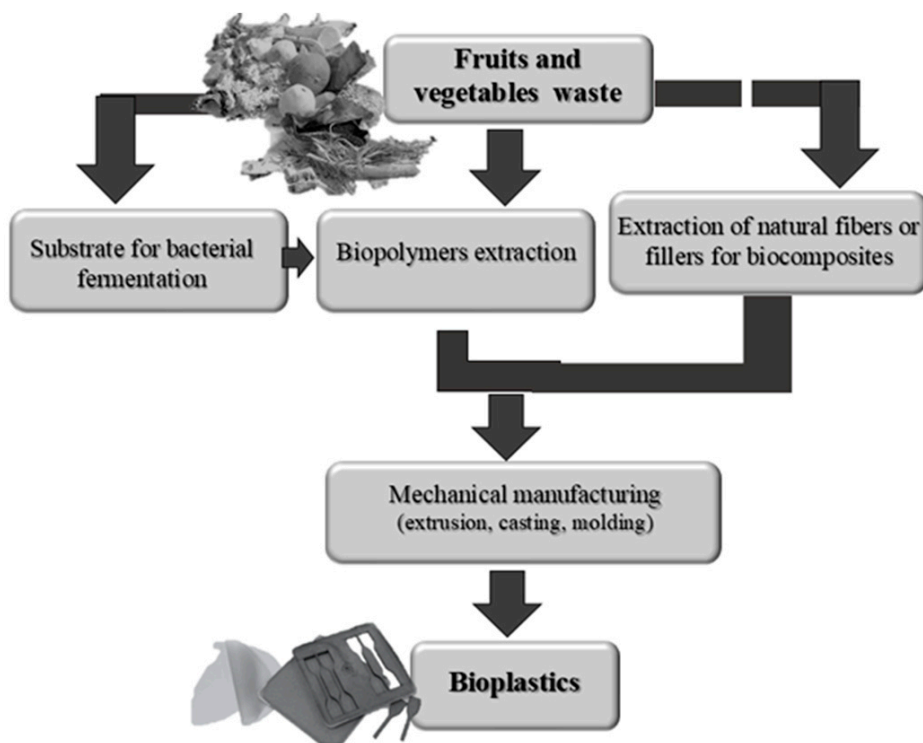


Figure 4. Conversion of food wastes into bioplastics could occur through biopolymers extraction and their mechanical manufacturing (extrusion, casting, molding, or combination of them). In more complex processes, food wastes are used as substrate for bacterial fermentation in order to produce biopolymers or as raw material for the extraction of other natural components, such as fibers, which act as reinforcing agents and/or natural filler of biocomposites.

It is often used as substrate for bacterial fermentation to obtain natural polyesters, namely PHA and polylactic acid (PLA). When used to produce PHAs, food waste is a prime candidate for an inexpensive carbon source, due to its widespread availability and the potential to solve significant waste problems. In this case, physical, thermochemical, and biological pre-treatments of the FW are requested. Briefly, as reported by Tsang et al. [19], a preliminary liberation of monomers from the FW (e.g., lignocellulosic components) with increasing accessibility of proteins, lipids, and polysaccharides (e.g., starch and cellulose), for subsequent enzymatic hydrolysis and fermentation, are essential. After the pre-treatment, the FW is ready for fermentation step in presence of bacteria, by using several cultivation strategies.

Other simple technologies for the production of bioplastics involve the direct extraction, from the food-waste-stream, of the biopolymeric components that are worked to give the finished products. More complex processes, on the other hand, require additional steps through which the biomass or the biopolymers extracted from it are used as reinforcements or fillers for the realization of biocomposites [98].

In many cases, the different “bioplastic formulations” need to be blended with additives in order to optimize some properties of the materials, such as thermal instability, high water vapor, brittleness, and low melt strength. Plasticizers, like glycerol, for example, are often required to improve the processability and the mechanical properties by interrupting hydrogen bonding and reducing the interactions between the biopolymers chains [81].

However, both formulations, biopolymeric and biocomposites, are lastly processed to obtain biofilms or three-dimensional objects by applying conventional mechanical techniques: extrusion, molding, casting, or a combination of them [88,99,100]. All these processing methods selected for the manufacture of food waste-based bioplastics play an important role in their final properties [101]. Extrusion is a highly efficient way for the continuous shaping of biomaterials, and it consists in pushing the bioplastic dough against an orifice with the desired geometry and dimensions. The mass of the dough inside the extrusion chamber is compacted, and the semi-finished product that comes out is cut to give the wanted length. Instead, with casting and molding, the dough is respectively poured or pressed against a rigid frame.

Compression molding technique has been widely employed for the development of biofilms or 3D objects without the use of any solvent or binder [88,102]. With this technique, the waste of interest or its dried extract is finely powdered and subjected to high temperatures and pressures through a heated press. Under this thermo-mechanical treatment, proteins undergo denaturation and dissociation leading to the formation of new links and their aggregation to new forms; in addition, biopolymers show a self-binding ability that is exploited to produce three-dimensional objects. Furthermore, the molding method is more suitable for industrial applications since it is characterized by lower energy demand and processing time compared to other techniques like solution casting [102].

In the last 10 years, several food wastes have been used as raw material for the production of bioplastics, including biocomposites; mostly fruit and vegetable wastes rich in polysaccharides (such as cellulose, starch, pectin) and in fibers [90,93,101,103–105] (Table A1). In the next paragraphs, a focus on the main uses of fruits and vegetables wastes for the production of bioplastics will be provided.

3.1. Biopolymers-Based Plastics

Biopolymers extracted from fruits and vegetables wastes show different characteristics and properties that make them more or less suitable for the production of eco-friendly materials (Table 1). The extraction of biopolymers from food waste could be achieved chemically or enzymatically. Enzymatic processes are widely considered “clean” since they are solvent-free [106]; however, this technology is still hindered by economic and technical limits, i.e., costly enzymes and long processing period. Because of the high cost and time-consuming nature, the production of bioplastics through sugar’s bacterial fermentation, occurring in agricultural waste, is disadvantageous. Therefore, chemical

extraction with solvents could be considered as the best solution at the lowest amount of energy.

Table 1. Properties associated with the main biopolymers extracted from fruits and vegetable wastes for bioplastics production.

Biopolymer Name	Biopolymer Type	Properties	Fruits and Vegetable Wastes Used as Biopolymer Source
<i>Cellulose</i>	Polysaccharide	Highly structured intermolecular hydrogen bonding network; impossibility of melting or dissolution by standard processes such as thermoforming.	Banana peels, carrots waste, cauliflower waste, cocoa pod husks, orange peels, parsley steams, radicchio waste, rice hulls, spinach steams, tea leaves waste.
<i>Starch</i>	Polysaccharide	Strong inter- and intra-molecular hydrogen bonding; water sensitivity and poor fowability; brittleness.	Banana peels, cassava peels, potato peels.
<i>Pectin</i>	Polysaccharide	Gelling ability but poor tensile and barrier properties; water sensitivity.	Apple pomace, banana peels, citrus waste, orange peels
<i>Cutin</i>	Polyester of hydroxy fatty acids	Amorphous and flexible three-dimensional polymer; hydrophobic, low water sensitivity.	Tomato waste

One of the main macromolecules extracted from fruits and vegetables waste and used for the production of biomaterials is the cellulose. The preparation of the pure cellulose bioplastics from bio-sources is not easy due to the highly structured intermolecular hydrogen bonding network of the polymer, which cannot be melted or dissolved by standard processes such as thermoforming [37,107]. Thus, the cellulose is usually used in industrial applications in the form of derivatives, such as esters or ethers, from which cellulose is then regenerated [108]. Nevertheless, in recent years, several biomaterials have been manufactured through amorphous cellulose extracted from vegetables by using different solvents. Bayer et al. [37] obtained amorphous cellulose-based biomaterial by digesting parsley and spinach stems, rice hulls, and cocoa pod husks wastes in trifluoroacetic acid (TFA), followed by casting and evaporation. TFA is a naturally occurring and biodegradable organic acid that can co-solubilize cellulose with other contained organic matter; it breaks the hydrogen bonds between neighboring cellulose chains (intersheet hydrogen bonds) and partial trifluoroacetylates OH groups of cellulose with formation of amorphous materials [109]. The mechanical properties of the produced cellulose-based biofilms were proved to be largely dependent on the starting biowaste. Indeed, cocoa pod husks biofilm displayed a tensile stress at break of approximately 30 MPa; whereas for the rice, the parsley, and the spinach-derived films, the obtained values were, respectively, 7 MPa, 5 MPa, and approximately 1 MPa, i.e., values close to elastomers and low density polyethylene thermoplastic [37]. Such higher stresses at break and strains for cocoa pod husks derived biomaterial were due to their significant number of triglycerides, i.e. oligomeric esters precursors of biopolymers. Instead, residual silica in the rice hulls derived material conferred a higher rigidity compared to parsley- and spinach-based biomaterials. UTS (ultimate tensile strength) at high Young's modulus comparable to poly(ethylene terephthalate) of bioplastics from cocoa pod husk could be compared with petroleum-based thermoplastics, such as high-density polyethylene and polypropylene. Rice straw was used also by Bilo et al. [110] to produce a new cellulose-based bioplastic material through a process that involved the digestion with TFA, preceded by an extraction pre-treatment performed in a rapid dynamic solid-liquid extractor. With this process, a bio-material with better mechanical properties,

compared to those evaluated by Bayer et al. [37], was obtained. Indeed, the tensile test of dried and wet dumbbell specimens allowed to ascertain tensile strengths and elongations at break equal to 45 MPa and 6.1% and 10 MPa and 63%, respectively (Table A1). The replacement of TFA with a diluted aqueous chloridric acid (HCl) solution has been found to be a better method to obtain biofilm evidencing higher stiffness and lower ductility. Perotto et al. [111] used this water-based process to convert carrot, parsley, radicchio, and cauliflower wastes into flexible bioplastic films made by cellulose crystals fused together, with some soluble components like pectin and sugars blended homogeneously acting as plasticizers. Compared to the oil-based polymers, the Young's Modulus (1.3 ± 0.2 GPa) and the UTS (38 ± 5 GPa) of the carrot bioplastics are similar to those of polypropylene, albeit with lower elongation. The mild conditions of the conversion process were demonstrated also to preserve the functional properties of the original vegetable, like the anti-oxidant activity [111]. An aqueous HCl solution was used also by Yaradoddi et al. [89] to produce a cellulose-based biofilm from banana peels; anyway, in this case, no mechanical tests were conducted in order to evaluate the strength of the material.

Although TFA and HCl are efficient acids for vegetable waste derived-cellulose dissolution, their utilization, and waste production remain problematic if considering the principles of green chemistry. Recently, a less harmful acid, i.e., citric acid, has been used by Liu et al. [112] in a green, non-toxic, waste-free method of synthesizing hydrophobic bioplastic films from spent tea leaves. The resultant material exhibited an ultimate tensile strength of 6.16 MPa and an elongation at break of 13.33%, thus it had a lower stiffness compared to oil-derived polymers, such as PP (Table A1). Since citric acid was found to not fully react with the tea waste matrix, the authors hypothesized that unreacted citric acid acted as a hygroscopic plasticizer in the bioplastic films.

In addition to cellulose, starch, i.e., a polymer consisting of a long chain of two glucose units joined together, namely branched polymerized amylopectin and amylose, can be considered as an effective eco-solution for the production of biomaterials, because it is inexpensive and easily available (Table 1). Starch for the production of biofilm have been obtain from different sources, principally potatoes, banana and cassava peels [90,113–118]. Arikani et al. [114] investigated the production of bioplastics from potato peels waste, obtaining satisfactory results in terms of biodegradability (the time requested for the complete biodegradation of the material was 28 days, see Table A1). However, native starch-based films are limited to high water affinity and brittleness, therefore other natural biopolymers are often added as fillers to modify and improve films' properties. As example, Dasumiati et al. [116] and Fathanah et al. [117] improved the mechanical properties of cassava peels derived starch by introducing chitosan as filler. In another work, proteins derived from soybeans waste were mixed with starch and glycerol as plasticizer, since proteins structure consists of stable three-dimensional networks which do not ensure material with enough plasticity [119]. Instead, Sultan et al. [90] developed bioplastic film from a combination of banana peels derived starch and different concentrations of corn starch (1% up to 5%) as co-biopolymer. Based on the results obtained, the film with 4% of corn starch gave the highest tensile strength 34.72 N/m^2 compared to other samples, while the authors stated that the biofilms with 3% of corn starch were resistant to water uptake by absorbing water up to 60.65% (Table A1). However, it should be considered that this value is considerably higher compared to conventional plastics such as PP, whose percentage of water absorption after 24 h of immersion ranges between 0.01 and 0.03.

Besides being a starch source, banana peels have been shown also to contain a good percentage of pectins [120]. Pectins are a family of covalently linked galacturonic acid-rich plant cell wall polysaccharides with functions in plant growth, morphology, and development; they also serves as gelling and stabilizing polymers in diverse foods [121]. The production of pectin-based biofilms typically involves the introduction of cellulose and hemicellulose components, since polysaccharidic films show poor tensile and barrier properties compared to those of petroleum-derived polymers. To this regard, Oliveira et al. [75] isolated pectin from banana peels in order to prepare a biofilm whose tensile strength was

increased through the addition of cellulose nanocrystals (CNCs) extracted from the same banana wastes (tensile strength values obtained were about 7 MPa, see Table A1). The tensile strength increase was due to favorable nanocrystal–pectin interactions as well as to the reinforcing effect through stress transfer at the nanocrystal–pectin interface [122].

Aside from the poor mechanical properties, the strong hydrophilic character of polysaccharidic films makes them dissolve in contact with water, limiting their applications [75]. To overcome the high water permeability, citric acid could be added, as it crosslinks polysaccharide films by forming covalent diester linkages between two of their carboxyl groups and hydroxyl groups of different polysaccharide chains [123]. In the previous mentioned work reported by Oliveira et al. [75], the presence of citric acid was ascertained to decrease the water vapor permeability from 3.31 to $3.10 \text{ g}\cdot\text{mm}\cdot\text{kPa}^{-1}\cdot\text{h}^{-1}\cdot\text{m}^{-2}$. Citric acid was used also for the processing of orange and apple wastes (OW and AW) in order to obtain a biodegradable material through a casting method in which cellulose and hemicelluloses were suspended in the pectin solution and further dried to a film [88,92]. In detail, Batori et al. [92] used a solution of citric acid and glycerol to form a biofilm from OW, exploiting the gelling ability of pectin and the strength of its cellulosic fibers. The tensile strengths of the films were 31.67 ± 4.21 and 34.76 ± 2.64 MPa, respectively, for the oven-dried and incubator-dried films. These values were within the range of different commodity plastics. In addition, anaerobic digestion was performed for testing the biodegradability of the material and a time of 15 day was requested to reach 90% of degradation. Instead, from a mixture of apple pomace waste (AW) and glycerol, a fluffier and connected structure (tensile strength 3.27 ± 0.31 MPa without including a washing step) was obtained by Gustaffson et al. [88], but with significant flexibility, similar to those of PP (elongation %: 55.41 ± 5.38 , Table A1).

The same authors [88] made an attempt to produce bioplastics by using solvent-free mechanical processing of AW. Compression molding technique has been widely employed for the development of pectin-based biofilm or 3D objects without the use of any solvent or binder [88,102]. Gurram et al. [102] applied a compression molding method for production of bioplastic films from citrus peel derived pectin. Moreover, free sugars and water-soluble nutrients were extracted from citrus waste and employed for cultivation of the filamentous fungus *Rhizopus oryzae*, whose biomass was incorporated into the pectin films. The addition of fungal biomass (up to 20%) enhanced the tensile strength (16.1–19.3 MPa) and reduced the water vapor permeability of the pectin films (Table A1).

In addition to the cellulose, starch, and pectine, a sustainable melt polycondensation of unsaturated and polyhydroxylated fatty acids recovered from tomato pomace agro-wastes, has been recently carried out in order to obtain an aliphatic polyester type of bioplastic without the use of solvents during the reaction [124]. Polyhydroxylated fatty acids are found in tomato pomace in the form of cutin, i.e., a biopolyester mainly composed of C_{16} and C_{18} fatty acids monomers linked together and forming an amorphous and flexible three-dimensional polymer matrix [125]. Since cutin isolation to produce bioplastics is a long multistep process and unsuitable for large-scale applications, a direct depolymerized of tomato pomace through alkaline hydrolysis, followed by monomers polycondensation, has been proposed by Heredia-Guerrero et al. [124] as a simpler and cheaper alternative. To that purpose, the influence of different temperatures, reaction times, and amounts of tin (II) 2-ethylhexanoate used as a catalyst, was evaluated. Synthesized tomato pomace bioplastics showed an amorphous molecular structure, whose mechanical properties were dependent on the degree of polymerization. In detail, an increase in hardness of the polyesters synthesized at higher reaction temperatures and amount of catalyst was detected (~ 1.8 MPa for biopolymers obtained at 125°C and 0 mmol of catalyst against ~ 26.3 MPa for biopolymers obtained at 175°C and 0.1 mmol of catalyst), since in those conditions a higher degree of polymerization was achieved. The water-contact angles of more polymerized samples were around 109° , which are values comparable to traditional hydrophobic polymers such as PDMS and PTFE. Concerning water uptakes, the obtained percentages were typical of low-absorbing plastics (2.1–61%).

3.2. Fruits and Vegetables Waste Usage for Biocomposites Production

More often, biopolymers extracted from fruits and vegetable wastes are blended with other polymers whose mechanical and physical properties are not suitable to accomplish commercially acceptable products [100], thus realizing composite materials known as biocomposites.

Biocomposite materials are usually made by a polymeric matrix coming from a renewable and available origin, such as polysaccharides, reinforced by natural fillers. Examples of natural fillers are layered silicates. They can be synthesized from silica naturally occurring in leaves, husks, blades, hulls, roots, and stems of many terrestrial and marine plants, including wheat, rice, horsetails, oats, barley, grasses, and algae. Among bio-wastes, one of the most silica-rich sources is rice husks, which is largely available, typically 20–22 wt% of rice grains. It is been used by Deng et al. [126] for layered silicates synthesis. Layered silicates (LSs) have hydrophilic characteristics owing to the presence of inorganic cations (Na^+ and Ca^{2+}) in the interlayer spacing; hence, they are miscible with different hydrophilic polymers, including starch and pectin, able to compensate their rheological property differences [100].

Despite not being recovered from vegetables wastes, Cokaygil et al. [100] used LSs as natural filler to prepare biocomposite films having corn starch and pectin extracted from orange peels as a polymeric matrix. Different pectin jelly-to-starch weight ratios (63/37, 60/40, 57/43, and 54/46 *w/w*) were considered when formulating the film ingredients. Furthermore, to enhance the compatibility and wettability among starch, LS, and pectin, starch and LSs were chemically modified through reaction with propylene oxide and hexadecyltrimethylammonium chloride, respectively. Among all the films considered, pectin jelly/modified starch-based biocomposite film (54/46 *w/w*) containing 0.25 wt % of LSs was found to be the most promising in terms of texture structure and mechanical integrity.

In the most recent years, wastes of agro-food industries have attracted attention also as sources of natural fibers exploitable as reinforcing elements of biodegradable biocomposite materials. Bio fibers, which are natural polymers, could be obtained from a large variety of fruits and vegetables [127], thus reflecting several characteristic properties unlike conventional fibers. Undoubtedly, conventional fibers for instance glass, carbon, and aramid can be produced with a definite range of properties, with a higher cost as well. In 2013, Schettini et al. [105] developed a novel biocomposite by using hemp and tomato peels and seeds fibers as natural reinforcement for sodium alginate polymer, in order to produce biodegradable pots in agriculture. Three different compositions of biocomposites were prepared by varying the percentage of tomato and hemp fibers added to sodium alginate water solution. By soaking the doughs with a calcium chloride solution, a three-dimensional and stable crosslinked network of calcium alginate was obtained as well and it was subjected to investigation of its functionality, physico-chemical and mechanical behavior. As reported by the authors, by increasing the hemp fibers content, a general enhancement of the mechanical parameters of both un-crosslinked and crosslinked samples was registered, since fibers from hemp strands are more rigid, stiff, and long in comparison to the more flexible and short fibers from tomato peels and seeds [128]. Moreover, crosslinked biocomposites showed a lower rigidity and strength with respect to their corresponding un-crosslinked counterparts (Young Modulus for un-crosslinked 100% tomato fibers biocomposite was 63.62 MPa; while for crosslinked 100% tomato fibers biocomposite Young Modulus was 48.05 MPa). Such a behavior was due to the loss of adhesive properties, which occurs when carboxylated and hydroxyl groups of alginate are strongly engaged in physical interaction with calcium ions during the crosslinking process, thus reducing the bonding strength between the matrix and the fibers [129]. However, these obtained values were all comparable to those of conventional plastics. Instead, Mathivanan et al. [130] used different percentages of pineapple leaf fibers to reinforce tapioca based bioplastic resin through a method based on extrusion followed by hot compression molding. The 30% composition showed the best average modulus value

among other composition, leading to the conclusion that the increase of pineapple leaf fibers increases the modulus strength of the composite.

Since passion fruit waste contains about 60% of fibers [131] that, when dried, could be used as reinforcement of thermoplastic starch, Moro et al. [132] tried to develop an extruded starchy bioplastic, reinforced with different content of passion fruit peel (0, 4, 10, 16, and 20%), glycerol and starch mix, recovered from corn and cassava. In this way, it was possible to obtain starch-based bioplastic with stronger and midterm elastic property (Tensile strength ranged between 1.6 MPa and 9.0 MPa, while the elongation at break values were between 24.7% and 54.5%, see Table A1). Despite this, the tensile strength values were lower of oil-derived polymers.

On the other hand, bio-blend of poly-butylene succinate (PBS) and poly-butylene-adipate-co-terephthalate (PBAT) has been recently proved to be strengthened in terms of higher modulus (3.0 GPa) and lower water absorption (3.4%) with the addition of Miscanthus fiber and oat hull followed by reactive extrusion of the dough [133]. Indeed, PBS alone has a tensile strength of around 26.5 MPa, elongation of 21.5%, and a modulus of ~48 MPa. The incorporation of fiber or cellulose remarkably improves the Young's modulus of neat PBS.

For their rich content in lipids, lignin, and fibrous polysaccharide components (cellulose, hemicellulose), peanut hulls and cocoa shell waste (CW) and hazelnut skin (HS) extracts have also been introduced into synthetic elastomers matrices as reinforcement fillers and plasticizers [76,134,135]. Battagazzore et al. [76] made selective and serial extractions from CW and HS to recover bio-components for producing high-added value PLA and PP plastics. Briefly, a first extraction with diethyl ether mainly separated lipids, phospholipids, and triglycerides, which were worked as plasticizers. In the second extracted fractions, instead, phenolic compounds and flavonoids, such as gallic acid and catechin, were distinguished by UV spectroscopy; therefore, those fractions served as antioxidant and photo-stabilizer for PP. In addition, they positively influenced the PP thermal stability in air; indeed, the temperature of its maximum weight loss was increased from 319 °C to 330 °C and 345 °C by adding HS and CW extracts, respectively. Finally, the last fractions extracted acted as reinforcement filler for PLA and PP; their content linearly influenced the oxygen permeability of the obtained biomaterials (Table A1). Instead, Tran et al. [135] introduced cocoa shell waste powder within an acetoxy-poly(dimethylsiloxane) silicone network through a process that involved a physical mixing with a nontoxic solvent and casting into a mold, with the advantage of direct utilization of CW without any extraction or purification steps. In this case, the antioxidant activity of the final cross-linked bioelastomers was investigated, demonstrating very effective radical scavenging activity against 2,2-diphenyl-1-picrylhydrazyl free radical and 2,2'-azinobis(3-ethylbenzothiazoline-6-sulfonic acid) radical cation.

As PLA reinforcement, cellulose extracted from pumpkins peels, and subsequently acetylated, has also been used [136]. In this case, the addition of 10% of acetylated cellulose enhanced the PLA's mechanical properties with an increase of the storage modulus at 40 °C of around 40%. More generally, cellulose or cellulose nanocrystals have been obtained from various vegetable or fruit waste, such as banana peels, pine flowers waste, rice straw, palm empty fruit bunch, sago waste, mangosteen peels, and also successfully employed as reinforcements of biopolymers, mainly starch [103,137–141]. In addition, banana pseudostems waste has been recently used to isolate nanocellulose employed for the production of green composites enriched with nano-fillers, such as graphene oxide and nanoclay, and glycerol as plasticizer [91]. As regard to rice straw, besides being considered as reinforcement, its fibers were proved to act as flame-retardant fillers in combination with PLA and lignin by Dahy et al. [142]. Typically, flame retardant used to reduce combustibility of the polymers, are halogen-based additives that act in the vapor phase by a radical mechanism to interrupt the exothermic processes, interfering with the combustion process during heating, pyrolysis, ignition, or flame spread. Instead, a more environmentally friendly alternative that contemplates the incorporation of natural

fillers, like rice straw derived fibers, mainly acts to dilute the polymer and reduce the concentration of decomposition gases [143].

4. Environmental Impacts of Agro-Food Waste Based Bioplastics Production

Nowadays, fruit and vegetable valorization is one of the main pillars of the circular economy; their use to substitute fossil resources for the production of plastics, is a widely accepted strategy towards sustainable development. In fact, the displacing of conventional plastics with food waste-based bioplastics can lead to considerable energy and GHGs emissions savings [19]. However, it should be noted that this is not always true. Further details about advantages and drawbacks related to the bioplastics use and production are given in Table 2. Despite being promoted as a safer alternative to their oil-based counterparts, bioplastics production involves major drawbacks. Indeed, bioplastics are generally not cost-competitive compared to conventional plastics and their production is plagued by low yields and being expensive. Moreover, some bioplastics have a shorter lifetime than oil-based plastics due to weaker mechanical and physical properties, such as greater water vapor permeability than standard plastic, being easy to tear like tissue paper, or being very brittle. Being compostable and biodegradable sounds great, but many bioplastics must follow a specific disposal procedure and require industrial composting in order to avoid being incinerated or going to landfill. On the other hand, biodegradable polymers require a controlled fate to kickstart the expected biodegradation process and as a result, it is nearly impossible to control and ensure the complete degradation of even potentially degradable plastic materials. Subsequently, when they are disposed of in an uncontrolled fashion, they will accumulate in the environment and fragment into microplastics (MPs). These MPs have proven to display diverse impacts over ingested organisms and ecosystem similar to those of conventional MPs, thus bioplastics could be a solution to MPs only if properly disposed of [144].

Table 2. Main advantages and drawbacks related to the production and the use of bioplastic materials.

	Advantages	Drawbacks
Production	Reduction of greenhouse gas emission; saving fossil fuels, possibility of using a local resource, less energy during the manufacturing cycle.	Use of croplands to produce items, not cost-competitive compared to conventional plastics
Use	No toxic, no release of chemicals into food if used as packaging	Often characterized by thermal instability, brittleness, low melt strength, high water vapor and oxygen permeability; when hydrophilic polymers are used, they possess low water vapor barrier and vulnerability to degradation.
Disposal	Biodegradable; broken down by naturally occurring bacteria; do not persist for many years in the environment.	Controlled fate in order to kickstart the expected biodegradation process; a specific disposal procedure must be followed to avoid they fragment into microplastics which accumulate in the environment.

As a matter of fact, the employment of fruits and vegetables waste as reinforcement of non-biodegradable polymers in drop-ins significantly increases the energy demand and CO₂ emission compared to biodegradable bioplastics [145].

Therefore, when the aim is the production of new bioplastic materials from agro-food waste, the effective sustainability of the process should be evaluated. The sustainability of bio-based plastics production depends on several factors that are often summarized in the life cycle assessments (LCAs) of the products [146]. Among them, there are availability of commercially viable quantities of renewable feedstock and agricultural waste, scalable and green production routes, cost and competition with synthetic polymers, and useful life and biodegradation/end of life treatment [21]. Many of these aspects are very often not

sufficiently deepened, thus making it difficult to assess environmental impacts associated with the agro-food waste-based bioplastics production.

The greenhouse gas emissions generated by food waste globally represent the third largest emitter in the world, thus any measure to reduce food waste, even to a small extent, may have a significant impact on overall environmental footprint [147]. However, even though the number of fruits and vegetable wasted every year are estimated to be around 484 million, the volume of waste produced does not predict the availability of agricultural waste for conversion into biomaterials. Indeed, a large quantity is employed in other competing applications such as bio-fertilizer and biogas production [148]. In addition, not all the routes proposed for obtaining bio-materials are applicable on a large scale, since sometimes they require extensive and advanced processing. This mainly concerns biocomposites production, which is often based on obtaining fillers and reinforcements, such as cellulose nanocrystals, through complex treatment of the agro-waste [103,122]. On the contrary, more feasible and scalable processes allow bioplastics production after chemical extraction of agro-polymers from the food waste stream. A low environmental impact is associated with this step, as no harsh chemicals, like pyridine and diethyl ether, are used for the production of PHA, and potential occupational hazards are covered.

Regarding the end of life of the agro-food waste = based bioplastics, reuse and recycling are preferred solutions to energy recovery or disposal. However, to date, for materials other than bio-PE or bio-PET, there is no recycling stream established yet [23]. An alternative is their composting, i.e., their aerobic biodegradation under controlled conditions of temperature, humidity, and aeration [72]. Compostability is a clear benefit of agro waste-based bioplastics compared to conventional plastics, resulting in the creation of more valuable compost.

5. Bioplastics Market

Currently, the number of bioplastics produced annually in all the world represents only about one percent of the 360 million tons of plastic materials produced globally. However, due to the growing sensitivity towards the adoption of a “green and circular economy” dependent policy, the global bioplastics production capacity is set to increase from around 2.11 million tons in 2019 to approximately 2.43 million tons in 2024 [23].

With a view to regional capacity development, Asia remains a major production hub with over 50 percent of bioplastics currently being produced there. Presently, only one-fifth of the production capacity is located in Europe. This share is predicted to grow to up to 27 percent by 2023. The expected growth will be supported by recently adopted policies in several European Member States, such as Italy and France.

Innovative biopolymers, such as bio-based PP, bio-based PET, bio-based PA, and PHAs continue to drive the growth in bioplastic production. To date, they make up for 40 percent (0.8 million tons) of the global bioplastics production capacities. Bioplastics materials are currently used in an increasing number of markets: From packaging, catering products, consumer electronics, automotive, agriculture/horticulture, and toys to textiles. Among these several market segments, electronics is the less developed (only about 2% of the global bioplastic production concerns this segment), while packaging remains the largest field of application for bioplastics since around 54% of the global bioplastic production is used to serve the packaging industry, including shopping bags producers, plastic bottles producers, and food packaging industry [23].

Biodegradable shopping bags are made of polymers that degrade, or decompose, when exposed to air, water, or sunlight. There are three main types of biodegradable bags, i.e., (1) biodegradable bags made from resins containing starches, polyethylene, and heavy metals such as cadmium, lead, and beryllium, (2) biodegradable bags made by using starches combined with biodegradable polymers such as PLA, and (3) oxo-biodegradable bags, which use Totally Degradable Plastics Additives (TDPA) to stimulate the breakdown of polymers and thus speed up the biodegradation process of conventional plastics.

As regard to food packaging, in the USA premarketing approval by the Food and Drug Administration is required to ensure that materials are wholesome, safe, and effective [149]. On the other hand, in Europe, food contact materials regulations sets specific manufacturing goals to assure a good quality control system and specifies the thresholds according to the form and composition of polymers, which shall explicitly be authorized in order to preserve food safety (European Commission, 2006; European Commission 2011). Anyway, biobased materials are mostly used to pack short shelf-life products or long shelf-life ones, which do not need very high oxygen and/or water barrier properties, such as fresh fruits, vegetables, pasta, and chips [150]. Actually, biomaterials available show such a wide range of properties, that they are also applicable as packaging materials for other food products, which request stricter conditions, like Modified Atmosphere Packaging (MAP).

Bioplastic materials also offer several advantages in the agriculture sector. Eight percent of the global production of bioplastics is covered by the agriculture and horticulture segment. Examples of bio-based products used in agriculture are mulching films and pots [105,151]. Soil mulching is a practice used in cultivation, which allows weed suppression, reduces the loss of moisture from the soil, and may promote the increasing of soil temperature. Ploughing-in of bio-based and biodegradable mulching films after use instead of collecting them from the field and cleaning off the soil is a more practical and time saving solution. In the same way, bio-based pots are used.

For the automotive field, instead, components made completely or partially from bioplastics can provide a safety standard, that is of ultimate importance in the transportation sector. The products include seat and airbag covers as well as steering wheels. Some of the bio-based plastics such as bio-based polyamides and bio-based polyesters are already successfully being used by leading automotive brands around the world today with the aim of reducing their products' environmental impact. For example, Toyota typically uses bio-based polypropylene/poly(lactic acid) (PP/PLA) composite derived from plant materials for the realization of up to 60% of the interior design of cars.

Biopolymers find applications in several housewares, such as kitchen tools and utensils, washable storage containers and cups, bathroom accessories, toys, hangers, and hooks. For example, hangers from United Colors of Benetton are made of biodegradable polymers. Nontoxic biodegradable polymers are also being used as sutures by surgeons in life-saving heart operations and other procedures. Easily sterilized, the sutures remain strong and intact until the surrounding tissues have healed. The sutures dissolve and are readily metabolized in the body leaving no trace. Moreover, there has been a surge of bioplastic products that are being introduced in the fast-moving consumer electronics sector, such as touch screen computer casings, loudspeakers, keyboard elements, mobile casings, vacuum cleaners, and a mouse for a laptop. SUPLA produced the first bioplastic touch screen computer by using PLA, in collaboration with a Taiwanese company (Kuender).

To date, a lot of companies have been identified as key players in the production of bioplastics and their distribution witnesses that the majority of them are located in Europe. Many of these companies produce sustainable bioplastics made from plant-based renewable resources, like corn, potatoes, and wheat. The land used to grow the renewable feedstock for the production of bioplastics is estimated to be 0.7 million hectares in 2021 and continues to account for 0.015 percent of the global agricultural area of 4.7 billion hectares. Despite the market growth predicted in the next five years, the land use share for bioplastics will only slightly increase to 0.02 percent.

Novamont SpA (www.novamont.com) is one of the major starch bioplastics producers. The trade name of their starch-based bioplastic is "Mater-Bi" and it is provided for a wide range of manufacturers, which use it to make bags, mulching film, disposable tableware, and packaging. Furthermore, Amynova Polymers GmbH (www.amynova.com) is engaged in the production of a starch-based substance named "CropCover". CropCover is an innovative "adhesive" non-toxic, non-combustible, and fully biodegradable applied together with pesticides and foliar fertilizers, in order to reduce their rinsing during heavy rainfall and to guarantee a longer stay time on the plant. Biotec Biologische Naturverpackungen

GmbH & Co. KG (www.biotec.de) and Cardia Bioplastics (www.cardiabioplastics.com) produce and sell a new generation of customized thermoplastic materials too, with various functional properties fully biodegradable and compostable according to EN 13432. Moreover, there are companies that exploit waste as feedstock for bioplastics production; an example is NaturePlast (www.natureplast.eu). Since 2015, NaturePlast has been producing and marketing a range of biocomposites consisting of by-products and plant fibers (such as hemp), sourced mostly from the French territory. The objective is to incorporate by-products or local waste materials in different polymers to ensure a circular economy and the reclamation of waste materials.

6. Conclusions

The valorization of food waste (FW) can create opportunities to produce new valuable bioplastics, which represent an eco-friendly alternative to conventional petroleum-based plastics. Bioplastics produced from fruits and vegetables waste are compatible with the “circular economy”, therefore with “zero waste” or more precisely aiming at a complete use of it; moreover, they could create positive synergies between industry and the agro-food sector, with considerable advantages for environmental pollution. This review highlights that the real challenge is to create new eco-friendly materials from food waste and not from specially grown crops, whose production comes at an environmental cost. As the FW potential as raw material for bioplastics production is well known, such a novel perspective focusing on the overall methods used for the design of biomaterials starting from both fruits and vegetables wastes, provided in this review, should be particularly helpful in the fields of the green chemistry and of the environmental sciences.

Author Contributions: Conceptualization, M.A.A.; investigation, M.A.A.; writing—original draft preparation, M.A.A.; review and editing, R.P.; supervision, G.M., M.B., and G.B. All authors have read and agreed to the published version of the manuscript.

Funding: This research received no external funding.

Informed Consent Statement: Not applicable.

Data Availability Statement: Data sharing not applicable.

Conflicts of Interest: The authors declare no conflict of interest.

Appendix A

Table A1. Fruits and vegetables wastes used in the last 10 years as raw material for the production of bioplastics. A full description of the methods used for the production of bioplastics (Technology and pre-treatment of the waste, processing), as well as the main physical and mechanical properties of the obtained materials are provided.

Food Waste Source	Technology and Pre-Treatment	Processing	Bioplastic Type	Bioplastic Mechanical and Physical Properties	Reference
Apple pomace	Apple pomace, either washed with water or not, was powdered. A mixture was prepared containing 2% (<i>w/v</i>) of powder and 7% glycerol (<i>w/w</i> of apple pomace powder) and dissolved in 1% (<i>w/v</i>) of citric acid solution under heating (70 °C) and constant magnetic stirring at 560 rpm. Then, the mixture was poured onto a non-sticky plate for casting. A mixture without glycerol was also used in order to prepare a biofilm.	Casting	Pectin based biofilm	Tensile strength (MPa): 3.27–16.49 Elongation at break: 10.77–55.41%	Gustaffson et al. [88]
	Apple pomace, either washed with water or not, was powdered. A mixture was prepared containing glycerol and apple pomace powder (70:30) was prepared. 40 g of the mixture was placed into a mold. A pressure of 8 MPa was applied for 20 min at 100 °C.	Molding	Pectin based 3D biomaterial	Tensile strength (MPa): 3.02–5.79 Young's Modulus (MPa): 367.1–633.4 Elongation at break: 0.93–1.56%	Gustaffson et al. [88]
	Banana peels were boiled in water for about 30 min; then, they were left to dry and squashed to obtain a paste. 25 g of banana paste were placed in a beaker with 3 mL of HCl (0.1 N) and 2 mL of glycerol and stirred. Subsequently, NaOH (0.1 N) was added in order to neutralize the pH up to 7.	Casting	Cellulose based biofilm	Weight loss after 13 days: 0.04 g Difference of weight after swelling test (g): 0.01–0.10	Yaradoddi et al. [89]
Banana peels and pseudostems	Banana peels were washed, sliced, and blended. Then, they were grounded and ground sample was heated at 150 °C for 2 h at 30 psi. The obtained paste was hydrolyzed (100 mL/50 g sample) by (HCl, 99%). The sample was filtrated and washed with water. 1000 g of sample were mixed with chlorinated paraffin liquid plasticizers (1:8 of sample), 5% acetic acid (5 mL/100 g sample), 5 mL/100 g of polyvinylchloride, cellulose (25%) and 25% starch powder, 5% toluene Phthalates ester and 10% water. Then, 10 mL/100 g of PVC and glycerine were added. The mixture was heated at 150 °C in the oven for 30 min at 30 psi pressure.	Casting	Biocomposite	Tensile strength (MPa/kg·m ³): 120.0 Tensile modulus (GPa): 1.1 Water absorption: 0.03%	Sharif Hossain et al. [139]

Table A1. Cont.

Food Waste Source	Technology and Pre-Treatment	Processing	Bioplastic Type	Bioplastic Mechanical and Physical Properties	Reference
	Banana peels were immersed in a Na ₂ S ₂ O ₅ solution (1% w/v) for 24 h, oven-dried at 60 °C and milled. 100 g of milled peels were washed three times with ethanol, then washed in 200 mL of acetone. The pectin was extracted with a citric acid solution at pH 2.0 at 87 °C for 160 min and then centrifuged. The supernatant pH was adjusted to 3.5 with KOH, added with ethanol, stirred for 30 min and left to precipitate at 4 °C. The pellet was washed with ethanol 70%, and dried at room temperature. Then, it was stirred and its pH adjusted to 7, and it was again dried and milled. For the extraction of cellulose nanocrystals (CNCs), the alcohol insoluble residue of banana peels was suspended in a mixture of 93 wt% acetic acid and 0.3 wt% HCl in distilled water. Subsequently, the pulp was rinsed and washed in more steps and an acid hydrolysis was conducted with a 30 v% H ₂ SO ₄ solution at 45 °C, for 150 min. After centrifugation-dilution-sonication cycles, the CNC suspension was dialyzed against deionized water. CNCs (at different wt%), 4.5 g of pectin, 1.35 g glycerol, citric acid, and distilled water were mixed to form biofilms.	Casting	Pectin based biofilm	Tensile strength (MPa) without citric acid: 7.36 ± 1.15 Tensile strength (MPa) with citric acid: 7.92 ± 1.21 Elongation at break (%)without citric acid: 4.69 ± 0.84 Elongation at break (%)with citric acid: 4.26 ± 0.77 Elastic modulus (MPa)without citric acid: 1586 ± 487 Elastic modulus (MPa)with citric acid: 1714 ± 452 Water vapor permeability(g·mm·kPa ⁻¹ ·h ⁻¹ ·m ⁻²) without citric acid: 3.31 ± 0.36 Water vapor permeability(g·mm·kPa ⁻¹ ·h ⁻¹ ·m ⁻²) with citric acid: 3.10 ± 0.33	Oliveira et al. [75]
	300 g of banana peels were dipped in acetic acid solution and then placed into a beaker containing 800 mL water and boiled for 30 min. The water was decanted off and the peels were left to dry. The banana peels were pureed. To 25 mL of the paste, 3 mL of 0.5 M HCl and 2 mL of 15% glycerol solution were added. The mixture was stirred, 3 mL of 1% corn starch and 3 mL of 0.5 M NaOH were added to the mixture and stirred again.	Casting	Starch based biofilm	Tensile strength (N/m ²): 12.22–34.72 Water uptake: 60.65–108.98%	Sultan et al. [90]

Table A1. Cont.

Food Waste Source	Technology and Pre-Treatment	Processing	Bioplastic Type	Bioplastic Mechanical and Physical Properties	Reference
	Banana pseudostem was sliced, dryer at 50 °C for 5 h and milled. Then, 10 g of pseudo-stem flour were soaked in 300 mL of 5% KOH, centrifuged and bleached with 200 mL of 1% NaClO ₂ at pH 5 for 1 h in 70 °C. 9 g of the bleached pseudo-stem were mixed with TEMPO solution and 22.5 mL of 12% NaClO. At the end of the reaction, the mixture was homogenized and sonicated. Water containing 0.7% solid nanocellulose was mixed with glycerol, nano-clay or graphene oxide in different proportions.	Casting	Biocomposite	Tensile strength (MPa): ~5--~39 Elongation at break (%): ~1--~9 Oxygen permeability (mL/m ² *day*Pa): 2×10^{-6} – 3.5×10^{-6} Water vapor permeability (g/m ² *day*Pa): ~0.007--~0.023 Contact angle at 20 s (°): 21.89–75.03	Faradilla et al. [91]
	Banana peels were boiled for 60 min and then left to dry and blended. In order to obtain a chemical-based material, 100 g of banana paste were mixed with 12 mL of HCl, 8 mL of glycerol and 12 mL of NaOH. The mixture was stirred for 5 min. Alternatively, a natural-based material was obtained by mixing 40 g of banana peels paste with, 1 g of sage, 12 g of glycerol, 12 g of potato starch, 12 g of corn starch and 38 g of water. The mixture was dried using the oven at a temperature of 120 °C for 3–4 h.	Casting	Biocomposite	Tensile strength for chemical-based material (KPa): 228 Tensile strength for natural-based material (KPa): 150 Young's Modulus for chemical-based material (MPa): 1.53 Young's Modulus for natural-based material (MPa): 1.88 Elongation at break for chemical-based material: 18.77% Elongation at break for natural-based material: 13.97%	Azieyanti et al. [138]
	Banana peels were boiled in water for about 30 min. Water was decanted and the peels were left to dry and then they were squashed to obtain a uniform paste. 25 g of banana paste were mixed with 3 mL of (0.1 N) HCl, 2 mL of glycerol and then 3 mL of 0.1 N NaOH to neutralize the pH up to 7.	Casting	Starch based biofilm	Not reported	Rizwana Beevi et al. [113]

Table A1. Cont.

Food Waste Source	Technology and Pre-Treatment	Processing	Bioplastic Type	Bioplastic Mechanical and Physical Properties	Reference
Carrots waste	Carrots waste powder was dispersed in a 5% (<i>w/w</i>) HCl water solution at a concentration of 50 mg/mL under vigorous stirring at 40 °C. After 12 h, the viscous dispersion was dialyzed using a 3500 MWCO membrane against MilliQ water for 72 h and then cast on a petri dish.	Casting	Cellulose based biofilm	Young's Modulus (MPa): ~1300 Elongation at break: 6% Ultimate strength (MPa): ~37 Water contact angle: >100° Oxygen permeability (cm ³ μm/m ² day kPa): 96 × 10 ⁴	Perotto et al. [111]
Cassava peels	100 g of cassava peels were washed and soaked in sodium metabisulphite 1%. Then, they were crushed with 100 mL of water. Slurry resulted was extracted with water (ratio of 1:1) two times. The extracts were precipitated for 3 h. The precipitate was dried; then 5 g were mixed with glacial acetic acid 1%, chitosan (20–50%), glycerol (30%), liquid smoke (0–2 mL) and stirred at 70 °C.	Casting	Biocomposite	Tensile strength (MPa): 35.28–96.04 Elongation at break (%): 14.87–52.27 Water resistance (%): 22.68–78.40	Fathanah et al. [117]
	5.0 g of dried cassava peels waste were mixed with 1.5 mL of glycerol, 0.5 mL of kaffir lime essential oil and 0.7 g of citric acid. The mixture was stirred for 45 min, and heated to 80 °C. Two other samples were prepared without essential oil and without citric acid, respectively.	Casting	Starch based biofilm	Tensile strength (N/cm): 0.3–2.5	Masruri et al. [115]
Cauliflower waste	Cassava peels were mashed into a pulp. Then, 10 g were extracted with 50 mL of water. The extract was washed with water. Then, the juice precipitated and dried under direct sunlight to form a flour or starch. 3 g of starch were mixed with glycerol (25% wt) and chitosan (2 and 3% wt). The mixture was heated at a 80–90 °C and stirred.	Casting	Biocomposite	Tensile strength (Kgf/cm ²): 4.16–27.41 Elongation at break (%): 30.37–94.25	Dasumiati et al. [116]
	Cauliflower waste powder was dispersed in a 5% (<i>w/w</i>) HCl water solution at a concentration of 50 mg/mL under vigorous stirring at 40 °C. After 12 h, the viscous dispersion was dialyzed using a 3500 MWCO membrane against MilliQ water for 72 h and then cast on a petri dish.	Casting	Cellulose based biofilm	Young's Modulus (MPa): ~500 Elongation at break: 4% Ultimate strength (MPa): ~7 Water contact angle: ~80°	Perotto et al. [111]

Table A1. Cont.

Food Waste Source	Technology and Pre-Treatment	Processing	Bioplastic Type	Bioplastic Mechanical and Physical Properties	Reference
Citrus waste	Citrus peel derived pectin powder was mixed with glycerol (30% (w/w)) for 2 min to get a uniform dough which was then formed into ball shape (total weight of 2.5 g). The obtained blend was placed in molding press. The compression molding process was performed for 10 min under operation conditions of 1.33 MPa and 120 °C. Pectin-based biomass films were also produced by incorporation of lyophilized and milled fungal biomass. Biomass concentrations varied in the range of 0–35% of the total mixture. Glycerol content was kept at 30%.	Molding	Pectin based biofilm	Tensile strength (MPa) without fungal biomass: 15.7 ± 0.5 Elongation at break without fungal biomass (%): 5.5 ± 1.7 Young's Modulus (MPa) without fungal biomass: 298 ± 58 Tensile strength (MPa) with fungal biomass: 5.2–19.3 Elongation at break with fungal biomass (%): 1.4–4.5 Young's Modulus (MPa) with fungal biomass: 187–1350 Water Vapor Permeability Coefficient ($(\text{kg}\cdot\text{s}^{-1}\cdot\text{m}^{-1}\cdot\text{Pa}^{-1}) \times 10^{13}$) without fungal biomass: 7 Water Vapor Permeability Coefficient ($(\text{kg}\cdot\text{s}^{-1}\cdot\text{m}^{-1}\cdot\text{Pa}^{-1}) \times 10^{13}$) with fungal biomass: ~2–4	Gurram et al. [102]
Cocoa pod husks	Cocoa pod husks were washed to remove residual sugars and alcohols and then dried in an oven at 40 °C overnight. Solutions of 3% by weight of solids in TFA were prepared in glass vials. Vials were sealed with Parafilm and were placed in a benchtop lab shaker for 29 days. The obtained solution was centrifuged in order to remove any residuals. 100 g of milled cocoa by-products were placed in 400 g of diethyl ether under stirring at room temperature for 24 h. After evaporation, the supernatant gave a first residue. In addition, the solid residue was separated by filtration and, subsequently, underwent the second extraction with 400 g of ethanol under stirring at room temperature for 24 h. Once again, the supernatant was evaporated and the second residue was collected. The third residue was used as obtained after filtration.	Casting	Cellulose based biofilm	Tensile stress at break (MPa): 70 Water adsorption %: <10 (at a relative humidity <50%) Water adsorption %: >10 (at a relative humidity >80%) Initial decomposition temperature under 44% of relative humidity (°C): ~200	Bayer et al. [37]
		Extrusion	Biocomposite	Oxygen permeability [$\text{cc}\cdot\text{mm}/(\text{m}^2\cdot\text{bar}\cdot 24\text{ h})$]: 844–1104 for PLA and 982–5784 for PP Wettability (contact angle): $88 \pm 2^\circ$	Battegazzore et al. [76]

Table A1. Cont.

Food Waste Source	Technology and Pre-Treatment	Processing	Bioplastic Type	Bioplastic Mechanical and Physical Properties	Reference
	Cocoa shell waste (CSW) was grinded. The micronized CSW powder was added to 10 mL of heptane and stirred for 2 min. Then, the silicone (Elastosil E43) was added to the CSW dispersion and vigorously stirred for further 5 min to obtain a homogenous blend.	Casting	Biocomposite	Tensile strain at break %: 15–250 Young Modulus (MPa): 1.96 ± 0.13 – 10.67 ± 0.19 Water vapor permeability (g (m d Pa)^{-1}): $1.51 \cdot 10^{-5}$ – $14.93 \cdot 10^{-5}$ BOD saturation level ($\text{mg O}_2/\text{L}$): 36.1–38.2	Tran et al. [135]
Hazelnut skin	50 g of hazelnut skin were placed in 400 g of diethyl ether under stirring at room temperature for 24 h. After evaporation, the supernatant gave a first residue. In addition, the solid residue was separated by filtration and, subsequently, underwent the second extraction with 400 g of ethanol under stirring at room temperature for 24 h. Once again, the supernatant was evaporated and the second residue was collected. The third residue was used as obtained after filtration.	Melt-blending extrusion	Biocomposite	Oxygen permeability [$\text{cc} \cdot \text{mm}/(\text{m}^2 \cdot \text{bar} \cdot 24 \text{ h})$]: 11.7–1875 for PLA and 122–338 for PP Wettability (contact angle): $80 \pm 2^\circ$	Battegazzore et al. [76]
Hemp fibers	Dried hemp fibers were aggregated with tomato fibers in different percentages (100% tomato fibers, 90% tomato fibers, 70% tomato fibers). 50.0 g of the aggregated were soaked in 100 mL of a 2% (w/v) sodium alginate water solution.	Molding	Biocomposite	Young Modulus (MPa): 62.51–97.08 Tensile stress at break (MPa): 0.46–1.20 Maximum load (N) *: 8.7–14.8 Displacement (mm) *: 3.22–4.75 Water up-take percentage $W_{st}\%$: 128–186 Time for complete biodegradation: 16 days after the transplanting	Schettini et al. [105]
Jackfruit seeds	Jackfruit seeds were removed from the skin of the arrows and then washed and powdered. The obtained powder was mixed with sorbitol (from 0 to 6 mL) and poly vinyl alcohol (from 0 to 3 g).	Not specified	Not specified	Tensile strength (MPa): 0–~2.2 Elongation at break: 0–7%	Lestari et al. [93]

Table A1. Cont.

Food Waste Source	Technology and Pre-Treatment	Processing	Bioplastic Type	Bioplastic Mechanical and Physical Properties	Reference
Mangosteen peels	Mangosteen peels were sun dried for about 48 h at room temperature. Then, they were grinded and sieved. To prepare cellulose fibers, about 50 g of the Mangosteen peels powder were treated with 700 mL of 0.1 M NaOH, under heating and stirring. Then the insoluble pulp was bleached with 500 mL of NaOCl buffered to a pH 5 and washed with distilled water. The cellulose fibers were air dried. Then 10 g of fibers were hydrolyzed in 100 mL of 95% H ₂ SO ₄ at 500 °C, then diluted with distilled water, centrifuged and sonicated. The resulting suspension cellulose nanocrystals (CNCs) were dried in a freeze drier at 3 °C. CNCs were mixed in different wt% (0–19%) with 10 g of cassava starch, 60 mL of distilled water, 5 mL of vinegar and 7 mL of glycerol. The mixture was stirred at 105 °C up to 200 °C.	Casting	Biocomposite	Tensile strength (MPa): ~1.3~2 Young's Modulus (GPa): ~15~26 Elongation at break (%): ~15~23	Muhammad et al. [103]
Miscanthus	Chopped 2 mm miscanthus were dried at 80 °C for at least 24 h. They were mixed with oat hull and blends of PBS/PBAT (80/20) in the presence of peroxide (0.02 phr) with feeder at 100 rpm and 180 °C.	Extrusion	Biocomposite	Tensile strength with 20% Mischatus fiber (MPa): 1.0 Tensile strength with 40% Mischatus fiber (MPa): 1.0 Young's Modulus with 20% Mischatus fiber (MPa): 64 Young's Modulus with 40% Mischatus fiber (MPa): 404 Water absorption with 20% Mischatus fiber: 1–3% Water absorption with 40% Mischatus fibre: 1–7%	Wu et al. [133]

Table A1. Cont.

Food Waste Source	Technology and Pre-Treatment	Processing	Bioplastic Type	Bioplastic Mechanical and Physical Properties	Reference
Oat Hull	Chopped 2 mm oat hull were dried at 80 °C for at least 24 h. They were mixed with miscanthus and blends of PBS/PBAT (80/20) in the presence of peroxide (0.02 phr) with feeder at 100 rpm and 180 °C.	Extrusion	Biocomposite	Tensile strength with 20% oat hull (MPa): 0.4 Tensile strength with 40% oat hull (MPa): 0.29 Young's Modulus with 20% oat hull (MPa): 54 Young's Modulus with 40% oat hull (MPa): 257 Water absorption with 20% oat hull: 1–5% Water absorption with 40% oat hull: 2–9%	Wu et al. [133]
Orange peels	Dried orange peels were washed with a HCl (0.03 N) at 60 °C and agitated for 30 min. The residue was hydrolyzed with HCl (0.04 N) at 90 °C for 20 min. Then, pectin extraction was performed with hot water at 90 °C and agitated for 30 min. The obtained pectin jelly was mixed with corn starch, layered silicates, glycerol and water; the mixture was left overnight in an oven at 70 °C.	Extrusion followed by casting	Biocomposite	Equilibrium recoverable compliance (m ² /N): 3.71 × 10 ⁻⁹ Water vapor transmission rate (g/m ² h): 9.87 Oxygen gas transmission rate (mL/m ² day): 1366 ± 194	Cokajgil et al. [100]
	Orange waste (OW) was washed with water then dried for 16 h at 40 °C and milled to a fine powder. A mixture of 2% (w/v) of OW powder was prepared in 1% (w/v) citric acid solution under constant magnetic stirring at 70 °C. The acid solution also contained 7% (w/w) glycerol and 1 drop of organic antifoam/100 mL solution. The suspension was sieved before it was poured onto PTFE plates and dried at 40 °C.	Casting	Pectin and cellulose based biofilm	Tensile strengths (MPa): 28–36 Time for 90% degradation: 15 days	Batori et al. [92]
Palm empty fruit bunch	Palm empty fruit bunch was dried, powdered and cooked for 8 h at 80 °C. 10% NaOH solution was added and the mixture was autoclaved for 15 min at 121 °C. The obtained mixture was added with 10% sodium hypochlorite processed using ultrafine grinder in wet milling method. 2% cellulose was mixed with 2 L of water and passed through the grinder for up to 30 cycles until a nanocellulose gel was formed. 5% of the produced nanocellulose was introduced in the Enviplast [®] formula.	Extrusion	Biocomposite	Tensile strength (kgf/cm ²): 191.30 Elongation at break (%): 197.12 Water Vapour Transmission Rate (g/m ² /24 h): 299.42	Iriani et al. [140]

Table A1. Cont.

Food Waste Source	Technology and Pre-Treatment	Processing	Bioplastic Type	Bioplastic Mechanical and Physical Properties	Reference
Parsley stems	Parsley stems were washed to remove residual sugars and alcohols and then dried in an oven at 40 °C overnight. Solutions of 3% by weight of solids in TFA were prepared in glass vials. Vials were sealed with Parafilm and were placed in a benchtop lab shaker for 29 days. The obtained solution was centrifuged in order to remove any residuals.	Casting	Cellulose based biofilm	Tensile stress at break (MPa): 5 Water adsorption %: <10 (at a relative humidity <50%) Water adsorption %: >10 (at a relative humidity >80%) Initial decomposition temperature under 44% of relative humidity (°C): ~200	Bayer et al. [37]
	Parsley stems powder was dispersed in a 5% (w/w) HCl water solution at a concentration of 50 mg/mL under vigorous stirring at 40 °C. After 12 h, the viscous dispersion was dialyzed using a 3500 MWCO membrane against MilliQ water for 72 h and then cast on a petri dish.	Casting	Cellulose based biofilm	Young's Modulus (MPa): ~200 Elongation at break: 10% Ultimate strength (MPa): ~7 Water contact angle: ~60	Perotto et al. [111]
Passion fruit peels	Passion fruits peels were dried and milled to fine flour. A mixture of corn and cassava starches, 45 and 55%, respectively, was placed in a homogenizer and blended for 10 min with the passion fruit peel. 2000 g of the mix was processed by the extruder. For the plasticizer solutions (1 L for each treatment), different amounts of glycerol and water were prepared (60, 64, 70, 76, and 80% glycerol content). The extrudates were cut into 5-g pieces, placed between Teflon sheets, compressed, and molded at 5 ton and 90 °C for 30 s.	Extrusion followed by molding	Biocomposite	Tensile strength (MPa): 1.6–9.0 Elongation at break: 24.7–54.5% Young's Modulus (MPa): 2.4–29.9 Water vapor permeability (g·mm/m ² ·h·kPa): 0.256–0.436 Water solubility index: 50.4–68.3% Contact angle (°): 5.3–72.2	Moro et al. [132]
Peanut hulls	Peanut hulls, were stored at 4 °C, and then reduce to powder. The mixture including 17 g of peanut hulls mashed to a size of around 100 microns was blended minutes, gradually adding potato flour from skins (30 g), whole milk (48 mL) and glycerol (5 mL). The mixed ingredients formed a compound that was cooked in a fan-assisted oven at 180 °C for 13 min.	Casting	Biocomposite	Weight loss %: 6.5 ± 0.5	Troiano et al. [134]

Table A1. Cont.

Food Waste Source	Technology and Pre-Treatment	Processing	Bioplastic Type	Bioplastic Mechanical and Physical Properties	Reference
Pine flower waste	Pine flowers were soaked water at 100 °C for 2 h, washed and dried for 24 h at 50 °C. Then, they were grounded and soaked in hot water for 4 h and roasted for 24 h at 60 °C. For cellulose isolation, 50 g of grounded pine flower were mixed with 500 mL of 6% NaOH at 70 °C for 4 h. After serial washing and filtration steps, 5 g of obtained cellulose were mixed with 10%, 30%, and 60% citric acid in 100 mL respectively and ultrasonicated. Then, a polyvinyl alcohol (PVA) solution was prepared by mixing 4% PVA, 25% glycerol, and 71% distilled water (<i>w/w</i>), and a starch solution by mixing 3% starch, 12% glycerol and 85% distilled water (<i>w/w</i>). Both solutions were mixed together (PVA: starch ratio of 80:20 (<i>w/w</i>)) and finally 1% nanocellulose, 10% turmeric extract and 10% natural dragon fruit extract were added.	Casting	Biocomposite	Not reported	Nasihin et al. [137]
Pineapple leaf	Pineapple leaf were scaffolded and then the fibers were cut into small sizes and grinded. The grinded fibers were then sieved to get the highest amount of fiber length available. Then they were placed in oven for 24 h and subsequently mixed with tapioca-based bioplastic resin (70–90% <i>w/w</i>). The mixture was first extruded into pellet at 160 °C. The pellets were then placed in the mold and hot pressed at 160 °C for 5 min at 8 MPa, and then cold pressed at room temperature for 5 min at 8 MPa.	Extrusion followed by molding	Biocomposite	Tensile Modulus (GPa): 1.029–1.145 Tensile strain (mm/mm): 0.007–0.011	Mathivanan et al. [130]
Potato peels	Potato peels were granulated and centrifuged at 15000 rpm for 20 min. The supernatant was filtered and the starch was obtained. 13.5 g of dried starch was extracted from 330 g wet potato peels. After filtration, starch was dried at 50 °C for 2 h. 13.5 g of starch were mixed with 135 mL of tap water, 16.2 mL of vinegar, and 10.8 mL of glycerin. The mixture was heated (100 °C) and kept waiting at that temperature for 20 min.	Casting	Starch based biofilm	Water absorption: 48.46% within two hours and 83.57% within 24 h Time for complete biodegradation: 28 days in moist soil.	Arikan et al. [114]

Table A1. Cont.

Food Waste Source	Technology and Pre-Treatment	Processing	Bioplastic Type	Bioplastic Mechanical and Physical Properties	Reference
	Potato peels were boiled with water and then the starch was extracted from the water by filtration. The starch was mixed with glycerine, vinegar and water in different ratio, at 105 °C.	Casting	Starch based biofilm	Resistance to compressive stress (MPa): 0.5–1.1	Samer et al. [118]
Pumpkin peels	1 g of dry pumpkin peel residue was suspended in 50 mL of 2 wt% NaOH solution and stirred for 4 h at 100 °C. Then 80 mL of 0.5 M NaOH containing 2% (v/v) of H ₂ O ₂ per each gram of material were added. The solution was stirred during 1 h. Then, 20 mL of 2 M NaOH solution was added and the suspension stirred during 5 h at 55 °C. Subsequently, the residue was washed with distilled water until achieve neutral pH. Finally, the residue was filtered and dried. 12 mL of [(BMIM)Cl] was used per each 0.25 g of material to dissolve cellulose. The isolated cellulose was acetylated and 0.02 g were added to a solution of PLA (0.18 g) in DCM (25 mL). The mixture was stirred for 1 h, at 50 °C and then it was casted.	Casting	Biocomposite	Storage Modulus (GPa): 1.85 at 40 °C	Coto et al. [136]
Radicchio waste	Radicchio waste powder was dispersed in a 5% (w/w) HCl water solution at a concentration of 50 mg/mL under vigorous stirring at 40 °C. After 12 h, the viscous dispersion was dialyzed using a 3500 MWCO membrane against MilliQ water for 72 h and then cast on a petri dish.	Casting	Cellulose based biofilm	Young's Modulus (MPa): ~200 Elongation at break: 5% Ultimate strength (MPa): ~5 Water contact angle: ~80°	Perotto et al. [111]
Rice straw and hulls	Rice hulls were washed to remove residual sugars and alcohols and then dried in an oven at 40 °C overnight. Solutions of 3% by weight of solids in TFA were prepared in glass vials. Vials were sealed with Parafilm and were placed in a benchtop lab shaker for 29 days. The obtained solution was centrifuged in order to remove any residuals.	Casting	Cellulose based biofilm	Tensile stress at break (MPa): 7 Water adsorption %: <10 (at a relative humidity <50%) Water adsorption %: >10 (at a relative humidity >80%) Initial decomposition temperature under 44% of relative humidity (°C): ~225	Bayer et al. [37]

Table A1. Cont.

Food Waste Source	Technology and Pre-Treatment	Processing	Bioplastic Type	Bioplastic Mechanical and Physical Properties	Reference
	200 g of dried rice straw samples were placed in a solid-liquid extractor with 1 L of Milli-Q water. Total extraction was performed for approximately 3 h and with 30 cycles and 12 strikes per cycle and the static phase for 10 min. Then, 10 g of the powdered and dried rice straw, previously washed and dried, was mixed with 200 mL of TFA and maintained under magnetic stirring (800 rpm) at room temperature for 3 days and, poured into a low edge crystallizing container maintained under laminar hood.	Casting	Cellulose based biofilm	Tensile strength at break (MPa): 45 (dried dumbbells) Elongation at break (%): 6.1 (dried dumbbells) Tensile strength at break (MPa): 10 (wet dumbbells) Elongation at break (%): 63 (wet dumbbells) Water adsorption %: 40.7–42.6 Time for complete biodegradation: 105 days in soil.	Bilo et al. [110]
	Rice straw was dried, powdered and cooked for 8 h at 80 °C. 10% NaOH solution was added and the mixture was autoclaved for 15 min at 121 °C. The obtained mixture was added with 10% sodium hypochlorite processed using ultrafine grinder in wet milling method. 2% cellulose was mixed with 2 L of water and passed through the grinder for up to 30 cycles until a nanocellulose gel was formed. 5% of the produced nanocellulose was introduced in the Enviplast® formula.	Extrusion	Biocomposite	Tensile strength (kgf/cm ²): 168.36 Elongation at break (%): 156.36 Water Vapour Transmission Rate (g/m ² /24 h): 301.06	Iriani et al. [140]
	Rice straw were chopped to prepare the fibres with lengths ranging from 0.5 to 2 mm. The fibers were dehydrated for 24 h within a vacuum oven at 105 °C. Three chosen polymers (PLA, Lignin, PP) were separately compounded with 20% of rice straw fiber.	Extrusion	Biocomposite	Not reported	Dahy et al. [142]
	Rice waste powdered. The powder of rice waste was mixed with chitosan (from 30 to 60%) and glycerol (from 0 to 3 mL), heated at 50–60 °C for 30 min.	Molding	Cellulose based biofilm	Tensile strength (MPa): ~0–60 Elongation at break: 2–4% Water resistance: 0.1–0.6%	Lestari et al. [93]

Table A1. Cont.

Food Waste Source	Technology and Pre-Treatment	Processing	Bioplastic Type	Bioplastic Mechanical and Physical Properties	Reference
Sago waste	Sago waste was soaked in hot water at 40 °C for 2 h and air dried. The sago waste was then treated with 2% NaOH aqueous solution at 60 °C for 1 h, filtered and washed. The samples were dried at 40 °C. The obtained fibers were bleached with NaClO ₂ /glacial CH ₃ COOH mixture at 80 °C. Then, they were washed with distilled water and dried at 60 °C. The cellulose fibers were dissolved in 10 mL of distilled water, stirred, ultrasonicated for 30 min and, subsequently, mixed with a sago starch 4% (<i>w/w</i>) solution.	Casting	Biocomposite	Tensile strength (MPa):86.66–123.03 Young's Modulus (MPa): 1710–2958 Elongation at break (%): 3.85–4.62 Water absorption (%): ~100--~200	Yacob et al. [141]
Soy waste	Soy waste was bleached with a solution of distilled water:sodium hypochlorite (70:30). Then, it was separated from the solvent, rinsed with distilled water and dried in the oven for one hour at 100 °C. Subsequently, it was powdered and 3.0 g were mixed with corn starch (9.5 g), glycerol (5 mL), vinegar (5 mL) and water (60 mL). The mixing process was carried out at 25 °C and 50 rpm for 10 min.	Casting	Biocomposite	Maximum value of force before fracture (N): 6.71 Water absorption (%): 114.17	Muhammad et al. [119]
Spinach steams	Spinach steams were washed to remove residual sugars and alcohols and then dried in an oven at 40 °C overnight. Solutions of 3% by weight of solids in TFA were prepared in glass vials. Vials were sealed with Parafilm and were placed in a benchtop lab shaker for 29 days. The obtained solution was centrifuged in order to remove any residuals.	Casting	Cellulose based biofilm	Tensile stress at break (MPa): 1 Water adsorption %: <10 (at a relative humidity <50%) Water adsorption %: >10 (at a relative humidity >80%) Initial decomposition temperature under 44% of relative humidity (°C): ~130	Bayer et al. [37]
Tea leaves waste	Tea leaves waste were dried under vacuum at 70 °C, grounded, and sifted. Tea waste powder (TW) was dried under vacuum at 70 °C. TW bioplastics were synthesized with 1 g of TW powder in 20 mL of 3% citric acid solution (TW-CA) or only with water (TW-H ₂ O). Carboxymethylcellulose sodium salt at 5% was investigated also as an additive to TW bioplastics (TW-CMC). All samples were magnetically stirred in an oil bath at 60 °C for 12 h, then casted.	Casting	Cellulose based biofilm	Ultimate tensile strength (MPa): 2--~6 Elongation at break: 0.5%--~13% Water contact angles (°): ~40--~120	Liu et al. [112]

Table A1. Cont.

Food Waste Source	Technology and Pre-Treatment	Processing	Bioplastic Type	Bioplastic Mechanical and Physical Properties	Reference
Tomato waste	After the extraction of polysaccharides, carotenoids and polyphenols from peels and seeds, the residual dried fibers were combined with hemp fibers in different percentages (0% hemp fibers, 10% hemp fibers, 30% hemp fibers). 50.0 g of the aggregated fibers were soaked in 100 mL of a 2% (<i>w/v</i>) sodium alginate water solution.	Molding	Biocomposite	Young Modulus (MPa): 62.51–97.08 Tensile stress at break (MPa): 0.46–1.20 Maximum load (N) *: 8.7–14.8 Displacement (mm) *: 3.22–4.75 Water up-take percentage W _{st} %: 128–186 Time for complete biodegradation: 16 days after the transplanting	Schettini et al. [105]
	Tomato pomace was subjected to alkaline hydrolysis (100 °C for 6 h with a NaOH 0.5 M solution in water) to obtain cutin monomers. The supernatant was discarded and the resulting solution was acidified with HCl 3 M up to final pH 3. 80.0 mg of tomato pomace monomers were blended with tin (II) 2-ethylhexanoate; the mixtures were placed on open carbon-doped Teflon molds and heated in air inside a convention oven.	Melt polycondensation	Aliphatic polyester	Young Modulus (MPa): 14–214 Hardness (MPa): 1.8–26.3 Water contact angle: 81°–109° Water up-take percentage: 2.1–6.1%	Heredia-Guarreiro et al. [124]

References

1. Plastics Europe An Analysis of European Plastics Production, Demand and Waste Data. Available online: https://www.plasticseurope.org/application/files/9715/7129/9584/FINAL_web_version_Plastics_the_facts2019_14102019.pdf (accessed on 6 April 2020).
2. Lee, A.; Liew, M.S. Ecologically derived waste management of conventional plastics. *J. Mater. Cycles Waste Manag.* **2020**, *22*, 1–10. [[CrossRef](#)]
3. Wright, S.L.; Kelly, F.J. Plastic and Human Health: A Micro Issue? *Environ. Sci. Technol.* **2017**, *51*, 6634–6647. [[CrossRef](#)] [[PubMed](#)]
4. Amodeo, C.; Sofo, A.; Tito, M.T.; Scopa, A.; Masi, S.; Pascale, R.; Mancini, I.M.; Caniani, D. Environmental factors influencing landfill gas biofiltration: Lab scale study on methanotrophic bacteria growth. *J. Environ. Sci. Health Part A* **2018**, *53*, 825–831. [[CrossRef](#)] [[PubMed](#)]
5. Caniani, D.; Caivano, M.; Pascale, R.; Bianco, G.; Mancini, I.M.; Masi, S.; Mazzone, G.; Firouzian, M.; Rosso, D. CO₂ and N₂O from water resource recovery facilities: Evaluation of emissions from biological treatment, settling, disinfection, and receiving water body. *Sci. Total Environ.* **2019**, *648*, 1130–1140. [[CrossRef](#)] [[PubMed](#)]
6. Caivano, M.; Pascale, R.; Mazzone, G.; Buchicchio, A.; Masi, S.; Bianco, G.; Caniani, D. N₂O and CO₂ Emissions from secondary settlers in WWTPs: Experimental results on full and pilot scale plants. In *Lecture Notes in Civil Engineering*; Springer: Cham, Switzerland, 2017; pp. 412–418.
7. Caivano, M.; Pascale, R.; Mazzone, G.; Masi, S.; Panariello, S.; Caniani, D. Disinfection unit of water resource recovery facilities: Critical issue for N₂O Emission. In *Lecture Notes in Civil Engineering*; Springer: Cham, Switzerland, 2017; pp. 444–450.
8. Pascale, R.; Caivano, M.; Buchicchio, A.; Mancini, I.M.; Bianco, G.; Caniani, D. Validation of an analytical method for simultaneous high-precision measurements of greenhouse gas emissions from wastewater treatment plants using a gas chromatography-barrier discharge detector system. *J. Chromatogr. A* **2017**, *1480*, 62–69. [[CrossRef](#)] [[PubMed](#)]
9. Bradney, L.; Wijesekara, H.; Palansooriya, K.N.; Obadamudalige, N.; Bolan, N.S.; Ok, Y.S.; Rinklebe, J.; Kim, K.H.; Kirkham, M.B. Particulate plastics as a vector for toxic trace-element uptake by aquatic and terrestrial organisms and human health risk. *Environ. Int.* **2019**, *131*, 104937. [[CrossRef](#)]
10. Hahladakis, J.N.; Velis, C.A.; Weber, R.; Iacovidou, E.; Purnell, P. An overview of chemical additives present in plastics: Migration, release, fate and environmental impact during their use, disposal and recycling. *J. Hazard. Mater.* **2018**, *344*, 179–199. [[CrossRef](#)]
11. Lots, F.A.E.; Behrens, P.; Vijver, M.G.; Horton, A.A.; Bosker, T. A large-scale investigation of microplastic contamination: Abundance and characteristics of microplastics in European beach sediment. *Mar. Pollut. Bull.* **2017**, *123*, 219–226. [[CrossRef](#)]
12. Okunola, A. A.; Kehinde, I. O.; Oluwaseun, A.; Olufiropo, E. A. Public and Environmental Health Effects of Plastic Wastes Disposal: A Review. *J. Toxicol. Risk Assess.* **2019**, *5*, 1–13. [[CrossRef](#)]
13. Gu, F.; Guo, J.; Zhang, W.; Summers, P.A.; Hall, P. From waste plastics to industrial raw materials: A life cycle assessment of mechanical plastic recycling practice based on a real-world case study. *Sci. Total Environ.* **2017**, *601–602*, 1192–1207. [[CrossRef](#)]
14. Yates, M.R.; Barlow, C.Y. Resources, Conservation and Recycling Life cycle assessments of biodegradable, commercial biopolymers—A critical review. *Resour. Conserv. Recycl.* **2013**, *78*, 54–66. [[CrossRef](#)]
15. Kumar, S.; Thakur, K. Bioplastics-classification, production and their potential food applications. *J. Hill Agric.* **2017**, *8*, 118. [[CrossRef](#)]
16. Polman, E.M.N.; Gruter, G.J.M.; Parsons, J.R.; Tietema, A. Comparison of the aerobic biodegradation of biopolymers and the corresponding bioplastics: A review. *Sci. Total Environ.* **2021**, *753*, 141953. [[CrossRef](#)] [[PubMed](#)]
17. Brodin, M.; Vallejos, M.; Opedal, M.T.; Area, M.C.; Chinga-Carrasco, G. Lignocellulosics as sustainable resources for production of bioplastics—A review. *J. Clean. Prod.* **2017**, *162*, 646–664. [[CrossRef](#)]
18. Karan, H.; Funk, C.; Grabert, M.; Oey, M.; Hankamer, B. Green Bioplastics as Part of a Circular Bioeconomy. *Trends Plant Sci.* **2019**, *24*, 237–249. [[CrossRef](#)]
19. Tsang, Y.F.; Kumar, V.; Samadar, P.; Yang, Y.; Lee, J.; Ok, Y.S.; Song, H.; Kim, K.H.; Kwon, E.E.; Jeon, Y.J. Production of bioplastic through food waste valorization. *Environ. Int.* **2019**, *127*, 625–644. [[CrossRef](#)]
20. Gowman, A.C.; Picard, M.C.; Lim, L.T.; Misra, M.; Mohanty, A.K. Fruit waste valorization for biodegradable biocomposite applications: A review. *BioResources* **2019**, *14*, 10047–10092. [[CrossRef](#)]
21. Maraveas, C. Production of sustainable and biodegradable polymers from agricultural waste. *Polymers* **2020**, *12*, 1127. [[CrossRef](#)]
22. Matheus, J.R.V.; Miyahira, R.F.; Fai, A.E.C. Biodegradable films based on fruit puree: A brief review. *Crit. Rev. Food Sci. Nutr.* **2020**, *1–8*. [[CrossRef](#)]
23. European Bioplastics Bioplastics Facts and Figures. Available online: https://docs.european-bioplastics.org/publications/EUBP_Facts_and_figures.pdf (accessed on 6 April 2020).
24. Janssen, L.P.B.M.; Moscicki, L. *Termoplastic Starch: A Green Material for Various Industries*, 1st ed.; Janssen, P.B.M., Moscicki, L., Eds.; Wiley-VCH Verlag GmbH & Co. KGaA: Weinheim, Germany, 2009; ISBN 9780470146835.
25. Reddy, R.L.; Reddy, V.S.; Gupta, G.A. Study of Bio-plastics As Green & Sustainable Alternative to Plastics. *Int. J. Emerg. Technol. Adv. Eng.* **2013**, *3*, 76–81.
26. Emadian, S.M.; Onay, T.T.; Demirel, B. Biodegradation of bioplastics in natural environments. *Waste Manag.* **2017**, *59*, 526–536. [[CrossRef](#)]

27. Ross, G.; Ross, S.; Tighe, B.J. Bioplastics: New Routes, New Products. In *Brydson's Plastics Materials*, 8th ed.; Elsevier: Oxford, UK, 2017; pp. 631–652. ISBN 9780323358248.
28. De Almeida Oroski, F.; Chaves Alves, F.; Bomtempo, V. Bioplastics Tipping Point: Drop-in or non-drop-in? *J. Bus. Chem.* **2014**, *11*, 42–50.
29. Xiao, B.; Zheng, M.; Pang, J.; Jiang, Y.; Wang, H.; Sun, R.; Wang, A.; Wang, X.; Zhang, T. Synthesis and Characterization of Poly(ethylene terephthalate) from Biomass-Based Ethylene Glycol: Effects of Miscellaneous Diols. *Ind. Eng. Chem. Res.* **2015**, *54*, 5862–5869. [[CrossRef](#)]
30. Chen, L.; Pelton, R.E.O.; Smith, T.M. Comparative life cycle assessment of fossil and bio-based polyethylene terephthalate (PET) bottles. *J. Clean. Prod.* **2016**, *137*, 667–676. [[CrossRef](#)]
31. Volanti, M.; Cespi, D.; Passarini, F.; Neri, E.; Cavani, F.; Mizsey, P.; Fozer, D. Terephthalic acid from renewable sources: Early-stage sustainability analysis of a bio-PET precursor. *Green Chem.* **2019**, *21*, 885–896. [[CrossRef](#)]
32. Soták, T.; Schmidt, T.; Hronec, M. Hydrogenolysis of polyalcohols in the presence of metal phosphide catalysts. *Appl. Catal. A Gen.* **2013**, *459*, 26–33. [[CrossRef](#)]
33. Yang, L.; Yan, X.; Wang, Q.; Wang, Q.; Xia, H. One-pot catalytic conversion of cellulose into polyols with Pt/CNTs catalysts. *Carbohydr. Res.* **2015**, *404*, 87–92. [[CrossRef](#)] [[PubMed](#)]
34. Pang, J.; Zheng, M.; Sun, R.; Wang, A.; Wang, X.; Zhang, T. Synthesis of ethylene glycol and terephthalic acid from biomass for producing PET. *Green Chem.* **2016**, *18*, 342–359. [[CrossRef](#)]
35. Jain, R.; Kosta, S.; Tiwari, A. Polyhydroxyalkanoates: A way to sustainable development of bioplastics. *Chron. Young Sci.* **2010**, *1*, 10–15. [[CrossRef](#)]
36. Koller, M. Poly(hydroxyalkanoates) for Food Packaging: Application and Attempts towards Implementation. *Appl. Food Biotechnol.* **2014**, *1*, 3–15.
37. Bayer, I.S.; Guzman-Puyol, S.; Heredia-Guerrero, J.A.; Ceseracciu, L.; Pignatelli, F.; Ruffilli, R.; Cingolani, R.; Athanassiou, A. Direct transformation of edible vegetable waste into bioplastics. *Macromolecules* **2014**, *47*, 5135–5143. [[CrossRef](#)]
38. Sharma, S.; Luzinov, I. Water Aided Fabrication of Whey and Albumin Plastics. *J. Polym. Environ.* **2012**, *20*, 681–689. [[CrossRef](#)]
39. Jiménez-Rosado, M.; Zarate-Ramírez, L.S.; Romero, A.; Bengoechea, C.; Partal, P.; Guerrero, A. Bioplastics based on wheat gluten processed by extrusion. *J. Clean. Prod.* **2019**, *239*, 1–8. [[CrossRef](#)]
40. Zárte-Ramírez, L.S.; Romero, A.; Bengoechea, C.; Partal, P.; Guerrero, A. Thermo-mechanical and hydrophilic properties of polysaccharide/gluten-based bioplastics. *Carbohydr. Polym.* **2014**, *112*, 16–23. [[CrossRef](#)]
41. Luengo, J.M.; García, B.; Sandoval, A.; Naharro, G.; Olivera, E.R. Bioplastics from microorganisms. *Curr. Opin. Microbiol.* **2003**, *6*, 251–260. [[CrossRef](#)]
42. Ribeiro, P.L.L.; da Silva, A.C.M.S.; Filho, J.A.M.; Druzian, J.I. Impact of different by-products from the biodiesel industry and bacterial strains on the production, composition, and properties of novel polyhydroxyalkanoates containing achiral building blocks. *Ind. Crops Prod.* **2015**, *69*, 212–223. [[CrossRef](#)]
43. Campos, M.I.; Figueiredo, T.V.B.; Sousa, L.S.; Druzian, J.I. The influence of crude glycerin and nitrogen concentrations on the production of PHA by *Cupriavidus necator* using a response surface methodology and its characterizations. *Ind. Crops Prod.* **2014**, *52*, 338–346. [[CrossRef](#)]
44. Chen, G.Q. A microbial polyhydroxyalkanoates (PHA) based bio- and materials industry. *Chem. Soc. Rev.* **2009**, *38*, 2434–2446. [[CrossRef](#)]
45. Costa, S.S.; Miranda, A.L.; de Moraes, M.G.; Costa, J.A.V.; Druzian, J.I. Microalgae as source of polyhydroxyalkanoates (PHAs) —A review. *Int. J. Biol. Macromol.* **2019**, *131*, 536–547. [[CrossRef](#)]
46. Delgado, M.; Felix, M.; Bengoechea, C. Development of bioplastic materials: From rapeseed oil industry by products to added-value biodegradable biocomposite materials. *Ind. Crops Prod.* **2018**, *125*, 401–407. [[CrossRef](#)]
47. Muthuraj, R.; Misra, M.; Defersha, F.; Mohanty, A.K. Influence of processing parameters on the impact strength of biocomposites: A statistical approach. *Compos. Part A Appl. Sci. Manuf.* **2016**, *83*, 120–129. [[CrossRef](#)]
48. Nguyen, H.T.H.; Qi, P.; Rostagno, M.; Feteha, A.; Mille, S.A. The quest for high glass transition temperature bioplastics. *J. Mater. Chem. A* **2013**, *1*, 1–38. [[CrossRef](#)]
49. Labet, M.; Thielemans, W. Synthesis of polycaprolactone: A review. *Chem. Soc. Rev.* **2009**, *38*, 3484–3504. [[CrossRef](#)] [[PubMed](#)]
50. Averous, L.; Moro, L.; Dole, P.; Fringant, C. Properties of thermoplastic blends: Starch-polycaprolactone. *Polymer* **2000**, *41*, 4157–4167. [[CrossRef](#)]
51. Bianco, G.; Agerbirk, N.; Losito, I.; Cataldi, T.R.I. Acylated glucosinolates with diverse acyl groups investigated by high resolution mass spectrometry and infrared multiphoton dissociation. *Phytochemistry* **2014**, *100*, 92–102. [[CrossRef](#)]
52. Cataldi, T.R.I.; Orlando, D.; Nardiello, D.; Rubino, A.; Bianco, G.; Abate, S.; Ciriello, R.; Guerrieri, A. A three-factor Doehlert matrix design in optimising the determination of octadecyltrimethylammonium bromide by cation-exchange chromatography with suppressed conductivity detection. *Anal. Chim. Acta* **2007**, *597*, 129–136. [[CrossRef](#)]
53. Zianni, R.; Bianco, G.; Lelario, F.; Losito, I.; Palmisano, F.; Cataldi, T.R.I. Fatty acid neutral losses observed in tandem mass spectrometry with collision-induced dissociation allows regiochemical assignment of sulfoquinovosyl-diacylglycerols. *J. Mass Spectrom.* **2013**, *48*, 205–215. [[CrossRef](#)]

54. Bianco, G.; Zianni, R.; Anzillotta, G.; Palma, A.; Vitacco, V.; Scrano, L.; Cataldi, T.R.I. Dibenzo-p-dioxins and dibenzofurans in human breast milk collected in the area of Taranto (Southern Italy): First case study. *Anal. Bioanal. Chem.* **2013**, *405*, 2405–2410. [[CrossRef](#)]
55. Pascale, R.; Onzo, A.; Ciriello, R.; Scrano, L.; Bufo, S.A.; Bianco, G. *LC/MS Based Food Metabolomics*; Elsevier: Oxford, UK, 2020; ISBN 9780081005965.
56. Cataldi, T.R.I.; Bianco, G.; Abate, S.; Losito, I. Identification of unsaturated N-acylhomoserine lactones in bacterial isolates of *Rhodobacter sphaeroides* by liquid chromatography coupled to electrospray ionization-hybrid linear ion trap-Fourier transform ion cyclotron resonance mass spectrometry. *Rapid Commun. Mass Spectrom.* **2011**, *25*, 1817–1826. [[CrossRef](#)]
57. Pascale, R.; Bianco, G.; Cataldi, T.R.I.; Kopplin, P.S.; Bosco, F.; Vignola, L.; Uhl, J.; Lucio, M.; Milella, L. Mass spectrometry-based phytochemical screening for hypoglycemic activity of Fagioli di Sarconi beans (*Phaseolus vulgaris* L.). *Food Chem.* **2018**, *242*, 497–504. [[CrossRef](#)]
58. Bianco, G.; Pascale, R.; Carbone, C.F.; Acquavia, M.A.; Cataldi, T.R.I.; Schmitt-Kopplin, P.; Buchicchio, A.; Russo, D.; Milella, L. Determination of soyasaponins in Fagioli di Sarconi beans (*Phaseolus vulgaris* L.) by LC-ESI-FTICR-MS and evaluation of their hypoglycemic activity. *Anal. Bioanal. Chem.* **2018**, *410*, 1561–1569. [[CrossRef](#)] [[PubMed](#)]
59. Pascale, R.; Bianco, G.; Cataldi, T.R.I.; Buchicchio, A.; Losito, I.; Altieri, G.; Genovese, F.; Tauriello, A.; Di Renzo, G.C.; Lafiosca, M.C. Investigation of the Effects of Virgin Olive Oil Cleaning Systems on the Secoiridoid Aglycone Content Using High Performance Liquid Chromatography–Mass Spectrometry. *JAOCS J. Am. Oil Chem. Soc.* **2018**, *95*, 665–671. [[CrossRef](#)]
60. Pascale, R.; Acquavia, M.A.; Cataldi, T.R.I.; Onzo, A.; Coviello, D.; Bufo, S.A.; Scrano, L.; Ciriello, R.; Guerrieri, A.; Bianco, G. Profiling of quercetin glycosides and acyl glycosides in sun-dried peperoni di Senise peppers (*Capsicum annuum* L.) by a combination of LC-ESI (-) -MS/MS and polarity prediction in reversed-phase separations. *Anal. Bioanal. Chem.* **2020**, *412*, 3005–3015. [[CrossRef](#)] [[PubMed](#)]
61. Pascale, R.; Bianco, G.; Coviello, D.; Cristina Lafiosca, M.; Masi, S.; Mancini, I.M.; Bufo, S.A.; Scrano, L.; Caniani, D. Validation of a liquid chromatography coupled with tandem mass spectrometry method for the determination of drugs in wastewater using a three-phase solvent system. *J. Sep. Sci.* **2020**, *43*, 886–895. [[CrossRef](#)] [[PubMed](#)]
62. Onzo, A.; Acquavia, M.A.; Cataldi, T.R.I.; Ligonzo, M.; Coviello, D.; Pascale, R.; Martelli, G.; Bondoni, M.; Scrano, L.; Bianco, G. Coceth sulfate characterization by electrospray ionization tandem mass spectrometry. *Rapid Commun. Mass Spectrom.* **2020**, *34*, 1–10. [[CrossRef](#)]
63. Thakur, S.; Chaudhary, J.; Sharma, B.; Tamulevicius, S.; Thakur, V.K. ScienceDirect Sustainability of bioplastics: Opportunities and challenges. *Curr. Opin. Green Sustain. Chem.* **2018**, *13*, 68–75. [[CrossRef](#)]
64. Quarta, G. Determination of the Biobased Content in Plastics by Radiocarbon. *Radiocarbon* **2013**, *55*, 1834–1844. [[CrossRef](#)]
65. Sherwood, J.; Clark, J.H.; Farmer, T.J.; Herrero-Davila, L.; Moity, L. Recirculation: A new concept to drive innovation in sustainable product design for bio-based products. *Molecules* **2017**, *22*, 48. [[CrossRef](#)]
66. Iwata, T. Biodegradable and bio-based polymers: Future prospects of eco-friendly plastics. *Angew. Chemie-Int. Ed.* **2015**, *54*, 3210–3215. [[CrossRef](#)]
67. Lucas, N.; Bienaime, C.; Belloy, C.; Queneudec, M.; Silvestre, F.; Nava-saucedo, J. Polymer biodegradation: Mechanisms and estimation techniques. *Chemosphere* **2008**, *73*, 429–442. [[CrossRef](#)]
68. Ruggero, F.; Gori, R.; Lubello, C. Methodologies to assess biodegradation of bioplastics during aerobic composting and anaerobic digestion: A review. *Waste Manag. Res.* **2019**, *37*, 959–975. [[CrossRef](#)] [[PubMed](#)]
69. Ciriello, R.; Lo Magro, S.; Guerrieri, A. Assay of serum cholinesterase activity by an amperometric biosensor based on a co-crosslinked choline oxidase/overoxidized polypyrrole bilayer. *Analyst* **2018**, *143*, 920–929. [[CrossRef](#)] [[PubMed](#)]
70. Ciriello, R.; De Gennaro, F.; Frascaro, S.; Guerrieri, A. A novel approach for the selective analysis of L-lysine in untreated human serum by a co-crosslinked L-lysine- α -oxidase/overoxidized polypyrrole bilayer based amperometric biosensor. *Bioelectrochemistry* **2018**, *124*, 47–56. [[CrossRef](#)] [[PubMed](#)]
71. Massardier-Nageotte, V.; Pestre, C.; Cruard-Pradet, T.; Bayard, R. Aerobic and anaerobic biodegradability of polymer films and physico-chemical characterization. *Polym. Degrad. Stab.* **2006**, *91*, 620–627. [[CrossRef](#)]
72. Kale, G.; Kijchavengkul, T.; Auras, R.; Rubino, M.; Selke, S.E.; Singh, S.P. Compostability of bioplastic packaging materials: An overview. *Macromol. Biosci.* **2007**, *7*, 255–277. [[CrossRef](#)]
73. Folino, A.; Karageorgiou, A.; Calabrò, P.S.; Komilis, D. Biodegradation of wasted bioplastics in natural and industrial environments: A review. *Sustainability* **2020**, *12*, 6030. [[CrossRef](#)]
74. Wang, K.; Wang, W.; Ye, R.; Liu, A.; Xiao, J.; Liu, Y.; Zhao, Y. Mechanical properties and solubility in water of corn starch-collagen composite films: Effect of starch type and concentrations. *Food Chem.* **2017**, *216*, 209–216. [[CrossRef](#)]
75. Oliveira, T.I.S.; Rosa, M.F.; Ridout, M.J.; Cross, K.; Brito, E.S.; Silva, L.M.A.; Mazzetto, S.E.; Waldron, K.W.; Azeredo, H.M.C. Bionanocomposite films based on polysaccharides from banana peels. *Int. J. Biol. Macromol.* **2017**, *101*, 1–8. [[CrossRef](#)]
76. Battegazzore, D.; Bocchini, S.; Alongi, J.; Frache, A. Plasticizers, antioxidants and reinforcement fillers from hazelnut skin and cocoa by-products: Extraction and use in PLA and PP. *Polym. Degrad. Stab.* **2014**, *108*, 297–306. [[CrossRef](#)]
77. Granda, L.A.; Espinach, X.; Méndez, J.A.; Tresserras, J.; Delgado-Aguilar, M.; Mutjé, P. Semichemical fibres of *Leucaena collinsii* reinforced polypropylene composites: Young's Modulus analysis and fibre diameter effect on the stiffness. *Compos. Part B Eng.* **2016**, *92*, 332–337. [[CrossRef](#)]

78. Palomba, D.; Vazquez, G.E.; Díaz, M.F. Chemometrics and Intelligent Laboratory Systems Prediction of elongation at break for linear polymers. *Chemom. Intell. Lab. Syst.* **2014**, *139*, 121–131. [[CrossRef](#)]
79. Sanjay, M.R.; Arpitha, G.R.; Yogesha, B. Study on Mechanical Properties of Natural-Glass Fibre Reinforced Polymer Hybrid Composites: A Review. *Mater. Today Proc.* **2015**, *2*, 2959–2967. [[CrossRef](#)]
80. Suderman, N.; Isa, M.I.N.; Sarbon, N.M. Food Bioscience The effect of plasticizers on the functional properties of biodegradable gelatin-based film: A review. *Food Biosci.* **2018**, *24*, 111–119. [[CrossRef](#)]
81. Vieira, G.M.A.; da Silva, A.M.; dos Santos, L.O.; Beppu, M.M. Natural-based plasticizers and biopolymer films: A review. *Eur. Polym. J.* **2011**, *47*, 254–263. [[CrossRef](#)]
82. Suyatma, N.E.; Tighzert, L.; Copinet, A.; Coma, V. Effects of hydrophilic plasticizers on mechanical, thermal, and surface properties of chitosan films. *J. Agric. Food Chem.* **2005**, *53*, 3950–3957. [[CrossRef](#)]
83. Di Gioia, L.; Guilbert, S. Corn protein-based thermoplastic resins: Effect of some polar and amphiphilic plasticizers. *J. Agric. Food Chem.* **1999**, *47*, 1254–1261. [[CrossRef](#)]
84. Santosa, F.X.B.; Padua, G.W. Tensile properties and water absorption of zein sheets plasticized with oleic and linoleic acids. *J. Agric. Food Chem.* **1999**, *47*, 2070–2074. [[CrossRef](#)]
85. Saberi, B.; Chockchaisawasdee, S.; Golding, J.B.; Scarlett, C.J.; Stathopoulos, C.E. Physical and mechanical properties of a new edible film made of pea starch and guar gum as affected by glycols, sugars and polyols. *Int. J. Biol. Macromol.* **2017**, *104*, 345–359. [[CrossRef](#)]
86. Ghasemlou, M.; Khodaiyan, F.; Oromiehie, A. Physical, mechanical, barrier, and thermal properties of polyol-plasticized biodegradable edible film made from kefiran. *Carbohydr. Polym.* **2011**, *84*, 477–483. [[CrossRef](#)]
87. Tihminlioglu, F.; Atik, I.D.; Ozen, B. Water vapor and oxygen-barrier performance of corn—Zein coated polypropylene films. *J. Food Eng.* **2010**, *96*, 342–347. [[CrossRef](#)]
88. Gustafsson, J.; Landberg, M.; Bátor, V.; Åkesson, D.; Taherzadeh, M.J.; Zamani, A. Development of bio-based films and 3D objects from apple pomace. *Polymers* **2019**, *11*, 289. [[CrossRef](#)] [[PubMed](#)]
89. Yaradoddi, J.; Patil, V.; Ganachari, S.; Banapurmath, N.; Hunashyal, A.; Shettar, A. Biodegradable plastic production from fruit waste material and its sustainable use for green applications. *Int. J. Pharm. Res. Allied Sci.* **2016**, *5*, 56–65.
90. Sultan, N.F.K.; Johari, W.L.W. The Development of Banana Peel/Corn Starch Bioplastic Film: A Preliminary Study. *Bioremediat. Sci. Technol. Res.* **2017**, *5*, 12–17.
91. Faradilla, R.H.F.; Lee, G.; Roberts, J.; Martens, P.; Stenzel, M.; Arcot, J. Effect of glycerol, nanoclay and graphene oxide on physicochemical properties of biodegradable nanocellulose plastic sourced from banana pseudo-stem. *Cellulose* **2018**, *25*, 399–416. [[CrossRef](#)]
92. Bátor, V.; Jabbari, M.; Åkesson, D.; Lennartsson, P.R.; Taherzadeh, M.J.; Zamani, A. Production of Pectin-Cellulose Biofilms: A New Approach for Citrus Waste Recycling. *Int. J. Polym. Sci.* **2017**, *2017*, 1–10. [[CrossRef](#)]
93. Lestari, R.A.S.; Kasmiyatun, M.; Dermawan, K.; Aini, A.N.; Riyati, N.; Putri, F.R. Bioplastic from Jackfruit Seeds and Rice. *IOP Conf. Ser. Mater. Sci. Eng.* **2020**, *835*, 1–10. [[CrossRef](#)]
94. Sun, S.; Song, Y.; Zheng, Q. Morphology and mechanical properties of thermo-molded bioplastics based on glycerol-plasticized wheat gliadins. *J. Cereal Sci.* **2008**, *48*, 613–618. [[CrossRef](#)]
95. Caner, C.; Vergano, P.J.; Wiles, J.L. Chitosan film mechanical and permeation properties as affected by acid, plasticizer, and storage. *J. Food Sci.* **1998**, *63*, 1049–1053. [[CrossRef](#)]
96. Aguilar, J.M.; Bengoechea, C.; Pérez, E.; Guerrero, A. Effect of different polyols as plasticizers in soy based bioplastics. *Ind. Crops Prod.* **2020**, *153*, 1–9. [[CrossRef](#)]
97. Alonso-González, M.; Ramos, M.; Bengoechea, C.; Romero, A.; Guerrero, A. Evaluation of Composition on Processability and Water Absorption of Wheat Gluten-Based Bioplastics. *J. Polym. Environ.* **2020**, 1–10. [[CrossRef](#)]
98. Bashir, A.S.M.; Manusamy, Y. Recent Developments in Biocomposites Reinforced with Natural Biofillers from Food Waste. *Polym. Plast. Technol. Eng.* **2015**, *54*, 87–99. [[CrossRef](#)]
99. Cinar, S.O.; Chong, Z.K.; Kucuker, M.A.; Wiczorek, N.; Cengiz, U.; Kuchta, K. Bioplastic Production from Microalgae: A Review. *Int. J. Environ. Res. Public Health* **2020**, *17*, 3842. [[CrossRef](#)]
100. Çokaygil, Z.; Banar, M.; Seyhan, A.T. Orange peel-derived pectin jelly and corn starch-based biocomposite film with layered silicates. *J. Appl. Polym. Sci.* **2014**, *131*, 1–12. [[CrossRef](#)]
101. González-Gutiérrez, J.; Partal, P.; García-Morales, M.; Gallegos, C. Effect of processing on the viscoelastic, tensile and optical properties of albumen/starch-based bioplastics. *Carbohydr. Polym.* **2011**, *84*, 308–315. [[CrossRef](#)]
102. Gurram, R.; Souza Filho, P.F.; Taherzadeh, M.J.; Zamani, A. A Solvent-Free Approach for Production of Films from Pectin and Fungal Biomass. *J. Polym. Environ.* **2018**, *26*, 4282–4292. [[CrossRef](#)]
103. Muhammad, A.; Roslan, A.; Sanusi, S.N.A.; Shahimi, M.Q.; Nazari, N.Z. Mechanical properties of bioplastic form cellulose nanocrystal (CNC) mangosteen peel using glycerol as plasticizer. *J. Phys. Conf. Ser.* **2019**, *1349*, 1–8. [[CrossRef](#)]
104. Oliveira, T.I.S.; Rosa, M.F.; Cavalcante, F.L.; Pereira, P.H.F.; Moates, G.K.; Wellner, N.; Mazzetto, S.E.; Waldron, K.W.; Azeredo, H.M.C. Optimization of pectin extraction from banana peels with citric acid by using response surface methodology. *Food Chem.* **2016**, *198*, 113–118. [[CrossRef](#)] [[PubMed](#)]

105. Schettini, E.; Santagata, G.; Malinconico, M.; Immirzi, B.; Scarascia Mugnozza, G.; Vox, G. Recycled wastes of tomato and hemp fibres for biodegradable pots: Physico-chemical characterization and field performance. *Resour. Conserv. Recycl.* **2013**, *70*, 9–19. [[CrossRef](#)]
106. Jha, A.; Kumar, A. Biobased technologies for the efficient extraction of biopolymers from waste biomass. *Bioprocess Biosyst. Eng.* **2019**, *42*, 1893–1901. [[CrossRef](#)]
107. Pingali, S.V.; Urban, V.S.; Heller, W.T.; McGaughey, J.; O'Neill, H.; Foston, M.B.; Li, H.; Wyman, C.E.; Myles, D.A.; Langan, P.; et al. Understanding Multiscale Structural Changes during Dilute Acid Pretreatment of Switchgrass and Poplar. *ACS Sustain. Chem. Eng.* **2017**, *5*, 426–435. [[CrossRef](#)]
108. Wang, S.; Lu, A.; Zhang, L. Recent advances in regenerated cellulose materials. *Prog. Polym. Sci.* **2016**, *53*, 169–206. [[CrossRef](#)]
109. Zhao, H.; Holladay, J.E.; Kwak, J.H.; Zhang, Z.C. Inverse Temperature-Dependent Pathway of Cellulose Decrystallization in Trifluoroacetic Acid. *J. Phys. Chem. B* **2007**, *111*, 5295–5300. [[CrossRef](#)] [[PubMed](#)]
110. Bilo, F.; Pandini, S.; Sartore, L.; Depero, L.E.; Gargiulo, G.; Bonassi, A.; Federici, S.; Bontempi, E. A sustainable bioplastic obtained from rice straw. *J. Clean. Prod.* **2018**, *200*, 357–368. [[CrossRef](#)]
111. Perotto, G.; Ceseracciu, L.; Simonutti, R.; Paul, U.C.; Guzman-Puyol, S.; Tran, T.N.; Bayer, I.S.; Athanassiou, A. Bioplastics from vegetable waste: Via an eco-friendly water-based process. *Green Chem.* **2018**, *20*, 894–902. [[CrossRef](#)]
112. Liu, M.; Arshadi, M.; Javi, F.; Lawrence, P.; Davachi, S.M.; Abbaspourrad, A. Green and facile preparation of hydrophobic bioplastics from tea waste. *J. Clean. Prod.* **2020**, *276*, 1–10. [[CrossRef](#)]
113. Rizwana Beevi, K.; Sameera Fathima, A.R.; Thahira Fathima, A.I.; Thameemunisa, N.; Noorjahan, C.M.; Deepika, T. Bioplastic Synthesis Using Banana Peels And Potato Starch And Characterization. *Int. J. Sci. Technol. Res.* **2020**, *9*, 1809–1814.
114. Arikan, E.B.; Bilgen, H.D. Production of bioplastic from potato peel waste and investigation of its biodegradability. *Int. Adv. Res. Eng. J.* **2019**, *03*, 093–097. [[CrossRef](#)]
115. Masruri, M.; Azhar, A.Z.; Rosyada, I.; Febrianto, A. The effect of kaffir lime (*Citrus hystrix* DC) essential oil on bioplastic derived from cassava peel waste. *J. Phys. Conf. Ser.* **2019**, *1374*, 1–6. [[CrossRef](#)]
116. Dasumiati; Saridewi, N.; Malik, M. Food packaging development of bioplastic from basic waste of cassava peel (*manihot utilisima*) and shrimp shell. *IOP Conf. Ser. Mater. Sci. Eng.* **2019**, *602*, 1–9. [[CrossRef](#)]
117. Fathanah, U.; Lubis, M.R.; Nasution, F.; Masyawi, M.S. Characterization of bioplastic based from cassava crisp home industrial waste incorporated with chitosan and liquid smoke. *IOP Conf. Ser. Mater. Sci. Eng.* **2018**, *334*, 1–8. [[CrossRef](#)]
118. Samer, M.; Khalefa, Z.; Abdelall, T.; Moawya, W.; Farouk, A.; Abdelaziz, S.; Soliman, N.; Salah, A.; Gomaa, M.; Mohamed, M. Bioplastics production from agricultural crop residues. *Agric. Eng. Int. CIGR J.* **2019**, *21*, 190–194.
119. Muhammad, A.; Rashidi, A.R.; Roslan, A.; Idris, S.A. Development of bio based plastic materials for packaging from soybeans waste. *AIP Conf. Proc.* **2017**, *1885*, 1–8. [[CrossRef](#)]
120. Emaga, T.H.; Robert, C.; Sebastien, N.R.; Wathélet, B.; Paquot, M. Dietary fibre components and pectin chemical features of peels during ripening in banana and plantain varieties. *Bioresour. Technol.* **2008**, *99*, 4346–4354. [[CrossRef](#)] [[PubMed](#)]
121. Mohnen, D. Pectin structure and biosynthesis. *Curr. Opin. Plant Biol.* **2008**, *11*, 266–277. [[CrossRef](#)]
122. Khan, A.; Khan, R.A.; Salmieri, S.; Le Tien, C.; Riedl, B.; Bouchard, J.; Chauve, G.; Tan, V.; Kamal, M.R.; Lacroix, M. Mechanical and barrier properties of nanocrystalline cellulose reinforced chitosan based nanocomposite films. *Carbohydr. Polym.* **2012**, *90*, 1601–1608. [[CrossRef](#)]
123. Olsson, E.; Hedenqvist, M.S.; Johansson, C.; Järnström, L. Influence of citric acid and curing on moisture sorption, diffusion and permeability of starch films. *Carbohydr. Polym.* **2013**, *94*, 765–772. [[CrossRef](#)]
124. Heredia-Guerrero, J.A.; Caputo, G.; Guzman-Puyol, S.; Tedeschi, G.; Heredia, A.; Ceseracciu, L.; Benitez, J.J.; Athanassiou, A. Sustainable polycondensation of multifunctional fatty acids from tomato pomace agro-waste catalyzed by tin (II) 2-ethylhexanoate. *Mater. Today Sustain.* **2019**, *3*, 1–10. [[CrossRef](#)]
125. Domínguez, E.; Heredia-Guerrero, J.A.; Heredia, A. Plant cutin genesis: Unanswered questions. *Trends Plant Sci.* **2015**, *20*, 551–558. [[CrossRef](#)]
126. Deng, M.; Zhang, G.; Zeng, Y.; Pei, X.; Huang, R.; Lin, J. Simple process for synthesis of layered sodium silicates using rice husk ash as silica source. *J. Alloys Compd.* **2016**, *683*, 412–417. [[CrossRef](#)]
127. Mohanty, A.K.; Misra, M.; Hinrichsen, G. Biofibres, biodegradable polymers and biocomposites: An overview. *Macromol. Mater. Eng.* **2000**, *276–277*, 1–24. [[CrossRef](#)]
128. Ashori, A.; Nourbakhsh, A. Bio-based composites from waste agricultural residues. *Waste Manag.* **2010**, *30*, 680–684. [[CrossRef](#)] [[PubMed](#)]
129. Russo, R.; Malinconico, M.; Santagata, G. Effect of cross-linking with calcium ions on the physical properties of alginate films. *Biomacromolecules* **2007**, *8*, 3193–3197. [[CrossRef](#)] [[PubMed](#)]
130. Mathivanan, D.; Norfazilah, H.; Siregar, J.P.; Rejab, M.R.M.; Bachtiar, D.; Cionita, T. The study of mechanical properties of pineapple leaf fibre reinforced tapioca based bioplastic resin composite. *MATEC Web Conf.* **2016**, *74*, 1–4. [[CrossRef](#)]
131. Yapo, B.M.; Koffi, K.L. Dietary fiber components in yellow passion fruit rind—A potential fiber source. *J. Agric. Food Chem.* **2008**, *56*, 5880–5883. [[CrossRef](#)] [[PubMed](#)]
132. Moro, T.M.A.; Ascheri, J.L.R.; Ortiz, J.A.R.; Carvalho, C.W.P.; Meléndez-Arévalo, A. Bioplastics of Native Starches Reinforced with Passion Fruit Peel. *Food Bioprocess Technol.* **2017**, *10*, 1798–1808. [[CrossRef](#)]

133. Wu, F.; Misra, M.; Mohanty, A.K. Sustainable green composites from biodegradable plastics blend and natural fibre with balanced performance: Synergy of nano-structured blend and reactive extrusion. *Compos. Sci. Technol.* **2020**, *200*, 1–8. [[CrossRef](#)]
134. Troiano, M.; Santulli, C.; Roselli, G.; Di Girolami, G.; Cinaglia, P.; Gkrilla, A. DIY Bioplastics from Peanut Hulls Waste in a Starch-Milk Based Matrix. *FME Trans.* **2018**, *46*, 503–512. [[CrossRef](#)]
135. Tran, T.N.; Heredia-Guerrero, J.A.; Mai, B.T.; Ceseracciu, L.; Marini, L.; Athanassiou, A.; Bayer, I.S. Bioelastomers Based on Cocoa Shell Waste with Antioxidant Ability. *Adv. Sustain. Syst.* **2017**, *1*, 1700002. [[CrossRef](#)]
136. Côtó, T.; Moura, I.; de Sá, A.; Vilarinho, C.; Machado, A.V. Sustainable materials based on cellulose from food sector agro-wastes. *J. Renew. Mater.* **2018**, *6*, 688–696. [[CrossRef](#)]
137. Nasihin, Z.D.; Masruri, M.; Warsito, W.; Srihardyastutie, A. Preparation of Nanocellulose Bioplastic with a Gradation Color of Red and Yellow. *IOP Conf. Ser. Mater. Sci. Eng.* **2020**, *833*, 1–6. [[CrossRef](#)]
138. Azieyanti, N.A.; Amirul, A.; Othman, S.Z.; Misran, H. Mechanical and Morphology Studies of Bioplastic-Based Banana Peels. *J. Phys. Conf. Ser.* **2020**, *1529*, 1–6. [[CrossRef](#)]
139. Sharif Hossain, A.B.M.; Ibrahim, N.A.; AlEissa, M.S. Nano-cellulose derived bioplastic biomaterial data for vehicle bio-bumper from banana peel waste biomass. *Data Brief* **2016**, *8*, 286–294. [[CrossRef](#)] [[PubMed](#)]
140. Iriani, E.S.; Permana, A.W.; Yuliani, S.; Kailaku, S.I.; Sulaiman, A.A. The effect of agricultural waste nanocellulose on the properties of bioplastic for fresh fruit packaging. *IOP Conf. Ser. Earth Environ. Sci.* **2019**, *309*, 1–7. [[CrossRef](#)]
141. Yacob, N.; Yusof, M.R.; Mohamed, A.Z.; Badri, K.H. Effect of cellulose fiber loading on the properties of starch-based films. *AIP Conf. Proc.* **2019**, *2111*, 1–7. [[CrossRef](#)]
142. Dahy, H. Efficient Fabrication of Sustainable Building Products from Annually Generated Non-wood Cellulosic Fibres and Bioplastics with Improved Flammability Resistance. *Waste Biomass Valoriz.* **2019**, *10*, 1167–1175. [[CrossRef](#)]
143. Lu, S.-T.; Hamerton, I. Recent developments in the chemistry of halogen-free flame retardant polymers. *Prog. Polym. Sci.* **2002**, *27*, 1661–1712. [[CrossRef](#)]
144. Shruti, V.C.; Kutralam-Muniasamy, G. Bioplastics: Missing link in the era of Microplastics. *Sci. Total Environ.* **2019**, *697*, 134139. [[CrossRef](#)]
145. Bhagwat, G.; Gray, K.; Wilson, S.P.; Muniyasamy, S.; Vincent, S.G.T.; Bush, R.; Palanisami, T. Benchmarking Bioplastics: A Natural Step Towards a Sustainable Future. *J. Polym. Environ.* **2020**, *28*, 3055–3075. [[CrossRef](#)]
146. Hottle, T.A.; Bilec, M.M.; Landis, A.E. Sustainability assessments of bio-based polymers. *Polym. Degrad. Stab.* **2013**, *98*, 1898–1907. [[CrossRef](#)]
147. Kakadellis, S.; Harris, Z.M. Don't scrap the waste: The need for broader system boundaries in bioplastic food packaging life-cycle assessment—A critical review. *J. Clean. Prod.* **2020**, *274*, 122831. [[CrossRef](#)]
148. Panuccio, M.R.; Attinà, E.; Basile, C.; Mallamaci, C.; Muscolo, A. Use of Recalcitrant Agriculture Wastes to Produce Biogas and Feasible Biofertilizer. *Waste Biomass Valoriz.* **2016**, *7*, 267–280. [[CrossRef](#)]
149. Heckman, J.H. Food packaging regulation in the United States and the European Union. *Regul. Toxicol. Pharmacol.* **2005**, *42*, 96–122. [[CrossRef](#)] [[PubMed](#)]
150. Peelman, N.; Ragaert, P.; De Meulenaer, B.; Adons, D.; Peeters, R.; Cardon, L.; Van Impe, F.; Devlieghere, F. Application of bioplastics for food packaging. *Trends Food Sci. Technol.* **2013**, *32*, 128–141. [[CrossRef](#)]
151. Malinconico, M.; Immirzi, B.; Santagata, G.; Schettini, E.; Vox, G.; Mugnozza, G.S. An overview on innovative biodegradable materials for agricultural applications. In *Progress in Polymer Degradation and Stability Research*; Moeller, H.W., Ed.; Nova Science Publishers: New York, NY, USA, 2008; pp. 69–114. ISBN 9781600218286.

Analysis of surfactants by mass spectrometry: Coming to grips with their diversity

Raffaella Pascale¹  | Maria A. Acquavia^{2,3}  | Alberto Onzo² |
Tommaso R. I. Cataldi^{4,5}  | Cosima D. Calvano⁶  | Giuliana Bianco² 

¹Gnosis by Lesaffre, Pisticci, Italy

²Dipartimento di Scienze, Università degli Studi della Basilicata, Potenza, Italy

³ALMAGISI S.r.l Corso Italia, Bolzano, Italy

⁴Università degli Studi di Bari Aldo Moro, Bari, Italy

⁵Dipartimento di Chimica, Bari, Italy

⁶Dipartimento di Farmacia-Scienze del Farmaco, Bari, Italy

Correspondence

Giuliana Bianco, Dipartimento di Scienze, Università della Basilicata, via dell'Ateneo Lucano, Potenza 10 85100, Italy.

Email: giuliana.bianco@unibas.it

Abstract

Surfactants are surface-active agents widely used in numerous applications in our daily lives as personal care products, domestic, and industrial detergents. To determine complex mixtures of surfactants and their degradation products, unselective and rather insensitive methods, based on colorimetric and complexometric analyses are no longer employable. Analytical methodologies able to determine low concentration levels of surfactants and closely related compounds in complex matrices are required. The recent introduction of robust, sensitive, and selective mass spectrometry (MS) techniques has led to the rapid expansion of the surfactant research field including complex mixtures of isomers, oligomers, and homologues of surfactants as well as their chemically and biodegradation products at trace levels. In this review, emphasis is given to the state-of-the-art MS-based analysis of surfactants and their degradation products with an overview of the current research landscape from traditional methods involving hyphenate techniques (gas chromatography-MS and liquid chromatography-MS) to the most innovative approaches, based on high-resolution MS. Finally, we outline a detailed explanation on the utilization of MS for mechanistic purposes, such as the study of micelle formation in different solvents.

Abbreviations: ABS, alkylbenzenesulfonates; AEO, ethoxylated alcohols; AES, alkyl ether sulfates; AFFF, aqueous film-forming foams; AOTNa, sodium bis (2-ethylhexyl)sulfosuccinate; AP, alkylphenols; APCI, atmospheric pressure chemical ionization; APEO, alkylphenol polyethoxylates; APG, alkyl polyglycosides; API, ambient pressure ionization; AS, alkyl sulfates; ATR, attenuated total reflectance; Auto-Abs, autoantibodies; BAC, benzalkonium chloride; CAPB, cocamidopropyl betaines; CE, capillary electrophoresis; CES, coceth sulfate; CI, chemical ionization; CID, collision induced dissociation; CMC, critical micellar concentration; CNPEC, carboxyalkylphenol ethoxycarboxylates; COVID-19, coronavirus disease 2019; Da, unit Dalton; DCI, desorption chemical ionization; EI, electron impact; ELISA, enzyme-linked immunosorbent assays; ELSD, evaporative light scattering detector; EO, ethylene oxide; ESI, electrospray ionization; FAB, fast atom bombardment; FD, field desorption; FIA, flow-injection analysis; FTAB, fluorotelomer sulfonamide alkylbetaine; FTIR, Fourier-transform infrared spectroscopy; GC, gas chromatography; GC×GC, two-dimensional gas chromatography; GC-MS, gas chromatography coupled to mass spectrometry; HAA, 3-(hydroxyalkanoxyloxy)alkanoic acid; HILIC, hydrophilic interaction liquid chromatography; HPLC, high pressure liquid chromatography; HRMS, high-resolution mass spectrometry; IC-CD, ion chromatography with suppressed or nonsuppressed conductivity detection; IgA, immunoglobulin A; IM, ion mobility; IRMPD, infrared multiphoton dissociation; KMD, Kendrick mass defect; LAE, linear alkyl ethoxylates; LAS, linear alkylbenzenesulfonates; LC, liquid chromatography; LC×LC, two-dimensional liquid chromatography; LOD, limits of detection; MALDI-ToF-MS, matrix-assisted laser desorption/ionization time-of-flight mass spectrometry; MS, mass spectrometry; MSI, mass spectrometry imaging; MS/MS, tandem mass spectrometry; NMR, nuclear magnetic resonance spectroscopy; NP, nonylphenol; NPEC, nonylphenol polyethoxycarboxylates; NPEO, nonylphenol polyethoxylate; OP, octylphenol; OPEO, octylphenol polyethoxylate; OTAB, octyl-trimethylammonium bromide; PEG, poly(ethylene glycol); PEO, polyethoxylates; PFAS, polyfluorinated alkyl surfactants; PICI, positive-ion chemical ionization; PS, pulmonary surfactants; RP, resolving power; SDME, single drop microextraction; SFC-MS, supercritical fluid chromatography coupled with mass spectrometry; SIM, selected ion monitoring; SPE, solid phase extraction; SP-A, surfactant proteins A; SP-B, surfactant proteins B; SP-C, surfactant proteins C; SP-D, surfactant proteins D; SRM, selected reaction monitoring.

KEYWORDS

gas chromatography-mass spectrometry, high resolution-mass spectrometry, liquid chromatography-mass spectrometry, surfactants, tandem mass spectrometry

1 | CHEMICAL-PHYSICAL PROPERTIES OF SURFACTANTS

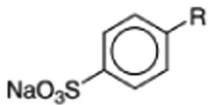
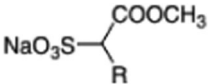
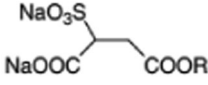
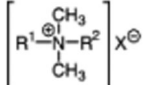
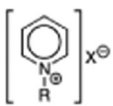
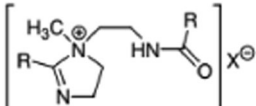
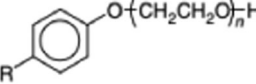
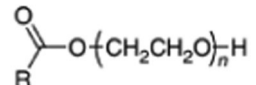
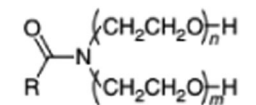
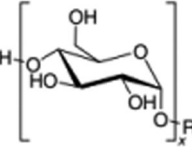
Surfactants or surface-active agents are a group of compounds used to modify the interfacial properties of aqueous and nonaqueous solutions. Each surfactant molecule has both hydrophilic and hydrophobic (or lipophilic) moieties (Broze, 1999; Morelli & Szajer, 2001, 2000). Typical structures of surfactant molecules comprise spatially separated polar and apolar parts, elongated shapes, large numbers of conformations and anisotropic surfactant–surfactant interactions. The polar group is localized in a small domain of the molecule and consists of an ionic, zwitterionic, or nonionic hydrophilic group (the so-called surfactant head), whereas the apolar portion is formed by one or more long flexible hydrocarbon or fluorocarbon chains, that is, the surfactant tail. As summarized in Table 1, the polar head group is used to distinguish surfactants into different categories: anionic, cationic, and nonionic.

Due to the competitive interplay of head–head, head–tail, and tail–tail interactions, triggered by surrounding molecules, surfactants can self-assemble leading to organized aggregates (see Figure 1), with coexistence of polar and apolar domains. When surfactant monomer molecules (Figure 1A) are dissolved in highly polar solvents (e.g., water), above a critical concentration, that is, the critical micellar concentration (CMC), they aggregate as micelles (Figure 1B), that is, supramolecules characterized by an apolar core of surfactant alkyl chains surrounded by an external layer of hydrophilic head groups in contact with solvent molecules (Broze, 1999; Hoffmann, 1994). The main driving force of the surfactant self-assembling is the hydrophobic effect. Yet, reverse micelles can also be formed when surfactants molecules are assembled in apolar media so that the head groups point toward the center of the aggregate while the alkyl chains are oriented toward the external (Figure 1C). This is because, in apolar media, interactions between polar groups dominate, being generally much stronger than those between apolar moieties (Allen et al., 2000). The presence of these aggregates dramatically influences the physicochemical properties of solutions at the liquid–air interface (Broze, 1999; Morelli & Szajer, 2000). Depending on

the nature of the hydrophilic moiety ensuring the water affinity of the molecule, major surfactants can be divided into anionic, cationic, amphoteric, and nonionic classes. Anionics are historically the earliest and the most common surfactants. Accordingly, they are produced with the highest volumes and most of them are relatively inexpensive. They are especially beneficial for their excellent deterative action and their efficacy to remove particulate soils, a benefit that relies on the fact that many substrates are negatively charged. Depending on the nature of the negatively charged head group, they show a variable resistance to bond cleavages, that is, C–C, C–S, C–O. Anionics are also enough sensitive to water hardness ions, thus limiting their use in hard waters. Some anionics have also the ability to generate viscous aqueous phases, thereby yielding self-thickened products (Bazel et al., 2014; Scheibel, 2004).

Cationics are characterized by very high affinity on various substrates, especially the negatively charged ones, and by the subsequent surface modifications. They are commonly used as conditioning agents in fabric care (i.e., dialkyl or diester quaternary ammonium salts [QAS] in rinse fabric softeners) and hair care products. Cationics form water-insoluble complexes with anionic surfactants. Some cationics are used as bactericides and fungicides too, such as dodecyl dimethylbenzyl ammonium chloride or cetyltrimethylammonium chloride (Carmona-Ribeiro et al., 2006; Fait et al., 2019; Zakharova et al., 2019). Amphoteric surfactants are usually used in conjunction with other surfactants (anionics or nonionics) to improve desired properties such as foam or detergency. Since the optimal surface activity and skin compatibility of amphoteric take place around neutral pH, they are suitable for mild detergent products like personal care ones, that is, shower gels, foam baths, shampoos, and so forth (Domsch & Jenni, 2004). Nonionics are especially useful because are minimally affected by water hardness and pH values. Since they are compatible with charged molecules, they are easily used in mixtures with other ionic surfactants, which often result in beneficial associations. For instance, nonionics can help to solubilize calcium or magnesium salts of anionic surfactants. These features, together with their low related costs, make nonionic surfactants widely used in detergent products (Bajpai & Tyagi, 2010; Lindman et al., 2016).

TABLE 1 Classification of surfactants in terms of class, chemical structure, and formula

Classes	Type	Structure	Formula
Anionic	Linear alkylbenzene sulfonates (LAS)		R = C ₁₀ –C ₁₃
	Alkylsulfonates	NaO ₃ S–R	R = C ₁₁ –C ₁₇
	α-Olefine sulfonates	NaO ₃ S–(CH ₂) _m HC=CH(CH ₂) _n CH ₃	m + n = 9–15
	Alkylsulfates	NaO ₃ S–O–R	R = C ₁₁ –C ₁₇
	Fatty alcohol ether sulfates	NaO ₃ S–O–(CH ₂ CH ₂ O) _n –R	R = C ₁₂ –C ₁₄ ; n = 1–4
	α-Sulfo fatty acid methyl esters		R = C ₁₄ –C ₁₆
	Sulfo succinate esters		R = C ₂ –C ₁₂
	Soaps	NaOOC–R	R = C ₁₂ –C ₁₆
Cationic	Tetraalkylammonium salts		R ¹ , R ² = C ₁ , C ₁₆ –C ₁₈ R ¹ , R ² = C ₁₆ –C ₁₈ R ¹ = C ₈ –C ₁₈ , R ² = CH ₂ C ₆ H ₅ X ⁻ = Cl ⁻ , Br ⁻
	Alkylpyridinium salts		R = C ₁₆ –C ₁₈ X ⁻ = Cl ⁻ , Br ⁻
	Imidazolium quaternary ammonium salts		R = C ₁₆ –C ₁₈ X ⁻ = Cl ⁻ , Br ⁻
Nonionic	Alkylphenoethoxylates (APEO)		R = C ₈ –C ₁₂ ; n = 3–40
	Alcoholoethoxylates (AEO)	R–O–(CH ₂ CH ₂ O) _n –H	R = C ₉ –C ₁₈ ; n = 1–40
	Fatty acid ethoxylates		R = C ₁₂ –C ₁₈ ; n = 4
	Fatty acid alkanolamide ethoxylates		R = C ₁₁ –C ₁₇ ; n = 1, 2; m = 0, 1
	Fatty alcohol polyglycol ethers	R–O–(CH ₂ CH ₂ O) _m –O–(CH ₂ CHO) _n –H CH ₃	R = C ₈ –C ₁₈ ; n = 3–6; m = 3–6
	Alkylpolyglucosides (APG)		R = C ₈ –C ₁₆ ; x = 1–4

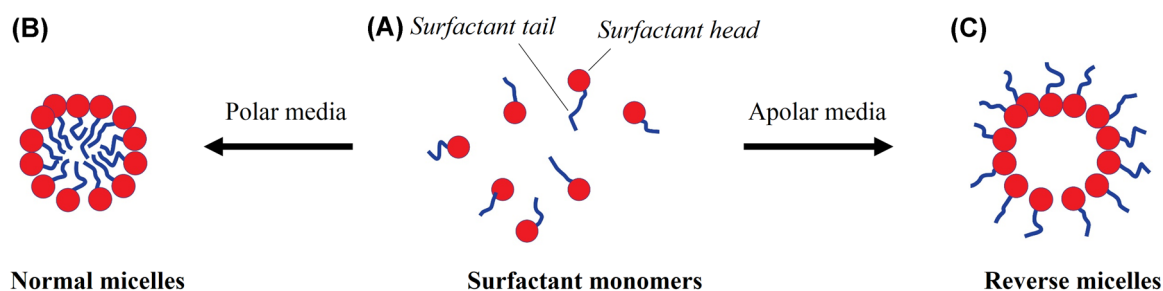


FIGURE 1 Schematic illustration of the reversible monomer-micelle thermodynamic equilibrium. The red circle represents the surfactant heads (hydrophilic moieties) and the blue curved lines represent the surfactant tails (hydrophobic moieties). When there is a large concentration of surfactants mixed in liquid phase, there may not be enough area at the phase surface for all the surfactant molecules to gather. In these cases, the surfactant monomers (A) will begin to gather in clumps, called normal micelles (B) in polar media and reverse micelles (C) in apolar ones [Color figure can be viewed at wileyonlinelibrary.com]

Surfactants are not chemically homogeneous being usually a mixture of compounds. For all types of surfactants, there may be a considerable distribution in the nonpolar part, different alkyl chain length, partial unsaturation, and so on, resulting from the fatty raw material used. As an example, coceth sulfate (CES), a commonly used surfactant in liquid cleaning formulations, is formally a blend of homologue molecules with hydrophobic tail C12 and C14, that is, $C_{12}H_{25}(OCH_2CH_2)_nOSO_3Na$ and $C_{14}H_{29}(OCH_2CH_2)_nOSO_3Na$ (Onzo et al., 2020). Moreover, the number of oxyethylene groups (n) may formally be two but the product will contain species with no oxyethylene units up to at least seven oxyethylene units.

The chemical structures of surfactants are very important to provide specific features to the final detergent products with the main aim to fully meet people needs. Degree of polymerization, presence of unsaturations and length of alkyl chain are examples of structure-related parameters that can be varied to tune the last product properties. For these reasons, knowing surfactant structure is important, to obtain more clues on the structure-properties relationship and to take advantage of this information to test new structural motifs (Gaudin et al., 2019). In 2020, the worldwide production of synthetic surfactants was estimated to be larger than 10 million tons; the anionics account for 50% of the total industrial surfactant output, cationics comprise only about 15%, while nonionics account for 30% (Morelli & Szajer, 2000).

As already mentioned, surfactants are widely used both industrially and domestically being currently ubiquitous into the environment (Caniani, Caivano, et al., 2019; Caniani, Esposito, et al., 2019). Recent works have demonstrated how surfactants, such as alkylphenol polyethoxylates (APEO), and their degradation products possess weakly estrogenic effects (Gaudin et al., 2019).

Apparently, APEO and closely related degradation products are of human health concerns, such as sperm production decrease and sexual reproductive issues (Acquavia et al., 2021; Sharpe & Skakkebaek, 1993). Moreover, halogenated compounds produced by biodegradation of most commonly used surfactants, including APEO and polyfluorinated alkyl surfactants (PFAS) are persistent and accumulate both in groundwater and sludge (Amodeo et al., 2018). Also the contamination of drinking water and foodstuffs is of great concern for human health (Montgomery-Brown & Reinhard, 2003; Trier et al., 2011). Conceivably, data about the total content of surfactants and their degradation products in environmental samples (Caivano, Pascale, Mazzone, Buchicchio, et al., 2017; Caivano, Pascale, Mazzone, Masi, et al., 2017) are critical in assessing the environmental impact of these compounds. Thus, information about the exact distribution of individual oligomers in environmental samples is important since it permits the identification of the sources of surfactants and the degree of degradation of the precursor compounds. For these reasons, much research is dedicated to developing more sensitive, specific, robust, and efficient analytical methods to identify, structurally characterize, and quantify these substances in a wide range of complex samples, also including biological systems where they play important roles comprising human physiology. This is the case of pulmonary surfactants (PS), which are involved in the efficient exchange of gases and the maintenance of the structural integrity of alveoli (Choi et al., 2020). PS are molecules of interest for several investigators wishing to understand bio-systems. Thus, sensitive analytical methods for their detection and characterization are needed as well. This review summarizes existing literature on the analysis of the different classes of surfactants by MS.

2 | THE CHALLENGES OF SURFACTANT ANALYSIS

The continued development of analytical tools and techniques has defined the field of surfactants, focusing on improvements mainly in analytical techniques. Currently, highly selective analytical methods are required to characterize and identify the plethora of surfactants occurring in industrial raw materials, manufactured products, and environmental samples. Because of the existence of many alkyl homologues, lack of chromophores, high polarity, and thermal instability, nonaromatic surfactants are difficult to analyse. Several techniques for their determination have been reported, including titration (Fielden & Claesson, 1998), Fourier-transform infrared spectroscopy (FTIR), nuclear magnetic resonance (NMR) spectroscopy (Jain et al., 2012; Lee et al., 2016), attenuated total reflectance with FTIR (Carolei & Gutz, 2005), ion chromatography with suppressed or nonsuppressed conductivity detection (IC-CD) (Cataldi et al., 2007; Levine et al., 2000), gas chromatography coupled to mass spectrometry (GC-MS) (Ding & Liao, 2001; Ding & Tsai, 2003), capillary electrophoresis with UV detection (Liu & Ding, 2004; Piera et al., 1997), high performance liquid chromatography coupled with mass spectrometry (HPLC-MS) or evaporative light scattering detector (HPLC-ELSD) (Crescenzi et al., 1995), and supercritical fluid chromatography coupled with mass spectrometry (SFC-MS) (Ma et al., 2019; Pan et al., 2020). Among the above-mentioned techniques, the chromatographic ones have many advantages for analysing surfactant mixtures. Albeit good resolution can be expected by using IC-CD, this analytical technique can only be applied to ionic compounds (Coviello et al., 2020). GC-MS with direct injection of ionic surfactants is not viable and derivatization or pyrolysis is required for their analysis (Pascale, Bianco, Calace, Masi, et al., 2018). Conversely, HPLC is applicable to surfactant mixtures regardless their molecular charge (Morelli & Szajer, 2001, 2000) and can be coupled with different detectors, such as mass spectrometers and UV-Vis diode array, without any derivatization reactions. However, low polymer solubility and increased solution viscosity, with the ensuing issues of sample injection and elution, as well as relatively low chromatographic resolution of individual oligomers, make its use challenging (Pan et al., 2020; Schmitt et al., 1990). As an alternative, stand-alone shotgun MS has been widely used for surfactant analysis, and MS provides a wide range of advantages, such as supplying key structural characterization by tandem mass spectrometry (MS/MS). A huge number of molecules can be quickly identified, thus making shotgun MS/MS somewhat useful for complex mixtures (Onzo et al.,

2020; Pascale, Bianco, Cataldi, Kopplin, et al., 2018). Matrix-assisted laser desorption/ionization time-of-flight mass spectrometry (MALDI/ToF/MS) has been also employed for nonionic surfactants (Sato et al., 2014, 2001; Treglia et al., 2020). Although it is a convenient and powerful technique, it can be rather cumbersome to identify low-molecular weight oligomers without a proper matrix selection (Calvano et al., 2018). Ion mobility mass spectrometry (IM/MS), which has a short analysis time and minimal solvent usage, has also been used to analyse oligomers (Katzenmeyer et al., 2016; Solak Erdem et al., 2014). Soft ionization techniques such as field desorption, fast atom bombardment (FAB), atmospheric pressure chemical ionization (APCI), and electrospray ionization (ESI) have been employed for a qualitative characterization of surfactant mixtures in environmental samples (Kühn & Neubert, 2004; Lyon, Crow, et al., 1984). Depending on the physicochemical properties of the surfactants such as polarity and molecular weights, operation in positive or negative ion mode can be selected. In addition, MS/MS outcomes have greatly increased the accessibility of surfactants to MS analysis; fragmentation patterns allow the isomer distribution examination along with other chemical information, such as location of unsaturations, occurrence of side chains and degree of branching (Onzo et al., 2020). The popularity of high-resolution MS (HRMS) has soared in the past decade and suggests that this technique has the potential to provide a significant boost to surfactant analysis. Here, rather than give a complete overview of surfactant MS analysis using uncommon ionization sources (e.g., FAB), we pursued the idea to give enough background of their useful information with a special look at the most popular atmospheric pressure ionization systems.

2.1 | MS in surfactant analysis

For several reasons, MS has become the most widely used tool in industrial laboratories to characterize and quantify surfactants and closely related degradation products in the last 20 years. First of all, MS represents a sensitive and highly selective technique for the analysis of complex mixture samples (Morelli & Szajer, 2001, 2000). Second, MS has the wide range of sample-related advantages, like the possibility to carried out direct-injection analyses of solution or to analyse directly solid samples without the need to recur to time-consuming sample pretreatment protocols. Third, the ability to isolate precursor ions by MS/MS and disclose the relevant fragmentation behavior (Bianco et al., 2017). Along with the possibility to couple MS with separation techniques,

makes this approach the most powerful analytical tool in every field of application, showing unsurpassed levels of specificity and selectivity (Pascale et al., 2021). MS technique has rapidly evolved during the past 30 years invading every discipline within the life and health sciences (Bianco et al., 2017; Pascale et al., 2021; Sun et al., 2020; Zhou et al., 2012), including surfactants field (Agozzino et al., 1986; García et al., 2019; Ma et al., 2019).

In this review, a survey of the most common approaches used in surfactant analysis by MS will be illustrated. Initially, a detailed description of the structural analysis by MS will be provided for each class of surfactants (see Table 1), including biosurfactants and PS. Then, the quantification of targeted surfactants will be discussed, focusing the attention on emerging compounds and their environmental concerns. Alternative and innovative approaches related to MS surfactant analysis will be listed to investigate complex mixtures of surfactant. Finally, a detailed explanation on the utilization of this technique for mechanistic purposes, such as the study of micelle formation in different solvents, will be presented.

3 | STRUCTURAL ANALYSIS OF SURFACTANTS BY MS

The structural characterization of surfactants and their degradation products is usually performed by flow-injection analysis with tandem mass spectrometry (FIA-MS/MS) or hyphenate techniques in which MS and MS/

MS is coupled to LC or GC. To shed light on the surfactant structure in complex samples, the loss of neutral fragments and the presence of diagnostic product ions in tandem MS experiments are decisive for the qualitative identification of surfactants. Taking into account that surfactants are not commercially available as individual compounds, MS is very useful to obtain their fingerprints, to recognize the chemical composition of commercial products and for traceability purposes as well. The fate of surfactants released into the environment along with their degradation products can be attempted by MS detection, thus possibly making the issue less challenging. Furthermore, the possibility to isolate selected product ions (i.e., diagnostic ions) in selected ion monitoring (SIM) and in selected reaction monitoring modes, allows to obtain good selectivity and sensitivity, thus demonstrating the suitability of MS for monitoring and quality control routine analyses (Crescenzi et al., 1995; Moody et al., 2001; Pascale, Bianco, et al., 2020; Petrović & Barceló, 2000). MS is widely used to characterize all classes of surfactants, viz., anionics, cationics, nonionics, amphoteric, and bioderivatives, as discussed below.

3.1 | Anionic surfactants

Anionic surfactants comprise the largest class of surfactants and account for ca. 50% of those used in Europe and ca. 60% in the United States. Most of them are high foaming but scarcely tolerant to hard water, thus

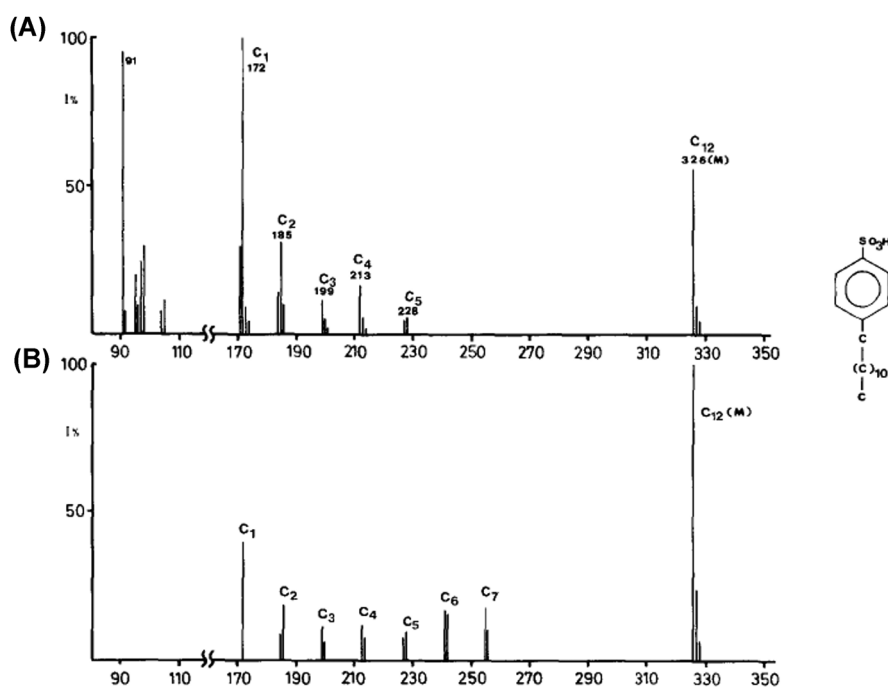


FIGURE 2 EI mass spectra of dodecylbenzenesulfonate at 75 eV (A) and 15 eV (B). Reproduced with the permission of Elsevier (Agozzino et al., 1986). EI, electron impact

requiring the addition of substances to complex calcium and magnesium ions, so called detergent builders. Anionic surfactants are more effective than other surfactants in particulate soil removal, especially from natural fabrics. As a rule, they are easily spray-dried and are chosen as detergent powders. Greater sensitivity and selectivity toward anionic surfactants are obtained by MS in negative ionization mode, even though works using positive ionization are also reported (Broze, 1999; Morelli & Szajer, 2001, 2000).

Alkylbenzenesulfonates (ABS) are anionic surfactants made of branched chains, which are only biodegradable with difficulty after long times. Except for specific applications, ABS are not used in developed countries as emulsifiers for agricultural chemicals. To facilitate the chemical and biodegradation under aerobic conditions, linear alkylbenzenesulfonates (LAS) have been introduced. LAS are synthesized by Friedel-Crafts alkylation of benzene using alkylation catalyst and ensuing sulfonation with oleum or sulfur trioxide, producing mainly the para isomers. Albeit LAS are enough sensitive to water hardness, they are plentifully used throughout the world because of their relatively low cost. GC-MS has been successfully applied to identify LAS homologs (Agozzino et al., 1986). The 75-eV electron impact (EI) mass spectrum of dodecylbenzenesulfonate with phenyl substitution in the C1 position (Figure 2A) show the tropylium ion, $[C_7H_7]^+$, at m/z 91 and the base peak at m/z 172 arises from the molecular ion by a benzylic cleavage with hydrogen rearrangement; the peak at m/z 171 is formed by a simple benzylic cleavage; both these fragmentations are consistent with unbranched α position. Other cleavages at different positions of the dodecyl chain yield the abundant ions at m/z 185, 199, 213, and 227 corresponding to C1, C2, C3, C4, and C5 fragments (the symbol C_n indicates the ions constituted by an alkyl chain of n carbon atoms linked to $-C_6H_4-SO_3H$). In the low electron beam energy (15 eV) spectrum, reported in Figure 2B, the rearrangement ion (m/z 172) is always the most abundant fragment, while the simple α cleavage reaction is completely quenched. This means that in 1-dodecylbenzenesulfonic acid the α cleavage reaction with H rearrangement is the process requiring lower energy.

LAS can be readily distinguished from the branched alkyl chains of tetrapropylene-based ABS by the different fragmentation patterns in tandem MS analysis of their precursor ions. The product ion at m/z 183 and chemical formula $[O_3SCH=CH_2]^-$ is diagnostic of LAS, while the corresponding ABS product ion $[O_3SC(CH_3)=CH_2]^-$ is detected at m/z 197. Both product ions exhibit the common loss of SO_2 to form species at m/z 119 and 133, respectively. Interesting examples of LC-MS analysis with ESI in the negative ion mode were reported by

González-Mazo et al. (1997) and Villar et al. (2007) with very careful determination of LAS along with their co-products and metabolites in wastewater.

Alkyl sulfates (AS), also called alcohol sulfates, are anionic surfactants formally obtained by sulfuric acid and linear alcohols. Alkyl chain lengths range from C10 to C18, and the properties of the final mixture vary with the alkyl chain length distribution. The alcohol source can be either natural (i.e., usually linear) or synthetic as oxo alcohols with some branching chains. The most used starting materials of fatty alcohols in the United States (ca. 15%) come from saponification of natural oil and fat. They tend to be sensitive to water hardness but are very widely used in cosmetics and detergents; lauryl alcohol sulfate is a major ingredient of hair shampoo (Broze, 1999). Since 1984, AS were structurally characterized by Lyon, Stebbings, et al. (1984) in positive and negative-ion mode by FAB/MS with collision induced dissociation (CID) experiments. However, FAB/MS lacks badly in sensitivity and the m/z value of the precursor ion is often not sufficient to provide an explicit characterization, thus either the LC coupling or tandem MS analysis are very useful for structural identification (Ogura et al., 1996; Popenoe et al., 1994).

Alkyl ether sulfates (AES), also called alcohol ethoxysulfates, are prepared by addition of one to four oxyethylene ($-OCH_2CH_2-$, 44.05 Da) groups to an organic compound that carries one hydroxyl functional group ($-OH$), which is then sulfated. Commercial AES consists of a very broad spectrum of compounds, broader than for most other surfactant types. Oxyethylation enhances water solubility and foaming activity over the analogous alcohol sulfate, giving rise to useful products in shampoos and in liquid as well as powdered detergents. The raw material for these products can be either natural fatty alcohols or primary/secondary synthetic alcohols, usually of C12–C18 chain length. However, ether sulfates are not less sensitive to water hardness than other anionic surfactants (Broze, 1999). The analogous alkylphenol (AP) ether sulfates are found in industrial applications. Because of their very low volatility, the analysis of AES can be fully accomplished by soft ionization sources, both in positive and negative ion modes. The typical two ions observed in ESI(+) for each individual AES component are $[M + Na]^+$ and the “desulfated” species $[M - SO_3 + H]^+$, whereas a single peak due to a desodiated molecule ($[M - Na]^-$) is observed for each compound in ESI(-). APCI(+) produces a protonated “desulfated” ion in the form of $[M - NaSO_3 + 2H]^+$ for each AES species in the mixture under relatively low cone voltage (10 V) conditions. The mass spectral ion intensities of each AES in either ESI(+) or APCI(+) can be used to obtain an estimation of relative abundance

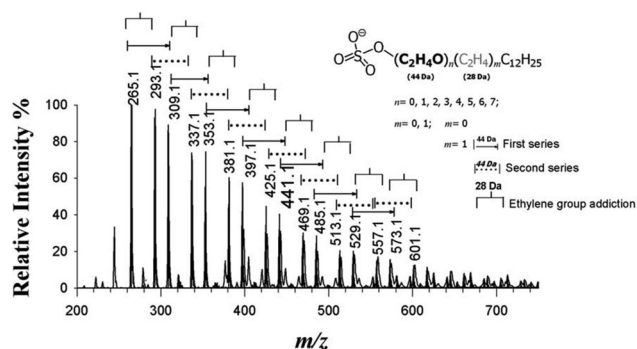


FIGURE 3 ESI(-)-MS spectrum obtained by direct injection of a methanolic solution of coceth sulfate. Inset: the general structure of CES whereby n indicates the number of oxyethylene units, between 0 and 7, and m (0 or 1) refers to the number of ethylene groups ($-\text{CH}_2\text{CH}_2-$, 28 Da) occurring in the alkyl chain of both series of oligomeric species, that is, $[\text{C}_{12}\text{H}_{25}(\text{OCH}_2\text{CH}_2)_n\text{OSO}_3]^-$ and $[\text{C}_{14}\text{H}_{29}(\text{OCH}_2\text{CH}_2)_n\text{OSO}_3]^-$. Reproduced with the permission of Elsevier (Onzo et al., 2020). CES, coceth sulfate; ESI, electrospray ionization; MS, mass spectrometry

in the mixture and an average ethylene oxide (EO) number of the sample. The precursor ions produced by positive or negative ESI, when subjected to low-energy (50 eV) collision-induced dissociation, do not fragment to give ions that provide adequate structural information. Conversely, protonated desulfated ions produced by APCI(+) generate fragment ions that disclose structural information of the precursor ions, including alkyl chain length and EO number, under similar conditions. Apparently, APCI(+) is less susceptible to matrix effects for quantitative work compared to ESI(+), thus APCI(+) provides an additional tool for the analysis of anionic surfactants such as AES, especially in complex mixtures where tandem MS is required for the identification of each component (Jewett et al., 1999). The use of ESI was demonstrated for LC-ESI/MS of AS and ethoxysulfates of C12–C15 alkyl chain length and 0–8 ethoxy groups: partial separation of alkyl chains was reported with quantification of individual homologs accomplished by MS in the negative ion mode (Popenoe et al., 1994). MS/MS of product ions in positive polarity produced rather uninformative spectra; for instance, whereas MS/MS of $[\text{R}(\text{OCH}_2\text{CH}_2)_n\text{OSO}_3\text{Na}_2]^+$ gives rise to Na^+ and $[\text{Na}_2\text{H-SO}_4]^+$ ions, the adduct $[\text{R}(\text{OCH}_2\text{CH}_2)_n\text{OH} + \text{Na}]^+$ yields just sodium ions as the main product ions. In the case of negative polarity, tandem MS of surfactant species with low degree of polymerization of alcohol ethoxysulfates (i.e., $[\text{R}(\text{OCH}_2\text{CH}_2)_n\text{OSO}_3]^-$) is also uninformative because the most common product ions $[\text{HSO}_4]^-$ at m/z 97, SO_3^- at m/z 80 and a low intensity peak signal at m/z 123 ($[\text{CH}_2=\text{CHOSO}_3]^-$) are reported (Attygalle et al., 2001). Remarkably, tandem mass spectra of AES with a high

degree of polymerization are more informative, showing fragmentation of monomeric units, whose product ions can be used to infer the number of EO units along with the alkyl chain (Onzo et al., 2020). CID of the precursor ion $[\text{R}(\text{OCH}_2\text{CH}_2)_n\text{OH} + \text{H}]^+$, produced by APCI, is more helpful as some important product ions can be obtained, corresponding to the alkyl group loss, namely $[\text{H}(\text{OCH}_2\text{CH}_2)_n\text{OH} + \text{H}]^+$, from which the alkyl group can be deduced. In addition, a series of ions of the form $[\text{C}_2\text{H}_4(\text{OCH}_2\text{CH}_2)_n\text{OH}]^+$ with $n = 1-4$, were observed in the corresponding mass spectra (Jewett et al., 1999). Very recently, the use of an ESI source in MS was found very effective to unveil the commercial formulas of AES. Alkyl chain lengths and degrees of ethoxylation of AES contained in CES solution were inferred from experimental data (Onzo et al., 2020). Single-stage ESI-MS analysis of CES allowed to distinguish two different series whose members differed in molecular mass by 28.05 Da, that is, the mass of the unit $-\text{CH}_2\text{CH}_2-$, thus suggesting the presence of C_x and $\text{C}_{(x+2)}$ alkyl homologues. For both series, a difference in the molecular mass of 44.05 Da, that is, the monomeric oxyethylene unit, was ascertained as shown in Figure 3, and the formulation fingerprint of CES was qualitatively used to check three commercial detergent formulations.

α -Olefin sulfonates are produced from the reaction between linear C11–C20 α -olefins and SO_3 . Whereas compounds with an alkyl chain length below C14 are used in liquid detergents, those above C14 are used in spray-dried powders. Enhanced water solubility is guaranteed by hydroxy groups, whereas double bonds make the mixture unstable to bleach. One of the most interesting features of α -olefin sulfonates is that they are less sensitive to water hardness than most anionic surfactants and are readily biodegradable (Broze, 1999). EI/MS spectra of methyl derivative of hexadecane sulfonates exhibit the highest m/z ion corresponding to the demethoxylated molecular ion $[\text{M} - \text{OCH}_3]^+$. Other peak signals corresponding to ions $[\text{C}_{16}\text{H}_{31}]^+$, $[\text{C}_{16}\text{H}_{29}]^+$, $[\text{SO}_2]^+$, and $[\text{CH}_3\text{SO}_2]^+$ were recognized (Taulli, 1969). The absence of the radical molecular ion peak signals is also common to methyl derivative of 2-hydroxyalkanesulfonate where the main peak at m/z 153 corresponds to the following fragment $[\text{CH}_3\text{O}=\text{CHCH}_2\text{-SO}_3\text{CH}_3]^+$ (Boyer et al., 1982) along with a peak at m/z 121 due to methanol loss. In ESI/MS instead, the deprotonated molecules of olefin sulfonates can be observed (Shi et al., 2014).

3.2 | Nonionic surfactants

Nonionic surfactants are generally more tolerant to water hardness compared to anionic ones. They tend to be

more effective than other surfactants for removal of oily soil from synthetic fabrics. Most nonionics are considered low-foaming products, possess good cold-water solubility and low CMC, making them effective even at low concentration. Their compatibility with cationic fabric softeners makes them preferable to anionics in certain formulations. These features and their low production costs make nonionic surfactants the most frequently detergent formulations, thus generating a strong environment impact (Bajpai & Tyagi, 2010; Cserhati, 1995).

Among nonionic surfactants, ethoxylated alcohols (AEO) are largely used as laundry detergents (Nitschke & Huber, 1993; Schmitt et al., 1990). The primary alcohol ethoxylates are the common item of commerce, but secondary alcohol ethoxylates are also available. The most important surfactant properties are controlled by the average EO percent and the average chain length of the starting alcohol (Hanton et al., 2006). Direct EI/MS analysis is handicapped because the ethoxylates of commercial interest are scarcely volatile. After derivatization, however, the identification of AEO can be performed from interpretation of the EI spectrum (Schneider et al., 1983; Vettori et al., 1988). Various types of nonionic surfactants have been analyzed by MS using ESI as ionization technique.

In detail, ESI/MS in the positive ionization mode is largely used in qualitative and quantitative analysis of nonionic surfactants because the hydroxyl deprotonation in the ionization source is rather negligible (Gomez et al., 2011). Also, negative ion mode ESI/MS experiments were conducted successfully on polyethoxylated surfactants, providing useful structural and mechanistic information: MS analysis of each peak provides data on the ethoxylated chain and identifying unambiguously each compound (Onzo et al., 2020). ESI and MALDI/MS generate protonated adducts $[M + H]^+$ reflecting the true molecular weight distribution (Hanton et al., 2006; Sherrard et al., 1994), which means that most intense peaks are at intervals of 44 Da, with peaks differing by 14 Da. When CID is applied to ions produced by ESI/MS, fragmentation of secondary AEO occurs more easily than primary one; with higher energy CID of secondary AEO compounds, the poly(ethylene glycol) (PEG) ions become dominant extending to the higher mass range. With APCI, positive ions of the form $[14n + 44x + 18]^+$, corresponding to the molecular ions, are observed. Environmental samples will also give ions for PEG, $[44x + 18]^+$, and mono- and di-carboxylated PEG, $[44x + 76]^+$ and $[44x + 134]^+$, respectively (Castillo & Barceló, 1999). APCI in negative ion mode of AEO generates deprotonated molecules.

APEO such as octylphenol polyethoxylate (OPEO) and nonylphenol polyethoxylate (NPEO) are commercially

important PEG-type nonionic surfactants, which have been widely used in industrial, agricultural, and domestic applications such as detergents, emulsifiers, pesticide additives and so on (Broze, 1999). Upon release into the environment, they undergo slow biodegradation processes and concern has increased about relatively stable degradation products of APEO, APs such as nonylphenol (NP) and octylphenol (OP) (Figure 4) (Zhang et al., 2009). AP have been classified together with lower ethoxylates (from mono- to tri-), as endocrine-disrupting compounds, because of their effects on the hormonal system of numerous organisms by competing with estrogen for binding receptors (Cserhati, 1995). APEO are preferentially detected in positive ion mode, while AP their self are detected with greatest sensitivity in negative ion mode (Shang et al., 1999). Electrospray MS of an acidic solution of NPEO as protonated adducts, $[M + H]^+$, reflects the true molecular weight distribution, with the main peaks differing by 44 Da, that is, the monomeric EO unit mass. The presence of sodium and potassium ions lead to the appearance of other peaks corresponding to sodiated and potassiated adducts, $[M + Na]^+$ and $[M + K]^+$ (Sherrard et al., 1994). Tandem MS shows product ions corresponding to the neutral loss of one EO unit (44 Da, $-CH_2CH_2O-$), 2 EO units (88 Da), and C_9H_{18} (126 Da). Likewise, tandem MS can be used to identify NPEO present in complex matrices by monitoring the product ion $[PhOCH=CH_2 + H]^+$ at m/z 121.16 for 1-4 EO units, and $[CH_2=CH-OCH_2CH_2-OCH_2CH_2-OH + H]^+$ at m/z 133.17 for higher ethoxylates (Figure 5) (Plomley et al., 1999).

APEO ions are dissociation resistant to low energy CID, showing very little fragmentation to form protonated PEG species (Sherrard et al., 1994). By increasing the collision energy, the formation of product ions corresponding to the loss of portions of both alkyl and ethoxy chains could be observed (see Figure 5). MALDI/ToF/MS was applied for APEO characterization, providing interesting information on the fate of these

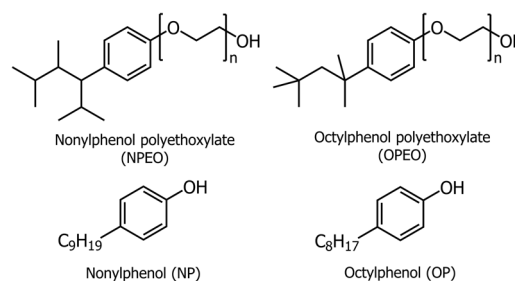


FIGURE 4 Representative APEO chemical structures and their metabolites NP and OP. APEO, alkylphenol polyethoxylates; NP, nonylphenol; OP, octylphenol

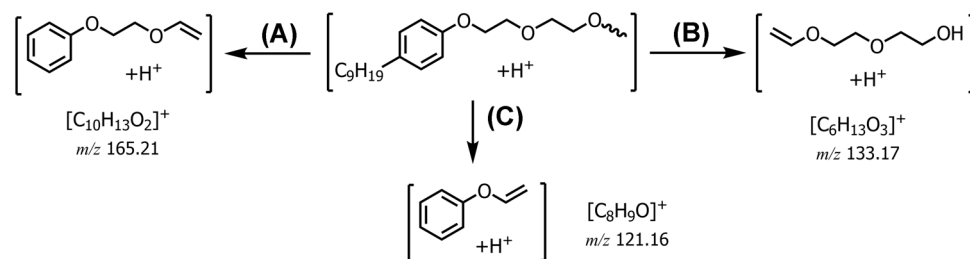


FIGURE 5 Proposed fragmentation pathways for the production of (A) m/z 165.21, (B) m/z 133.17, and (C) m/z 121.16, representative of the formation of product ions of general formula $[NPE_x + H]^+$. Reproduced with the permission of Elsevier (Plomley et al., 1999)

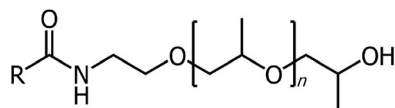


FIGURE 6 General formula of fatty acid alkanolamides wherein R represents a C10–C18 alkyl group and n a number from 1 to 3

substances in environment samples. For example, *Pseudomonas* sp. biodegradation intermediates of OPEO isolated from a paddy field soil and examined by MALDI/MS showed mass spectrum whereby a hydroxyl end-group and several EO units, distributed mostly from 4 to 17, with maximum intensity peak at 9 EO units. The gradual shortening by biodegradation processes was successfully monitored by MALDI/MS, where the maximum of the ion peak distributions of OPEO decreased from 9 EO units down to 3. Furthermore, among the biodegradation intermediates, the formation of OPEO oligomers with a carboxyl terminal of EO chain was also noted under m/z 600. These observations agreed with an exo-scission of EO chain accompanied with oxidation of the hydroxyl terminal side (Sato et al., 2001). Moreover, MALDI/MS alone was used for quantification of NPEO in commercial products too, showing good results by choosing a proper internal standard (Hanton et al., 2006).

PEG are polyols used in a wide range of industrial applications including surfactants and precursors for grafted polymers. The characterization of PEG is of

significance in correlating compositions and structures with their properties and, for this purpose, the combination of MALDI/ToF/MS, ESI/MS, and MS/MS demonstrated to be the approach of choice to obtain compositional information required for problem solving. Indeed, Chen et al. (2001) analysed four EO/PO copolymers to unequivocally demonstrate that one of the samples had a small variation in copolymer composition, thus explaining its abnormal activity. Moreover, two samples, displaying similar properties and activities, were found to be two different PEG blends.

Fatty acid alkanolamides (Figure 6), useful for increasing the viscosity of liquid formulations including shampoo (from ca. 0.5% to 5% by weight), were investigated by EI and positive-ion chemical ionization (PCI) MS. The discussion of the fragmentation pattern is made in correlation with the methyl branch position in aliphatic compounds and the double bond position in monounsaturated compounds. A quantitative correlation of the ratio $[M-H_2O+H]^+/[M-H_2O-H]^+$, in the PCI mass spectra, with the number of double bonds, C atoms, and aliphatic H atoms is made from the authors (Moldovan et al., 1997).

Belonging to the nonionic surfactant class are the alkyl polyglycosides (see Figure 7), obtained by acid-catalyzed condensation of a fatty alcohol with hexoses such as glucose. Alkyl polyglycosides (APG) typically have single alkyl chains with length in the C8–C16 range, with an average degree of polymerization of the glycoside

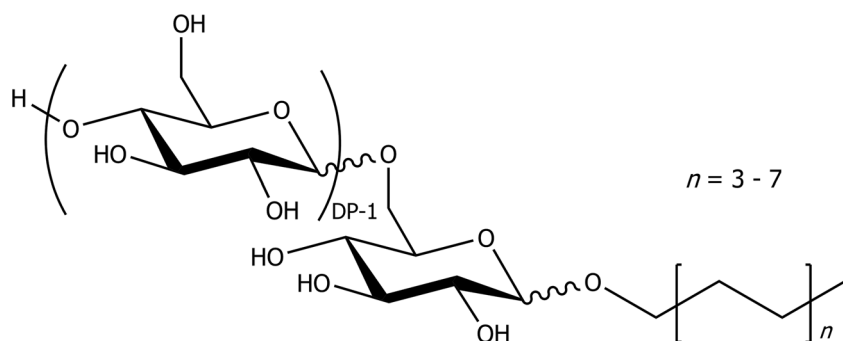


FIGURE 7 General formula of alkyl polyglycosides whereby DP is the degree of polymerization

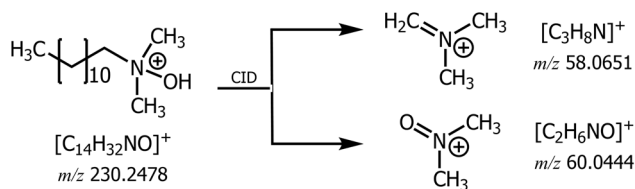


FIGURE 8 Protonated dodecyl (i.e., coco or lauryl) dimethylamine oxide and the schematic formation of product ions at m/z 58 and 60

moiety between 1 and 4. For their natural origin, they are mainly encountered in applications where mildness and good detergency property are important, such as cosmetics and personal care products (Bajpai & Tyagi, 2010; Broze, 1999). EI/MS of underivatized glycosides provides characteristic fragments of the sugar, fragments of the alkyl chain without the molecular ions. Thus, the identity of the alkyl chain cannot be inferred from these spectra alone. Ambient pressure ionization was applied for direct analysis of APG and esters of APG (Facino et al., 1995). LC-ESI/MS of deprotonated APG molecules ($[\text{M} - \text{H}]^-$) showed a uniform response and good results in SIM mode (Kühn & Neubert, 2004).

Amine oxides are synthesized by oxidation of tertiary amines with hydrogen peroxide in aqueous solution. They are useful as foam stabilizers and are used extensively in cosmetics as well as household products. FAB/MS of amine oxides gives positive ions corresponding to protonated molecules and dimer ions (Lyon, Crow, et al., 1984). For example, the mass spectrum of cocodimethylamine oxides exhibited intense $[\text{M} + \text{H}]^+$ ions at m/z 230, 258, and 286 for C12, C14, and C16 homologues, respectively and the relative abundances mirror the commercial product composition, that is, dodecyl (70%), tetradecyl (25%) and hexadecyl (5%). Proton bound dimers of the form $[2\text{M} + \text{H}]^+$ corresponding to each component appeared at m/z 459 (20%), 487 (15%) and 515 (6%). Loss of water from the protonated molecule (m/z 230) to yield a peak signal at m/z 212, occurs upon CID too. As depicted in Figure 8, the most abundant fragment ion at m/z 58 come from cleavage of the long β alkyl chain to the nitrogen together with the loss of the -OH group from the precursor ion. Another fragment at m/z 60 is formed by direct cleavage of the C-N bond of the dodecyl moiety with the oxygen remaining attached to the nitrogen (35% relative abundance).

3.3 | Cationic surfactants

Cationic surfactants are useful as fabric softeners, corrosion inhibitors, and antimicrobial agents. They are not

used in general purpose detergents because they do not provide effective cleaning at neutral pH values. In general, only nitrogen-based compounds are used as cationic surfactants, most of them being QAS (Broze, 1999; Morelli & Szajer, 2000; Zakharova et al., 2019). Under EI or CI conditions, quaternary amines normally decompose to tertiary amines, which can be ionized or protonated for MS detection. Thus, ordinary MS shows only fragments and rearrangement product ions, and its use is rather limited in the analysis of unknown mixture compounds (Tsai & Ding, 2004). FAB tandem mass spectra of aliphatic amines show diagnostic ions useful to infer the alkyl chain length by considering related fragment ions. Both negative and positive ionization modes were successfully performed on QAS and ethoxylated quaternary amines to identify the composition of the commercial product Arquad 12-50 and Ethoquad 18/12 (Lyon, Crow, et al., 1984).

3.4 | Amphoteric surfactants

Amphoteric surfactants contain both anionic and cationic functional group in the same molecule, therefore they can act either as anionic or cationic surfactants, depending on the solution pH. Their production is more costly than ionic and amphoteric surfactants, representing just 3% of surfactants in Europe and less than 1% in the United States. They are less irritating than other materials and are largely used in personal care products. Bond cleavage amphoteric compounds usually occurs before volatilization in conventional EI or CI sources. Apparently, ESI as a soft ionization source is more suitable for MS analysis (Eichhorn & Knepper, 2001; Lyon, Crow, et al., 1984) and their di-functionality can be inferred by the existence of diagnostic ions.

3.5 | Biosurfactants

Currently, MS is the most exploited technique to study biosurfactants, which are surface active substances derived from natural sources even though frequently biosurfactant refers specifically to the surfactants produced directly by microorganisms. Biosurfactants represent an ecofriendly and innovative alternative, as they are typically of lower toxicity than synthetic surfactants (Hayes & Smith, 2019). Since biosurfactants boast a lower environmental impact, they have found application in the production of fine chemicals, as surface coatings, additives for environmental remediation and in biological control (Kitamoto et al., 2002; Pacwa-Płociniczak et al., 2011). Biosurfactants are amphiphilic compounds

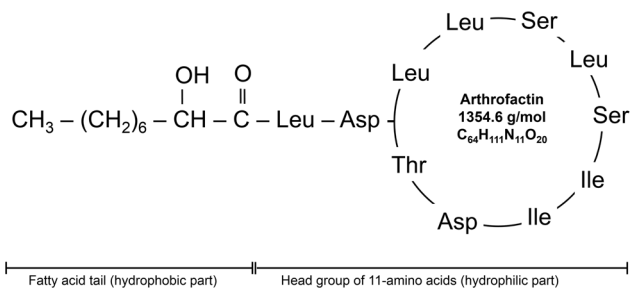


FIGURE 9 Schematic structure of arthrofactin

produced in living spaces or excreted as extracellular hydrophobic and hydrophilic moieties that confer on the organism the ability to accumulate between fluid phases, thus reducing surface and interfacial tension. They are produced by several microorganisms, bacteria, fungi, and yeasts which include *Acinetobacter* sp., *Bacillus* sp., *Candida antarctica*, and *Pseudomonas aeruginosa*. Biosurfactants are glycolipids, lipoamino acids, lipopeptides, lipoproteins, lipopolysaccharides, phospholipids, mono-glycerides, and diglycerides. During the last few decades, the increasing interest in biological surfactants led to an

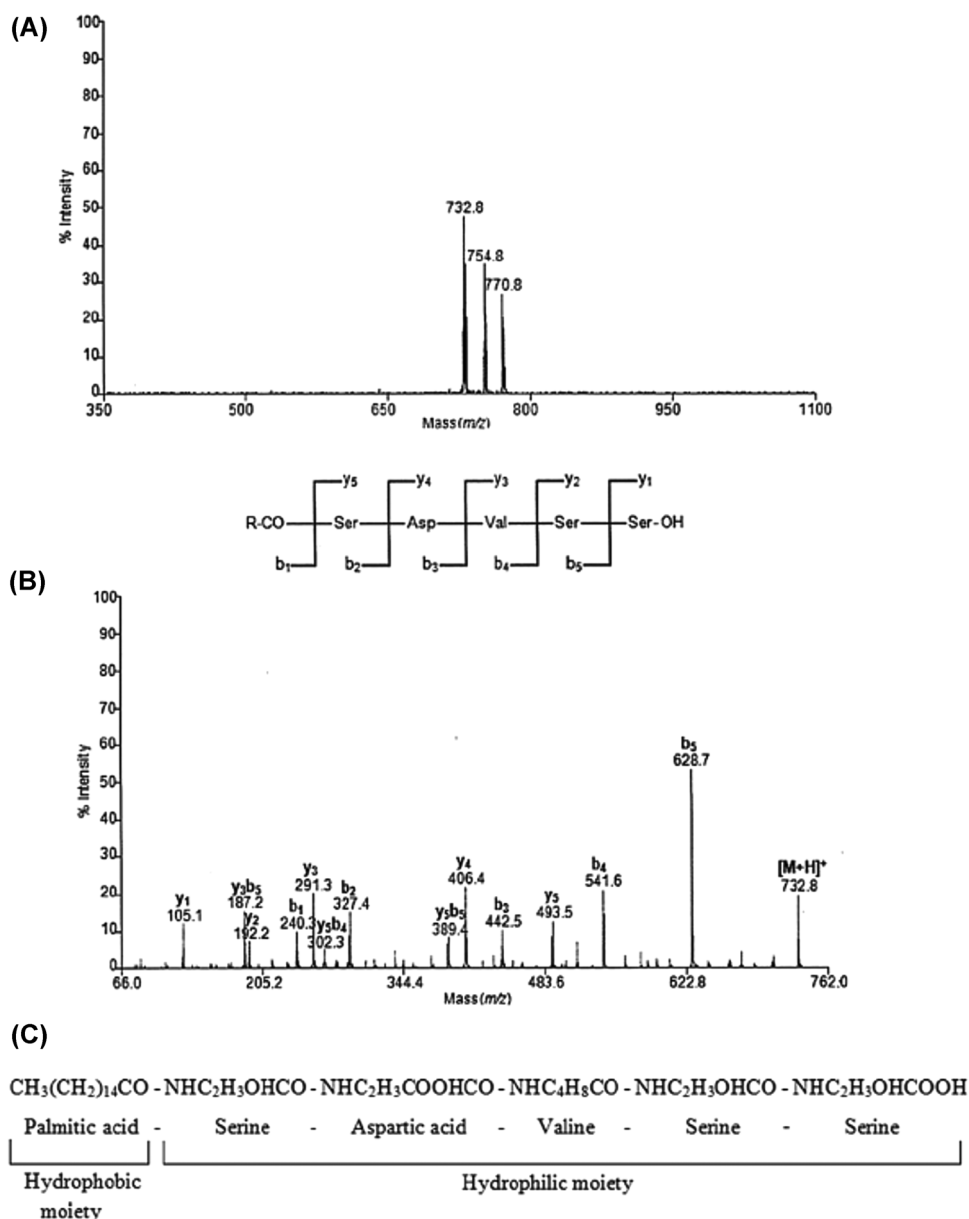


FIGURE 10 (A) MALDI-TOF-MS spectrum of the purified lipopeptide biosurfactant from *Pontibacter korensis* SBK-47. (B) Tandem MS spectrum of the protonated precursor ion $[M + H]^+$ at m/z 732.8 and (C) deduced structure of the purified lipopeptide biosurfactant from *P. korensis* SBK-47. Reproduced with the permission of Elsevier (Balan et al., 2016). MALDI-ToF-MS, matrix-assisted laser desorption/ionization time-of-flight mass spectrometry

intensification of research for the cost-efficient production of biosurfactants compared with traditional petrochemical surface-active components. The request of alternative production strains has been also associated with new demands on biosurfactant analysis. MS/MS testing is extensively employed to figure out the biosurfactant chain units. For example, arthrofactin, a biosurfactant produced by *Arthrobacter* species strain MIS38, was analysed by FAB/CID/MS and identified as 3-hydroxydecanoyl-D-leucyl-D-asparagyl-D-threonyl-D-leucyl-D-leucyl-D-seryl-L-leucyl-D-seryl-L-isoleucyl-L-isoleucyl-L-asparagyl lactone (Morikawa et al., 1993) (see Figure 9).

MALDI/ToF/MS was used to characterize a biosurfactant produced by a novel marine bacterium *Pontibacter korlensis* SBK47 showing significant properties like excellent surface tension reduction, CMC and emulsification activity (Balan et al., 2016). Mass spectra revealed a cluster of three peaks at m/z 732.8, 754.8, and 770.8, recognized as protonated, Na^+ and K^+ adducts (Figure 10a). The tandem MS analysis of the precursor ion at m/z 732.8 revealed the amino acid sequence as Ser-Asp-Val-Ser-Ser (Figure 10b). The authors assigned the ion at m/z 240.3 to $\text{C}_{16}\text{H}_{32}\text{O}^{+}$, thus suggesting the presence of a fatty acyl chain. Based on these data and their interpretation, the structure of the lipopeptide biosurfactant was elucidated as Palmitoyl-Ser-Asp-Val-Ser-Ser (Figure 10c), which represents a new lipopeptide biosurfactant named *pontifactin*.

HPLC-ESI/MS was used by Costa et al. (2006) to characterize the rhamnolipids produced by *P. aeruginosa* LBI in several Brazilian plants. Rhamnolipids have a glycosyl head group, in this case a rhamnose moiety, and a 3-(hydroxyalkanoyloxy)alkanoic acid (HAA) fatty acid tail. Specifically, there are two main classes of rhamnolipids (Rha_x): mono-rhamnolipids and di-rhamnolipids, which consist of one or two rhamnose groups respectively (Rha and Rha_2). They are also heterogeneous in the length and degree of branching of the HAA moiety (indicated as C_yC_z where y and z are the length of fatty acids).

MS analysis revealed the presence of two major components detected as the anions of m/z 649.40 and 503.34, which corresponds to the deprotonated molecules $[\text{M}-\text{H}]^-$ of the dirhamnolipid ($\text{Rha}_2\text{C}_{10}\text{C}_{10}$) and mono-rhamnolipid ($\text{RhaC}_{10}\text{C}_{10}$), respectively, with the latter (m/z 503.34) being the predominant ion in all samples analyzed. Mass selection of these anions followed by CID-MS/MS produced characteristic spectra (Figure 11) that confirm the structural assignments. For instance, $[\text{RhaC}_{10}\text{C}_{10}-\text{H}]^-$ at m/z 503.34 generated two major product ions by the gas-phase neutral loss of a mono-unsaturated C10 acyl chain to form $[\text{RhaC}_{10}-\text{H}]^-$ at m/z 333.21, and m/z 169.14 by the neutral loss of RhaC_{10}H and formation of $[\text{unsaturated C}_{10}-\text{H}]^-$ (Figure 11b). Likewise, $[\text{Rha}_2\text{C}_{10}\text{C}_{10}-\text{H}]^-$ of m/z 649.40 dissociates to generate two major product ions at m/z 479.28 and 169.15 (Figure 11a).

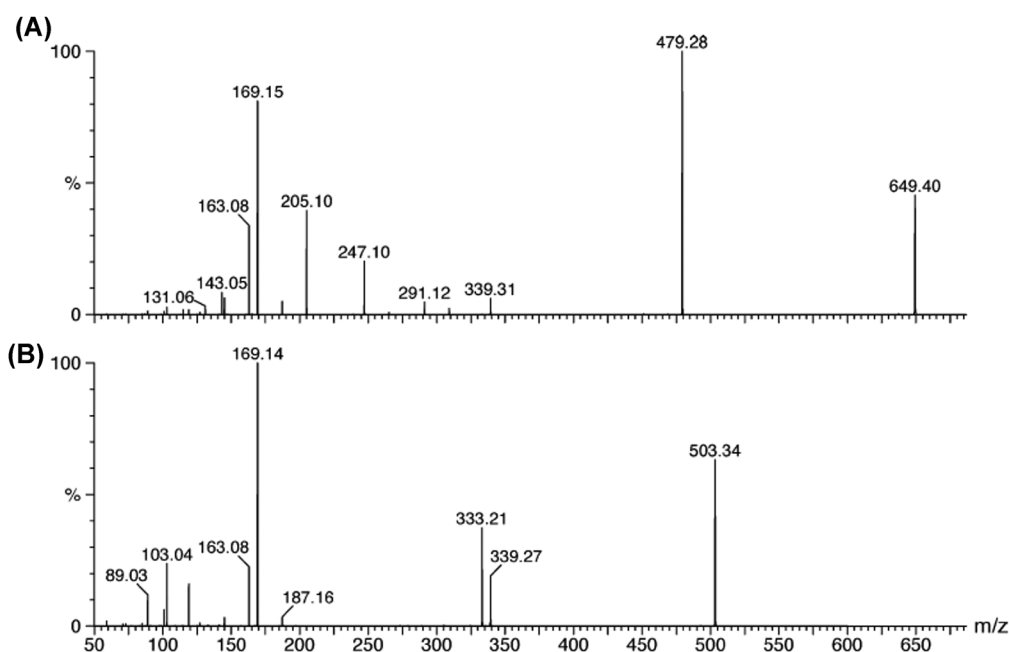


FIGURE 11 ESI tandem mass spectra of: (A) $[\text{Rha}_2\text{C}_{10}\text{C}_{10}-\text{H}]^-$ of m/z 649.40 and (B) $[\text{RhaC}_{10}\text{C}_{10}-\text{H}]^-$ of m/z 503.34. Reproduced with the permission of Elsevier (Costa et al., 2006). ESI, electrospray ionization

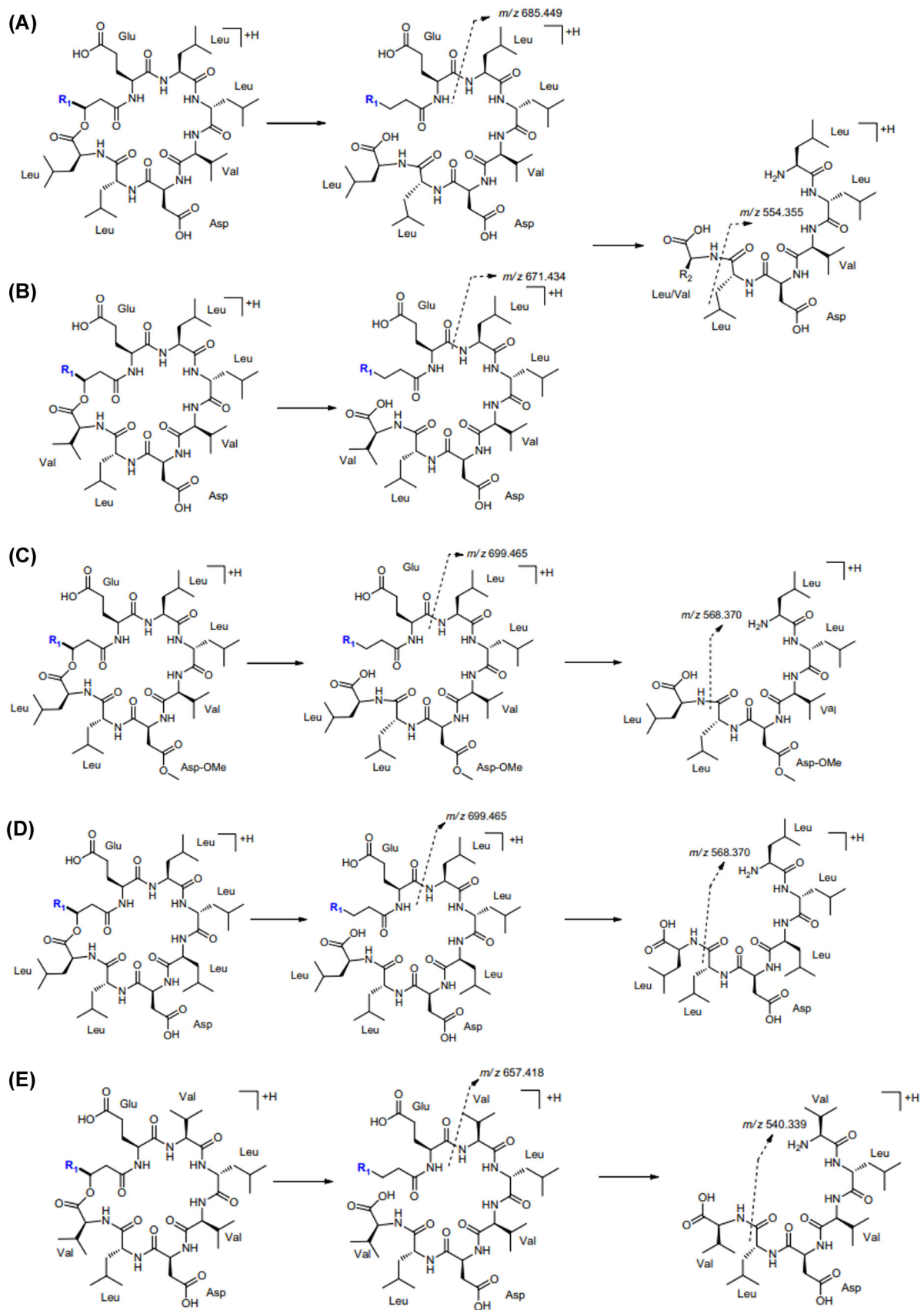


FIGURE 12 (See caption on next page)

In a recent study of Moro et al. (2018) on bacteria related to the *Bacillus* genus, surfactin isoforms were identified through ultra-high-performance LC coupled with HRMS. The surfactins are a mixture of isoforms, in which an amino acid of the cyclic peptide chain of surfactin Glu-Leu-Leu-Val-Asp-Leu-Leu is replaced by another amino acid. These isoforms may be differentiated according to their fragmentation pattern and structural features (Figure 12A–E). In detail, the MS/MS spectra of surfactin isoforms present some common fragments of $[M+H]^+$ at m/z 685.44, 671.43, and 699.46, which are due to protonated amino acid sequences of Val-Leu-Asp-Val-Leu-Leu, Leu-Leu-Asp-Val-Leu-Leu and Leu-Leu-Asp-OMe-Val-Leu-Leu, respectively. Common fragments of an isoform with primary structure Val-Leu-Asp-Val-Leu-Leu was found and proposed in Figure 12E, suggesting the occurrence of a new surfactin component (Moro et al., 2018).

For structural characterization of surfactin (C14/Leu7) produced by *Bacillus subtilis* isolate LSFM-05 grown on raw glycerol from the biodiesel industry, De Faria et al. (2011) used ESI/FTICR/MS, followed by CID for fragments of higher m/z , and infrared multiphoton dissociation (IRMPD) for fragments of lower m/z values. Dissociation produced ions of m/z 923, 810, 695, 596, 483, 370, and 227. These fragments corresponded to the sequential losses of the amino acid residues Leu/Leu/Asp/Val/Leu/Leu/GluOMe. The loss of a 143 Da residue from the fragment of m/z 370 to that of m/z 227. A mass of 143 Da corresponds to that of methylated glutamic acid (Glu-OMe), confirming that the glutamic acid residue is the methyl esterified amino acid. The ion of m/z 227 corresponds to an aliphatic fatty acid chain containing 14 carbons in the normal, iso or anteiso forms. This dissociation profile indicates that this lipopeptide is a seven-residue peptide with a Glu(O-Me)-Leu-Leu-Val-Asp-Leu-Leu sequence with a lactone bond linking the terminal Leu (position 7 on the peptide moiety) to the β -hydroxyl fatty acid moiety containing 14 carbons, creating a cyclopeptide. Other researchers (Moro et al., 2018) showed the characterization of surfactin isomers with amino acid sequences analogous to that reported in the work De Faria et al. (2011).

3.6 | Pulmonary surfactants

Several MS-based approaches have been exploited to characterize PS. PS are mixtures of lipids and proteins occurring in the alveolar surface of lungs, which form a layer between the aqueous airway liquid and the inspired air (Choi et al., 2020). Due to their essential role in preventing the collapse of lungs, a PS deficiency could contribute to the etiology of persistent or severe respiratory distress (e.g., newborn respiratory distress syndrome, NRDS) (Akella et al., 2013). In the last years, many natural mixtures of lipids and proteins have been proposed for the pharmacological treatment or prophylaxis of distress syndromes associated with PS deficiency.

The composition of Curosurf, a PS made up of 99% of polar and neutral lipids and about 1% of low molecular weight hydrophobic apoproteins, has been extensively investigated by Pelizzi et al. (2002). These authors developed a rapid and selective ESI-MS/MS method without preliminary derivatization or chromatographic separation; the following phospholipids were qualitatively identified: phosphatidylcholines, lysophosphatidylcholines, sphingomyelins, phosphatidylethanolamines, phosphatidylglycerols and phosphatidylinositols. Tandem MS experiments proved to be very useful for the unequivocal discrimination of phospholipids.

Bai et al. (2004) performed identification of surfactant protein SP-A and SP-D modifications in proteinosis and cystic fibrosis patients, by using MALDI/FTICR/MS analysis. Although isoforms of these surfactant proteins were detected, the IRMPD-FT-ICR MS/MS data clearly presented a new level of information. Of particular interest was the result obtained for an isoform of SP-A (mass 35 kDa, pI 4.6) after reduction, alkylation, in-gel deglycosylation and in-gel tryptic digestion. In contrast to all other matched tryptic digest peaks, a new peptide fragment peak at m/z 1736.7593 was assigned to the Asn-187-deamidated peptide, $^{180}\text{YSDGTPVDYTNWYR}^{193}$. The peaks denoted were identified as y_2 , y_3 , y_6 , y_{11} and b_3 fragment ions of m/z 1736, and demonstrated that the glycosylated Asn-187 was deamidated to form Asp. Therefore, analysis of bronchoalveolar lavage fluid proteins from adults with cystic fibrosis showed a decreased content of intact SP-A.

FIGURE 12 Fragmentation pattern for surfactin isoforms. (A) Surfactin A, fragment ions with m/z 685.449 and 554.355. (B) Surfactin B, fragments ions with m/z 671.434 and 554.355. (C) Surfactin monomethyl ester, fragments ions with m/z 699.465 and 568.370. (D) [Leu4] surfactin, fragments ions with m/z 699.465 and 568.370. (E) Isoform surfactin, fragments ions with m/z 657.418 and 540.339. Groups R1: $(\text{CH}_2)_5\text{-11CH}(\text{CH}_3)_2$. Reproduced under the terms of the Creative Commons Attribution License, which permits use, distribution and reproduction in any medium, provided the original open access work is properly cited (Moro et al., 2018) [Color figure can be viewed at wileyonlinelibrary.com]

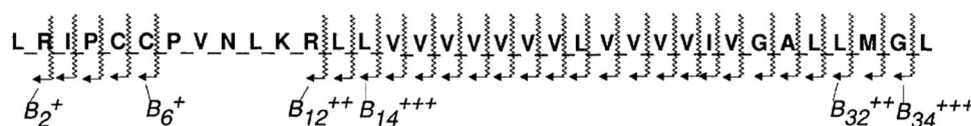


FIGURE 13 Fragmentation scheme of SP-C. The start and end of B-type fragment ion series are indicated. Reproduced with the permission of Wiley (Griffiths et al., 1998). SP-C, surfactant proteins C

Liu et al. (2008) used nano ESI/MS/MS to characterize the amino acid sequence of bovine surfactant proteins B (SP-B) and C (SP-C), that is, other natural surfactants used for the treatment of respiratory distress. It should be noted that, to determine the amino acid sequences, SP-B was first digested with trypsin and then analyzed by tandem MS, after a preliminary chromatographic separation. From the LC-MS/MS analysis of the protein digest, six unique peptides and some mis-cleaved peptides were detected. By assembling the peptides together and by considering SP-B from other species as templates, the complete sequence of bovine SP-B was obtained, namely FPIPI-PYCWL-CRTLI-KRIQA-VIPKG-VLAMT-VAQVC-HVVPL-LVGGI-CQCLV-ERYSV-ILLDT-LLGRM-LPQLV-CGLVL-RCSS. Thus, seven cysteine residues (C) were identified for the first time in the amino acid sequence.

Porcine pulmonary phospholipids (SP-C) have been widely used as well as natural surfactants. Their native form was investigated by plasma desorption MS, showing a lipopeptidic structure with two palmitoylated cysteine residues (Curstedt et al., 1990). In addition to plasma desorption MS, ESI/MS has been used as well for the analysis of porcine SP-C preparation, demonstrating the existence of extended forms of pulmonary SP-C including histidine and methionine as C-terminal residues (Griffiths et al., 1998). To obtain structural information, Griffiths et al. (1998) fragmented $[M + 3H]^{3+}$ ion of methionine oxidized C-terminally methylated SP-C, by using CID. In the tandem MS spectrum, three major product ions series were observed consisting of B_{12}^{2+} - B_{32}^{2+} , B_{14}^{3+} - B_{34}^{3+} and B_2^+ - B_6^+ , B_{17}^+ - B_{22}^+ (Figure 13). The sequence ion B_{34}^{3+} allowed to locate the site of methylation on the C-terminal amino acid. Moreover, the masses of sequence ions B_{33}^{3+} and B_{32}^{3+} enabled the identification of an oxidized methionine residue as amino acid 33. Instead, the B^+ ion series allowed to identify the palmitoylation sites on 5 and 6 cysteine residues.

The amount of surfactant deposited in the lungs and its overall pulmonary distribution determine the therapeutic outcome of surfactant replacement therapy. Most of the currently available methods to determine the intrapulmonary distribution of surfactant are time-consuming and require surfactant labeling. Zecchi et al. (2019) used mass spectrometry imaging (MSI) as a

label-free technique for evaluating the pulmonary distribution of exogenous surfactant in premature lambs. The authors successfully imaged and quantified SP-C analog and SP-B analog, by means of MSI in the peripheral lungs of all animals, treated with CHF5633. CHF5633 is a synthetic surfactant containing phospholipids and two synthetic peptides mimicking key sequences of SP-B and SP-C. Native human SP-B and SP-C have 79 and 35 amino acids, whereas SP-B analog and SP-C analog have 34 and 33 residues, respectively. Therefore, differences in number and type of amino acids endow SP-B analog and SP-C analog with distinct m/z ratios, which facilitated their detection by means of MSI and allowed to perform an accurate study of the intrapulmonary localization of CHF5633 surfactant. Distribution maps show the presence of both peptides in all samples of surfactant-treated animals. In untreated animals, however, the intensity of the signal is remarkably low and corresponds to background noise. SP-C analog shows a fairly uniform distribution across the lung sections of surfactant-treated animals with some local accumulation of this peptide in central areas. The distribution maps of SP-B analog show a lower intensity, mainly due to its relatively poor MALDI ionization yield. As for the SP-C analog, spots of local accumulation of the SP-B analog are also evident in the distribution maps. The investigation of the analog signals as a function of distance from the tissue border suggests reduced accessibility of peripheral lung regions to the drug, correlated well with the physiologic response as assessed by the area under the curves of the individual arterial partial oxygen pressure and dynamic lung compliance curves of the lambs.

Another recent MS application on PS, concerns complications affecting the lung due to severe coronavirus disease 2019 (COVID-19) (Acquavia et al., 2021). While there is evidence for autoimmunity in severe COVID-19, the exact mechanisms remain unknown. Sinnberg et al. (2021) established a prospective observational cohort to study lung specific autoantibodies (auto-Abs). Incubation of plasma from severe COVID-19 patients with healthy human lung tissue revealed the presence of Immunoglobulin A (IgA) antibodies binding to surfactant-producing pneumocytes. Enzyme-linked immunosorbent assays (ELISA) and protein pull-downs

using porcine surfactant confirmed the presence of auto-Abs binding to surfactant proteins in severe COVID-19 patients. MS and ELISAs with recombinant proteins identified IgA auto-Abs that target human surfactant proteins B and C. In line with these findings, lungs of deceased COVID-19 patients showed reduced PS. These data suggest that IgA-driven autoimmunity against surfactant may result in disease progression of COVID-19 (Sinnberg et al., 2021).

4 | QUANTITATIVE ANALYSIS OF SURFACTANTS BY USING MS

To determinate very low content of targeted compounds such as surfactants in complex mixtures, the MS quantitative analysis needs high sensitivity and selectivity. MS coupled to GC or LC markedly improves its ability to cope with complex matrices (Bianco et al., 2013, 2010; Pascale, Acquavia, et al., 2020) and targeted MS/MS experiments increase even more the selectivity (Pascale, Acquavia, et al., 2020). Both chromatographic step and tandem mass experiments reduce background noise, thus reaching outstanding levels of sensitivity and selectivity as well (Pascale, Bianco, et al., 2020; Ventura et al., 2019). Most scientific efforts have triggered the development of methods mainly concentrated on specific classes of surfactants, for their toxicity or their occurrence in common commercial products. Among these compounds, the discussion was focused on nonionic APEO, anionic LAS, PFAS, and cationic surfactants as QAS.

4.1 | Nonionic surfactants: The case of APEO

Non-ionic APEO deserve special attention because of their massive use and ubiquitous occurrence in the environment. The global production of APEO is well over 300.000 tons/year and have been extensively used in the last 40 years as detergents, emulsifiers, dispersants, antifoamers, and pesticide adjuvants. Approximately 60% of APEO that enter mechanical and biological sewage and sewage sludge treatment are subsequently released into the environment (Cserhati, 1995; Petrovic et al., 2002). Some of these surfactants biodegrade before reaching the environment: primary degradation (chain oxidation) may be 90% complete within a few hours to 1 month under favorable laboratory conditions, and treatment plants often remove more than 95% of the higher ethoxylates through secondary treatments (Ying et al., 2002). Initial degradation proceeds as an attack on the long ethoxy chain to produce short chain nonylphenol ethoxylates (NP_nEO, with *n* = number of ethoxy units) or carboxylic

acids. Apparently, these APEO metabolic intermediates are more toxic than their precursor compounds and more bio-accumulative in aquatic environments (Marcomini et al., 1990; Petrović & Barceló, 2000). Their environment degradation is highly variable with the result that the effluent concentrations of NPEO and metabolites are also highly variable. As expected, These compounds are potential endocrine disrupters and are able to enter the environment after pouring out from treatment plants (Petrović & Barceló, 2000). Considering the toxicity, the large production volumes and likely persistence, APEO and especially NPEO have emerged as a leading issue in Europe where a withdrawal for many uses largely occurred (Ying et al., 2002). All these worries lead to the need to improve and standardize analytical methods for their determination in complex environmental matrices. In this sense, the use of GC-MS was a turning point for APEO and relative derivative quantitation, because of higher sensitivities and specificities obtained in comparison to other techniques used on a routine basis for quality control purposes, like UV/Vis spectroscopy. Indeed, Stephanou and Giger (1982) successfully identified and quantified NP and NPEO with one and two oxyethylene groups in the effluents of six mechanical-biological sewage treatment plants. In detail, limits of detection (LOD) in µg/L range were obtained, thus allowing the quantitation of analytes from 36 to 202 µg/L, representing from 0.5% to 2.3% of the total residual dissolved organic carbon. The same approach was exploited by Ding et al. for the targeted analysis of nonylphenol polyethoxycarboxylates (NPEC) and their related degradation products (i.e., carboxyalkylphenol ethoxycarboxylates, CNPEC) in water samples. The method involved an extraction step using graphitized carbon black cartridges, and the direct derivatization with tetraalkylammonium salts in the GC injection-port by using a large-volume (10–20 ml) direct sample introduction device. The analytes were identified and quantitated, while on-line derivatization technique provided sensitive, fast and reproducible results for NPEC and their metabolites, with good recoveries ranging from 90% to 108% (Ding & Chen, 1999).

Thus, for nonionic surfactants, the employment of GC-MS either with EI or CI has proved to be useful for the analysis of these compounds with a low number of polyethoxylation degree. However, several drawbacks are associated with GC-MS, which is not suitable for the analysis of compounds with high degree of polymerization and high polarity, because of their low volatilities. Adding derivatization steps during the sample preparation process is a good solution in few cases and without accounting the completeness of reactions, the analysis is labor and time demanding, making the GC-MS of surfactant not suitable for routine work (Tsai & Ding, 2004).

Compared with GC-MS, HPLC with ESI/MS detection offers excellent sensitivity for ionic and polar molecules,

making it an ideal candidate for the quantitative determination of low volatile APEO metabolites. For example, a very sensitive and specific analytical procedure for determining nonionic polyethoxylate surfactants, such as AEO and NPEO in aqueous environmental samples using LC-ESI/MS was developed by Crescenzi et al (Crescenzi et al., 1995). The LODs were 0.6, 0.02, 0.002, and 0.0002 $\mu\text{g/L}$ for NPEOs and each AEO homologue in the influents and effluents of sewage treatment plants, river water, and drinking water, respectively. Recoveries of the analytes ranged between 85% and 97% and the liquid chromatographic conditions were adjusted for eluting all the oligomers of NPEO and of the various AEO homologues as single peaks to enhance detection levels and simplify quantification. LC-MS was also used for the analysis of APEO in solid samples, sediments, and sludges, with LODs values in the low ppb level. Pivotal for the analysis of complex solid matrices was the use of SPE cartridges during sample preparation step, which turned out to be the perfect solution for the matrix effect, one of the major LC-MS related problems (Pascale, Bianco, Cataldi, Buchicchio, et al., 2018). Finally, aquatic organism samples were analysed to find APEO and related derivatives, thus shedding some light on the fate of these substances once released into the environment.

4.2 | Anionic surfactants: The case of linear AS and PFAS

Among anionic surfactants of environmental interest, LAS and PFAS represent the emerging contaminants due to their occurrence in humans and wildlife and their bioaccumulative, nondegradative, and toxic properties (Giesy & Kannan, 2001; Grandjean & Clapp, 2015). GC-MS was successfully employed for LAS analysis. In detail, these compounds were found and quantified in anaerobically and aerobically stabilized sewage sludges. Sulfonyl chloride species were properly formed and separated by high-resolution gas chromatography (HRGC) coupled with either flame ionization detection or EI/MS and CI/MS modes (McEvoy & Giger, 1986). The total LAS concentrations ranged from 0.3% to 1.2% of dry sludge with only minor variations in the relative composition of LAS homologues and isomers. These concentrations were considerably larger than those of other pollutants that have been reported in sewage sludges. Although LAS are soluble in water, the sorption of these amphiphilic chemicals onto suspended particles in sewage seems to be significant. In contrast to their biodegradability in the aqueous phase, LAS are apparently enough resistant to biodegradation during sludge treatment.

LC-MS was applied for the PFAS analysis. Fluorinated alkyl surfactants as well as hydrocarbon surfactants are used as “active ingredients” in aqueous film-forming foams

(AFFF), which are used to fight hydrocarbon-fueled fires. The fluorinated alkyl substances present in AFFF decrease the surface tension, thus smothering the flames, preventing air from reaching flammable materials, and therefore, suppressing reignition of the fire (Moody et al., 2003). Formulations of AFFF contain mixtures of fluorosurfactants produced by either electrochemical fluorination or fluorotelomerization as well as hydrocarbon surfactants, cosolvents, and solvents. Although AFFF compose only a small percent of the total fluorosurfactant production, repeated applications of AFFF during fire training activities conducted at military bases have led to groundwater contamination by AFFF chemicals, unspent fuels, and solvents. Due to this wide spreading of fluorinated surfactant, LC-MS/MS was employed in various investigations to analyse perfluoroalkyl carboxylates and sulfonates in human sera (Olsen et al., 2003), animal tissues (Kannan et al., 2002) and surface water (Moody et al., 2001) showing low LOD (in the $\mu\text{g/L}$ and ng/g ranges, respectively) and recoveries higher than 90%.

4.3 | Cationic surfactants: The case of QAS

Fewer papers were dedicated to the quantitative analysis of cationic surfactants, mostly because of the lower frequency of use in the everyday life as detergents. For QAS, hyphenated MS techniques are able to reach high sensitivity in the $\mu\text{-}$ and ng/L dimensions for water samples and in the low-ppb one for solid ones, with recoveries ranging from 70% to 90% (Ferrer & Furlong, 2001; Ford et al., 2002; Radke et al., 1999; Sütterlin et al., 2008; Tsai & Ding, 2004). For example, the determination of alkyl (C12, C14, and C16) dimethylbenzylammonium chloride (benzalkonium chloride or BAC) in water samples was performed by the identification of the main ions at m/z of 304, 332, and 360, corresponding to the molecular ions of the C12, C14, and C16 alkyl BAC, respectively (Ferrer & Furlong, 2001). The unequivocal structural identification of these compounds in water samples was performed by LC-MS/MS after the isolation and the subsequent fragmentation of each quaternary ammonium ion. The main product ion observed of all the three different homologues corresponded to the loss of the toluyl group in the chemical structure, which led to the fragment ions at m/z 212, 240, and 268 and a tropylium ion, characteristic of all homologues, at m/z 91.

An interesting example of cationic surfactant examined by MALDI/MS was reported by Shrivastava and Wu (2007). A rapid, simple, sensitive, and effective quantitative method for the simultaneous determination of cationic surfactants from river and municipal wastewater

was successfully developed by combining single-drop microextraction (SDME), with atmospheric pressure (AP)/MALDI MS, without any separation step. SDME uses a microdrop (about 1–3 μl) of organic solvent suspended at the tip of a microsyringe for the extraction of analytes from the aqueous phase, thus allowing the suppression of matrix ions (background interferences) and, consequently, a signal-to-noise increase. This method was found to yield a linear calibration curve in the concentration range from 50 to 1500 $\mu\text{g/L}$ with LOD of 10 $\mu\text{g/L}$. The relative recoveries in river and municipal wastewater were found to be 93.8%–103.6% and 91.0%–98.7%, respectively.

5 | INNOVATIVE APPROACHES OF SURFACTANT ANALYSIS BY MS

The most modern advances in MS instrumentation provide the possibility to distinguish isomeric and even isobaric m/z values of surfactant complex mixtures by HRMS along with IM/MS coupled to two-dimensional (2D) separations or SFC.

5.1 | High resolution MS

The high resolving power (RP) of HRMS instruments reduces interferences and the high mass accuracy allows the prediction of molecular formulas from the m/z signals (Bianco et al., 2018; Kind & Fiehn, 2007; Pascale et al., 2016). Other important advances include fast full-scanning rates (i.e., >1 Hz), which allows for on-line coupling to chromatography, and high sensitivity, thereby allowing the detection of trace contaminants at femtogram levels in the full-scan operation mode. Commercially available HRMS apparatuses include various time-of-flight instruments (TOF-MS, $\text{RP} \geq 20,000$, mass accuracy ≤ 3 ppm, scan rate up to 200 Hz), Fourier-transform orbital trap (Orbitrap-FTMS, $\geq 240,000$, ≤ 2 ppm; up to 40 Hz) and Fourier-transform ion cyclotron resonance (FTICR-MS, $\geq 1,000,000$, ≤ 1 ppm, ≤ 1 Hz) (Pascale, Bianco, Cataldi, Kopplin, et al., 2018; Santarsiero et al., 2020).

Moe et al. (2012) proposed a HPLC-ESI/QToF/HRMS method for the structural characterization of a commercial detergent named Forafac[®]1157, composed of novel fluorinated surfactants developed by the DuPont company. The combined information from the ^1H , ^{13}C ,

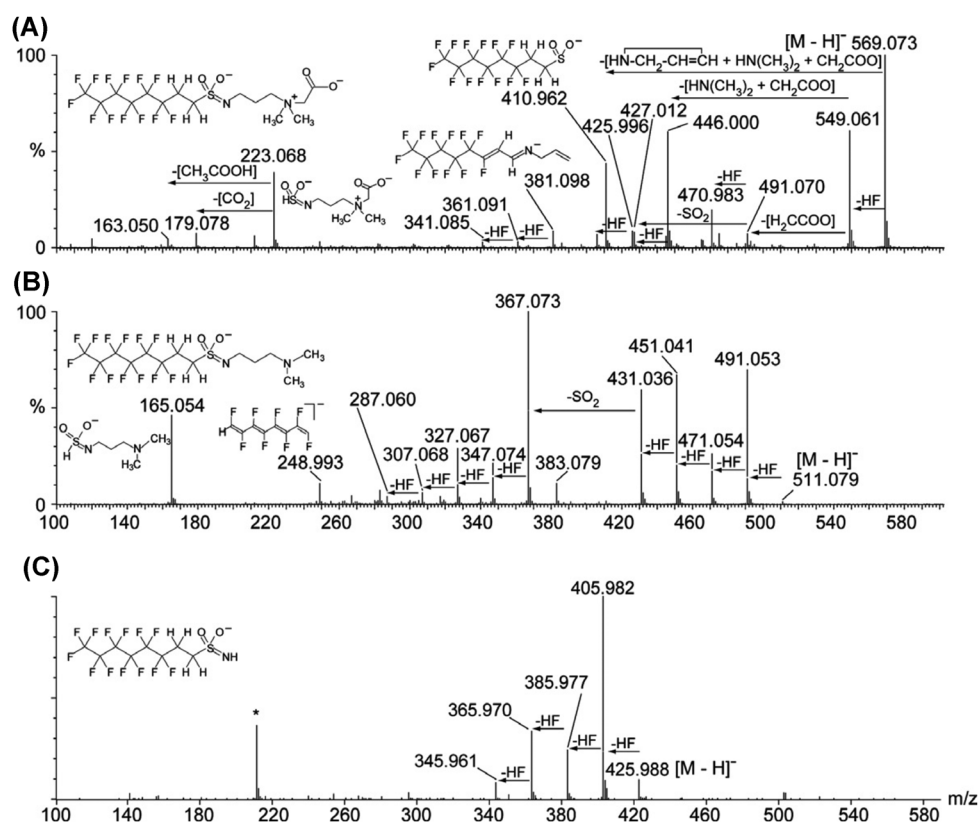


FIGURE 14 Mass spectra of deprotonated (A) 6:2 FTAB; (B) the major metabolite from mussel and turbot, and the major photolytic transformation product; (C) the 6:2 fluorotelomersulfonamide by-product was produced by turbot, mussel, and photolysis. All spectra were recorded at CV 35 V. Reproduced with the permission of Elsevier (Moe et al., 2012). FTAB, fluorotelomer sulfonamide alkylbetaine

^{19}F , ^1H - ^1H correlation spectroscopy, NMR spectra and m/z values allowed the chemical formula assignment of the observed ion at m/z 571.094 in positive ion mode, that is, $[\text{C}_{15}\text{H}_{20}\text{F}_{13}\text{N}_2\text{O}_4\text{S}]^+$ ($\Delta m = 1.1$ ppm) to a 6:2 fluorotelomer sulfonamide alkylbetaine. The same findings were experienced in negative ion mode where the m/z 569.073 was isolated and fragmented as reported in plot of Figure 14. The same approach was employed for its major metabolites extracted from turbot and mussel, both exposed to the commercial product treated with simulated UV light. The tandem MS spectrum of the precursor ion at m/z 511.079 is illustrated in plot b (Figure 14), which is 58.005 Da lower than the precursor compound, suggesting the neutral loss of oxiran-2-one ($\text{C}_2\text{H}_2\text{O}_2$, 58.005) from the betaine moiety and the generation of a secondary N,N -dimethylamine. Photolysis also yielded one by-product, whose $[\text{M}-\text{H}]^-$ ion was observed at m/z 425.983 (Figure 14c; $\Delta m = 2.5$ ppm): the interpretation of tandem mass spectrum in Figure 14c allowed to identify the compound as 6:2 fluorotelomer sulfonamide.

Chiesa et al. (2018) developed and validated a sensitive method by HPLC-HRMS to monitor the occurrence of 16 PFAS in eels from the Gard Lake (Italy). The LOD were in the order of pg/g and the recoveries were between 80% and 101%. MS/MS targeted analysis was used to improve analyte identification by chemical formula calculation of precursor and product ions.

Despite these great advantages, HRMS produces a huge amount of data, which require an effective data processing strategy. Kendrick mass defect (KMD) analysis is one of the most common approach, used for the identification of homologous series, that is, a series of MS signals differing only by a number of previously chosen base units, such as those present in surfactants, demonstrating to be fully suitable for the by-products identification of unknown surfactants (Fouquet & Sato, 2017; Gaiffe et al., 2018; Hughey et al., 2001; Tziotis et al., 2011). Thurman et al. (2014) used LC-QToF/MS to perform studies of ethoxylated surfactants in groundwater and surface water. Since this class of surfactants contains long chains of EO units, the KMD analysis was very

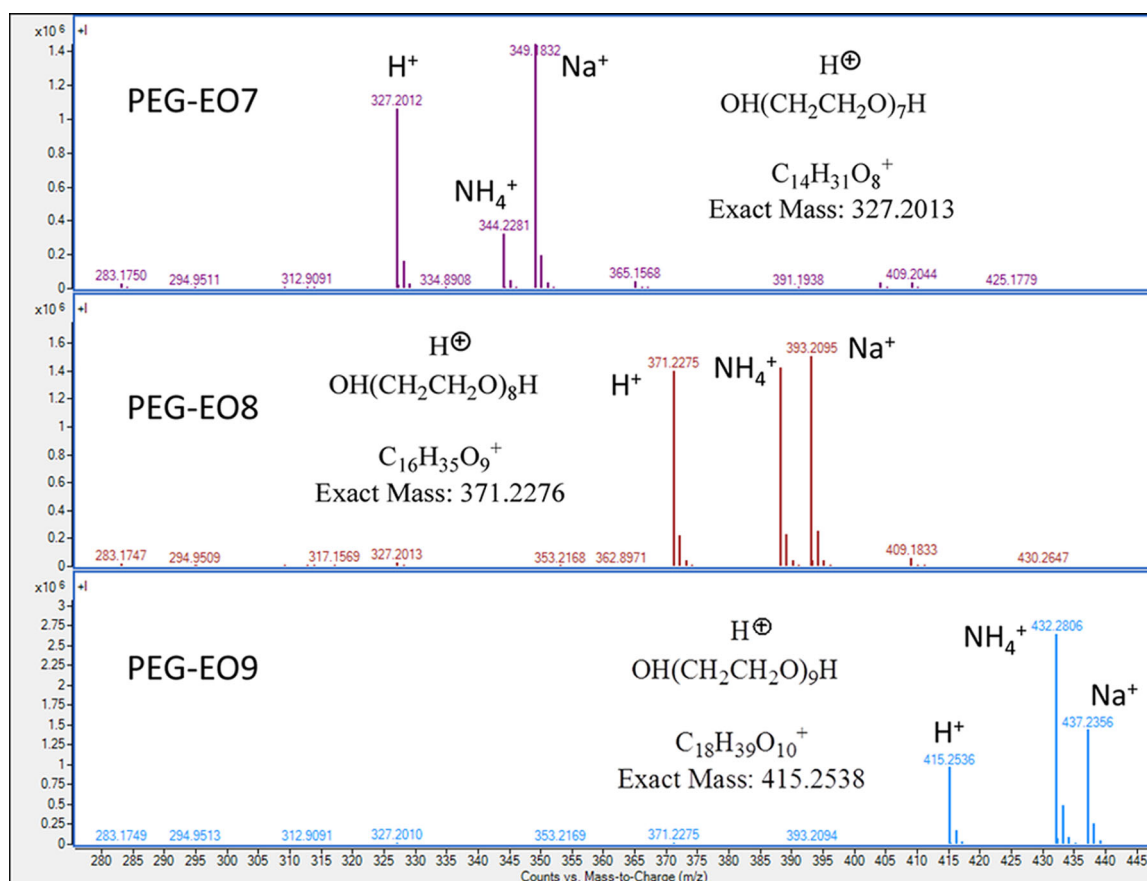


FIGURE 15 Mass spectra of putative structures for PEG-EO7, -EO8, and -EO9 with calculated exact masses showing accuracies of 0.3–0.5 ppm for the $[\text{M} + \text{H}]^+$. Overall, the mass accuracies are less than 1 ppm. Reproduced with the permission of Elsevier (Thurman et al., 2014) [Color figure can be viewed at wileyonlinelibrary.com]

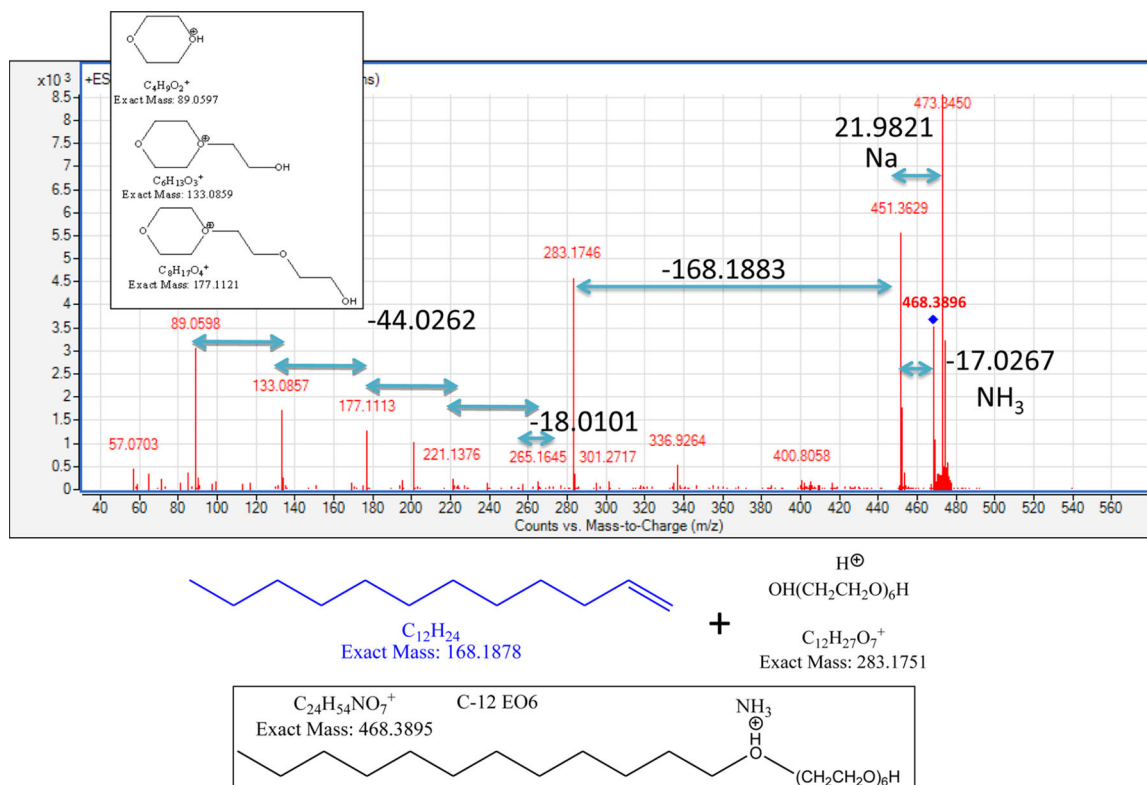


FIGURE 16 Tandem MS spectrum at m/z 468 with a putative identification of C12 and $n_{EO} = 6$ $[M + NH_4]^+$. Mass accuracies are 0.2 ppm for NH_4^+ adduct and 1.5 ppm for the major fragment ion at m/z 283.1746. Reproduced with the permission of Elsevier (Thurman et al., 2014). MS, mass spectrometry [Color figure can be viewed at wileyonlinelibrary.com]

useful. A mixture of PEG with EO number, n_{EO} , from 3 up to 33 and linear alkyl ethoxylates (LAE) C9–C15 with $n_{EO} = 3–28$ were identified in hydraulic fracturing flowback and produced water. It was noted that upon changing the chain length from $n_{EO} = 7$ to $n_{EO} = 9$, the predominant adduct of PEG changed from Na^+ to NH_4^+ with the protonated adduct also existing (see Figure 15). Whereas all these adducts were investigated by tandem MS, in Figure 16 is shown the ammonium adduct at m/z 468. As expected, the accurate mass differences between the ammoniated/sodiated and protonated adducts were 17.0267 Da and 21.9821 Da, confirming the designation of m/z 451.3629 as $[M + H]^+$.

A major purpose of the study was the identification of the EO surfactants and the construction of a database with accurate masses and retention times to solve the mass spectral complexity of surfactant mixtures employed in hydraulic fracturing fluids. Over 500 accurate mass assignments were used as a fingerprint chromatogram of the water samples. The same approach was applied to a series of flowback and produced water samples to demonstrate the usefulness of ethoxylate “fingerprinting” to monitor water quality that results from fluids used in hydraulic fracturing. Interestingly, KMD analysis was also used in conjunction to LC-MS/MS to fully

characterize the unknown fluorinated pollutants of fire-fighting foams in environmental samples (Chiesa et al., 2018; D’Agostino & Mabury, 2014; García et al., 2019). Despite the great advantages of using KMD plots for HRMS data processing, there are still some shortcomings such as the low isotopic resolution and the poor distinction of some homologous series. The finite resolution and mass accuracy of the MS analysis and the intrinsically low variations of the KMD values account for a fuzzy appearance and a limited RP of the KMD plot, respectively. To overcome this pitfall, the concept of a fractional base unit was introduced; instead of using a molecule or part of a molecule as the base unit for the calculation of Kendrick masses, a fraction of the repeat unit, that is (repeat unit)/X with X being an integer, was proposed. Albeit this base unit has no chemical meaning, it is still mathematically acceptable. This mathematical trick significantly amplifies the variation of KMD values and improves the resolution of the KMD plots without interfering with the basics of a KMD analysis such as the point alignments of homologue ions (horizontal or oblique) (Fouquet, Cody, et al., 2017).

This new high resolution KMD (HRKMD) analysis was used, together with MALDI/HRMS, to characterize nonionic surfactants made of a polyethoxylates (PEO)

core capped by esters of fatty acids (Fouquet, Shimada, et al., 2017). More specifically, a PEO monostearate surfactant was first analysed as a proof of principle of the HRKMD analysis conducted with a fraction of EO as the base unit (EO/X with X being an integer). KMD plots allowed the formula assignment in an easier and faster way. Moreover, HRKMD plots permitted to observe the presence of more homologous series, which are hardly identified in MALDI full spectrum because of low intensities. Data visualization was greatly enhanced, and the distributions detected in the MALDI mass spectrum were successfully assigned to a pristine (H, OH)-PEO as well as mono- and di-esterified PEO chains with palmitate and stearate end-groups in HRKMD plots computed with EO/45. The MALDI/HRMS/HRKMD analysis was successfully applied to the more complex case of ethoxylated hydrogenated castor oil, found to contain many hydrogenated ricinoleate moieties (up to 14) in its HRKMD plot computed with EO/43, departing from the expected triglyceride structure.

5.2 | Surfactant analysis by ion mobility-MS

Due to complementary separation capability and elevated peak capacity, LC in conjunction with IM/MS is becoming increasingly popular for complex mixture analysis. IM/MS is a gas phase electrophoretic technique that allows ionized target molecules to be separated relying on their mobility in the presence of an inert carrier gas and under the influence of an electric field of ~ 200 V/cm (Kanu et al., 2008). The LC-IM/MS enables the initial separation of components by LC, the transfer and dispersion of the generated ions according to their differing mobility and m/z registration. Hence, a 2D separation can be accomplished in a reasonably short time. Particularly, a hydrophilic interaction liquid chromatography (HILIC) column was chosen using a porous silica stationary phase and acetonitrile–water gradient elution, which is readily compatible with ESI, obtaining the separation of APEO oligomers on the basis of their ethoxy chain lengths (Ma et al., 2012). The IM/MS employed a hybrid quadrupole ion mobility ToF mass spectrometer coupled with an orthogonal separation of APEO that is based on size, shape, and electric charge, and lasting roughly 13.0 ms. The high-throughput IM approach demonstrates a promising alternative to traditional chromatographic separation ones for removing the effects of isobaric interferences. The same method was applied to analyse other types of nonionic surfactants such as complex mixtures of PEO conjugated with a glucose core and esterified with stearic acid, and to better resolve the

composition of commercial surfactant products like polysorbate 85 (Katzenmeyer et al., 2016; Solak Erdem et al., 2014).

5.3 | 2D chromatographic separation techniques

Despite numerous reports, one-dimensional (1D) LC and GC analyses of complex surfactant mixtures, in particular when compounds that belong to different families are present simultaneously, is still not an easy task. One reason for this is the inherent complexity of the individual analytes, which most of the time are not a single well defined molecule but rather a mixture of homologues. These 2D techniques capture all sample constituents and not only a limited number of fractions of the first dimension. In addition, the orthogonality of 2D applications is often high, because of different separation mechanisms in two dimensions, which result in high peak capacities.

Among hyphenated MS technique, the coupling of MS with 2D chromatographic separation techniques has led to a marked boost of chromatographic peak resolutions (Gilar et al., 2005; Guiochon et al., 2008; Phillips & Beens, 1999). Different conjunctions were explored for surfactant analysis, each of them demonstrating superior capability in comparison to common 1D separation counterparts. In addition, 2D chromatographic systems are nowadays commercially available from several instrument manufacturers and have successfully solved many separation problems in recent years (Mondello et al., 2008).

The high peak capacity of 2D gas chromatography (GC \times GC) clearly reduces co-elution, so that time- and cost-intensive sample preparation largely become less important (Phillips & Beens, 1999). GC \times GC coupled with time-of-flight MS allowed the qualitative and quantitative determination of AG, FAEO, FAS, FAES, and cocamidopropyl betaines (CAPB) in shower gel and cleaning agents (Hübner et al., 2007). 2D chromatograms were obtained from the analysis of standard solutions and used as fingerprints to identify and quantify surfactants in commercial samples. This method allowed the simultaneous determination of all GC-accessible components including those present at low concentrations, with no undesirable matrix effects.

GC \times GC–EI/ToF/MS was also used for the simultaneous determination of fatty alcohols, fatty alcohol sulfates and alkyl polyglucosides in complex industrial cleaners (Wulf et al., 2010). Because the derivatization procedure formed decomposition products of some surfactants in the GC injector, the number of analyte

components increased. However, the identification of such GC-atypical analytes was performed by their decomposition products and it was possible because GC × GC reduced mixture complexity.

GC × GC application present the same problems of all GC analyses: silylation of surfactants is often necessary; high-molecular-weight surfactants have extremely low vapor pressures or undergo thermolysis in the GC injector; time- and cost-intensive sample preparation is required.

2D HPLC was applied for the first time to the analysis of complex surfactant mixtures by Haefliger (2003), bypassing disadvantages of GC. In the first dimension, ion chromatographic-type separations were performed on a diol column eluted by an acetonitrile/water (0.1% trifluoroacetic acid) gradient. Using this new technique, cationic, and amphoteric surfactants were not retained at all, nonionic surfactants exhibited a weak and essentially unspecific retention, and anionic surfactants were retained mainly according to their functional group. Rather than detecting the analytes immediately after this first separation, successive fractions were automatically and quantitatively transferred to parallel C2 (dimethyl) and C4 (butyl) reversed-phase columns using an innovative setup. The second dimension of the separation then took place, by which the analytes were separated according to their hydrophobicity. Surfactants from all four classes, cationic, amphoteric, nonionic, and anionic, were separated simultaneously in single 54-min 2D HPLC runs.

Elsner et al. (2012) performed a simultaneous separation of anionic (fatty alcohol sulfates, fatty alcohol ether sulfates), nonionic (alkyl polyglucosides, fatty alcohol ethoxylates) and amphoteric (CAPB) surfactants by comprehensive 2D liquid chromatography (LC × LC) utilizing a ZIC®-HILIC column in the first dimension, a Reprosphere 100 C8-Aqua column in the second dimension and a 10-port two position valve as the interface. In the first dimension, a gradient of acetonitrile and an ammonium acetate buffer was used to separate polyethoxylated surfactants by their EO number whereas in the second dimension, a separation by alkyl chain was performed using a methanol/ammonium acetate buffer gradient. A baseline separation of the above mentioned surfactants according to both EO number and alkyl chain was achieved.

5.4 | The supercritical fluid chromatography

Instead of LC and GC, some applications of surfactant analysis by SFC coupled to MS also exist. SFC has the advantages of low-cost, green, fast separations, high

resolution, and low viscosity (Hofstetter et al., 2019). As compared with LC, hydrophobic moieties of compounds favor the fast elution in SFC. Whist different series can be separated by LC, homologue compounds of the same series can be better separated by SFC, which coupled with MS provided very useful structural information (Pan et al., 2020). The SFC-MS was used to analyse alkyl polyglyceryl ethers (Fan et al., 2015), offering further understanding on the product surfactant composition after etherification and it was also developed for the fast determination of alkylphenol ethoxylates in leafy vegetables (Jiang et al., 2017), thus demonstrating its usefulness for anionic surfactant analysis. Takahashi et al. (2013) optimized the SFC-MS experimental parameters of a synthetic mixture of nonionic surfactant poly(ethylene glycol) nonylphenyl ethers and Pan et al. (2016; Takahashi et al., 2013) reported the characterization of commercial polysorbate 80 by ultra-high performance SFC and quadrupole time-of-flight MS.

An interesting example of SFC-IM/MS was reported by Ma et al. (2019) for nonionic surfactants, including APEO, for example, OP ethoxylates and FAE, for example, lauryl alcohol ethoxylates. A column packed with sub-2- μm diol particles was used for the chromatographic separation before ESI as first-dimensional SFC exploiting the differences in ethoxy chain, and IM as the second one. A significant enhancement in peak capacity was achieved by SFC-IM/MS, namely more than 40- and 160-fold than those of SFC and IM/MS alone, respectively.

6 | MECHANISTIC STUDY ON SURFACTANTS

In addition to qualitative and quantitative studies, MS techniques are useful to investigate micelle formation from aggregation processes to aggregate structure and their reactivity/stability (Ceraulo et al., 2011). Despite the possibility of studying surfactant aggregates with MS, an answer to the question of whether aggregates produced in the gas phase mirror those formed in solution is not obvious. Soft ionization sources (e.g., FAB, ESI, and MALDI) are important, being able to produce charged aggregates of surfactants, with a survival life long enough to be studied. This leads to gaining much important information on the aggregation processes, on the structure of the aggregates and on their reactivity and stability. Up to now, several surfactants have been investigated using a wide variety of MS techniques.

Among the various ionization mechanisms, the ESI technique is the most suited for the generation of charged supramolecular aggregates with minimal

dissociative impact on the integrity of surfactant molecules as well as on their associated forms. Moreover, since ESI works best with polar solvents, it is capable of separating charges in solution, enriching the small droplets either in positive or in negative species and favoring the formation of the corresponding charged aggregates. The progressive concentration increase in the surfactant due to solvent evaporation is also a process that favors micelle generation and/or conservation in the gas phase, with a minimum amount of internal energy excess. Large aggregates are thus easily detected with this technique, even using solutions where the surfactant concentration is below its CMC. As well as ESI, the MALDI technique proved to be a useful tool to evidence surfactant aggregation pathways during the ionization process. This technique can be considered a true alternative to ESI, which struggles with apolar media, when the information on supramolecular aggregates are acquired from lipophilic solvents. MS/MS and energy resolved mass spectrometry (ER-MS) are both useful and mostly complementary techniques to gather information on the aggregate structure, stability and fragmentation pathways.

IRMPD spectroscopy is a technique that, by applying a wavelength tunable IR laser to fragment molecules in the gas phase, allows structural information to be obtained about selected ions. Recently, IRMPD has been used in MS applications as a method to induce wavelength-dependent fragmentation on noncovalently self-assembled aggregates.

IMMS is able to separate charged species with the same m/z value and different shape, exploiting their drift time in a gaseous environment under the same electric field; thus also allowing the determination of an interesting structural parameter, that is, their collision cross section.

For example, octyl-trimethylammonium bromide (OTAB) with chemical formula $C_8H_{17}N(CH_3)_3Br$ was examined by ESI-MS to evaluate the molecular weight of micelles formed in water alone, without any additive. From the measurement of the m/z of the doubly or triply charged ions, it was revealed that the micelle of OTAB exhibited an almost symmetrical and polydisperse distribution about the mean molecular weight of 5000–5500 Da (Nohara et al., 1998).

Useful hints on the binding affinity of surfactants with metallic ions were also reported. Using sodium dodecylcarboxylate and dodecyltrimethylammonium bromide in the presence of different salts, Vlachy et al. (2008) showed how the binding tendency of Li^+ was greater than $Na^+ > K^+$ > Cationic surfactant. This binding tendency affects the types and dimensions of formed micelles, and consequently their behaviors into aqueous solutions.

Bongiorno et al. (2005) studied the structure of sodium bis(2-ethylhexyl)sulfosuccinate (AOTNa) aggregates in the gas phase by ESI-MS and MALDI-MS. Large surfactant clusters with an aggregation number close to that found in apolar media were observed either as positive or negative ions. Moreover, the marked predominance of singly charged species as well as preliminary theoretical calculations strongly suggests an aggregate structure characterized by an internal hydrophilic core hosting the extra charge surrounded by an apolar shell constituted by the surfactant alkyl chains. This structure is like that of the more familiar reversed micelles, formed when an appropriate surfactant is solubilized in apolar solvents, which together with the idea that gas phase can be considered an apolar environment, strongly indicates that self-assembling of the surfactant molecules occurs during the evaporation step (Bongiorno et al., 2011). The formation of reverse micelle-like structures in gas phase was also evidenced by Giorgi et al. (2011). Close similarity between ESI-IRMPD spectra of AOTNa aggregates in the gas phase and infrared spectra of AOTNa reverse micelles in carbon tetrachloride has been found. Spectral shifts of surfactant head group signals have consistently been attributed to some differences, mainly due to the charge state, between the small aggregates sampled in the gas phase and those in CCl_4 solution.

7 | CONCLUSIONS AND OUTLOOK

MS-based surfactant analysis, including shotgun approaches, has reached a high level of maturity with respect to sample processing, data acquisition and data analysis. The literature screening demonstrated MS is an indispensable tool for the identification and quantification of surfactants. Emphasis was placed on the description and value of existing methods as well as on the most recent innovation of MS. Traditional hyphenated techniques are widely used to resolve complex surfactants mixture; HPLC/MS has been widely used for surfactant analysis, without any derivatization steps, compared to GC/MS. In addition, tandem MS instruments have greatly increased the accessibility of surfactants to MS analysis: fragmentation patterns allow the determination of isomer distribution and other chemical information, such as location of unsaturation, location of side chains, and degree of branching. However, several significant challenges remain. They are primarily related to the complexity of surfactants, which has so far precluded true surfactant analyses (i.e., the analysis of all the components of a sample) and generated partially overlapping datasets from identical samples, suggesting poor reproducibility of the technology.

Secondarily, these challenges are related to the analysis of surfactants and degradation products in environmental samples. In combination, these problems have created the impression that published surfactant data are at times of dubious quality. Overall, mature MS technologies are available today for surfactants analysis. The most significant improvements, however, will come from HRMS, ion mobility MS, 2D- and superfluid chromatographic approaches. Stand-alone and coupled MS techniques are reliable, highly reproducible and can analyse hundreds to thousands of samples in a short period of time. MS, HRMS and tandem MS are not labor intensive and time consuming, being highly accurate and can discover the presence of impurities, including truncated chains that are often overlooked when using less sensitive and selective approaches. Great strides have been made and we can anticipate continued improvements and cost reductions in the future.

ORCID

Raffaella Pascale  <https://orcid.org/0000-0002-7650-653X>

Maria A. Acquavia  <https://orcid.org/0000-0001-6103-8860>

Tommaso R. I. Cataldi  <https://orcid.org/0000-0003-4811-8959>

Cosima D. Calvano  <https://orcid.org/0000-0001-8832-7072>

Giuliana Bianco  <https://orcid.org/0000-0001-9427-2274>

REFERENCES

- Acquavia, M.A., Foti, L., Pascale, R., Nicolò, A., Brancaleone, V., Cataldi, T.R.I., Martelli, G., Scrano, L., Bianco, G., 2021. Detection and quantification of COVID-19 antiviral drugs in biological fluids and tissues. *Talanta* 224, 121862. <https://doi.org/10.1016/j.talanta.2020.121862>
- Agozzino, P., Ceraulo, L., Ferrugia, M., Caponetti, E., Intravaia, F., Triolo, R., 1986. Sodium p-alkylbenzenesulfonates: A simple and fast characterization by electron impact mass spectrometry. *J. Colloid Interface Sci.* 114, 26–31. [https://doi.org/10.1016/0021-9797\(86\)90237-7](https://doi.org/10.1016/0021-9797(86)90237-7)
- Akella, A., Shripad, &, Deshpande, B., 2013. Pulmonary surfactants and their role in pathophysiology of lung disorders. *Indian J. Exp. Biol.* 51, 5–22.
- Allen, R., Bandyopadhyay, S., Klein, M.L., 2000. C12E2 reverse micelle: A molecular dynamics study. *Langmuir* 16, 10547–10552. <https://doi.org/10.1021/la001182d>
- Amodeo, C., Sofo, A., Tito, M.T., Scopa, A., Masi, S., Pascale, R., Mancini, I.M., Caniani, D., 2018. Environmental factors influencing landfill gas biofiltration: Lab scale study on methanotrophic bacteria growth. *J. Environ. Sci. Heal. - Part A Toxic/Hazardous Subst. Environ. Eng.* 53, 825–831. <https://doi.org/10.1080/10934529.2018.1455342>
- Attygalle, A.B., García-Rubio, S., Ta, J., Meinwald, J., 2001. Collisionally-induced dissociation mass spectra of organic sulfate anions. *J. Chem. Soc. Perkin Trans. 2* 2, 498–506. <https://doi.org/10.1039/b009019k>
- Bai, Y., Galetskiy, D., Damoc, E., Paschen, C., Liu, Z., Griese, M., Liu, S., Przybylski, M., Kinderspital, H., 2004. High resolution mass spectrometric alveolar proteomics: Identification of surfactant protein SP-A and SP-D modifications in proteinosis and cystic fibrosis patients. *Proteomics* 4, 2300–23009. <https://doi.org/10.1002/pmic.200400855>
- Bajpai, D., Tyagi, V.K., 2010. Nonionic surfactants: An overview. *Tenside, Surfactants, Deterg.* 47, 190–196. <https://doi.org/10.3139/113.110062>
- Balan, S.S., Kumar, C.G., Jayalakshmi, S., 2016. Pontifactin, a new lipopeptide biosurfactant produced by a marine *Pontibacter korensis* strain SBK-47: Purification, characterization and its biological evaluation. *Process Biochem* 51, 2198–2207. <https://doi.org/10.1016/j.procbio.2016.09.009>
- Bazel, Y.R., Antal, I.P., Lavra, V.M., Kormosh, Z.A., 2014. Methods for the determination of anionic surfactants. *J. Anal. Chem.* 69, 211–236. <https://doi.org/10.1134/S1061934814010043>
- Bianco, G., Novario, G., Anzilotta, G., Palma, A., Mangone, A., Cataldi, T.R.I., 2010. Polybrominated diphenyl ethers (PBDEs) in Mediterranean mussels (*Mytilus galloprovincialis*) from selected Apulia coastal sites evaluated by GC-HRMS. *J. Mass Spectrom.* 45, 1046–1055. <https://doi.org/10.1002/jms.1799>
- Bianco, G., Pascale, R., Carbone, C.F., Acquavia, M.A., Cataldi, T.R.I., Schmitt-Kopplin, P., Buchicchio, A., Russo, D., Milella, L., 2018. Determination of soyasaponins in Fagioli di Sarconi beans (*Phaseolus vulgaris* L.) by LC-ESI-FTICR-MS and evaluation of their hypoglycemic activity. *Anal. Bioanal. Chem.* 410, 1561–1569. <https://doi.org/10.1007/s00216-017-0806-8>
- Bianco, G., Pascale, R., Lelario, F., Bufo, S.A., Cataldi, T.R.I., 2017. Investigation of glucosinolates by mass spectrometry, in: J.-M. Mérillon, K.G.R. (Ed.), *Glucosinolates, reference series in phytochemistry*. Springer, Cham, Switzerland, pp. 431–461. https://doi.org/10.1007/978-3-319-25462-3_12
- Bianco, G., Zianni, R., Anzilotta, G., Palma, A., Vitacco, V., Scrano, L., Cataldi, T.R.I., 2013. Dibenzo-p-dioxins and dibenzofurans in human breast milk collected in the area of Taranto (Southern Italy): First case study. *Anal. Bioanal. Chem.* 405, 2405–2410. <https://doi.org/10.1007/s00216-013-6706-7>
- Bongiorno, D., Ceraulo, L., Giorgi, G., Indelicato, S., Turco Liveri, V., 2011. Do electrospray mass spectra of surfactants mirror their aggregation state in solution? *J. Mass Spectrom.* 46, 1263–1268. <https://doi.org/10.1002/jms.2013>
- Bongiorno, D., Ceraulo, L., Ruggirello, A., Liveri, V.T., Basso, E., Seraglia, R., Traldi, P., 2005. Surfactant self-assembling in gas phase: Electrospray ionization- and matrix-assisted laser desorption/ionization-mass spectrometry of singly charged AOT clusters. *J. Mass Spectrom.* 40, 1618–1625. <https://doi.org/10.1002/jms.965>
- Boyer, J.L., Canselier, J.P., Castro, V., 1982. Analysis of SO₃-Sulfonation products of 1-Alkenes by spectrometric methods. *J. Am. Oil Chem. Soc.* 59, 458–464. <https://doi.org/10.1007/BF02634434>
- Broze, G., 1999. *Handbook of detergents, Part A: Properties, First edit. ed, Surfactant Science Series 82*. CRC Press, Boca Raton.

- Caivano, M., Pascale, R., Mazzone, G., Buchicchio, A., Masi, S., Bianco, G., Caniani, D., 2017a. N₂O and CO₂ Emissions from secondary settlers in WWTPs: Experimental results on full and pilot scale plants, in: *Lecture Notes in Civil Engineering*. pp. 412–418. https://doi.org/10.1007/978-3-319-58421-8_65
- Caivano, M., Pascale, R., Mazzone, G., Masi, S., Panariello, S., Caniani, D., 2017b. Disinfection unit of water resource recovery facilities: Critical issue for N₂O emission, in: *Lecture notes in civil engineering*. Springer, Cham, pp. 444–450. https://doi.org/10.1007/978-3-319-58421-8_70
- Calvano, C.D., Monopoli, A., Cataldi, T.R.I., Palmisano, F., 2018. MALDI matrices for low molecular weight compounds: An endless story? *Anal. Bioanal. Chem* 410, 4015–4038 <https://doi.org/10.1007/s00216-018-1014-x>
- Caniani, D., Caivano, M., Pascale, R., Bianco, G., Mancini, I.M., Masi, S., Mazzone, G., Firouzian, M., Rosso, D., 2019a. CO₂ and N₂O from water resource recovery facilities: Evaluation of emissions from biological treatment, settling, disinfection, and receiving water body. *Sci. Total Environ.* 648, 1130–1140. <https://doi.org/10.1016/j.scitotenv.2018.08.150>
- Caniani, D., Esposito, G., Gori, R., Caretti, C., Bellandi, G., Mancini, I.M., Caivano, M., Pascale, R., Cosenza, A., Abouissa, H., Mannina, G., 2019b. Toward a new plant-wide experimental and modeling approach for reduction of greenhouse gas emission from wastewater treatment plants. *J. Environ. Eng.* 145, 04019043. [https://doi.org/10.1061/\(asce\)ee.1943-7870.0001538](https://doi.org/10.1061/(asce)ee.1943-7870.0001538)
- Carmona-Ribeiro, A.M., Vieira, D.B., Lincopan, N., 2006. Cationic surfactants and lipids as anti-infective agents. *Antiinfect. Agents Med. Chem.* 5, 33–51. <https://doi.org/10.2174/187152106774755572>
- Carolei, L., Gutz, I.G.R., 2005. Simultaneous determination of three surfactants and water in shampoo and liquid soap by ATR-FTIR. *Talanta* 66, 118–124. <https://doi.org/10.1016/j.talanta.2004.10.005>
- Castillo, M., Barceló, D., 1999. Identification of polar toxicants in industrial wastewaters using toxicity-based fractionation with liquid chromatography/mass spectrometry. *Anal. Chem.* 71, 3769–3776. <https://doi.org/10.1021/ac990364d>
- Cataldi, T.R.I., Orlando, D., Nardiello, D., Rubino, A., Bianco, G., Abate, S., Ciriello, R., Guerrieri, A., 2007. A three-factor Doehlert matrix design in optimising the determination of octadecyltrimethylammonium bromide by cation-exchange chromatography with suppressed conductivity detection. *Anal. Chim. Acta* 597, 129–136. <https://doi.org/10.1016/j.aca.2007.06.038>
- Ceraulo, L., Giorgi, G., Liveri, V.T., Bongiorno, D., Indelicato, Serena, Gaudio, F. Di, Indelicato, S., 2011. Mass spectrometry of surfactant aggregates. *Eur. J. Mass Spectrom.* 17, 525–541. <https://doi.org/10.1255/ejms.1158>
- Chen, R., Tseng, A.M., Uhing, M., Li, L., 2001. Application of an integrated matrix-assisted laser desorption/ionization time-of-flight, electrospray ionization mass spectrometry and tandem mass spectrometry approach to characterizing complex polyol mixtures. *J. Am. Soc. Mass Spectrom.* 12, 55–60. [https://doi.org/10.1016/S1044-0305\(00\)00200-2](https://doi.org/10.1016/S1044-0305(00)00200-2)
- Chiesa, L.M., Nobile, M., Pasquale, E., Balzaretto, C., Cagnardi, P., Tedesco, D., Panseri, S., Arioli, F., 2018. Detection of perfluoroalkyl acids and sulphonates in Italian eel samples by HPLC-HRMS Orbitrap. *Chemosphere* 193, 358–364. <https://doi.org/10.1016/j.chemosphere.2017.10.082>
- Choi, Y., Jang, J., Park, H.S., 2020. Pulmonary surfactants: A new therapeutic target in asthma. *Curr. Allergy Asthma Rep* 20, 70. <https://doi.org/10.1007/s11882-020-00968-8>
- Costa, S.G.V.A.O., Nitschke, M., Haddad, R., Eberlin, M.N., Contiero, J., 2006. Production of *Pseudomonas aeruginosa* LBI rhamnolipids following growth on Brazilian native oils. *Process Biochem.* 41, 483–488. <https://doi.org/10.1016/j.procbio.2005.07.002>
- Coviello, D., Pascale, R., Ciriello, R., Salvi, A.M., Guerrieri, A., Contursi, M., Scrano, L., Bufo, S.A., Cataldi, T.R.I., Bianco, G., 2020. Validation of an analytical method for nitrite and nitrate determination in meat foods for infants by ion chromatography with conductivity detection. *Foods* 9, 1238. <https://doi.org/10.3390/foods9091238>
- Crescenzi, C., Corola, A. Di, Samperi, R., Marcomini, A., 1995. Determination of nonionic polyethoxylate surfactants in environmental waters by liquid chromatography/electrospray mass spectrometry. *Anal. Chem.* 67, 1797–1804. <https://doi.org/10.1021/ac00107a008>
- Cserhati, T., 1995. Alkyl ethoxylated and alkylphenol ethoxylated nonionic surfactants: Interaction with bioactive compounds and biological effects. *Environ. Health Perspect.* 103, 358–364. <https://doi.org/10.1289/ehp.95103358>
- Curstedt, T., Johansson, J., Persson, P., Eklund, A., Robertson, B., Löwenadler, B., Jörnvall, H., 1990. Hydrophobic surfactant-associated polypeptides: SP-C is a lipopeptide with two palmitoylated cysteine residues, whereas SP-B lacks covalently linked fatty acyl groups. *Proc. Natl. Acad. Sci. USA.* 87, 2985–2989. <https://doi.org/10.1073/pnas.87.8.2985>
- D'Agostino, L.A., Mabury, S.A., 2014. Identification of novel fluorinated surfactants in aqueous film forming foams and commercial surfactant concentrates. *Environ. Sci. Technol.* 48, 121–129. <https://doi.org/10.1021/es403729e>
- De Faria, A.F., Teodoro-Martinez, D.S., De Oliveira Barbosa, G.N., Gontijo Vaz, B., Serrano Silva, Í., Garcia, J.S., Tótola, M.R., Eberlin, M.N., Grossman, M., Alves, O.L., Regina Durrant, L., 2011. Production and structural characterization of surfactin (C14/Leu7) produced by *Bacillus subtilis* isolate LSFM-05 grown on raw glycerol from the biodiesel industry. *Process Biochem.* 46, 1951–1957. <https://doi.org/10.1016/J.PROCBIO.2011.07.001>
- Ding, W.H., Chen, C.T., 1999. Analysis of nonylphenol polyethoxycarboxylates and their related metabolites by on-line derivatization and ion-trap gas chromatography-mass spectrometry. *J. Chromatogr. A* 862, 113–120. [https://doi.org/10.1016/S0021-9673\(99\)00895-X](https://doi.org/10.1016/S0021-9673(99)00895-X)
- Ding, W.H., Liao, Y.H., 2001. Determination of alkylbenzylidimethyl ammonium chlorides in river water and sewage effluent by solid-phase extraction and gas chromatography/mass spectrometry. *Anal. Chem.* 73, 36–40. <https://doi.org/10.1021/ac000655i>
- Ding, W.H., Tsai, P.C., 2003. Determination of alkyltrimethyl ammonium chlorides in river water by gas chromatography/ion trap mass spectrometry with electron impact and chemical ionization. *Anal. Chem.* 75, 1792–1797. <https://doi.org/10.1021/ac020536y>
- Domsch, A., Jenni, K., 2004. Biodegradability of amphoteric surfactants, In: U., Zoller (Ed.), *Handbook of Detergents*,

- Part B: Environmental Impact. Springer: Netherlands, pp. 231–254. <https://doi.org/10.1201/9780203020500>
- Eichhorn, P., Knepper, T.P., 2001. Electrospray ionization mass spectrometric studies on the amphoteric surfactant cocamidopropylbetaine. *J. Mass Spectrom.* 36, 677–684. <https://doi.org/10.1002/jms.170>
- Elsner, V., Laun, S., Melchior, D., Köhler, M., Schmitz, O.J., 2012. Analysis of fatty alcohol derivatives with comprehensive two-dimensional liquid chromatography coupled with mass spectrometry. *J. Chromatogr. A* 1268, 22–28. <https://doi.org/10.1016/J.CHROMA.2012.09.072>
- Facino, R.M., Carini, M., Depta, G., Bernardi, P., Casetta, B., 1995. Atmospheric-pressure ionization mass-spectrometric analysis of new anionic surfactants: The alkylpolyglucoside esters. *J. Am. Oil Chem. Soc.* 72, 1–9. <https://doi.org/10.1007/BF02635771>
- Fait, M.E., Bakas, L., Garrote, G.L., Morcelle, S.R., Saparrat, M.C.N., 2019. Cationic surfactants as antifungal agents. *Appl. Microbiol. Biotechnol.* 103, 97–112. <https://doi.org/10.1007/s00253-018-9467-6>
- Fan, Z., Zhao, Y., Preda, F., Clacens, J.M., Shi, H., Wang, L., Feng, X., De Campo, F., 2015. Preparation of bio-based surfactants from glycerol and dodecanol by direct etherification. *Green Chem.* 17, 882–892. <https://doi.org/10.1039/c4gc00818a>
- Ferrer, I., Furlong, E.T., 2001. Identification of alkyl dimethylbenzylammonium surfactants in water samples by solid-phase extraction followed by ion trap LC/MS and LC/MS/MS. *Environ. Sci. Technol.* 35, 2583–2588. <https://doi.org/10.1021/es001742v>
- Fielden, M.L., Claesson, P.M., 1998. A comparison of three methods for the convenient determination of sodium dodecyl sulfate in aqueous solutions. *J. Colloid Interface Sci.* 198, 261–265. <https://doi.org/10.1006/jcis.1997.5241>
- Ford, M.J., Tetler, L.W., White, J., Rimmer, D., 2002. Determination of alkyl benzyl and dialkyl dimethyl quaternary ammonium biocides in occupational hygiene and environmental media by liquid chromatography with electrospray ionisation mass spectrometry and tandem mass spectrometry. *J. Chromatogr. A* 952, 165–172. [https://doi.org/10.1016/S0021-9673\(02\)00082-1](https://doi.org/10.1016/S0021-9673(02)00082-1)
- Fouquet, T., Cody, R.B., Sato, H., 2017. Capabilities of the remainders of nominal Kendrick masses and the referenced Kendrick mass defects for copolymer ions. *J. Mass Spectrom.* 52, 618–624. <https://doi.org/10.1002/jms.3963>
- Fouquet, T., Sato, H., 2017. Improving the resolution of Kendrick mass defect analysis for polymer ions with fractional base units. *Mass Spectrom.* 6, A0055. <https://doi.org/10.5702/massspectrometry.a0055>
- Fouquet, T., Shimada, H., Maeno, K., Ito, K., Ozeki, Y., Kitagawa, S., Ohtani, H., Sato, H., 2017. High-resolution Kendrick mass defect analysis of poly(ethylene oxide)-based non-ionic surfactants and their degradation products. *J. Oleo Sci.* 66, 1061–1072. <https://doi.org/10.5650/jos.ess17096>
- Gaiffé, G., Cole, R.B., Lacpatia, S., Bridoux, M.C., 2018. Characterization of fluorinated polymers by atmospheric-solid-analysis-probe high-resolution mass spectrometry (ASAP/HRMS) combined with Kendrick-mass-defect analysis. *Anal. Chem.* 90, 6035–6042. <https://doi.org/10.1021/acs.analchem.7b05116>
- García, R.A., Chiaia-Hernández, A.C., Lara-Martin, P.A., Loos, M., Hollender, J., Oetjen, K., Higgins, C.P., Field, J.A., 2019. Suspect screening of hydrocarbon surfactants in AFFFs and AFFF-contaminated groundwater by high-resolution mass spectrometry. *Environ. Sci. Technol.* 53, 8068–8077. <https://doi.org/10.1021/acs.est.9b01895>
- Gaudin, T., Lu, H., Fayet, G., Berthaud-Drelich, A., Rotureau, P., Pourceau, G., Wadouachi, A., Van Hecke, E., Nesterenko, A., Pezron, I., 2019. Impact of the chemical structure on amphiphilic properties of sugar-based surfactants: A literature overview. *Adv. Colloid Interface Sci.* 270, 87–100. <https://doi.org/10.1016/j.cis.2019.06.003>
- Giesy, J.P., Kannan, K., 2001. Global distribution of perfluorooctane sulfonate in wildlife. *Environ. Sci. Technol.* 35, 1339–1342. <https://doi.org/10.1021/es001834k>
- Gilar, M., Olivova, P., Daly, A.E., Gebler, J.C., 2005. Orthogonality of separation in two-dimensional liquid chromatography. *Anal. Chem.* 77, 6426–6434. <https://doi.org/10.1021/ac050923i>
- Giorgi, G., Ceraulo, L., Berden, G., Oomens, J., Liveri, V.T., 2011. Gas phase infrared multiple photon dissociation spectra of positively charged sodium bis(2-ethylhexyl)sulfosuccinate reverse micelle-like aggregates. *J. Phys. Chem. B* 115, 2282–2286. <https://doi.org/10.1021/JP110941P>
- Gomez, V., Ferreres, L., Pocurull, E., Borrull, F., 2011. Determination of non-ionic and anionic surfactants in environmental water matrices. *Talanta.* 84, 859–866. <https://doi.org/10.1016/j.talanta.2011.02.009>
- González-Mazo, E., Honing, M., Barceló, D., Gómez-Parra, A., 1997. Monitoring long-chain intermediate products item the degradation of linear alkylbenzene sulfonates in the marine environment by solid-phase extraction followed by liquid chromatography/ion spray mass spectrometry. *Environ. Sci. Technol.* 31, 504–510. <https://doi.org/10.1021/es960333p>
- Grandjean, P., Clapp, R., 2015. Perfluorinated alkyl substances: Emerging insights into health risks. *New Solut. a J. Environ. Occup. Heal. policy* 25, 147–163. <https://doi.org/10.1177/1048291115590506>
- Griffiths, W.J., Gustafsson, M., Yang, Y., Curstedt, T., Sjövall, J., Johansson, J., 1998. Analysis of variant forms of porcine surfactant polypeptide-C by nano-electrospray mass spectrometry - Griffiths - 1998 - Rapid Communications in Mass Spectrometry - Wiley Online Library. *Rapid Commun. Mass Spectrom.* 12, 1104–1114.
- Guiochon, G., Marchetti, N., Mriziq, K., Shalliker, R.A., 2008. Implementations of two-dimensional liquid chromatography. *J. Chromatogr. A* 1189, 109–168. <https://doi.org/10.1016/j.chroma.2008.01.086>
- Haefliger, O.P., 2003. Universal two-dimensional HPLC technique for the chemical analysis of complex surfactant mixtures. *Anal. Chem. Chem* 75, 371–378. <https://doi.org/10.1021/ac020534d>
- Hanton, S.D., Parees, D.M., Zweigenbaum, J., 2006. The fragmentation of ethoxylated surfactants by AP-MALDI-QIT. *J. Am. Soc. Mass Spectrom.* 17, 453–458. <https://doi.org/10.1016/j.jasms.2005.11.013>
- Hayes, D.G., Smith, G.A., 2019. Biobased surfactants: Overview and industrial state of the art. *Biobased Surfactants* 3–38. <https://doi.org/10.1016/b978-0-12-812705-6.00001-0>

- Hoffmann, H., 1994. Hundred years of colloid science fascinating phenomena in surfactant solutions. *Berichte der Bunsengesellschaft/Physical Chem. Chem. Phys.* 98, 1433–1455. <https://doi.org/10.1002/bbpc.19940981111>
- Hofstetter, R.K., Hasan, M., Eckert, C., Link, A., 2019. Supercritical fluid chromatography: From science fiction to scientific fact. *ChemTexts* 5, 13. <https://doi.org/10.1007/s40828-019-0087-2>
- Hübner, J., Taheri, R., Melchior, D., Kling, H.-W., Gäb, S., Schmitz, O.J., 2007. Analysis of tensides in complex samples with comprehensive two-dimensional gas chromatography coupled with time-of-flight mass spectrometry. *Anal. Bioanal. Chem.* 388, 1755–1762. <https://doi.org/10.1007/s00216-007-1376-y>
- Hughey, C.A., Hendrickson, C.L., Rodgers, R.P., Marshall, A.G., Qian, K., 2001. Kendrick mass defect spectrum: A compact visual analysis for ultrahigh-resolution broadband mass spectra. *Anal. Chem.* 73, 4676–4681. <https://doi.org/10.1021/ac010560w>
- Jain, R.M., Mody, K., Mishra, A., Jha, B., 2012. Physicochemical characterization of biosurfactant and its potential to remove oil from soil and cotton cloth. *Carbohydr. Polym.* 89, 1110–1116. <https://doi.org/10.1016/j.carbpol.2012.03.077>
- Jewett, B.N., Ramaley, L., Kwak, J.C.T., 1999. Atmospheric pressure ionization mass spectrometry techniques for the analysis of alkyl ethoxysulfate mixtures. *J. Am. Soc. Mass Spectrom.* 10, 529–536. [https://doi.org/10.1016/S1044-0305\(99\)00017-3](https://doi.org/10.1016/S1044-0305(99)00017-3)
- Jiang, Z.J., Cao, X.L., Li, H., Zhang, C., Abd El-Aty, A.M., Jin, F., Shao, H., Jin, M.J., Wang, S.S., She, Y.X., Wang, J., 2017. Fast determination of alkylphenol ethoxylates in leafy vegetables using a modified quick, easy, cheap, effective, rugged, and safe method and ultra-high performance supercritical fluid chromatography–tandem mass spectrometry. *J. Chromatogr. A* 1525, 161–172. <https://doi.org/10.1016/j.chroma.2017.10.035>
- Kannan, K., Corsolini, S., Falandyisz, J., Oehme, G., Focardi, S., Giesy, J.P., 2002. Perfluorooctanesulfonate and related fluorinated hydrocarbons in marine mammals, fishes, and birds from coasts of the Baltic and the Mediterranean Seas. *Environ. Sci. Technol.* 36, 3210–3216. <https://doi.org/10.1021/es020519q>
- Kanu, A.B., Dwivedi, P., Tam, M., Matz, L., Hill, H.H., 2008. Ion mobility-mass spectrometry. *J. Mass Spectrom.* 43, 1–22. <https://doi.org/10.1002/jms.1383>
- Katzenmeyer, B.C., Hague, S.F., Wesdemiotis, C., 2016. Multidimensional mass spectrometry coupled with separation by polarity or shape for the characterization of sugar-based nonionic surfactants. *Anal. Chem.* 88, 851–857. <https://doi.org/10.1021/acs.analchem.5b03400>
- Kind, T., Fiehn, O., 2007. Seven Golden Rules for heuristic filtering of molecular formulas obtained by accurate mass spectrometry. *BMC Bioinformatics* 8, 105. <https://doi.org/10.1186/1471-2105-8-105>
- Kitamoto, D., Isoda, H., Nakahara, T., 2002. Functions and potential applications of glycolipid biosurfactants—From energy-saving materials to gene delivery carriers. *J. Biosci. Bioeng.* 94, 187–201. [https://doi.org/10.1016/s1389-1723\(02\)80149-9](https://doi.org/10.1016/s1389-1723(02)80149-9)
- Kühn, A. V., Neubert, R.H.H., 2004. Characterization of mixtures of alkyl polyglycosides (plantacare) by liquid chromatography-electrospray ionization quadrupole time-of-flight mass spectrometry. *Pharm. Res.* 21, 2347–2353. <https://doi.org/10.1007/s11095-004-7688-0>
- Lee, S.M., Lee, J.Y., Yu, H.P., Lim, J.C., 2016. Synthesis of environment friendly nonionic surfactants from sugar base and characterization of interfacial properties for detergent application. *J. Ind. Eng. Chem.* 38, 157–166. <https://doi.org/10.1016/j.jiec.2016.04.019>
- Levine, L.H., Judkins, J.E., Garland, J.L., 2000. Determination of anionic surfactants during wastewater recycling process by ion pair chromatography with suppressed conductivity detection. *J. Chromatogr. A* 874, 207–215. [https://doi.org/10.1016/S0021-9673\(00\)00155-2](https://doi.org/10.1016/S0021-9673(00)00155-2)
- Lindman, B., Medronho, B., Karlström, G., 2016. Clouding of nonionic surfactants. *Curr. Opin. Colloid Interface Sci.* 22, 23–29. <https://doi.org/10.1016/j.cocis.2016.01.005>
- Liu, H.Y., Ding, W.H., 2004. Determination of homologues of quaternary ammonium surfactants by capillary electrophoresis using indirect UV detection. *J. Chromatogr. A* 1025, 303–312. <https://doi.org/10.1016/j.chroma.2003.10.108>
- Liu, S., Zhao, L., Manzanares, D., Doherty-Kirby, A., Zhang, C., Possmayer, F., Lajoie, G.A., 2008. Characterization of bovine surfactant proteins B and C by electrospray ionization mass spectrometry. *Rapid Commun. Mass Spectrom.* 22, 197–203. <https://doi.org/10.1002/rcm.3345>
- Lyon, P.A., Crow, F.W., Tomer, K.B., Gross, M.L., 1984. Analysis of cationic surfactants by mass spectrometry/mass spectrometry with fast atom bombardment. *Anal. Chem.* 56, 2278–2284. <https://doi.org/10.1021/ac00277a004>
- Lyon, P.A., Stebbings, W.L., Crow, F.W., Tomer, K.B., Lippstreu, D.L., Gross, M.L., 1984. Analysis of anionic surfactants by mass spectrometry/mass spectrometry with fast atom bombardment. *Anal. Chem.* 56, 8–13. <https://doi.org/10.1021/ac00265a004>
- Ma, Q., Xi, G.C., Wang, C., Bai, H., Zhang, Q., Xi, H.W., Wang, Z.M., Guo, L.H., 2012. Comprehensive two-dimensional separation for the analysis of alkylphenol ethoxylates employing hydrophilic interaction chromatography coupled with ion mobility-mass spectrometry. *Int. J. Mass Spectrom.* 315, 31–39. <https://doi.org/10.1016/j.ijms.2012.02.010>
- Ma, Q., Zhang, Y., Zhai, J., Chen, X., Du, Z., Li, W., Bai, H., 2019. Characterization and analysis of non-ionic surfactants by supercritical fluid chromatography combined with ion mobility spectrometry-mass spectrometry. *Anal. Bioanal. Chem.* 411, 2759–2765. <https://doi.org/10.1007/s00216-019-01777-3>
- Marcomini, A., Pavoni, B., Sfriso, A., Orio, A.A., 1990. Persistent metabolites of alkylphenol polyethoxylates in the marine environment. *Mar. Chem.* 29, 307–323. [https://doi.org/10.1016/0304-4203\(90\)90020-D](https://doi.org/10.1016/0304-4203(90)90020-D)
- McEvoy, J., Giger, W., 1986. Determination of linear alkylbenzenesulfonates in sewage sludge by high-resolution gas chromatography/mass spectrometry. *Environ. Sci. Technol.* 20, 376–383. <https://doi.org/10.1021/es00146a009>
- Moe, M.K., Huber, S., Svenson, J., Hagenaaers, A., Pabon, M., Trümper, M., Berger, U., Knapen, D., Herzke, D., 2012. The structure of the fire fighting foam surfactant Forafac®1157 and its biological and photolytic transformation products. *Chemosphere* 89, 869–875. <https://doi.org/10.1016/j.chemosphere.2012.05.012>
- Moldovan, Z., Maldonado, C., Bayona, J.M., 1997. Electron ionization and positive-ion chemical ionization mass spectra

- of N-(2-hydroxyethyl) alkylamides. *Rapid Commun. Mass Spectrom.* **11**, 1077–1082. [https://doi.org/10.1002/\(sici\)1097-0231\(19970630\)11:10%3C1077::aid-rcm912%3E3.0.co;2-1](https://doi.org/10.1002/(sici)1097-0231(19970630)11:10%3C1077::aid-rcm912%3E3.0.co;2-1)
- Mondello, L., Tranchida, P.Q., Dugo, P., Dugo, G., 2008. Comprehensive two-dimensional gas chromatography-mass spectrometry: A review. *Mass Spectrom. Rev.* **27**, 101–124. <https://doi.org/10.1002/MAS.20158>
- Montgomery-Brown, J., Reinhard, M., 2003. Occurrence and behavior of alkylphenol polyethoxylates in the environment. *Environ. Eng. Sci.* **20**, 471–486. <https://doi.org/10.1089/109287503768335940>
- Moody, C.A., Hebert, G.N., Strauss, S.H., Field, J.A., 2003. Occurrence and persistence of perfluorooctanesulfonate and other perfluorinated surfactants in groundwater at a fire-training area at Wurtsmith Air Force Base, Michigan, USA. *J. Environ. Monit.* **5**, 341–345. <https://doi.org/10.1039/b212497a>
- Moody, C.A., Wai Chi Kwan, Martin, J.W., Muir, D.C.G., Mabury, S.A., 2001. Determination of perfluorinated surfactants in surface water samples by two independent analytical techniques: Liquid chromatography/tandem mass spectrometry and ¹⁹F NMR. *Anal. Chem.* **73**, 2200–2206. <https://doi.org/10.1021/ac0100648>
- Morelli, J.J., Szajer, G., 2000. Analysis of surfactants: Part I. *J. Surfactants Deterg.* **3**, 539–552. <https://doi.org/10.1007/s11743-000-0154-8>
- Morelli, J.J., Szajer, G., 2001. Analysis of surfactants: Part II. *J. Surfactants Deterg.* **4**, 75–83. <https://doi.org/10.1007/s11743-001-0163-7>
- Morikawa, M., Daido, H., Takao, T., Murata, S., Shimonishi, Y., Imanaka, T., 1993. A new lipopeptide biosurfactant produced by *Arthrobacter* sp. strain MIS38. *J. Bacteriol.* **175**, 6459–6466. <https://doi.org/10.1128/jb.175.20.6459-6466.1993>
- Moro, G. V., Almeida, R.T.R., Napp, A.P., Porto, C., Pilau, E.J., Lüdtkke, D.S., Moro, A. V., Vainstein, M.H., 2018. Identification and ultra-high-performance liquid chromatography coupled with high-resolution mass spectrometry characterization of biosurfactants, including a new surfactin, isolated from oil-contaminated environments. *Microb. Biotechnol.* **11**, 759–769. <https://doi.org/10.1111/1751-7915.13276>
- Nitschke, L., Huber, L., 1993. Analysis of ethoxylated alcohol surfactants in water by HPLC. *Fresenius. J. Anal. Chem.* **345**, 585–588. <https://doi.org/10.1007/BF00325804>
- Nohara, D., Ohkoshi, T., Sakai, T., 1998. The possibility of the direct measurement of micelle weight by electrospray ionization mass spectrometry. *Rapid Commun. Mass Spectrom.* **12**, 1933–1935. [https://doi.org/10.1002/\(SICI\)1097-0231\(19981215\)12:23%3C1933::AID-RCM410%3E3.0.CO;2-N](https://doi.org/10.1002/(SICI)1097-0231(19981215)12:23%3C1933::AID-RCM410%3E3.0.CO;2-N)
- Ogura, I., DuVal, D.L., Kawakami, S., Miyajima, K., 1996. Identification and quantisation of surfactants in consumer products by ion-spray mass spectrometry. *J. Am. Oil Chem. Soc.* **73**, 137–142. <https://doi.org/10.1007/BF02523461>
- Olsen, G.W., Hansen, K.J., Stevenson, L.A., Burris, J.M., Mandel, J.H., 2003. Human donor liver and serum concentrations of perfluorooctanesulfonate and other perfluorochemicals. *Environ. Sci. Technol.* **37**, 888–891. <https://doi.org/10.1021/es020955c>
- Onzo, A., Acquavia, M.A., Cataldi, T.R.I., Ligonzo, M., Coviello, D., Pascale, R., Martelli, G., Bondoni, M., Scrano, L., Bianco, G., 2020. Coceth sulfate characterization by electrospray ionization tandem mass spectrometry. *Rapid Commun. Mass Spectrom.* **34**, e8884. <https://doi.org/10.1002/rcm.8884>
- Pacwa-Płociniczak, M., Płaza, G.A., Piotrowska-Seget, Z., Cameotra, S.S., 2011. Environmental applications of biosurfactants: Recent advances. *Int. J. Mol. Sci.* **12**, 633–654. <https://doi.org/10.3390/ijms12010633>
- Pan, J., Ji, Y., Du, Z., Zhang, J., 2016. Rapid characterization of commercial polysorbate 80 by ultra-high performance supercritical fluid chromatography combined with quadrupole time-of-flight mass spectrometry. *J. Chromatogr. A* **1465**, 190–196. <https://doi.org/10.1016/j.chroma.2016.08.051>
- Pan, J., Tang, Y., Shen, Z., Du, Z., 2020. Development of supercritical fluid chromatography coupled with mass spectrometry method for characterization of a nonionic surfactant and comparison with liquid chromatography coupled with mass spectrometry method. *J. Mass Spectrom.* **55**, e4499. <https://doi.org/10.1002/jms.4499>
- Pascale, R., Acquavia, M.A., Cataldi, T.R.I., Onzo, A., Coviello, D., Bufo, S.A., Scrano, L., Ciriello, R., Guerrieri, A., Bianco, G., 2020. Profiling of quercetin glycosides and acyl glycosides in sun-dried peperoni di Senise peppers (*Capsicum annuum* L.) by a combination of LC-ESI(-)-MS/MS and polarity prediction in reversed-phase separations. *Anal. Bioanal. Chem.* **412** 1–11. <https://doi.org/10.1007/s00216-020-02547-2>
- Pascale, R., Bianco, G., Calace, S., Masi, S., Mancini, I.M., Mazzone, G., Caniani, D., 2018. Method development and optimization for the determination of benzene, toluene, ethylbenzene and xylenes in water at trace levels by static headspace extraction coupled to gas chromatography–barrier ionization discharge detection. *J. Chromatogr. A* **1548**, 10–18. <https://doi.org/10.1016/j.chroma.2018.03.018>
- Pascale, R., Bianco, G., Cataldi, T.R.I., Buchicchio, A., Losito, I., Altieri, G., Genovese, F., Tauriello, A., Di Renzo, G.C., Lafiosca, M.C., 2018. Investigation of the effects of virgin olive oil cleaning systems on the secoiridoid aglycone content using high performance liquid chromatography–mass spectrometry. *J. Am. Oil Chem. Soc.* **95**, 665–671. <https://doi.org/10.1002/aocs.12072>
- Pascale, R., Bianco, G., Cataldi, T.R.I., Kopplin, P.S., Bosco, F., Vignola, L., Uhl, J., Lucio, M., Milella, L., 2018. Mass spectrometry-based phytochemical screening for hypoglycemic activity of Fagioli di Sarconi beans (*Phaseolus vulgaris* L.). *Food Chem.* **242**, 497–504. <https://doi.org/10.1016/j.foodchem.2017.09.091>
- Pascale, R., Bianco, G., Coviello, D., Cristina Lafiosca, M., Masi, S., Mancini, I.M., Bufo, S.A., Scrano, L., Caniani, D., 2020. Validation of a liquid chromatography coupled with tandem mass spectrometry method for the determination of drugs in wastewater using a three-phase solvent system. *J. Sep. Sci.* **43**, 886–895. <https://doi.org/10.1002/jssc.201900509>
- Pascale, R., Grossi, G., Cruciani, G., Mecca, G., Santoro, D., Calace, R.S., Falabella, P., Bianco, G., 2016. Sequence protein identification by randomized sequence database and transcriptome mass spectrometry (SPIDER-TMS): From manual to automatic application of a “de novo sequencing” approach. *Eur. J. Mass Spectrom.* **22**, 193–198. <https://doi.org/10.1255/ejms.1434>
- Pascale, R., Onzo, A., Ciriello, R., Scrano, L., Bufo, S.A., Bianco, G., 2021. LC/MS based food metabolomics, in: *Comprehensive*

- foodomics*. Elsevier, pp. 39–53. <https://doi.org/10.1016/b978-0-08-100596-5.22774-1>
- Pelizzi, N., Catinella, S., Barbosa, S., Zanol, M., 2002. Different electrospray tandem mass spectrometric approaches for rapid characterization of phospholipid classes of Curosurf®, a natural pulmonary surfactant. *Rapid Commun. Mass Spectrom.* 16, 2215–2220. <https://doi.org/10.1002/rcm.844>
- Petrović, M., Barceló, D., 2000. Determination of anionic and nonionic surfactants, their degradation products, and endocrine-disrupting compounds in sewage sludge by liquid chromatography/mass spectrometry. *Anal. Chem.* 72, 4560–4567. <https://doi.org/10.1021/ac000306o>
- Petrovic, M., Lacorte, S., Viana, P., Barceló, D., 2002. Pressurized liquid extraction followed by liquid chromatography-mass spectrometry for the determination of alkylphenolic compounds in river sediment. *J. Chromatogr. A* 959, 15–23. [https://doi.org/10.1016/S0021-9673\(02\)00407-7](https://doi.org/10.1016/S0021-9673(02)00407-7)
- Phillips, J.B., Beens, J., 1999. Comprehensive two-dimensional gas chromatography: A hyphenated method with strong coupling between the two dimensions. *J. Chromatogr. A* 856, 331–347. [https://doi.org/10.1016/S0021-9673\(99\)00815-8](https://doi.org/10.1016/S0021-9673(99)00815-8)
- Piera, E., Erra, P., Infante, M.R., 1997. Analysis of cationic surfactants by capillary electrophoresis. *J. Chromatogr. A* 757, 275–280. [https://doi.org/10.1016/S0021-9673\(96\)00663-2](https://doi.org/10.1016/S0021-9673(96)00663-2)
- Plomley, J.B., Crozier, P.W., Taguchi, V.Y., 1999. Characterization of nonyl phenol ethoxylates in sewage treatment plants by combined precursor ion scanning and multiple reaction monitoring. *J. Chromatogr. A* 854, 245–257. [https://doi.org/10.1016/S0021-9673\(99\)00314-3](https://doi.org/10.1016/S0021-9673(99)00314-3)
- Popenoe, D.D., Morris, S.J., Horn, P.S., Norwood, K.T., 1994. Determination of alkyl sulfates and alkyl ethoxysulfates in wastewater treatment plant influents and effluents and in river water using liquid chromatography/ion spray mass spectrometry. *Anal. Chem.* 66, 1620–1629. <https://doi.org/10.1021/ac00082a005>
- Radke, M., Behrends, T., Förster, J., Herrmann, R., 1999. Analysis of cationic surfactants by microbore high-performance liquid chromatography-electrospray mass spectrometry. *Anal. Chem.* 71, 5362–5366. <https://doi.org/10.1021/ac990453q>
- Santarsiero, A., Onzo, A., Pascale, R., Acquavia, M.A., Coviello, M., Convertini, P., Todisco, S., Marsico, M., Pifano, C., Iannece, P., Gaeta, C., D'Angelo, S., Padula, M.C., Bianco, G., Infantino, V., Martelli, G., 2020. Pistacia lentiscus hydrosol: Untargeted metabolomic analysis and anti-inflammatory activity mediated by NF- κ B and the citrate pathway. *Oxid. Med. Cell. Longev.* 2020 1–14. <https://doi.org/10.1155/2020/4264815>
- Sato, H., Nakamura, S., Teramoto, K., Sato, T., 2014. Structural characterization of polymers by MALDI spiral-TOF mass spectrometry combined with Kendrick mass defect analysis. *J. Am. Soc. Mass Spectrom.* 25, 1346–1355. <https://doi.org/10.1007/s13361-014-0915-y>
- Sato, H., Shibata, A., Wang, Y., Yoshikawa, H., Tamura, H., 2001. Characterization of biodegradation intermediates of non-ionic surfactants by matrix-assisted laser desorption/ionization-mass spectrometry 1. Bacterial biodegradation of octylphenol polyethoxylate under aerobic conditions. *Polym. Degrad. Stab.* 74, 69–75. [https://doi.org/10.1016/S0141-3910\(01\)00102-1](https://doi.org/10.1016/S0141-3910(01)00102-1)
- Scheibel, J.J., 2004. The evolution of anionic surfactant technology to meet the requirements of the laundry detergent industry. *J. Surfactants Deterg.* 7, 319–328. <https://doi.org/10.1007/s11743-004-0317-7>
- Schmitt, T.M., Allen, M.C., Brain, D.K., Guin, K.F., Lemmel, D.E., Osburn, Q.W., 1990. HPLC determination of ethoxylated alcohol surfactants in wastewater. *J. Am. Oil Chem. Soc.* 67, 103–109. <https://doi.org/10.1007/BF02540636>
- Schneider, E., Levsen, K., Dähling, P., Röllgen, F.W., 1983. Analysis of surfactants by newer mass spectrometric techniques-Part I. Cationic and non-ionic surfactants. *Fresenius' Zeitschrift für Anal. Chemie* 316, 27–285. <https://doi.org/10.1007/BF00468920>
- Shang, D.Y., Ikononou, M.G., MacDonald, R.W., 1999. Quantitative determination of nonylphenol polyethoxylate surfactants in marine sediment using normal-phase liquid chromatography-electrospray mass spectrometry. *J. Chromatogr. A* 849, 467–482. [https://doi.org/10.1016/S0021-9673\(99\)00563-4](https://doi.org/10.1016/S0021-9673(99)00563-4)
- Sharpe, R.M., Skakkebaek, N.E., 1993. Are oestrogens involved in falling sperm counts and disorders of the male reproductive tract? *Lancet* 341, 1392–1396. [https://doi.org/10.1016/0140-6736\(93\)90953-E](https://doi.org/10.1016/0140-6736(93)90953-E)
- Sherrard, K.B., Marriott, P.J., McCormick, M.J., Colton, R., Smith, G., 1994. Electrospray mass spectrometric analysis and photocatalytic degradation of polyethoxylate surfactants used in wool scouring. *Anal. Chem.* 66, 3394–3399. <https://doi.org/10.1021/ac00092a016>
- Shi, C., Liao, G., Liu, W., 2014. Synthesis of internal olefin sulfonate and its application in oil recovery. *Arab. J. Sci. Eng.* 39, 37–41. <https://doi.org/10.1007/s13369-013-0841-5>
- Shrivastava, K., Wu, H.F., 2007. A rapid, sensitive and effective quantitative method for simultaneous determination of cationic surfactant mixtures from river and municipal wastewater by direct combination of single-drop microextraction with AP-MALDI mass spectrometry. *J. Mass Spectrom.* 42, 1637–1644. <https://doi.org/10.1002/jms.1266>
- Sinnberg, T., Lichtensteiger, C., Hasan Ali, O., Pop, O.T., Gilardi, M., Risch, L., Bomze, D., Kohler, P., Vernazza, P., Albrich, W.C., Kahlert, C.R., Brugger, S.D., Abdou, M.-T., Zinner, C., Röcken, M., Kern, L., Brutsche, M.H., Kalbacher, H., Velic, A., Maček, B., Penninger, J.M., Matter, M.S., Flatz Lukas, 2021. IgA autoantibodies target pulmonary surfactant in patients with severe COVID-19. *medRxiv* 17, 1–19. <https://doi.org/10.1101/2021.02.02.21250940>
- Solak Erdem, N., Alawani, N., Wesdemiotis, C., 2014. Characterization of polysorbate 85, a nonionic surfactant, by liquid chromatography vs. ion mobility separation coupled with tandem mass spectrometry. *Anal. Chim. Acta* 808, 83–93. <https://doi.org/10.1016/j.aca.2013.07.026>
- Stephanou, E., Giger, W., 1982. Persistent organic chemicals in sewage effluents. 2. Quantitative determinations of nonylphenols and nonylphenol ethoxylates by glass capillary gas chromatography. *Environ. Sci. Technol.* 16, 800–805. <https://doi.org/10.1021/es00105a014>
- Sun, T., Wang, X., Cong, P., Xu, J., Xue, C., 2020. Mass spectrometry-based lipidomics in food science and nutritional health: A comprehensive review. *Compr. Rev. Food Sci. Food Saf.* 19, 2530–2558. <https://doi.org/10.1111/1541-4337.12603>
- Sütterlin, H., Alexy, R., Coker, A., Kümmerer, K., 2008. Mixtures of quaternary ammonium compounds and anionic organic

- compounds in the aquatic environment: Elimination and biodegradability in the closed bottle test monitored by LC-MS/MS. *Chemosphere* 72, 479–484. <https://doi.org/10.1016/j.chemosphere.2008.03.008>
- Takahashi, K., Takahashi, R., Horikawa, Y., Matsuyama, S., Kinugasa, S., Ehara, K., 2013. Optimization of experimental parameters for separation of nonionic surfactants by supercritical fluid chromatography. *J. Supercrit. Fluids* 82, 256–262. <https://doi.org/10.1016/j.supflu.2013.08.007>
- Taulli, T.A., 1969. Evaluation of isomeric sodium alkenesulfonates via methylation and gas chromatography. *J. Chromatogr. Sci.* 7, 671–673. <https://doi.org/10.1093/chromsci/7.11.671>
- Thurman, E.M., Ferrer, I., Blotevogel, J., Borch, T., 2014. Analysis of hydraulic fracturing flowback and produced waters using accurate mass: Identification of ethoxylated surfactants. *Anal. Chem.* 86, 9653–9661. <https://doi.org/10.1021/ac502163k>
- Treglia, A., Palumbo, F., Gristina, R., Calvano, C.D., Cataldi, T., Fracassi, F., Favia, P., 2020. Novel aerosol assisted plasma deposition of PEG containing coatings for non-fouling application. *Appl. Surf. Sci.* 527, 146698. <https://doi.org/10.1016/j.apsusc.2020.146698>
- Trier, X., Granby, K., Christensen, J.H., 2011. Polyfluorinated surfactants (PFS) in paper and board coatings for food packaging. *Environ. Sci. Pollut. Res.* 18, 1108–1120. <https://doi.org/10.1007/s11356-010-0439-3>
- Tsai, P.C., Ding, W.H., 2004. Determination of alkyltrimethylammonium surfactants in hair conditioners and fabric softeners by gas chromatography-mass spectrometry with electron-impact and chemical ionization. *J. Chromatogr. A* 1027, 103–108. <https://doi.org/10.1016/j.chroma.2003.10.047>
- Tziotis, D., Hertkorn, N., Schmitt-Kopplin, P., 2011. Kendrick-analogous network visualisation of ion cyclotron resonance Fourier transform mass spectra: Improved options for the assignment of elemental compositions and the classification of organic molecular complexity. *Eur. J. Mass Spectrom.* 17, 415–421. <https://doi.org/10.1255/ejms.1135>
- Ventura, G., Calvano, C.D., Losito, I., Bianco, G., Pascale, R., Palmisano, F., Cataldi, T.R.I., 2019. Effect of pH and mobile phase additives on the chromatographic behaviour of an amide-embedded stationary phase: Cyanocobalamin and its diaminemonochloro-platinum(II) conjugate as a case study. *J. Sep. Sci.* 42, 1155–1162. <https://doi.org/10.1002/jssc.201801060>
- Vettori, U., Issa, S., Facino, R.M., Carini, M., 1988. Analysis of ethoxylated fatty alcohols, non-ionic surfactants, in raw materials by capillary column gas chromatography/electron impact mass spectrometry. *Biol. Mass Spectrom.* 17, 193–204. <https://doi.org/10.1002/bms.1200170308>
- Villar, M., Callejón, M., Jiménez, J.C., Alonso, E., Guiráum, A., 2007. Optimization and validation of a new method for analysis of linear alkylbenzene sulfonates in sewage sludge by liquid chromatography after microwave-assisted extraction. *Anal. Chim. Acta* 599, 92–97. <https://doi.org/10.1016/j.aca.2007.07.065>
- Vlachy, N., Drechsler, M., Verbavatz, J.M., Touraud, D., Kunz, W., 2008. Role of the surfactant headgroup on the counterion specificity in the micelle-to-vesicle transition through salt addition. *J. Colloid Interface Sci.* 319, 542–548. <https://doi.org/10.1016/j.jcis.2007.11.048>
- Wulf, V., Wienand, N., Wirtz, M., Kling, H.-W., Gäb, S., Schmitz, O.J., 2010. Analysis of special surfactants by comprehensive two-dimensional gas chromatography coupled to time-of-flight mass spectrometry. *J. Chromatogr. A* 1217, 749–754. <https://doi.org/10.1016/j.chroma.2009.11.093>
- Ying, G.G., Williams, B., Kookana, R., 2002. Environmental fate of alkylphenols and alkylphenol ethoxylates - A review. *Environ. Int.* 28, 215–226. [https://doi.org/10.1016/S0160-4120\(02\)00017-X](https://doi.org/10.1016/S0160-4120(02)00017-X)
- Zakharova, L.Y., Pashirova, T.N., Doktorovova, S., Fernandes, A.R., Sanchez-Lopez, E., Silva, A.M., Souto, S.B., Souto, E.B., 2019. Cationic surfactants: Self-assembly, structure-activity correlation and their biological applications. *Int. J. Mol. Sci.* 20, 5534. <https://doi.org/10.3390/ijms20225534>
- Zecchi, R., Franceschi, P., Tigli, L., Ricci, F., Boscaro, F., Pioselli, B., Mileo, V., Murgia, X., Bianco, F., Salomone, F., Schmidt, A.F., Hillman, N.H., Kemp, M.W., Jobe, A.H., 2019. Mass spectrometry imaging as a tool for evaluating the pulmonary distribution of exogenous surfactant in premature lambs. *Respir. Res.* 20, 1–12. <https://doi.org/10.1186/s12931-019-1144-5>
- Zhang, Y.Z., Tang, C.Y., Song, X.F., Li, F.D., 2009. Behavior and fate of alkylphenols in surface water of the Jialu River, Henan Province, China. *Chemosphere* 77, 559–565. <https://doi.org/10.1016/j.chemosphere.2009.07.005>
- Zhou, B., Xiao, J.F., Tuli, L., Resson, H.W., 2012. LC-MS-based metabolomics. *Mol. Biosyst.* 8, 470–481. <https://doi.org/10.1039/c1mb05350g>

AUTHOR BIOGRAPHIES



Raffaella Pascale obtained a master's degree in Chemical Sciences at the University of Basilicata and she is a Doctor of Philosophy (PhD) in Engineering for Innovation and Sustainable Development (XXXI Cycle) at the University of Basilicata. Her research work concerns, mainly, the validation of GC-MS and HPLC-MS analytical methods according to the ICH, EURACHEM, and AOAC guidelines. In addition to academic experience, she worked in an environmental laboratory for the analysis of organic and inorganic pollutants in environmental matrices, applying the EPA and ISO standardized methods. She is currently an IPC-QC Analyst for the quality control at an Italian pharmaceutical industry.



Maria A. Acquavia hold a master's degree in Chemical Sciences in 2019, at the University of the Basilicata. Currently, she is attending the International Doctoral School of Research in Applied Biology and Environmental Safeguard (XXXV Cycle), at the same university, as PhD student and employee researcher of the company ALMAGISI S.r.l. (Bolzano). Her expertise deal with the determination of nutritional foods labeling, as well as the analysis of environmental samples by using accredited official methods. She mainly uses chromatographic and mass spectrometry techniques, as well as hyphenate techniques, for the quantification and/or characterization of organic and inorganic molecules in complex matrices.



Alberto Onzo hold a master's degree in Chemical Sciences at the University of Salerno (Italy) and he is currently a Doctor of Philosophy (PhD) in Analytical Chemistry (XXXIII cycle). His research work is related to the targeted and untargeted metabolomic analysis of food products by means of hyphenated Mass Spectrometry techniques and Fourier Transform Ion Cyclotron Resonance Mass Spectrometry and the development of open source software for Mass Spectrometry data elaboration and visualization. Nowadays, he is working as a QC analyst in a private italian laboratory, dealing with the analysis of environmental and food matrices.



Tommaso R. I. Cataldi Full Professor at University of Bari (Department of Chemistry). His research work is focused on the use of LC-MS to identify and quantify relevant metabolites with a special focus on the lipidome of biological fluids, bacteria, vegetables and seafood. The main aim is to investigate and understand the fundamental mechanisms whereby lipids (e.g., phospholipids, sulfolipids, etc.) are involved in the regulation of metabolic processes, including abiotic stress of

bacteria, nutraceutical properties of farmed and wild fishes, and human neurodegenerative disorders.



Cosima D. Calvano Assistant Professor of Analytical Chemistry at University of Bari in the Master's Degree Course in Pharmacy and teacher of Applied Mass Spectrometry in the Master's Degree Course in Chemical Sciences. Her current scientific interests relate to the use of mass spectrometry for proteomics and lipidomics applied to clinical, food and cultural heritage fields. Another important research activity concerns the development of new matrices for MALDI MS (second generation ionic liquids, nanostructured materials, binary matrices, strong organic bases, newly synthesized matrices derived from conventional ones).



Giuliana Bianco Assistant Professor at University of Basilicata of Analytical Chemistry in the Master's Degree Course in Pharmacy and of Analytical Methods for Environmental Analysis in the Master's Degree Course in Chemical Sciences. The research field concerns mainly the development of new analytical methodologies based on the use of separative techniques as liquid chromatography (LC), gas chromatography (GC), capillary electrophoresis (CE), the most modern spectrometry techniques mass (MS) as well as combined techniques (LC-MS, GC-MS, CE-MS) for the determination of compounds of interest in biotechnology, biomedical, agro-food, environmental and microbiological, and so forth.

How to cite this article: Pascale R, Acquavia MA, Onzo A, Cataldi TRI, Calvano CD, Bianco G. Analysis of surfactants by mass spectrometry: Coming to grips with their diversity. *Mass Spectrometry Reviews*, (2021);1–32.
<https://doi.org/10.1002/mas.21735>

Review

Analytical Methods for Extraction and Identification of Primary and Secondary Metabolites of Apple (*Malus domestica*) Fruits: A Review

Maria Assunta Acquavia ^{1,2}, Raffaella Pascale ³ , Luca Foti ¹, Giuseppe Carlucci ¹, Laura Scrano ⁴ , Giuseppe Martelli ¹, Monica Brienza ¹, Donatella Coviello ⁵, Giuliana Bianco ^{1,*}  and Filomena Lelario ¹

- ¹ Dipartimento di Scienze, Università degli Studi della Basilicata, Via dell'Ateneo Lucano 10, 85100 Potenza, Italy; maria.acquavia@unibas.it (M.A.A.); luca.foti@unibas.it (L.F.); giuseppe.carlucci89@gmail.com (G.C.); giuseppe.martelli@unibas.it (G.M.); monica.brienza@unibas.it (M.B.); filomena.lelario@unibas.it (F.L.)
- ² ALMAGISI S.r.l Corso Italia, 27, 39100 Bolzano, Italy
- ³ Gnosis by Lesaffre, Pisticci, 75015 Matera, Italy; raff.pascale@gmail.com
- ⁴ Dipartimento delle Culture Europee e del Mediterraneo: Arch., Università degli Studi della Basilicata, Ambiente, Patrimoni Culturali, Via Lanera, 20-75100 Matera, Italy; laura.scrano@unibas.it
- ⁵ Centro Direzionale, Dipartimento di Ingegneria, Università degli Studi di Napoli Parthenope, Isola C/4, 80143 Napoli, Italy; donatella.coviello@unibas.it
- * Correspondence: giuliana.bianco@unibas.it



Citation: Acquavia, M.A.; Pascale, R.; Foti, L.; Carlucci, G.; Scrano, L.; Martelli, G.; Brienza, M.; Coviello, D.; Bianco, G.; Lelario, F. Analytical Methods for Extraction and Identification of Primary and Secondary Metabolites of Apple (*Malus domestica*) Fruits: A Review. *Separations* **2021**, *8*, 91. <https://doi.org/10.3390/separations8070091>

Academic Editor: Mihaly Dernovics

Received: 7 June 2021

Accepted: 23 June 2021

Published: 25 June 2021

Publisher's Note: MDPI stays neutral with regard to jurisdictional claims in published maps and institutional affiliations.



Copyright: © 2021 by the authors. Licensee MDPI, Basel, Switzerland. This article is an open access article distributed under the terms and conditions of the Creative Commons Attribution (CC BY) license (<https://creativecommons.org/licenses/by/4.0/>).

Abstract: Apples represent a greater proportion of the worldwide fruit supply, due to their availability on the market and to the high number of existing cultivar varieties and apple-based products (fresh fruit, fruit juice, cider and crushed apples). Several studies on apple fruit metabolites are available, with most of them focusing on their healthy properties' evaluation. In general, the metabolic profile of apple fruits strongly correlates with most of their peculiar characteristics, such as taste, flavor and color. At the same time, many bioactive molecules could be identified as markers of a specific apple variety. Therefore, a complete description of the analytical protocols commonly used for apple metabolites' characterization and quantification could be useful for researchers involved in the identification of new phytochemical compounds from different apple varieties. This review describes the analytical methods published in the last ten years, in order to analyze the most important primary and secondary metabolites of *Malus domestica* fruits. In detail, this review gives an account of the spectrophotometric, chromatographic and mass spectrometric methods. A discussion on the quantitative and qualitative analytical shortcomings for the identification of sugars, fatty acids, polyphenols, organic acids, carotenoids and terpenes found in apple fruits is reported.

Keywords: apple; metabolites; polyphenols; mass spectrometry-based analytical methods; GC-MS; LC-MS; LC-MS/MS

1. Introduction

Due to the beneficial properties of metabolites, the interest in the characterization and quantification of the metabolites—both primary and secondary—of plant-based foods is growing, and it often aims at the definition of food nutritional value, as well as of its quality and authenticity. In this context, foodomics technologies have emerged [1]. Foodomics has been defined as a new discipline that studies the food and nutrition domains through the application of advanced omics technologies for improving consumers' well-being, health and confidence [2]. Considering a large number of plant primary and secondary metabolites and their different properties, several analysis techniques have been developed for each class of compounds, which differ already starting from the extraction phase of metabolites [3]. The interest in nutritional parameters, such as sugars content, often identified as being responsible for obesity or diseases such as diabetes, determined

the attention to develop analytical methods for the determination of simple sugars and polysaccharides [4]. Anyway, each class of metabolite, whether primary or secondary, needs a dedicated extraction and analysis method to offer the consumer as much information as possible regarding the functional values of the individual foods.

Malus domestica fruits, commonly known as apples, are one of the most consumed fruits worldwide, and they are generally recognized as an outstanding source of biologically active compounds, related to both functional and nutraceutical values [5] (Figure 1).

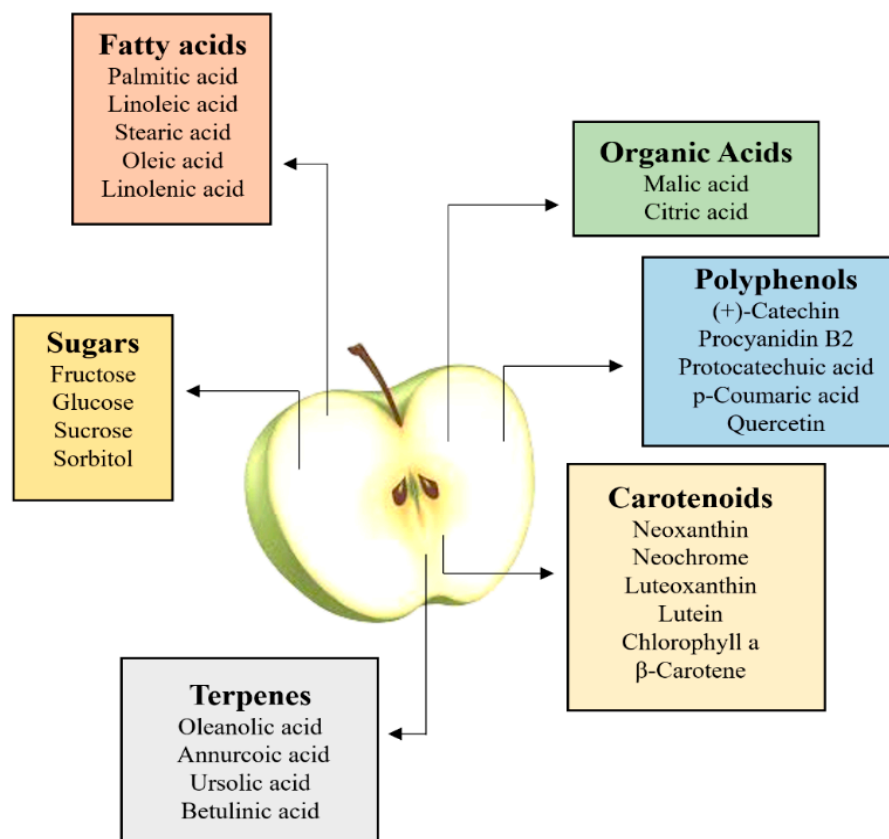


Figure 1. Main primary and secondary metabolites related to functional and nutraceutical values of apples.

Apples have a varied and well-balanced composition; more than 84% of their weight is represented by water, in which minerals such as K, Mg, Ca and Na and trace elements such as Zn, Mn, Cu, Fe, B, F, Se and Mo are dissolved [6]. Proteins and lipids represent a small energetic supply contribution to *Malus domestica* fruits, due to their relatively small concentrations [6]. On the contrary, the content of fibers, i.e., complex polysaccharides such as pectin, celluloses, hemicelluloses and lignin, is high in apples when compared with other fresh fruits [7]. Although a large variety of vitamins are present, the B complex vitamins are the most abundant. Moreover, apples are considered an important source of polyphenols, which are responsible for their well-known antioxidant properties [5].

Apples are commonly considered as healthy plant-based foods. They have a very low caloric impact. From a nutritional point of view, they contain a high number of sugars, balanced by the concentration of fibers [8]. In the last ten years, apples have been the subject of research and studies aiming to evaluate their effects on human health [9]. The daily intake of apples and apples-related products is often proposed in with weight control diets and has proved to have a statistically significant impact on weight reduction [10]. Recent epidemiological research shows how the risk of cardiovascular diseases and cancers could be reduced by the regular consumption of apples [11,12], due to their phenolic acids and flavonoids, i.e., molecules with antioxidant properties [12]. The nutritional value and

health-related properties of apples depend on the bioavailability and daily intake of their nutrients and phytochemicals, as well as on their concentration [13]. Therefore, a complete evaluation of the apple's metabolites distribution is desirable.

Over the years, many new *Malus domestica* species have been produced through new grafts and hybridizations, thus obtaining apple fruits with different chemical–physical characteristics and organoleptic properties [14]. The first evaluation regards the pulp, which usually has a yellow/white color and can be crunchy, pasty or floury, based on the percentage of pectin and cellulose [15]. The crunchiness or mellowness of the apple is affected by the water content, too, which is generally around the 85%. By varying this percentage, greater or less juiciness results [6]. The flavor that distinguishes the various apples species depends on the quantity of organic acids and sugars present in the pulp [16]. All the qualitative, physical and organoleptic parameters characterizing the existing apple varieties are listed in Table 1.

Table 1. Qualitative, physical and organoleptic parameters characterizing all the existing apple fruit varieties.

Apple Variety	Color	Dimension	Pulp	Flavor
Renetta	Yellow, tending to the green	Medium	Soft and pasty	Acid, medium sweetened
Golden Delicious	Gold yellow	Large	Crunchy and juicy	Very sweet
Stark Delicious	Bright red	Large	Crunchy and juicy	Sweet, little acidic
Granny Smith	Green	Medium	Crunchy	Acid
Fuji	Reddish with yellow-green streaks	Large	Crunchy and juicy	Sweet, little acidic
Pink Lady	Reddish/red	Medium	Crunchy	Sweet
Annurca	Bright red	Small	Crunchy	Acid
Royal Gala	Red with streaks	Small	Crunchy and juicy	Very sweet
Kanzi	Intense red or yellow	Medium	Hard and crunchy	Medium sweet and acid
Braeburn	Brown red	Medium–large	Crunchy	Medium sweet/acid
Morgenduft	Red with clear patches	Medium	Hard and juicy	Sweet and slightly acid

In addition to the apple fruit varieties listed in Table 1, some other types result from crosses between them [17]. Moreover, it should be considered that some small variations in each apple variety could occur, due to grafts and environmental conditions [16]. All the existing varieties of apple fruits show a characteristic profile of phytochemical components [18].

Like all fruits, apples have to meet commercial-quality parameters established by the European Commission Regulation (CE) N. 85/2004 15 January 2004. In detail, an apple fruit must be whole, healthy, clean, free of pathogens and free of flavors or odors other than usual, in order to be considered qualitatively relevant, from a commercial point of view.

In general, the phytochemical profile of apple fruits strongly correlates with most of their peculiar characteristics, such as taste, flavor and color. As previously said, it is difficult to estimate the number of the existing apple varieties among the world, due to the continuous changes and hybridizations performed [6].

However, it is possible to determine the phytochemical profile of apples to provide the real quantities of all natural compounds [19]. At the same time, new bioactive molecules could be identified as markers of a specific apple variety. Thus, an investigation of the complete metabolic profile of these fruits is mandatory. In this review, a discussion on the main analytical methods, differing in their extraction and detection protocols, developed in the last ten years for the investigation of primary and secondary metabolites occurring in apple fruits is provided. Particular attention is given to the more recent and cutting-edge techniques, thus making the readers could easily choose the methods that best suit their needs.

2. Apple Metabolites Analysis

Sugars, proteins, lipids, carotenoids, polyphenols and triterpenoids are present with different concentrations in apple fruits [20]. Since these phytochemical constituents have received greater attention in the last years, thanks to their beneficial properties, an overview of the main analytical methods applied for their analysis in apple fruits is useful [21]. Due to the pronounced chemo-variability observed in apple fruits, the availability of an update and comprehensive review dedicated to analytical methods, such as that reported in the present study, could be a useful tool in the standardization of apple fruit extracts, to be used in studies for various purposes. All the existing methods include a preliminary step, during which the extraction of the metabolites of interest from apple fruits is carried out. Successful metabolomic research, in fact, requires effective metabolite extraction. The sample pretreatment, which precedes metabolites analysis can widely vary depending on the type of matrix of interest (Table 2). If the samples are liquid, they can be analyzed directly after filtration and/or centrifugation; for solid samples, preliminary freeze-drying, grinding and extraction phases are required [22]. The extraction procedure is aimed at maximizing the amount and concentration of the compounds of interest and must be chosen according to the type of metabolites [23]. For this reason, extraction is probably the most critical step in the analysis of the plant and fruit metabolites. An ideal extraction should allow us to recover all metabolites of interest, without any chemical modifications. The extraction procedures differ according to the physicochemical properties of the compounds to be extracted, i.e., polarity and solubility [24]. Furthermore, after the extraction of metabolites, several methods could be employed in order to quantify them. Usually, spectrophotometric assays are used as a preliminary screening of the major classes of metabolites occurring in the fruits. They allow a general evaluation of the content of a specific metabolite class; however, they do not provide quantitative information about individual compounds [25]. On the other hand, higher sensitive and selective analytical techniques, such as mass spectrometry [26,27] or liquid chromatography coupled to mass spectrometry (LC–MS), are exploited for the separation and the detection of individual compounds, as well as for their structural characterization [28]. LC–MS is one of the most used techniques in foodomics, as well as in drugs analyses and in the environmental fields [29]. Starting from primary metabolites, with a special focus on sugars and fatty acids, a description of the extraction protocols of the different classes of metabolites occurring in apple fruits, as well as of the analytical techniques used for their analysis, is provided in the following sections. Particular attention will be addressed to secondary metabolites' extraction, detection and quantification, as they are the main compounds responsible for the well-known healthy properties of *Malus* fruits.

Table 2. Main extraction and detection methods used for apples primary and secondary metabolites, with their recommendations.

		Extraction and Detection Methods	Recommendations
Primary Metabolites	Sugars	Extraction LSE extraction with water as solvent Analysis HPLC–RI; HPLC–ELSD	<ul style="list-style-type: none"> • A preliminary immersion in methanol/water solution is important to avoid the hydrolysis of sucrose into free sugars; • HPLC–RI and HPLC–ELSD based methods are destructive, require the use of hazardous chemicals and are labor intensive. As an alternative, FT-NIR and ATR–FT-NIR are more rapid and simple to be used.
	Fatty acids	Extraction LSE extraction with hexane as solvent; Soxhlet extraction with petroleum ether Analysis GC–FID; GC–MS	<ul style="list-style-type: none"> • The derivatization is requested, because most fatty acids have high boiling points, thus being difficult to evaporate, and have a low FID response.

Table 2. Cont.

		Extraction and Detection Methods	Recommendations
Secondary Metabolites	Phenolics and organic acids	Extraction MAE or UAE extraction; Analysis HPLC–DAD; LC–MS/MS	<ul style="list-style-type: none"> No single wavelength is ideal for monitoring all classes of phenolics, because they display absorbency maxima at different wavelengths; As phenolic compounds are often linked to saccharidic moieties that are not UV-active, the correct polyphenols identification with LC–UV is not often feasible; LC–MS/MS allow sensitive and selective analysis.
	Carotenoids	Extraction LSE extraction Analysis HPLC–DAD; LC–MS/MS	<ul style="list-style-type: none"> Carotenoids are strongly susceptible to oxidative degradation, due to the high number of conjugated double bonds, thus extraction must be performed in dark conditions or by adding antioxidant compounds; The λ_{max} of individual carotenoids can vary depending on functional groups.
	Terpenes	Extraction SPME and SBSE extraction for volatile terpenes; UAE extraction for non-volatile triterpenoids; Analysis GC–FID; GC–MS for volatile terpenes; HPLC–DAD; LC–MS/MS for non-volatile triterpenoids	<ul style="list-style-type: none"> It is highly recommended the combined use of retention index values (RI) and MS spectrum for the univocal peak assignment during analysis of volatile terpenes; LC–DAD is often not useful, as these compounds absorb UV radiation weakly and only at wavelength of 200 nm.

3. Primary Metabolites: Extraction and Analysis

Primary metabolites are defined as chemical compounds which are necessary for plant growth, development and reproduction [30]. There are, basically, four main groups of primary metabolites in plant-based foods: sugars, amino-acids, fatty acids and nucleotides. Among them, sugars and fatty acids deserve special attention for apples, because they play a role in fruits' taste.

3.1. Sugars

For many fruits and vegetables, sweetness is an important parameter influencing their quality and is determined by the level of soluble sugars. Therefore, the determination of sugars and sweetness are of great importance in many fields of plant-food-science research [4]. In apples, sweetness is one of the most important quality parameters that determines the overall acceptability of the fruit, and it is affected mainly by fructose, glucose, sucrose and sorbitol concentrations [31]. Sorbitol and sucrose are biosynthesized in the leaves, and then they are translocated into the fruits, where they can be converted into fructose, glucose, malic acid and starch depending on the stage of fruit development. Sorbitol and sucrose represent almost the total translocated carbohydrates [31]. Although the individual sugar content may vary greatly between and within apple cultivars, during fruit storage, the concentrations of sucrose tend to decrease due to the conversion to fructose and glucose [31].

Sugars quantification in apples is preceded by their extraction from the fruit tissues. The extraction of sugars is usually performed by using water as an extraction solvent, since it yields more reliable results. Indeed, Karkacier et al. [32] found that, with alcoholic extraction, some sugars may not adequately dissolve in proportion to their true concen-

tration because of solvent vaporization, even at low temperatures. However, in general, a preliminary immersion in methanol/water solution of the fruit tissues before the extraction, is important to inhibit the invertase activity, thus avoiding the hydrolysis of sucrose into free sugars (glucose and fructose) [3].

As traditional colorimetric and iodometric methods are unable to quantitate sugars individually, non-structural carbohydrates in apples are analyzed by HPLC coupled with suitable columns and detectors, including refractive index detector (RI), evaporative light scattering detector (ELSD) and pulsed amperometric detector (PAD) [32–34]. HPLC coupled to diode-array detector is quite limited, as sugars do not absorb UV light at a wavelength longer than 200 nm [32]. Although less common, GC–MS-based methods for sugars' analysis have also been proposed. In these cases, preliminary derivatization stages with methoxyamine hydrochloride and N-methyl-N-trimethylsilyl-trifluoroacetamide (MSTFA) are needed [35].

One of the most used methods for the quantification of soluble carbohydrates, is HPLC–RI, being simple, rapid and economical [34]. In fact, an accurate HPLC–RI method for the simultaneous determination of glucose, fructose, sucrose and sorbitol in leaf and/or fruit peel from different apple cultivars was developed and validated by Filip et al. [34]. This method was found to be reproducible and sensitive. The HPLC–RI method was successfully applied to qualitative and quantitative establish the sugars of seven apple cultivars and two rootstocks originating from a germplasm collection [34]. Instead, Ma et al. [33] developed an HPLC–ELSD method to analyze sugars without derivatizations, with short analysis times (25 min) and good chromatographic separations. Recently, Yang et al. [36] also used the same method to quantify glucose, fructose, sucrose and sorbitol in “Orin” apples, founding that their content generally increased during the fruit-ripening periods and reached the maximum at full-ripening stage of 180 days after full-bloom stage [36]. ELSD does not suffer of limitations such as composition, flow rate of mobile phase and temperature. In this case, the detection is based on the ability of particles to cause photon scattering, thus with ELSD most compounds less volatile than the mobile phase could be detected, regardless the optical properties of the analytes.

The methods discussed above require considerable financial investment, advanced analytical skills and time. Moreover, they are destructive and require the use of hazardous chemicals and are labor intensive. As an alternative, more rapid, simple and non-destructive techniques, i.e., Fourier transform near-infrared (FT-NIR) spectroscopy with attenuated total reflection (ATR–FT-NIR), have been used to determine the sweetness as an internal quality attribute of fresh apples [37,38]. By comparison of HPLC and FT-NIR for quantification of glucose, fructose and sucrose in intact apple fruit [37], it emerged that FT-NIR is more flexible and much faster than HPLC method.

3.2. Fatty Acids

The mesocarp, or pulp, of apples generally contains very low levels of lipid material (0.2–0.6%), and therefore it is not an important source of edible or industrial fats and oils [39]. Saturated and unsaturated fatty acids are, in fact, degraded to precursor molecules for straight-chain esters. However, despite their low levels of concentration, fatty acids (FAs) and lipids are important structural and metabolic constituents [40]. Indeed, alterations of the lipids constituting the cellular membranes, could cause serious problems to the cell's adaptability to stress conditions, thus resulting in fruit storage disorders. Moreover, FAs and lipids often play a crucial role as precursors of important volatile aroma and regulatory compounds cells [41]. Although there are differences among varieties and ripening stage, the content of saturated fatty acids is generally higher than that of the unsaturated ones in each apple variety. The optimal value of the ratio between the content of the latter and the former is around 30/70 or less [42]. Among the saturated and unsaturated FAs classes, palmitic acid (C16:0) and linoleic acid (C18:2) are the dominant compounds, respectively [42]. In addition to palmitic and linoleic acid, there are C18:0 (stearic acid), C18:1(oleic acid) and C18:3 (linolenic acid), whose concentration levels dynamically fluctuate.

tuates during fruit growth and development. Other FAs, such as C20:0 (arachidonic acid), show only small variations, which may indicate that they are constituents of the fruit cuticle, rather than participants in actual fruit metabolism [41].

Gas chromatography (GC) coupled to flame ionization detector (FID) or mass spectrometric detector (MS) is the most commonly used technology for the detection of fatty acids in apples. The analysis of fatty acids by GC–FID and GC–MS-based analytical methods involve three main steps, i.e., their extraction from the sample matrix, their derivatization, and the GC–FID or GC–MS analysis [43]. Lipids extraction from apple tissues is performed with hexane, and it is often followed by filtration of the supernatant through anhydrous sodium sulfate [44,45]. Soxhlet extraction with petroleum ether has also been used [45,46]. The derivatization is requested, because most fatty acids have high boiling points, thus being difficult to evaporate, and have a low FID response [47]. Fatty acids in apples are usually analyzed by GC–FID and GC–MS as methyl ester derivatives. The derivatization is typically made by treating apple extract with methanol and sulfuric acid under a stream of nitrogen, before the GC–MS analysis. Five fatty acids were identified as their methyl esters with this approach by Walia et al. [45] in apple fruits, i.e., oleic acid, linoleic acid, palmitic acid, stearic acid and arachidic acids. Since mass spectra of derivatized fatty acids rarely contain ions indicative of structural features (the positions of double bonds in the aliphatic chain, for example, cannot be determined), retention indices (RI) of the compounds relative to a mixture of n-alkanes are calculated and are typically used for their identification, alongside with a comparison of their mass spectral data with Wiley, NIST, NBS library and the literature data [45].

4. Secondary Metabolites

To date, the structures and the average content of primary metabolites occurring in apples, are well known, for their nutritional value [42]. Therefore, in recent years, research has been most focused on the extraction of secondary metabolites to be used in pharmacological studies for their beneficial properties [21]. Food and pharmaceutical studies have addressed their attention on fruits and vegetables' bioactive components considered healthy for the treatment and prevention of human diseases. Among the different classes of apples, secondary metabolites, polyphenols, carotenoids, organic acids and terpenes are the main phytochemicals [6].

Although several classes of bioactive compounds occurring in apples, their well-known antioxidant properties are mainly attributed to phenolic compounds. These compounds exhibit several of double bonds and hydroxyl groups in their structures, which are responsible of their antioxidant activity [48]. There are five major groups of polyphenolic compounds found in apples: hydroxycinnamic acids (primarily chlorogenic acid), flavan-3-ols, i.e., (+)-catechin, (–)-epicatechin and anthocyanidins, flavonols (mainly different quercetin glycosides), dihydrochalcones (such as phloridzin) and anthocyanins [49–51] (Figure 2). A high percentage (60%) of the total phenolic concentration in apple peel is represented by the monomeric and polymeric flavan-3-ols, while flavonols, hydroxycinnamic acids, dihydrochalcones and anthocyanins account, respectively, for the 18%, 9%, 8% and 5% of the total phenol content [52].

Carotenoid pigments in the skin of apples contribute to fruit coloration, and therefore to their attractiveness, but in the flesh, their concentrations are low. Indeed, fruits of commercial apple cultivars show relatively low concentrations of carotenoids (<2.5 µg/g of fresh weight), in comparison with non-commercial apples, such as the rootstock cultivar "Aotea", that show relatively high carotenoid concentrations [53].

Alongside with sugars, aromatic volatile compounds and organic acids are responsible for the taste and flavor of apples (Figure 3). In addition, organic acids are the main soluble constituents that influence the shelf life of fresh fruits and ripeness; consequently, they can be used as an index of consumer acceptability [54]. In cultivated apple, malic acid is the predominantly detectable organic acid, while malic acid and citric acid are the predominant organic acids in wild apple species [55]. In regard to apple aroma profiles,

many volatile organic compounds (VOCs) contribute to the overall sensory quality. These compounds include carboxylic esters, alcohols, aldehydes and ketones. Various terpenes have also been identified; however, they only contribute a relatively minor component of total VOCs produced [56]. Some of the terpenes occurring in apples are α -farnesene, geranyl acetone and farnesol [57,58]. α -farnesene, which is an acyclic branched sesquiterpene, is highly occurring in ripe fruits; moreover, other monoterpenes, cyclic sesquiterpenes and terpene derivatives have also been identified in floral and vegetative tissues. Many of these compounds are constitutively produced in relatively low amounts also as a response to insect infestation and they could directly affect apple pest behavior [56]. More polar and less volatile terpenes, i.e., triterpenoid compounds, have been also identified in apples, namely pomaceic, annurcoic, euscaphic, pomolic, corosolic, maslinic, oleanolic, betulinic and ursolic acid [59].

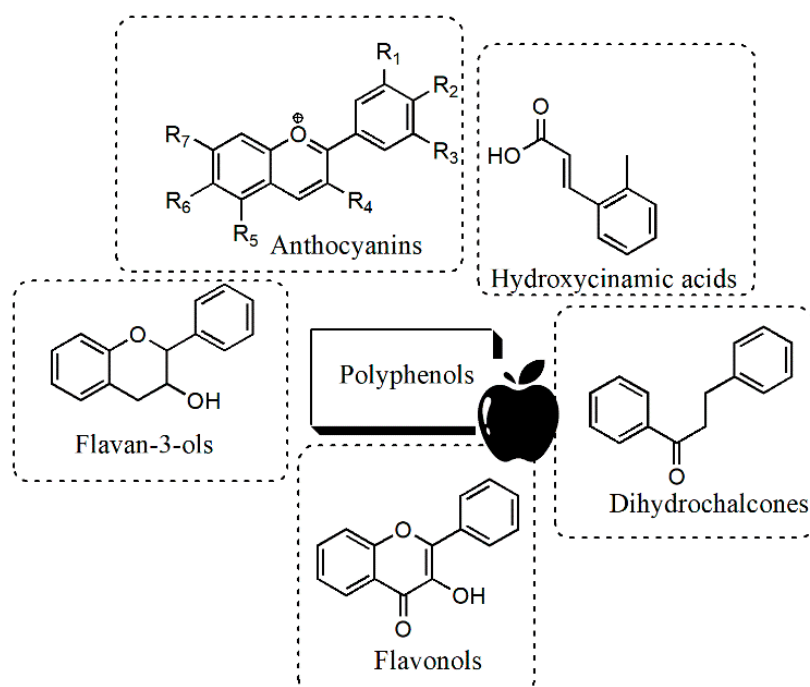


Figure 2. Main classes of polyphenols occurring in apples.

4.1. Extraction

Phytochemical compounds from apples were extracted by using various extraction methods based on the application of different solvents and by heating and/or mixing. The most used techniques were Soxhlet extraction, maceration and hydro-distillation [60–62]. Conventional Soxhlet extraction still remains one of the most relevant approaches to extract volatile compounds from apples [62]. The sample is placed in a thimble-holder, where it's slowly filled with condensed solvent from a distillation flask. Once the liquid has reached an overflow level, the whole contents of the thimble-holder is aspirated by a siphon, which unloads it back into the distillation flask, leaving the extracted analytes in the bulk liquid [45]. On the contrary, during maceration, the sample is immersed for a variable time in a solvent inside an airtight container in order to allow the analyte transferring [63]. Vacuum hydro-distillation, instead, uses water vapor to recover volatile and apolar components from fruit tissues, and, as Soxhlet, it has been mainly used for the extraction of apple aroma, because it gave the extracts closest to the fresh fruit [60]. The duration of the extraction process, and the large number of organic solvents used are the major drawbacks of these techniques. In fact, alternative approaches have emerged in an attempt to mitigate limitations of the conventional ones. The innovation is largely focused on finding technological solutions to diminish or even prevent the use of organic

solvents in extraction processes, in order to obtain more highly purified products containing fewer additional toxins [64]. The new methods include solid–liquid extractions (namely microwave-assisted extraction (MAE) and ultrasound-assisted extraction (UAE), accelerated solvent extraction (ASE), supercritical fluid extraction (SFE)) and solid-phase microextraction (SPME) (Table 3). Organic solvents, such as hexane, acetone, methanol, ethanol or water, have been generally used under atmospheric pressure. The choice of the solvent largely depended on the polarity of the analytes.

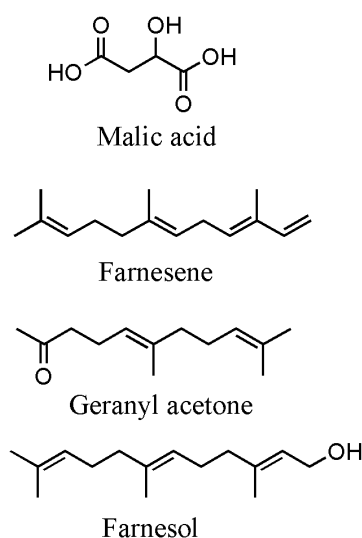


Figure 3. Main compounds responsible for the taste and flavor of apples.

Extraction of polyphenols from apples has been carried out by using methods that differ for many variables, such as solvent, time, temperature and number of extractions; therefore, the data reported in the literature are not always easily comparable. According to Bai et al. [65], the extraction of polyphenols from apples can easily be achieved via MAE, by using ethanol as extracting solvent, in a ratio to raw material of 22.9/1. Microwave-assisted extraction is based on the use of microwave energy to heat solvents in contact with a sample to allow the analytes partitioning from the sample matrix into the solvent [66]. Compared to Soxhlet and maceration, MAE results in a greater efficiency at a shorter time for the extraction of phenolic compounds from apple pomace. Moreover, accelerated operation can be regarded as a major advantage of MAE, which is useful especially at the industrial scale [61]. Bekele et al. [24] used a methanol extraction by adding pre-chilled MeOH (−20 °C) to apple pulp and extracting at 70 °C in a homogenizer. The extract was then centrifuged and dried under nitrogen flow. This extraction method was not selective for polyphenols; in fact, it allowed the extraction of many hydrophilic metabolites. Furthermore, this protocol of extraction was found to be not very efficient for complete extraction of all apple polyphenols, because less polar molecules could remain inside the matrix, which is discarded. In order to avoid this problem, a multi-step extraction can be used [67,68]. A first step involves the treatment of the dried apples cortex with hexane, to remove lipids, carotenoids and chlorophyll. Then, an extraction with methanol dissolves sugars, organic acids and phenolic compounds of low molecular weight. Lastly, the resulting residue is treated with aqueous acetone (4:6), in order to extract polymerized polyphenols. Sanoner et al. [67] applied this protocol by blending the apple powder with each solvent for 5 min, using an Ultra-Turrax blender, and the mixture was filtered through a G3 sintered glass filter. Moreover, UAE, ASE and SFE play an important role as real potential sustainable technique for industrial applications for polyphenols extraction. In recent works, ASE conditions have been optimized for the extraction of polyphenols from apple peel and pulp, achieving good recovery and repeatability. ASE allows to reduce the volume of solvent required for the extraction, to shorten the analysis time and the handling

necessary to obtain precise results [69]. As regard to SFE, several works aimed to recover phenolic compounds applying CO₂ in supercritical conditions without and with ethanol (5%) as co-solvent. As CO₂ is non-polar, it is not a favorable solvent for polar polyphenols. However, the addition of organic co-solvents which could improve the solvating power and the yield of the extraction, such as ethanol, methanol and acetone, could be a suitable strategy [70]. Instead, Stefova et al. [71] used UAE with a methanol: water mixture for the extraction of polyphenols. Ultrasound can reduce the operating temperature of extraction for thermolabile compounds; moreover, the cavitation process that occurs during sonication causes the rupture of cell walls, thus enhancing solvent contact with available extractable cell material [72]. UAE has also been used for the extraction of organic acids; water or alcoholic mixtures were used as extraction solvents [42,55,73,74].

In regard to carotenoids and vitamins, their extraction from apple skin and pomace is usually carried out with acetone or a solution of acetone/petroleum ether as solvent [3,53]. Since carotenoids are strongly susceptible to oxidative degradation, due to the high number of conjugated double bonds, extraction must be performed in dark conditions or by adding antioxidant compounds, such as butylated hydroxytoluene (BHT), to the extraction solvent, in order to prevent photo-isomerization phenomena [75].

Unlike apple polar triterpenoids, such as betulinic and ursolic acid, whose extraction is carried out by using polar solvents (i.e., methanol and acetone) [76], a separate discussion is needed for the extraction of terpenes from apple tissues. As they are non-polar and highly volatile compounds, the better method for their extraction is the solid-phase microextraction (SPME), followed by their analysis by gas chromatographic (GC) methods. With SPME, the analytes are absorbed from the liquid or gaseous sample onto an absorbent coated fused silica fiber, which is part of the syringe needle, for a fixed time. The fiber is then inserted directly into a GC injection port for thermal desorption [77]. Other advantages of this technique are the absence of solvents and the possibility to separate and pre-concentrate the analytes in a single step [78]. Therefore, it is really helpful for the extraction of volatile compounds from apples, due to their low concentration and the complexity of the matrix [79]. As fiber coatings, DVB/CAR/PDMS (Divinylbenzene/Carboxen/Polydimethylsiloxane) and PDMS/DVB have been mainly used because they offer higher extraction efficiency and a clear pattern of volatile compounds [57,80]. Despite its several advantages, the limited amount of stationary phase on the fused silica fiber used for the SPME often does not ensure enough sensitivity and reproducibility. To overcome this problem, Madrera et al. [81] successfully applied stir bar sorption extraction (SBSE), a variation of SPME consisting on the use of magnetized bars covered with an absorbent polymer, for the extraction of apple pomace aroma. SBSE has the same advantages than SPME, but its sensibility increases around 100-fold because it uses a greater amount of stationary phase.

4.2. Analytical Methods

The interest in the characterization and quantification of secondary metabolites of plant-based foods is growing and it often aims at the definition of food nutritional value as well as its quality and authenticity. Considering the large number of plant primary and secondary metabolites and their different properties and structures, different analytical techniques have been developed for each group or subgroup of phytochemicals [12]. Spectrophotometric assays have been largely used for the rough quantification of polyphenols and flavonoids. In the last decade, there has been an increasing request of more reliable and accurate analytical methods, with reduced operational time and costs, as well as with minimized use of hazardous chemicals [82–85], according to the green chemistry objectives [86]. The most common analytical methods used for the detection and/or quantification of the main classes of apples phytochemicals are the chromatographic ones.

4.2.1. Spectrophotometric Assays

The extraction of secondary metabolites is followed by their qualitative and/or quantitative analysis. Although the separation techniques, coupled with different detectors,

play a key role in the analysis of bioactive compounds, a number of spectrophotometric methods have been developed, in order to verify their presence or to quantify them in plant-based foods [87]. These assays are based on different principles and are mainly used to determine polyphenols and flavonoids.

For the rough quantification of polyphenols in apple fruits extract, colorimetric methods are widely used, due to their simplicity and high sensitivity. These include the Folin–Ciocalteu methods, used for the analysis of total polyphenols content (TPC), and the aluminum chloride (AlCl₃) assay for flavonoids determination [5,10,88,89]. The Folin–Ciocalteu assay is based on an electron-transfer reaction between the Folin–Ciocalteu reagent, which is a mixture of phosphomolybdic and phosphotungstic acid, with the polyphenol-based extract. In presence of phenols, under basic conditions, phosphomolybdic and phosphotungstic acid reduce themselves. Their reduced forms confer to the sample a blue color ($\lambda_{\max} = 495 \text{ nm}$). By evaluating the absorbance of the extract at 765 nm, it is possible to determine the total phenols concentration [10]. Viera et al. [10] used this assay in order to quantify the TPC in Fuji, Galaxy and other traditional Brazilian apples varieties. A great variation in terms of total phenolic content was observed by the authors among the apple cultivars (105.4–269.7 mg of gallic acid equivalents per 100 g of fresh matter). One of the main limits related to the quantification of total polyphenols through spectrophotometric assay, is due to interfering compounds, such as sugars, amino acids and ascorbic acid, which absorb in the same polyphenols region [90]. To avoid this problem, Vrhovsek et al. [88] made a cleanup procedure on a C-18 cartridge, prior TPC analysis. The average content of total polyphenols in the apple, evaluated by the Folin–Ciocalteu assay, was 110.2 mg/100 g of fresh fruit with significant differences depending on the apple variety.

Table 3. Overview of the methods used for the extraction of the main phytochemical classes occurring in apples.

Class	Extraction Technique	Solvents	References
Phenolics	Microwave-assisted extraction	• Ethanol	[61,65,67–72]
	Solid–liquid extraction	• Methanol	
	Ultrasound-assisted extraction	• Acetone:water	
	Accelerated solvent extraction	• Methanol:water	
	Supercritical fluid extraction		
Organic acids	Ultrasound-assisted extraction	• Water	[42,55,73,74]
		• Ethanol:water	
		• Methanol:water	
Carotenoids	Solid–liquid extraction	• Acetone + BHT	[32,53]
		• Acetone/petroleum ether + BHT	
Terpenes	Solid-phase microextraction	• /	[56,57,76,80]
	Stir bar sorption extraction	• /	
	Ultrasound-assisted extraction	• Methanol • Acetone	

Instead, the principle involved in AlCl₃ colorimetric method is that AlCl₃ forms acid stable complexes with the C-4 keto groups and either the C-3 or C-5 hydroxyl group of flavones and flavonol, which show maximum of absorbance at 415 nm. The total flavonoid content of *Malus* fruits is generally, around 110–120 mg of catechin equivalents per 100 g of fresh matter [89].

Although these spectrophotometric assays are often used as preliminary test to evaluate the content of a specific metabolite class of apples, they are not selective and not useful for a sensitive quantification of individual compounds. Therefore, in the last years, more sensitive and selective methods, based on chromatographic techniques, have been continuously developed.

4.2.2. Chromatographic Methods

The determination of secondary metabolites in plant-based foods remains an analytical challenge, due to their low concentration and the complexity and diversity of their structures. The structural complexity of secondary metabolites often hinders most attempts to quantify these compounds by analytical methods not including preliminary separation steps [12,91]. In effect, to conduct a reliable detection and quantification of the main phytochemicals occurring in fruits, chromatographic methods (both LC and GC) either coupled with UV–Vis, fluorescence, or mass spectrometry (MS) detection, represent the gold standards methods [92–96]. The following paragraphs deepen on the chromatographic methods that have been used for the determination of the main apple secondary metabolites, i.e., phenolics, organic acids, carotenoids and terpenes.

Phenolics and Organic Acids

The most common method for the separation and analysis of polyphenols and organic acids occurring in apple fruits is the high-performance liquid chromatography (HPLC) due to its high-resolution, efficiency, reproducibility and relatively short analysis time, without derivatization and no restriction on sample volatility [97–102]. Recent advances in apple phytochemicals analysis show a tendency for the application of environmentally friendly and faster techniques. This is evidenced, for example by the recently developed separative techniques, such as Ultrahigh-Performance Liquid Chromatography (UHPLC) and Ultra-Fast Liquid Chromatography that came from the evolution of packing materials used to improve resolution, and also contributed to such advances. Recently, UHPLC has been proposed for the analysis of polyphenols [103–108]. In general, peak efficiency and chromatographic resolution provided in UHPLC are higher than conventional HPLC. In addition, UHPLC methods can be considered more cost-effective because they typically need 80% less organic solvents than conventional HPLC methods [91]. Both HPLC and UHPLC can be easily coupled to a variety of detectors for polyphenols detection, including UV–Vis and MS.

To date, no single chromatographic methods capable of separating the different types of phenolic compounds, occurring in apples, are available. It is necessary to optimize the stationary phase, mobile phase, gradient elution, temperature and flow rate for each group of compounds [109]. Moreover, polyphenols stereochemistry, molecular weight, polarity and degree of polymerization could influence compounds retention. However, the reported methods for the separation of phenolics, as well as their glycosides, have been carried out mainly by reverse phase liquid chromatography (RPLC), on silica-based C18-bonded phase columns [71,106,110,111]. The average particle diameter of HPLC packings is typically 3–10 μm . With columns of smaller particle size, a larger number of plates per unit time is provided, with respect to columns with larger particle size [112]. As mobile phase, binary mixtures of aqueous formic acid or acetic acid and acetonitrile (ACN) or methanol (MeOH) as organic modifiers have been employed [71,106,110,111]. Typically, gradient elutions have been preferred, since multiple-step gradients are more suitable for complex mixtures, such as apple extracts. Although RPLC has been mostly chosen for apple polyphenols separation, Hollands et al. [113] used hydrophilic interaction chromatography (HILIC) to develop a robust and reliable analytical method for the extraction, separation and identification of monomeric and oligomeric procyanidins in apple extracts. HILIC separation mechanism is opposite to that of RP systems: polar stationary phase retains polar analytes, which are eluted by mixture of organic solvent (usually acetonitrile) and water [114]. Due to the complexity of procyanidins oligomers structures in the apple extract, normal phase silica columns were found to be not suitable for quantification purposes, particularly at a higher degree of polymerization. Instead, HILIC column ensured a better resolution of the chromatographic peaks [113].

As for phenolic compounds, reverse phase liquid chromatography is used also for the detection of organic acids by C18-bonded phase column. However, a method based on the use of an Aminex HPX cation-exchange column and an elution solvent consisting

of sulfuric acid in bi-distilled water has been also reported for the quantification of malic acid [115]. The Aminex HPX-series of strong cation-exchange resins are prepared from a sulfonated polystyrene-divinylbenzene copolymer and are available in prepacked columns. One of the major problems experienced with the use of these columns are related to the co-elution of non-acid components and the poor resolution of the chromatographic peaks, thus limiting their use. Moreover, the ion exchange’s separation mechanism implies that organic acids should be in their ionic form, so that a severe control of pH is required [116].

As regard detection, the most commonly used detector for HPLC is a variable-wavelength UV or UV-Vis detector, because both phenolics and organic acids absorb very well in the UV region [21,28,35,111,117–121]. The use of low UV detection wavelength, which ranged between 185 nm and 254 nm, allows to achieve high sensitivities in the determination of organic acids [122]. Moreover, for phenol compounds, HPLC–DAD provides extensive information; however, no single wavelength is ideal for monitoring all classes of phenolics, because they display absorbency maxima at different wavelengths (Table 4).

Table 4. Absorption maximum (λ_{max}) of polyphenols occurring in apples and belonging to flavanols, phenolics acids, dihydrochalcones and flavonols classes. Reproduced under the terms of the Creative Common CC BY license which permits reuse in any medium, provided the original open access work is properly cited [21].

Group of Polyphenols	Phenolic Compound	λ_{max} (nm)
Flavanols	Procyanidin B1	281
	(+)-Catechin	281
	Procyanidin B2	281
	Procyanidin C1	275
	(–)-Epicatechin	280
	Procyanidin A2	280
Phenolic acids	Gallic acid	272
	Protocatechuic acid	261, 298
	5-O-Caffeoylquinic acid	326
	Caffeic acid	324
	p-Coumaric acid	310
	Ferulic acid	324
Dihydrochalcones	Phloretin-2-O- β -glucoside	287
Flavonols	Quercetin-3-O-galactoside	259, 348
	Quercetin-3-O-glucoside	259, 351
	Quercetin-3-O-rutinoside	259, 348
	Quercetin-3-O-xyloside	260, 348
	Quercetin-3-O-arabinoside	260, 347
	Quercetin-3-O-rhamnoside	260, 347
	Quercetin	256, 372

For comprehensive and simultaneous monitoring of different groups of polyphenols, Kschonsek et al. [21] set the detector at 254, 280 and 320 nm to identify and quantify, into fifteen different apple cultivars, twenty polyphenolic compounds belonging to flavanols, phenolics acids, dihydrochalcones and flavonols. Among them, quercetin glycosides were found to be the main polyphenols in the peel (203 ± 108 mg/100 g) and phenolic acids (10 ± 5 mg/100 g) in the flesh. Instead, by Liaudanskas et al. [117] flavonols were quantitated at 360 nm. The method implemented by these authors allowed the identification of 11 analytes: procyanidin B1, (+)-catechin, chlorogenic acid, procyanidin B2, (–)-epicatechin, rutin, hyperoside, isoquercitrin, avicularin, quercitrin and phloridzin. The elution order of quercetin-3-O-glycosides was as follows: quercetin-3-O-rutinoside (rutin), quercetin-3-O-galactoside (hyperoside), quercetin-3-O-glucoside (iso-quercitrin), quercetin-3-O-arabinoside (avicularin) and quercetin-3-O-rhamnoside (quercitrin), mainly according to other studies aimed at the evaluation of the quercetin derivatives profile in food extracts [92].

HPLC–UV for the quantification of polyphenols on *Malus* extracts allowed to reach limits of detection (LOD) and limits of quantification (LOQ) in the range 0.2–5.8 $\mu\text{g}/\text{mL}$ and 0.1–7.1 $\mu\text{g}/\text{mL}$, respectively. Fluorescence detector (FL) in some cases offers higher selectivity and sensitivity compared to UV–Vis detection methods, so that it could be offered as a robust and reliable alternative or to be complementary to UV–Vis detection systems. For example, Teleszko et al. [106] determined the polyphenolic profile in leaves and fruits of 2 cultivars of *Malus domestica* by UPLC–PDA–FL. In this case, the identification was also achieved, by using LC–MS/MS. Although LC–UV–Vis or LC–UV–FL are cheap and robust techniques for the quantification of polyphenols, their identification could be uniquely achieved through the comparison of retention times and UV–Vis spectra with those of authentic standards. Moreover, phenolic compounds are often linked to saccharidic moieties that are not UV-active, thus preventing the correct polyphenols identification.

Considering these difficulties, in many cases, it is necessary to use a more sensitive and selective detector such as a mass spectrometer to an LC system (LC–MS), as it allows unequivocal identification of the analytes thanks to the possibility to conduct MS/MS experiments [95,109,123–126]. Liquid chromatography coupled to mass spectrometry (LC–MS) or tandem mass spectrometry (LC–MS/MS) are among the most widely used techniques for the analysis of polyphenols occurring in apple fruits [127–131]. The employment of these methods is particularly helpful not only for their quantitative determination but also for their characterization and structural elucidation, especially when MS^n fragmentation can be achieved [91]. For the ionization of apple polyphenols in LC–MS, electrospray ionization (ESI) in negative mode has been, by far, the most generalized interface employed [128,130,132]. The negative ionization mode provides the highest sensitivity and results in limited fragmentation of flavonoids. Instead, for the identification of anthocyanins, positive ionization mode is mainly chosen, as it gives the best results [133]. As an extra-certainty to the molecular mass determination, the combination of both ionization modes (positive and negative) in MS^n scan could be implemented [13]. Other less common techniques used in the analysis of polyphenols are atmospheric pressure ionization techniques, such as atmospheric pressure chemical ionization (APCI). For instance, LC–APCI–MS in positive ionization mode was proposed for the characterization of apple polyphenols by Alonso-Salces et al. [134], who reported for the first time five isorhamnetin glycosides, two hydroxyphloretin glycosides and quercetin in apple peel.

As mass analyzers, multiple types are available and have been proposed for phenols detection, among them triple quadrupole (QqQ) [135], linear ion-trap [103], time-of-flight [103], Orbitrap [105] and QTrap [136], among others. QTrap mass analyzers are hybrid instruments combining a quadrupole and a linear ion-trap in a similar configuration to a QqQ instrument and they are gaining popularity for the analysis of food products. LC–MS methods offer a better selectivity compared to LC–UV methods. In this regard, Verdu et al. [128] developed an UHPLC–UV and UHPLC–MS/MS for the quantification of phenolic compounds in apple juices. The developed methods were validated for 15 major compounds based on linearity, limits of detection and quantification, recovery and precision tests (see Supplementary Materials Table S1). A comparison of the quantifications showed that both UHPLC–UV and UHPLC–MS/MS had an excellent correlation for major compounds, quantified in 120 different samples. However, the slope value showed an overestimation of the UV detector for chlorogenic acid, explained by the co-elution of unknown UV-absorbing minor compounds, highlighting the advantage of using MS as detector and the selected reaction monitoring (SRM) mode to quantify highly concentrated samples. LC coupled to high-resolution mass spectrometry (HRMS), which provides accurate mass measurements, has recently obtained popularity due to its ability to give more comprehensive information concerning the exact molecular mass, elemental composition and detailed molecular structure of a given compound. LC–HRMS provides data of exceptional quality regarding apple metabolites. Indeed, it is currently used to aid in the identification of a broader range of phenolic compounds. High-resolution MS/MS has several advantages; indeed, they greatly improve the sensitivity and the accuracy of the mass measurements,

thus allowing a simplified identification of the analytes and a differentiation between molecular formulas having the same nominal masses [130].

UV and MS are, often, both used for the identification and quantification of apple polyphenols [137,138]. Bizjak et al. [137] studied the changes of the concentrations of sugars, organic acids and a wide range of polyphenols as well as total phenolic compounds in the “Braeburn” apple peel during the advanced maturation of apples in two growing, by coupling HPLC to both detectors. A total of 21 phenolics, belonging to five groups, namely hydroxycinnamic acids, dihydrochalcones, flavonols, flavanols and anthocyanins, were identified and quantified. Identification was performed by comparing the retention times and their UV–Vis spectra from 200 to 600 nm and confirmed by MS and MS² data that were acquired in positive and negative ions mode by using full-scan-data-dependent MS scanning from m/z 115 to 2000. The results obtained could be useful to understand the evolution and highest concentration of primary and secondary metabolites in the last stages of apple ripening and their relation as well. Instead, Ramirez-Ambrosi et al. [13] used ultrahigh performance liquid chromatography with diode array detection coupled to electrospray ionization and quadrupole time-of-flight mass spectrometry (UHPLC–DAD–ESI–Q–ToF–MS), in order to obtain polyphenolic profile of apples, apple pomace and apple juice from Asturian cider apples, in a single run of 22 min. This method allowed the automatic and simultaneous acquisition of accurate mass to charge values, overcoming chromatographic co-elution problems. With this technique, a large number of phenolic acids, organic acids and flavonoids were identified (see Supplementary Materials Table S1) [13].

Carotenoids

The diversified structural characteristic of apple carotenoids requires accurate methods for their separation and identification. To date, many chromatographic techniques are available for the determination of carotenoids in plant-based foods; however, their characterization is more challenging due to similar molecular mass (structural isomers or geometrical isomers) and other derivatives [139]. Routinely, HPLC with UV–Vis, are used for the separation and quantification of carotenoids, occurring in apples [11,140,141], as these compounds show absorption in the visible region (400 and 500 nm), due to the long-conjugated double-bond system [142]. However, the λ_{\max} of individual carotenoids can vary depending on functional groups (see Table 5). To confirm the occurrence of unknown carotenoids in a given sample, single run by HPLC (normal or reversed-phase) systems with isocratic or gradient elution are used. Typically, chromatographic separation of carotenoids is based on HPLC analysis using C18 and C30 columns. In general, C30 and C18 stationary phases are extremely employed for the separation of geometrical isomers. As regard the composition of the mobile phase, Perry et al. [11] quantified carotenoids in apples with a HPLC–UV–Vis (DAD) method, which involved the use of methanol/MTBE (2-methoxy-2-methylpropane)/water (95:3:2, v/v , with 1.5% ammonium acetate in water) and methanol/MTBE/water (8:90:2, v/v , with 1.0% ammonium acetate in water). Instead, a binary-gradient elution with acetone and deionized water was used by Delgado-Pelayo et al. [140] for the characterization and the quantification of chlorophyll and carotenoid pigments in the peel and flesh of thirteen commercial apple cultivars, including red-skinned varieties (Ariane, Fuji (I) from Italy, Fuji (F) from France, Pink Lady, Royal Gala and Starking Red Chief), green-skinned varieties (Granny Smith, Green Doncella, Green Golden Delicious and Reina de Reineta), yellow-skinned and yellow-green and varieties (Golden Montaña, Golden Delicious and Golden Rosett). It should be noted that, for more reliable results, the identification of the pigment profile is often performed not only by comparing the UV–visible spectra and retention time, but also by comparing mass spectra with those of standard pigments and data in the literature [11,141]. Indeed, closely related carotenoids and their metabolites could co-elute in various analytical methods. Thus, although spectral confirmation of these carotenoids is based on characteristic UV–Vis spectra, obtained by PDA/DAD, additional characterization is required by MS analysis [139]. Remarkable milestones are provided by the development of analytical methods

for qualitative and quantitative analysis of carotenoids, through liquid chromatography coupled to mass spectrometry; first of all, the possibility to confirm their structures through tandem mass spectrometric experiments. MS/MS is used in order to find out the characteristic/typical fragmentation pattern of carotenoids, thus allowing their identification. The fragmentation patterns of the main carotenoids occurring in apples are reported in Table 5. Most of the MS analysis of carotenoids is performed, by using positive ion mode. APCI (atmospheric pressure chemical ionization) has become the most widely used ionization technique for various carotenoids in apples, because of high sensitivity [139]. Recently, also ultrahigh-performance liquid chromatography (UHPLC) technology has been used for the analysis of carotenoids in *Malus* fruits. As the UHPLC C30 stationary phase columns are not commercially available, C18 columns have been used [143].

Table 5. Wavelengths of maximum absorption λ_{max} and characteristic fragmentation pattern of the main carotenoids occurring in apples. Reproduced with the permission of Elsevier [140].

Pigment	λ_{max} (nm)	HPLC/MS (APCI+) Fragmentation Pattern <i>m/z</i>	
		[M + H] ⁺	Characteristic Fragments
all- <i>trans</i> -Neoxanthin	419, 444, 472	601	583 ([M + H – 18] ⁺), 565 ([M + H – 18 – 18] ⁺), 547 ([M + H – 18 – 18 – 18] ⁺)
9'- <i>cis</i> -Neoxanthin	415, 439, 468	601	583 ([M + H – 18] ⁺), 565 ([M + H – 18 – 18] ⁺), 547 ([M + H – 18 – 18 – 18] ⁺)
Neochrome	401, 424, 452	601	583 ([M + H – 18] ⁺), 565 ([M + H – 18 – 18] ⁺), 547 ([M + H – 18 – 18 – 18] ⁺)
all- <i>trans</i> -Violaxanthin	418, 443, 472	601	583 ([M + H – 18] ⁺), 565 ([M + H – 18 – 18] ⁺)
9- <i>cis</i> -Violaxanthin	411, 436, 468	601	583 ([M + H – 18] ⁺), 565 ([M + H – 18 – 18] ⁺)
13- <i>cis</i> -Violaxanthin	410, 435, 466	601	583 ([M + H – 18] ⁺), 565 ([M + H – 18 – 18] ⁺)
Luteoxanthin	400, 424, 451	601	583 ([M + H – 18] ⁺), 565 ([M + H – 18 – 18] ⁺)
all- <i>trans</i> -Antheraxanthin	424, 448, 476	585	567 ([M + H – 18] ⁺), 549 ([M + H – 18 – 18] ⁺), 505 ([M + H – 80] ⁺)
all- <i>trans</i> -Zeaxanthin	428, 455, 481	569	551 ([M + H – 18] ⁺), 533 ([M + H – 18 – 18] ⁺)
all- <i>trans</i> -Lutein	428, 448, 476	569	551 ([M + H – 18] ⁺), 533 ([M + H – 18 – 18] ⁺)
9- <i>cis</i> -Lutein	330, 420, 444, 472	569	551 ([M + H – 18] ⁺), 533 ([M + H – 18 – 18] ⁺)
13- <i>cis</i> -lutein	334, 418, 441, 470	569	551 ([M + H – 18] ⁺), 533 ([M + H – 18 – 18] ⁺)
Chlorophyll b	457, 646	907	629 ([M + H – 278] ⁺)
Chlorophyll b'	457, 646	907	629 ([M + H – 278] ⁺)
Chlorophyll a	430, 662	893	615 ([M + H – 278] ⁺)
Chlorophyll a'	430, 662	893	629 ([M + H – 278] ⁺)
all- <i>trans</i> - β -Carotene	427, 454, 479	537	445 ([M + H – 92] ⁺)

Terpenes

Terpenes are secondary metabolites obtained by the combinations of several isoprene units (C₅) and they can be grouped, based on the number of carbon atoms, in monoterpenes (C₁₀), sesquiterpenes (C₁₅), diterpenes (C₂₀) and triterpenes (C₃₀). Terpenes with 15 carbons or less are typically volatile compounds, due to their small size and low polarity, and they represent in apples a minor component of total volatile organic compounds (VOCs), responsible for the fruits' aroma [56]. Some interesting triterpenoids, occurring in *Malus* fruits, are more polar and less volatile molecules, because they are linked to one or multiple polar groups: among them, oleanolic, annurcoic, ursolic and betulinic acid are the most important polar triterpenoids [144].

The detection and quantification of volatile terpenes in apples are widely performed through the use of the GC coupled to mass spectrometry (MS). Few works were based on GC coupled to flame ionization detector (FID) method [145,146]; however, GC-FID is one of the most used detectors in the flavor and fragrance field, due to its low cost and simplicity. More commonly, the nature of terpenes is investigated by using single quadrupole MS detectors [57,81,147]. The easy electron impact (EI) ionization ensures high reliability in compounds detection. However, problems in identification of monoterpenes and sesquiterpenes could be found, due to their structural similarities, which result in

similar MS spectra. To overcome these problems retention index values (RI) and MS spectrum interpretation should be used for a univocal peak assignment [92]. Compounds are identified using mass spectral libraries and linear retention indices, calculated from a series of n-alkanes from C₆ to C₃₀. Such an approach was used by Ferreira et al. [57] to identify several terpenes occurring in different apple varieties of *Malus domestica* Borkh from different geographic regions at Madeira Islands, including farnesol and α -farnesene. The authors found that for the whole fruit, terpenes accounted for 3.10% of the total GC peak area of the chromatograms. In order to increase the selectivity and sensitivity of the analytical method, Vrhovsek et al. [148] used tandem mass spectrometry (QqQ) for metabolite profiling of volatile compounds, including terpenes, in apples. The developed analytical method allowed the separation of co-eluted terpenes, with the same nominal masses, which could be not identified by conventional detectors such as FID and/or qMS. In this work, the triple quadrupole mass spectrometer operated in multiple selected reaction monitoring mode (MRM) and at the optimal collision energy for a given compound, the most intense fragmentation ion was chosen as a quantifier (Q) and the second most intense as a qualifier (q). The confirmation of molecules identity was achieved by comparing the q/Q ratio of samples and those of reference standards. The choose of two selected ions transition, one for quantification and one for confirmation, during MRM, ensured high selectivity and sensitivity, using the q/Q ratio as a confirmatory parameter.

As triterpenoids such as betulinic acid (BA) and ursolic acid (UA) are polar metabolites, they are not efficiently volatilized for analysis using GC. Thus, LC-MS is more suitable for their analysis [59,149–151]. LC coupled with ultraviolet (UV) or diode array detectors found a limited application in the study of apples triterpenes, as these compounds absorb UV radiation weakly and only at wavelength of 200 nm. Thus, only few studies reported the use of LC-DAD for triterpenoids analysis in apple fruits [152]. On the contrary, LC-MS/MS has been widely preferred, as it allows compounds unequivocal identification by examining their fragment ions, obtained through MS/MS experiments [153]. Sut and colleagues [59] investigated the fragmentation pathways of apple triterpenes, i.e., pomaceic, annurcoic, euscaphic, pomolic, corosolic, maslinic, betulinic, ursolic and oleanolic acid by LC-APCI-MS/MS, in order to allow their fast identification without the use of reference standards. Negative ion mode was the polarity chosen for the analytes. The main ions observed in ion trap and Q-TOF measurements for the considered triterpene acids are summarized in Table 6. The application of LC-MS/MS for triterpenoids analysis also ensures more sensitive quantification. Wildner et al. [149] developed a practical and reliable analytical method for the extraction, identification and quantification of UA and BA in apple peel extracts, by using LC coupled to MS with positive electrospray ionization mode (ESI+). An isocratic run, consisting of 80% acetonitrile and 20% ammonium acetate 10 mM pH 6.0, allowed the separation of the analytes. The developed method was validated in terms of sensibility, precision and accuracy. The LOD and LOQ values were 0.087 and 0.266 $\mu\text{g}/\text{mL}$ for BA and 0.398 and 2.117 $\mu\text{g}/\text{mL}$ for UA. For betulinic acid, LOD and LOQ values were lower compared to those obtained with the LC-DAD method developed by Butkevičiūtė et al. [152] (LOD: 0.15 $\mu\text{g}/\text{mL}$ and LOQ: 0.45 $\mu\text{g}/\text{mL}$).

Table 6. Main fragments observed for the considered apple triterpene acids, low-resolution species were detected in ion trap (LR-IT), while high-resolution species were detected using Q-TOF (HR-Q-TOF). Reproduced with the permission of John Wiley and Sons [59].

Ion	Pomaceic Acid	Annurcoic Acid	Euscaphic Acid	Pomolic Acid	Corosolic Acid	Maslinic Acid	Betulinic Acid	Oleanolic Acid	Ursolic Acid
HR-MSQ-TOF	501.3222 ($\Delta + 1.2$ ppm for $C_{30}H_{45}O_6$ 501.3216)	485.3281 ($\Delta + 2.9$ ppm for $C_{30}H_{45}O_5$ 485.3267)	487.3415 ($\Delta - 1.6$ ppm for $C_{30}H_{47}O_5$ 487.3423)	471.3474 ($\Delta + 0.4$ ppm for $C_{30}H_{47}O_4$ 471.3473)	471.3475 ($\Delta + 0.4$ ppm for $C_{30}H_{47}O_4$ 471.3473)	471.3475 ($\Delta + 0.6$ ppm for $C_{30}H_{47}O_4$ 471.3473)	455.3529 ($\Delta + 0.9$ ppm for $C_{30}H_{47}O_3$ 455.3525)	455.3522 ($\Delta - 0.7$ ppm for $C_{30}H_{47}O_3$ 455.3525)	455.3531 ($\Delta + 1.3$ ppm for $C_{30}H_{47}O_3$ 455.3525)
MS ²									
[M-H-18] ⁻	483.3110 ($\Delta - 3.9$ ppm for $C_{30}H_{43}O_5$ 483.3111)	467.3170 ($\Delta + 0.9$ ppm for $C_{30}H_{43}O_4$ 467.3161)	469.3304 ($\Delta - 3.0$ ppm for $C_{30}H_{45}O_4$ 469.3318)	453.3359 ($\Delta - 2.2$ ppm for $C_{30}H_{45}O_3$ 453.3369)					
[M-H-40] ⁻							415.3181 ($\Delta - 7.5$ ppm for $C_{27}H_{43}O_3$ 415.3212)		
[M-H-44] ⁻	457.3303 ($\Delta - 3.3$ ppm for $C_{29}H_{45}O_4$ 457.3318)	441.3355 ($\Delta - 3.2$ ppm for $C_{29}H_{45}O_3$ 441.3369)							
[M-H-46] ⁻	455.3160 ($\Delta - 0.3$ ppm for $C_{30}H_{43}O_4$ 455.3161)						409.3423 ($\Delta - 10.0$ ppm for $C_{29}H_{45}O$ 409.3470)		
[M-H-48] ⁻					423.3250 ($\Delta - 3.1$ ppm for $C_{29}H_{43}O_2$ 423.3263)	423.3253 ($\Delta + 2.4$ ppm for $C_{29}H_{43}O_2$ 423.3263)	407.3314 ($\Delta - 3.2$ ppm for $C_{29}H_{43}O$ 407.3314)	407.3314 ($\Delta - 3.2$ ppm for $C_{29}H_{43}O$ 407.3314)	407.3304 ($\Delta - 2.5$ ppm for $C_{29}H_{43}O$ 407.3314)
[M-H-60] ⁻	441.2984 ($\Delta - 4.8$ ppm for $C_{28}H_{41}O_4$ 441.3005)			411.3250 ($\Delta - 3.2$ ppm for $C_{28}H_{43}O_2$ 411.3263)					
[M-H-62] ⁻	439.2848 ($\Delta + 0.9$ ppm for $C_{28}H_{39}O_4$ 439.2848)	423.3259 ($\Delta - 0.9$ ppm for $C_{29}H_{43}O_2$ 423.3263)	425.3420 ($\Delta - 5.4$ ppm for $C_{29}H_{45}O_2$ 425.3420)	409.3095 ($\Delta - 2.9$ ppm for $C_{28}H_{41}O_2$ 409.3107)			393.3143 ($\Delta - 8.5$ ppm for $C_{28}H_{41}O$ 393.3157)		

Table 6. Cont.

Ion	Pomaceic Acid	Annurcoic Acid	Euscaphic Acid	Pomolic Acid	Corosolic Acid	Maslinic Acid	Betulinic Acid	Oleanolic Acid	Ursolic Acid
[M-H-64] ⁻				407.3313 (Δ - 0.3 ppm for C ₂₉ H ₄₃ O 407.3314)	407.2914 (Δ - 8.8 ppm for C ₂₈ H ₃₉ O ₂ 407.2950)	407.6			
[M-H-66] ⁻					405.5	405.5			
[M-H-78] ⁻					393.3157 (Δ - 0.1 ppm for C ₂₈ H ₄₁ O 393.3157)	393.6	377.5		
[M-H-80] ⁻		405.3149 (Δ - 2.0 ppm for C ₂₉ H ₄₁ O 405.3157)	407.2934 (Δ - 3.9 ppm for C ₂₈ H ₃₉ O ₂ 407.2934)						
[M-H-93] ⁻	409.3107 (Δ - 5.9 ppm for C ₂₈ H ₄₁ O ₂ 409.3107)	393.3157 (Δ - 1.3 ppm for C ₂₈ H ₄₁ O 393.3157)							
MS ³ *									
	409.6→379.5	423.6→405.7 423.6→393.6	425.6→407.6 425.6→405.6 425.6→393.5		423.5→407.5 423.5→405.5 423.5→393.5			407.6→391.6 407.6→377.6 407.6→365.4 407.6→363.4	407.6→391.5 407.6→378.5 407.6→377.5 407.6→206.6
MS ⁴ **									
	379.5→363.8 379.5→361.8 379.5→190.3 379.5→137.3	393.6→377.6 393.6→189.3	393.5→377.5 393.5→189.3		393.5→377.6 393.5→375.5 393.5→202.5				

* Fragment ions obtained by fragmentation of the precursor ion (left of the arrow), during MS³ experiments. ** Fragment ions obtained by fragmentation of the precursor ion (left of the arrow), during MS⁴ experiments.

5. Conclusions

In this review, a comprehensive description of extraction approaches and analytical methods, used for the determination of primary and secondary metabolites of apple fruits (*Malus domestica*), was provided. In detail, the extraction method mostly employed for the extraction of primary metabolites from apple tissues is the traditional extraction with solvent (LSE); for secondary metabolites, extraction with solvents at different polarities, assisted by microwave (MAE) or ultrasound (UAE), are commonly used. After extraction, spectrophotometric assays are often used to quantify apple phytochemicals, mainly polyphenols and flavonoids. However, spectrophotometric methods are not selective; therefore, chromatographic methods (LC and GC coupled to MS) are used, too. Overall, an analysis based on the LC–MS reaches a greater sensitivity, thus allowing us to identify the phytochemical components occurring in apples at very low concentrations.

Supplementary Materials: The following are available online at <https://www.mdpi.com/article/10.3390/separations8070091/s1>. Table S1: Overview of the analytical techniques used in the last 10 years (reported in chronological order) for the extraction and the analysis of secondary metabolites occurring in *Malus Domestica*.

Author Contributions: Writing—original draft preparation, M.A.A., F.L.; investigation, L.F., G.C.; writing—review and editing; R.P., D.C., M.B.; supervision G.M., L.S., G.B. All authors have read and agreed to the published version of the manuscript.

Funding: This research received no external funding.

Conflicts of Interest: The authors declare no conflict of interest.

References

1. Bevilacqua, M.; Bro, R.; Marini, F.; Rinnan, Å.; Rasmussen, M.A.; Skov, T. Recent chemometrics advances for foodomics. *TrAC Trends Anal. Chem.* **2017**, *96*, 42–51. [[CrossRef](#)]
2. Herrero, M.; Simò, C.; Garcia-Canasa, V.; Ibanez, E.; Cifuentes, A. Foodomics: MS-based strategies in modern food science and nutrition. *Mass Spectrom. Rev.* **2012**, *31*, 49–69. [[CrossRef](#)]
3. Giordani, E.; Doumet, S.; Nin, S.; Del Bubba, M. Selected primary and secondary metabolites in fresh persimmon (*Diospyros kaki* Thunb.): A review of analytical methods and current knowledge of fruit composition and health benefits. *Food Res. Int.* **2011**, *44*, 1752–1767. [[CrossRef](#)]
4. Magwaza, L.S.; Opara, U.L. Analytical methods for determination of sugars and sweetness of horticultural products—A review. *Sci. Hortic.* **2015**, *184*, 179–192. [[CrossRef](#)]
5. Huber, G.M.; Rupasinghe, H.P.V. Phenolic profiles and antioxidant properties of apple skin extracts. *J. Food Sci.* **2009**, *74*, 693–700. [[CrossRef](#)]
6. Feliciano, R.P.; Antunes, C.; Ramos, A.; Serra, A.T.; Figueira, M.E.; Duarte, C.M.M.; de Carvalho, A.; Bronze, M.R. Characterization of traditional and exotic apple varieties from Portugal. Part 1—Nutritional, phytochemical and sensory evaluation. *J. Funct. Foods* **2010**, *2*, 35–45. [[CrossRef](#)]
7. Figuerola, F.; Hurtado, M.L.; Estévez, A.M.; Chiffelle, I.; Asenjo, F. Fibre concentrates from apple pomace and citrus peel as potential fibre sources for food enrichment. *Food Chem.* **2005**, *91*, 395–401. [[CrossRef](#)]
8. Mohanta, S.; Singh, S.K.; Kumar, B.; Gulati, M.; Jyoti, J.; Som, S.; Panchal, S.; Melkani, I.; Banerjee, M.; Sinha, S.K.; et al. Solidification of liquid Modified Apple Polysaccharide by its adsorption on solid porous carriers through spray drying and evaluation of its potential as binding agent for tablets. *Int. J. Biol. Macromol.* **2018**, *120*, 1975–1998. [[CrossRef](#)]
9. Ajanaku, C.; Echeme, J.; Mordi, R.; Bolade, O.; Okoye, S.; Jonathan, H.; Ejilude, O. In-vitro antibacterial, phytochemical, antimycobacterial activities and GC-MS analyses of *Bidens pilosa* leaf extract. *J. Microbiol. Biotechnol. Food Sci.* **2018**, *8*, 721–725. [[CrossRef](#)]
10. Vieira, F.G.K.; Borges, G.D.S.C.; Copetti, C.; Amboni, R.D.D.M.C.; Denardi, F.; Fett, R. Physico-chemical and antioxidant properties of six apple cultivars (*Malus domestica* Borkh) grown in southern Brazil. *Sci. Hortic.* **2009**, *122*, 421–425. [[CrossRef](#)]
11. Perry, A.; Rasmussen, H.; Johnson, E.J. Xanthophyll (lutein, zeaxanthin) content in fruits, vegetables and corn and egg products. *J. Food Compos. Anal.* **2009**, *22*, 9–15. [[CrossRef](#)]
12. Ignat, I.; Volf, I.; Popa, V.I. A critical review of methods for characterisation of polyphenolic compounds in fruits and vegetables. *Food Chem.* **2011**, *126*, 1821–1835. [[CrossRef](#)]
13. Ramirez-Ambrosi, M.; Abad-Garcia, B.; Vilorio-Bernal, M.; Garmon-Lobato, S.; Berrueta, L.A.; Gallo, B. A new ultrahigh performance liquid chromatography with diode array detection coupled to electrospray ionization and quadrupole time-of-flight mass spectrometry analytical strategy for fast analysis and improved characterization of phenolic compounds in ap. *J. Chromatogr. A* **2013**, *1316*, 78–91. [[CrossRef](#)]

14. Uzun, A.; Kantemiz, A.; Pinar, H. Evaluation of Yield and Fruit Quality of Some Apple. *Curr. Trends Nat. Sci.* **2019**, *8*, 36–40.
15. Bonany, J.; Brugger, C.; Buehler, A.; Carbó, J.; Codarin, S.; Donati, F.; Echeverria, G.; Egger, S.; Guerra, W.; Hilaire, C.; et al. Preference mapping of apple varieties in Europe. *Food Qual. Prefer.* **2014**, *32*, 317–329. [[CrossRef](#)]
16. Shippy, W.B. Influence of Environment on the Callusing of Apple Cuttings and Grafts. *Am. J. Bot.* **1930**, *17*, 290–327. [[CrossRef](#)]
17. Harker, F.R.; White, A.; Gunson, F.A.; Hallett, I.C.; De Silva, H.N. Instrumental measurement of apple texture: A comparison of the single-edge notched bend test and the penetrometer. *Postharvest Biol. Technol.* **2006**, *39*, 185–192. [[CrossRef](#)]
18. Francini, A.; Sebastiani, L. Phenolic compounds in apple (*Malus x domestica* borkh.): Compounds characterization and stability during postharvest and after processing. *Antioxidants* **2013**, *2*, 181–193. [[CrossRef](#)]
19. Rana, S.; Kumar, S.; Rana, A.; Sharma, V.; Katoch, P.; Padwad, Y.; Bhushan, S. Phenolic constituents from apple tree leaves and their in vitro biological activity. *Ind. Crops Prod.* **2016**, *90*, 118–125. [[CrossRef](#)]
20. Petkovsek, M.M.; Stampar, F.; Veberic, R. Parameters of inner quality of the apple scab resistant and susceptible apple cultivars (*Malus domestica* Borkh.). *Sci. Hortic.* **2007**, *114*, 37–44. [[CrossRef](#)]
21. Kschonsek, J.; Wolfram, T.; Stöckl, A.; Böhm, V. Polyphenolic compounds analysis of old and new apple cultivars and contribution of polyphenolic profile to the in vitro antioxidant capacity. *Antioxidants* **2018**, *7*, 20. [[CrossRef](#)]
22. Pascale, R.; Onzo, A.; Ciriello, R.; Scrano, L.; Bufo, S.A.; Bianco, G. *LC/MS Based Food Metabolomics*; Elsevier: Amsterdam, The Netherlands, 2020; ISBN 9780081005965.
23. Fukusaki, E.; Kobayashi, A. Plant metabolomics: Potential for practical operation. *J. Biosci. Bioeng.* **2005**, *100*, 347–354. [[CrossRef](#)]
24. Bekele, E.A.; Annaratone, C.E.P.; Hertog, M.L.A.T.M.; Nicolai, B.M.; Geeraerd, A.H. Multi-response optimization of the extraction and derivatization protocol of selected polar metabolites from apple fruit tissue for GC-MS analysis. *Anal. Chim. Acta* **2014**, *824*, 42–56. [[CrossRef](#)] [[PubMed](#)]
25. Bouayed, J.; Hoffmann, L.; Bohn, T. Total phenolics, flavonoids, anthocyanins and antioxidant activity following simulated gastrointestinal digestion and dialysis of apple varieties: Bioaccessibility and potential uptake. *Food Chem.* **2011**, *128*, 14–21. [[CrossRef](#)]
26. Santarsiero, A.; Onzo, A.; Pascale, R.; Acquavia, M.A.; Coviello, M.; Convertini, P.; Todisco, S.; Marsico, M.; Pifano, C.; Iannece, P.; et al. Pistacia lentiscus Hydrosol: Untargeted Metabolomic Analysis and Anti-Inflammatory Activity Mediated by NF- κ B and the Citrate Pathway. *Oxid. Med. Cell. Longev.* **2020**, *2020*. [[CrossRef](#)] [[PubMed](#)]
27. Onzo, A.; Pascale, R.; Acquavia, M.A.; Cosma, P.; Gubitosa, J.; Gaeta, C.; Iannece, P.; Tsybin, Y.; Rizzi, V.; Guerrieri, A.; et al. Untargeted analysis of pure snail slime and snail slime-induced Au nanoparticles metabolome with MALDI FT-ICR MS. *J. Mass Spectrom.* **2021**, *56*. [[CrossRef](#)] [[PubMed](#)]
28. Arnous, A.; Meyer, A.S. Comparison of methods for compositional characterization of grape (*Vitis vinifera* L.) and apple (*Malus domestica*) skins. *Food Bioprod. Process.* **2008**, *86*, 79–86. [[CrossRef](#)]
29. Acquavia, M.A.; Foti, L.; Pascale, R.; Nicolò, A.; Brancalone, V.; Cataldi, T.R.I.; Martelli, G.; Scrano, L.; Bianco, G. Detection and quantification of Covid-19 antiviral drugs in biological fluids and tissues. *Talanta* **2021**, *224*. [[CrossRef](#)]
30. Canarini, A.; Kaiser, C.; Merchant, A.; Richter, A.; Wanek, W. Root exudation of primary metabolites: Mechanisms and their roles in plant responses to environmental stimuli. *Front. Plant Sci.* **2019**, *10*. [[CrossRef](#)]
31. Guan, Y.; Peace, C.; Rudell, D.; Verma, S.; Evans, K. QTLs detected for individual sugars and soluble solids content in apple. *Mol. Breed.* **2015**, *35*, 1–13. [[CrossRef](#)]
32. Karkacier, M.; Erbas, M.; Uslu, M.K.; Aksu, M. Comparison of different extraction and detection methods for sugars using amino-bonded phase HPLC. *J. Chromatogr. Sci.* **2003**, *41*, 331–333. [[CrossRef](#)] [[PubMed](#)]
33. Ma, C.; Sun, Z.; Chen, C.; Zhang, L.; Zhu, S. Simultaneous separation and determination of fructose, sorbitol, glucose and sucrose in fruits by HPLC-ELSD. *Food Chem.* **2014**, *145*, 784–788. [[CrossRef](#)]
34. Filip, M.; Vlassa, M.; Coman, V.; Halmagyi, A. Simultaneous determination of glucose, fructose, sucrose and sorbitol in the leaf and fruit peel of different apple cultivars by the HPLC-RI optimized method. *Food Chem.* **2016**, *199*, 653–659. [[CrossRef](#)] [[PubMed](#)]
35. Zhang, Y.; Li, P.; Cheng, L. Developmental changes of carbohydrates, organic acids, amino acids, and phenolic compounds in “Honeycrisp” apple flesh. *Food Chem.* **2010**, *123*, 1013–1018. [[CrossRef](#)]
36. Yang, S.; Meng, Z.; Li, Y.; Chen, R.; Yang, Y.; Zhao, Z. Evaluation of Physiological Characteristics, Soluble Sugars, Organic Acids and Volatile Compounds in “Orin” Apples (*Malus domestica*) at Different Ripening Stages. *Molecules* **2021**, *26*, 807. [[CrossRef](#)] [[PubMed](#)]
37. Liu, Y.; Ying, Y.; Yu, H.; Fu, X. Comparison of the HPLC method and FT-NIR analysis for quantification of glucose, fructose, and sucrose in intact apple fruits. *J. Agric. Food Chem.* **2006**, *54*, 2810–2815. [[CrossRef](#)] [[PubMed](#)]
38. Liu, Y.-d.; Ying, Y. Bin Measurement of sugar content in Fuji apples by FT-NIR spectroscopy. *J. Zhejiang Univ. Sci.* **2004**, *5*, 651–655. [[CrossRef](#)]
39. Arain, S.; Sherazi, S.T.H.; Bhangar, M.I.; Memon, N.; Mahesar, S.A.; Rajput, M.T. Prospects of fatty acid profile and bioactive composition from lipid seeds for the discrimination of apple varieties with the application of chemometrics. *Grasas y Aceites* **2012**, *63*, 175–183. [[CrossRef](#)]
40. Baeza-Jiménez, R.; López-Martínez, L.X.; García-Varela, R.; García, H.S. Lipids in fruits and vegetables: Chemistry and biological activities. *Fruit Veg. Phytochem. Chem. Hum. Health Second Ed.* **2017**, *1*, 423–449. [[CrossRef](#)]
41. Song, J.; Bangerth, F. Fatty acids as precursors for aroma volatile biosynthesis in pre-climacteric and climacteric apple fruit. *Postharvest Biol. Technol.* **2003**, *30*, 113–121. [[CrossRef](#)]

42. Wu, J.; Gao, H.; Zhao, L.; Liao, X.; Chen, F.; Wang, Z.; Hu, X. Chemical compositional characterization of some apple cultivars. *Food Chem.* **2007**, *103*, 88–93. [[CrossRef](#)]
43. Chiu, H.H.; Kuo, C.H. Gas chromatography-mass spectrometry-based analytical strategies for fatty acid analysis in biological samples. *J. Food Drug Anal.* **2020**, *28*, 60–73. [[CrossRef](#)]
44. Duroňová, K.; Márová, I.; Čertík, M.; Obruča, S. Changes in lipid composition of apple surface layer during long-term storage in controlled atmosphere. *Chem. Pap.* **2012**, *66*, 940–948. [[CrossRef](#)]
45. Walia, M.; Rawat, K.; Bhushan, S.; Padwad, Y.S.; Singh, B. Fatty acid composition, physicochemical properties, antioxidant and cytotoxic activity of apple seed oil obtained from apple pomace. *J. Sci. Food Agric.* **2014**, *94*, 929–934. [[CrossRef](#)]
46. Radenkova, V.; Kviesis, J.; Juhnevica-Radenkova, K.; Valdovska, A.; Püssa, T.; Klavins, M.; Drudze, I. Valorization of wild apple (*Malus* spp.) by-products as a source of essential fatty acids, tocopherols and phytosterols with antimicrobial activity. *Plants* **2018**, *7*, 90. [[CrossRef](#)]
47. Seppanen-Laakso, T.; Laakso, I.; Hiltunen, R. Analysis of fatty acids by gas chromatography, and its relevance to research on health and nutrition. *Anal. Chim. Acta* **2002**, *465*, 39–62. [[CrossRef](#)]
48. Wojdyło, A.; Oszmiański, J.; Laskowski, P. Polyphenolic compounds and antioxidant activity of new and old apple varieties. *J. Agric. Food Chem.* **2008**, *56*, 6520–6530. [[CrossRef](#)]
49. Tsao, R.; Yang, R.; Young, J.C.; Zhu, H. Polyphenolic profiles in eight apple cultivars using high-performance liquid chromatography (HPLC). *J. Agric. Food Chem.* **2003**, *51*, 6347–6353. [[CrossRef](#)]
50. Alonso-Salces, R.M.; Barranco, A.; Abad, B.; Berrueta, L.A.; Gallo, B.; Vicente, F. Polyphenolic Profiles of Basque Cider Apple Cultivars and Their Technological Properties. *J. Agric. Food Chem.* **2004**, *52*, 2938–2952. [[CrossRef](#)] [[PubMed](#)]
51. Vanzani, P.; Rossetto, M.; Rigo, A.; Vrhovsek, U.; Mattivi, F.; D’Amato, E.; Scarpa, A.M. Major phytochemicals in apple cultivars: Contribution to peroxy radical trapping efficiency. *J. Agric. Food Chem.* **2005**, *53*, 3377–3382. [[CrossRef](#)] [[PubMed](#)]
52. Łata, B.; Trampczynska, A.; Paczesna, J. Cultivar variation in apple peel and whole fruit phenolic composition. *Sci. Hortic.* **2009**, *121*, 176–181. [[CrossRef](#)]
53. Ampomah-Dwamena, C.; Deinoprat, S.; Lewis, D.; Sutherland, P.; Volz, R.; Allan, A.C. Metabolic and gene expression analysis of apple (*Malus × domestica*) carotenogenesis. *J. Exp. Bot.* **2012**, *63*, 4497–4511. [[CrossRef](#)] [[PubMed](#)]
54. Mikulic-Petkovsek, M.; Schmitzer, V.; Slatnar, A.; Stampar, F.; Veberic, R. Composition of Sugars, Organic Acids, and Total Phenolics in 25 Wild or Cultivated Berry Species. *J. Food Sci.* **2012**, *77*, 1064–1070. [[CrossRef](#)] [[PubMed](#)]
55. Ma, B.; Yuan, Y.; Gao, M.; Li, C.; Ogutu, C.; Li, M.; Ma, F. Determination of predominant organic acid components in malus species: Correlation with apple domestication. *Metabolites* **2018**, *8*, 74. [[CrossRef](#)]
56. Nieuwenhuizen, N.J.; Green, S.A.; Chen, X.; Bailleul, E.J.D.; Matich, A.J.; Wang, M.Y.; Atkinson, R.G. Functional Genomics Reveals That a Compact Terpene Synthase Gene Family Can Account for Terpene Volatile Production in Apple. *Plant Physiol.* **2020**, *161*, 787–804. [[CrossRef](#)]
57. Ferreira, L.; Perestrelo, R.; Caldeira, M.; Câmara, J.S. Characterization of volatile substances in apples from Rosaceae family by headspace solid-phase microextraction followed by GC-qMS. *J. Sep. Sci.* **2009**, *32*, 1875–1888. [[CrossRef](#)]
58. Mehinagic, E.; Prost, C.; Demaimay, M. Optimization of extraction of apple aroma by dynamic headspace and influence of saliva on extraction of volatiles. *J. Agric. Food Chem.* **2004**, *52*, 5175–5182. [[CrossRef](#)]
59. Sut, S.; Poloniato, G.; Malagoli, M.; Dall’acqua, S. Fragmentation of the main triterpene acids of apple by LC-APCI-MSn. *J. Mass Spectrom.* **2018**, *53*, 882–892. [[CrossRef](#)]
60. Mehinagic, E.; Prost, C.; Demaimay, M. Representativeness of Apple Aroma Extract Obtained by Vacuum Hydrodistillation: Comparison of Two Concentration Techniques. *J. Food Sci.* **2003**, *68*, 2411–2415. [[CrossRef](#)]
61. Rezaei, S.; Rezaei, K.; Haghighi, M.; Labbafi, M. Solvent and Solvent to Sample Ratio as Main Parameters in the Microwave-assisted Extraction of Polyphenolic Compounds from Apple Pomace. *Food Sci. Biotechnol.* **2013**, *22*, 1269–1274. [[CrossRef](#)]
62. Rowan, D.D. Volatile metabolites. *Metabolites* **2011**, *1*, 41–63. [[CrossRef](#)]
63. Müller, E.; Berger, R.; Blass, E.; Sluyts, D.; Pfennig, A. Liquid-liquid Extraction. *Encicl. Ind. Chem.* **2000**, *21*, 250–303. [[CrossRef](#)]
64. Naboulsi, I.; Aboulmouhajir, A. Plants extracts and secondary metabolites, their extraction methods and use in agriculture for controlling crop stresses and improving productivity: A review. *Acad. J. Med. Plants* **2018**, *6*, 223–240. [[CrossRef](#)]
65. Bai, X.L.; Yue, T.L.; Yuan, Y.H.; Zhang, H.W. Optimization of microwave-assisted extraction of polyphenols from apple pomace using response surface methodology and HPLC analysis. *J. Sep. Sci.* **2010**, *33*, 3751–3758. [[CrossRef](#)]
66. Eskilsson, C.S.; Bjorklund, E. Analytical-scale microwave-assisted extraction. *J. Chromatogr. A* **2000**, *902*, 227–250. [[CrossRef](#)]
67. Sanoner, P.; Guyot, S.; Marnet, N.; Molle, D.; Drilleau, J.F. Polyphenol profiles of French cider apple varieties (*Malus domestica* sp.). *J. Agric. Food Chem.* **1999**, *47*, 4847–4853. [[CrossRef](#)] [[PubMed](#)]
68. Guyot, S.; Marnet, N.; Laraba, D.; Sanoner, P.; Drilleau, J.F. Reversed-Phase HPLC following Thiolysis for Quantitative Estimation and Characterization of the Four Main Classes of Phenolic Compounds in Different Tissue Zones of a French Cider Apple Variety (*Malus domestica* Var. Kermerrien). *J. Agric. Food Chem.* **1998**, *46*, 1698–1705. [[CrossRef](#)]
69. Alonso-Salces, R.M.; Korta, E.; Barranco, A.; Berrueta, L.A.; Gallo, B.; Vicente, F. Determination of polyphenolic profiles of Basque cider apple varieties using accelerated solvent extraction. *J. Agric. Food Chem.* **2001**, *49*, 3761–3767. [[CrossRef](#)] [[PubMed](#)]
70. Ferrentino, G.; Morozova, K.; Mosibo, O.K.; Ramezani, M.; Scampicchio, M. Biorecovery of antioxidants from apple pomace by supercritical fluid extraction. *J. Clean. Prod.* **2018**, *186*, 253–261. [[CrossRef](#)]

71. Stefova, M.; Petkovska, A.; Ugarkovic, S.; Stanoeva, J.P. Strategy for optimized use of LC-MSn for determination of the polyphenolic profiles of apple peel, flesh and leaves. *Arab. J. Chem.* **2019**, *12*, 5180–5186. [[CrossRef](#)]
72. Pingret, D.; Fabiano-Tixier, A.S.; Le Bourvellec, C.; Renard, C.M.G.C.; Chemat, F. Lab and pilot-scale ultrasound-assisted water extraction of polyphenols from apple pomace. *J. Food Eng.* **2012**, *111*, 73–81. [[CrossRef](#)]
73. Bizjak, J.; Weber, N.; Mikulic-Petkovsek, M.; Slatnar, A.; Stampar, F.; Alam, Z.; Stich, K.; Halbwirth, H.; Veberic, R. Influence of phostrade Ca on color development and anthocyanin content of “Braeburn” apple (*Malus domestica* Borkh.). *HortScience* **2013**, *48*, 193–199. [[CrossRef](#)]
74. Feng, F.; Li, M.; Ma, F.; Cheng, L. Effects of location within the tree canopy on carbohydrates, organic acids, amino acids and phenolic compounds in the fruit peel and flesh from three apple (*Malus domestica*) cultivars. *Hortic. Res.* **2014**, *1*, 1–7. [[CrossRef](#)] [[PubMed](#)]
75. Rodríguez-Bernaldo de Quirós, A.; Costa, H.S. Analysis of carotenoids in vegetable and plasma samples: A review. *J. Food Compos. Anal.* **2006**, *19*, 97–111. [[CrossRef](#)]
76. Fan, J.; Liao, D.; Zhang, X. Ultrasonic assisted extraction of ursolic acid from apple pomace: A novel and facile technique. *Sep. Sci. Technol.* **2016**, *6395*, 1344–1350. [[CrossRef](#)]
77. Prosen, H.; Zupančič-Kralj, L. Solid-phase microextraction. *TrAC Trends Anal. Chem.* **1999**, *18*, 272–282. [[CrossRef](#)]
78. Bianco, G.; Novario, G.; Zianni, R.; Cataldi, T.R.I. Comparison of two SPME fibers for the extraction of some off-flavor cork-taint compounds in bottled wines investigated by GC-HRMS. *Anal. Bioanal. Chem.* **2009**, *393*, 2019–2027. [[CrossRef](#)]
79. Schmutzer, G.R.; Magdas, A.D.; David, L.I.; Moldovan, Z. Determination of the Volatile Components of Apple Juice Using Solid Phase Microextraction and Gas Chromatography-Mass Spectrometry. *Anal. Lett.* **2014**, *47*, 1683–1696. [[CrossRef](#)]
80. Risticvic, S.; Souza-Silva, E.A.; Gionfriddo, E.; DeEll, J.R.; Cochran, J.; Hopkins, W.S.; Pawliszyn, J. Application of in vivo solid phase microextraction (SPME) in capturing metabolome of apple (*Malus domestica* Borkh.) fruit. *Sci. Rep.* **2020**, *10*, 1–11. [[CrossRef](#)]
81. Sbse-gc-ms, S.; Rodr, R. Determination of Volatile Compounds in Apple Pomace by Stir Bar Sorptive Extraction and Gas Chromatography-Mass. *J. Food Sci.* **2011**, *76*, C1326–C1334. [[CrossRef](#)]
82. Caivano, M.; Pascale, R.; Mazzone, G.; Masi, S.; Panariello, S.; Caniani, D. Disinfection unit of water resource recovery facilities: Critical issue for N₂O Emission. In *Frontiers in Wastewater Treatment and Modelling*; Mannina, G., Ed.; Springer: Milano, Italy, 2017; pp. 444–449. ISBN 978-3-319-58421-8.
83. Caivano, M.; Pascale, R.; Mazzone, G.; Buchicchio, A.; Masi, S.; Bianco, G.; Caniani, D. N₂O and CO₂ Emissions from secondary settlers in WWTPs: Experimental results on full and pilot scale plants. In *Frontiers in Wastewater Treatment and Modelling*; Mannina, G., Ed.; Springer: Milano, Italy, 2017; pp. 412–418.
84. Caniani, D.; Esposito, G.; Gori, R.; Caretti, C.; Bellandi, G.; Mancini, I.M.; Caivano, M.; Pascale, R.; Cosenza, A.; Abouissa, H.; et al. Toward a New Plant-Wide Experimental and Modeling Approach for Reduction of Greenhouse Gas Emission from Wastewater Treatment Plants. *J. Environ. Eng.* **2019**, *145*, 1–12. [[CrossRef](#)]
85. Caniani, D.; Caivano, M.; Pascale, R.; Bianco, G.; Mancini, I.M.; Masi, S.; Mazzone, G.; Firouzian, M.; Rosso, D. CO₂ and N₂O from water resource recovery facilities: Evaluation of emissions from biological treatment, settling, disinfection, and receiving water body. *Sci. Total Environ.* **2019**, *648*, 1130–1140. [[CrossRef](#)]
86. Acquavia, M.A.; Pascale, R.; Martelli, G.; Bondoni, M.; Bianco, G. Natural polymeric materials: A solution to plastic pollution from the agro-food sector. *Polymers* **2021**, *13*, 158. [[CrossRef](#)] [[PubMed](#)]
87. Harnafi, H.; Amrani, S. Spectrophotometric Methods for Determination of Plant Polyphenols Content and their Antioxidant Activity Assessment: An Overview. *Mol. Nutr. Food Res.* **2008**, *2*, 20–22.
88. Vrhovsek, U.; Rigo, A.; Tonon, D.; Mattivi, F. Quantitation of polyphenols in different apple varieties. *J. Agric. Food Chem.* **2004**, *52*, 6532–6538. [[CrossRef](#)]
89. Mitić, S.S.; Stojanović, B.T.; Stojković, M.B.; Mitić, M.N.; Pavlović, J.L. Total phenolics, flavonoids and antioxidant activity of different apple cultivars. *Bulg. Chem. Commun.* **2013**, *45*, 326–331.
90. Bastola, K.P.; Guragain, Y.N.; Bhadriraju, V.; Vadlani, P.V. Evaluation of Standards and Interfering Compounds in the Determination of Phenolics by Folin-Ciocalteu Assay Method for Effective Bioprocessing of Biomass. *Am. J. Anal. Chem.* **2017**, *8*, 416–431. [[CrossRef](#)]
91. Lucci, P.; Saurina, J.; Núñez, O. Trends in LC-MS and LC-HRMS analysis and characterization of polyphenols in food. *TrAC Trends Anal. Chem.* **2017**, *88*, 1–24. [[CrossRef](#)]
92. Pascale, R.; Acquavia, M.A.; Cataldi, T.R.I.; Onzo, A.; Coviello, D.; Bufo, S.A.; Scrano, L.; Ciriello, R.; Guerrieri, A.; Bianco, G. Profiling of quercetin glycosides and acyl glycosides in sun-dried peperoni di Senise peppers (*Capsicum annum* L.) by a combination of LC-ESI (—)MS/MS and polarity prediction in reversed-phase separations. *Anal. Bioanal. Chem.* **2020**, *412*, 3005–3015. [[CrossRef](#)]
93. Pascale, R.; Bianco, G.; Cataldi, T.R.I.; Buchicchio, A.; Losito, I.; Altieri, G.; Genovese, F.; Tauriello, A.; Di Renzo, G.C.; Lafiosca, M.C. Investigation of the Effects of Virgin Olive Oil Cleaning Systems on the Secoiridoid Aglycone Content Using High Performance Liquid Chromatography–Mass Spectrometry. *J. Am. Oil Chem. Soc.* **2018**, *95*, 665–671. [[CrossRef](#)]
94. Pascale, R.; Bianco, G.; Cataldi, T.R.I.; Kopplin, P.S.; Bosco, F.; Vignola, L.; Uhl, J.; Lucio, M.; Milella, L. Mass spectrometry-based phytochemical screening for hypoglycemic activity of Fagioli di Sarconi beans (*Phaseolus vulgaris* L.). *Food Chem.* **2018**, *242*, 497–504. [[CrossRef](#)]

95. Bianco, G.; Pascale, R.; Carbone, C.F.; Acquavia, M.A.; Cataldi, T.R.I.; Schmitt-Kopplin, P.; Buchicchio, A.; Russo, D.; Milella, L. Determination of soyasaponins in Fagioli di Sarconi beans (*Phaseolus vulgaris* L.) by LC-ESI-FTICR-MS and evaluation of their hypoglycemic activity. *Anal. Bioanal. Chem.* **2018**, *410*, 1561–1569. [[CrossRef](#)]
96. Bianco, G.; Pascale, R.; Lelario, F.; Bufo, S.A.; Cataldi, T.R.I. Investigation of Glucosinolates by Mass Spectrometry. In *Glucosinolates*; Mérillon, J.-M., Ramawat, K.G., Eds.; Springer International Publishing: Cham, Switzerland, 2017; pp. 431–461, ISBN 978-3-319-25462-3.
97. Ventura, G.; Calvano, C.D.; Losito, I.; Bianco, G.; Pascale, R.; Palmisano, F.; Cataldi, T.R.I. Effect of pH and mobile phase additives on the chromatographic behaviour of an amide-embedded stationary phase: Cyanocobalamin and its diamine monochloro-platinum(II) conjugate as a case study. *J. Sep. Sci.* **2019**, *42*, 1155–1162. [[CrossRef](#)] [[PubMed](#)]
98. Pascale, R.; Bianco, G.; Coviello, D.; Cristina Lafiosca, M.; Masi, S.; Mancini, I.M.; Bufo, S.A.; Scranò, L.; Caniani, D. Validation of a liquid chromatography coupled with tandem mass spectrometry method for the determination of drugs in wastewater using a three-phase solvent system. *J. Sep. Sci.* **2020**, *43*, 886–895. [[CrossRef](#)]
99. Natale, A.; Nardiello, D.; Palermo, C.; Muscarella, M.; Quinto, M.; Centonze, D. Development of an analytical method for the determination of polyphenolic compounds in vegetable origin samples by liquid chromatography and pulsed amperometric detection at a glassy carbon electrode. *J. Chromatogr. A* **2015**, *1420*, 66–73. [[CrossRef](#)] [[PubMed](#)]
100. Dordevic, B.; Durovic, D.; Zec, G.; Radovic, A.; Vulic, T. Bio-chemical properties and susceptibility to fire blight (*Erwinia amylovora* Burrill) of scab-resistant apple cultivars (*Malus domestica* Borkh.). *Folia Hortic.* **2019**, *31*, 253–261. [[CrossRef](#)]
101. Petkovska, A.; Gjamovski, V.; Stanoeva, J.P.; Stefova, M. Characterization of the polyphenolic profiles of peel, flesh and leaves of *Malus domestica* cultivars using UHPLC-DAD-HESI-MSn. *Nat. Prod. Commun.* **2017**, *12*, 35–42. [[CrossRef](#)]
102. Marks, S.C.; Mullen, W.; Crozier, A. Flavonoid and chlorogenic acid profiles of English cider apples. *J. Sci. Food Agric.* **2007**, *87*, 719–728. [[CrossRef](#)]
103. Jakobek, L.; García-Villalba, R.; Tomás-Barberán, F.A. Polyphenolic characterisation of old local apple varieties from Southeastern European region. *J. Food Compos. Anal.* **2013**, *31*, 199–211. [[CrossRef](#)]
104. De Paepe, D.; Servaes, K.; Noten, B.; Diels, L.; De Loose, M.; Van Droogenbroeck, B.; Voorspoels, S. An improved mass spectrometric method for identification and quantification of phenolic compounds in apple fruits. *Food Chem.* **2013**, *136*, 368–375. [[CrossRef](#)] [[PubMed](#)]
105. Navarro, M.; Moreira, I.; Arnaez, E.; Quesada, S.; Azofeifa, G.; Vargas, F.; Alvarado, D.; Chen, P. Polyphenolic characterization and antioxidant activity of *malus domestica* and *prunus domestica* cultivars from Costa Rica. *Foods* **2018**, *7*, 15. [[CrossRef](#)]
106. Teleszko, M.; Wojdyło, A. Comparison of phenolic compounds and antioxidant potential between selected edible fruits and their leaves. *J. Funct. Foods* **2015**, *14*, 736–746. [[CrossRef](#)]
107. Raudone, L.; Raudonis, R.; Liaudanskas, M.; Viskelis, J.; Pukalskas, A.; Janulis, V. Phenolic Profiles and Contribution of Individual Compounds to Antioxidant Activity of Apple Powders. *J. Food Sci.* **2016**, *81*, C1055–C1061. [[CrossRef](#)] [[PubMed](#)]
108. Oszmiański, J.; Wojdyło, A.; Kolniak, J. Effect of pectinase treatment on extraction of antioxidant phenols from pomace, for the production of puree-enriched cloudy apple juices. *Food Chem.* **2011**, *127*, 623–631. [[CrossRef](#)] [[PubMed](#)]
109. López-fernández, O.; Domínguez, R.; Pateiro, M.; Munekata, P.E.S.; Rocchetti, G.; Lorenzo, J.M. Determination of polyphenols using liquid chromatography–tandem mass spectrometry technique (LC–MS/MS): A review. *Antioxidants* **2020**, *9*, 479. [[CrossRef](#)]
110. Serni, E.; Venir, E.; Romano, G.; Guerra, W.; Robatscher, P. Determination of Major Phenolics Content in Dried Apples from Three New Cultivars (*Malus domestica* Borkh.) Using HPLC-UV-FL with Pentafluorophenyl Stationary Phase. *Food Anal. Methods* **2020**, *13*, 863–871. [[CrossRef](#)]
111. Wojdyło, A.; Oszmiański, J. Antioxidant activity modulated by polyphenol contents in apple and leaves during fruit development and ripening. *Antioxidants* **2020**, *9*, 567. [[CrossRef](#)]
112. Wollgast, J.; Anklam, E. Review on polyphenols in Theobroma cacao: Changes in composition during the manufacture of chocolate and methodology for identification and quantification. *Food Res. Int.* **2000**, *33*, 423–447. [[CrossRef](#)]
113. Hollands, W.J.; Voorspoels, S.; Jacobs, G.; Aaby, K.; Meisland, A.; Garcia-Villalba, R.; Tomas-Barberan, F.; Piskula, M.K.; Mawson, D.; Vovk, I.; et al. Development, validation and evaluation of an analytical method for the determination of monomeric and oligomeric procyanidins in apple extracts. *J. Chromatogr. A* **2017**, *1495*, 46–56. [[CrossRef](#)]
114. Bernal, J.; Ares, A.M.; Pól, J.; Wiedmer, S.K. Hydrophilic interaction liquid chromatography in food analysis. *J. Chromatogr. A* **2011**, *1218*, 7438–7452. [[CrossRef](#)]
115. Veberic, R.; Schmitzer, V.; Petkovsek, M.M.; Stampar, F. Impact of Shelf Life on Content of Primary and Secondary Metabolites in Apple (*Malus domestica* Borkh.). *J. Food Sci.* **2010**, *75*, 461–468. [[CrossRef](#)]
116. Blake, J.D.; Clarke, M.L.; Richards, G.N. Determination of organic acids in sugar cane process juice by high-performance liquid chromatography: Improved resolution using dual aminex HPX-87H cation-exchange columns equilibrated to different temperatures. *J. Chromatogr. A* **1987**, *398*, 265–277. [[CrossRef](#)]
117. Liaudanskas, M.; Viškelis, P.; Jakštās, V.; Raudonis, R.; Kviklys, D.; Milašius, A.; Janulis, V. Application of an optimized HPLC method for the detection of various phenolic compounds in apples from Lithuanian cultivars. *J. Chem.* **2014**, *2014*. [[CrossRef](#)]
118. Sowa, A.; Zgórk, G.; Szykuba, A.; Franciczek, R.; Gbikowska, B.; Gamian, A.; Sroka, Z. Analysis of polyphenolic compounds in extracts from leaves of some *malus domestica* cultivars: Antiradical and antimicrobial analysis of these extracts. *BioMed Res. Int.* **2016**, *2016*. [[CrossRef](#)]
119. Le Bourvellec, C.; Bouzerzour, K.; Ginies, C.; Regis, S.; Plé, Y.; Renard, C.M.G.C. Phenolic and polysaccharidic composition of applesauce is close to that of apple flesh. *J. Food Compos. Anal.* **2011**, *24*, 537–547. [[CrossRef](#)]

120. Le Bourvellec, C.; Bureau, S.; Renard, C.M.G.C.; Plenet, D.; Gautier, H.; Touloumet, L.; Girard, T.; Simon, S. Cultivar and year rather than agricultural practices affect primary and secondary metabolites in apple fruit. *PLoS ONE* **2015**, *10*, e0141916. [[CrossRef](#)]
121. Zhang, L.; Xu, Q.; You, Y.; Chen, W.; Xiao, Z.; Li, P.; Ma, F. Characterization of quercetin and its glycoside derivatives in *Malus germplasm*. *Hortic. Environ. Biotechnol.* **2018**, *59*, 909–917. [[CrossRef](#)]
122. Mato, I.; Suárez-Luque, S.; Huidobro, J.F. A review of the analytical methods to determine organic acids in grape juices and wines. *Food Res. Int.* **2005**, *38*, 1175–1188. [[CrossRef](#)]
123. Pascale, R.; Bianco, G.; Calace, S.; Masi, S.; Mancini, I.M.; Mazzone, G.; Caniani, D. Method development and optimization for the determination of benzene, toluene, ethylbenzene and xylenes in water at trace levels by static headspace extraction coupled to gas chromatography–barrier ionization discharge detection. *J. Chromatogr. A* **2018**, *1548*, 10–18. [[CrossRef](#)] [[PubMed](#)]
124. Onzo, A.; Acquavia, M.A.; Cataldi, T.R.I.; Ligonzo, M.; Coviello, D.; Pascale, R.; Martelli, G.; Bondoni, M.; Scrano, L.; Bianco, G. Coceth sulfate characterization by electrospray ionization tandem mass spectrometry. *Rapid Commun. Mass Spectrom.* **2020**, *34*, 1–10. [[CrossRef](#)]
125. Lelario, F.; De Maria, S.; Rivelli, A.R.; Russo, D.; Milella, L.; Bufo, S.A.; Scrano, L. LC-FTICR-MS and IRMPD in a Commercial Variety and their Anticholinesterase and Antioxidant Activities. *Toxins* **2019**, *11*, 230. [[CrossRef](#)]
126. Lelario, F.; Labella, C.; Napolitano, G.; Scrano, L.; Bufo, S.A. Fragmentation study of major spirosolane-type glycoalkaloids by collision-induced dissociation linear ion trap and infrared multiphoton dissociation Fourier transform ion cyclotron resonance mass spectrometry. *Rapid Commun. Mass Spectrom.* **2016**, *30*, 2395–2406. [[CrossRef](#)]
127. Šavikin, K.; Živković, J.; Zdunić, G.; Godevac, D.; Dordević, B.; Dojčinović, B.; Dordević, N. Phenolic and mineral profiles of four Balkan indigenous apple cultivars monitored at two different maturity stages. *J. Food Compos. Anal.* **2014**, *35*, 101–111. [[CrossRef](#)]
128. Verdu, C.F.; Gatto, J.; Freuze, I.; Richomme, P.; Laurens, F.; Guilet, D. Comparison of two methods, UHPLC-UV and UHPLC-MS/MS, for the quantification of polyphenols in cider apple juices. *Molecules* **2013**, *18*, 10213–10227. [[CrossRef](#)] [[PubMed](#)]
129. Kolniak-Ostek, J.; Oszmiański, J.; Wojdyło, A. Effect of l-ascorbic acid addition on quality, polyphenolic compounds and antioxidant capacity of cloudy apple juices. *Eur. Food Res. Technol.* **2013**, *236*, 777–798. [[CrossRef](#)]
130. Lee, J.; Chan, B.L.S.; Mitchell, A.E. Identification/quantification of free and bound phenolic acids in peel and pulp of apples (*Malus domestica*) using high resolution mass spectrometry (HRMS). *Food Chem.* **2017**, *215*, 301–310. [[CrossRef](#)] [[PubMed](#)]
131. Reis, S.F.; Rai, D.K.; Abu-Ghannam, N. Water at room temperature as a solvent for the extraction of apple pomace phenolic compounds. *Food Chem.* **2012**, *135*, 1991–1998. [[CrossRef](#)] [[PubMed](#)]
132. Malec, M.; Le Quéré, J.M.; Sotin, H.; Kolodziejczyk, K.; Bauduin, R.; Guyot, S. Polyphenol profiling of a red-fleshed apple cultivar and evaluation of the color extractability and stability in the juice. *J. Agric. Food Chem.* **2014**, *62*, 6944–6954. [[CrossRef](#)]
133. Giomaro, G.; Karioti, A.; Bilia, A.R.; Bucchini, A.; Giamperi, L.; Ricci, D.; Fraternali, D. Polyphenols profile and antioxidant activity of skin and pulp of a rare apple from Marche region (Italy). *Chem. Cent. J.* **2014**, *8*, 1–10. [[CrossRef](#)] [[PubMed](#)]
134. Alonso-Salces, R.M.; Ndjoko, K.; Queiroz, E.F.; Ioset, J.R.; Hostettmann, K.; Berrueta, L.A.; Gallo, B.; Vicente, F. On-line characterisation of apple polyphenols by liquid chromatography coupled with mass spectrometry and ultraviolet absorbance detection. *J. Chromatogr. A* **2004**, *1046*, 89–100. [[CrossRef](#)]
135. Denis, M.C.; Furtos, A.; Dudonné, S.; Montoudis, A.; Garofalo, C.; Desjardins, Y.; Delvin, E.; Levy, E. Apple Peel Polyphenols and Their Beneficial Actions on Oxidative Stress and Inflammation. *PLoS ONE* **2013**, *8*, e53725. [[CrossRef](#)]
136. Todea, D.; Cadar, O.; Simedru, D.; Roman, C.; Tanaselia, C.; Suatean, I.; Naghiu, A. Determination of major-to-trace minerals and polyphenols in different apple cultivars. *Not. Bot. Horti Agrobot. Cluj Napoca* **2014**, *42*, 523–529. [[CrossRef](#)]
137. Bizjak, J.; Mikulic-Petkovsek, M.; Stampar, F.; Veberic, R. Changes in primary metabolites and polyphenols in the peel of “braeburn” Apples (*Malus domestica* Borkh.) during advanced maturation. *J. Agric. Food Chem.* **2013**, *61*, 10283–10292. [[CrossRef](#)]
138. De Bernonville, T.D.; Gaucher, M.; Guyot, S.; Durel, C.E.; Dat, J.F.; Brisset, M.N. The constitutive phenolic composition of two *Malus domestica* genotypes is not responsible for their contrasted susceptibilities to fire blight. *Environ. Exp. Bot.* **2011**, *74*, 65–73. [[CrossRef](#)]
139. Arathi, B.P.; Sowmya, P.R.R.; Vijay, K.; Baskaran, V.; Lakshminarayana, R. Metabolomics of carotenoids: The challenges and prospects—A review. *Trends Food Sci. Technol.* **2015**, *45*, 105–117. [[CrossRef](#)]
140. Delgado-Pelayo, R.; Gallardo-Guerrero, L.; Hornero-Méndez, D. Chlorophyll and carotenoid pigments in the peel and flesh of commercial apple fruit varieties. *Food Res. Int.* **2014**, *65*, 272–281. [[CrossRef](#)]
141. Fromm, M.; Bayha, S.; Kammerer, D.R.; Carle, R. Identification and quantitation of carotenoids and tocopherols in seed oils recovered from different rosaceae species. *J. Agric. Food Chem.* **2012**, *60*, 10733–10742. [[CrossRef](#)] [[PubMed](#)]
142. Saini, R.K.; Nile, S.H.; Park, S.W. *Carotenoids from Fruits and Vegetables: Chemistry, Analysis, Occurrence, Bioavailability and Biological Activities*; Elsevier: Amsterdam, The Netherlands, 2015; Volume 76, ISBN 8224503739.
143. Delpino-Rius, A.; Eras, J.; Marsol-Vall, A.; Vilaró, F.; Balcells, M.; Canela-Garayoa, R. Ultra performance liquid chromatography analysis to study the changes in the carotenoid profile of commercial monovarietal fruit juices. *J. Chromatogr. A* **2014**, *1331*, 90–99. [[CrossRef](#)] [[PubMed](#)]
144. Cargnin, S.T.; Gnoatto, S.B. Ursolic acid from apple pomace and traditional plants: A valuable triterpenoid with functional properties. *Food Chem.* **2016**, *220*, 477–489. [[CrossRef](#)]
145. Song, J.; Gardner, B.D.; Holland, J.F.; Beaudry, R.M. Rapid Analysis of Volatile Flavor Compounds in Apple Fruit Using SPME and GC/Time-of-Flight Mass Spectrometry. *J. Agric. Food Chem.* **1997**, *45*, 1801–1807. [[CrossRef](#)]

146. Januszek, M.; Satora, P. Oenological Characteristics of Fermented Apple Musts and Volatile Profile of Brandies Obtained from Different Apple Cultivars. *Biomolecules* **2020**, *10*, 853. [[CrossRef](#)]
147. Giannetti, V.; Boccacci Mariani, M.; Mannino, P.; Marini, F. Volatile fraction analysis by HS-SPME/GC-MS and chemometric modeling for traceability of apples cultivated in the Northeast Italy. *Food Control* **2017**, *78*, 215–221. [[CrossRef](#)]
148. Vrhovsek, U.; Lotti, C.; Masuero, D.; Carlin, S.; Weingart, G.; Mattivi, F. Quantitative metabolic profiling of grape, apple and raspberry volatile compounds (VOCs) using a GC/MS/MS method. *J. Chromatogr. B Anal. Technol. Biomed. Life Sci.* **2014**, *966*, 132–139. [[CrossRef](#)]
149. Wildner, A.C.; Ferreira, P.L.; Oliveira, S.S.; Gnoatto, S.B.; Bergold, A.M. Variation of ursolic and betulinic acid in five *Malus × domestica* clones from Southern Brazil. *J. Appl. Pharm. Sci.* **2018**, *8*, 158–165. [[CrossRef](#)]
150. Viškelis, J.; Uselis, N.; Liaudanskas, M.; Janulis, V.; Bielicki, P.; Univer, T.; Lepsis, J.; Kviklys, D. Triterpenic acid content in the fruit peel of *Malus × domestica* Borkh. depends on the growing technology. *Zemdirb.-Agric.* **2018**, *105*, 71–78. [[CrossRef](#)]
151. Sut, S.; Zengin, G.; Maggi, F.; Malagoli, M.; Dall'Acqua, S. Triterpene acid and phenolics from ancient apples of Friuli Venezia Giulia as nutraceutical ingredients: LC-MS study and in vitro activities. *Molecules* **2019**, *24*, 1109. [[CrossRef](#)]
152. Butkevičiūtė, A.; Liaudanskas, M.; Kviklys, D.; Zymonė, K.; Raudonis, R.; Viškelis, J.; Uselis, N.; Janulis, V. Detection and analysis of triterpenic compounds in apple extracts. *Int. J. Food Prop.* **2018**, *21*, 1716–1727. [[CrossRef](#)]
153. McGhie, T.K.; Hudault, S.; Lunken, R.C.M.; Christeller, J.T. Apple peels, from seven cultivars, have lipase-inhibitory activity and contain numerous ursenoic acids as identified by LC-ESI-QTOF-HRMS. *J. Agric. Food Chem.* **2012**, *60*, 482–491. [[CrossRef](#)] [[PubMed](#)]

Article

Characterization of Quercetin Derivatives in Crossing Combination of Habanero White and *Capsicum annuum* Peppers and of Anti-Inflammatory and Cytotoxic Activity

Maria Assunta Acquavia^{1,2}, Raffaella Pascale^{3,*}, Iliara Pappalardo^{1,4}, Anna Santarsiero¹, Giuseppe Martelli¹ and Giuliana Bianco¹

- ¹ Dipartimento di Scienze, Università degli Studi della Basilicata, Via dell'Ateneo Lucano 10, 85100 Potenza, Italy; maria.acquavia@unibas.it (M.A.A.); ilaria.pappalardo@unibas.it (I.P.); anna.santarsiero@unibas.it (A.S.); giuseppe.martelli@unibas.it (G.M.); giuliana.bianco@unibas.it (G.B.)
- ² ALMAGISI s.r.l Corso Italia, 27, 39100 Bolzano, Italy
- ³ Gnosis by Lesaffre, Pisticci, 75015 Matera, Italy
- ⁴ KAMABIO Srl, Via Al Boschetto 4/B, 39100 Bolzano, Italy
- * Correspondence: raff.pascale@gmail.com; Tel.: +39-347-799-4159

Abstract: The overproduction of reactive oxygen species and the exposure of the human body to free radicals contribute to the aetiology of many chronic health problems, such as cardiovascular disease and cancer. Supplementation with natural antioxidants could be helpful, preventing free-radical-induced tissue damage through the inhibition of the radicals' formation. Quercetin derivatives have recently been shown to inhibit the production of inflammatory mediators and to reduce the proliferation of tumoral cells, thus being valid compounds to be promoted as dietary supplements. In this work, an HPLC-MS/MS investigation on the derivatives of quercetin in a methanolic extract of peppers deriving from an original crossing combination between Habanero white and *Capsicum annuum* revealed the occurrence of nine glycoconjugates, either monosaccharide, disaccharide or trisaccharide, as well as an acylated disaccharidic derivative (i.e., quercetin rhamnoside-(feruloyl-hexoside)). Due to the great variability in the quercetin derivatives' profiles, the Habanero white hybrid pepper extract was subjected to in vitro cytotoxicity assays. The pepper extract under study was proved to have anti-inflammatory activity comparable to that shown by a *Capsicum annuum* pepper extract since it reduced ROS levels compared to activated cells. Due to its beneficial effects, it could be exploited as a natural constituent of nutraceutical formulations.

Keywords: Habanero white peppers; *Capsicum annuum*; HPLC-MS/MS; quercetin derivatives; anti-inflammatory properties



Citation: Acquavia, M.A.; Pascale, R.; Pappalardo, I.; Santarsiero, A.; Martelli, G.; Bianco, G. Characterization of Quercetin Derivatives in Crossing Combination of Habanero White and *Capsicum annuum* Peppers and of Anti-Inflammatory and Cytotoxic Activity. *Separations* **2021**, *8*, 90. <https://doi.org/10.3390/separations8070090>

Academic Editor: Francisco J. Barba

Received: 5 May 2021

Accepted: 17 June 2021

Published: 24 June 2021

Publisher's Note: MDPI stays neutral with regard to jurisdictional claims in published maps and institutional affiliations.



Copyright: © 2021 by the authors. Licensee MDPI, Basel, Switzerland. This article is an open access article distributed under the terms and conditions of the Creative Commons Attribution (CC BY) license (<https://creativecommons.org/licenses/by/4.0/>).

1. Introduction

In recent years there has been a great deal of attention to nutraceuticals, that is, bioactive ingredients extractable from food sources that have scientifically proven health benefits for both the treatment and prevention of many disease [1,2], covering a broad range of biological activities (e.g., antioxidant, anti-inflammatory, antimicrobial, anticancer, hypoglycaemic, cardioprotective and neuroprotective) [3,4]. Nutraceuticals are often referred to as pharma-foods, since they are a powerful toolbox to be used beyond the diet and before pharmaceuticals [5]. As such, the search for new compounds, for new plant sources from which they could be extracted, and for information on their activity is continuously increasing, making use of targeted and untargeted metabolomics analyses [6–8].

Interestingly, common peppers (*Capsicum*) are an important source of many bioactive molecules [9–11]. Indeed, there are several groups of valuable phytochemicals in *Capsicum* species, including carbohydrates, which constitute approximately 85% of the dry matter (dm); polyphenols and flavonoids (~0.5% dm); and minor yet important bioactive capsaicinoids, carotenoids and vitamins [9]. Polyphenols and flavonoids deserve

special mention because of their well-known antioxidant activity, which they express by reducing free radicals and reactive oxygen species (ROS) in the organism, thus avoiding inflammatory diseases [12]. ROS and other free radicals are produced as part of normal cellular metabolism, and in response to environmental factors such as ultraviolet irradiation. The over-accumulation of these highly reactive molecules in cells can damage cellular components such as lipids, membranes, nucleic acids and proteins. This oxidative stress can directly and/or indirectly lead to human diseases such as cardiovascular disease and cancer [13]. The human body is equipped with an antioxidant defence system that deactivates these highly reactive free radicals. Nevertheless, dietary supplementation with nutrients that contain antioxidants may be important for additional protection against oxidative stress and cell damage caused by ROS over-production, since they can act as radical scavengers, reducing agents and quenchers of singlet oxygen formation and form complexes with pro-oxidant metals [14]. Among the species belonging to the *Capsicum* genus, *C. annuum* and *C. chinense*, including the Habanero white which is considered as one of the hottest existing pepper species [15], have been promoted as a conspicuous source of flavonoids [16]. Although significant variation of the total flavonoid profile can be registered at every stage of maturity [17], in a typical flavonoid analysis, quercetin and luteolin are usually the two most prevalent compounds identified within fruit tissue [18–20]. Quercetin is a flavonoid with very pronounced anti-carcinogenic effects, derived from its anti-inflammatory and anti-oxidative activities, which in turn are a result of its effective free-radical scavenging attributes [21,22]. It has been recently proposed as potential inhibitor of SARS-CoV-2 replication, thus becoming a possible therapeutic agent against coronavirus disease 2019 (COVID-19), in addition to pharmaceuticals already supplied to hospitalized patients [23–25]. Quercetin is a candidate of first choice as an antioxidant and anti-inflammatory supplement in the form of capsules, tablets, gel and creams. However, due to its poor solubility and slow dissolution rate, this molecule has limited bioavailability [26], and various formulation approaches have been used to increase its pharmaceutical application. Glycosylation generally increases the polarity of the quercetin molecule, which is necessary for aglycone bioavailability and, consequently, for the corresponding biological activity [27]. Therefore, research interest in the structural characterization of quercetin derivatives has been growing due to their pharmacological properties.

In the present work, an investigation on the occurrence of quercetin glycoconjugate derivatives in a methanolic extract of a selected genotype obtained from an original crossing combination between Habanero white and *Capsicum annuum* was conducted through the liquid chromatography coupled with tandem mass spectrometry (LC-MS/MS), widely used in environmental and food science [6,28,29]. This investigation was followed by an *in vitro* assay for the establishment of the cytotoxic properties of the extract on human monoblastic leukemia cells, in addition to the study of its anti-inflammatory activity through ROS production inhibition. Moreover, a comparison of the cytotoxic and anti-inflammatory properties of the Habanero white hybrid pepper extract (WC) and those of a methanolic extract of peppers belonging to the *Capsicum annuum* spp. (RC) was conducted.

2. Materials and Methods

2.1. Reagents and Chemicals

Analytical standard materials ($\geq 95\%$) used for the LC-MS/MS analysis were purchased from Chem Faces (i.e., quercetin-3-O-rutinoside) and Sigma–Aldrich (i.e., quercetin 7-rhamnoside, quercetin and quercetin 7-glucoside). Acetonitrile and methanol (LC-MS grade) were obtained from Sigma–Aldrich (Schnelldorf, Germany). Ultra-pure water was produced using a Milli-Q RG system from Millipore (Bedford, MA, USA). Pure nitrogen (99.996%) was delivered to the LC-MS system as sheath gas. The ion-trap pressure was maintained with helium 99.999%; helium was used for trapping and for the collisional activation of trapped ions. L-Glutamine, penicillin/streptomycin solution, lipopolysaccharide from *Salmonella enterica* serotype Typhimurium (LPS) and Roswell Park Memorial Institute 1640 (RPMI 1640) were purchased from Sigma–Aldrich (St. Louis, MO, USA). 6-Carboxy-

2',7'-dichlorodihydrofluorescein diacetate (DCF-DA) was obtained from Thermo Fisher Scientific (San Jose, CA, USA).

2.2. Plant Material and Extraction

A pepper species obtained from a genotype from a specific breeding programme conducted by Bioinnova (Potenza, Italy) underwent LC-MS/MS and in vitro assays in this work. The genotype used is a selected backcross 1 (BC1) obtained in Potenza in August 2020, starting from an original crossing combination between Habanero white x P4 A2–16 (selected genotype of *Capsicum annuum*), where P4 A2–16 is the recurrent parental. The abbreviation WC (White *Capsicum*) is used to refer to peppers belonging to this crossing combination. The extraction protocol for the derivatives of quercetin occurring in the peppers was optimized from Wahyuni et al. [30]. Briefly, 3 mL of methanol was added to 0.5 g of lyophilized peppers. The samples were sonicated for 15 min ($T = 25\text{ }^{\circ}\text{C}$) in a Sonorex Super RK 100/H sonicator (Bandelin electronic, Berlin, Germany). After filtration through 0.20 μm nylon filters, the Habanero white hybrid pepper extract was analysed by LC-MS in order to evaluate the profile of quercetin derivatives. To carry out the cytotoxicity assays, the WC methanolic extract was subjected to solvent evaporation (Laborota 4000 efficient, Heidolph, Schwabach, Germany), then the sample was solubilized in DMSO at a concentration of 50 mg/mL. Concentrations tested were 0.025 mg/mL and 0.005 mg/mL. The results of the assays were compared to those obtained for the extract of traditional sun-dried peppers, namely Peperoni di Senise (*Capsicum annuum* L.) protected with the Protected Geographical Indication mark. This pepper species, referred to by the abbreviation RC (Red *Capsicum*), was lyophilized and ground before the methanolic extraction. The extract was then subjected to solvent evaporation and solubilized in DMSO at a concentration of 50 mg/mL in order to conduct the in vitro assays. Concentrations tested were 0.005 mg/mL and 0.025 mg/mL.

2.3. Mass Spectrometry Analysis

WC extract (25 μL) was subjected to LC-ESI-MS analysis using an LC system coupled to a mass spectrometer (Thermo Fisher Scientific, Bremen, Germany) with a linear trap quadrupole (LTQ) analyzer. Chromatographic separation was performed at room temperature on an RP Luna C18 (2) column (150 \times 4.6 mm i.d., 3.0 μm , 100 \AA), through a previously developed and optimized method [6]. Briefly, water (solvent A) and acetonitrile (solvent B) were used as mobile phases. Starting from 100% A, a composition of 70:30 (A:B) of the mobile phase was reached within 15 min, then passed to 65% A in 25 min and held for 5 min. Following this, the composition was 60:40 (A: B) at 40 min and 15:85 (A: B) after 50 min. A reconditioning time of 10 min was employed. Due to the better sensitivity, the negative-ion mode was the polarity chosen for the quercetin derivatives' ionization [31]. The source voltage, the temperature of the heated capillary, the tube lens voltage and the sheath gas (N_2) flow rate were set, respectively, to 4.5 kV, 350 $^{\circ}\text{C}$, -45 V , -75 V and 5 arbitrary units (a.u). m/z 100–1500 was the range chosen for the full-scan MS experiments. Ions corresponding to quercetin derivatives found in WC extract were selected for MS² experiments by collision-induced dissociation (CID), in order to confirm their identity, using helium as the collision gas. Collision energy was optimized for each precursor ion, between 18% and 30% of the normalized collision energy (NCE). The Xcalibur software package (version 2.0 SR1 Thermo Electron) was used for the acquisition and analysis of the MS and MS/MS data.

2.4. Cell Culture and Treatments

Human monoblastic leukaemia U937 cell line (ICLC HTL94002-Interlab Cell Line Collection) was grown in suspension in the Roswell Park Memorial Institute 1640 medium (RPMI 1640) supplemented with 10% (*v/v*) foetal bovine serum, 2 mM L-glutamine, 100 U/mL penicillin and 100 $\mu\text{g/mL}$ streptomycin at 37 $^{\circ}\text{C}$ in 5% CO_2 in a water-saturated atmosphere. HEK293 kidney immortalized cell line was purchased from the European

Type Culture Collection and maintained as described by Convertini et al. [32]. U937 and HEK293 cells were treated with White *Capsicum* (WC) or Red *Capsicum* (RC) (0.005 mg/mL and 0.025 mg/mL) and, where indicated, stimulated with 100 ng/mL of lipopolysaccharide from *Salmonella enterica* serotype typhimurium (LPS, Sigma–Aldrich, St. Louis, MO, USA).

2.5. Cytotoxicity Assay

The effects of WC and RC on HEK293 and U937 cells' proliferation were determined by MTT assay or by cell counting. In brief, cells were cultured into 96-well plates (1.5×10^4 and 5×10^4 cells/well, respectively) and treated with WC or RC (0.005 mg/mL and 0.025 mg/mL) for 72 h. HEK293 cell viability was measured spectrophotometrically using MTT as a substrate. After treatment, fresh MTT was added and resuspended in phosphate-buffered saline (PBS) (final concentration 0.5 mg/mL), and the plate was incubated at 37 °C for 3 h in a humidified 5% CO₂ incubator. Then, the media were removed, and the formazan crystals were dissolved in 100 µL of DMSO-EtOH (1:1) (Sigma–Aldrich, St. Louis, MO, USA). The optical density was measured at 570 nm with a GloMax plate reader (Promega, Madison, WI, USA). U937 cell viability was carried out by using the automated handheld Scepter 2.0 Cell Counter (Merck Millipore, Milano, Italy), according to the manufacturer's instructions.

2.6. ROS Detection

To evaluate reactive oxygen species (ROS) levels, U937 cells were triggered by 100 ng/mL of LPS in the presence or absence of WC or RC (0.005 mg/mL and 0.025 mg/mL). Following 24 h, ROS concentration was measured using 6-carboxy-2',7'-dichlorodihydrofluorescein diacetate (DCF-DA, Thermo Fisher Scientific, San Jose, CA, USA). The fluorescence was revealed using a GloMax plate reader, a 96-well microplate reader (Promega, Madison, WI, USA).

2.7. Statistical Analysis

Statistical significance of differences was determined by using one-way analysis of variance (ANOVA) followed by Student's *t*-test for multiple comparisons. Results are shown as means \pm SDs of three independent experiments. Differences were considered as significant (* $p < 0.05$, * versus LPS), very significant (##, ** $p < 0.01$, # versus control) and highly significant (### $p < 0.001$).

3. Results and Discussion

Among the countless flavonoids occurring in foodstuffs, quercetin is well known for its great therapeutic potential in the prevention and treatment of many diseases [33]. Despite being often suggested as a dietary supplement, quercetin's bioavailability is very low, mostly due to its extensive metabolism [26]. On the other hand, quercetin derivatives, mainly β -glycosidic derivatives of various sugars, are more easily absorbed and metabolized throughout the body since the attached substituents change the biochemical activity and bioavailability of the molecules when compared to the aglycone [34]. In light of the efficient metabolism of quercetin derivatives, the interest in the evaluation of their occurrence in fruits and vegetables is growing.

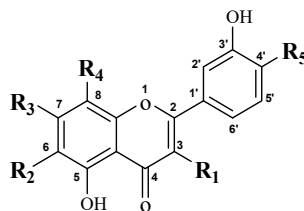
A profiling of the quercetin derivatives occurring in the modified genotype of the Habanero white pepper extract under study was conducted using an HPLC-MS/MS method previously developed by Pascale et al. [6]. In detail, these authors proposed a method for the screening of quercetin glycol conjugates in traditional peppers (*Capsicum annuum* L.), based on a cubic regression model which correlated chromatographic retention times and partition coefficients (log P) of the analytes, in addition to MS/MS data and an exact masses list provided by a database developed in-house (named QUEdb). A similar method was applied here to provide a deep qualitative profile of the quercetin glycoconjugates occurring in the WC methanolic extract. Table 1 reports all of the identified compounds (Q1–Q10) with their corresponding retention times. All the derivatives eluted

before quercetin aglycone, as they were monosaccharidic, disaccharidic or trisaccharidic glycoconjugates, namely, more hydrophilic molecules linked respectively to one, two or three sugar moieties.

In detail, compounds Q5 (m/z 463.0 [M–H][−]), Q7 (m/z 609.1 [M–H][−]), Q8 (m/z 447.1 [M–H][−]) and Q10 (m/z 301.0 [M–H][−]) were identified, respectively, as quercetin-7-*O*-glucoside, quercetin-3-*O*-rutinose, quercetin-7-*O*-rhamnoside and quercetin aglycone (Figure 1A). Quercetin aglycone fragmentation gave the typical ion fragments resulting from losses of CO (−28 Da) and CO₂ (−44 Da) and from rearrangements of the molecular ion at m/z 301.0 ([C₁₅H₉O₇][−]) [31]. Notice that the occurrence of the fragment ion at m/z 301.0 in the MS/MS spectra of the quercetin derivatives was diagnostic to establish the nature of the aglycone, and it was further subjected to MS² experiments in order to confirm the quercetin fragmentation pattern.

Since no reference standards were available, for derivatives Q1 (m/z 595.1 [M–H][−]) and Q3 (m/z 433.1 [M–H][−]) (Figure 1B), tandem mass spectra interpretation was conducted to determine the nature of the aglycone substituents. As the ion fragments detected in the MS/MS spectrum of the molecular ion at m/z 595.1 were compatible with the fragmentation of hexose (ions at m/z 415.0 [M–H–120–60][−], m/z 385.0 [M–H–120–90][−] and m/z 355.0 [M–H–120–120][−]) and a pentose moiety (ions at m/z 505.0 [M–H–90][−], m/z 487.1 [M–H–108][−] and m/z 475.0 [M–H–120][−]), Q1 was identified as quercetin-6-*C*-hexoside-8-*C*-pentoside/apioside [35,36]. Notice that the more pronounced fragmentation of the sugars, rather than their neutral losses, suggest the existence of *C*-glycosidic bonds with the aglycone. Instead, the neutral loss of 132 Da from the molecular ion at m/z 433.1, allowed the identification of Q3 as a monosaccharidic derivative, namely quercetin-7-*O*-pentoside/apioside. The 7-glycosylation position was revealed by the higher relative abundance of the aglycone ion Y₀[−] (at m/z 301.0), compared to the relative abundance of the radical aglycone ion [Y₀–H]^{−•} at m/z 300.0 [37].

For compounds Q2, Q4, Q6 and Q9, tandem mass data were not enough to achieve an unambiguous identification, therefore making a distinction between putative quercetin glycosides and acyl glycosides with the same nominal mass more complicated (Figure 1C). Thus, a cubic regression model which correlated the standard quercetin derivatives' experimental RT with their hydrophobicity (log P values) was used as a valuable approach for their characterization. Compounds Q2 (m/z 609.1 [M–H][−]) and Q6 (m/z 609.1 [M–H][−]) were identified as two di-*O*-glycosyl isomers (i.e., quercetin-4'-rhamnoside-7-hexoside and quercetin-3-*O*-rhamnoside-7-*O*-hexoside), since they showed retention times shorter than that of the more hydrophobic quercetin standard (23.7 min). A further quercetin rhamnoside-hexoside isomer (Q9, m/z 785.1 [M–H][−]), with an additional acyl group on the hexose moiety, was also identified in the Habanero white pepper extract. The fragment ion at m/z 447.0 ([M–H–162–176][−]) occurring in its MS/MS spectrum supported the evidence of a feruloyl-hexose substituent of the aglycone. Thus, Q9 was identified as quercetin rhamnoside-(feruloyl-hexoside), a derivative found for the first time in *Capsicum annum* extracts [6]. A trisaccharidic derivative, the compound eluted at 15.5 min (Q4, m/z 741.3 [M–H][−]), was identified as quercetin-3-*O*-pentosyl/apiosyl-rhamnosyl-hexoside, due to the occurrence in the CID MS spectrum of product ions at m/z 595.1 ([M–146][−]), m/z 463.0 ([M–146–132][−]) and m/z 300.9 ([M–146–132–162][−]), which were obtained after neutral losses of rhamnose (−146), pentose/apiose (−132) and hexose (−162). The validity of the assignment was confirmed by the cubic regression model, which predicts RTs which are too high for the other isomeric candidates possible from the MS/MS spectrum [6].

Table 1. Quercetin derivatives identified in the methanolic extract of peppers derived from a crossing combination between Habanero white and *Capsicum annuum* spp.

Compound n.	RT (min)	Name	Aglycone Substituents	<i>m/z</i> [M–H] [–]	CID (%NCE)
Q1	10.3	Quercetin-6-C-hexoside-8-C-pentoside/apioside	R ₁ : OH; R ₂ : Hex; R ₃ : OH; R ₄ : Pent; R ₅ : OH	595.1	18%
Q2	13.3	Quercetin-4'-rhamnoside-7-hexoside	R ₁ : OH; R ₂ : H; R ₃ : O-Hex; R ₄ : H; R ₅ : O-Rha	609.1	18%
Q3	13.4	Quercetin-7-O-pentoside/apioside	R ₁ : OH; R ₂ : H; R ₃ : O-Pent/Api; R ₄ : H; R ₅ : OH	433.1	18%
Q4	15.5	Quercetin-3-O-pentosyl/apiosyl-rhamnosyl-hexoside	R ₁ : O-Pent/Api-Rha-Hex; R ₂ : H; R ₃ : OH; R ₄ : H; R ₅ : OH	741.3	19%
Q5	15.9	Quercetin-7-O-glucoside	R ₁ : OH; R ₂ : H; R ₃ : O-Glu; R ₄ : H; R ₅ : OH	463.0	18%
Q6	16.0	Quercetin-3-O-rhamnoside-7-O-hexoside	R ₁ : O-Rha; R ₂ : H; R ₃ : O-Hex; R ₄ : H; R ₅ : OH	609.1	18%
Q7	17.5	Quercetin-3-O-rutinose	R ₁ : O-Glu-Rha; R ₂ : H; R ₃ : OH; R ₄ : H; R ₅ : OH	609.1	18%
Q8	19.5	Quercetin-7-O-rhamnoside	R ₁ : OH; R ₂ : H; R ₃ : O-Rha; R ₄ : H; R ₅ : OH	447.1	18%
Q9	23.1	Quercetin rhamnoside-(feruloyl-hexoside)	R _x ² : O-Rha-Hex-Fer; R ₁ : OH; R ₂ : H; R ₃ : OH; R ₄ : H; R ₅ : OH	785.1	20%
Q10	23.7	Quercetin	R ₁ : OH; R ₂ : H; R ₃ : OH; R ₄ : H; R ₅ : OH	301.0	30%

Abbreviations: Hex (hexose); Pent (pentose); Rha (rhamnose); Glu (glucose); Api (apiose); Fer (feruloyl). R_x is used for substituents whose position on the aglycone was not defined according to the MS/MS spectrum.

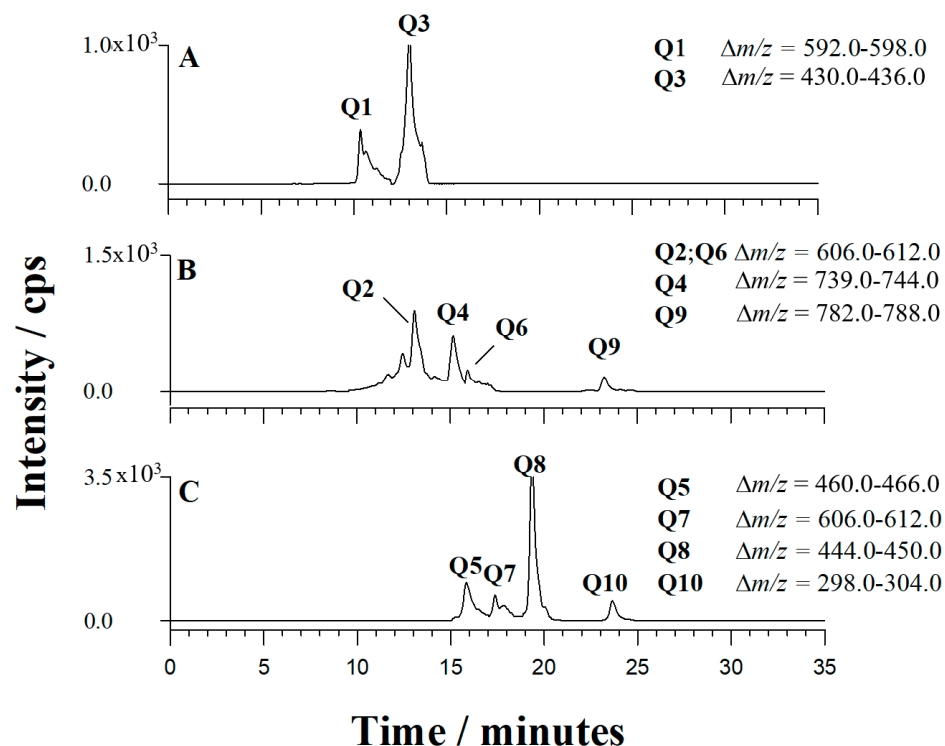


Figure 1. Extracted ion current (XIC) chromatograms by LC-ESI(-)-LTQ-MS of quercetin derivatives occurring in methanolic extract of peppers belonging to a modified genotype of the Habanero white and identified through the use of commercially available standards (A), tandem mass spectra interpretation (B), Log P-RT correlation (C). A window of ± 3.0 m/z unit centred around the selected $[M-H]^-$ ion was chosen. Peak numbers correspond to (Q1) quercetin-6-C-hexoside-8-C-pentoside/apioside, (Q2) quercetin-4'-rhamnoside-7-hexoside, (Q3) quercetin-7-O-pentoside/apioside, (Q4) quercetin-3-O-pentosyl/apiosyl-rhamnosyl-hexoside, (Q5) quercetin-7-O-glucoside, (Q6) quercetin-3-O-rhamnoside-7-O-hexoside, (Q7) quercetin-3-O-rutinoside, (Q8) quercetin-7-O-rhamnoside, (Q9) quercetin rhamnoside-(feruloyl-hexoside) and (Q10) quercetin.

Quercetin and its derivatives are known for exerting a direct pro-apoptotic effect on tumor cells, thus blocking the growth of several cancer cell lines at different phases of the cell cycle. Both of these effects have been documented in a wide variety of cellular models and in animal models [38]. Several studies demonstrated a significant role of quercetin in the growth inhibition of breast, colon, prostate, ovary, endometrium and lung cancer cells [39]. As the LC-MS/MS analysis showed that several quercetin derivatives were present in the WC extract, the extract's cytotoxic activity was evaluated. The *in vitro* cytotoxicity was first studied against the human monoblastic leukaemia U937 cell line for two extract concentrations (0.005 and 0.025 mg/mL) by cell counting, and compared with DMSO used as a control. As illustrated in Figure 2A, WC did not significantly alter cell viability at the tested concentrations. Moreover, surprisingly, the number of dead cells did not increase with the increase in the concentration of the extract. The effect on cell viability was also evaluated for RC extract, whose previously targeted LC-MS/MS analysis showed its rich quercetin profile [6]. As expected, cell viability decreased by increasing the extract concentration. Indeed, RC reduced cell viability by approximately 12% and 6% at 0.025 mg/mL and 0.005 mg/mL concentrations, respectively (Figure 2B).

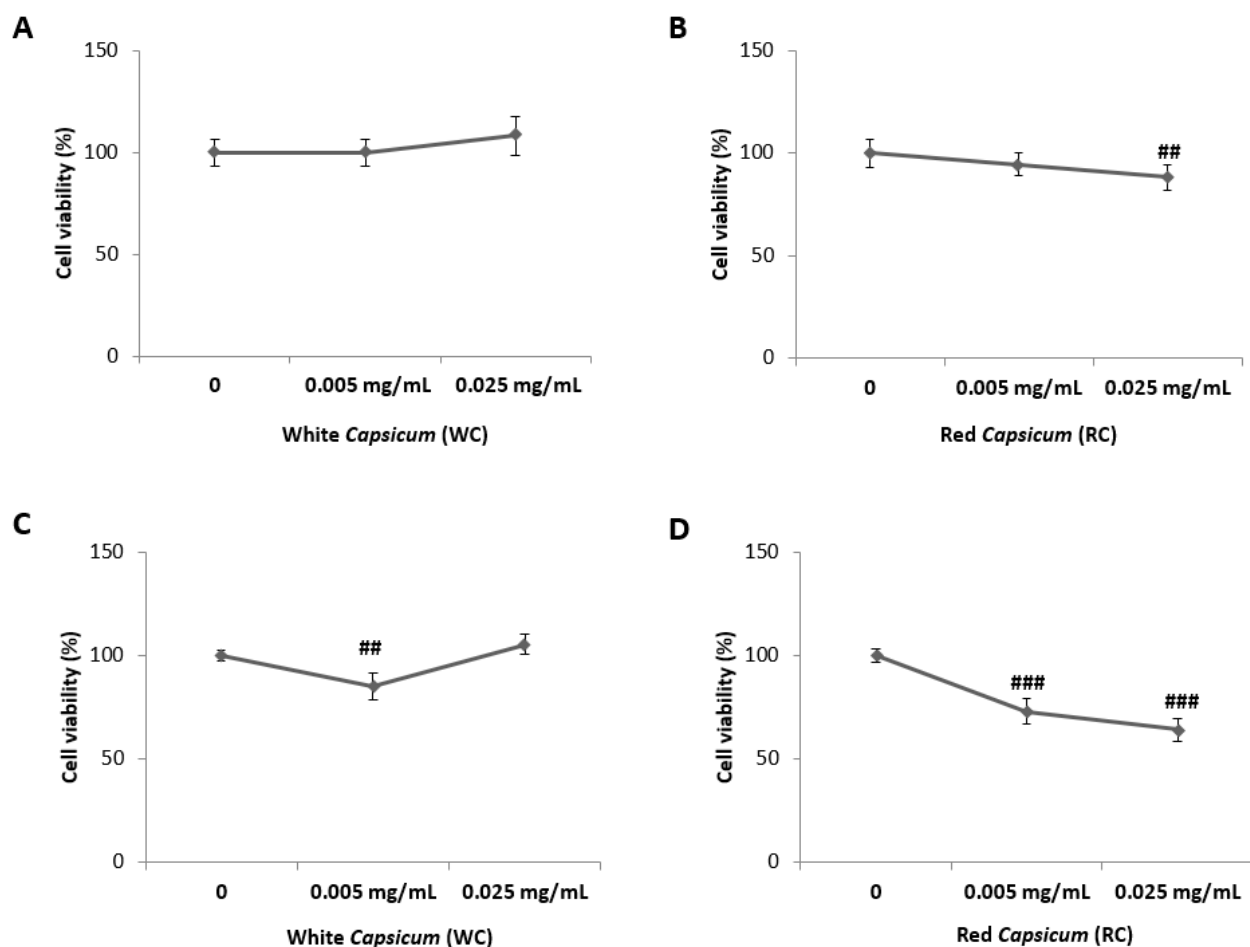


Figure 2. Effect of WC and RC on U937 (A,B) and HEK293 (C,D) cells' viability. U937 and HEK293 cells were treated with WC or RC (0.050 mg/mL and 0.025 mg/mL) as indicated for 72 h. Cell viability was measured using an MTT assay or a Millipore Scepter™ handheld automated cell counter. Results are presented as means \pm SDs from three independent experiments. ### $p < 0.001$, ## $p < 0.01$ versus control (one-way analysis of variance, ANOVA followed by Student's *t*-test for multiple comparisons).

Cytotoxicity was also evaluated in HEK293, a non-tumorigenic cell line, by MTT assay and compared with DMSO used as a control. As illustrated in Figure 2C, WC slightly reduced cell viability only at the lowest concentration (0.005 mg/mL). Instead, the RC extract significantly reduced cell viability in a dose-dependent manner. RC decreased cell viability by approximately 35% and 25% at concentrations of 0.025 mg/mL and 0.005 mg/mL, respectively (Figure 2D). Thus, the RC extract turned out to not have potential for use in nutraceutical formulations.

Several studies have proposed ROS generation inhibition as a possible mechanism through which quercetin and its derivatives express their anti-inflammatory activity [40,41]. Overall, quercetin derivatives' anti-inflammatory activity was found to be comparable to that of the aglycone [42], thus suggesting the potential of these flavonoids as useful constituents of nutraceutical formulations. As both WC and RC extracts showed a wide quercetin derivatives profile, and they did not significantly reduce the U937 cells' viability, their anti-inflammatory activity was evaluated by testing their inhibitory effects on the production of inflammatory mediators, that is, reactive oxygen species (ROS). ROS are typically generated by tightly regulated enzymes, such as NAD(P)H oxidase isoforms. At moderate concentrations, ROS play an important role as regulatory mediators in signaling processes. Many of the ROS-mediated responses actually protect cells against oxidative stress and re-establish "redox homeostasis". However, excessive amounts of ROS may arise either from the excessive stimulation of NAD(P)H oxidases or from less-well-regulated

sources such as the mitochondrial electron-transport chain [43]. Here, the intracellular ROS generation in U937 cells treated with WC and RC extracts was evaluated by fluorescence spectrophotometer after the cells were triggered by lipopolysaccharide. LPS induces the reactive oxygen species-producing enzymes' inducible nitric oxide synthase and reduced nicotinamide adenine dinucleotide phosphate oxidase in monocytes and macrophages, leading to the extensive production of NO, O_2^- , peroxynitrite and other ROS or reactive nitrogen species [44]. ROS activate activating transcription factors such as nuclear factor κ -B (NF- κ b) and activator protein-1, which in turn induce not only more ROS but also proinflammatory cytokines such as TNF- α . Because TNF- α can also activate NF- κ b, a feedforward mechanism resulting in the increased production of both cytokines and ROS is set in motion with LPS exposure [45]. Figure 3A,B shows the percentage of ROS levels for control, cells triggered with LPS and cells either treated with LPS and WC or RC extract, respectively. ROS levels were increased by about 30% in the cells treated with LPS as compared to untreated control cells. Instead, WC reduced ROS levels compared to activated cells at a concentration of 0.025 mg/mL (about 20%) (Figure 3A). RC also showed an inhibitory effect toward ROS, especially at the 0.005 mg/mL concentration (about 10% vs. LPS) (Figure 3B). The results were comparable to the ROS production inhibition capability reported in the literature for quercetin [46]. Because ROS generation is an important factor in the progression of the inflammatory process, these results indicate that both WC and RC extracts could exert health benefits for inflammation-related diseases. However, it should be considered that RC extract is slightly cytotoxic to healthy cell lines. Moreover, according to the cytotoxicity data on non-tumorigenic cell line, WC extract could be used for nutraceutical formulations only at a concentration higher than 0.005 mg/mL.

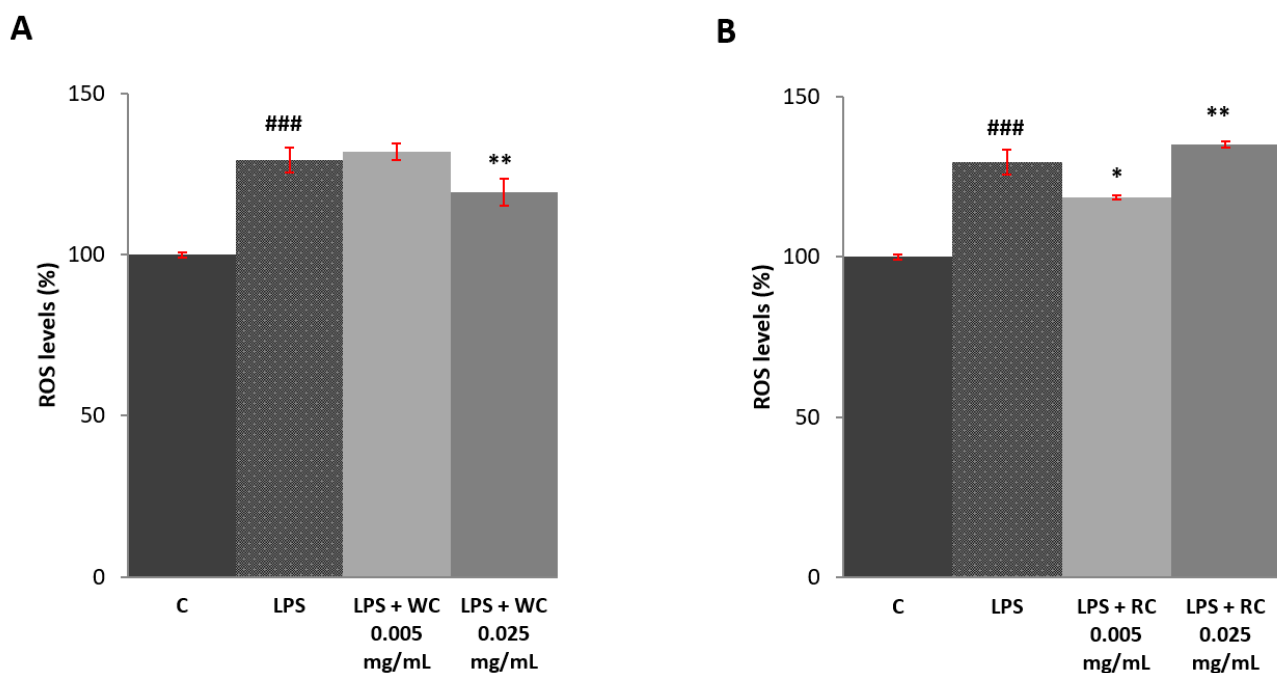


Figure 3. Effect of WC (panel A) and RC (panel B) on ROS production. U937 cells were triggered by 100 ng/mL of LPS in the presence or absence of WC or RC (0.025 mg/mL and 0.005 mg/mL). After 24 h, ROS levels were quantified. Results are presented as means \pm SDs from three independent experiments. The comparison between the results are expressed as follows: * $p < 0.05$ vs LPS, ** $p < 0.01$ vs LPS, ### $p < 0.001$ vs control.

4. Conclusions

In recent years, many nutraceuticals have appeared on the market in different pharmaceutical forms, containing food bioactive compounds as active principles. Many of them are quercetin-based nutraceuticals. Here, a comprehensive profiling of the quercetin

glycoconjugates occurring in a methanolic extract of a new genotype of peppers coming from an original crossing combination of Habanero white and *Capsicum annuum* was conducted. Nine quercetin derivatives were identified by LC-MS/MS along with a correlation between chromatographic data and log P values. An evaluation of the ability of the extract to inhibit the ROS production was conducted here for the first time, showing that the extract is potentially suitable for nutraceutical formulations at concentrations higher than 0.005 mg/mL with anti-inflammatory properties, as it was effectively able to reduce ROS levels in activated cells.

Author Contributions: Formal analysis, I.P. and A.S.; methodology, R.P.; project administration, G.M.; supervision, G.B.; writing—original draft, M.A.A. All authors have read and agreed to the published version of the manuscript.

Funding: This research received no external funding.

Conflicts of Interest: The authors declare no conflict of interest.

References

1. Dillard, C.J.; German, J.B. Phytochemicals: Nutraceuticals and human health. *J. Sci. Food Agric.* **2000**, *80*, 1744–1756. [[CrossRef](#)]
2. Espín, J.C.; García-Conesa, M.T.; Tomás-Barberán, F.A. Nutraceuticals: Facts and fiction. *Phytochemistry* **2007**, *68*, 2986–3008. [[CrossRef](#)]
3. Valentino, G.; Graziani, V.; D’Abrosca, B.; Pacifico, S.; Fiorentino, A.; Scognamiglio, M. NMR-based plant metabolomics in nutraceutical research: An overview. *Molecules* **2020**, *25*, 1444. [[CrossRef](#)]
4. Wang, L.; Weller, C.L. Recent advances in extraction of nutraceuticals from plants. *Trends Food Sci. Technol.* **2006**, *17*, 300–312. [[CrossRef](#)]
5. Daliu, P.; Santini, A.; Novellino, E. From pharmaceuticals to nutraceuticals: Bridging disease prevention and management. *Expert Rev. Clin. Pharmacol.* **2019**, *12*, 1–7. [[CrossRef](#)]
6. Pascale, R.; Acquavia, M.A.; Cataldi, T.R.I.; Onzo, A.; Coviello, D.; Bufo, S.A.; Scrano, L.; Ciriello, R.; Guerrieri, A.; Bianco, G. Profiling of quercetin glycosides and acyl glycosides in sun-dried peperoni di Senise peppers (*Capsicum annuum* L.) by a combination of LC-ESI (-) -MS/MS and polarity prediction in reversed-phase separations. *Anal. Bioanal. Chem.* **2020**, *412*, 3005–3015. [[CrossRef](#)]
7. Onzo, A.; Acquavia, M.A.; Cataldi, T.R.I.; Ligonzo, M.; Coviello, D.; Pascale, R.; Martelli, G.; Bondoni, M.; Scrano, L.; Bianco, G. Coceth sulfate characterization by electrospray ionization tandem mass spectrometry. *Rapid Commun. Mass Spectrom.* **2020**, *34*, 1–10. [[CrossRef](#)] [[PubMed](#)]
8. Santarsiero, A.; Onzo, A.; Pascale, R.; Acquavia, M.A.; Coviello, M.; Convertini, P.; Todisco, S.; Marsico, M.; Pifano, C.; Iannece, P.; et al. Pistacia lentiscus Hydrosol: Untargeted Metabolomic Analysis and Anti-Inflammatory Activity Mediated by NF- κ B and the Citrate Pathway. *Oxid. Med. Cell. Longev.* **2020**, *2020*. [[CrossRef](#)]
9. Asnin, L.; Park, S.W. Isolation and Analysis of Bioactive Compounds in Capsicum Peppers. *Crit. Rev. Food Sci. Nutr.* **2015**, *55*, 254–289. [[CrossRef](#)] [[PubMed](#)]
10. Farhoudi, R.; Mehrnia, M.A.; Lee, D.J. Antioxidant activities and bioactive compounds of five Jalopeno peppers (*Capsicum annuum*) cultivars. *Nat. Prod. Res.* **2019**, *33*, 871–874. [[CrossRef](#)]
11. Hernández-Pérez, T.; Gómez-García, M.d.R.; Valverde, M.E.; Paredes-López, O. *Capsicum annuum* (hot pepper): An ancient Latin-American crop with outstanding bioactive compounds and nutraceutical potential. A review. *Compr. Rev. Food Sci. Food Saf.* **2020**, *19*, 2972–2993. [[CrossRef](#)]
12. Cho, S.Y.; Kim, H.W.; Lee, M.K.; Kim, H.J.; Kim, J.B.; Choe, J.S.; Lee, Y.M.; Jang, H.H. Antioxidant and anti-inflammatory activities in relation to the flavonoids composition of pepper (*Capsicum annuum* L.). *Antioxidants* **2020**, *9*, 986. [[CrossRef](#)]
13. Panth, N.; Paudel, K.R.; Parajuli, K. Reactive Oxygen Species: A Key Hallmark of Cardiovascular Disease. *Adv. Med.* **2016**, *2016*, 1–12. [[CrossRef](#)]
14. Cammisotto, V.; Nocella, C.; Bartimoccia, S.; Sanguigni, V.; Francomano, D.; Sciarretta, S.; Pastori, D.; Peruzzi, M.; Cavarretta, E.; D’Amico, A.; et al. The role of antioxidants supplementation in clinical practice: Focus on cardiovascular risk factors. *Antioxidants* **2021**, *10*, 146. [[CrossRef](#)]
15. Muñoz-Ramírez, L.S.; Peña-Yam, L.P.; Álvarez-Gil, M.A.; Iglesias-Andreu, L.G.; Avilés-Viñas, S.A.; Canto-Flick, A.; Guzmán-Antonio, A.; Santana-Buzzy, N. Selection of habanero pepper f1 hybrids (*Capsicum chinense jacq.*) at the yucatan peninsula, mexico with a high potential for different markets. *Agriculture* **2020**, *10*, 478. [[CrossRef](#)]
16. Campos, M.R.S.; Gómez, K.R.; Ordoñez, Y.M.; Ancona, D.B. Polyphenols, Ascorbic Acid and Carotenoids Contents and Antioxidant Properties of Habanero Pepper (*Capsicum chinense*) Fruit. *Food Nutr. Sci.* **2013**, *4*, 47–54. [[CrossRef](#)]
17. Siddiqui, M.W.; Momin, C.M.; Acharya, P.; Kabir, J.; Debnath, M.K.; Dhua, R.S. Dynamics of changes in bioactive molecules and antioxidant potential of *Capsicum chinense* Jacq. cv. Habanero at nine maturity stages. *Acta Physiol. Plant.* **2013**, *35*, 1141–1148. [[CrossRef](#)]

18. Oney-Montalvo, J.; Uc-Varguez, A.; Ramírez-Rivera, E.; Ramírez-Sucre, M.; Rodríguez-Buenfil, I. Influence of soil composition on the profile and content of polyphenols in habanero peppers (*Capsicum chinense* Jacq.). *Agronomy* **2020**, *10*, 1234. [[CrossRef](#)]
19. Lee, Y.; Howard, L.R.; Villalón, B. Flavonoids and Antioxidant Activity of Fresh Pepper (*Capsicum annuum*) Cultivars. *J. Food Sci.* **1995**, *60*, 473–476. [[CrossRef](#)]
20. Butcher, J.D.; Crosby, K.M.; Yoo, K.S.; Patil, B.S.; Ibrahim, A.M.H.; Leskovar, D.I.; Jifon, J.L. Environmental and genotypic variation of capsaicinoid and flavonoid concentrations in Habanero (*Capsicum chinense*) peppers. *HortScience* **2012**, *47*, 574–579. [[CrossRef](#)]
21. Ezzati, M.; Yousefi, B.; Velaei, K.; Safa, A. A review on anti-cancer properties of Quercetin in breast cancer. *Life Sci.* **2020**, *248*, 1–12. [[CrossRef](#)] [[PubMed](#)]
22. Mertens-Talcott, S.U.; Talcott, S.T.; Percival, S.S. Low concentrations of quercetin and ellagic acid synergistically influence proliferation, cytotoxicity and apoptosis in MOLT-4 human leukemia cells. *J. Nutr.* **2003**, *133*, 2669–2674. [[CrossRef](#)] [[PubMed](#)]
23. Abian, O.; Ortega-Alarcon, D.; Jimenez-Alesanco, A.; Ceballos-Laita, L.; Vega, S.; Reyburn, H.T.; Rizzuti, B.; Velazquez-Campoy, A. Structural stability of SARS-CoV-2 3CLpro and identification of quercetin as an inhibitor by experimental screening. *Int. J. Biol. Macromol.* **2020**, *164*, 1693–1703. [[CrossRef](#)] [[PubMed](#)]
24. Schoot, T.S.; Kerckhoffs, A.P.M.; Hilbrands, L.B.; van Marum, R.J. Immunosuppressive Drugs and COVID-19: A Review. *Front. Pharmacol.* **2020**, *11*, 1333. [[CrossRef](#)] [[PubMed](#)]
25. Acquavia, M.A.; Foti, P.; Pascale, R.; Nicolò, A.; Brancaleone, V.; Cataldi, T.R.I.; Martelli, G.; Scranò, L.; Bianco, G. Detection and quantification of Covid-19 antiviral drugs in biological fluids and tissues. *Talanta* **2021**, *24*, R713–R715. [[CrossRef](#)] [[PubMed](#)]
26. Lauro, M.R.; Torre, M.L.; Maggi, L.; De Simone, F.; Conte, U.; Aquino, R.P. Fast- and slow-release tablets for oral administration of flavonoids: Rutin and quercetin. *Drug Dev. Ind. Pharm.* **2002**, *28*, 371–379. [[CrossRef](#)]
27. Arts, I.C.W.; Sesink, A.L.A.; Faassen-Peters, M.; Hollman, P.C.H. The type of sugar moiety is a major determinant of the small intestinal uptake and subsequent biliary excretion of dietary quercetin glycosides. *Br. J. Nutr.* **2004**, *91*, 841–847. [[CrossRef](#)]
28. Pascale, R.; Bianco, G.; Coviello, D.; Lafiosca, M.C.; Masi, S.; Mancini, I.M.; Bufo, S.A.; Scranò, L.; Caniani, D. Validation of a liquid chromatography coupled with tandem mass spectrometry method for the determination of drugs in wastewater using a three-phase solvent system. *J. Sep. Sci.* **2020**, *43*, 886–895. [[CrossRef](#)]
29. Bianco, G.; Pascale, R.; Lelario, F.; Bufo, S.A.; Cataldi, T.R.I. Investigation of Glucosinolates by Mass Spectrometry. In *Glucosinolates*; Mérillon, J.-M., Ramawat, K.G., Eds.; Springer: Cham, Switzerland, 2017; pp. 431–461, ISBN 978-3-319-25462-3.
30. Wahyuni, Y.; Ballester, A.R.; Tikunov, Y.; de Vos, R.C.H.; Pelgrom, K.T.B.; Maharijaya, A.; Sudarmonowati, E.; Bino, R.J.; Bovy, A.G. Metabolomics and molecular marker analysis to explore pepper (*Capsicum* sp.) biodiversity. *Metabolomics* **2013**, *9*, 130–144. [[CrossRef](#)]
31. Fabre, N.; Rustan, I.; De Hoffmann, E.; Quetin-Leclercq, J. Determination of flavone, flavonol, and flavanone aglycones by negative ion liquid chromatography electrospray ion trap mass spectrometry. *J. Am. Soc. Mass Spectrom.* **2001**, *12*, 707–715. [[CrossRef](#)]
32. Convertini, P.; Todisco, S.; De Santis, F.; Pappalardo, I.; Iacobazzi, D.; Morelli, M.A.C.; Fondufe-Mittendorf, Y.N.; Martelli, G.; Palmieri, F.; Infantino, V. Transcriptional Regulation Factors of the Human Mitochondrial Aspartate/Glutamate Carrier Gene, Isoform 2 (SLC25A13): USF1 as Basal Factor and FOXA2 as Activator in Liver Cells. *Int. J. Mol. Sci.* **2019**, *20*, 1888. [[CrossRef](#)]
33. Rauf, A.; Imran, M.; Khan, I.A.; ur-Rehman, M.; Gilani, S.A.; Mehmood, Z.; Mubarak, M.S. Anticancer potential of quercetin: A comprehensive review. *Phyther. Res.* **2018**, *32*, 2109–2130. [[CrossRef](#)]
34. Murota, K.; Terao, J. Antioxidative flavonoid quercetin: Implication of its intestinal absorption and metabolism. *Arch. Biochem. Biophys.* **2003**, *417*, 12–17. [[CrossRef](#)]
35. Cuyckens, F.; Claeys, M. Mass spectrometry in the structural analysis of flavonoids. *J. Mass Spectrom.* **2004**, *39*, 1–15. [[CrossRef](#)]
36. Pinheiro, P.F.; Goncalon, C.J. Structural Analysis of Flavonoids and Related Compounds—A Review of Spectroscopic Applications. In *Phytochemicals—A Global Perspective of Their Role in Nutrition and Health*; InTech: London, UK, 2012.
37. Ablajan, K.; Abliz, Z.; Shang, X.Y.; He, J.M.; Zhang, R.P.; Shi, J.G. Structural characterization of flavonol 3,7-di-O-glycosides and determination of the glycosylation position by using negative ion electrospray ionization tandem mass spectrometry. *J. Mass Spectrom.* **2006**, *41*, 352–360. [[CrossRef](#)]
38. Danihelová, M.; Veverka, M.; Šturdík, E.; Jantová, S. Antioxidant action and cytotoxicity on HeLa and NIH-3T3 cells of new quercetin derivatives. *Interdiscip. Toxicol.* **2013**, *6*, 209–216. [[CrossRef](#)] [[PubMed](#)]
39. Baghel, S.S.; Shrivastava, N.; Baghel, R.S.; Rajput, S. A Review of Quercetin: Antioxidant and Anticancer Properties. *World J. Pharm. Pharm. Sci.* **2012**, *1*, 146–160.
40. Boots, A.W.; Wilms, L.C.; Swennen, E.L.R.; Kleinjans, J.C.S.; Bast, A.; Haenen, G.R.M.M. In vitro and ex vivo anti-inflammatory activity of quercetin in healthy volunteers. *Nutrition* **2008**, *24*, 703–710. [[CrossRef](#)] [[PubMed](#)]
41. Gibellini, L.; Pinti, M.; Nasi, M.; de Biasi, S.; Roat, E.; Bertocelli, L.; Cossarizza, A. Interfering with ROS metabolism in cancer cells: The potential role of quercetin. *Cancers* **2010**, *2*, 1288–1311. [[CrossRef](#)] [[PubMed](#)]
42. Lesjak, M.; Beara, I.; Simin, N.; Pintač, D.; Majkić, T.; Bekvalac, K.; Orčić, D.; Mimica-Dukić, N. Antioxidant and anti-inflammatory activities of quercetin and its derivatives. *J. Funct. Foods* **2018**, *40*, 68–75. [[CrossRef](#)]
43. Wolin, M.S. Interactions of oxidants with vascular signaling systems. *Arterioscler. Thromb. Vasc. Biol.* **2000**, *20*, 1430–1442. [[CrossRef](#)] [[PubMed](#)]
44. Khanduja, K.L.; Sohi, K.K.; Pathak, C.M.; Kaushik, G. Nimesulide inhibits lipopolysaccharide-induced production of superoxide anions and nitric oxide and iNOS expression in alveolar macrophages. *Life Sci.* **2006**, *78*, 1662–1669. [[CrossRef](#)] [[PubMed](#)]

-
45. Rahman, I. Oxidative stress, transcription factors and chromatin remodelling in lung inflammation. *Biochem. Pharmacol.* **2002**, *64*, 935–942. [[CrossRef](#)]
 46. Tiwari, M.; Dwivedi, U.N.; Kakkar, P. Suppression of oxidative stress and pro-inflammatory mediators by *Cymbopogon citratus* D. Stapf extract in lipopolysaccharide stimulated murine alveolar macrophages. *Food Chem. Toxicol.* **2010**, *48*, 2913–2919. [[CrossRef](#)]



Article

Exploiting the Anti-Inflammatory Potential of White *Capsicum* Extract by the Nanoformulation in Phospholipid Vesicles

Iliara Pappalardo ^{1,2,†}, Anna Santarsiero ^{1,†}, Maria De Luca ^{1,3}, Maria Assunta Acquavia ^{1,4}, Simona Todisco ¹, Carla Caddeo ^{5,*}, Giuliana Bianco ¹, Vittoria Infantino ¹, Giuseppe Martelli ^{1,‡} and Antonio Vassallo ^{1,6,‡}

¹ Department of Science, University of Basilicata, Viale dell'Ateneo Lucano 10, 85100 Potenza, Italy; ilia.pappalardo@unibas.it (I.P.); anna.santarsiero@unibas.it (A.S.); maria.deluca@unibas.it (M.D.L.); maria.acquavia@unibas.it (M.A.A.); simona.todisco@unibas.it (S.T.); giuliana.bianco@unibas.it (G.B.); vittoria.infantino@unibas.it (V.I.); giuseppe.martelli@unibas.it (G.M.); antonio.vassallo@unibas.it (A.V.)

² ALMACABIO Srl, C/so Italia 27, 39100 Bolzano, Italy

³ KAMABIO Srl, Via Al Boschetto 4/B, 39100 Bolzano, Italy

⁴ Thema Informatik Srl, Via Ressel 2/F, 39100 Bolzano, Italy

⁵ Department of Scienze della Vita e dell'Ambiente, Sezione di Scienze del Farmaco, University of Cagliari, Via Ospedale 72, 09124 Cagliari, Italy

⁶ Spinoff TNcKILLERS s.r.l., Viale dell'Ateneo Lucano 10, 85100 Potenza, Italy

* Correspondence: caddeoc@unica.it; Tel.: +39-0706-758-462

† These authors contributed equally to this work.

‡ These authors contributed equally to this work.



Citation: Pappalardo, I.; Santarsiero, A.; De Luca, M.; Acquavia, M.A.; Todisco, S.; Caddeo, C.; Bianco, G.; Infantino, V.; Martelli, G.; Vassallo, A. Exploiting the Anti-Inflammatory Potential of White *Capsicum* Extract by the Nanoformulation in Phospholipid Vesicles. *Antioxidants* **2021**, *10*, 1683. <https://doi.org/10.3390/antiox10111683>

Academic Editor: Elisabetta Esposito

Received: 18 September 2021

Accepted: 23 October 2021

Published: 25 October 2021

Publisher's Note: MDPI stays neutral with regard to jurisdictional claims in published maps and institutional affiliations.



Copyright: © 2021 by the authors. Licensee MDPI, Basel, Switzerland. This article is an open access article distributed under the terms and conditions of the Creative Commons Attribution (CC BY) license (<https://creativecommons.org/licenses/by/4.0/>).

Abstract: The peppers of the *Capsicum* species are exploited in many fields, as flavoring agents in food industry, or as decorative and therapeutic plants. Peppers show a diversified phytochemical content responsible for different biological activities. Synergic activity exerted by high levels of antioxidant compounds is responsible for their important anti-inflammatory property. A methanolic extract was obtained from a new pepper genotype and tested for anti-inflammatory activity. The extract was incorporated into phospholipid vesicles to increase the bioavailability of its bioactive components. Two types of phospholipid vesicles were produced, conventional liposomes and Penetration Enhancer containing Vesicles (PEVs). They were tested in human monoblastic leukemia U937 cell line, showing no cytotoxic effect. The intracellular reactive oxygen species (ROS) and nitric oxide (NO) levels were measured to value the in vitro efficacy of the vesicles in regulating inflammatory responses. Liposomal incorporation significantly reduced ROS levels in extract-treated LPS-activated cells. Furthermore, LC-MS/MS analyses demonstrated that liposomes facilitated the transport of the extract components across the cell membrane and their accumulation into the cytoplasm.

Keywords: white *Capsicum* extract; phospholipid vesicles; anti-inflammatory; ROS; NO; cells

1. Introduction

Plants are an important source of chemical compounds mainly derived from their secondary metabolites with valuable properties to consumers [1].

Peppers (*Capsicum* spp.) are among the oldest cultivated crops in warm climate regions worldwide and are a fundamental reservoir of bioactive compounds that contribute to the taste, color, and flavor of the fruits. *Capsicum* species are annual herbaceous plants belonging to the Solanaceae family, including domesticated species such as *C. baccatum*, *C. annuum*, *C. pubescens*, *C. frutescens*, and *C. chinense*, which display a wide range of fruit size, shape, color, and pungency [2].

Common peppers are mainly used in the food sector, as flavoring agents, for example, but they are also cultivated as decorative and therapeutic plants. Peppers show different biological activities due to their high and diverse phytochemical content, which includes capsaicinoids, carotenoids, phenolic compounds, vitamins, and minerals, and whose expression profile depends on the fruit part, the genotype, the ripening stage, the climatic

conditions, the processing and storage practices [3,4]. Capsaicinoids are a group of alkaloids produced in variable amounts in hot peppers and their chemical structure influences the pungency of *Capsicum* species. They are probably produced as deterrents against certain herbivores and fungi, and major representatives are capsaicin and dihydrocapsaicin. Capsaicinoids have a rather strong biological activity and a potential pharmacological and clinical application for the treatment of neurological and musculoskeletal pain, and inflammatory and oxidative diseases [5–14].

Recently, capsinoids have been found in some varieties of peppers. They are non-pungent compounds with a similar structure to capsaicinoids. Their mechanisms of action are poorly understood, but they have shown some interesting properties, such as antimicrobial activity [4].

Peppers are also good sources of vitamins, showing high levels of vitamin C, E, provitamin A, and folate, and they are also rich in minerals, including iron, calcium, and manganese [15]. Mostly, *Capsicum* fruits contain high levels of antioxidants primarily responsible for the antiseptic, antimetastatic, antifungal, antiviral, anti-inflammatory, and immunomodulatory properties of peppers [3,4]. The radical scavenging activity of peppers is also influenced by the synergism between the total antioxidants. Peppers are generally rich in different types of carotenoids, such as β -carotene, capsanthin, violaxanthin, lutein, zeaxanthin, capsorubin, antheraxanthin, and others [3,16,17]. The excellent antioxidant properties of these compounds, which protect cells from free radicals by scavenging reactive oxygen species (ROS), are due to the presence of a conjugated double bond system in their chemical structure [4]. Peppers are also rich in phenolic compounds, mostly flavonoids and phenolic acid derivatives that have health-promoting effects, as they protect the body from the damage produced by oxidative agents [18,19]. Among phenolics, quercetin is one of the most potent compounds. It is a flavonol with anticancer, antiviral, antiprotozoal, anti-hypertensive, anti-inflammatory and antimicrobial effects [20], also employed for the treatment of eye and cardiovascular diseases, arthritis, allergic, metabolic, and inflammatory disorders [21–24].

Inflammation is a defence mechanism of the body against detrimental stimuli including pathogens (bacteria, viruses, and parasites) and/or toxins released by pathogens, trauma, heat, or damaged cells [25]. The immune system eliminates the harmful agents responsible for tissue damage and initiates the healing process to restore homeostasis. The unconstrained acute inflammatory response could evolve in chronic inflammation, which may increase the risk for different chronic diseases, such as diabetes, cardiovascular diseases, cancer, arthritis, and joint diseases [26]. Immune cells resident in the damaged tissues, mostly resident macrophages and dendritic cells, recognize the noxious agents thanks to pattern recognition receptors on their cell surface. Subsequently, inflammatory signaling pathways (i.e., NF- κ B signaling cascade) are activated with consequent changes in vascular permeability, leukocytes chemotaxis to the site of damage, and the release of inflammatory mediators [27].

Under inflammatory conditions, triggered immune cells undergo metabolic shifts to fulfil the new cellular demands of energy and biomolecules [28,29]. Metabolites produced could act as signaling molecules or be used for the synthesis of inflammatory mediators. In lipopolysaccharide (LPS)-triggered macrophages, as a consequence of the rewired Krebs cycle, there is an accumulation of different metabolites among which is citrate [30]. Citrate represents a key signal for the activation and functions of immune cells and has a central role in the inflammatory cascade [31]. In fact, citrate contributes to the synthesis of chemical mediators of inflammation, namely ROS, nitric oxide (NO), and prostaglandin E₂ (PGE₂), and can affect cytokine secretion [32–34]. The inhibition of the citrate pathway, composed of citrate, mitochondrial citrate carrier and ATP citrate lyase (ACLY), by synthetic [35,36] and natural compounds, such as hydroxycitric acid (HCA) [18,34,37], counteracts inflammation and oxidative stress.

Non-steroidal anti-inflammatory drugs (NSAIDs) are commonly used to control inflammation by inhibition of PGE₂ biosynthesis, but they can cause serious side effects.

There is ongoing research for new anti-inflammatory compounds that can be associated with or can replace NSAIDs and can act on other targets of the inflammatory cascade. Plant secondary metabolites have attracted the interest of several researchers over the last few years for their numerous biological activities including anti-inflammatory properties, especially phenolic compounds and quercetin. Unfortunately, they are generally poorly soluble and bioavailable, and chemically unstable. The incorporation of bioactive compounds or extracts from plants into nanocarriers has been shown to protect from degradation, and to increase solubility and bioavailability [38–40]. For example, the nanoencapsulation of ACLY inhibitor HCA into liposomes enhanced its anti-inflammatory activity by increasing its intracellular uptake [41]. Nanocarriers, such as phospholipid vesicles, represent a huge amount of promise for drug delivery, since they allow the successful treatment of diseases with minimal side effects. They are nanosized particles with elevated surface area to volume ratio. Thanks to their versatile and tunable composition and structure, phospholipid vesicles improve pharmacokinetics, pharmacodynamics, solubility and stability of drugs, decrease their toxicity, and guarantee site-specific delivery [42,43]. Intensive research has been devoted to the development of new classes of phospholipid vesicles that are capable of enhancing the efficacy of the payload in the skin, such as transfersomes, ethosomes and PEVs (Penetration Enhancer containing Vesicles) [44].

In a previous work [45], we conducted a comprehensive phytochemical profiling of a methanolic extract of a new pepper genotype deriving from an original crossing combination between Habanero white, from *C. chinense*, and *C. annuum*. Furthermore, we demonstrated the anti-inflammatory properties of the extract, as it was able to reduce ROS levels in LPS-activated cells. In the present study, we investigated the anti-inflammatory activity of this white *Capsicum* extract incorporated into phospholipid vesicles to evaluate a potential enhancement of its biological activity.

2. Materials and Methods

2.1. Materials

Phospholipon90G (>90% phosphatidylcholine; P90G) was purchased from Lipoid GmbH (Ludwigshafen, Germany). Propylene glycol was purchased from Galeno (Carmignano, Prato, Italy). LC-MS grade acetonitrile was obtained from Sigma-Aldrich (Milan, Italy). Formic acid (99%), used as additive of aqueous mobile phase, was purchased from Carlo Erba Srl (Milan, Italy). Deionized water was obtained with a Milli-Q RG system (Millipore, Bedford, MA, USA).

L-glutamine, penicillin/streptomycin solution, lipopolysaccharide from *Salmonella enterica* serotype typhimurium (LPS), fetal bovine serum (FBS), Roswell Park Memorial Institute 1640 (RPMI 1640), and phorbol 12-myristate 13-acetate (PMA) were purchased from Sigma-Aldrich (St. Louis, MO, USA). Furthermore, 6-Carboxy-2',7'-Dichlorodihydrofluorescein Diacetate (DCF-DA) and 4-amino-5-methylamino-2',7'-difluorofluorescein diacetate (DAF-FM Diacetate) were obtained from Thermo Fisher Scientific (San Jose, CA, USA).

2.2. Extract Preparation

In a previous work [45], we reported the preparation of an extract from a pepper species obtained from a specific breeding program. The white *Capsicum* extract was prepared by optimizing the protocol of Wahyuni et al. [46]: 3 mL of methanol was added to 0.5 g of lyophilized peppers; the sample was sonicated for 15 min (25 °C) in a Sonorex Super RK 100/H sonicator (Bandelin electronic, Berlin, Germany); and the methanolic extract was filtered through 0.20 µm nylon filters, which are recommended for methanolic matrices as they do not procure changes in flow rate or bubble point of the membrane, nor visible chemical attack. The extract was subjected to solvent evaporation (Laborota 4000 efficient, Heidolph, Schwabach, Germany).

2.3. Vesicle Preparation and Characterization

For the preparation of conventional liposomes, P90G and white *Capsicum* extract were weighed in a glass vial and dispersed in water (Table 1). The dispersion was sonicated (10 cycles 5 s on/2 s off + 10 cycles 3 s on/2 s off; 13 microns of probe amplitude) with a Soniprep 150 (MSE Crowley, London, UK). For the preparation of Penetration Enhancer containing Vesicles (PEVs), propylene glycol (PG) was dispersed in water along with P90G and the extract (Table 1). Thereafter, the dispersion was sonicated as reported above for the preparation of liposomes.

Table 1. Composition of vesicle formulations.

Formulation	P90G ¹	PG ²	WC ³ Extract	H ₂ O
Empty liposomes	120 mg			1 mL
WC liposomes	120 mg		2 mg	1 mL
Empty PG-PEVs	120 mg	0.05 mL		0.95 mL
WC PG-PEVs	120 mg	0.05 mL	2 mg	1 mL

¹ P90G, phospholipid; ² PG, propylene glycol; ³ WC, white *Capsicum*.

For comparative purposes, empty vesicles and empty PG-PEVs were prepared following the above procedure, but without the addition of white *Capsicum* extract (Table 1).

The average diameter, polydispersity index (PI, a measure of the width of size distribution), and zeta potential of the vesicles were determined via dynamic and electrophoretic light scattering using a Zetasizer nano-ZS (Malvern Panalytical, Worcestershire, UK). Samples ($n > 10$) were diluted with water (1:100) and analyzed at 25 °C.

The stability of the formulations was evaluated by monitoring vesicle mean size, PI, and zeta potential over three months at 4 ± 2 °C.

The vesicle dispersions were purified from the non-incorporated active compounds by dialysis. Each sample (1 mL) was loaded into Spectra/Por[®] tubing (12–14 kDa MW cut-off; Spectrum Laboratories Inc., DG Breda, The Netherlands), previously rinsed in water, and dialyzed against water (2 L) for 2 h to allow the removal of the non-incorporated components of the extract. Unpurified and purified vesicles were disrupted with methanol (1:100) [47,48] and dried under N₂ flow. The solid residues were redissolved in 80 µL of MeOH and filtered through 0.20 µm nylon filters before injection in a liquid chromatography coupled to a tandem mass spectrometry (LC-MS/MS) system (see Section 2.7). The content of capsaicin was determined, and the entrapment efficiency (E) was calculated as the percentage of the amount of capsaicin in purified vesicles, according to the following Formula (1):

$$E = \left(\frac{\text{amount of Capsaicin in purified vesicles}}{\text{amount of Capsaicin in unpurified vesicles}} \right) \times 100 \quad (1)$$

2.4. Cell Culture and Treatments

Human monoblastic leukemia U937 cell line (HTL94002-Interlab Cell Line Collection, IRCCS San Martino Hospital, Genoa, Italy) was maintained in RPMI 1640 medium supplemented with 10% (v/v) fetal bovine serum, 2 mM L-glutamine, 100 U/mL penicillin, and 100 µg/mL streptomycin at 37 °C in 5% CO₂ in a water-saturated atmosphere. U937 cells were differentiated to macrophages by using 10 ng/mL PMA. U937/PMA cells were treated with 5 or 25 µg/mL free white *Capsicum* (WC) extract, WC liposomes or WC PG-PEVs (both non-dialyzed), and, where appropriate, stimulated with 200 ng/mL LPS. The vesicle formulations were sterilized by using 0.22 µm syringe filters (STARLAB, Milan, Italy).

2.5. Cytotoxicity Assay

Cells were cultured into 96-well plates (5×10^4 cells/well) and treated with free WC, WC liposomes or WC PG-PEVs (both non-dialyzed). The effects on the U937 cell number

were determined using a Millipore Scepter™ handheld automated cell counter (Merck Millipore, Darmstadt, Germany) after 48 h of incubation, according to the manufacturer's instructions.

2.6. ROS and NO Detection

To evaluate ROS and NO levels, U937 cells were seeded at the density of 1×10^5 cells/well, differentiated with 10 ng/mL PMA, and triggered by 200 ng/mL of LPS in both the presence and absence of free WC, WC liposomes or WC PG-PEVs (both non-dialyzed).

After 24 h, intracellular total ROS were detected by using DCF-DA, a chemically reduced form of fluorescein used as a probe for ROS in cells. After cleavage of the acetate groups by intracellular esterases and oxidation, the non-fluorescent H₂DCFDA is converted to highly fluorescent 2',7'-dichlorofluorescein (DCF, Ex/Em: ~492–495/517–527 nm) [49]. At the end of treatments, the cell culture medium was removed, and DCF-DA was added to the cell pellet at the final concentration of 10 μM. After 30 min incubation at 37 °C in the dark, 100 μL of samples were transferred into a black microtiter plate in triplicate and the fluorescence was revealed using the GloMax plate reader (Promega, Madison, WI, USA).

NO concentrations were measured by using DAF-FM Diacetate, after 24 h from the beginning of treatments. DAF-FM diacetate is non-fluorescent until it reacts with NO to form a fluorescent benzotriazole (Ex/Em of DAF-FM: ~495/515 nm) [49]. U937/PMA cells were incubated with 2.24 μM DAF-FM diacetate for 30 min in the dark. The fluorescence was measured using GloMax plate reader. Each experiment was performed in triplicate.

2.7. LC-MS/MS Analysis

To quantify the cellular uptake of the white *Capsicum* extract, U937/PMA cells were seeded into 6-well plates at a density of 2.5×10^5 cells/well, treated with 5 μg/mL and 25 μg/mL of extract (as free or incorporated in liposomes and PG-PEVs) for 24 h, and pelleted at 1200 rpm for 5 min. Supernatants were removed. To pull out the extract, 500 μL of 40% MeOH with 0.1% (v/v) formic acid was added to the cells, which were lysed by sonication (1 min on/1 min off, 10 min total), mixed, and placed on ice for 15 min. Lysates were then centrifuged at 1500 rpm for 5 min. Supernatants were collected for LC-MS analysis. To ensure that all of the extract was pulled out from cells, another amount of 250 μL of 40% MeOH with 0.1% (v/v) formic acid was added to the cell pellets and suspended again. After 15 min on ice, the suspensions were centrifuged at 14,000 rpm for 5 min, and all supernatants were pooled together [20,41]. The supernatants were dried with vacuum-centrifugation using a Concentrator plus (Eppendorf AG, Hamburg, Germany). Before the cellular uptake quantification, samples were reconstituted with 80 μL of LC-MS grade MeOH, filtered through 0.20 μm nylon filters and 15 μL aliquots were injected in the LC-MS system. The protein concentration in each sample was determined by the Bradford assay [50], and cell lysates were checked to verify success of the lyses step and to normalize multiple samples for side-by-side comparison.

Capsaicin content, for both entrapment efficiency evaluation and intracellular uptake quantification, was assayed using an HPLC system coupled with a linear ion trap quadrupole (LTQ) mass spectrometer equipped with an electrospray ionization source, both from Thermo Fisher Scientific (Bremen, Germany). The chromatographic separation was performed on a reversed-phase Luna C18 (2) column (150 × 4.6 mm internal diameter, 3.0 μm particle size, 100 Å pore size from Phenomenex Torrance, CA, USA). The mobile phase consisted of water containing 0.1% v/v of formic acid (solvent A) and acetonitrile (solvent B). The gradient elution program was adapted from previous works [45,51] as follows: from 0% B and increased to 35% B over 5 min. After holding at 35% for 5 min, mobile phase B was increased to 40% over 5 min. Then, the composition was linearly increased to 85% B in 15 min, to return to initial conditions at min 32.0. The initial conditions were held for 8 min in order to recondition the column. The sample injection volume was set at 15 μL and the flow rate was 0.8 mL min⁻¹, with a 4:1 post-column split, thus allowing 200 μL/min to enter the ESI source, operating in positive ionization mode. MS analyses were performed by using product ion scan mode. Precursor ion at

m/z 306.0, corresponding to the protonated ion of capsaicin $[M + H]^+$, was selected for the screening of capsaicin in the samples of interest. All fragment ions, obtained by Collision Induced Dissociation (CID) of the precursor ion, were scanned in the range 80–650 m/z . Pure nitrogen (99.996%) was used as sheath gas, at a flow of 60 arbitrary units (a.u.). The following parameters were applied for MS ionization: needle voltage, +4.50 kV; capillary voltage, +13.0 V; and capillary temperature, 350 °C. An isolation window of 6 m/z and a collision energy of 5.2 eV (15%) were used for precursor ion fragmentation. All the data were exported and processed with Xcalibur 2.2 software (Thermo Fisher Scientific) [52].

2.8. Statistical Analysis of Data

Statistical significance of differences was determined by using one-way analysis of variance (ANOVA) followed by Dunnett's test or Tukey's post hoc test for multiple comparisons. For LC-MS analysis, Student's t -test was used. Results are shown as mean \pm standard deviation (S.D.) of three independent experiments. The statistical method employed is detailed in each figure legend. Asterisks indicate the significance: * $p < 0.05$, ** $p < 0.01$, and *** $p < 0.001$. When Tukey's test was performed, different letters in figures denote significant differences between treatments at $p < 0.05$.

3. Results

3.1. Vesicle Design and Characterization

The present study aimed to develop a vesicular formulation for the delivery of white *Capsicum* extract to the skin. Two types of phospholipid vesicles, liposomes, and PEVs, were produced to enhance the bioavailability of the extract components through nanoincorporation and facilitate the interaction with cells to achieve an increased intracellular accumulation and consequent biological response.

In order to discriminate between the activity of the white *Capsicum* extract and the effect of the nanocarriers, WC-loaded liposomes and PG-PEVs were prepared, characterized, and compared with empty liposomes, empty PG-PEVs, and free WC extract.

Light scattering results, summarized in Table 2, showed that empty liposomes were small (~100 nm). These liposomes were also characterized by slight inhomogeneity (PI 0.36) and negative zeta potential (−16 mV), due to the charge carried by P90G. Quite similar results were obtained for empty PG-PEVs (Table 2). It is worth noting that, for both liposomes and PEVs, the incorporation of the extract induced an increase in size (115 nm, $p < 0.05$; Table 2), with a significant improvement of the homogeneity of the systems, as the polydispersity index values were around 0.27 ($p < 0.05$; Table 2). No relevant variations of the zeta potential values were detected ($p > 0.05$; Table 2).

Table 2. Characteristics of empty and white *Capsicum* (WC) loaded vesicles: mean diameter (MD), polydispersity index (PI), zeta potential (ZP), and entrapment efficiency (E). Each value represents the mean \pm S.D. ($n > 10$). *, ° values statistically different ($p < 0.05$) from empty liposomes and empty PG-PEVs, respectively.

Formulation	MD nm \pm SD	PI \pm SD	ZP mV \pm SD	E % \pm SD
Empty liposomes	104 \pm 9.6	0.36 \pm 0.04	−16 \pm 2.5	–
WC liposomes	* 114 \pm 7.1	* 0.27 \pm 0.01	−14 \pm 1.5	Capsaicin 86 \pm 6.0
Empty PG-PEVs	102 \pm 10.7	0.38 \pm 0.05	−16 \pm 3.0	–
WC PG-PEVs	° 115 \pm 7.6	° 0.28 \pm 0.02	−18 \pm 5.1	Capsaicin 89 \pm 2.2

The entrapment efficiency of the vesicles was calculated based on the content of capsaicin, one of the most abundant components of the white *Capsicum* extract, widely responsible for the pungency of the pepper fruits [53]. The entrapment efficiency was >85% for both vesicle systems ($p > 0.05$; Table 2), which points to their great capability of loading a complex, multicomponent plant extract, such as the white *Capsicum* extract. These values were higher than those obtained in other studies available in the literature, which investigated the encapsulation of black pepper extract [54].

The stability of the white *Capsicum* formulations was evaluated for three months by monitoring the mean diameter, PI, and zeta potential of the vesicles. The results showed no statistically significant variations of the three examined parameters ($p > 0.05$; Figure 1).

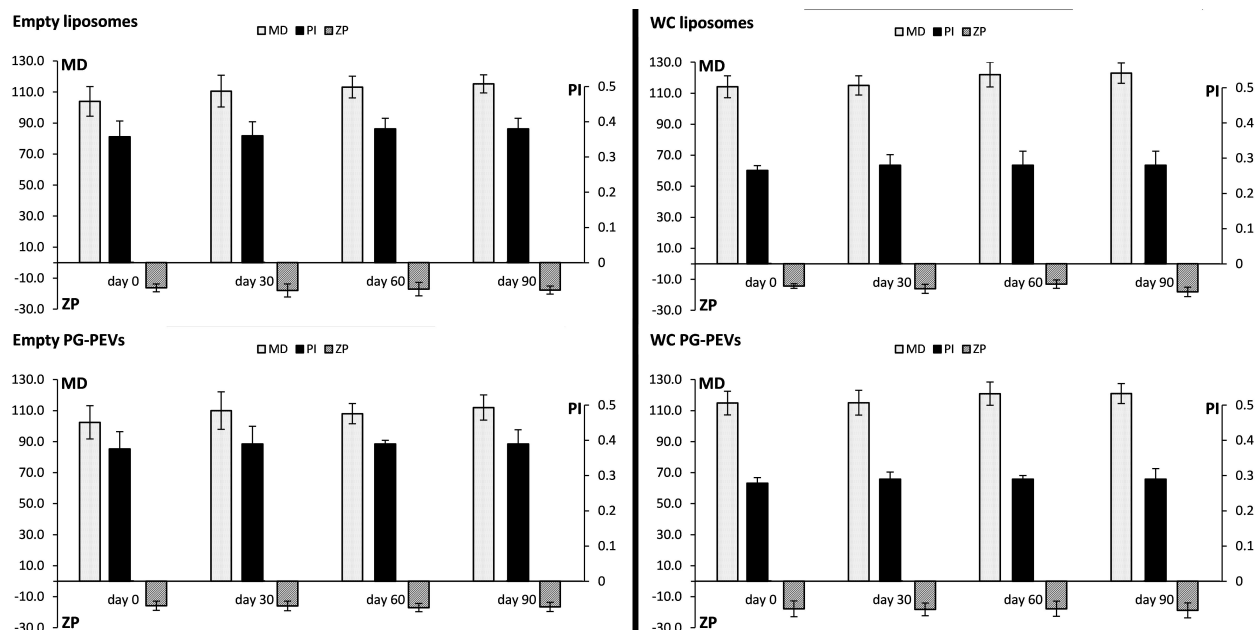


Figure 1. Long-term stability of the vesicle formulations assessed by monitoring mean diameter (MD), polydispersity index (PI), and zeta potential (ZP) for 90 days.

3.2. Effect of WC Nano Incorporation in Phospholipid Vesicles on Cell Viability

The effect of the white *Capsicum* extract, either free or incorporated in liposomes and PG-PEVs, was assessed in cells. The exposure to free WC for 48 h did not affect cell viability, as no differences from the control (i.e., untreated cells = 0 WC) were detected at the two tested concentrations (Figure 2A).

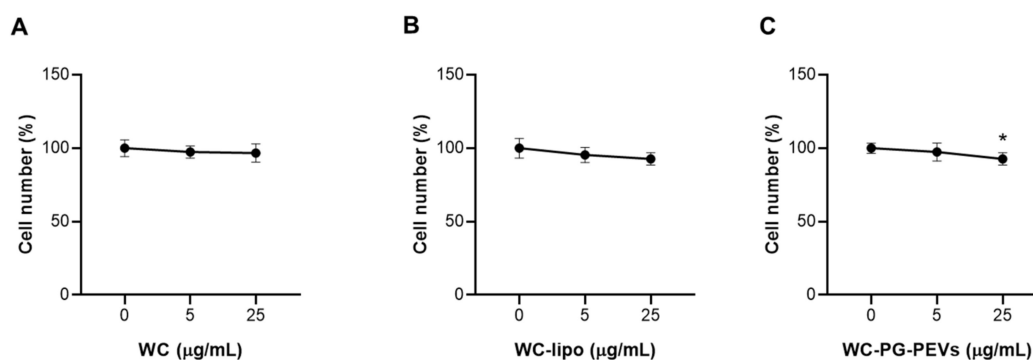


Figure 2. Effect of free WC (A), WC liposomes (B), and WC PG-PEVs (C) on cell viability. U937 cells were counted after 48 h exposure to WC, WC liposomes, and WC PG-PEVs (5 and 25 µg/mL). Means \pm S.D. of three replicate independent experiments are shown. Statistical significance of differences was determined by one-way ANOVA followed by Dunnett's test; * $p < 0.05$. Abbreviations: WC, free WC; and WC-lipo, WC liposomes.

The incorporation of the extract in both liposomes and PG-PEVs had no effect on the number of viable cells (Figure 2B,C). In particular, WC liposomes did not affect cell viability at both tested concentrations in a significant manner (Figure 2B), while at 25 µg/mL, WC PG-PEVs decreased the cell number by about 10% with respect to untreated cells

(Figure 2C), but they cannot be considered toxic. Thus, equivalent doses of free and vesicular WC in both liposomes and PG-PEVs were safe for U937 cells.

3.3. Effect of WC Nanoincorporation in Phospholipid Vesicles on ROS Production

In LPS-triggered U937/PMA cells, the white *Capsicum* extract reduced intracellular ROS levels of about 8% only at the highest tested concentration (25 $\mu\text{g}/\text{mL}$) (Figure 3) [45]. No effect on ROS production was observed when cells were treated with the lower concentration (5 $\mu\text{g}/\text{mL}$), as ROS levels were approximately the same as in cells activated with LPS (Figure 3) [45]. The aim of this study was to exploit phospholipid vesicles to enhance the bioavailability of the bioactive compounds present in the white *Capsicum* extract and to facilitate the entry into cells in order to increase the biological response, specifically the anti-inflammatory activity. To this end, we evaluated the effect of WC liposomes and WC PG-PEVs on ROS production induced by LPS in U937/PMA cells. As shown in Figure 3, empty liposomes and empty PG-PEVs did not affect ROS levels after 24 h treatment, in both the presence and absence of LPS. ROS levels increased only when LPS was added, with values around 30% in all the sets of experiments (Figure 3). When WC was incorporated in PG-PEVs, a reduction of about 20% in ROS levels was recorded in cells treated with 25 $\mu\text{g}/\text{mL}$ of WC PG-PEVs; 5 $\mu\text{g}/\text{mL}$ of WC PG-PEVs was not enough to influence ROS production induced by LPS.

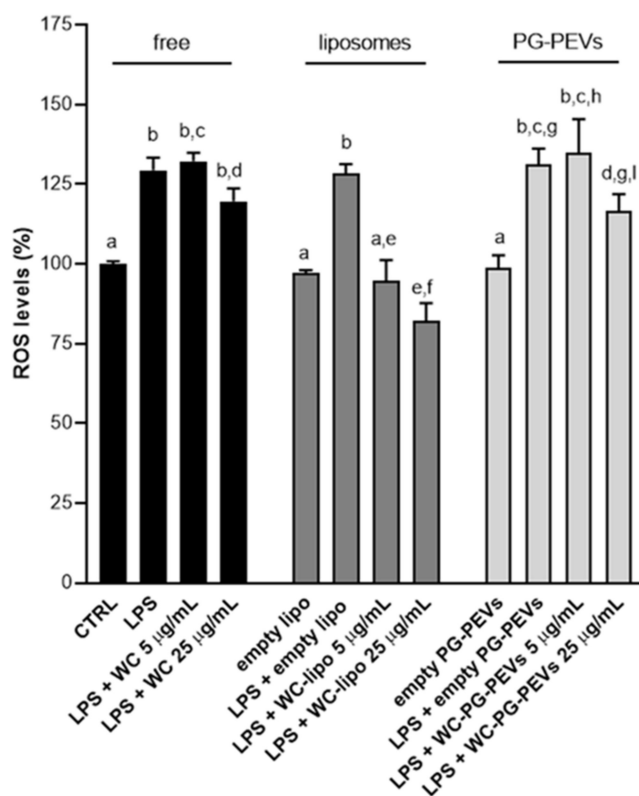


Figure 3. Effect of free WC, WC liposomes, and WC PG-PEVs on ROS production. U937/PMA cells were activated by LPS in both the presence and absence of WC, WC liposomes, and WC PG-PEVs (5 and 25 $\mu\text{g}/\text{mL}$). After 24 h, ROS levels were quantified. Means \pm S.D. of four replicate independent experiments are shown. According to one-way ANOVA, differences were significant ($p < 0.05$). Thus, Tukey's test for multiple comparisons was performed and different letters above the bars indicate significant differences between treatments at $p < 0.05$. Abbreviations: CTRL, untreated cells; WC, free WC; empty lipo, empty liposomes; and WC-lipo, WC liposomes.

When the cells were treated with WC liposomes, a dose-dependent reduction and a re-establishment of physiological conditions were observed (Figure 3). In more detail, in the presence of 5 µg/mL of WC liposomes, ROS levels were the same as in both unstimulated (CTRL) and empty liposomes-treated cells, which means that the effect of LPS was abolished (Figure 3). Furthermore, at the higher tested concentration (25 µg/mL), WC liposomes reduced ROS levels below physiological values (Figure 3). Hence, liposomal formulation was proved to be the best delivery system for WC to control inflammation induced by LPS by hindering ROS production.

3.4. Effect of WC Nanoincorporation in Phospholipid Vesicles on NO Levels

In consideration of the remarkable ability of WC to reduce ROS levels, we also evaluated the effect of free WC, WC liposomes, and WC PG-PEVs on NO, which has a relevant role in the onset and progression of inflammation. As shown in Figure 4, WC, both in the free and vesicular forms, was able to reduce NO levels in a dose-dependent manner, but not always in a significant way. In particular, free WC restored the physiological conditions, since NO levels were lower than those of LPS-triggered cells (Figure 4). However, even if 5 µg/mL of free WC reduced NO levels of about 20%, differences between “LPS” and “LPS + WC 5 µg/mL” were not statistically significant according to Tukey’s post hoc test (Figure 4). A significant reduction was observed at the higher tested concentration (LPS + WC 25 µg/mL; Figure 4) in comparison to LPS-activated cells. Both empty liposomes and PG-PEVs induced NO release, even if differences between “CTRL” and “empty lipo” were not statistically significant (Figure 4). Empty PG-PEVs had a more marked effect on rising NO levels (Figure 4). WC liposomes decreased NO production in a significant manner of about 15 and 20% at 5 and 25 µg/mL, respectively, in comparison to LPS-stimulated cells. The treatment with 25 µg/mL of WC PG-PEVs significantly inhibited LPS-induced NO increase by approximately 15% with respect to cells treated with LPS only (Figure 4). The decrease in NO levels induced by 5 µg/mL of WC PG-PEVs was around 8%, but not significant (Figure 4). Overall findings suggested that WC incorporated in liposomes had a stronger ability to reduce NO production than PG-PEVs.

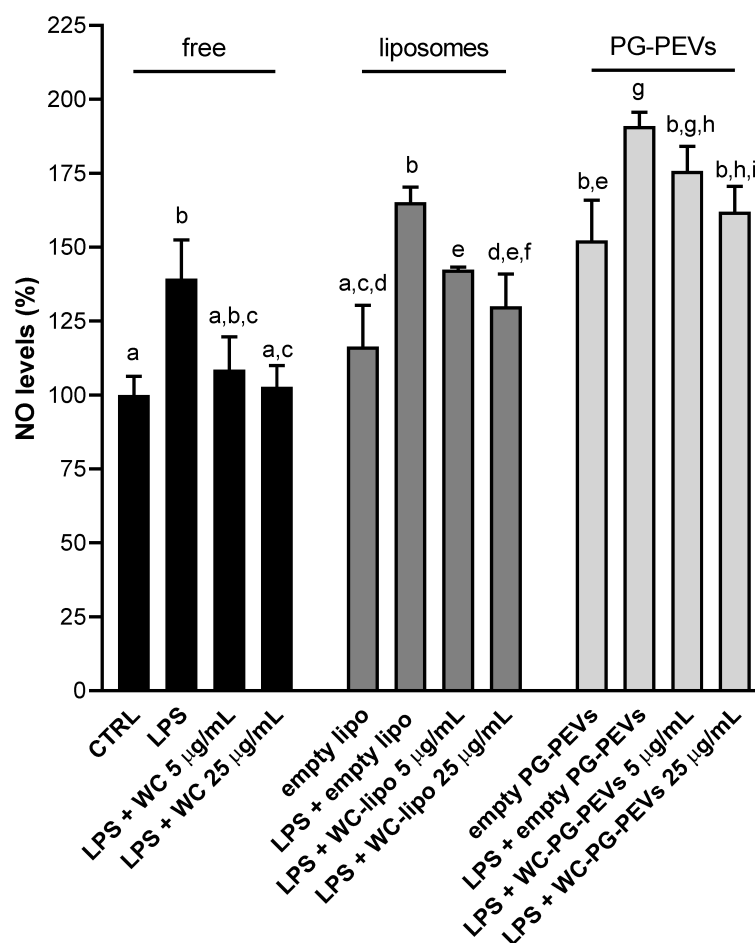


Figure 4. Effect of free WC, WC liposomes, and WC PG-PEVs on NO production. LPS-triggered U937/PMA cells were treated with 5 and 25 µg/mL of WC, WC liposomes, and WC PG-PEVs. After 24 h, NO levels were quantified. Means ± S.D. of four replicate independent experiments are shown. Since differences were statistically significant (one-way ANOVA, $p < 0.05$), Tukey's test was performed and different letters above the bars indicate significant differences between treatments at $p < 0.05$. Abbreviations: CTRL, untreated cells; WC, free WC; empty lipo, empty liposomes; and WC-lipo, WC liposomes.

3.5. Intracellular Accumulation of White Capsicum Extract

The intracellular uptake of the white *Capsicum* extract delivered by the phospholipid vesicles was assessed and compared with the uptake values obtained after incubation of cells with the free extract. LC-MS/MS analyses were carried out and capsaicin was used as marker compound for relative quantification purposes. Two different concentrations of the extract were tested, 5 µg/mL and 25 µg/mL. The results obtained clearly showed that the intracellular uptake of the extract was higher when it was formulated in liposomes and PG-PEVs (Figure 5). Indeed, the amount of capsaicin detected within the cells increased (~2 fold) when the extract was incorporated into the vesicles, rather than in solution, at the two tested concentrations. Among the investigated formulations, slightly higher values of intracellular accumulation were obtained for WC liposomes (~2 and 2.5 fold vs. free extract) compared to WC PG-PEVs (~1.8 and 2.3 fold vs. free extract).

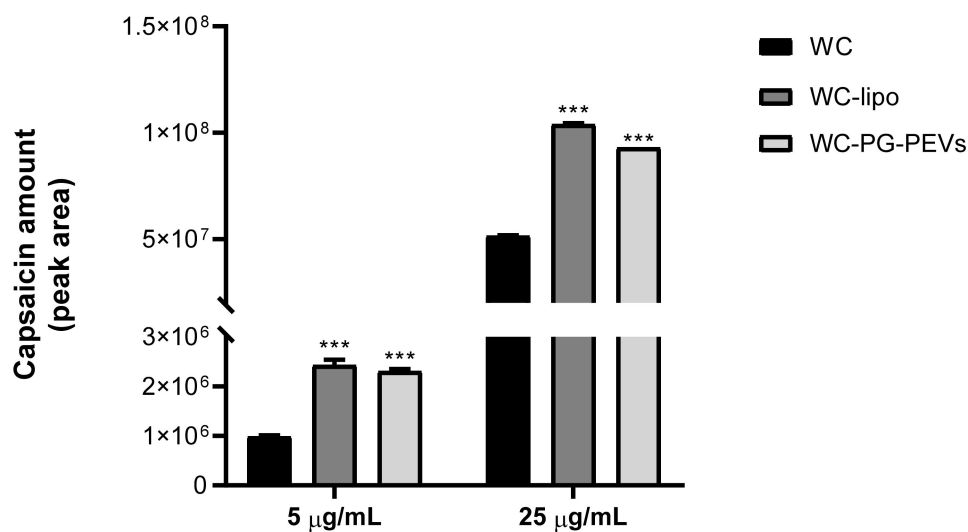


Figure 5. Amount of white *Capsicum* extract, reported as an area of the chromatographic peak of capsaicin, accumulated in U937/PMA cells as free or incorporated into liposomes and PG-PEVs. Two different concentrations of the extract were tested (5 µg/mL and 25 µg/mL). Results are reported as means of three independent replicates ± S.D. ($n = 3$). Statistical significance of differences was determined by using Student's *t*-test, *** $p < 0.001$ (5 µg/mL WC-lipo vs. 5 µg/mL WC, 5 µg/mL WC PG-PEVs vs. 5 µg/mL WC, 25 µg/mL WC-lipo vs. 25 µg/mL WC, and 25 µg/mL WC PG-PEVs vs. 25 µg/mL WC). Abbreviations: WC, free WC; and WC-lipo, WC liposomes.

It is worth noting that an approximate 50-fold increase in capsaicin content was detected in cells treated with the higher WC concentration with respect to the lower concentration (25 vs. 5 µg/mL), which did not correspond to the only 5-fold more concentrated extract samples. This could be due to a matrix effect, which gave rise to a higher suppression of the capsaicin signal within the less concentrated sample (5 µg/mL) [55].

These results indicate that liposomes were more efficient than PG-PEVs in transporting the white *Capsicum* extract into the cells and promoting the accumulation of its components into the cytoplasm. This might explain the superior anti-inflammatory activity of WC liposomes, as shown by ROS and NO inhibition studies.

4. Discussion

Capsicum peppers are recognized as a source of capsaicinoids, phenolic compounds, and antioxidants. Epidemiological studies have shown the benefits of pepper consumption in reducing mortality and improving the quality of health [56]. Many nutraceutical benefits are associated with the consumption of chili peppers, including anti-inflammatory [57], analgesic [58], blood glucose regulation [59], and antioxidant benefits [60,61]. *Capsicum* peppers are frequently attributed functional properties mainly because these foods are sources of carotenoids, vitamin C, vitamin E, alkaloids, flavonoids, and capsaicinoids, which are the predominant phenolic compounds [56]. However, the levels of these bioactive compounds can vary in relation to various factors, such as genotype, stage of maturation, and conditions of growth and harvest [56].

In the present work, the *in vitro* efficacy of different formulations (free form and vesicle-based) of a methanolic extract of a new pepper genotype in regulating inflammatory responses was evaluated. Liposomal encapsulation strategy has been demonstrated in various studies to improve the therapeutic indices and pharmacological activities of conventional drug formulations [41,62]. In addition, the use of lipid-based nanoparticles has become increasingly popular due to their ability to alter the biopharmacological properties of entrapped hydrophobic drugs (e.g., by improving drug solubility, dissolution kinetics, and bioavailability) [63–65].

We investigated the ability of the white *Capsicum* extract to inhibit ROS and NO inflammatory mediators using a sensitive LPS-stimulated macrophage model. ROS and NO are two radical species with well-defined roles in the onset and progression of the inflammatory process. ROS, both as byproducts of numerous enzymatic reactions in different cell compartments, and as generated by specific enzymes such as NADPH oxidase, mediate both physiological and pathological signal transduction [66,67]. NO is a molecule used as a signaling or toxic agent between cells. It plays physiological roles in mammals, acting as a vascular relaxant, neurotransmitter, and inhibitor of platelet aggregation. NO is also generated during immune and inflammatory responses [68]. Therefore, as inflammatory mediators, ROS and NO are important targets in the treatment of inflammatory diseases.

In a previous work [45], we evaluated the anti-inflammatory activity of raw white *Capsicum* extract, the results showing that WC was not toxic to U937 cells at 5 and 25 µg/mL concentrations. In the present study, similar results of non-toxicity were obtained when the cells were treated with WC incorporated into phospholipid vesicles (Figure 2).

Furthermore, liposome incorporation strongly improved the ability of WC to dampen ROS and NO levels in a dose-dependent fashion. Indeed, we observed a good efficiency in bringing ROS back to levels of unstimulated cells, already at the lower tested concentration (5 µg/mL) and an even more marked efficacy was detected at the higher tested concentration of WC (25 µg/mL) (Figure 3). In addition, we found that 5 µg/mL of WC liposomes reduced NO levels in LPS-activated U937/PMA cells in a similar percentage to free WC, but in a statistically significant way. At the concentration of 25 µg/mL, the reduction was more marked, so as to bring NO levels back almost to physiological levels (Figure 4). On the other hand, the incorporation into PG-PEVs did not significantly strengthen the anti-inflammatory properties of WC.

The delivery of WC by liposomes was found to facilitate the transport of the extract components across the cell membrane and their accumulation into the cytoplasm, as demonstrated by a double amount of capsaicin detected within the cells after the exposure to WC liposomes in comparison with WC solution, and slightly higher than that obtained with PG-PEVs (Figure 5). This was reflected in a dose-dependent reduction mostly in ROS levels stimulated by LPS and a re-establishment of physiological conditions.

5. Conclusions

To the best of our knowledge, this is the first study that reports the incorporation of the new white *Capsicum* genotype extract into phospholipid vesicles and the assessment of its anti-inflammatory activity in cells. The results showed the potential of liposomes in facilitating the entrance of the extract components into cells and the consequent counteraction of ROS and NO deleterious intracellular damage. Further research will be needed to investigate the mechanisms through which white *Capsicum* extract loaded liposomes work, with the identification of the molecular pathways involved in the observed anti-inflammatory activity.

Author Contributions: Conceptualization, A.V. and G.M.; methodology, I.P., A.S., S.T., A.V., V.I., C.C. and G.B.; software, A.S. and M.D.L.; validation, all authors; investigation, I.P., S.T., A.V., C.C., V.I. and M.A.A.; resources, A.V., G.M., C.C. and V.I.; data curation, all authors; writing—original draft preparation, all authors; writing—review and editing, A.S., M.D.L., C.C., V.I. and A.V.; funding acquisition, A.V., V.I. and G.M. All authors have read and agreed to the published version of the manuscript.

Funding: Funding for Basic Research from the Italian Ministry of Education, University and Research (grant number 102050101) to Vittoria Infantino and Antonio Vassallo.

Institutional Review Board Statement: Not applicable.

Informed Consent Statement: Not applicable.

Data Availability Statement: The data presented in this study are available in article.

Acknowledgments: The Authors would like to thank Bioinnova srls for giving them the opportunity to study and characterize the white *Capsicum* genotype, and Angelica Rebecca Zizzamia for her support in LC-MS/MS analyses.

Conflicts of Interest: The authors declare no conflict of interest.

References

1. Naves, E.R.; de Ávila Silva, L.; Sulpice, R.; Araújo, W.L.; Nunes-Nesi, A.; Peres, L.E.P.; Zsögön, A. Capsaicinoids: Pungency beyond *Capsicum*. *Trends Plant Sci.* **2019**, *24*, 109–120. [[CrossRef](#)] [[PubMed](#)]
2. Batiha, G.E.S.; Alqahtani, A.; Ojo, O.A.; Shaheen, H.M.; Wasef, L.; Elzeiny, M.; Ismail, M.; Shalaby, M.; Murata, T.; Zaragoza-Bastida, A.; et al. Biological properties, bioactive constituents, and pharmacokinetics of some *Capsicum* spp. and capsaicinoids. *Int. J. Mol. Sci.* **2020**, *21*, 5179. [[CrossRef](#)] [[PubMed](#)]
3. Villa-Rivera, M.G.; Ochoa-Alejo, N. Chili pepper carotenoids: Nutraceutical properties and mechanisms of action. *Molecules* **2020**, *25*, 5573. [[CrossRef](#)] [[PubMed](#)]
4. Baenas, N.; Belović, M.; Ilic, N.; Moreno, D.A.; García-Viguera, C. Industrial use of pepper (*Capsicum annum* L.) derived products: Technological benefits and biological advantages. *Food Chem.* **2019**, *274*, 872–885. [[CrossRef](#)] [[PubMed](#)]
5. Srinivasan, K. Biological activities of red pepper (*Capsicum annum*) and its pungent principle capsaicin: A review. *Crit. Rev. Food Sci. Nutr.* **2016**, *56*, 1488–1500. [[CrossRef](#)] [[PubMed](#)]
6. Adaszek, Ł.; Gadomska, D.; Mazurek, Ł.; Łyp, P.; Madany, J.; Winiarczyk, S. Properties of capsaicin and its utility in veterinary and human medicine. *Res. Vet. Sci.* **2019**, *123*, 14–19. [[CrossRef](#)]
7. Ilie, M.; Caruntu, C.; Tampa, M.; Georgescu, S.-R.; Matei, C.; Negrei, C.; Ion, R.-M.; Constantin, C.; Neagu, M.; Boda, D. Capsaicin: Physicochemical properties, cutaneous reactions and potential applications in painful and inflammatory conditions (Review). *Exp. Ther. Med.* **2019**, *18*, 916–925. [[CrossRef](#)] [[PubMed](#)]
8. Afroz, M.; Akter, S.; Ahmed, A.; Rouf, R.; Shilpi, J.A.; Tiralongo, E.; Sarker, S.D.; Göransson, U.; Uddin, S.J. Ethnobotany and antimicrobial peptides from plants of the *Solanaceae* family: An update and future prospects. *Front. Pharmacol.* **2020**, *11*, 565. [[CrossRef](#)]
9. Tavares, W.R.; Barreto, M.D.C.; Seca, A.M.L. Aqueous and ethanolic plant extracts as bio-insecticides—Establishing a bridge between raw scientific data and practical reality. *Plants* **2021**, *10*, 920. [[CrossRef](#)] [[PubMed](#)]
10. Zheng, J.; Zhou, Y.; Li, Y.; Xu, D.P.; Li, S.; Li, H. Bin Spices for prevention and treatment of cancers. *Nutrients* **2016**, *8*, 495. [[CrossRef](#)] [[PubMed](#)]
11. Chapa-Oliver, A.M.; Mejía-Teniente, L. Capsaicin: From plants to a cancer-suppressing agent. *Molecules* **2016**, *21*, 931. [[CrossRef](#)]
12. Cunha, M.R.; Tavares, M.T.; Fernandes, T.B.; Parise-Filho, R. Peppers: A “hot” natural source for antitumor compounds. *Molecules* **2021**, *26*, 1521. [[CrossRef](#)] [[PubMed](#)]
13. Basith, S.; Cui, M.; Hong, S.; Choi, S. Harnessing the therapeutic potential of capsaicin and its analogues in pain and other diseases. *Molecules* **2016**, *21*, 966. [[CrossRef](#)]
14. Zheng, J.; Zheng, S.; Feng, Q.; Zhang, Q.; Xiao, X. Dietary capsaicin and its anti-obesity potency: From mechanism to clinical implications. *Biosci. Rep.* **2017**, *37*, BSR20170286. [[CrossRef](#)] [[PubMed](#)]
15. Olatunji, T.L.; Afolayan, A.J. The suitability of chili pepper (*Capsicum annum* L.) for alleviating human micronutrient dietary deficiencies: A review. *Food Sci. Nutr.* **2018**, *6*, 2239–2251. [[CrossRef](#)] [[PubMed](#)]
16. Hassan, N.M.; Yusof, N.A.; Yahaya, A.F.; Rozali, N.N.M.; Othman, R. Carotenoids of *capsicum* fruits: Pigment profile and health-promoting functional attributes. *Antioxidants* **2019**, *8*, 469. [[CrossRef](#)]
17. Sinisgalli, C.; Faraone, I.; Vassallo, A.; Caddeo, C.; Bisaccia, F.; Armentano, M.F.; Milella, L.; Ostuni, A. Phytochemical profile of *Capsicum annum* l. Cv senise, incorporation into liposomes, and evaluation of cellular antioxidant activity. *Antioxidants* **2020**, *9*, 428. [[CrossRef](#)]
18. Santarsiero, A.; Convertini, P.; Vassallo, A.; Santoro, V.; Todisco, S.; Iacobazzi, D.; Fondufe-Mittendorf, Y.; Martelli, G.; De Oliveira, M.R.; Montanaro, R.; et al. Phenolic compounds of red wine Aglianico del Vulture modulate the functional activity of macrophages via inhibition of NF-κB and the citrate pathway. *Oxid. Med. Cell. Longev.* **2021**, *2021*, 5533793. [[CrossRef](#)]
19. Parisi, V.; Vassallo, A.; Pisano, C.; Signorino, G.; Cardile, F.; Sorrentino, M.; Colelli, F.; Fucci, A.; D’Andrea, E.L.; De Tommasi, N.; et al. A herbal mixture from propolis, pomegranate, and grape pomace endowed with anti-inflammatory activity in an in vivo rheumatoid arthritis model. *Molecules* **2020**, *25*, 2255. [[CrossRef](#)]
20. Caddeo, C.; Nacher, A.; Vassallo, A.; Armentano, M.F.; Pons, R.; Fernández-Busquets, X.; Carbone, C.; Valenti, D.; Fadda, A.M.; Manconi, M. Effect of quercetin and resveratrol co-incorporated in liposomes against inflammatory/oxidative response associated with skin cancer. *Int. J. Pharm.* **2016**, *513*, 153–163. [[CrossRef](#)]
21. El-Saber Batiha, G.; Beshbishy, A.M.; Ikram, M.; Mulla, Z.S.; Abd El-Hack, M.E.; Taha, A.E.; Algammal, A.M.; Ali Elewa, Y.H. The pharmacological activity, biochemical properties, and pharmacokinetics of the major natural polyphenolic flavonoid: Quercetin. *Foods* **2020**, *9*, 374. [[CrossRef](#)] [[PubMed](#)]
22. Haddad, P.; Eid, H. The antidiabetic potential of quercetin: Underlying mechanisms. *Curr. Med. Chem.* **2016**, *24*, 355–364. [[CrossRef](#)]
23. Jafarinia, M.; Sadat Hosseini, M.; Kasiri, N.; Fazel, N.; Fathi, F.; Ganjalikhani Hakemi, M.; Eskandari, N. Quercetin with the potential effect on allergic diseases. *Allergy Asthma Clin. Immunol.* **2020**, *16*, 36. [[CrossRef](#)] [[PubMed](#)]

24. Sato, S.; Mukai, Y. Modulation of chronic inflammation by quercetin: The beneficial effects on obesity. *J. Inflamm. Res.* **2020**, *13*, 421–431. [[CrossRef](#)]
25. Medzhitov, R. Inflammation 2010: New adventures of an old flame. *Cell* **2010**, *140*, 771–776. [[CrossRef](#)]
26. Pahwa, R.; Goyal, A.; Bansal, P.; Jialal, I. *Chronic Inflammation*; StatPearls Publishing: Treasure Island, FL, USA, 2021.
27. Chen, L.; Deng, H.; Cui, H.; Fang, J.; Zuo, Z.; Deng, J.; Li, Y.; Wang, X.; Zhao, L. Inflammatory responses and inflammation-associated diseases in organs. *Oncotarget* **2018**, *9*, 7204–7218. [[CrossRef](#)] [[PubMed](#)]
28. Loftus, R.M.; Finlay, D.K. Immunometabolism: Cellular metabolism turns immune regulator. *J. Biol. Chem.* **2016**, *291*, 1–10. [[CrossRef](#)]
29. O'Neill, L.A.J.; Kishton, R.J.; Rathmell, J. A guide to immunometabolism for immunologists. *Nat. Rev. Immunol.* **2016**, *16*, 553–565. [[CrossRef](#)]
30. Ryan, D.G.; O'Neill, L.A.J. Krebs cycle rewired for macrophage and dendritic cell effector functions. *FEBS Lett.* **2017**, *591*, 2992–3006. [[CrossRef](#)]
31. Williams, N.C.; O'Neill, L.A.J. A role for the krebs cycle intermediate citrate in metabolic reprogramming in innate immunity and inflammation. *Front. Immunol.* **2018**, *9*, 141. [[CrossRef](#)]
32. Infantino, V.; Convertini, P.; Cucci, L.; Panaro, M.A.; Di Noia, M.A.; Calvello, R.; Palmieri, F.; Iacobazzi, V. The mitochondrial citrate carrier: A new player in inflammation. *Biochem. J.* **2011**, *438*, 433–436. [[CrossRef](#)] [[PubMed](#)]
33. Infantino, V.; Iacobazzi, V.; Menga, A.; Avantiaggiati, M.L.; Palmieri, F. A key role of the mitochondrial citrate carrier (SLC25A1) in TNF α - and IFN γ -triggered inflammation. *Biochim. Biophys. Acta* **2014**, *23*, 1217–1225. [[CrossRef](#)] [[PubMed](#)]
34. Infantino, V.; Iacobazzi, V.; Palmieri, F.; Menga, A. ATP-citrate lyase is essential for macrophage inflammatory response. *Biochem. Biophys. Res. Commun.* **2013**, *440*, 105–111. [[CrossRef](#)] [[PubMed](#)]
35. Laurita, T.; Pappalardo, I.; Chiummiento, L.; D'Orsi, R.; Funicello, M.; Santarsiero, A.; Marsico, M.; Infantino, V.; Todisco, S.; Lupattelli, P. Synthesis of new methoxy derivatives of trans 2,3-diaryl-2,3-dihydrobenzofurans and evaluation of their anti-inflammatory activity. *Bioorg. Med. Chem. Lett.* **2021**, *49*, 128264. [[CrossRef](#)] [[PubMed](#)]
36. Wellen, K.E.; Hatzivassiliou, G.; Sachdeva, U.M.; Bui, T.V.; Cross, J.R.; Thompson, C.B. ATP-citrate lyase links cellular metabolism to histone acetylation. *Science* **2009**, *324*, 1076–1080. [[CrossRef](#)]
37. Santarsiero, A.; Onzo, A.; Pascale, R.; Acquavia, M.A.; Coviello, M.; Convertini, P.; Todisco, S.; Marsico, M.; Pifano, C.; Iannece, P.; et al. Pistacia lentiscus hydrosol: Untargeted metabolomic analysis and anti-inflammatory activity mediated by NF- κ B and the citrate pathway. *Oxid. Med. Cell. Longev.* **2020**, *2020*, 4264815. [[CrossRef](#)]
38. Assadpour, E.; Mahdi Jafari, S. A systematic review on nanoencapsulation of food bioactive ingredients and nutraceuticals by various nanocarriers. *Crit. Rev. Food Sci. Nutr.* **2019**, *59*, 3129–3151. [[CrossRef](#)]
39. Ozkan, G.; Kostka, T.; Esatbeyoglu, T.; Capanoglu, E. Effects of lipid-based encapsulation on the bioaccessibility and bioavailability of phenolic compounds. *Molecules* **2020**, *25*, 5545. [[CrossRef](#)]
40. McClements, D.J.; Xiao, H. Designing food structure and composition to enhance nutraceutical bioactivity to support cancer inhibition. *Semin. Cancer Biol.* **2017**, *46*, 215–226. [[CrossRef](#)]
41. Vassallo, A.; Santoro, V.; Pappalardo, I.; Santarsiero, A.; Convertini, P.; De Luca, M.; Martelli, G.; Infantino, V.; Caddeo, C. Liposome-mediated inhibition of inflammation by hydroxycitrate. *Nanomaterials* **2020**, *10*, 2080. [[CrossRef](#)]
42. Mishra, B.; Patel, B.B.; Tiwari, S. Colloidal nanocarriers: A review on formulation technology, types and applications toward targeted drug delivery. *Nanomed. Nanotechnol. Biol. Med.* **2010**, *6*, 9–24. [[CrossRef](#)] [[PubMed](#)]
43. Ud Din, F.; Waqar, A.; Ullah, I.; Qureshi, O.S.; Mustapha, O.; Shafique, S.; Zeb, A. Effective use of nanocarriers as drug delivery systems for the treatment of selected tumors. *Int. J. Nanomed.* **2017**, *12*, 7291–7309. [[CrossRef](#)] [[PubMed](#)]
44. Lai, F.; Caddeo, C.; Manca, M.L.; Manconi, M.; Sinico, C.; Fadda, A.M. What's new in the field of phospholipid vesicular nanocarriers for skin drug delivery. *Int. J. Pharm.* **2020**, *583*, 119398. [[CrossRef](#)] [[PubMed](#)]
45. Acquavia, M.A.; Pascale, R.; Pappalardo, I.; Santarsiero, A.; Martelli, G.; Bianco, G. Characterization of quercetin derivatives in crossing combination of habanero white and *Capsicum annuum* peppers and of anti-inflammatory and cytotoxic activity. *Separations* **2021**, *8*, 90. [[CrossRef](#)]
46. Wahyuni, Y.; Ballester, A.R.; Tikunov, Y.; de Vos, R.C.H.; Pelgrom, K.T.B.; Maharijaya, A.; Sudarmonowati, E.; Bino, R.J.; Bovy, A.G. Metabolomics and molecular marker analysis to explore pepper (*Capsicum* sp.) biodiversity. *Metabolomics* **2013**, *9*, 130–144. [[CrossRef](#)] [[PubMed](#)]
47. Caddeo, C.; Chessa, M.; Vassallo, A.; Pons, R.; Diez-Sales, O.; Fadda, A.M.; Manconi, M. Extraction, purification and nanoformulation of natural phycocyanin (from Klamath algae) for dermal and deeper soft tissue delivery. *J. Biomed. Nanotechnol.* **2013**, *9*, 1929–1938. [[CrossRef](#)]
48. Caddeo, C.; Pucci, L.; Gabriele, M.; Carbone, C.; Fernández-Busquets, X.; Valenti, D.; Pons, R.; Vassallo, A.; Fadda, A.M.; Manconi, M. Stability, biocompatibility and antioxidant activity of PEG-modified liposomes containing resveratrol. *Int. J. Pharm.* **2018**, *538*, 40–47. [[CrossRef](#)] [[PubMed](#)]
49. Gardiner, B.; Dougherty, J.A.; Ponnalagu, D.; Singh, H.; Angelos, M.; Chen, C.-A.; Khan, M. Measurement of oxidative stress markers in vitro using commercially available kits. In *Measuring Oxidants and Oxidative Stress in Biological Systems*; Springer: Cham, Switzerland, 2020; pp. 39–60.
50. Bradford, M.M. A rapid and sensitive method for the quantitation of microgram quantities of protein utilizing the principle of protein-dye binding. *Anal. Biochem.* **1976**, *72*, 248–254. [[CrossRef](#)]

51. Pascale, R.; Acquavia, M.A.; Cataldi, T.R.I.; Onzo, A.; Coviello, D.; Bufo, S.A.; Scrano, L.; Ciriello, R.; Guerrieri, A.; Bianco, G. Profiling of quercetin glycosides and acyl glycosides in sun-dried peperoni di Senise peppers (*Capsicum annuum* L.) by a combination of LC-ESI(-)-MS/MS and polarity prediction in reversed-phase separations. *Anal. Bioanal. Chem.* **2020**, *412*, 3005–3015. [[CrossRef](#)]
52. Cioffi, G.; Dal Piaz, F.; Vassallo, A.; Venturella, F.; De Caprariis, P.; De Simone, F.; De Tommasi, N. Antiproliferative oleanane saponins from *Meryta denhamii*. *J. Nat. Prod.* **2008**, *71*, 1000–1004. [[CrossRef](#)]
53. Cisneros-Pineda, O.; Torres-Tapia, L.W.; Gutiérrez-Pacheco, L.C.; Contreras-Martín, F.; González-Estrada, T.; Peraza-Sánchez, S.R. Capsaicinoids quantification in chili peppers cultivated in the state of Yucatan, Mexico. *Food Chem.* **2007**, *104*, 1755–1760. [[CrossRef](#)]
54. Dutta, S.; Bhattacharjee, P. Nanoliposomal encapsulates of piperine-rich black pepper extract obtained by enzyme-assisted supercritical carbon dioxide extraction. *J. Food Eng.* **2017**, *201*, 49–56. [[CrossRef](#)]
55. Van Hout, M.W.J.; Hofland, C.M.; Niederländer, H.A.G.; De Jong, G.J. On-line coupling of solid-phase extraction with mass spectrometry for the analysis of biological samples. II. Determination of clenbuterol in urine using multiple-stage mass spectrometry in an ion-trap mass spectrometer. *Rapid Commun. Mass Spectrom.* **2000**, *14*, 2103–2111. [[CrossRef](#)]
56. Bogusz, S.; Libardi, S.H.; Dias, F.F.G.; Coutinho, J.P.; Bochi, V.C.; Rodrigues, D.; Melo, A.M.T.; Godoy, H.T. Brazilian capsicum peppers: Capsaicinoid content and antioxidant activity. *J. Sci. Food Agric.* **2018**, *98*, 217–224. [[CrossRef](#)]
57. Cho, S.Y.; Kim, H.W.; Lee, M.K.; Kim, H.J.; Kim, J.B.; Choe, J.S.; Lee, Y.M.; Jang, H.H. Antioxidant and anti-inflammatory activities in relation to the flavonoids composition of pepper (*Capsicum annuum* L.). *Antioxidants* **2020**, *9*, 986. [[CrossRef](#)] [[PubMed](#)]
58. Evangelista, S. Novel therapeutics in the field of capsaicin and pain. *Expert Rev. Clin. Pharmacol.* **2015**, *8*, 373–375. [[CrossRef](#)]
59. Panchal, S.K.; Bliss, E.; Brown, L. Capsaicin in metabolic syndrome. *Nutrients* **2018**, *10*, 630. [[CrossRef](#)] [[PubMed](#)]
60. Sora, G.T.S.; Haminiuk, C.W.I.; da Silva, M.V.; Zielinski, A.A.F.; Gonçalves, G.A.; Bracht, A.; Peralta, R.M. A comparative study of the capsaicinoid and phenolic contents and in vitro antioxidant activities of the peppers of the genus *Capsicum*: An application of chemometrics. *J. Food Sci. Technol.* **2015**, *52*, 8086–8094. [[CrossRef](#)]
61. Shahidi, F.; Ambigaipalan, P. Phenolics and polyphenolics in foods, beverages and spices: Antioxidant activity and health effects—A review. *J. Funct. Foods* **2015**, *18*, 820–897. [[CrossRef](#)]
62. Chiong, H.S.; Yong, Y.K.; Ahmad, Z.; Sulaiman, M.R.; Zakaria, Z.A.; Yuen, K.H.; Nazrul Hakim, M. Cytoprotective and enhanced anti-inflammatory activities of liposomal piroxicam formulation in lipopolysaccharide-stimulated RAW 264.7 macrophages. *Int. J. Nanomed.* **2013**, *8*, 1245–1255. [[CrossRef](#)]
63. Chen, H.; Khemtong, C.; Yang, X.; Chang, X.; Gao, J. Nanonization strategies for poorly water-soluble drugs. *Drug Discov. Today* **2011**, *16*, 354–360. [[CrossRef](#)] [[PubMed](#)]
64. Fricker, G.; Kromp, T.; Wendel, A.; Blume, A.; Zirkel, J.; Rebmann, H.; Setzer, C.; Quinkert, R.O.; Martin, F.; Müller-Goymann, C. Phospholipids and lipid-based formulations in oral drug delivery. *Pharm. Res.* **2010**, *27*, 1469–1486. [[CrossRef](#)]
65. Chakraborty, S.; Shukla, D.; Mishra, B.; Singh, S. Lipid—An emerging platform for oral delivery of drugs with poor bioavailability. *Eur. J. Pharm. Biopharm.* **2009**, *73*, 1–15. [[CrossRef](#)]
66. Forrester, S.J.; Kikuchi, D.S.; Hernandez, M.S.; Xu, Q.; Griendling, K.K. Reactive oxygen species in metabolic and inflammatory signaling. *Circ. Res.* **2018**, *122*, 877–902. [[CrossRef](#)]
67. Brieger, K.; Schiavone, S.; Miller, F.J.; Krause, K.H. Reactive oxygen species: From health to disease. *Swiss Med. Wkly.* **2012**, *142*, 13659. [[CrossRef](#)] [[PubMed](#)]
68. Coleman, J.W. Nitric oxide in immunity and inflammation. *Int. Immunopharmacol.* **2001**, *1*, 1397–1406. [[CrossRef](#)]



Metabolic profiling of Peperoni di Senise PGI bell peppers with ultra-high resolution absorption mode Fourier transform ion cyclotron resonance mass spectrometry



Alberto Onzo, Ph.D.^a, Maria Assunta Acquavia, Master^{a, b}, Raffaella Pascale, Ph.D.^c, Patrizia Iannece^d, Carmine Gaeta^d, Konstantin O. Nagornov^e, Yury O. Tsybin^e, Giuliana Bianco, Professor^{a, *}

^a Università Degli Studi Della Basilicata, Dipartimento di Scienze, Via Dell'Ateneo Lucano 10, Potenza, Italy

^b ALMAGISI s.r.l Corso Italia, 27-39100, Bolzano, Italy

^c Gnosis by Lesaffre, Pisticci, 75015, Matera, Italy

^d Università Degli Studi di Salerno, Dipartimento di Chimica e Biologia, Via Giovanni Paolo II 132, Fisciano, Italy

^e Spectroswiss, 1015 Lausanne, Switzerland

ARTICLE INFO

Article history:

Received 26 May 2021

Received in revised form

30 September 2021

Accepted 2 October 2021

Available online 5 October 2021

Keywords:

Capsicum annuum L.

Metabolomics

Untargeted

High-resolution mass spectrometry

Absorption mode mass spectrum

ABSTRACT

Bell peppers (genus *Capsicum*) are an excellent source of health-related compounds, such as ascorbic acid (vitamin C), carotenoids (provitamin A), tocopherols (vitamin E), flavonoids and capsaicinoids. These compounds are known for their biological activities, including antioxidant, anti-inflammatory and anticarcinogenic properties. Over the past decade, there has been an increasing number of studies focused on metabolite profiling of bell peppers. However, none of the direct analysis methods exploited in these studies were capable of simultaneously detecting compounds belonging to more than four metabolite classes (and possible derivatives of model compounds) present in bell peppers, i.e. mainly amino acids, sugars, polyphenols and organic acids. We have attempted to profile a higher number of metabolite classes by performing a direct-injection analysis with a Fourier transform ion cyclotron resonance mass spectrometry (FT-ICR MS), on *Peperoni di Senise* bell peppers (*Capsicum annuum* L.). These bell peppers are a typical food product cultivated in Basilicata (Southern Italy), protected with a protected geographical indication (PGI) quality mark and known for their unique taste. To increase the performance of the FT-ICR MS method, we processed the recorded time-domain ion signals (transients) into the absorption mode FT-ICR mass spectra. The latter was achieved by the use of the dedicated software package, AutoVectis Pro. Mass spectral representation in absorption mode produced a more comprehensive description of the metabolic profile of *Peperoni di Senise PGI* by improving results reliability via artifacts removal and identifying a higher number of compounds.

© 2021 Elsevier B.V. All rights reserved.

1. Introduction

As many as 30 wild and cultivated plant species belong to the genus *Capsicum*. They belong to the family of *Solanaceae* and are grown all over the world, principally in tropical and subtropical

countries [1,2] *Capsicum annuum* L. (bell pepper) is one of the five major cultivated and marketed species (*Capsicum chinense* Jacq., *Capsicum frutescens* L., *Capsicum baccatum* L., and *Capsicum pubescens* are the others). The market for *Capsicum* has seen a remarkable expansion during the last years [3]. For example, world pepper production in 2018 reached ~0.8 million tons [4]. Bell peppers are used as a raw or cooked vegetable, as a condiment, or a spice. In addition, the industry uses peppers as a spice or coloring agent in food products.

Capsicum fruits are a rich source of capsaicinoids, carotenoids (some of them with provitamin A activity), flavonoids, and vitamins, such as ascorbic acid (vitamin C) and tocopherols (vitamin E)

* Corresponding author.

E-mail addresses: albertoonzo@gmail.com (A. Onzo), maria.acquavia@unibas.it (M.A. Acquavia), raff.pascale@gmail.com (R. Pascale), piannece@unisa.it (P. Iannece), cgaeta@unisa.it (C. Gaeta), nagornov@spectroswiss.ch (K.O. Nagornov), tsybin@spectroswiss.ch (Y.O. Tsybin), giuliana.bianco@unibas.it (G. Bianco).

[5,6]. The amount and composition of these metabolites vary among genotypes and are affected by many conditions such as fruit ripening, cultivation systems, geographical origin, and processing methods [7,8].

The biochemical content of *Capsicum annuum* L. species is not only valuable for the plant itself but may also be advantageous for human health, which led scientific community to put more effort on metabolite profile uncovering of different *Capsicum annuum* L. cultivars. To date, different techniques have been used to provide insights on the metabolomics profile of bell peppers, such as ultraviolet/visible (UV/Vis), infrared (IR), and nuclear magnetic resonance (NMR) spectroscopies [9–12]. However, the direct analysis methods exploited in these studies were not capable of simultaneously detecting compounds belonging to more than four metabolite classes present in bell peppers, i.e., mainly amino acids, sugars, polyphenols, and organic acids [13]. The satisfying levels of specificity and sensitivity were reached only after the breakthrough of chromatographic techniques, i.e., gas and liquid chromatography, hyphenated to mass spectrometry (GC-MS and LC-MS). The GC/LC-MS methods allowed the separation of matrix components, ensuring more accurate identification and quantification of specific metabolites [14–25]. Enhanced knowledge of the metabolite derivatives made it possible to understand to which kind of biochemical pathways specific types of bio-compounds are related.

Contemporary, extraction techniques could be optimized to isolate one or more particular metabolites, required to prepare efficient nutraceutical products [14,20,26–29]. However, these techniques are not generally applied in the metabolomic analysis as they carry a series of drawbacks. The latter include long analysis times and high costs, related to the consumption of large volumes of solvents, a series of features which make untargeted metabolomic analysis of peppers far to be a routine analysis.

Ultra-high resolution Fourier transform ion cyclotron resonance mass spectrometry (FT-ICR MS) can provide the most comprehensive information on classes of metabolites present in analyzed samples. It is capable of identifying an enormous number of ionic species simultaneously, in a fast and straightforward direct analysis, and giving information on the entity of the diversity related to each metabolic class [30–34]. The promises of this approach are remarkable; simplifying and accelerating metabolomic experimental designs for biomechanistic and nutraceutical formulation purposes [30–34]. Despite this, particular attention should be paid to FT-ICR MS data pre-treatment. Raw mass spectral data could contain artifacts, such as wiggles, i.e., Gibbs oscillations, and harmonics, which could lead to the wrong formula assignment [35–37]. Moreover, information loss could occur due to the chemical and electronic noise often present in mass spectra of complex matrices [38]. This latter drawback could make it difficult or impossible to distinguish low-intensity ionic species from noise peaks. To diminish these problems, mass spectral representation in the absorption Fourier transform (aFT) mode could be employed, instead of the more common magnitude Fourier transform (mFT) mode representation [39]. The aFT representation offers a two-fold higher resolution, lower levels of noise, and may reveal spectral artifacts [35]. However, obtaining an artifact-free aFT mass spectrum is not straightforward. A proper correction of the ions' phase shifting should be made prior to result formulation [35]. Thus, the use of dedicated software tools is compulsory to perform an appropriate data pre-treatment processing and extrapolate a useable aFT mass spectrum from raw time-domain data (transients) which remains cumbersome with current commercial FT-ICR MS instrumentation [35,36].

In this work, a comprehensive profile of the metabolite classes of a methanolic extract of *Peperoni di Senise PGI* peppers was obtained by the use of FT-ICR MS. We employed a direct-injection

approach and processed the unreduced (raw) time-domain data (transients) with the dedicated FT-ICR MS data processing software, AutoVectis Pro. This software tool performed the phase correction step in few milliseconds to obtain the aFT mass spectra. Consequently, a higher number of ionic species could be assigned to molecular formulas. Moreover, the use of a well-known visualization means, i.e., van Krevelen plots (e.g., O/C versus H/C scatter plots), allowed us to interpret our results better.

2. Materials and methods

2.1. Chemicals

Sodium trifluoroacetate (NaTFA, 98%) and methanol (LC-MS purity grade) were purchased from Sigma-Aldrich (Milano, Italy). Pure nitrogen (99.996%) was delivered to the MS system as the sheath gas.

2.2. Sample preparation

Extracts of *Peperoni di Senise PGI* sun-dried bell peppers (*Capsicum annuum* L.) were obtained by following an optimized procedure based on a previously reported method [20]. Peppers were grounded to a fine powder using a home miller, and residual water was eliminated by lyophilization (24 h). 500 mg of each sample were extracted by using 1.5 mL of MeOH as a solvent. Metabolites were extracted utilizing the Ultrasound-Assisted Extraction (UAE) technique for 15 min at room temperature with a 35 kHz automatic frequency control and a high-frequency power of 80 W (Sonorex Super RK 100/H sonicator; Bandelin electronic, Berlin, Germany). Extracts were passed through a polytetrafluoroethylene (PTFE) 0.22 μm filter and were injected into the MS system without any further pre-treatment. 1.5 mL of MeOH were used as a blank sample and subjected to the same treatments as the sun-dried bell peppers sample.

2.3. Mass spectrometry

The negative ion mode electrospray ionization (ESI) FT-ICR MS technique was used in the untargeted analysis mode. High-resolution ESI mass spectra were acquired with a 7 T solariX XR FT-ICR MS (Bruker Daltonik GmbH, Bremen, Germany). The capillary voltage was set to 3.9 kV, with a nebulizer gas pressure of 1.2 bar and dry gas flow rate of 4 L/min at 200 °C. Mass spectra were acquired in a mass range of 100–2000 m/z using a time-domain ion signal size of 16 mega-words (the corresponding transient length: 1.63 s; mFT resolution of 1,141,061 at 400 m/z), and an ion accumulation time of 0.1 s. The number of scans was set to 50. Before the analysis, the mass spectrometer was externally calibrated with NaTFA. High mass accuracies were reached for the NaTFA calibration datasets, with a root mean square (RMS) error lower than 0.1 ppm. Once recorded, FT-ICR mass spectra were submitted to several data treatment steps. More specifically, recorded time-domain ion signals (transients) were apodized with a sine function (full window) and zero-filled twice. The corresponding mass spectra were obtained in both absorption and magnitude FT modes (aFT and mFT, respectively). On the former, phase correction, mass recalibration, and baseline correction have been performed. The latter was processed by means of smoothing, choosing the Savitzki-Golay algorithm with a 0.001 m/z range and performing 10 cycles to reduce the number of peak wiggles. Finally, noise thresholding has been performed on mass spectra by following the N-Sigma methodology approach [38]. More specifically, the noise level has been estimated as the mean of the low-intensity signal distribution [38], and peaks showing a signal-to-noise ratio (S/N) higher than 2 were

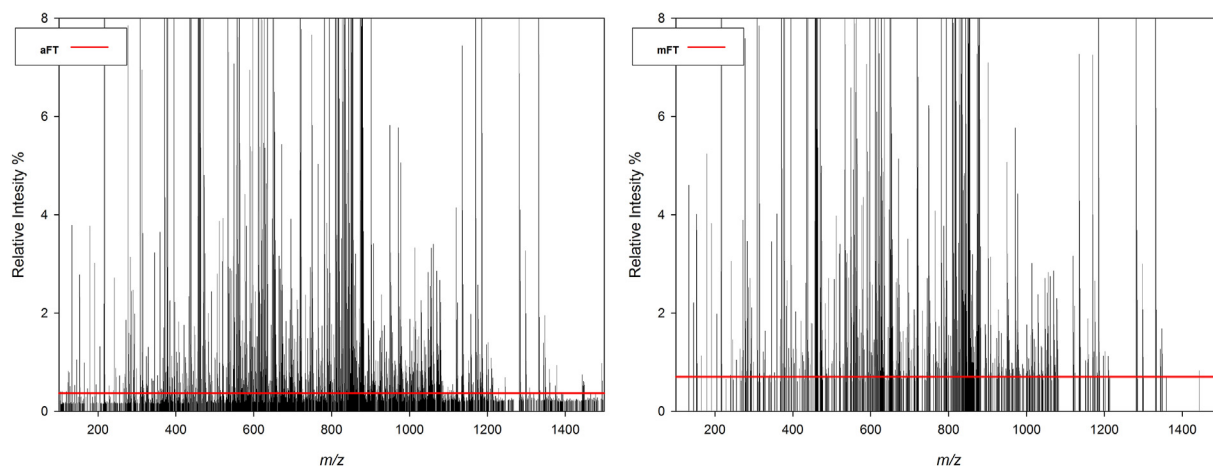


Fig. 1. Noise thresholding levels for aFT and mFT mass spectra. As the noise was different, noise thresholding was set to 0.37% and 0.70% of the base peak for aFT and mFT, respectively. Noise levels are highlighted as red horizontal lines.

retained (Fig. 1). The obtained FT-ICR mass spectra were exported to peak lists. Overall, the mFT-ICR MS was obtained and pre-processed by using the Bruker DataAnalysis software (v. 4.2). The aFT-ICR MS data were processed by using AutoVectis Pro (v.8.9, Spectroswiss, Lausanne, Switzerland).

2.4. Data analysis

The possible elemental formulas were calculated for each MS signal. To obtain the unequivocal formulas, several constraints were applied, such as atoms number limitations, i.e., $C \leq 100$, $H \leq 200$, $O \leq 80$, $N \leq 5$ and $S \leq 1^{34}$, restrictions on atoms to carbon number ratios, i.e., $0.2 \leq H/C \leq 3.1$, $O/C \leq 2$, $N/C \leq 1.3$, and $S/C \leq 0.8$, as well as $RDBE > 0$, nitrogen rule (for m/z ratio values lower or equal to 500) and isotopic pattern filtering [39]. Moreover, Kendrick mass defect (KMD) calculations were performed to help formulas assignment for both mFT and aFT mass spectra. For the KMD analysis, building blocks with a higher number of occurrences were identified and chosen for the analysis. For this step, values of the experimentally observed mass differences were examined and only those comprised in the range ± 1 mDa of the building block exact mass were considered [40–43]. To further improve the reliability of results, building blocks with occurrences lower than a threshold value were excluded. Indeed, it is known that rare mass differences are related to lower probabilities of appearance and could occur as random factors, thus making necessary the setting of an occurrence threshold value, which depends on the mass spectrum peak density [44]. Thus, this threshold was set to 30 for the mFT, whereas it was set to 200 for the aFT. Overall, the FT-ICR MS data analysis was performed with R software (v3.63, www.r-project.org).

3. Results and discussion

Direct-injection ultra-high-resolution ESI(–)-FT-ICR MS data were used to obtain a general description of the metabolome of *Peperoni di Senise* PGI peppers, since they allowed to simultaneously detect compounds belonging to different metabolite classes, i.e. amino acids, sugars, polyphenols, organic acids and carotenoids. The obtained mass spectra showed a high density of peaks, revealing the sample's high complexity. However, some of these signals could be related to noise and artifacts, thus hampering metabolites' identification by formula assignment [35,36]. It is, therefore, essential to face several data treatment steps to obtain

more reliable peak lists, from which an accurate metabolic profile could be deduced. In this context, the choice of working with absorption (aFT) or magnitude (mFT) mass spectra representation could make the difference. aFT mass spectra are obtained as a result of the free induction decay signal pre-processing step, through the application of the Fourier Transformation [45]. Through proper ion phase correction, the resulting aFT mass spectrum shows a much narrower peak shape, with an increase of ~ 2 -fold in resolution, 2-fold in mass accuracy, and $\sqrt{2}$ -fold in the signal-to-noise ratio (S/N) simultaneously, throughout the entire m/z range compared to the conventional magnitude-mode spectra. The use of aFT mode improves peak resolution and S/N ratios and boosts the number of species identified with a single direct analysis. Moreover, artifact designation, including electronic noise peak identification, may be possible with aFT. Despite all these advantages, a number of challenges made the employment of aFT for scientific purposes impractical for at least 40 years [35]. Indeed, deviations and dispersion in the ion initial phases can introduce errors into the aFT mass spectra and render them ambiguous. The aFT mass spectra artifacts include baseline roll, peak asymmetry, peak splitting, abundance, and mass errors [45]. Moreover, phase shifting depends on the cyclotron frequency (m/z). Therefore, the phase correction function demonstrates frequency (or m/z) dependence [35,36]. These features make obtaining aFT mass spectra of complex matrices cumbersome without the utilization of a dedicated tool, with which full control of the transient elaboration should be possible. Consequently, using a new software tool, AutoVectis Pro, was crucial for efficient data treatment, allowing us to work directly on the transient, starting from apodization to aFT phase correction [46–48]. In addition, full control of the peak peaking process was possible, allowing tuning of related parameters such as the magnitude of points interval to consider for centroid calculation. Both aFT and mFT could be readily calculated from the transient apodized with the user-specified apodization function (full or half, symmetric or asymmetric apodization windows) (Fig. 2A). The AutoVectis Pro software, thus, permitted direct comparison between the aFT and mFT outputs. In this way, it was possible to appreciate resolution improvement, which characterizes aFT, and artifact depletion (Fig. 2B). By considering the latter, it is possible to perform a more reliable peak quality evaluation that is not always possible by looking at the mFT alone. Obtainment of the aFT mass spectra not only led to a marked reduction of artifacts, like wiggles and harmonics, but to the enhancement of peak resolution and S/N

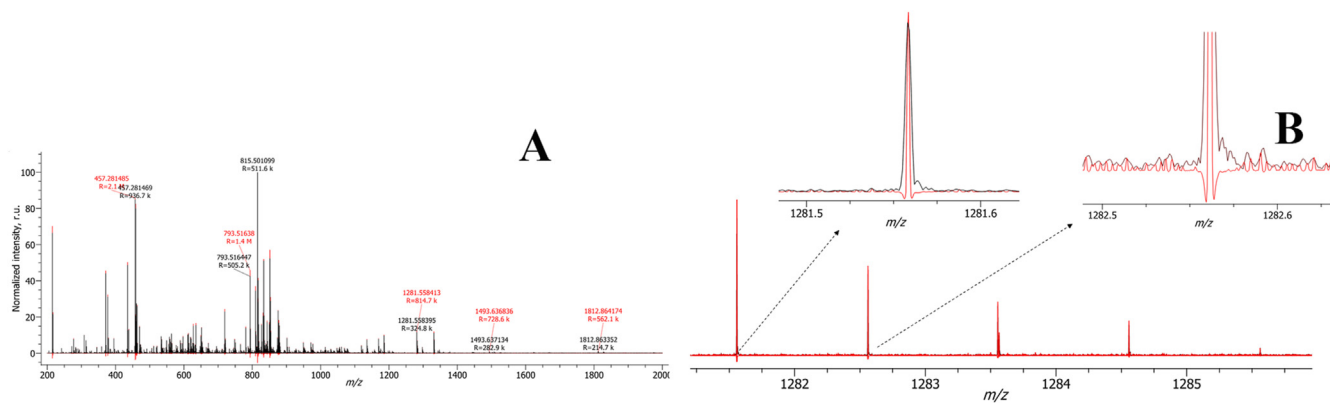


Fig. 2. The ESI(-)-FT-ICR MS analysis of a sample of sun-dried Peperoni di Senise (PGI) peppers showing (A) magnitude mode (black line) and absorption mode (red line) mass spectra. In plot B, a detail of the mass spectra, in which an improvement of peak resolution and a reduction of related wiggles (artifacts, see text) can be appreciated.

ratios too, leading to the lowering of the noise thresholding level and thus increasing the number of resolved MS signals and identified ion species. Moreover, it was not possible to compare the results obtained by AutoVectis Pro software with those obtained by the other existing common software because, as far as we know, no one is suitable for these purposes.

Proper phase correction is a key to the artifact-free aFT mass spectra. During the last years, several approaches have been optimized to solve the phase correction problem [35]. However, some of them need to utilize a dedicated MS apparatus, whereas others are shown to be time-consuming because of the higher number of computational steps. AutoVectis Pro employs a genetic algorithm to optimize the phase calibration coefficients in a few milliseconds [48]. In detail, it generates several phase correction functions starting from a predefined one (which order is defined by the user) and applying random mutation on related frequency values. After the best phase correction function from the initial population has been identified, the step is iterated until complete optimization is obtained [48].

In the aFT spectrum, more ionic species could be distinguished and identified and more complete information on the analyzed sample's metabolic profile could be retrieved. This last aspect was evident during the formula assignment step. Indeed, an m/z peak list of 4906 entries could be extracted from the aFT data, a marked improvement compared to the 901 peaks obtained from the mFT data. Such a difference could be due to the lower noise thresholding level, which was set to 0.37% and 0.70% of the base peak for aFT and mFT spectra, respectively (Fig. 1).

In each case, however, the number of MS signals is high, making it necessary to introduce additional ways to rationalize the results to simplify their analysis and to obtain desired information from mass spectra. In light of this, accurate m/z values were subjected to the KMD analysis [43] to identify the present homologous series and to simplify molecular formula assignment. It is worth noting how aFT analysis provided a more complete information of the sample's metabolic profile by leading to the discovery of new homologous series and related members, as can be noticed by the analysis of corresponding Kendrick plots (Fig. 3). Moreover, the latter feature helped identify other high-frequency building blocks (Table 1), which could be chosen to perform other KMD analyses to extend the range of assigned peaks. For aFT, 1175 unique formulas were obtained, a marked improvement compared to the 351 formulas obtained for the mFT.

To better interpret our results, a well-known visualization method was assumed, i.e., van Krevelen diagrams, in which

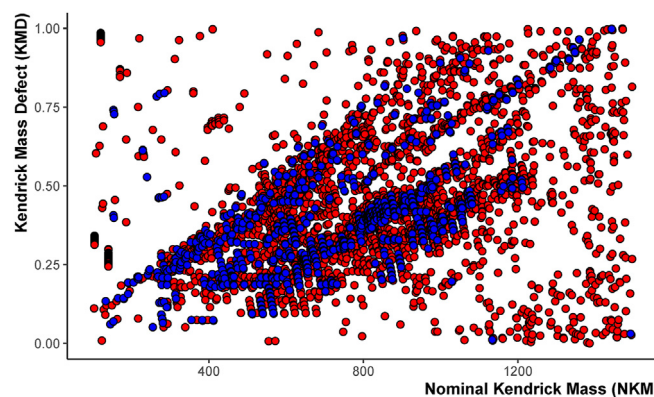
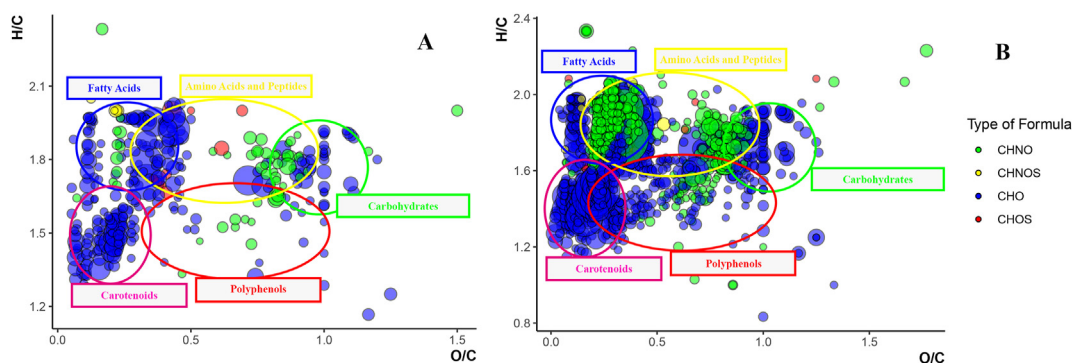


Fig. 3. Kendrick plot obtained from absorption (red dots) and magnitude (blue dots) mode FT-ICR mass spectra, by choosing CH_2 as a building block.

elemental compositions are plotted depending on their O/C and H/C ratios [30–34]. Thanks to these plots, by merely looking at the spots' positions, it is possible to relate the observed metabolite to a specific metabolic class [30–34]. From the analysis of aFT and mFT-derived van Krevelen plots (Fig. 4), the presence of the same important classes of metabolites could be deduced, i.e., fatty acids and related derivatives, carotenoids, amino acids and peptides, carbohydrates, and polyphenols. As can be deduced from the analysis of the obtained van Krevelen plots, sun-dried *Peperoni di Senise PGI* peppers still show a wide diversity of metabolites to which several beneficial health properties have been associated [49], thus supporting the hypothesis of retainment of macroscopic health-promoting properties of these fruits. Moreover, a comparison of aFT and mFT related van Krevelen plots highlighted the advantages provided by the former, supporting what was already argued from the analysis of related Kendrick plots. Indeed, point density is higher for the aFT data, providing a better idea of the range of different metabolites belonging to a specific class. Indeed, the analysis of the aFT spectrum revealed the presence of a higher number of polyphenol derivatives, suggested by central spots in van Krevelen diagram. In detail, some of them showed higher O/C ratios, thus suggesting the presence of glycoside moieties connected to the corresponding aglycones. Some of these compounds were already found into red pepper samples, like quercetin glycosides derivatives [22]. The range of different carotenoid derivatives was

Table 1Building block occurrences in both absorption and magnitude mode mass spectra. Mass differences in the range ± 1 mDa of the building block exact mass were considered.

Building Block	Exact mass	Reaction	Magnitude Mode MS	Absorption Mode MS
CH ₂	14.016	Methylation	54	441
H ₂	2.016	Hydrogenation	104	1033
C ₁	12.000	C-insertion	31	340
O ₁	15.995	O-insertion	42	455
CO ₂	43.990	Carboxylation	37	253
C ₂ H ₂	26016	Decarboxylative Condensation	73	537
H ₂ O	18.011	Hydrolysis/Condensation	43	355
C ₂ H ₄	28.032	Alkylation	48	645
C ₆ H ₁₀ O ₅	162.053	Glucose addition	62	291
CH ₂ O	30.011	Hydroxymethyl transfer	39	380
C ₂ H ₂ O	42.011	Hydroxypyruvic acid addition	0	310
CO	27.995	Formyl transfer	0	288
C ₂ H ₄ O	44.026	Pyruvic Acid addition	0	246
C ₂ H ₄ O ₂	60.021	Hydroxypyruvic acid addition/hydrogenation	0	206
C ₃ H ₂ O ₂	70.006	2-Ketosuccinate addition	0	206
C ₃ H ₆ O ₂	74.037	3-Hydroxy-2-oxobutanoic acid addition	0	275
C ₅ H ₈ O ₄	132.043	Pentose addition (condensation)	0	212

**Fig. 4.** Van Krevelen plots of a sun-dried *Peperoni di Senise* (PGI) peppers extract (*Capsicum Annuum* L.), obtained from the elaboration of the magnitude (plot A) and absorption (plot B) mode FT-ICR mass spectra, respectively. Types of the formula are distinguished by colors, i.e., blue for CHO, green for CHON, red for CHONS, and yellow for CHOS type.

remarkable too, as highlighted by the huge density of points on the left-lower part of the diagram. This was expected for *Capsicum annuum* L. cultivars, since they are recognized as carotenoids-rich non-leafy vegetables. Actually, these compounds are responsible for pepper color and their composition and concentration vary among ripening stages [7,8]. Generally, red pepper is unique for its high xanthophylls content and composition, showing the most diverse carotenoid profile, consisting mainly of the yellow carotenoids namely β -carotene, violaxanthin, antheraxanthin, zeaxanthin, and the characteristic intense red ketocarotenoids, which are capsanthin, capsorubin and capsanthin-5,6-epoxide. Some assigned formulas reflect this general trend, like [C₄₀H₅₃O₄]⁻ and [C₄₀H₅₉O₅]⁻, which could be related to xanthophyll derivatives. On the other hand, spot spreading suggests that these compounds could undergo to different biochemical pathways, such as H₂ and CH addition, as already found through the literature [50], but also decarboxylative condensation and glycosylation, the latter of which occurs in some leaf species to regulate the synthesis of carotenoids [51].

Among fatty acids found in *Peperoni di Senise* PGI peppers, related to spots located on the left-upper part of Van Krevelen plot, there are species like [C₁₆H₃₁O₂]⁻, [C₁₈H₃₃O₂]⁻ and [C₁₈H₃₁O₂]⁻, probably corresponding to the most abundant fatty acids in red pepper, i.e. palmitic, oleic and linoleic acids, respectively [52], whose everyone is connected to other spots by different building blocks, such as H₂ (hydrogenation), CH₂ (methylene addition) and C₆H₁₀O₅ (hexose addition), thus suggesting there is more to

discover about fatty acid profile of this kind of sample. The presence of a high number of CHNO-type compounds on this part of the plot is interesting, and probably its related to amino acid fatty acid conjugates found in our sample, a type of compound never reported for red peppers, as far as we know. Amino acid and peptide glycosides seem to be present too, seen the presence of high O/C ratio CHNO-type compounds, and the presence of other spots of the same kind on the central area of the plot suggests that amino acid addition could occur for phenolic compounds too. So, through the van Krevelen plot it was possible to highlight how *Peperoni di Senise* PGI peppers show common features to other red pepper cultivars too, but its analysis suggested the presence of a higher number of derivatives belonging to identified metabolite classes, supporting the idea that red pepper metabolites could undergo to unexplored biochemical pathways.

4. Conclusions

This work underlines how the implementation of absorption mode FT mass spectra representation is necessary to obtain a comprehensive overview of the metabolic profile of a methanolic extract of *Peperoni di Senise* PGI bell peppers. The recently developed AutoVectis Pro software was crucial in maximizing the reliable information provided by a single ultra-high resolution mass spectrum obtained from a very complex matrix analysis and, by working directly on the recorded transients, it allowed to calculate absorption mode FT-ICR mass spectra in a few seconds. The

utilization of the aFT mass spectral representation led to identifying a substantially higher number of species, as could be supported by the related Kendrick and van Krevelen plots, minimizing loss of information and allowing the in-depth characterization of the metabolic profile of the sample. Expansion of the aFT mass spectra representation to the combination of on-line separation methods, such as LC-MS, with the high-resolution FT-ICR MS, should bring further insights into the metabolic profiles of complex food matrices.

Author statement

Alberto Onzo: Investigation, Data Curation, Writing-Original Draft, Maria Assunta Acquavia: Writing - Review & Editing, Raffaella Pascale: Writing - Review & Editing, Patrizia Iannece: Writing - Review & Editing, Carmine Gaeta: Supervision, Konstantin Nagornov: Software, Validation, Yury O. Tsybin: Software, Validation, Supervision, Giuliana Bianco: Supervision.

Declaration of competing interest

The authors declare that they have no known competing financial interests or personal relationships that could have appeared to influence the work reported in this paper.

References

- [1] S.K. Basu, A.K. De, in: A.K. De (Ed.), *Capsicum: the Genus Capsicum*, Taylor & Francis Group, London, 2003.
- [2] F. Di Dato, M. Parisi, T. Cardì, P. Tripodi, Genetic diversity and assessment of markers linked to resistance and pungency genes in *Capsicum* germplasm, *Euphytica* 204 (2015) 103–119. <https://doi.org/10.1007/s10681-014-1345-4>.
- [3] *Product and Market Development: World Markets in the Spice Trade 2000–2004*, 2006. Geneva.
- [4] FAOSTAT.
- [5] L.R. Howard, R.E.C. Wildman, *Handbook of Nutraceuticals and Functional Foods*, CRC Press, Boca Raton, FL, 2007.
- [6] Y. Wahyuni, A.R. Ballester, E. Sudarmonowati, R.J. Bino, A.G. Bovy, Metabolite biodiversity in pepper (*Capsicum*) fruits of thirty-two diverse accessions: variation in health-related compounds and implications for breeding, *Phytochemistry* 72 (2011) 1358–1370. <https://doi.org/10.1016/j.phytochem.2011.03.016>.
- [7] L.R. Howard, S.T. Talcott, C.H. Brenes, B. Villalon, Changes in phytochemical and antioxidant activity of selected pepper cultivars (*Capsicum* species) as influenced by maturity, *J. Agric. Food Chem.* 48 (2000) 1713–1720. <https://doi.org/10.1021/jf990916t>.
- [8] F. Márkus, H.G. Daoud, J. Kapitány, P.A. Biacs, Change in the carotenoid and antioxidant content of spice red pepper (*Paprika*) as a function of ripening and some technological factors, *J. Agric. Food Chem.* 47 (1999) 100–107. <https://doi.org/10.1021/jf980485z>.
- [9] J. Lim, G. Kim, C. Mo, M. Kim, Design and fabrication of a real-time measurement system for the capsaicinoid content of Korean red pepper (*Capsicum annuum* L.) powder by visible and near-infrared spectroscopy, *Sensors* 15 (2015) 27420–27435. <https://doi.org/10.3390/s151127420>.
- [10] I. Domínguez-Martínez, O.G. Meza-Márquez, G. Osorio-Revilla, J. Proal-Nájera, T. Gallardo-Velázquez, Determination of capsaicin, ascorbic acid, total phenolic compounds and antioxidant activity of *Capsicum annuum* L. var. serrano by mid infrared spectroscopy (Mid-FTIR) and chemometric analysis, *J. Korean Soc. Appl. Biol. Chem.* 57 (2014) 133–142. <https://doi.org/10.1007/s13765-013-4295-y>.
- [11] D. Lee, M. Kim, B.H. Kim, S. Ahn, Identification of the geographical origin of asian red pepper (*Capsicum annuum* L.) powders using ^1H NMR spectroscopy, *Bull. Kor. Chem. Soc.* 41 (2020) 317–322. <https://doi.org/10.1002/bkcs.11974>.
- [12] M. Ritota, F. Marini, P. Sequi, M. Valentini, Metabolomic characterization of Italian sweet pepper (*Capsicum annuum* L.) by means of HRMAS-NMR spectroscopy and multivariate analysis, *J. Agric. Food Chem.* 58 (2010) 9675–9684. <https://doi.org/10.1021/jf1015957>.
- [13] E. Fiorentino-Ramos, N. Villa-Ruano, D. Hidalgo-Martínez, M. Ramírez-Meraz, R. Méndez-Aguilar, R. Velásquez-Valle, L.G. Zepeda-Vallejo, N. Pérez-Hernández, E. Becerra-Martínez, ^1H NMR-based fingerprinting of eleven Mexican *Capsicum annuum* cultivars, *Food Res. Int.* 121 (2019) 12–19. <https://doi.org/10.1016/j.foodres.2019.03.025>.
- [14] G. Bianco, R. Pascale, C.F. Carbone, M.A. Acquavia, T.R.I. Cataldi, P. Schmitt-Kopplin, A. Buchicchio, D. Russo, L. Milella, Determination of soyasaponins in Fagioli di Sarconi beans (*Phaseolus vulgaris* L.) by LC-ESI-FTICR-MS and evaluation of their hypoglycemic activity, *Anal. Bioanal. Chem.* 410 (2018) 1561–1569. <https://doi.org/10.1007/s00216-017-0806-8>.
- [15] G. Bianco, A. Buchicchio, T.R.I. Cataldi, Structural characterization of major soyasaponins in traditional cultivars of Fagioli di Sarconi beans investigated by high-resolution tandem mass spectrometry, *Anal. Bioanal. Chem.* 407 (2015) 6381–6389. <https://doi.org/10.1007/s00216-015-8810-3>.
- [16] M.A. Acquavia, L. Foti, R. Pascale, A. Nicolò, V. Brancaleone, T.R.I. Cataldi, G. Martelli, L. Scrano, G. Bianco, Detection and quantification of Covid-19 antiviral drugs in biological fluids and tissues, *Talanta* (2021) 224. <https://doi.org/10.1016/j.talanta.2020.121862>.
- [17] R. Pascale, G. Bianco, D. Coviello, M. Cristina Lafiosca, S. Masi, I.M. Mancini, S.A. Bufo, L. Scrano, D. Caniani, Validation of a liquid chromatography coupled with tandem mass spectrometry method for the determination of drugs in wastewater using a three-phase solvent system, *J. Separ. Sci.* 43 (2020) 886–895. <https://doi.org/10.1002/jssc.201900509>.
- [18] A. Buchicchio, G. Bianco, A. Sofo, S. Masi, D. Caniani, Biodegradation of carbamazepine and clarithromycin by *Trichoderma harzianum* and *Pleurotus ostreatus* investigated by liquid chromatography - high-resolution tandem mass spectrometry (FTICR MS-IRMPD), *Sci. Total Environ.* 557–558 (2016) 733–739. <https://doi.org/10.1016/j.scitotenv.2016.03.119>.
- [19] G. Bianco, N. Agerbirk, I. Losito, T.R.I. Cataldi, Acylated glucosinolates with diverse acyl groups investigated by high resolution mass spectrometry and infrared multiphoton dissociation, *Phytochemistry* 100 (2014) 92–102. <https://doi.org/10.1016/j.phytochem.2014.01.010>.
- [20] G. Bianco, R. Zianni, G. Anzillotta, A. Palma, V. Vitacco, L. Scrano, T.R.I. Cataldi, Dibenzo-p-dioxins and dibenzofurans in human breast milk collected in the area of Taranto (Southern Italy): first case study, *Anal. Bioanal. Chem.* 405 (2013) 2405–2410. <https://doi.org/10.1007/s00216-013-6706-7>.
- [21] G. Bianco, G. Novario, G. Anzillotta, A. Palma, A. Mangone, T.R.I. Cataldi, Polybrominated diphenyl ethers (PBDEs) in Mediterranean mussels (*Mytilus galloprovincialis*) from selected Apulia coastal sites evaluated by GC-HRMS, *J. Mass Spectrom.* 45 (2010) 1046–1055. <https://doi.org/10.1002/jms.1799>.
- [22] R. Pascale, M.A. Acquavia, T.R.I. Cataldi, A. Onzo, D. Coviello, S.A. Bufo, L. Scrano, R. Ciriello, A. Guerrieri, G. Bianco, Profiling of quercetin glycosides and acyl glycosides in sun-dried perononi di Senise peppers (*Capsicum annuum* L.) by a combination of LC-ESI (-) -MS/MS and polarity prediction in reversed-phase separations, *Anal. Bioanal. Chem.* 412 (2020) 3005–3015. <https://doi.org/10.1007/s00216-020-02547-2>.
- [23] G. Ventura, C.D. Calvano, I. Losito, G. Bianco, R. Pascale, F. Palmisano, T.R.I. Cataldi, Effect of pH and mobile phase additives on the chromatographic behaviour of an amide-embedded stationary phase: cyanocobalamin and its diaminechloro-platinum(II) conjugate as a case study, *J. Separ. Sci.* 42 (2019) 1155–1162. <https://doi.org/10.1002/jssc.201801060>.
- [24] F. Lelario, G. Bianco, S.A. Bufo, T.R.I. Cataldi, Establishing the occurrence of major and minor glucosinolates in Brassicaceae by LC-ESI-hybrid linear ion trap and Fourier-transform ion cyclotron resonance mass spectrometry, *Phytochemistry* 73 (2012) 74–83. <https://doi.org/10.1016/j.phytochem.2011.09.010>.
- [25] G. Bianco, F. Lelario, F.G. Battista, S.A. Bufo, T.R.I. Cataldi, Identification of glucosinolates in capers by LC-ESI-hybrid linear ion trap with Fourier transform ion cyclotron resonance mass spectrometry (LC-ESI-LTQ-FTICR MS) and infrared multiphoton dissociation, *J. Mass Spectrom.* 47 (2012) 1160–1169. <https://doi.org/10.1002/jms.2996>.
- [26] M.H. Sarafian, M. Gaudin, M.R. Lewis, F.P. Martin, E. Holmes, J.K. Nicholson, M.E. Dumas, Objective set of criteria for optimization of sample preparation procedures for ultra-high throughput untargeted blood plasma lipid profiling by ultra performance liquid chromatography-mass spectrometry, *Anal. Chem.* 86 (2014) 5766–5774. <https://doi.org/10.1021/ac500317c>.
- [27] S. Malovaná, F.J. García Montelongo, J.P. Pérez, M.A. Rodríguez-Delgado, Optimisation of sample preparation for the determination of trans-resveratrol and other polyphenolic compounds in wines by high performance liquid chromatography, *Anal. Chim. Acta* 428 (2001) 245–253. [https://doi.org/10.1016/S0003-2670\(00\)01231-9](https://doi.org/10.1016/S0003-2670(00)01231-9).
- [28] S. Kim, D.Y. Lee, G. Wohlgenuth, H.S. Park, O. Fiehn, K.H. Kim, Evaluation and optimization of metabolome sample preparation methods for *Saccharomyces cerevisiae*, *Anal. Chem.* 85 (2013) 2169–2176. <https://doi.org/10.1021/ac302881e>.
- [29] S. Ferrari, Biological elicitors of plant secondary metabolites, *Adv. Exp. Med. Biol.* 698 (2010) 144–151. <https://doi.org/10.1007/978-1-4419-7347-4>.
- [30] R.D. Gougeon, M. Lucio, L. Boutegrabet, D. Peyron, F. Feuillat, D. Chassagne, H. Alexandre, A. Voilley, P. Cayot, I. Gebeffigi, et al., Authentication approach of the chemodiversity of grape and wine by FTICR-MS. *Proceedings of the ACS Symposium Series*, 2011.
- [31] C. Roullier-Gall, M. Witting, R.D. Gougeon, P. Schmitt-Kopplin, High precision mass measurements for wine metabolomics, *Front. Chem.* 2 (2014) 1–9. <https://doi.org/10.3389/fchem.2014.00102>.
- [32] C. Roullier-Gall, D. Hemmler, M. Gonsior, Y. Li, M. Nikolantonaki, A. Ron, C. Coelho, R.D. Gougeon, P. Schmitt-Kopplin, Sulfites and the wine metabolome, *Food Chem.* 237 (2017) 106–113. <https://doi.org/10.1016/j.foodchem.2017.05.039>.
- [33] A. Santarsiero, A. Onzo, R. Pascale, M.A. Acquavia, M. Coviello, P. Convertini, S. Todisco, M. Marsico, C. Pifano, P. Iannece, et al., Pistacia lentiscus hydrosol: untargeted metabolomic analysis and anti-inflammatory activity mediated by NF- κ B and the citrate pathway, *Oxid. Med. Cell. Longev.* (2020) 2020. <https://doi.org/10.1155/2020/4264815>.

- [34] R. Pascale, G. Bianco, T.R.I. Cataldi, P.S. Kopplin, F. Bosco, L. Vignola, J. Uhl, M. Lucio, L. Milella, Mass spectrometry-based phytochemical screening for hypoglycemic activity of Fagioli di Sarconi beans (*Phaseolus vulgaris* L.), *Food Chem.* 242 (2018) 497–504, <https://doi.org/10.1016/j.foodchem.2017.09.091>.
- [35] Y. Qi, P.B. O' Connor, Data processing in Fourier transform ion cyclotron resonance mass spectrometry, *Mass Spectrom. Rev.* 33 (2014) 333–352, <https://doi.org/10.1002/mas.21414>.
- [36] E.N. Nikolaev, Y.I. Kostyukevich, G.N. Vladimirov, Fourier transform ion cyclotron resonance (FT ICR) mass spectrometry: theory and simulations, *Mass Spectrom. Rev.* 35 (2016) 219–258, <https://doi.org/10.1002/mas.21422>.
- [37] B. Kanawati, K.P. Wanczek, P. Schmitt-kopplin, *Data Processing and Automation in Fourier Transform Mass Spectrometry*, Elsevier Inc., 2019, ISBN 9780128140130, pp. 133–185. *Fundamentals and Applications of Fourier Transform Mass Spectrometry*.
- [38] A.T. Zielinski, I. Kourtchev, C. Bortolini, S.J. Fuller, C. Giorio, O.A.M. Popoola, S. Bogianni, A. Tapparo, R.L. Jones, M. Kalberer, A new processing scheme for ultra-high resolution direct infusion mass spectrometry data, *Atmos. Environ.* 178 (2018) 129–139, <https://doi.org/10.1016/j.atmosenv.2018.01.034>.
- [39] Osterholz, H.; Kilgour, D.; Storey, D.S.; Lavik, G.; Ferdelman, T.; Niggemann, J. Accumulation of DOC in the south pacific subtropical gyre from a molecular perspective. *Mar. Chem.* 2021, 103955, doi:10.1016/j.marchem.2021.103955.
- [40] K. Longnecker, E.B. Kujawinski, Using network analysis to discern compositional patterns in ultrahigh-resolution mass spectrometry data of dissolved organic matter, *Rapid Commun. Mass Spectrom.* (2016) 2388–2394, <https://doi.org/10.1002/rcm.7719>.
- [41] A.G. Marshall, R.P. Rodgers, *Petroleomics*, The next grand challenge for chemical analysis, *Acc. Chem. Res.* 37 (2004) 53–59, <https://doi.org/10.1021/ar020177t>.
- [42] F. Moritz, M. Kaling, J.P. Schnitzler, P. Schmitt-Kopplin, Characterization of poplar metabolotypes via mass difference enrichment analysis, *Plant Cell Environ.* 40 (2017) 1057–1073, <https://doi.org/10.1111/pce.12878>.
- [43] K. Qian, R.P. Rodgers, C.L. Hendrickson, C.A. Hughey, A.G. Marshall, Kendrick mass defect spectrum: a compact visual analysis for ultrahigh-resolution broadband mass spectra, *Anal. Chem.* 73 (2002) 4676–4681, <https://doi.org/10.1021/ac010560w>.
- [44] E.V. Kunenkov, A.S. Kononikhin, I.V. Perminova, N. Hertkorn, A. Gaspar, P. Schmitt-Kopplin, I.A. Popov, A.V. Garmash, E.N. Nikolaev, Total mass difference statistics algorithm: a new approach to identification of high-mass building blocks in electrospray ionization fourier transform ion cyclotron mass spectrometry data of natural organic matter, *Anal. Chem.* 81 (2009) 10106–10115, <https://doi.org/10.1021/ac901476u>.
- [45] E.C. Craig, I. Santos, A.G. Marshall, N.M.M. Nibbering, Dispersion versus absorption (DISPA) method for automatic phasing of fourier transform ion cyclotron resonance mass spectra, *Rapid Commun. Mass Spectrom.* 1 (1987) 33–37, <https://doi.org/10.1002/rcm.1290010209>.
- [46] D.P.A. Kilgour, S.L. Van Orden, Absorption mode Fourier transform mass spectrometry with no baseline correction using a novel asymmetric apodization function, *Rapid Commun. Mass Spectrom.* 29 (2015) 1009–1018, <https://doi.org/10.1002/rcm.7190>.
- [47] D.P.A. Kilgour, R. Wills, Y. Qi, P.B. O'Connor, Autophaser: an algorithm for automated generation of absorption mode spectra for FT-ICR MS, *Anal. Chem.* 85 (2013) 3903–3911, <https://doi.org/10.1021/ac303289c>.
- [48] D.P.A. Kilgour, M.J. Neal, A.J. Soulbey, P.B. O'Connor, Improved optimization of the Fourier transform ion cyclotron resonance mass spectrometry phase correction function using a genetic algorithm, *Rapid Commun. Mass Spectrom.* 27 (2013) 1977–1982, <https://doi.org/10.1002/rcm.6658>.
- [49] K. Singletary, Red pepper: overview of potential health benefits, *Nutr. Today* 46 (2011) 33–47, <https://doi.org/10.1097/NT.0b013e3182076ff2>.
- [50] M. Gómez-García, R. del N. Ochoa-Alejo, *Biochemistry and Molecular Biology of carotenoid biosynthesis in chili peppers (Capsicum spp.)*, *Int. J. Mol. Sci.* 14 (2013) 19025–19053, <https://doi.org/10.3390/ijms140919025>.
- [51] K. Lätari, F. Wüst, M. Hübner, P. Schaub, K.G. Beisel, S. Matsubara, P. Beyer, R. Welsch, Tissue-specific apocarotenoid glycosylation contributes to carotenoid homeostasis in arabidopsis leaves, *Plant Physiol.* 168 (2015) 1550–1562, <https://doi.org/10.1104/pp.15.00243>.
- [52] G.T. de Souza Sora, A.H.P. Souza, A.A.F. Zielinski, C.W.I. Haminiuk, M. Matsushita, R.M. Peralta, Fatty acid composition of Capsicum genus peppers, *Cienc. E Agrotecnol* 39 (2015) 372–380, <https://doi.org/10.1590/s1413-70542015000400008>.

Review

An Overview of Methods for L-Dopa Extraction and Analytical Determination in Plant Matrices

Carmen Tesoro¹, Filomena Lelario¹ , Rosanna Ciriello¹, Giuliana Bianco¹ , Angela Di Capua^{1,*} 
and Maria Assunta Acquavia^{1,2}

¹ Dipartimento di Scienze, Università degli Studi della Basilicata, Via dell'Ateneo Lucano 10, 85100 Potenza, Italy

² Thema Informatik S.R.L, Via Ressel 2/F, 39100 Bolzano, Italy

* Correspondence: angela.dicapua@unibas.it

Abstract: L-dopa is a precursor of dopamine used as the most effective symptomatic drug treatment for Parkinson's disease. Most of the L-dopa isolated is either synthesized chemically or from natural sources, but only some plants belonging to the Fabaceae family contain significant amounts of L-dopa. Due to its low stability, the unambiguous determination of L-dopa in plant matrices requires appropriate technologies. Several analytical methods have been developed for the determination of L-dopa in different plants. The most used for quantification of L-dopa are mainly based on capillary electrophoresis or chromatographic methods, i.e., high-performance liquid chromatography (HPLC), coupled to ultraviolet-visible or mass spectrometric detection. HPLC is most often used. This paper aims to give information on the latest developments in the chemical study of L-dopa, emphasizing the extraction, separation and characterization of this compound by chromatographic, electrochemical and spectral techniques. This study can help select the best possible strategy for determining L-dopa in plant matrices using advanced analytical methods.

Keywords: levodopa; plant matrices; extraction; review; chromatographic methods



Citation: Tesoro, C.; Lelario, F.; Ciriello, R.; Bianco, G.; Di Capua, A.; Acquavia, M.A. An Overview of Methods for L-Dopa Extraction and Analytical Determination in Plant Matrices. *Separations* **2022**, *9*, 224. <https://doi.org/10.3390/separations9080224>

Academic Editor: Alena Kubatova

Received: 31 July 2022

Accepted: 15 August 2022

Published: 17 August 2022

Publisher's Note: MDPI stays neutral with regard to jurisdictional claims in published maps and institutional affiliations.



Copyright: © 2022 by the authors. Licensee MDPI, Basel, Switzerland. This article is an open access article distributed under the terms and conditions of the Creative Commons Attribution (CC BY) license (<https://creativecommons.org/licenses/by/4.0/>).

1. Introduction

L-Dopa or levodopa (LD) is an amino acid analogue belonging to the class of catecholamine compounds. It is a precursor of dopamine (DP) and norepinephrine that act as neurotransmitters in brain areas related to psychomotor and emotional functions. LD is currently considered the most effective oral dopaminergic treatment for the main motor symptoms of Parkinson's disease (PD). This latter is the most widespread neurodegenerative movement disorder in the world: only Europe has a prevalence rate of around 108–257/100,000 and an incidence rate of 11–19/100,000 per year [1,2]. PD arises when the substantia nigra neuronal cells die and cannot biosynthesize dopamine (DA), a fundamental neurotransmitter, as it plays an essential role in physiological motor control. The symptoms of PD can be kept under control with strategies to replace or improve dopamine [1]. The LD pharmacological treatment is based on its replacement for DP to increase its bioavailability at the peripheral synaptic level, where the LD is decarboxylated to DP because of the amino acid aromatic decarboxylase (AADC) enzyme [3]. The pharmacological efficacy decreases after a certain period of intake; serious side effects such as motor fluctuations (commonly called on-off phenomenon), orthostatic hypotension, hallucinations and dyskinesias occur after a half-life time $t_{1/2}$ of 50 to 90 min. These reasons led to the development of extended-release LD formulations, combined with other drugs, to extend the half-life and bioavailability and reduce side effects [2,4–8].

The LD drug is chemically synthesized through a process that requires a costly metal catalyst and advanced technologies [9]. There are also natural sources, and the production of LD from different plants has advantages compared to chemical methods, such as a pure enantiomerically compound and low-cost approach. LD from natural sources also

reduces the secondary effects and helps slow the disease's progression. Some plants belonging to the Fabaceae family naturally contain significant amounts of LD [10]. Among these, the genus *Mucuna* includes the highest concentration of LD, which explains its widespread use in the management of Parkinson disease. The *Mucuna pruriens* is the most considered, containing up to 10% of LD in its seeds [11,12]. However, the seeds are covered by stinging hairs, and the beans contain elevated levels of tryptamines which may cause hallucinations in humans, so other plant matrices as a natural source of LD are also investigated. The control of crucial human body functions can be affected by a lack or excess of LD and its metabolites. Consequently, it is necessary to monitor the concentration of LD in all plant matrices destined for human consumption.

LD's low molecular weight and polar nature generally make its determination by reversed phase liquid chromatography challenging. A possible solution is to use an ion pair reagent to increase retention time. In general, it is necessary to work below the pK_a of the compound, where it will be protonated and not charged, and to decrease the organic content of the mobile phase [13]. In addition, LD aqueous solutions are unstable and degrade naturally over time, so the extraction procedure also requires special attention [13]. This review summarizes several analytical techniques developed in the last twenty years to analyze and quantify LD in plants consumed by animals and humans. It offers an entry into the extensive analytical literature on this compound, emphasizing the advantages and drawbacks of the proposed extraction, separation and characterization approaches. The described methods should make it possible to measure the content and changes in the concentrations of this biologically active plant compound in different plant matrices to evaluate their nutritional and toxicology aspects following consumption by animals and humans. Before introducing the main analytical techniques employed for LD extraction and detection in plant matrices, a brief description of its chemical and physical properties and its metabolic pathway in plants is provided, highlighting the main compounds involved during the biosynthetic routes both as LD precursors and as its conversion products. Among all, those characterized by chemical–physical properties more similar to LD are likely to be found in the extracts at an appreciable content and therefore must be taken into due consideration during its detection.

1.1. Chemical and Physical Properties

LD structure is characterized by the catechol moiety bonded to the amino acid functionality ($-\text{CH}_2\text{NH}_2\text{COOH}$) in -meta and -para positions to the hydroxyl groups in positions 3 and 4, respectively (Figure 1). The main chemical and physical properties are summarized in Figure 1.

Chemical Properties

Formula $\text{C}_9\text{H}_{11}\text{NO}_4$

Exact Mass: 197.069

Mol. Wt.: 197.188

Boiling Point: 537.89 [°C]

Melting Point: 396.26 [°C]

Log P: 0.05

Critical Temp: 588.32 [°C]

Critical Pres: 59.26 [Bar]

Critical Vol: 510.5 [cm^3/mol]

Gibbs Energy: -451.83 [kJ/mol]

Heat of Form: -668.94 [kJ/mol]

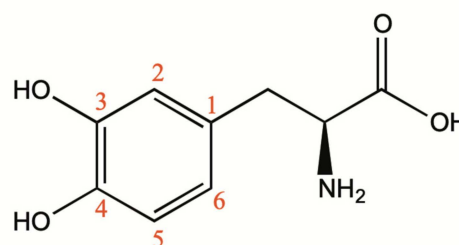


Figure 1. L-Dopa, (3,4-dihydroxyphenyl)-L-alanine, structure and its chemical and physical properties.

Furthermore, LD has three ionizable groups (Figure 2). When the pH value is on average between $pK_{a1} = 2.3$ and $pK_{a2} = 8.11$, LD is present as zwitterion that forms a network of intermolecular bonds where the protonated amine groups and the deprotonated carboxylic acid groups are linked. For this reason, LD is not very soluble in this pH range (LD solubility in water is 3.3 g/L), and acids are required to prepare aqueous solutions. This point is especially crucial regarding LD pharmacological bioavailability along the gastrointestinal lumen as well [14,15].

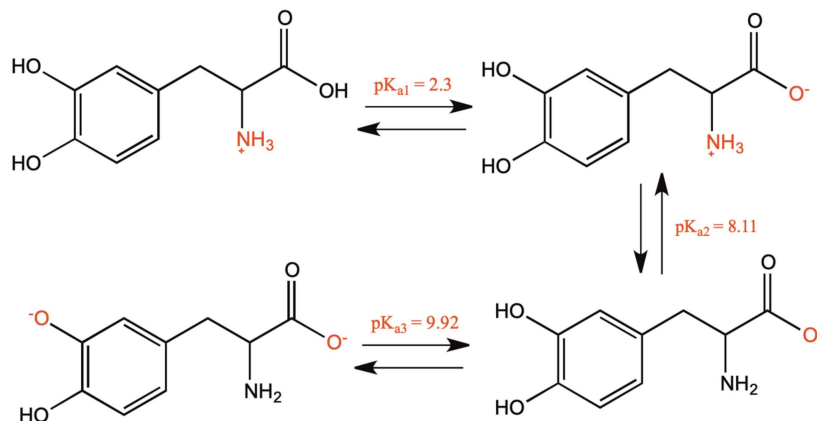


Figure 2. Ionization of L-Dopa at various pH values.

1.2. Biosynthesis and Conversion Routes of Levodopa in Plants

Plants produce hundreds of non-protein amino acids, among which LD, a secondary metabolite belonging to the class of catecholamines. Metabolism refers to the whole regulatory aspects implied in the biosynthesis of functional compounds, generally called metabolites. Metabolism in plants can be primary or secondary: primary metabolism generates all the essential compounds for the organism’s growth (primary metabolites); secondary metabolism produces all compounds that are considered not essential for the organism’s growth (secondary metabolites) but are equally important since directly involved in the interaction with the external environment [16,17]. Among catecholamines, norepinephrine (NE), epinephrine (EP), dopamine (DP) and normetanephrine (NMP) are other secondary metabolites whose structures are shown in Figure 3.

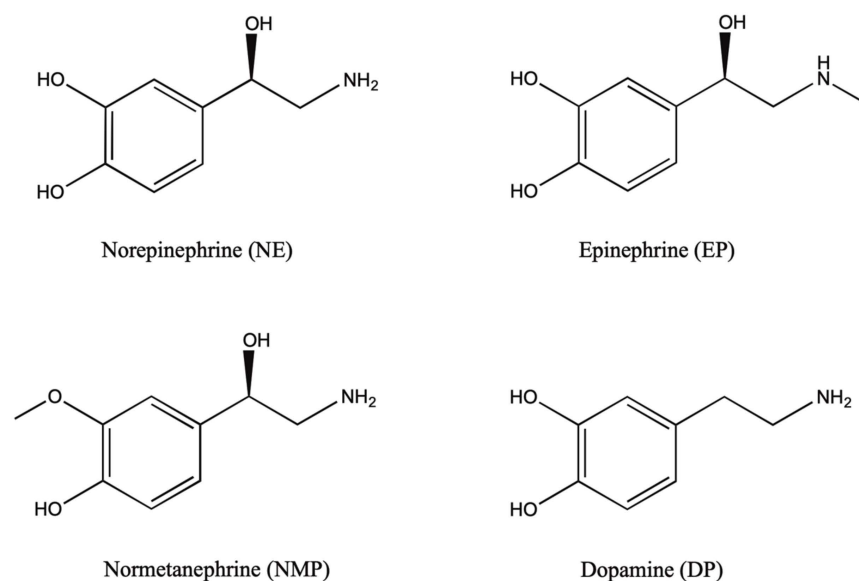


Figure 3. Norepinephrine (NE), epinephrine (EP), dopamine (DP) and normetanephrine (NMP) structures.

Shikimic acid pathway is the most important metabolic pathway of secondary metabolites in plants, and it represents the plant's biosynthetic key for L-tyrosine [16,18]. Like in mammals, L-tyrosine is involved in plants as a precursor for the catecholamines' biosynthetic pathway.

L-tyrosine can be converted into LD by tyrosine hydroxylase, or in tyramine upon decarboxylation of the same substrate. DP can derive both from tyramine hydroxylation and L-dopa decarboxylation (Figure 4) [16,19]. This last synthetic route has been reported in plants such as *Cytisus scoparius* Scottish broom, *Monostroma fuscum* marine alga, *Lophophora williamsii* peyote cactus and *Portulaca callus* [19,20].

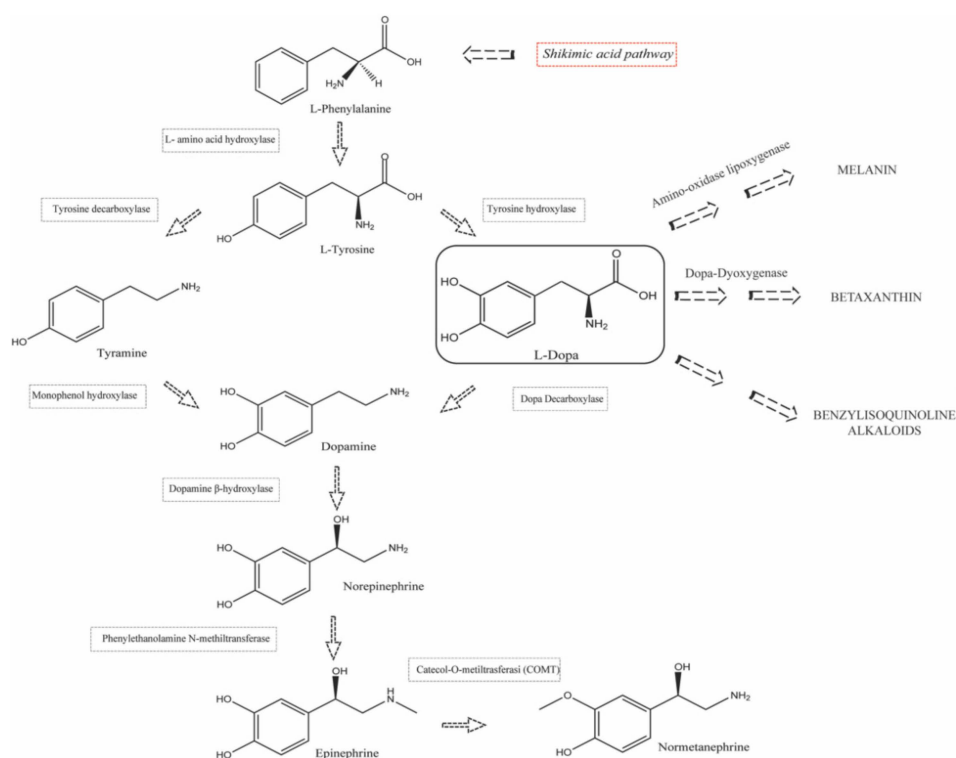


Figure 4. Plant catecholamine synthesis pathway.

In plant organisms, LD plays an important role as a precursor for other classes of compounds. LD can be converted by 4,5-DOPA dioxygenase into betalamic acid, which is a key compound in the biosynthesis of betalaines, red-purple and yellow pigments found in plants of the order *Caryophyllales* and two genera of fungi: *Amanita* and *Hygrocybe* [21–23]. Furthermore, it can be oxidized toward melanin: at first, LD is oxidized to dopaquinone by the enzyme polyphenol oxidase (PPO), and then it is metabolized to melanin by the plant lipoxigenase [18,19,24]. LD also represents a key precursor in the biosynthesis of benzylisoquinoline alkaloids, involved in specific plants (like basal eudicots in the order *Ranunculales*) for defense against herbivores and pathogens [21]. As far as the defense is concerned, in some legumes (e.g., *Mucuna pruriens*), LD plays an important role as an allelopathic compound that is exuded from the roots in order to inhibit the growth of surrounding plants [18,21,24,25]. The catecholamines catabolism in some plant species also involves their methylation: this is the case of the peyote cactus, *Lophophora williamsii*, in which LD is decarboxylated to dopamine and subsequently leads to the biosynthesis of mescaline, a hallucinogenic alkaloid, through the key compound 4-hydroxy-3-methoxyphenethylamine [26].

2. Levodopa Extraction Techniques

As it was previously outlined, extraction from natural products is nowadays considered the method of choice for providing LD over chemical synthesis which is time consuming, requires expensive and harmful chemicals and generates a racemic mixture of

LD. This justifies the growing interest in developing an extraction protocol to ensure LD recoveries are as high as possible, to remove interfering endogenous compounds and to be quick, easy and cheap.

In a general workflow, analytes are extracted directly from the plant matrices after undergoing simple pre-treatment steps consisting of homogenization and freeze drying. Homogenization, in particular, was found to be effective in increasing LD concentration in extracts from *Mucuna pruriens* seeds with respect to the extract obtained without any pre-conditioning ($151.5 \pm 5.1 \mu\text{g/g dw}$ vs. $146.0 \pm 4.5 \mu\text{g/g dw}$) [15].

Typical steps within food sample preparation after pre-treatment and extraction generally include clean-up and concentration. To this regard, literature data show that in the case of plant matrices, LD pre-concentration and clean-up steps are rarely provided. In contrast, for biological samples (e.g., plasma, blood, animal tissues or urine), a sample pre-concentration step or solid phase extraction (SPE) is always required. Such a distinction in sample preparation may be ascribed to the different content of LD in biological and plant samples. For samples containing low levels of LD, like biological ones, pre-concentration and SPE are essential in order to guarantee the minimum levels for analyte detection and quantification [27–34]. On the other hand, plant samples mainly involved in LD extraction studies, e.g., different varieties of *Mucuna pruriens* seeds and *Vicia faba* broad beans, are rich in this analyte. To get an idea of the LD content in plants, an average concentration of 4.96 and 4.39 g/100 g were estimated, respectively, in white and black variety of *Mucuna pruriens* seeds [35], whereas an average concentration of 7.68 mg/g dw was found in *Vicia faba* seeds [36]).

The extraction techniques used for LD, whose specifications are reported in Table 1, range from the traditional liquid–solid extraction (LSE), Soxhlet extraction, maceration extraction and reflux extraction to the latest and less used microwave-assisted extraction (MAE) and ultrasound-assisted extraction (UAE). The last two techniques involve substantial improvements in terms of automation and solvent consumption so to be referred as green techniques.

Regardless of the particular extraction technique used, in all cases the transferring of LD from the solid plant matrix into the extracting liquid phase revealed to be highly dependent on the pH: the extracting solutions used are all acidic in order to inhibit the LD oxidation process and avoid the formation of its zwitterionic form, which is poorly soluble. Controversies arise about the appropriateness of using solutions slightly acidified with acetic/formic acid or strongly acidified with hydrochloric/perchloric acid. The use of mineral or concentrated organic acids for L-dopa extraction is surely efficient but it is limited by the requirement of costly and energy-demanding downstream processes. The potential degradation of L-dopa in a strongly acidic environment is also to be considered. Acids of moderate strength meet the need to find more sustainable solvents even if they could be less efficient in preserving LD stability towards oxidation or formation of aggregated structures.

While the pH strongly influences the extraction yield, on the other hand, the sample ionic strength does not seem to affect the extraction process. IUPAC defines the salting-out effect as “the addition of particular electrolytes to an aqueous phase in order to increase the distribution ratio of a particular solute” [37]. It is usually exploited to improve the extraction efficiency (as it generally occurs for solid-phase microextraction SPME), but in the case of LD extraction from plant matrices it seemed to play no role.

Starting from these general considerations, the main extraction techniques listed above will be described in detail and critically discussed with reference to the most significant applications reported in the literature.

Table 1. Overview of the methods used for LD extraction occurring in plant samples.

Extraction Technique	Matrix	Variety	Solvents and Optimized Conditions	Recovery Percent (Mean Value Percent)	References
Solid–liquid extraction (LSE)	<i>Mucuna pruriens</i> dehulled and whole seed	White and black var. utilis	HCl 0.1 M; solvent: sample ratio 100:1 (<i>v/w</i>), extraction time 2 × (30 sec under homogenization and 1 h under stirring); extraction temperature 22 °C	101.8%	[35]
	Broad bean, cocoa and beans	//	HClO ₄ 0.2 M, solvent: sample ratio 5:1 (<i>v/w</i>), extraction time 24 h under shaking time for time; extraction temperature 25 °C	Within-day 84.4–96.0% Between-day 84.0–83.1%	[38]
	<i>Vicia faba</i> seeds (cotyledons and embryo axis)	var. Alameda var. Brocal	HClO ₄ 0.83 mol/kg; solvent: sample ratio 100:1 (<i>v/w</i>); extraction time 1 min under homogenization; extraction temperature 4 °C	//	[25]
	<i>Vicia faba</i> broad beans	Iambola, San Francesco, FV5, Cegliese, Extra-early purple and Aguadulce supersimonia	5% <i>w/v</i> HClO ₄ solution; solvent: sample ratio 10:1 (<i>v/w</i>); extraction time 5 min under homogenization; extraction temperature 4 °C	//	[39]
	<i>Vicia Faba</i> roots, sprouts and seeds	//	Formic acid:ethanol (1:1 <i>v/v</i>); solvent: sample ratio (10–40):1 (<i>v/w</i>); extraction time 5 × 120 min at 120 rpm; extraction temperature 4 °C	94.1–116.6%	[40]
	<i>Mucuna pruriens</i> seed cooked and raw	//	Water; solvent: sample ratio 400:1 (<i>v/w</i>); extraction time 20 min under stirring; extraction temperature 25 °C	//	[41]
	<i>Avena sativa</i> seeds	GK Iringo, GK Kormorán and GK Zalán	Aqueous solution of 0.1% (<i>m/v</i>) ascorbic acid and 1% (<i>v/v</i>) MeOH; solvent: sample ratio 6:1 (<i>v/w</i>); extraction time 5 h under shaking; extraction temperature 25 °C	95.2–99.6%	[42]

Table 1. Cont.

Extraction Technique	Matrix	Variety	Solvents and Optimized Conditions	Recovery Percent (Mean Value Percent)	References
	<i>Vicia Faba</i> roots, sprouts, leaf, seedling, pod, flower, stem	//	Ethanol solution 95% (v/v); solvent: sample ratio //; extraction time 72 h in freezer; extraction temperature −18 °C	//	[43]
	<i>Vicia Faba</i> sprouts	//	Ethanol solution 95% (v/v); solvent: sample ratio //; extraction time 48–72 h; extraction temperature −18 °C	//	[44]
	<i>Mucuna and Stizolobium pruriens</i> seed	<i>M. sempervirens</i> , <i>M. birdwoodiana</i> , <i>M. macrocarpa</i> , <i>M. interrupta</i> , <i>M. paohwashanica</i> , <i>Stizolobium pruriens</i> var. <i>pruriens</i> , <i>S. pruriens</i> var. <i>utilis</i>	HCl 0.1 M; solvent: sample ratio 20:1 (v/w); extraction time 2 × 5–10 min; extraction temperature 100 °C with a steam bath.	//	[45]
	<i>Mucuna pruriens</i> seed	//	0.1 M phosphate-buffered solution (pH = 7.0); solvent: sample ratio 5000:1(v/w); extraction time 5 h; extraction temperature 25 °C under stirring.	99.35%	[46]
	<i>Mucuna pruriens</i> leaves	//	0.1 M phosphate-buffered solution (pH = 7.0); solvent: sample ratio 500:1 (v/w); extraction time 5 h; extraction temperature 25 °C under stirring	98.30%	
	<i>Mucuna pruriens</i> seed	//	Citric acid 58% (wt%); solvent: sample ratio 7:1; extraction time 90 min; extraction temperature 60 °C	80–84%	[47]

Table 1. Cont.

Extraction Technique	Matrix	Variety	Solvents and Optimized Conditions	Recovery Percent (Mean Value Percent)	References
Ultrasound-assisted solvent extraction (UASE)	<i>Mucuna pruriens</i> seed	<i>Arka Dhanwantri</i>	Water acidified with 0.1 M HCl (pH: 2.6); solvent: sample ratio 10:1 (v/w); frequency 35 kHz; extraction time 5, 10, 15 min; extraction temperature 25 °C.	(5 min) 30.7% (10 min) 25.6% (15 min) 31.5%	[48]
		<i>Arka Ashwini</i>		(5 min) 29.0% (10 min) 27.7% (15 min) 26.8%	
		<i>White</i>		(5 min) 29.3% (10 min) 31.4% (15 min) 30.8%	
		<i>Brown</i>		(5 min) 23.9% (10 min) 28.7% (15 min) 30.6%	
	<i>Vicia faba</i> sprouts and seeds	//	MeOH and water mixture (80:20); solvent: sample ratio 1:5 (v/w); frequency //; extraction time 30 min; extraction temperature 25 °C.	//	[49]
	<i>Vicia faba</i> flowers, fruits and leaves	//	Water boiling deionized; solvent: sample ratio 50:1 (v/w); frequency //; extraction time 15 min; extraction temperature 100 °C.	100.32%	[36]
	<i>Vicia Faba</i> seeds	//	HCl 10 mM 5 mL; solvent: sample ratio // (v/w); frequency //; extraction time 2 × 60 min; extraction temperature 25 °C.	99.8%	[50]
	<i>Lens culinaris</i> seeds			105.0%	
	<i>Vicia Faba</i> sprouts, leaves, flowers, pods, roots	//	Aqueous MeOH 50% (v/v); solvent: sample ratio 200:1 (v/w); frequency //; extraction time 30 min; extraction temperature below 40 °C.	//	[51]

Table 1. Cont.

Extraction Technique	Matrix	Variety	Solvents and Optimized Conditions	Recovery Percent (Mean Value Percent)	References
	<i>Vicia faba</i> seeds	<i>Bachus, Bolero White, Windsor Bonus, Rambo Amigo, Olga Granit, Albus Fernando, Amulet</i>	Aqueous CH ₃ COOH 0.2% (v/v); solvent: sample ratio 25:1 (v/w); frequency 40 kHz; extraction time 2 × 20 min; extraction temperature 25 °C.	//	[15]
	Wild type legume grain	<i>Acacia nilotica, Bauhinia purpurea, Canavalia ensiformis, Cassia hirsuta, Caesalpinia bonducella, Erythrina indica, Mucuna gigantea, Pongamia pinnata, Sebania sesban, Xylia xylocarpa</i>	HCl 0.1 M; solvent: sample ratio 10:1 (v/w); frequency // kHz; extraction time 30 min and stirring for 1 h. extraction temperature 25 °C.	//	[52]
	<i>Mucuna sanjappae</i> seed	//	HCl 0.1 M; solvent: sample ratio 300:1 (v/w); frequency // kHz; extraction time 20 min; extraction temperature 25 °C.	//	[53]
	<i>M. pruriens</i> seeds	<i>Macrocarpa</i>	HCl 0.1 M; solvent: sample ratio 300:1 (v/w); frequency // kHz; extraction time 20 min; extraction temperature 25 °C.	//	[54]
Microwave-assisted solvent extraction (MASE)	<i>Mucuna pruriens</i> seed	<i>Arka Dhanwantri</i>	Water acidified with 0.1 M HCl (pH = 2.6); solvent: sample ratio 10:1 (v/w); MW power 400 W; irradiation time 5, 10, 15 min; extraction temperature 60 °C.	(5 min) 53.5% (10 min) 58.7% (15 min) 58.4%	[48]
		<i>Arka Ashwini</i>		(5 min) 50.6% (10 min) 59.6% (15 min) 54.0%	
		<i>White</i>		(5 min) 50.5% (10 min) 49.6% (15 min) 58.5%	

Table 1. Cont.

Extraction Technique	Matrix	Variety	Solvents and Optimized Conditions	Recovery Percent (Mean Value Percent)	References
		Brown		(5 min) 56.1% (10 min) 54.9% (15 min) 54.8%	
	<i>Mucuna pruriens</i> seed	<i>Arka Dhanwantri</i>	Water acidified with 0.1 M HCl (pH = 2.6); solvent: sample ratio 10:1 (v/w); extraction time 300 min, extraction temperature 100 °C	60.2%	[48]
		<i>Arka Ashwini</i>		65.7%	
		White		57.2%	
		Brown		59.8%	
Reflux extraction	<i>Mucuna pruriens</i> powder and extracts	//	MeOH and 0.1 M HCl mixture (70:30); solvent: sample ratio 100:1 (v/w); extraction time 30 min; extraction temperature 25 °C	98.83%	[55]
	<i>Mucuna pruriens</i> seed	<i>Preta Kaunch</i>	HCl 0.1 M; solvent: sample ratio 2:1 (v/w); extraction time 180 min; extraction temperature 25 °C	98.1–106.7%	[56]
	<i>Mucuna pruriens</i> powder formulation	//	Water and EtOH mixture (30:70); solvent: sample ratio //; extraction time 7 days; extraction temperature cold	94.5%	[57]
Maceration	<i>Phaseolus vulgaris</i> dried seed, seeding and callus	//	HCl 0.1 M and EtOH mixture (1:1); solvent: sample ratio 1:10; extraction time 5 days; extraction temperature 25 °C	99.55–100.27%	[58]
Soxhlet extraction	<i>Mucuna utilis</i> seed	//	MeOH; solvent: sample ratio //; extraction Soxhlet time //; extract obtained sonication for 60 min with 100 mL HCl 0.1 M; extraction temperature 25 °C	98.67–100.4%	[59]

// This indicates that values were not reported.

2.1. Liquid–Solid Extraction (LSE)

Liquid–solid extraction (LSE) is one of the most widely used extraction methods. At first, it involves the penetration of the extracting solution into the solid sample with subsequent analytes dissolution into the solution, followed by analytes diffusion out of the solid sample and, finally, their collection. The physical-chemical properties of the extraction solvent, the solid sample granulometry, the solvent–solid ratio, the temperature and the extraction time are parameters that must be taken into consideration in order to optimize the efficiency of the extraction process [60]. As it was previously discussed, all liquid–solid extraction methods include a pre-treatment step of the finely grounded solid sample and, sometimes, they also require a possible homogenization of the solid with the extracting solution in order to increase the surface contact area and facilitate the liquid extraction, improving the passage of LD in the solution [25,35,39].

Solvent selection is generally based on the law of similarity and inter-miscibility so that solvents with polarity values similar to the solute are likely to perform better. Alcohols, such as ethanol and methanol, are universal solvents for phytochemical investigation [60]; despite this, LD appears to be insoluble in ethanol and methanol as well as not very soluble in water for the reasons previously explained [15]. Accordingly, the choice of 95% ethanol [43,44] or water as extracting solutions [41] is doubtful, especially if neither sample homogenization nor agitation is foreseen in the extraction procedure.

The solid–solvent ratios used are quite different, strongly depending on the concentration of the analyte of interest in the plant sample. Large ratios are needed for matrices rich in LD. As an example, for *Mucuna pruriens* extraction, ratios values of 5000:1 *v/w* for seeds or 500:1 *v/w* for fresh leaves both in 0.1 M phosphate-buffered solution pH = 7.0 have been reported [46]. Intermediate ratios are used for matrices with a medium content of LD (e.g., for *Vicia faba* the ratio 10:1 *v/w* in 5% *w/v* HClO₄ solution was used [39]) and, finally, small ratios suggest minor LD quantities (e.g., for *Avena sativa* a ratio of 6:1 *v/w* in aqueous solution of 0.1% ascorbic acid and 1% methanol was reported [42], for cacao and broad beans the ratio used was 5:1 *v/w* in HClO₄ 0.2 M [38]).

Regarding the extraction temperature, stability studies conducted by Zhou et al. [14] have shown that the oxidation kinetics of LD is favored at high temperatures and in a neutral pH environment: despite the acidic environment (pH = 2), at 80 °C the analyte already starts showing degradation after less than 100 h of treatment. For this reason, although high temperatures increase diffusion and solubility, in the specific case of LD it is advisable to proceed at low extraction temperatures or at least at room temperatures, as mostly reported, with some exceptions such as the work of Yang et al. [45], where a surprisingly high temperature of 100 °C was adopted for LD extraction. A prolonged extraction time is another parameter that might negatively influence LD stability and therefore its content in the final extract.

The values of the LSE percentage recoveries are not always reported. A high percentage recovery of 101.8% was achieved for LD extraction from *Mucuna pruriens* dehulled and whole seed [35]. Appreciable values of 94.1 to 116.6% were also reported for the extractions from *Vicia faba* roots, sprouts and seeds [40].

An extraction efficiency of 9.2 ± 0.1 wt% of LD was achieved from *Mucuna pruriens* seeds by employing citric acid as solvent extraction. In order to find more sustainable solvents, the authors demonstrated that organic acids, such as citric acid, have hydrotropic properties: in acidic environments, they interact with protonated compounds characterized by low solubility. Thanks to the intermolecular interactions between the solvent and LD, a high extraction selectivity was assured, with relative purities of levodopa higher than 90%.

2.2. Ultrasound-Assisted Solvent Extraction (UAE)

The ultrasound-assisted extraction (UAE) is based on the ultrasonic energy waves that generate acoustic cavitation in the liquid medium and allow the cells' disruption: this method improves analyte dissolution and its mass-transfer to the solution [60,61].

Based on the literature, the UAE method for the extraction of LD from plant matrices is more commonly used compared to reflux, maceration or microwave-assisted extraction (MAE) extraction methods. The extracting solutions used are mostly acidified solutions such as water acidified with 0.1 M HCl (pH = 2.6), HCl 0.1 M, HCl 10 mM, aqueous CH₃COOH 0.2% (v/v) [48,50,52–54]. The extraction times are usually in a range between 15 and 30 min, with the exception of the work of Chen et al. [50], where a UAE extraction of LD from *Lens culinaris* and *Vicia faba* seeds matrices was applied in duplicate for 60 min by using a 10 mM HCl extracting solution. The percentage recovery values obtained from the two matrices are 99.8% for *Vicia faba* and 105.0% for *Lens culinaris*: these values suggest that the methodology used allows high recoveries and therefore shows high extraction efficiency.

Generally, a long-term exposure of the extraction matrix to ultrasounds is discouraged. Palonowska et al. [15] conducted a study on the optimization of LD extraction from *Vicia faba* and pointed out that a prolonged exposure of the plant matrix to ultrasounds has a negative effect. They demonstrated that the content of LD extracted from dry beans of *Vicia faba* var. major Bachus decreased from $74.8 \pm 1.4 \mu\text{g/g}$ (dw) to $71.9 \pm 0.7 \mu\text{g/g}$ (dw), by switching ultrasonic extraction time from 10 to 60 min, respectively. Initially, a positive effect of ultrasounds employment was observed up to 10 min of treatment. A further increase in the sonication time decreased the LD content in the extract. A possible explanation for these results might be that ultrasounds cause overheating, thus promoting the thermal degradation of LD. It is therefore advisable to shorten the sonication time as much as possible or at least to take precautions aimed at reducing overheating, such as water circulation in the ultrasonic bath [48].

2.3. Microwave-Assisted Extraction (MAE)

Microwave-assisted extraction (MAE) is an extraction technique that involves the use of microwaves in order to heat the sample–solvent mixture and thus facilitate the extraction of the analyte. The microwave heat source has the advantage of acting on the entire volume by interacting with polar compounds (e.g., water and some organic components) present in the plant matrix based on ionic conduction and dipole rotation mechanisms [60,62].

In the literature, there is only one work by Dahnani et al. [48] where MAE was used for LD extraction from *Mucuna pruriens* seeds. In this work, the performances of the conventional extraction method of refluxing were compared with those of two green methods, namely ultrasound and microwave-assisted solvent extraction (MASE). The MASE recovery percentages obtained on four *Mucuna pruriens* seeds (Arka Dhanwantri, Arka Ashwini, White, Brown) fall within the range of 54.0–58.5% for 15 min of extraction. These values are encouraging when compared with the percentages recorded on the same matrices by using UAE extraction treatment, which were comprised in the range of 26.8–31.5%. Better recoveries of 57.2 to 65.7% were obtained with a reflux extraction. The higher extraction yield obtained using refluxing in comparison to UAE and MAE was justified by the authors in terms of the exhaustive extraction by refluxing. It is worth noting that extraction times of the order of 5 to 15 min were employed for UAE and MAE against the 5 h employed for reflux. In general, higher extract yields were obtained with UAE and MAE by increasing the extraction time, even if a definite trend was not derived. The authors concluded their study pointing out that, among the three extraction methods explored, the microwave-assisted extraction provided overall the best results in terms of yield and quality of *Mucuna pruriens* extract by employing shorter times and with minimal solvent consumption.

2.4. Reflux Extraction

Reflux extraction is a common solid–liquid extraction process that takes place at a constant temperature and is based on repeated cycles of evaporation and subsequent condensation of the solvent over a given period of time. This process is efficient, simple, economical and very popular at an industrial scale [63]. As reported in Table 1, there are few works where a reflux extraction protocol has been performed, although notable recovery percentages ranging in the interval of 98.1–106.7% were achieved for LD extraction from

Mucuna pruriens seeds var. Preta Kaunch [56]. For this extraction, the following conditions have been used: HCl 0.1 M; solvent: sample ratio 2:1 (*v/w*); extraction time 180 min; extraction temperature: 25 °C. The long extraction time adopted is to be noticed, for it constitutes a disadvantage of this technique (extraction times generally range from a minimum of 30 min [55] to a maximum of 300 min [48]) along with the higher solvent volumes needed compared to UAE, MASE or LSE extractions.

2.5. Maceration and Soxhlet Extraction

Maceration is a simple and low-cost extraction technique which has some drawbacks such as low extraction yield and need of large amounts of solvents. The extraction starts by grinding the plant sample into smaller particles to increase the surface area and improve the mixing with solvent. Then, the material–solvent mixture plant is kept for a long time, agitated at different intervals and finally filtered through a filtration medium.

The Soxhlet extraction is an automatic continuous extraction method which makes it possible to achieve a high extraction efficiency. A small amount of dry sample is placed in a thimble-holder, located in a distillation flask containing the extraction solvent. When an overflow level is reached, the solution of the thimble is aspirated by a siphon and is delivered back into the distillation flask, carrying the extracted solutes into the bulk liquid. The solute remains in the distillation flask, whereas the solvent comes back to the solid sample. The process is repeated until complete extraction takes place.

Due to the need for larger amounts of solvents and longer extraction times compared to UAE, MAE or LSE techniques, there are only a few works in the literature where maceration and Soxhlet extractions are used, as it is possible to see from Table 1. In particular, maceration has been reported for LD extraction from *Mucuna pruriens* powder formulation with a recovery percentage of 94.5% [57] and from *Phaseolus vulgaris* dried seed, seeding and callus with recoveries in the range of 99.55–100.27% [58]. In both cases, the high recovery percentages were achieved at the expense of the extraction times that were extended up to 7 days and 5 days, respectively. Singh et al. used the Soxhlet method for LD extraction from *Mucuna pruriens* seeds, obtaining recovery percentage values in the range of 98.67–100.4% [59].

3. Levodopa Detection Methods

In the last 20 years, many attractive papers have been published showing the optimized techniques used to identify and quantify the LD in plant matrices (Table 2). Most of these require a preliminary separation step, and the HPLC is most often used; others allow a direct detection of the analyte.

Table 2. Analytical methods and operation conditions employed in the last twenty years for the LD detection with their main strengths and drawbacks.

Methods	Sample Source	LOD Range	Stationary Phase	Mobile Phase	Detection Mode	Strengths	Drawbacks	References
HPLC-UV	Broad bean, cocoa and beans	10 ng/mL–15 µg/mL	RP-C18 (mean particle diameter 5 µm, 125 × 3 mm I.D.)	Solvent (A): acetate buffer, pH = 4.66; solvent (B): methanol	Photodiode array detector (DAD)	It is highly reproducible, rapid and efficient	Sensitivity is rather limited so it is suitable for plant matrices with medium and high concentrations of LD. Selectivity is also limited since it does not allow the unambiguous identification of structurally similar molecules.	[38]
	<i>Mucuna pruriens</i> dehulled and whole seed			Solvent (A): water/methanol/phosphoric acid 975.5:19.5:1 (v/v/v), pH = 2.0; solvent (B): 70% methanol.				[35]
	<i>Vicia faba</i> seeds (cotyledons and embryo axis)			Ammonium phosphate buffer (0.05 mol/kg, pH = 2.0)				[25]
	<i>Vicia faba</i> broad beans			Water (H ₂ O) and acetonitrile (ACN) both containing 0.1% (v/v%) acid formic				[39]
	<i>Vicia faba</i> roots, sprouts, seedling, leaf, flower, pod, stem			Solvent (A): 0.1% acetic (98%); Solvent (B): methanol (2%).				[43]
	<i>Vicia faba</i> sprouts			Solvent (A): 82% buffer solution (32 mM citric acid, 54.3 mM sodium acetate, 0.074 mM Na ₂ EDTA, 0.215 mM octyl sulphate pH = 4); Solvent (B): 18% methanol				[44]
	<i>Mucuna</i> and <i>Stizolobium pruriens</i> seed			Solvent (A): 0.1 N acetic acid (90%); Solvent (B): methanol (10%)				[45]
	<i>Mucuna pruriens</i> seed			Solvent (A): 0.1% formic acid (98%); Solvent (B): methanol (2%)				[48]
	<i>Vicia faba</i> flowers, fruits and leaves			Solution of 50 mM potassium dihydrogen phosphate (pH = 2.3)				[36]
	<i>Vicia faba</i> sprouts, leaves, flowers, pods, roots			Solvent (A): water with 0.3% formic acid; Solvent (B): acetonitrile with 0.3% formic acid				[51]

Table 2. Cont.

Methods	Sample Source	LOD Range	Stationary Phase	Mobile Phase	Detection Mode	Strengths	Drawbacks	References
	<i>Vicia faba</i> seeds			Solvent (A): 97% v/v of an aqueous solution of 0.2% v/v acetic acid; Solvent (B): 3% v/v methanol				[15]
	<i>M. pruriens</i> seeds			Water, methanol and acetonitrile (5:3:2) containing 0.2% triethylamine, pH = 3.3				[54]
	<i>Mucuna pruriens</i> powder formulation			Solvent (A): water 80% v/v; Solvent (B): methanol 20% v/v				[57]
	<i>Mucuna pruriens</i> powder and extracts		RP-C18 (mean particle diameter 5 µm)	Water: Methanol: Acetonitrile (100:60:40) containing 0.2% Triethylamine, pH = 3.3				[55]
	<i>Mucuna sanjappae</i> Seed		RP-C18 (250 × 4.6 mm I.D.)	Methanol				[53]
	<i>Mucuna utilis</i> seed		RP-C18 (250 × 4.0 mm I.D.)	Solvent (A):0.5% v/v of acetic acid 30%; Solvent (B): methanol 70%				[59]
LC-MS	<i>Vicia faba</i> roots, sprouts and seeds	18 µg/Kg	RP-C18 (mean particle diameter 2.6 µm, 100 × 4.6 mm I.D.)	Solvent (A): ultrapure water with 0.5% (v/v) formic acid 50%; Solvent (B): methanol 50%	Photo diode array detector (DAD) and triple quadrupole (TQ) mass spectrometer	Robust analytical technique that provides higher sensitivity and selectivity than LC-UV methods. It allows to unambiguously identify the compounds under analysis, through the possibility of fragmentation.	It is a technique susceptible to matrix effects: co-eluting compounds could interfere with the ionization of the analyte under examination. Detection in MRM mode is to be preferred.	[40]
			Not reported	Not reported	Photo diode array detector (DAD) and quadrupole-time-of-flight (QTOF)-mass spectrometer			[49]
	0.01 µg/mL	RP-C18 (mean particle diameter 4 µm, 250 × 2 mm I.D.)	Solvent (A): solution 0.1% (v/v) of formic acid (97%); Solvent (B): ACN/MeOH 75/25 containing 0.1% (v/v) formic acid (3%)	Ion Trap mass spectrometer	[42]			

Table 2. Cont.

Methods	Sample Source	LOD Range	Stationary Phase	Mobile Phase	Detection Mode	Strengths	Drawbacks	References
HPTLC	<i>M. pruriens</i> seeds	Not reported	Silica-coated aluminum sheet (10 cm × 10 cm with 0.2 mm thickness)	n-butanol, acetic acid and water were used as mobile phase at 4:1:1	UV-Vis thin layer scanner	It makes it possible to obtain a preliminary separation of the analytes in a fast, efficient, easy and low cost analysis	It is generally employed only for qualitative analysis. It is poorly reproducible, as it works in an open system, whose environmental conditions could alter the results.	[54]
CE-UV	<i>Vicia faba</i> seeds <i>Lens culinaris</i> seeds	LOD value 0.7 µg/mL.	47 cm (40 cm from inlet to the detector) × 75 µm i.d. fused-silica capillary	35 mM NaH ₂ PO ₄ , pH = 4.55, 17.5 kV and 30 °C.	Photo diode array detector (DAD)	It allows faster analysis and higher efficiency than LC-UV	It is less sensitive than HPLC-UV	[50]
Electrochemical methods	<i>Mucuna pruriens</i> seed, leaves	LOD value 1.54 µM	Working electrode: gold modified pencil graphite	Supporting electrolyte: 0.1 M phosphate-buffered solution (pH = 7.0)	Differential pulse voltammetry (DPV)	It makes it possible to identify and quantify the analyte in a fast and economical way, through the use of conventional or modified nanostructured electrodes, which permits a better selectivity and sensitivity of analysis.	The technique still shows limitations especially related to the problem of electrode poisoning and oxidizable interfering compounds in the same range of anode potential.	[46]
	<i>Mucuna pruriens</i> seed cooked and raw	LOD value 5.12 ng/mL	RP-C18 (mean particle diameter 3.5 µm, 150 × 2.1 mm I.D.) Working electrode: Glassy carbon	Eluent/supporting electrolyte: 103 mM sodium acetate, 0.88 mM citric acid, 2.14 mM 1-octanesulphonic acid sodium salt with pH adjusted to 2.38 by orthophosphoric acid	Amperometric detection at a potential of +0.7 V after micro-high performance liquid chromatography separation			[41]
	<i>Sunflower seed, sesame seed, pumpkin seed and fava bean seed</i>	LOD value 14.3 nmol/L	Working electrode: glassy carbon modified by graphene quantum dots decorated with Fe ₃ O ₄ nanoparticles/functionalized multiwalled carbon nanotubes	Supporting electrolyte: 0.1 mol/L PBS at pH = 5.5	Differential Pulse Voltammetry (DPV)			[64]
	<i>Sweet potato</i>	17 nM	Working electrode: nitrogen-doped graphene supported with nickel oxide nanocomposite	Supporting electrolyte: 0.05 M PBS at pH = 7	Differential pulse voltammetry (DPV)			[65]

Table 2. Cont.

Methods	Sample Source	LOD Range	Stationary Phase	Mobile Phase	Detection Mode	Strengths	Drawbacks	References
Spectrophotometry UV-Vis	Wild type legume grain	LOD 1.12 µg/mL	//	//	//	It is an easy to use and low-cost technique that allows both qualitative and quantitative evaluation	It is generally not preceded by a separation step. This implies that the sample can contain interfering compounds causing potential false positives.	[52]
	<i>Phaseolus vulgaris</i> dried seed, seeding and callus							[58]
NMR	<i>Mucuna pruriens</i> seed	LOD value 0.0175 mg/g	//	//	//	It is a highly reproducible technique. It makes it possible to get structural details of the compounds under examination.	Requires expensive equipment and provides low sensitivity compared to LC-MS. It is hardly used for quantification, due to the chemical noise and signal overlapping.	[56]

// This indicates that values were not reported.

3.1. High Performance Liquid Chromatography Coupled to UV–Vis (HPLC-UV)

The most widely used analytical method to detect LD from plant matrices is high performance liquid chromatography (HPLC) coupled to diode array detection (DAD) set at 280 nm. Generally, HPLC-UV requires an analyte concentration in the sample greater than that needed for LC-MS, as the sensitivity is limited. Similar molecules could absorb at the same wavelength value too (especially metabolites deriving from the same synthesis pathways or degradation products of a precursor metabolite); therefore, the HPLC-UV selectivity is lower than that of LC-MS which can instead provide a unique and unambiguous identification.

As far as the plant matrices reported in the references are concerned, LD is structurally similar to tyrosine, dopaquinone or dopamine, which at a wavelength of 280 nm can still give absorption and generate chromatographic peaks whose absorption spectrum is not unambiguously identifying the analyte. In this case, the use of standards and the comparison of retention times are more helpful than the only analysis of UV absorption spectra to validate the separation method and confirm the identity of the compounds.

Despite these disadvantages, HPLC-UV remains the most widely used technique since it is highly reproducible, rapid (in all methods proposed, LD peak can be observed up to 10 min into the chromatogram), efficient, very robust and has better sensitivity compared to UV–Visible spectrophotometry as well as being less expensive than LC-MS.

Regarding the chromatography separation conditions, all the works report the employment of columns with a classic C-18 stationary phase (although the most suitable chromatographic columns for the separation of small and polar molecules, such as LD, are different, e.g., the ZORBAX Eclipse Plus Phenyl-Hexyl [13]); instead, the most used mobile phases are acidified aqueous solutions with a pH range between 2 and 4.6 mixed with methanol or acetonitrile. Figure 5 shows an example of chromatographic separation conducted by Duan et al. [51], where LD was detected in faba tissues at different growth stages and separated from vicine and convicine ((A) 8-day-old sprout; (B) New leaf at vegetative stage; (C) Old leaf at vegetative stage; (D) Flower bud; (E) Pod hull at S4 stage; (F) Bean at S4 stage; (G) Stem at ripening; (H) Root at ripening stage; (I) Standard peaks of vicine and L-dopa, see Table 2 for operation conditions).

The limit of detection (LOD) reported for the different methods developed goes from 10 ng/mL [38] up to 15 µg/mL [48]. The best LOD/LOQ values are obtained by Baranowska et al. [38], respectively, 10/30 ng/mL on broad bean, cocoa and bean samples. The HPLC analyses were performed using gradient elution with acetate buffer (pH = 4.66) and methanol, with a DAD detector and fluorescence detector as well, which provides lower limits of quantification and detection because they are more sensitive and selective than the first detector. This is the only work that uses the fluorescent detector coupled to DAD. In fact, all other works report higher LOD/LOQ values because only DAD detectors are employed, e.g., LOD/LOQ 0.115/0.348 µg/mL by Kasture et al. [57] are better than the others that only use the DAD detector, by employing a RP-C18 (250 mm × 4.6 mm × 5 µm) column and water–methanol 80:20 as mobile phase.

Kasture et al. [57] and Baranowska et al. [38] showed the most suitable values of LOD/LOQ, so they theoretically provide methods that allow a more selective and sensitive quantification and separation of LD in plant matrices (in the specific case of Kasture et al. [57], on *Mucuna pruriens* samples).

Nevertheless, despite the good LOD/LOQ values, the choice of the water and methanol mix as mobile phase by Kasture et al. [57] is in contradiction with most of the works reported here, where acidified mobile phase are largely applicated. Among all, three of them used a phosphate buffer as mobile phase for LD separation (e.g., Goyoaga et al. [25] proposed a separation method with only ammonium phosphate buffer 0.05 mol/kg, pH = 2.0), although it is not the best choice for instrument maintenance because it can reduce the column life, due to precipitation of phosphate salts. For this latter reason, acidified aqueous solutions (e.g., water: acetonitrile both containing 0.1% (v/v%) acid formic by Renna et al. [39], 0.1% formic acid: methanol 98:2 by Duan et al. [51]) are preferred, because they allow a more efficient LD separation (LD chromatographic peaks appreciably resolved in the

chromatograms of the *Vicia faba* samples reported by Renna et al. [39] and Duan et al. [51] in comparison to Kasture et al. [57] who do not show any chromatogram) and a more efficient LD quantification than the only use of organic phase (e.g., Patil et al. [53] reported the LD separation from *Mucuna sanjappae* seeds by using only methanol on a RP-C18, 250 × 4.6 mm I.D. column.) or only water use as aqueous phase [57]. The reason for the use acidic solutions mobile phases could be the ion pair formation between analyte and counter-ion of the acid used, which provides better analyte stabilization and better separation than other matrix compounds. This is especially helpful for the analysis of plant matrices with a medium and low content of LD, where a best resolution and selectivity of chromatographic peaks are required.

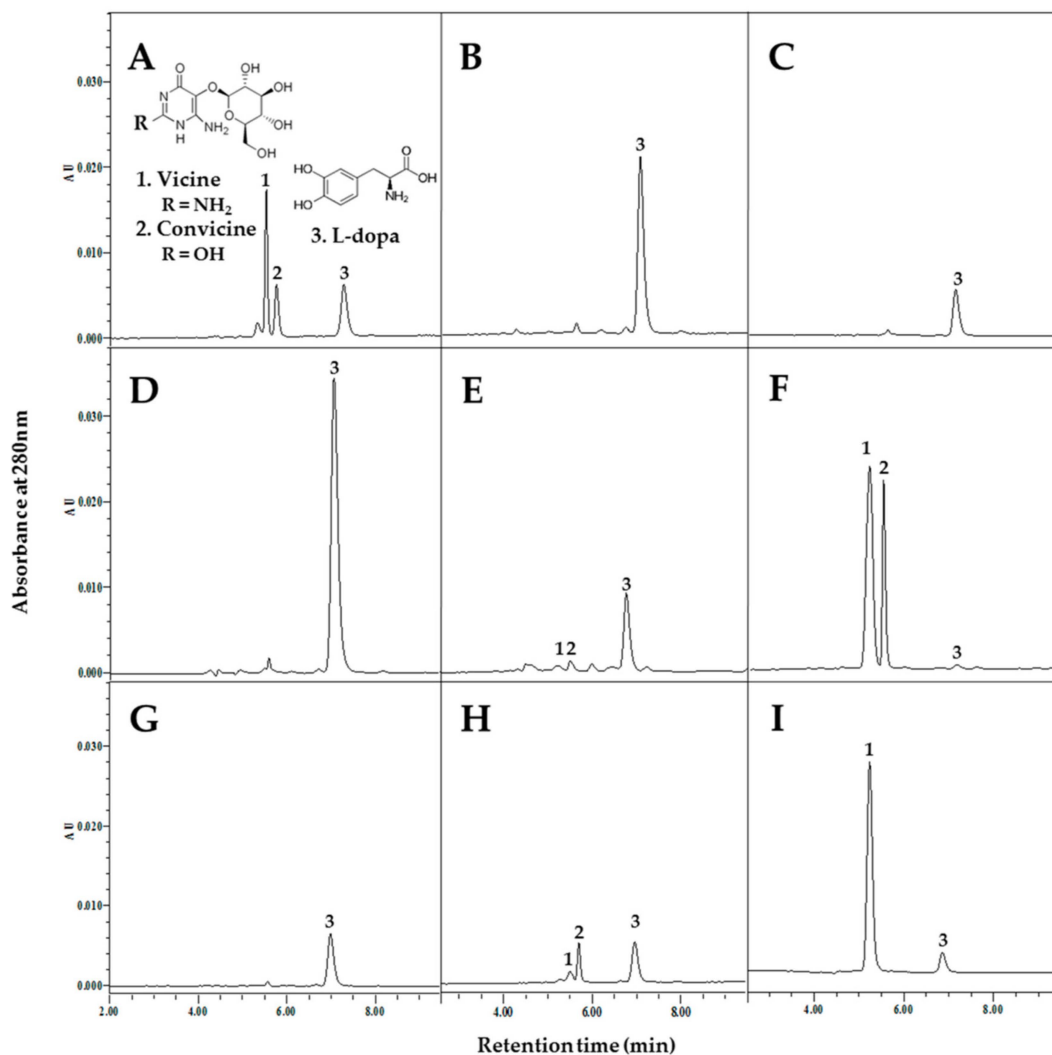


Figure 5. HPLC chromatograms of extracts from different faba bean tissues. (A) 8-day-old sprout; (B) New leaf at vegetative stage; (C) Old leaf at vegetative stage; (D) Flower bud; (E) Pod hull at S4 stage; (F) Bean at S4 stage; (G) Stem at ripening; (H) Root at ripening stage; (I) Standard peaks of vicine and L-dopa. Reprinted with permission from Ref. [51].

In addition, the lack of analytical method validation for all reported papers (Rathod et al. [55], Singh et al. [59], Kasture et al. [57] are the only ones who validated the method performed by following the International Council for Harmonization ICH guidelines) represents a disadvantage for those who approach the choice of an appropriate HPLC-UV LD analysis method, which is consistent and satisfying the analytical requirements for different plant matrices.

3.2. Ultra-High-Performance Liquid Chromatography Coupled to Mass Spectrometry (UHPLC-MS)

Ultra-high-performance liquid chromatography coupled to mass spectrometry (UHPLC-MS) is a valid method to determine the presence of specific compounds in a matrix. So far, only a few examples have been published in the literature where LC-MS has been used to determine LD presence in plant matrices. Varga et al. [42] determined LD in extracts from *Avena sativa* seeds by using a UHPLC coupled with an electrospray ionization ion trap mass spectrometer (ESI-ITMS). Separation was performed under gradient elution by using Eluent A consisting of 0.1% (*v/v*) formic acid and 3% (*v/v*) of Eluent B, containing ACN/MeOH at a volume ratio of 75/25 containing 0.1% (*v/v*) formic acid on a Synergi Hydro-RP250 \times 2 mm I.D., mean particle diameter 4 μ m analytical column. They reported the most abundant fragmentation of protonated precursor ion [(M+H)]⁺ at *m/z* 198: [(M+H)-NH₃]⁺ at *m/z* 181 and [(M+H)-H₂O-CO]⁺ at *m/z* 152. For MS analysis, they optimized ESI conditions. They found that a good peak intensity is reached with a gas pressure of 60 psi and a drying gas pressure of 25 psi at a nebulizing gas temperature of 350 °C. For this validated method, RSD% was reported as better than 4%. Furthermore, the high specificity allowed to obtain lower LODs is 18 μ g/kg. In this way, Varga et al. [42] have been able to detect LD in different species of oat, where LD concentration is three times lower than in *M. pruriens*.

Pavòn-Perèz et al. [40] determined the presence of LD from *Vicia faba* roots, sprouts and seeds. In this case, separation was carried out on a Phenomenex (Torrance, CA, USA) Kinetex XB Core-Shell C₁₈ column (100 mm \times 4.6 mm, 2.6 μ m), thermostated at 35 °C, using a mobile phase composed of 50% ultrapure water with 0.5% (*v/v*) formic acid and 50% methanol. LD detection was carried out by using an SPD-M20A diode array detector (DAD) and an LCMS-8030 triple quadrupole mass spectrometer. The separation method was validated following the ICH guidelines. Repeatability showed an RSD value of 1.40%, while recovery yield values were recorded from 94.14 to 116.62%, with RSD values \leq 5.66%. For the MS analysis, full spectra were acquired in a 50–1200 *m/z* range. They applied a multiple reaction monitoring (MRM) method for quantification using the transition *m/z* 198 \rightarrow *m/z* 152. The method developed by Pavòn-Perèz et al. [40] shows detection and quantification limits of 0.01 and 0.05 μ g/mL: these values are much lower than those reported by Kasture et al. [57] for HPLC/UV method (LOD/LOQ 0.115/0.348 μ g/mL). Compared to HPLC-UV alone, the opportunity to couple an HPLC system with the mass spectrometry makes it possible to identify compounds under investigation, based not only on their retention time but also on the mass. Furthermore, the possibility of applying fragmentation is helpful for characterization, in particular for the natural extract analyses, where the presence of isomers with similar retention times is possible.

3.3. High Performance Thin Layer Chromatography (HPTLC)

High performance thin layer chromatography (HPTLC) is a simple, robust, rapid and efficient analytical technique in quantitative analysis. HPTLC allows for a better separation than TLC, and the separation can be further improved with bidimensional HPTLC. Aware et al. [54] used HPTLC to determine LD presence on extracts from *M. macrocarpa* beans. The sample was spotted on a silica-coated aluminum sheet (10 cm \times 10 cm with 0.2 mm thickness), and LD was separated with a mixture of n-butanol: acetic acid: water (4:1:1). Although HPTLC provides a better resolution and a visual result, it can only be used as a preliminary step as a complementary method for quantitative analysis is still required.

3.4. Capillary Electrophoresis Coupled to UV-Vis (CE-UV)

Chen et al. [50] reported a simple method to determine LD from broad beans and lentils. Experiments were performed by using a Beckman P/ACE system 5510 coupled to a photodiode array (PDA) detector, set at 210 nm. For this separation, a 47 cm \times 75 μ m i.d. fused-silica capillary was employed.

The authors stressed the influence of pH on the LD charge state and then on its stability and solubility. In this regard, capillary electrophoresis revealed a powerful tool to

determine the pK_a values of LD (2.30, 8.11 and 9.92) along with its isoelectric point (5.20). The appearance of pseudo-peaks in electropherograms registered at neutral and basic pH confirmed LD instability in these conditions and the requirement for an acidic environment for its determination, in accordance with the pK_a values derived. The separation conditions were optimized by using as running buffer 35 mM NaH_2PO_4 , pH = 4.55. Column was kept at 30 °C and a voltage of 17.5 kV was applied for the separation. For this method, a LOD of 0.7 $\mu\text{g}/\text{mL}$ was calculated. The method was validated for the quantification of LD in beans.

Generally, CE allows for faster analysis, higher efficiency and lower sensitivity than LC-UV even if in the present case comparable performances were observed considering that a LOD of 0.7 $\mu\text{g}/\text{mL}$ was achieved and that migration times of about 10 min were observed and then of the same order of the elution times reported in Table 2 for HPLC methods. The use of an aqueous buffer without organic solvent and the reduced cost of reagents and capillaries compared with that of HPLC solvents and columns are undoubted advantages of the proposed electrophoretic method.

3.5. UV-Vis Spectrophotometry

UV-Vis spectrophotometry is an analytical technique that is easy to use and low cost. Generally, it is used as a direct method without a preliminary separation step. This implies the risk of occurring in false results or inaccurate measurements, as the technique cannot really ascertain the compound identity and purity.

Vadivel et al. [52] determined the LD content in wild type legume grains collected from South India by measuring the ultra-violet light absorption at 282 nm. The LD content varied in the range of 1.34–5.45 g/100 g of dry matter. The samples of *Mucuna gigantea* showed the maximum content of LD. The spectrophotometric method adopted was not discussed at all, and there are no data concerning selectivity, accuracy and precision. The authors focused their interest on studying the effect of processing techniques used by Indian tribal groups on the level of LD. As an example, a drastic reduction of LD (29–46%) was observed during soaking and cooking in an alkaline solution due to the enhanced seed coat permeability increasing the leaching out of LD. Furthermore, alkaline conditions promoted the chemical conversion of LD into melanin pigments. Sprouting and oil-frying treatment also caused a significant decrease in LD content (34–48%), suggesting that enzymes able to metabolize LD, such as polyphenol oxidase, could be synthesized upon germination of seeds.

Rahami-Nezhad et al. [58] developed a UV-spectrophotometric method based on a nitrosation reaction of LD in an acidic medium and then a treatment with NaOH to form a stable red compound which absorbs at a wavelength of 470 nm. The method revealed to be highly selective for the detection of LD comparing with phenolic compounds such as resorcinol, pyrogallol, phenol and tyrosine. The authors stressed the selectivity towards LD by showing that the formation of the deep red color in the reaction solution was not observed for the other compounds investigated. Indeed, tyrosine gave no coloration whereas resorcinol, pyrogallol and phenol gave less intense coloration. In order to exclude that the method can generate a false positive in the determination of LD, besides the visual inspection of the reaction solutions, it would have been desirable to demonstrate the lack of absorbance from the phenolic compounds upon reaction at the detection wavelength.

The method has been fully validated showing good performances. Percentage RSD values of intra- and inter-day were found between 0.24 and 0.36% as well as 0.08 and 0.36%, respectively, indicating satisfactory precision. It was successfully applied to the quantification of LD in 33 biotypes of *P. vulgaris* seeds. No significant differences were observed by comparing the results obtained by the proposed method with those deriving from a reference HPLC method. Among the tested biotypes, black seeds possessed higher amounts of LD in comparison to yellow and brown types. LD content was determined also in seed dark germination and callus culture of *Phaseolus vulgaris* in different conditions. The results obtained show that tyrosine significantly increased the concentration of LD and thus could be exploited for the large-scale production of LD.

3.6. Electrochemical Methods

Electrochemical methods are of considerable interest for the analysis of biological compounds since they offer important advantages compared to classical methods such as fast response time, simple equipment, low cost, high sensitivity and even selectivity without samples pretreatment. The modification of conventional electrodes by nanomaterials such as metal nanoparticles, graphene oxide and carbon nanotubes, makes it possible to achieve detection limits at the nanomolar level, high precision and accuracy by substantially improving the response selectivity.

To date, considering the ease of LD to oxidize, there are a plethora of electrochemical sensors for LD anodic determination in areas such as the pharmaceutical or clinical, whereas there are few applications to the analysis of food samples. Amperometric detection was firstly apply to LD detection in raw and cooked *Mucuna* bean seeds by Mwatseteza et al. [41] by applying a constant potential of +0.70 V vs. Ag/AgCl at a glassy carbon electrode. It is worth noting that the employment of an unmodified electrode was possible thanks to a preliminary micro-high performance liquid chromatography separation that nullifies the feasibility of electrochemical techniques for direct sample analysis. Detection of low concentration of L-dopa up to 5.12 ng/mL was achieved even if no data are reported on the method's accuracy.

A gold modified pencil graphite electrode was employed for LD detection by differential pulse voltammetry (DPV) in *Mucuna pruriens* leaves and seeds [46]. The detection limit for L-dopa was 1.54 μ M. The appreciable separation of the LD current peak from that of ascorbic acid, along with the good recoveries evaluated in all the real samples, indicated the successful applicability of the method for determinations in complex matrices.

A glassy carbon electrode modified with a new nanocomposite consisting of graphene quantum dots decorated with magnetic nanoparticles and carboxylated multiwalled carbon nanotubes was employed as a new sensing platform for the electrochemical determination of L-dopa by DPV in sunflower seed, sesame seed, pumpkin seed and fava bean seed [64]. Good sensitivity and selectivity with low overpotential for the determination of LD and a detection limit of 14.3 nmol/L were obtained. The influence of some coexistent interfering substances was examined, setting their tolerance limit as the amount of foreign ion causing $\pm 10\%$ error in the determination of LD. The lowest value was obtained for dopamine, as it would be expected considering its similar structure with LD. The results obtained on LD quantification in the real samples were in good agreement with those obtained by a reference spectrophotometric method.

Finally, a nitrogen-doped graphene oxide incorporated nickel oxide modified electrode was applied for the sensitive determination of LD by DPV in sweet potato with a limit of detection of 17 nM. The selective determination of LD was achieved in the presence of common interferents, displaying a minor response from uric acid, acetaminophen and L-cysteine. The recovery percentages from sweet potato (*Ipomoea batatas*) samples were in the range of 97.8–101.5% [65].

3.7. Nuclear Magnetic Resonance Spectroscopy (NMR)

Nuclear magnetic resonance spectroscopy (NMR) has been largely used to determine the chemical structure of compounds isolated from different food matrices. It is a simple, robust, rapid and not disruptive method, although it requires very expensive instrumentation. Furthermore, it is barely used for quantification analysis as an internal standard need to be added to the sample's solution. In this way, the sample cannot be directly recovered after analysis. For the LD identification, there is only one publication where they used this technique. Fernandez-Pastor et al. [56] were able to quantify the presence of LD from different *Mucuna pruriens* seeds. NMR analyses were performed by using 600 MHz Varian Direct Drive NMR spectrometer. Samples were dissolved in a mixture of 0.1 M HCl:H₂O:D₂O:DMSO-*d*₆ (8:1:1) and syringic acid was added as internal standard. In this work, they were able to set values of 0.0175 mg/g for LOD and 0.0578 mg/g for LOQ.

4. Conclusions and Outlook

In the last twenty years, some progress has been made in developing sensitive and selective extraction and detection methods for the unambiguous identification of LD in plant matrices, mainly *Vicia faba* and *Mucuna pruriens* seeds and green parts. However, one major difficulty in LD determination is quantitatively extracting the compound of interest. Using efficient extraction methods can improve the use of natural products with high levels of this bioactive compound in the Parkinson's disease.

LSE, UASE, MASE techniques are the most widely used, although the different procedures proposed still show some contradictions concerning extracting solutions, time and temperature values. Extraction efficiency typically increases by applying more acidic extraction conditions. Chromatographic separations based on a single separation step can show limited selectivity in complex matrices. In the future, the application of multidimensional techniques could considerably reduce the matrix effects and thus significantly improve the analytical performances. Regarding detection techniques, the DAD is typically the method of choice for medium and high content of LD matrices due to its high versatility and diffusion.

Nevertheless, tandem mass spectrometry offers some advantages since characteristic fragments can be generated, thus providing the structural information necessary for LD characterization. A step forward could be done by the validation of LC-MS/MS method for LD quantification in different plant matrices since this analytical technique remains the most sensitive, with LOD and LOQ values lower than those from other analytical techniques reported in the literature. In conclusion, advances have been achieved in LD analysis; however, further efforts are required to establish analytical protocols that can be applied for routine determinations of this compound.

Author Contributions: C.T., first draft, writing, editing, conceptualization, reviewing; F.L. and R.C., writing, editing, conceptualization, reviewing; A.D.C., G.B. and M.A.A., writing, editing, reviewing. All authors have read and agreed to the published version of the manuscript.

Funding: This research received no external funding.

Institutional Review Board Statement: Not applicable.

Informed Consent Statement: Not applicable.

Data Availability Statement: Not applicable.

Conflicts of Interest: The authors declare no conflict of interest.

References

1. Balestrino, R.; Schapira, A.H.V. Parkinson disease. *Eur. J. Neurol.* **2020**, *27*, 27–42. [[CrossRef](#)] [[PubMed](#)]
2. Khan, S.T.; Ahmed, S.; Gul, S.; Khan, A.; Al-Harrasi, A. Search for safer and potent natural inhibitors of Parkinson's disease. *Neurochem. Int.* **2021**, *149*, 105135. [[CrossRef](#)] [[PubMed](#)]
3. Hall, M.F.E.; Church, F.C. Integrative Medicine and Health Therapy for Parkinson Disease. *Top. Geriatr. Rehabil.* **2020**, *36*, 176–186. [[CrossRef](#)]
4. Rezak, M. Current Pharmacotherapeutic Treatment Options in Parkinson's Disease. *Disease-A-Month* **2007**, *53*, 214–222. [[CrossRef](#)]
5. Nutt, J.G. Pharmacokinetics and pharmacodynamics of levodopa. *Mov. Disord.* **2008**, *23*, 580–584. [[CrossRef](#)]
6. Tizabi, Y.; Getachew, B.; Aschner, M. Novel Pharmacotherapies in Parkinson's Disease. *Neurotox. Res.* **2021**, *39*, 1381–1390. [[CrossRef](#)]
7. Poewe, W.; Antonini, A. Novel formulations and modes of delivery of levodopa. *Mov. Disord.* **2015**, *30*, 114–120. [[CrossRef](#)]
8. Müller, T. Catechol-O-methyltransferase inhibitors in Parkinson's disease. *Drugs* **2015**, *75*, 157–174. [[CrossRef](#)]
9. Valdés, R.H.; Puzer, L.; Gomes, M.; Marques, C.E.S.J.; Aranda, D.A.G.; Bastos, M.L.; Gemal, A.L.; Antunes, O.A.C. Production of L-DOPA under heterogeneous asymmetric catalysis. *Catal. Commun.* **2004**, *5*, 631–634. [[CrossRef](#)]
10. Patil, S.A.; Apine, O.A.; Surwase, S.N.; Jadhav, J.P. Biological sources of L-DOPA: An alternative approach. *Adv. Park. Dis.* **2013**, *2*, 81–87. [[CrossRef](#)]
11. Lampariello, L.; Cortelazzo, A.; Guerranti, R.; Sticozzi, C.; Valacchi, G. The magic velvet bean of mucuna pruriens. *J. Tradit. Complement. Med.* **2012**, *2*, 331–339. [[CrossRef](#)]
12. Denne, T. Analysis of Levodopa Content in Commercial Formulations of *Mucuna pruriens* Seeds Used in Integrative Treatment of Parkinson's Disease. *Mov. Disord.* **2019**, *34*, S37–S38.

13. Long, W.J.; Brooks, A.E.; Biazzo, W. Analysis of Polar Compounds Using 100% Aqueous Mobile Phases with Agilent ZORBAX Eclipse Plus Phenyl-Hexyl and Other ZORBAX Phenyl Columns. *Appl. Note Pharm. Food* **2009**, 1–8.
14. Zhou, Y.Z.; Alany, R.G.; Chuang, V.; Wen, J. Studies of the rate constant of L-DOPA oxidation and decarboxylation by HPLC. *Chromatographia* **2012**, *75*, 597–606. [[CrossRef](#)]
15. Polanowska, K.; Łukasik, R.M.; Kuligowski, M. Development of a Sustainable, Simple, and Robust Method for Efficient L-DOPA Extraction. *Molecules* **2019**, *24*, 2325. [[CrossRef](#)] [[PubMed](#)]
16. Płonka, J.; Górny, A.; Kokoszka, K.; Barchanska, H. Metabolic profiles in the course of the shikimic acid pathway of *Raphanus sativus* var. *longipinnatus* exposed to mesotrione and its degradation products. *Chemosphere* **2020**, *245*, 125616. [[CrossRef](#)] [[PubMed](#)]
17. Kroymann, J. Natural diversity and adaptation in plant secondary metabolism. *Curr. Opin. Plant. Biol.* **2011**, *14*, 246–251. [[CrossRef](#)] [[PubMed](#)]
18. Soares, A.R.; Marchiosi, R.; de Cássia Siqueira-Soares, R.; de Lima, R.B.; dos Santos, W.D.; Ferrarese-Filho, O. The role of L-DOPA in plants. *Plant. Signal. Behav.* **2014**, *9*, e28275. [[CrossRef](#)]
19. Kulma, A.; Szopa, J. Catecholamines are active compounds in plants. *Plant. Sci.* **2007**, *172*, 433–440. [[CrossRef](#)]
20. Szopa, J.; Wilczyński, G.; Fiehn, O.; Wenzel, A.; Willmitzer, L. Identification and quantification of catecholamines in potato plants (*Solanum tuberosum*) by GC-MS. *Phytochemistry* **2001**, *58*, 315–320. [[CrossRef](#)]
21. Schenck, C.A.; Maeda, H.A. Tyrosine biosynthesis, metabolism, and catabolism in plants. *Phytochemistry* **2018**, *149*, 82–102. [[CrossRef](#)] [[PubMed](#)]
22. Hatlestad, G.J.; Sunnadeniya, R.M.; Akhavan, N.A.; Gonzalez, A.; Goldman, I.L.; McGrath, J.M.; Lloyd, A.M. The beet R locus encodes a new cytochrome P450 required for red betalain production. *Nat. Genet.* **2012**, *44*, 816–820. [[CrossRef](#)]
23. Tanaka, Y.; Sasaki, N.; Ohmiya, A. Biosynthesis of plant pigments: Anthocyanins, betalains and carotenoids. *Plant. J.* **2008**, *54*, 733–749. [[CrossRef](#)] [[PubMed](#)]
24. Hachinohe, M.; Matsumoto, H. Mechanism of selective phytotoxicity of L-3,4-dihydroxyphenylalanine (L-dopa) in barnyardgrass and lettuce. *J. Chem. Ecol.* **2007**, *33*, 1919–1926. [[CrossRef](#)] [[PubMed](#)]
25. Goyoaga, C.; Burbano, C.; Cuadrado, C.; Varela, A.; Guillamón, E.; Pedrosa, M.M.; Muzquiz, M. Content and distribution of vicine, convicine and L-DOPA during germination and seedling growth of two *Vicia faba* L. varieties. *Eur. Food Res. Technol.* **2008**, *227*, 1537–1542. [[CrossRef](#)]
26. Kuklin, A.I.; Conger, B.V. Catecholamines in Plants. *J. Plant. Growth Regul.* **1995**, *14*, 91–97. [[CrossRef](#)]
27. Ribeiro, R.P.; Gasparetto, J.C.; De Oliveira Vilhena, R.; De Francisco, T.M.G.; Martins, C.A.F.; Cardoso, M.A.; Pontarolo, R. Simultaneous determination of levodopa, carbidopa, entacapone, tolcapone, 3-O-methyldopa and dopamine in human plasma by an HPLC-MS/MS method. *Bioanalysis* **2015**, *7*, 207–220. [[CrossRef](#)]
28. Azaryan, A.; Ligor, T.; Buszewski, B.; Temerdashev, A.; Dmitrieva, E.; Gashimova, E. LC-MS/MS Determination of Catecholamines in Urine Using FMOC-Cl Derivatization on Solid-Phase Extraction Cartridge. *Chromatographia* **2018**, *81*, 1487–1494. [[CrossRef](#)]
29. Bergmann, M.L.; Schmedes, A. Highly sensitive LC-MS/MS analysis of catecholamines in plasma. *Clin. Biochem.* **2020**, *82*, 51–57. [[CrossRef](#)]
30. Bugamelli, F.; Marcheselli, C.; Barba, E.; Raggi, M.A. Determination of l-dopa, carbidopa, 3-O-methyldopa and entacapone in human plasma by HPLC-ED. *J. Pharm. Biomed. Anal.* **2011**, *54*, 562–567. [[CrossRef](#)]
31. Van Faassen, M.; Bischoff, R.; Eijkelenkamp, K.; De Jong, W.H.A.; Van Der Ley, C.P.; Kema, I.P. In Matrix Derivatization Combined with LC-MS/MS Results in Ultrasensitive Quantification of Plasma Free Metanephrines and Catecholamines. *Anal. Chem.* **2020**, *92*, 9072–9078. [[CrossRef](#)] [[PubMed](#)]
32. Kakarla, S.; Kodali, G.; Seru, G. Selective and rapid LC-MS/MS method for the simultaneous quantitation of levodopa and carbidopa in human plasma using alumina SPE cartridges. *Indo Am. J. Pharm. Sci.* **2016**, *3*, 905–915.
33. Li, W.; Rossi, D.T.; Fountain, S.T. Development and validation of a semi-automated method for L-dopa and dopamine in rat plasma using electrospray LC/MS/MS. *J. Pharm. Biomed. Anal.* **2000**, *24*, 325–333. [[CrossRef](#)]
34. Tampu, R.; Tampu, C.; Elfakir, C. Optimization of SPE method for the extraction of 12 neurotransmitters from sheep brain. *Ovidius Univ. Ann. Chem.* **2020**, *31*, 110–121. [[CrossRef](#)]
35. Siddhuraju, P.; Becker, K. Rapid reversed-phase high performance liquid chromatographic method for the quantification of L-Dopa (L-3,4-dihydroxyphenylalanine), non-methylated and methylated tetrahydroisoquinoline compounds from *Mucuna* beans. *Food Chem.* **2001**, *72*, 389–394. [[CrossRef](#)]
36. Bulduk, İ.; Topal, N. Development and Validation of a Quantification Method for L-DOPA in Plants and Pharmaceutical Materials. *Hacet. J. Biol. Chem.* **2020**, *49*, 1–10. [[CrossRef](#)]
37. IUPAC. *IUPAC Compendium of Chemical Terminology*; IUPAC: Research Triangle Park, NC, USA, 2009. [[CrossRef](#)]
38. Baranowska, I.; Płonka, J. Simultaneous Determination of Biogenic Amines and Methylxanthines in Foodstuff—Sample Preparation with HPLC-DAD-FL Analysis. *Food Anal. Methods* **2015**, *8*, 963–972. [[CrossRef](#)]
39. Renna, M.; De Cillis, F.; Leoni, B.; Acciardi, E.; Santamaria, P. From by-product to unconventional vegetable: Preliminary evaluation of fresh fava hulls highlights richness in L-DOPA and low content of anti-nutritional factor. *Foods* **2020**, *9*, 159. [[CrossRef](#)]

40. Pavón-Pérez, J.; Oviedo, C.A.; Elso-Freudenberg, M.; Henríquez-Aedo, K.; Aranda, M. LC-MS/MS Method For L-Dopa Quantification in Different Tissues of *Vicia Faba*. *J. Chil. Chem. Soc.* **2019**, *64*, 4–6. [[CrossRef](#)]
41. Mwatseteza, J.; Torto, N. Amperometric detection of 3-(3,4-dihydroxyphenyl)-L-alanine (L-dopa) in raw and cooked *Mucuna* bean seeds employing micro-HPLC. *Chromatographia* **2007**, *66*, 811–813. [[CrossRef](#)]
42. Varga, E.; Varga, M. Development and validation of an LC-MS/MS method for the analysis of L-DOPA in oat. *Acta Biol. Szeged.* **2014**, *58*, 133–137.
43. Etemadi, F.; Hashemi, M.; Randhir, R.; Zandvakili, O.; Ebadi, A. Accumulation of L-DOPA in various organs of faba bean and influence of drought, nitrogen stress, and processing methods on L-DOPA yield. *Crop. J.* **2018**, *6*, 426–434. [[CrossRef](#)]
44. Randhir, R.; Shetty, P.; Shetty, K. L-DOPA and total phenolic stimulation in dark germinated faba bean in response to peptide and phytochemical elicitors. *Process. Biochem.* **2002**, *37*, 1247–1256. [[CrossRef](#)]
45. Yang, X.; Zhang, X.; Zhou, R. Determination of L-Dopa content and other significant nitrogenous compounds in the seeds of seven *Mucuna* and *Stizolobium* species in China. *Pharm. Biol.* **2001**, *39*, 312–316. [[CrossRef](#)]
46. Kalachar, H.C.B.; Basavanna, S.; Viswanatha, R.; Arthoba Naik, Y.; Ananda Raj, D.; Sudha, P.N. Electrochemical determination of l-dopa in *Mucuna pruriens* seeds, leaves and commercial siddha product using gold modified pencil graphite electrode. *Electroanalysis* **2011**, *23*, 1107–1115. [[CrossRef](#)]
47. Benfica, J.; Morais, E.S.; Miranda, J.S.; Freire, M.G.; de Cássia Superbi de Sousa, R.; Coutinho, J.A.P. Aqueous solutions of organic acids as effective solvents for levodopa extraction from *Mucuna pruriens* seeds. *Sep. Purif. Technol.* **2021**, *274*, 119084. [[CrossRef](#)]
48. Dhanani, T.; Singh, R.; Shah, S.; Kumari, P.; Kumar, S. Comparison of green extraction methods with conventional extraction method for extract yield, L-DOPA concentration and antioxidant activity of *Mucuna pruriens* seed. *Green Chem. Lett. Rev.* **2015**, *8*, 43–48. [[CrossRef](#)]
49. Abdel-Sattar, E.; Mahrous, E.A.; Thabet, M.M.; Elnaggar, D.M.Y.; Youssef, A.M.; Elhawary, R.; Zaitone, S.A.; Rodríguez-Pérez, C.; Segura-Carretero, A.; Mekky, R.H. Methanolic extracts of a selected Egyptian *Vicia faba* cultivar mitigate the oxidative/inflammatory burden and afford neuroprotection in a mouse model of Parkinson's disease. *Inflammopharmacology* **2021**, *29*, 221–235. [[CrossRef](#)]
50. Chen, X.; Zhang, J.; Zhai, H.; Chen, X.; Hu, Z. Determination of levodopa by capillary zone electrophoresis using an acidic phosphate buffer and its application in the analysis of beans. *Food Chem.* **2005**, *92*, 381–386. [[CrossRef](#)]
51. Duan, S.; Kwon, S.J.; Lim, Y.J.; Gil, C.S.; Jin, C.; Eom, S.H. L-3,4-dihydroxyphenylalanine accumulation in faba bean (*Vicia faba* L.) tissues during different growth stages. *Agronomy* **2021**, *11*, 502. [[CrossRef](#)]
52. Vadivel, V.; Biesalski, H.K. Effect of certain indigenous processing methods on the bioactive compounds of ten different wild type legume grains. *J. Food Sci. Technol.* **2012**, *49*, 673–684. [[CrossRef](#)] [[PubMed](#)]
53. Patil, R.R.; Gholave, A.R.; Jadhav, J.P.; Yadav, S.R.; Bapat, V.A. *Mucuna sanjappae* Aitawade et Yadav: A new species of *Mucuna* with promising yield of anti-Parkinson's drug L-DOPA. *Genet. Resour. Crop. Evol.* **2015**, *62*, 155–162. [[CrossRef](#)]
54. Aware, C.; Patil, R.; Gaikwad, S.; Yadav, S.; Bapat, V.; Jadhav, J. Evaluation of L-dopa, proximate composition with in vitro anti-inflammatory and antioxidant activity of *Mucuna macrocarpa* beans: A future drug for Parkinson treatment. *Asian Pac. J. Trop. Biomed.* **2017**, *7*, 1097–1106. [[CrossRef](#)]
55. Rathod, B.G.; Patel, N.M. Development of validated RP-HPLC method for the estimation of L-Dopa from *Mucuna pruriens*, its extracts and in Aphrodisiac formulation. *Int. J. Pharma Sci. Res.* **2014**, *5*, 508–513.
56. Fernandez-Pastor, I.; Luque-Muñoz, A.; Rivas, F.; O'Donnell, M.; Martinez, A.; Gonzalez-Maldonado, R.; Haidour, A.; Parra, A. Quantitative NMR analysis of L-Dopa in seeds from two varieties of *Mucuna pruriens*. *Phytochem. Anal.* **2019**, *30*, 89–94. [[CrossRef](#)]
57. Kasture, V.; Sonar, V.P.; Patil, P.P.; Musmade, D. Quantitative Estimation of L-Dopa from Polyhebal Formulation by using RP-HPLC. *Am. J. PharmTech Res.* **2014**, *4*, 408–414.
58. Rahmani-Nezhad, S.; Dianat, S.; Saeedi, M.; Barazandeh, M.; Ghadiri, A. Evaluating the accumulation trend of L-dopa in dark-germinated seeds and suspension cultures of *Phaseolus vulgaris* L. by an efficient uv-spectrophotometric method. *Quim. Nova* **2018**, *41*, 386–393. [[CrossRef](#)]
59. Singh, R.; Saini, P.; Mathur, S.; Singh, G.; Kumar, S. Application of high performance liquid chromatography to the determination and validation of levodopa in methanolic extract of *Mucuna utilis*. *Int. J. Green Pharm.* **2010**, *4*, 156–158. [[CrossRef](#)]
60. Zhang, Q.W.; Lin, L.G.; Ye, W.C. Techniques for extraction and isolation of natural products: A comprehensive review. *Chin. Med.* **2018**, *13*, 20. [[CrossRef](#)]
61. Chemat, F.; Rombaut, N.; Sicaire, A.G.; Meullemiestre, A.; Fabiano-Tixier, A.S.; Abert-Vian, M. Ultrasound assisted extraction of food and natural products. Mechanisms, techniques, combinations, protocols and applications. A review. *Ultrason. Sonochem.* **2017**, *34*, 540–560. [[CrossRef](#)]
62. Conte, L.; Moret, S.; Purcaro, G. *Il Campione per l'Analisi Chimica*; Springer: Berlin/Heidelberg, Germany, 2014; Chapter 4; pp. 81–82.
63. Chua, L.S.; Latiff, N.A.; Mohamad, M. Reflux extraction and cleanup process by column chromatography for high yield of andrographolide enriched extract. *J. Appl. Res. Med. Aromat. Plants* **2016**, *3*, 64–70. [[CrossRef](#)]

64. Arvand, M.; Abbasnejad, S.; Ghodsi, N. Graphene quantum dots decorated with Fe₃O₄ nanoparticles/functionalized multiwalled carbon nanotubes as a new sensing platform for electrochemical determination of l-DOPA in agricultural products. *Anal. Methods* **2016**, *8*, 5861–5868. [[CrossRef](#)]
65. Renganathan, V.; Sasikumar, R.; Chen, S.M.; Chen, T.W.; Rwei, S.P.; Lee, S.Y.; Chang, W.H.; Lou, B.S. Detection of neurotransmitter (Levodopa) in vegetables using nitrogen-doped graphene oxide incorporated Nickel oxide modified electrode. *Int. J. Electrochem. Sci.* **2018**, *13*, 7206–7217. [[CrossRef](#)]



Untargeted metabolomic analysis by ultra-high-resolution mass spectrometry for the profiling of new Italian wine varieties

Alberto Onzo^{1,2} · Maria Assunta Acquavia^{1,3} · Raffaella Pascale⁴ · Patrizia Iannece⁵ · Carmine Gaeta⁵ · Filomena Lelario¹ · Rosanna Ciriello¹ · Carmen Tesoro¹ · Giuliana Bianco¹ · Angela Di Capua¹

Received: 21 July 2022 / Revised: 23 August 2022 / Accepted: 31 August 2022 / Published online: 19 September 2022
© Springer-Verlag GmbH Germany, part of Springer Nature 2022

Abstract

The chemical composition of wine samples comprises numerous bioactive compounds responsible for unique flavor and health-promoting properties. Thus, it's important to have a complete overview of the metabolic profile of new wine products in order to obtain peculiar information in terms of their phytochemical composition, quality, and traceability. To achieve this aim, in this work, a mass spectrometry-based phytochemical screening was performed on seven new wine products from Villa D'Agri in the Basilicata region (Italy), i.e., *Aglianico Bianco*, *Plavina*, *Guisana*, *Giosana*, *Malvasia ad acino piccolo*, *Colata Murro* and *Santa Sofia*. Ultra-high-resolution mass spectrometry data were processed into absorption mode FT-ICR mass spectra, in order to remove artifacts and achieve a higher resolution and lower levels of noise. Accurate mass-to-charge ratio (m/z) values were converted into putative elemental formulas. Therefore, 2D van Krevelen diagrams were used as a tool to obtain molecular formula maps useful to perform a rapid and more comprehensive analysis of the wine sample metabolome. The presence of important metabolite classes, i.e., fatty acid derivatives, amino acids and peptides, carbohydrates and phenolic derivatives, was assessed. Moreover, the comparison of obtained metabolomic maps revealed some differences among profiles, suggesting their employment as metabolic fingerprints. This study shed some light on the metabolic composition of seven new Italian wine varieties, improving their value in terms of related bioactive compound content. Moreover, different metabolomic fingerprints were obtained for each of them, suggesting the use of molecular maps as innovative tool to ascertain their unique metabolic profile.

Keywords Wine · Metabolomics · Untargeted · High-resolution mass spectrometry · Van Krevelen

Introduction

Wine has been a part of human culture for 6000 years, being employed for dietary and socio-religious purposes [1, 2]. Its first production goes back to antiquity, as does

the discovery of its healthful benefits, now largely attributed to the antimicrobial activity of ethanol [2]. Today, wine is a cultural symbol for many countries, a form of entertainment and a beverage of choice for supporters of its health benefits. Regardless of the region in which the wine is produced or the economic status of the consumer, all wines are expected to be pleasant experiences [3]. In most of wine regions of the world, at least until around the middle of the 1980s, wine was obtained from grapes, following a complex process known as “winemaking,” based on the fermentation of grape must with the indigenous yeasts present on the grapes when harvested or introduced from the equipment and cellar during the vinification process [4–7]. Nowadays, the practice of adding selected yeasts to slightly sulfited musts has been widely used to ensure a rapid and complete must fermentation and to produce wines of reproducible characteristics and quality [5, 7, 8]. Winemaking is a biological process characterized

✉ Maria Assunta Acquavia
maria.acquavia@unibas.it

¹ Dipartimento Di Scienze, Università Degli Studi Della Basilicata, Via dell'Ateneo Lucano 10, Potenza, Italy

² Present Address: Agilent Technologies, Via Piero Gobetti, 2c, 20063 Cernusco sul Naviglio, Milan, Italy

³ Thema Informatik S.R.L., Via Ressel 2/F, 39100 Bolzano, Italy

⁴ Gnosis By Lesaffre, Pisticci, 75015 Matera, Italy

⁵ Dipartimento Di Chimica e Biologia, Università Degli Studi Di Salerno, Via Giovanni Paolo II 132, Fisciano, Italy

by a series of biochemical transformations that involve enzymes from different microorganisms, especially yeasts, which are responsible for the principal part of the process, i.e., the alcoholic fermentation [4, 7]. The result of the winemaking process is the production of specific bio-compounds that are considered responsible of the most appreciated properties of this beloved product, such as its taste and its related biological activity [9, 10]. For this reason, a lot of effort has been spent in recent years to improve the knowledge of the metabolic profiles of different wine varieties. This information would be helpful in terms of process optimization, to enhance specific wine properties [8, 10–13]. The use of the modern chromatographic techniques, both gas chromatography (GC) and high-pressure liquid chromatography (HPLC) coupled to mass spectrometry as detection system [14–19], supported by other less sensitive techniques such as thin-layer chromatography (TLC), infrared spectroscopy (IRS), and nuclear magnetic resonance (NMR) [20–28], has allowed the identification of more than 500 compounds in wine, with concentrations ranging between 10^{-1} and 10^{-6} mg/L. Although at low levels, all these compounds greatly contribute to wine aroma and taste [29–31]. In detail, the taste is mainly due to a few compounds that are usually present individually at concentrations higher than 100 mg/L, like water, ethanol, organic acids, sugars, and glycerol [32, 33]. However, also other alcohols, volatile acids, and fatty acid esters are important for wine aroma, and they are produced by yeast during fermentation [34, 35]. Among them, alcohols often cover the higher and more concentrated percentage of all the volatile substances [16, 17]. On the contrary, carbonyls, polyphenols, lactones, terpenes, acetals, hydrocarbons, sulfur, and nitrogen compounds and B vitamins are present in much lower concentrations [36–38]. With regard to B vitamins, among which there's riboflavin (RF), they are released during vinification, and they are strain-dependent. RF wine content is generally up to 0.2 mg/L [39, 40]. Tannins are found in red wine and rarely in significant amounts in white wines [41, 42]. A comprehensive characterization of the wine metabolome could be accomplished using hyphenated techniques by following an untargeted analysis approach [43]. Despite high costs and long analysis times associated to their routine employment for this task, high-resolution mass spectrometry (HRMS) technique is the method of choice for untargeted metabolomic analysis, even if used by following a shotgun, or direct injection, approach [44–47]. Indeed, HRMS has been already used for wine characterization, allowing the identification of thousands of metabolites by using a single direct analysis, with labor times of a few minutes [31, 44, 45]. Moreover, related results provided useful biochemical mechanistic information, highlighting metabolic differences among

samples subjected to different winemaking conditions [31, 44, 45].

In this study, data acquired by using Fourier transform ion cyclotron resonance mass spectrometry (FT-ICR MS) and processed into absorption mode FT-ICR (aFT) mass spectra were employed to characterize for the first time the general molecular profile of seven new Italian wine varieties, i.e., *Aglianico Bianco*, *Plavina*, *Guisana*, *Giosana*, *Malvasia ad acino piccolo*, *Colata Murro* and *Santa Sofia*, produced in Villa D'Agri in the Basilicata region (Italy). These seven wines (five white wines and two red wines) represent the new main local grape varieties identified in the Basilicata region. Registered species and new species have been classified and reported in the chapter 5 of *Basivin_SUD* [48], and the general characteristics of grapes and vines have been summarized in Table S1 (see Supplementary information). Since raw data often contain artifacts, ultra-high-resolution mass spectra were processed into absorption mode FT-ICR mass spectra, in order to achieve a higher resolution and lower levels of noise, thus avoiding wrong molecular formula assignment. Considering the huge diversity of organic compounds present in wine varieties and their synergic activity resulting in pleased macroscopic properties, together with the deep correlation between compound levels and winemaking process, it's of great interest to obtain a general metabolomic profile of new wine varieties. Here, the molecular maps of main metabolites were proposed and discussed, with the aim to suggest their use as innovative tool to ascertain wines' unique metabolic profiles.

Materials and methods

Wine samples

Wine samples were obtained from new germplasms cultivated in the Pollino region, a natural area located in Basilicata (Italy), and were provided by the Agency for Development and Innovation in Agriculture (ALSIA, Agenzia Lucana di Sviluppo e di Innovazione in Agricoltura). The studied samples varied in terms of their type (i.e., red and white). Key features of these new wine varieties, together with a detailed organoleptic description, are described elsewhere [48].

Chemicals

Sodium trifluoroacetate (NaTFA, 98%) and methanol (MeOH, LC–MS grade) were purchased from Sigma-Aldrich

(Milano, Italy). Pure nitrogen (99.996%) was delivered to the MS system as the sheath gas.

Sample preparation

The procedure adopted in this work for the sample preparation was described by Roullier-Gall et al. [45]. In detail, 20 μL of sample were diluted by adding 1 mL of MeOH. The solution was vortexed, passed through a PTFE 0.22- μm syringe filter, and directly injected into the HRMS instrument. For each sample, 3 replicates have been prepared, together with a blank sample obtained by subjecting 20 μL of MeOH to the whole sample preparation step.

Mass spectrometry analysis

ESI (\pm) Fourier transform ion cyclotron resonance mass spectrometry (ESI-FT-ICR MS) technique was used for the untargeted analysis of the sample. High-resolution mass spectra were acquired on a Bruker (Bruker Daltonik GmbH, Bremen, Germany) solariX XR Fourier transform ion cyclotron resonance mass spectrometer (FT-ICR-MS) equipped with a 7 T superconducting magnet and an ESI source. The capillary voltage was set to 3.9 and -4.5 kV for negative and positive ionization modes, respectively, with a nebulizer gas pressure of 1.2 bar and dry gas flow rate of 4 L/min at 200 $^{\circ}\text{C}$. Samples were analyzed by direct infusion, with syringe flow rate of 5.0 $\mu\text{L}/\text{h}$. Spectra were acquired with a time domain size of 16 mega-word, an accumulation time of 0.1 s, and a mass range of 100–2000 m/z . For each sample, the number of scans was set to 50. Before the analysis, the mass spectrometer was externally calibrated with NaTFA. High accuracies were reached, with a root mean square (RMS) error lower than 0.1 ppm. FT-ICR mass spectra were subjected to several data pre-treatment steps. In detail, recorded free induction decays (FIDs) were subjected to apodization, and related absorption mode mass spectra were obtained. Phase correction, mass recalibration, and baseline correction have been performed, together with blank subtraction [49, 50] and noise filtering by following the N-Sigma methodology approach [51, 52]. More specifically, noise level has been estimated, and peaks showing a signal-to-noise ratio (S/N) higher than 2 were retained. Thus, the obtained FT-ICR mass spectra were exported to peak lists. From these, possible elemental formulas were calculated for each MS signal. To obtain unequivocal formulas, several constraints were applied, such as atoms number limitations, i.e., $C \leq 100$, $H \leq 200$, $O \leq 80$, $N \leq 5$, and $S \leq 1$ [44–47], restrictions on atoms to carbon number ratios, i.e., $0.2 \leq H/C \leq 3.1$, $O/C \leq 2$, $N/C \leq 1.3$, and $S/C \leq 0.8$, $\text{RDBE} > 0$, nitrogen rule (for m/z ratio values lower or equal to 500), and isotopic pattern filtering. Moreover, Kendrick mass defect (KMD) was performed to help formula

assignment [44, 45]. In detail, building blocks with a higher number of occurrences were identified and chosen for the analysis. For this step, experimental mass differences values were examined, and only those in the range ± 1 mDa of the building block exact mass were considered [53, 54]. To further improve the reliability of results, building blocks with occurrences lower than a threshold value (properly chosen to remove all the noisy data) were excluded, being higher the probability for these to have occurred randomly [55]. The absorption mode FT-ICR MS data obtained from both positive and negative mode analysis of all wine samples were processed by using AutoVectis Pro (v.8.9, Spectroswiss, Lausanne, Switzerland). R software (v3.6.3, www.r-project.org) was used for FT-ICR MS data analysis, in order to plot the van Krevelen 2D diagrams.

Results and discussion

Ultra-high-resolution ESI(\pm)-FT-ICR MS data acquired by direct injection were used to obtain a general description of metabolome of new Italian wine variety samples. In detail, five types of white wines, i.e., *Aglianico Bianco*, *Guisana*, *Giosana*, *Malvasia ad acino piccolo*, and *Santa Sofia*, and two types of red ones, i.e., *Colata Murro* and *Plavina*, were analyzed. A huge number of peaks (data not shown) were detected from our wine samples in both positive and negative mode. Through the analysis, nearly 500 signals were selected and included in our data (a maximum of 421 signals for the *Malvasia ad acino piccolo* wine), thus revealing the wide diversity of metabolites present in wine samples. However, it should be pointed out that possible artifacts can occur during FT-ICR data acquisition [56, 57] and, at the same time, background/noisy signal can interfere with hamper the identification of low intensity ionic species, thus making overall data elaboration more complex. Working with absorption mode mass spectra turned out to be the best solution to overcome these issues. Indeed, peak resolution and signal-to-noise ratios (S/N) were markedly improved, leading to the identification of a higher number of ionic species. The use of specific tools to accomplish this task, i.e., the AutoVectis Pro software, was crucial to perform a quick phase correction step efficiently and, thus, to obtain a readable absorption mode mass spectrum, task that couldn't be achieved for almost 40 years [49, 52, 56, 58]. Indeed, the use of absorption mode in FT-ICR mass spectrometry has been required for a long time either specially adapted instrumentation or a manually intensive process of phase correction. Instead, AutoVectis pro software allows to automatically do phase correction and baseline deviation removal, thus greatly reducing user interaction. In detail, AutoVectis Pro software performs the phase correction step in few milliseconds to obtain aFT mass spectra, by employing

a genetic algorithm to optimize the phase calibration. Once the user has defined the order of a predefined phase correction function, several others are generated by this software by applying random mutation on related frequency values. An identification of the best phase correction function is done by reiteration, until the complete optimization has been reached. Despite the advantages provided by the absorption mode mass spectrum, it's still difficult to deduce something by simply looking at full MS spectra. To better understand our results, MS signals were assigned to unique elemental formulas (see Materials and methods), and a well-known visualization tool, i.e., the van Krevelen plot, was employed to plot our results on a 2D diagram, by setting the H/C and the O/C ratios as the y- and the x-axis, respectively [44–46]. Based on H/C and O/C ratio, ionic species obtained from MS spectra will occupy a well-defined area on the van Krevelen 2D plot, and their position is helpful to classify them in one of the major metabolite classes. Briefly, the lipid region is located at the highest H/C ratio ($1.3 < \text{H/C} < 2.2$) and lowest O/C ratio ($0 < \text{O/C} < 0.3$) (e.g., palmitic acid H/C ratio = 2, O/C = 0.12). The peptide region overlaps with the lipid region but is located at higher O/C ratios ($0.1 < \text{O/C} < 0.5$) (e.g., methionine H/C ratio = 2.2, O/C ratio = 0.4). Instead, carbohydrate and polyphenol regions are located in the range $1.5 < \text{H/C} < 2.2$, $0.6 < \text{O/C} < 1.2$, and $0.4 < \text{H/C} < 1.4$ and $0.2 < \text{O/C} < 0.7$, respectively (e.g., glucose H/C ratio = 2, O/C ratio = 1 quercetin H/C ratio = 0.67, O/C ratio = 0.47) [59, 60]. Based on the results obtained from van Krevelen plots, the presence of specific types of metabolites in wine samples was proposed, i.e., carbohydrates, polyphenols, amino acids, and peptides and unsaturated fatty acids (Fig. 1, Figs. S1–S6).

From the van Krevelen plots analysis, it is possible to notice differences among metabolic profiles, some of them reflecting what was already found in the literature [45]. By

checking the results acquired in negative mode (Fig. 1) (see also Supplementary information Figs. S1A, S2A, S3, S4A, S5A), we can observe that there is a high-density population on the upper right part of the plot (usually assigned to carbohydrates, amino sugars, and peptides [60]), indicating a wider diversity of carbohydrates and glycoconjugates, and this aspect is common for both red and white wines that we analyzed. Furthermore, red wines seem to contain a higher amount of unsaturated glycoconjugate compounds, supporting what was already found regarding the presence of phenolic compounds in wine as glycoconjugates [6, 9, 61–63]. A higher density of points in the middle part of van Krevelen plot of red wines, moreover, indicates the presence of more phenolic derivatives [44, 45]. Polyphenols are important for the characteristics and quality of red wines. Their concentration in white wine is much lower. Polyphenols and related compounds can affect the appearance, taste, mouth-feel, fragrance, and antimicrobial properties of wine [61]. The two primary phenol groups that occur in grapes and wine are the flavonoids and the non-flavonoids. The most common flavonoids in wine are flavonols, catechins, and flavan-3-ols and, in red wines, anthocyanins too [62–64]. Flavonoids come primarily from the skins, seeds, and stems of the fruit [65]. In red wines, they commonly constitute up to 85% of the phenol content, while, in white wines, flavonoids are typically lower than 20% of the total phenolic content. The amount of flavonoids extracted during vinification is influenced by many factors, including temperature, length of skin contact, mixing, type of fermentation vessel, ethanol concentrations, SO_2 yeast strain, and pH [66–70]. The concentration of phenolics in wine increases during skin fermentation and subsequently begins to fall as phenols aggregate and precipitate with proteins and yeast cell remnants [37, 38]. As regard to white wines, they showed a little cluster in the middle left part of the plot (Fig. 1B),

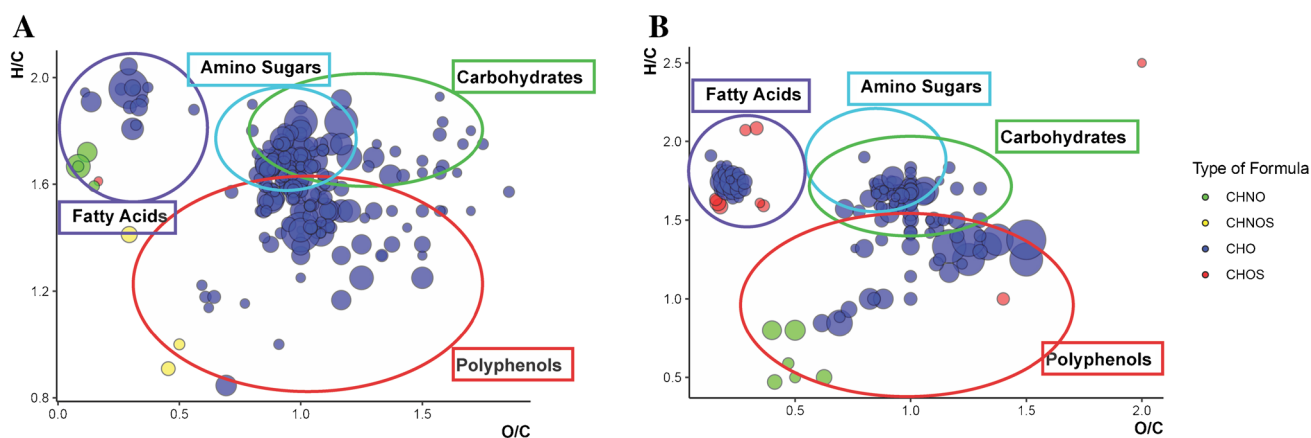


Fig. 1 van Krevelen plots of *Colata Murro* (A) and *Aglianico Bianco* (B) red and white wine samples, respectively, obtained from related ESI(-)FT-ICR MS data. The types of formula are distinguished by colors (green for CHNO, yellow for CHNOS, blue for CHO, and red for CHOS)

not observed for red wine varieties, which could be related to the presence of low oxygen content phenolic acids, such as hydroxycinnamic acid derivatives, known to be responsible for the typical yellowish color of white wines [71, 72]. Hydroxycinnamic acid derivatives commonly occur esterified to sugars, organic acids, or various alcohols. The principal grape sugars are glucose and fructose, and they occur in roughly equal proportions at maturity, whereas overripe grapes often have a higher proportion of fructose [73, 74]. As the most important and abundant alcohol in wine is ethanol [75, 76], several ethyl derivatives could be detected. Under standard fermentation conditions, ethanol can accumulate up to ~14–15%, but generally ethanol concentrations in wine range between 10 and 13% [75, 76]. Other potentially significant higher alcohols in wine are the straight-chain alcohols: 1-propanol, 2-methyl-1-propanol, 2-methyl-1-butanol, and 3-methyl-1-butanol [61]. The formation of higher alcohols occurs as a by-product of yeast fermentation and is markedly influenced by vinification parameters, such as temperature, presence of oxygen, suspended solids, and yeast strain [5, 6, 10]. With regard to organic acid, tartaric, malic, lactic, succinic, oxalic, fumaric, and citric acids control the pH of wine [73, 77].

Among the same types of wine, differences could be spotted related to the absence and the presence of points in specific van Krevelen plots, suggesting the fact that some classes of derivatives are present only in some wine samples, just like the unsaturated CHNO formula type compounds present for the *Giosana* and *Santa Sofia* white wines (see Supplementary information) or the aliphatic amides present in the *Colata Murro* red wine sample only. van Krevelen plots obtained from the analysis of data acquired in positive ionization mode results show a similar profile among all

analyzed samples (Fig. 2) (see also Supplementary information Figs. S1B, S2B, S4B, S5B, S6).

In this case, amino acids and peptides, together with their aliphatic derivatives, and aliphatic amides seem to be predominant, as well as other CHO formula type compounds, probably related to unsaturated fatty acid derivatives. Generally, fatty acids as well as their ethyl esters are produced in the first days of the fermentation; after that, their concentration levels decrease. Since a lower amount of external sterols is detectable in the medium during the clarification process of the white wines, these ones show a higher content in fatty acids than red wines [78], as proved by the analyzes made in this work (Fig. 2). It is interesting to notice that, except for the lipidic class, van Krevelen plots do not reveal other remarkable differences between red and white wine metabolic profiles acquired in positive mode. Instead, some differences could be detected by comparing all the results obtained for the white wines. As an example, the *Malvasia ad acino piccolo* van Krevelen plot (Fig. 2B) shows the highest density of points (421 signals), suggesting the presence of several clusters, while in the *Santa Sofia* white wine plot (see Supplementary information Fig. S4B), we observe a uniform distribution with a lower number of points (81 signals). The lower number of compounds reported on in the *Santa Sofia* molecular map as amino acids and fatty acids, compared to those occurring in the *Malvasia ad acino piccolo* one, could be dependent on the winemaking practices and not only on the wine type, i.e., red or white [79]. For the two red wine *Colata Murro* (Fig. 1A) and *Plavina* (Fig. S5A), instead, van Krevelen plots show a similar distribution, suggesting a similar metabolic profile that includes fatty acids, carbohydrates, and polyphenols. For this similarity, a higher number of points could be detected in the

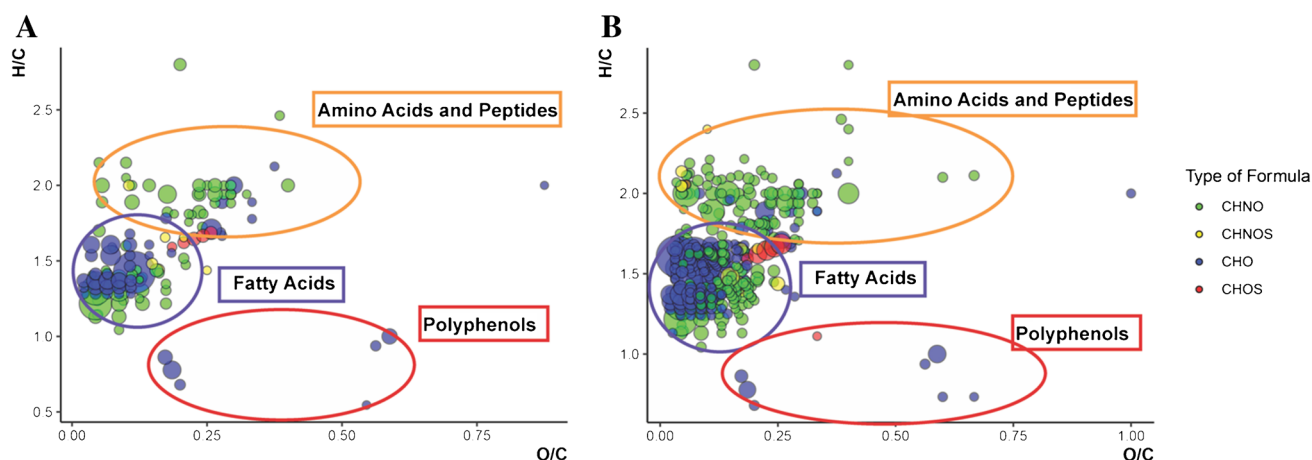


Fig. 2 van Krevelen plots of *Colata Murro* (A) and *Malvasia ad acino piccolo* (B) red and white wine samples, respectively, obtained from related ESI(+)-FT-ICR MS data. The types of formula are dis-

tinguished by colors (green for CHNO, yellow for CHNOS, blue for CHO, and red for CHOS)

carbohydrate and polyphenol regions for the *Colata Murro* red wine, confirming that the polyphenolic composition varies among different wines according to different factors, and the type of grape used is one of the most important ones [80]. Overall, the use of van Krevelen plots provided a comprehensive metabolic fingerprint of the seven wine samples based on data acquired in full-scan mode and allowed to identify the different metabolite classes. This strategy will also provide a hint for further investigation of putative markers by performing MS/MS analysis.

Conclusions

High-resolution mass spectrometry technique was successfully used in this work for the characterization of the metabolome of new Italian type wine varieties, thus confirming its suitability for quick and efficient untargeted metabolic analysis of natural samples. Useful information about types of metabolites present in wine samples were obtained, since a classification of identified species has been made possible by the utilization of the van Krevelen plot, a well-known visualization tool useful for HRMS data interpretation. Results helped to identify principal classes of metabolites and to spot principal differences among related metabolic profiles. Thus, they are very promising as innovative tool to ascertain their unique metabolic profile.

Supplementary Information The online version contains supplementary material available at <https://doi.org/10.1007/s00216-022-04314-x>.

Funding The authors would like to thank ALSIA (Agenzia Lucana di Sviluppo e di Innovazione in Agricoltura) for providing the samples analyzed within this work and Yury O. Tsybin and Konstantin O. Nagornov for their support in the processing of recorded time domain ion signals into absorption mode FT-ICR mass spectra.

Declarations

Competing interests The authors declare no competing interests.

References

1. Soleas GJ, Diamandis EP, Goldberg DM. Wine as a biological fluid: history, production, and role in disease prevention. *J Clin Lab Anal.* 1997;11:287–313. [https://doi.org/10.1002/\(SICI\)1098-2825\(1997\)11:5%3c287::AID-JCLA6%3e3.0.CO;2-4](https://doi.org/10.1002/(SICI)1098-2825(1997)11:5%3c287::AID-JCLA6%3e3.0.CO;2-4).
2. JB G, Walzem RL. The health benefits of wine. *Annu Rev Nutr.* 2000;20:561
3. Zoecklein B, Fugelsang KC, Gump BH, & Nury FS. Wine analysis and production. Springer Science & Business Media. 2013.
4. Boulton RB, Singleton VL, Bisson LF, Kunee RE. Principles and practices of winemaking. US: Springer; 1999.
5. Ciani M, Comitini F. Yeast ecology of wine production. In *Yeasts in the Production of Wine.* 2019;1–42. Springer, New York, NY.
6. Augustyn O, Pretorius I, Jolly N. Winemaking biochemistry and microbiology: current knowledge and future trends. *Crit Rev Food Sci Nutr.* 2005;45:265–86.
7. Chambers PJ, Pretorius IS. Winemaking, Science and Yeast Research. *EMBO Rep.* 2010;11:914–20.
8. Suárez-Lepe JA, Morata A. New trends in yeast selection for winemaking. *Trends Food Sci Technol.* 2012;23:39–50. <https://doi.org/10.1016/j.tifs.2011.08.005>.
9. Moreno-Arribas MV, Polo MC. Wine chemistry and biochemistry. New York. 2009
10. Kritzinger EC, Bauer FF, Du Toit WJ. Role of glutathione in winemaking: a review. *J Agric Food Chem.* 2013;61:269–77. <https://doi.org/10.1021/jf303665z>.
11. Sacchi KL, Bisson LF, Adams DO. A review of the effect of winemaking techniques on.pdf. *Am J Enol Vitic.* 2005;48:197–206.
12. Di Lorenzo A, Bloise N, Meneghini S, Suredda A, Tenore GC, Visai L, Arciola CR, Daglia M. Effect of winemaking on the composition of red wine as a source of polyphenols for anti-infective biomaterials. *Materials (Basel).* 2016;9:<https://doi.org/10.3390/ma9050316>
13. Ayestarán B, Martínez-Lapuente L, Guadalupe Z, Canals C, Adell E, Vilanova M. Effect of the winemaking process on the volatile composition and aromatic profile of Tempranillo Blanco wines. *Food Chem.* 2019;276:187–94. <https://doi.org/10.1016/j.foodchem.2018.10.013>.
14. Wang Y, Catana F, Yang Y, Roderick R, Van Breemen RB. An LC-MS method for analyzing total resveratrol in grape juice, cranberry juice, and in wine. *J Agric Food Chem.* 2002;50:431–5. <https://doi.org/10.1021/jf010812u>.
15. Jaitz L, Siegl K, Eder R, Rak G, Abranko L, Koellensperger G, Hann S. LC-MS/MS analysis of phenols for classification of red wine according to geographic origin, grape variety and vintage. *Food Chem.* 2010;122:366–72. <https://doi.org/10.1016/j.foodchem.2010.02.053>.
16. Aznar M, López R, Cacho JF, Ferreira V. Identification and quantification of impact odorants of aged red wines from Rioja, GC-olfactometry, quantitative GC-MS, and odor evaluation of HPLC fractions. *J Agric Food Chem.* 2001;49:2924–9. <https://doi.org/10.1021/jf001372u>.
17. Bosch-Fusté J, Riu-Aumatell M, Guadayo JM, Caixach J, López-Tamames E, Buxaderas S. Volatile profiles of sparkling wines obtained by three extraction methods and gas chromatography-mass spectrometry (GC-MS) analysis. *Food Chem.* 2007;105:428–35. <https://doi.org/10.1016/j.foodchem.2006.12.053>.
18. Acquavia MA, Pascale R, Pappalardo I, Santarsiero A, Martelli G, Bianco G. Characterization of quercetin derivatives in crossing combination of habanero white and Capsicum annum peppers and of anti-inflammatory and cytotoxic activity. *Separations.* 2021; 8:<https://doi.org/10.3390/separations8070090>
19. Pascale R, Acquavia MA, Onzo A, Cataldi TRI, Calvano CD, Bianco G. Analysis of surfactants by mass spectrometry: coming to grips with their diversity. *Mass Spectrom Rev.* 2021;1–32<https://doi.org/10.1002/mas.21735>
20. Agatonovic-Kustrin S, Hettiarachchi CG, Morton DW, Rasic S. Analysis of phenolics in wine by high performance thin-layer chromatography with gradient elution and high resolution plate imaging. *J Pharm Biomed Anal.* 2015;102:93–9. <https://doi.org/10.1016/j.jpba.2014.08.031>.
21. Romano A, Klebanowski H, La Guerche S, Beneduce L, Spano G, Murat ML, Lucas P. Determination of biogenic amines in wine by thin-layer chromatography/ densitometry. *Food Chem.* 2012;135:1392–6. <https://doi.org/10.1016/j.foodchem.2012.06.022>.
22. Revilla E, Ryan JM. Analysis of several phenolic compounds with potential antioxidant properties in grape extracts and wines by

- high-performance liquid chromatography-photodiode array detection without sample preparation. *J Chromatogr A*. 2000;881:461–9. [https://doi.org/10.1016/S0021-9673\(00\)00269-7](https://doi.org/10.1016/S0021-9673(00)00269-7).
23. Visconti A, Pascale M, Centonze G. Determination of ochratoxin A in wine by means of immunoaffinity column clean-up and high-performance liquid chromatography. *J Chromatogr A*. 1999;864:89–101. [https://doi.org/10.1016/S0021-9673\(99\)00996-6](https://doi.org/10.1016/S0021-9673(99)00996-6).
 24. Culleré L, Escudero A, Cacho J, Ferreira V. Gas chromatography-olfactometry and chemical quantitative study of the aroma of six premium quality Spanish aged red wines. *J Agric Food Chem*. 2004;52:1653–60. <https://doi.org/10.1021/jf0350820>.
 25. López R, Aznar M, Cacho J, Ferreira V. Determination of minor and trace volatile compounds in wine by solid-phase extraction and gas chromatography with mass spectrometric detection. *J Chromatogr A*. 2002;966:167–77. [https://doi.org/10.1016/S0021-9673\(02\)00696-9](https://doi.org/10.1016/S0021-9673(02)00696-9).
 26. Godelmann R, Fang F, Humpfer E, Schütz B, Banschach M, Schäfer H, Spraul M. Targeted and nontargeted wine analysis by 1H NMR spectroscopy combined with multivariate statistical analysis. Differentiation of important parameters: grape variety, geographical origin, year of vintage. *J Agric Food Chem*. 2013;61:5610–9. <https://doi.org/10.1021/jf400800d>.
 27. Son HS, Hwang GS, Kim KM, Ahn HJ, Park WM, Van Den Berg F, Hong YS, Lee CH. Metabolomic studies on geographical grapes and their wines using 1H NMR analysis coupled with multivariate statistics. *J Agric Food Chem*. 2009;57:1481–90. <https://doi.org/10.1021/jf803388w>.
 28. Cozzolino D, Kwiatkowski MJ, Parker M, Cynkar WU, Damberg RG, Gishen M, Herderich MJ. Prediction of phenolic compounds in red wine fermentations by visible and near infrared spectroscopy. *Anal Chim Acta*. 2004;513:73–80. <https://doi.org/10.1016/j.aca.2003.08.066>.
 29. Bokulich NA, Collins T, Masarweh C, Allen G, Heymann H, Ebeler SE, Mills DA. Fermentation behavior suggest microbial contribution to regional. *MBio*. 2016;7:1–12. <https://doi.org/10.1128/mBio.00631-16>. [Bokulich](https://doi.org/10.1128/mBio.00631-16).
 30. Cuadros-Inostroza A, Giavalisco P, Hummel J, Eckardt A, Willmitzer L, Peña-Cortés H. Discrimination of wine attributes by metabolome analysis. *Anal Chem*. 2010;82:3573–80. <https://doi.org/10.1021/ac902678t>.
 31. Roullier-Gall C, Hemmler D, Gonsior M, Li Y, Nikolantonaki M, Aron A, Coelho C, Gougeon RD, Schmitt-Kopplin P. Sulfites and the wine metabolome. *Food Chem*. 2017;237:106–13. <https://doi.org/10.1016/j.foodchem.2017.05.039>.
 32. Vidal S, Francis L, Guyot S, Marnet N, Kwiatkowski M, Gawel R, Cheynier V, Waters EJ. The mouth-feel properties of grape and apple proanthocyanidins in a wine-like medium. *J Sci Food Agric*. 2003;83:564–73. <https://doi.org/10.1002/jsfa.1394>.
 33. Vidal S, Courcoux P, Francis L, Kwiatkowski M, Gawel R, Williams P, Waters E, Cheynier V. Use of an experimental design approach for evaluation of key wine components on mouth-feel perception. *Food Qual Prefer*. 2004;15:209–17. [https://doi.org/10.1016/S0950-3293\(03\)00059-4](https://doi.org/10.1016/S0950-3293(03)00059-4).
 34. Peinado RA, Moreno J, Bueno JE, Moreno JA, Mauricio JC. Comparative study of aromatic compounds in two young white wines subjected to pre-fermentative cryomaceration. *Food Chem*. 2004;84:585–90. [https://doi.org/10.1016/S0308-8146\(03\)00282-6](https://doi.org/10.1016/S0308-8146(03)00282-6).
 35. Vilanova M, Martínez C. First study of determination of aromatic compounds of red wine from *Vitis vinifera* cv. Castañal grown in Galicia (NW Spain). *Eur Food Res Technol*. 2007;224:431–6. <https://doi.org/10.1007/s00217-006-0322-0>.
 36. Longo R, Blackman JW, Torley PJ, Rogiers SY, Schmidtke LM. Changes in volatile composition and sensory attributes of wines during alcohol content reduction. *J Sci Food Agric*. 2017;97:8–16. <https://doi.org/10.1002/jsfa.7757>.
 37. Harrison R. Practical interventions that influence the sensory attributes of red wines related to the phenolic composition of grapes: a review. *Int J Food Sci Technol*. 2018;53:3–18. <https://doi.org/10.1111/ijfs.13480>.
 38. Coetzee C, Du Toit WJ. Sauvignon blanc wine: contribution of ageing and oxygen on aromatic and non-aromatic compounds and sensory composition: a review. *South African J Enol Vitic*. 2015;36:347–365. <https://doi.org/10.21548/36-3-968>.
 39. Cataldi TRI, Nardiello D, Scranò L, Scopa A. Assay of riboflavin in sample wines by capillary zone electrophoresis and laser-induced fluorescence detection. *J Agric Food Chem*. 2002;50:6643–7. <https://doi.org/10.1021/jf020212a>.
 40. Fracassetti D, Limbo S, Tirelli A. Formation and prevention of light-struck taste in white wine. *Vino Anal Sci*. 2017;1:50316674. <https://doi.org/10.1111/ajgw.12295>. **ACKNOWLEDGMENT**.
 41. Nel AP. Tannins and anthocyanins: from their origin to wine analysis - a review. *South African J Enol Vitic*. 2018;39:1–20. <https://doi.org/10.21548/39-1-1503>.
 42. Herderich MJ, Smith PA. Analysis of grape and wine tannins: methods, applications and challenges. *Aust J Grape Wine Res*. 2005;11:205–14. <https://doi.org/10.1111/j.1755-0238.2005.tb00288.x>.
 43. Nunes-Miranda JD, Igrejas G, Araujo E, M. R-J, Capelo JL. Mass spectrometry-based fingerprinting of proteins and peptides in wine quality control: a critical overview. *Crit Rev Food Sci Nutr*. 2013;53:751–759. <https://doi.org/10.1080/10408398.2011.557514>.
 44. Roullier-Gall C, Witting M, Tziotis D, Ruf A, Gougeon RD, Schmitt-Kopplin P. Integrating analytical resolutions in non-targeted wine metabolomics. *Tetrahedron*. 2015;71:2983–90. <https://doi.org/10.1016/j.tet.2015.02.054>.
 45. Roullier-Gall C, Witting M, Gougeon RD, Schmitt-Kopplin P. High precision mass measurements for wine metabolomics. *Front Chem*. 2014;2:1–9. <https://doi.org/10.3389/fchem.2014.00102>.
 46. Pascale R, Bianco G, Cataldi TRI, Kopplin PS, Bosco F, Vignola L, Uhl J, Lucio M, Milella L. Mass spectrometry-based phytochemical screening for hypoglycemic activity of Fagioli di Sarconi beans (*Phaseolus vulgaris* L.). *Food Chem*. 2018;242:497–504. <https://doi.org/10.1016/j.foodchem.2017.09.091>.
 47. Santarsiero A, Onzo A, Pascale R, Acquavia MA, Coviello M, Convertini P, Todisco S, Marsico M, Pifano C, Iannece P, Gaeta C, D'Angelo S, Padula MC, Bianco G, Infantino V, Martelli G. Pistacia lentiscus hydrosol: untargeted metabolomic analysis and anti-inflammatory activity mediated by NF- κ B and the citrate pathway. *Oxid Med Cell Longev*. 2020;2020:<https://doi.org/10.1155/2020/4264815>.
 48. Alba V, Bergamini C, Gasparro M, Mazzone F, Roccotelli S, Antonacci D, Caputo AR. Basivin_SUD: la ricerca del germoplasma viticolo in Basilicata. Maria Adda Editore. 2016.
 49. Kilgour DPA, Wills R, Qi Y, O'Connor PB. Autophaser: an algorithm for automated generation of absorption mode spectra for FT-ICR MS. *Anal Chem*. 2013;85:3903–11. <https://doi.org/10.1021/ac303289c>.
 50. Kilgour DPA, Neal MJ, Soulby AJ, O'Connor PB. Improved optimization of the Fourier transform ion cyclotron resonance mass spectrometry phase correction function using a genetic algorithm. *Rapid Commun Mass Spectrom*. 2013;27:1977–82. <https://doi.org/10.1002/rcm.6658>.
 51. Zielinski AT, Kourtchev I, Bortolini C, Fuller SJ, Giorio C, Popoola OAM, Bogianni S, Tapparo A, Jones RL, Kalberer M. A new processing scheme for ultra-high resolution direct infusion mass spectrometry data. *Atmos Environ*. 2018;178:129–39. <https://doi.org/10.1016/j.atmosenv.2018.01.034>.
 52. Onzo A, Acquavia MA, Pascale R, Iannece P, Gaeta C, Nagornov KO, Tsybin YO, Bianco G. Metabolic profiling of Peperoni di Senise PGI bell peppers with ultra-high resolution absorption mode Fourier transform ion cyclotron resonance mass

- spectrometry. *Int J Mass Spectrom.* 2021;470: 116722. <https://doi.org/10.1016/j.ijms.2021.116722>.
53. Longnecker K, Kujawinski EB. Using network analysis to discern compositional patterns in ultrahigh-resolution mass spectrometry data of dissolved organic matter. *Rapid Commun Mass Spectrom.* 2016; 2388–2394. <https://doi.org/10.1002/rcm.7719>
 54. Moritz F, Kaling M, Schnitzler JP, Schmitt-Kopplin P. Characterization of poplar metabolotypes via mass difference enrichment analysis. *Plant Cell Environ.* 2017;40:1057–73. <https://doi.org/10.1111/pce.12878>.
 55. Kunenkov EV, Kononikhin AS, Perminova IV, Hertkorn N, Gaspar A, Schmitt-Kopplin P, Popov IA, Garmash AV, Nikolaev EN. Total mass difference statistics algorithm: a new approach to identification of high-mass building blocks in electrospray ionization Fourier transform ion cyclotron mass spectrometry data of natural organic matter. *Anal Chem.* 2009;81:10106–15. <https://doi.org/10.1021/ac901476u>.
 56. Qi Y, O' Connor PB. Data processing in Fourier transform ion cyclotron resonance mass spectrometry. *Mass Spectrom Rev.* 2014;33:333–52. <https://doi.org/10.1002/mas.21414>.
 57. Nikolaev EN, Kostyukevich YI, Vladimirov GN. Fourier transform ion cyclotron resonance (FT ICR) mass spectrometry: theory and simulations. *Mass Spectrom Rev.* 2016;35:219–58. <https://doi.org/10.1002/mas.21422>.
 58. Kilgour DPA, Van Orden SL. Absorption mode Fourier transform mass spectrometry with no baseline correction using a novel asymmetric apodization function. *Rapid Commun Mass Spectrom.* 2015;29:1009–18. <https://doi.org/10.1002/rcm.7190>.
 59. Kuhnert N, Dairpoosh F, Yassin G, Golon A, Jaiswal R. What is under the hump? Mass spectrometry based analysis of complex mixtures in processed food—lessons from the characterisation of black tea thearubigins, coffee melanoidines and caramel. *Food Funct.* 2013;4:1130–47. <https://doi.org/10.1039/c3fo30385c>.
 60. Laszakovits JR, MacKay AA. Data-based chemical class regions for Van Krevelen diagrams. *J Am Soc Mass Spectrom.* 2022;33:198–202. <https://doi.org/10.1021/jasms.1c00230>.
 61. Čiča KH, Pezer M, Mrvčić J, Stanzer D, Čačić J, Jurak V, Krajnović M, Kljusurić JG. Identification of phenolic and alcoholic compounds in wine spirits and their classification by use of multivariate analysis. *J Serbian Chem Soc.* 2019;84:663–77. <https://doi.org/10.2298/JSC190115020H>.
 62. Castillo-Muñoz N, Gómez-Alonso S, García-Romero E, Hermosín-Gutiérrez I. Flavonol profiles of *Vitis vinifera* red grapes and their single-cultivar wines. *J Agric Food Chem.* 2007;55:992–1002. <https://doi.org/10.1021/jf062800k>.
 63. Castillo GAGR gomez; VH-G. Flavonol 3-O-glycosides series of *Vitis vinifera* Cv. 2009;209–219
 64. Boulton R. The copigmentation of anthocyanins and its role in the color of red wine: a critical review. *Am J Enol Vitic.* 2001;52:67–87.
 65. Fernandes I, Pérez-Gregorio R, Soares S, Mateus N, De Freitas V, Santos-Buelga C, Feliciano AS. Wine flavonoids in health and disease prevention. *Molecules.* 2017;22:<https://doi.org/10.3390/molecules22020292>
 66. Cohen SD, Tarara JM, Gambetta GA, Matthews MA, Kennedy JA. Impact of diurnal temperature variation on grape berry development, proanthocyanidin accumulation, and the expression of flavonoid pathway genes. *J Exp Bot.* 2012;63:2655–65. <https://doi.org/10.1093/jxb/err449>.
 67. Kennedy JA, Matthews MA, Waterhouse AL. Effect of maturity and vine water status on grape skin and wine flavonoids. *Am J Enol Vitic.* 2002;53:268–74.
 68. Fang F, Li JM, Pan QH, Huang WD. Determination of red wine flavonoids by HPLC and effect of aging. *Food Chem.* 2007;101:428–33. <https://doi.org/10.1016/j.foodchem.2005.12.036>.
 69. Fang F, Li JM, Zhang P, Tang K, Wang W, Pan QH, Huang WD. Effects of grape variety, harvest date, fermentation vessel and wine ageing on flavonoid concentration in red wines. *Food Res Int.* 2008;41:53–60. <https://doi.org/10.1016/j.foodres.2007.09.004>.
 70. Nardini M, Garaguso I. Effect of sulfites on antioxidant activity, total polyphenols, and flavonoid measurements in white wine. *Foods.* 2018;7:<https://doi.org/10.3390/foods703003>
 71. Ortega AF, Lopez-Toledano A, Mayen M, Merida J, Medina M. Changes in color and phenolic compounds during oxidative aging of sherry white wine. *J Food Sci.* 2003;68:2461–8. <https://doi.org/10.1111/j.1365-2621.2003.tb07046.x>.
 72. Recamales ÁF, Sayago A, González-Miret ML, Hernanz D. The effect of time and storage conditions on the phenolic composition and colour of white wine. *Food Res Int.* 2006;39:220–9. <https://doi.org/10.1016/j.foodres.2005.07.009>.
 73. Calull M, Marcé RM, Borrull F. Determination of carboxylic acids, sugars, glycerol and ethanol in wine and grape must by ion-exchange high-performance liquid chromatography with refractive index detection. *J Chromatogr A.* 1992;590:215–22. [https://doi.org/10.1016/0021-9673\(92\)85384-](https://doi.org/10.1016/0021-9673(92)85384-).
 74. Falqué López E, Fernández Gómez E. Simultaneous determination of the major organic acids, sugars, glycerol, and ethanol by HPLC in grape musts and white wines. *J Chromatogr Sci.* 1996;34:254–7. <https://doi.org/10.1093/chromsci/34.5.254>.
 75. Nieto-Villegas R, Rabadán A, Bernabéu R. Ethanol, wine, and experimental cardioprotection in ischemia/reperfusion: role of the prooxidant/antioxidant balance. *Antioxidants Redox Signal.* 2004;6:431–8. <https://doi.org/10.1089/152308604322899503>.
 76. Iriti M, Varoni EM. Moderate red wine consumption in cardiovascular disease: ethanol versus polyphenols, in: *Mediterr. Diet An Evidence-Based Approach.* 2015.
 77. Tusseau D, Benoit C. Routine high-performance liquid chromatographic determination of carboxylic acids in wines and champagne. *J Chromatogr A.* 1987;395:323–33. [https://doi.org/10.1016/S0021-9673\(01\)94121-4](https://doi.org/10.1016/S0021-9673(01)94121-4).
 78. Tesnière C. Importance and role of lipids in wine yeast fermentation. *Appl Microbiol Biotechnol.* 2019;103:8293–300. <https://doi.org/10.1007/s00253-019-10029-4>.
 79. Phan Q, Dubois A, Osborne J, Tomasino E. Effects of yeast product addition and fermentation temperature on lipid composition, taste and mouthfeel characteristics of pinot noir wine. *Horticulturae.* 2022; 8:<https://doi.org/10.3390/horticulturae8010052>
 80. Cordova AC, Sumpio BE. Polyphenols are medicine: is it time to prescribe red wine for our patients? *Int J Angiol.* 2009;18:111–7. <https://doi.org/10.1055/s-0031-1278336>.
- Part of the results of this research has been shared as oral communication in occasion of the 4thMS Italian Wine Day Conference (June 22–24th, Carlentini, Sicily, Italy).

Publisher's note Springer Nature remains neutral with regard to jurisdictional claims in published maps and institutional affiliations.

Springer Nature or its licensor holds exclusive rights to this article under a publishing agreement with the author(s) or other rightsholder(s); author self-archiving of the accepted manuscript version of this article is solely governed by the terms of such publishing agreement and applicable law.

Article

Development and Validation of a Reversed-Phase HPLC Method with UV Detection for the Determination of L-Dopa in *Vicia faba* L. Broad Beans

Carmen Tesoro ¹, Rosanna Ciriello ¹, Filomena Lelario ^{1,*} , Angela Di Capua ^{1,*} , Raffaella Pascale ² , Giuliana Bianco ¹ , Mario Dell'Agli ³ , Stefano Piazza ³ , Antonio Guerrieri ¹ , Laura Scrano ⁴ , Sabino A. Bufo ^{1,5}  and Maria Assunta Acquavia ^{1,6} 

¹ Department of Sciences, University of Basilicata, Via dell'Ateneo Lucano 10, 85100 Potenza, Italy

² Gnosis Bioresearch by Lesaffre, 75015 Pisticci, Italy

³ Department of Pharmacological and Biomolecular Sciences, University of Milan, Via Balzaretti 9, 20133 Milano, Italy

⁴ Department of the European Cultures (DICEM), University of Basilicata, Via Lanera 20, 85100 Matera, Italy

⁵ Department of Geography, Environmental Management & Energy Studies, University of Johannesburg, Johannesburg 2092, South Africa

⁶ Thema Informatik S.R.L., Via Ressel 2/F, 39100 Bolzano, Italy

* Correspondence: filomena.lelario@unibas.it (F.L.); angela.dicapua@unibas.it (A.D.C.)



Citation: Tesoro, C.; Ciriello, R.; Lelario, F.; Di Capua, A.; Pascale, R.; Bianco, G.; Dell'Agli, M.; Piazza, S.; Guerrieri, A.; Scrano, L.; et al. Development and Validation of a Reversed-Phase HPLC Method with UV Detection for the Determination of L-Dopa in *Vicia faba* L. Broad Beans. *Molecules* **2022**, *27*, 7468. <https://doi.org/10.3390/molecules27217468>

Academic Editors: Mario-Livio Jeličić, Ana Mornar and Daniela Amidžić Klarić

Received: 8 October 2022

Accepted: 28 October 2022

Published: 2 November 2022

Publisher's Note: MDPI stays neutral with regard to jurisdictional claims in published maps and institutional affiliations.



Copyright: © 2022 by the authors. Licensee MDPI, Basel, Switzerland. This article is an open access article distributed under the terms and conditions of the Creative Commons Attribution (CC BY) license (<https://creativecommons.org/licenses/by/4.0/>).

Abstract: L-Dopa (LD), a substance used medically in the treatment of Parkinson's disease, is found in several natural products, such as *Vicia faba* L., also known as broad beans. Due to its low chemical stability, LD analysis in plant matrices requires an appropriate optimization of the chosen analytical method to obtain reliable results. This work proposes an HPLC-UV method, validated according to EURACHEM guidelines as regards linearity, limits of detection and quantification, precision, accuracy, and matrix effect. The LD extraction was studied by evaluating its aqueous stability over 3 months. The best chromatographic conditions were found by systematically testing several C₁₈ stationary phases and acidic mobile phases. In addition, the assessment of the best storage treatment of *Vicia faba* L. broad beans able to preserve a high LD content was performed. The best LD determination conditions include sun-drying storage, extraction in HCl 0.1 M, chromatographic separation with a Discovery C₁₈ column, 250 × 4.6 mm, 5 μm particle size, and 99% formic acid 0.2% v/v and 1% methanol as the mobile phase. The optimized method proposed here overcomes the problems linked to LD stability and separation, thus contributing to the improvement of its analytical determination.

Keywords: drugs; bioactive compound; liquid chromatography; UV detection; broad beans; aqueous stability; EURACHEM guidelines; storage conditions

1. Introduction

Broad bean (*Vicia faba* L.) has been identified as a rich source of L-Dopa or levodopa (LD), a dopamine precursor and first-line treatment for Parkinson's disease (PD) symptoms, usually characterized by slowness of movement (bradykinesia), tremor at rest, muscle rigidity, and postural fragility [1–6]. PD affects nerve cells and their function in producing the neurotransmitter dopamine. In contrast to dopamine, LD can cross the blood-brain barrier and enter into the nerve cells, where it is decarboxylated to dopamine. In cells, LD can also be oxidized toward melanin, producing leucodopachrome and dopachrome by auto-oxidation or with the aid of tyrosinases, also known as polyphenol oxidases (PPO) (Figure 1A). During these reactions, reactive oxygen species (ROS) such as hydrogen peroxide (H₂O₂), superoxide anion (O₂^{•−}), and hydroxyl radical (HO[•]) can be produced. Some studies report that the beneficial effect of LD drugs in PD is counterbalanced by the strong oxidative damage generated over a long period of drug treatment [7]. Furthermore,

patients with advanced PD generally experience an unbalanced response pattern to L-Dopa because of fluctuating drug delivery to the brain. In the most severe form, motor fluctuations produce the typical “on-off” syndrome. Thus, the consumption of vegetables containing LD, such as broad beans or botanicals food supplements, could be recommended as adjuvants for patients with PD [7,8]. In fact, as reported by Apaydin et al. [9], the “on” period was prolonged in patients consuming a *Vicia faba* broad bean meal.

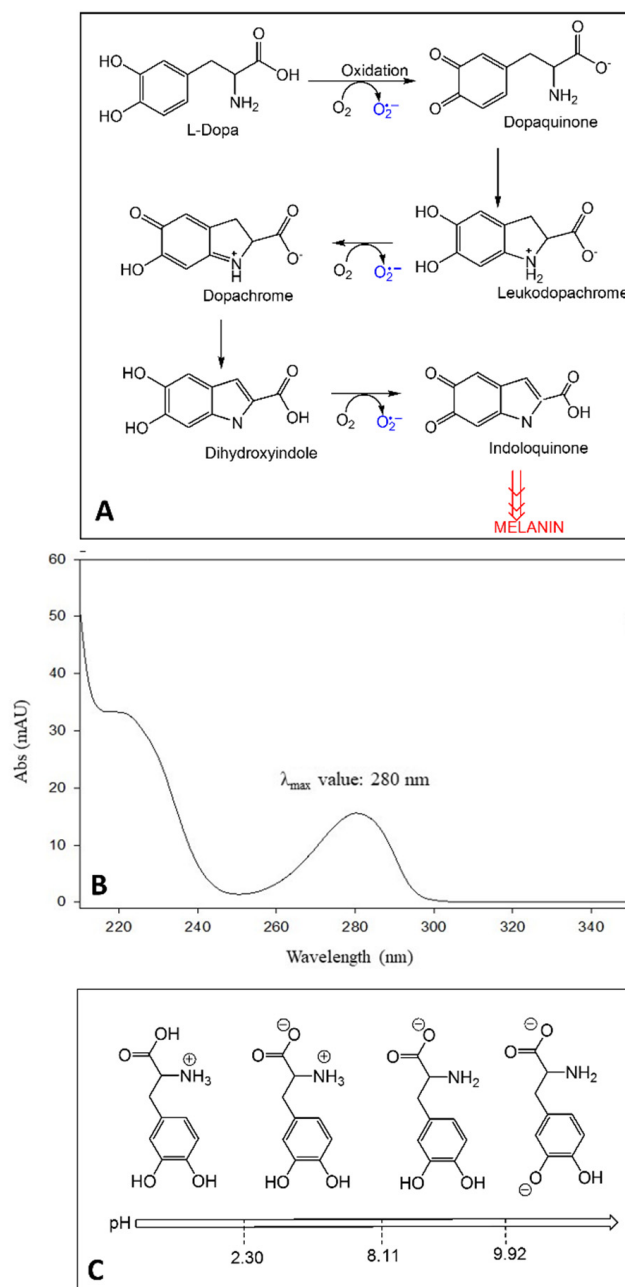


Figure 1. Auto-oxidation reactions of LD and ROS production (A); UV absorption spectrum of LD (B); LD structures at different pH and corresponding pKa values (C).

The presence of the catechol moiety in the chemical structure characterizes LD as a chromophore with a λ_{max} value of 280 nm and allows us to obtain UV detection results sufficiently sensitive for LD determination in vegetable matrices [10]. Since the absorption spectrum of LD is highly characteristic (Figure 1B), its determination by spectrum acquisition (LC-UV analysis) is also selective. Although several scientific works reported the

separation and quantification of LD in *Vicia faba* L. by using liquid chromatography coupled to a UV-Vis detector (LC/UV-Vis) [8,10–25], there are still some limitations regarding LD extraction/stability, chromatographic conditions, and method validation.

Firstly, LD is unstable in aqueous solutions and naturally degrades over time [26–36]: for this reason, it is crucial to identify the best conditions to avoid LD degradation over all the analytical steps. LD instability will also influence the choice of the extraction technique. Typical extraction techniques include liquid–solid extraction, Soxhlet extraction, microwave-assisted extraction, and ultrasound-assisted extraction [10]. However, the latter two techniques, although significantly improving the extraction procedure in terms of automation and solvent consumption, are less used because thermal effects can reduce the final concentration of L-Dopa [11].

Secondly, low-molecular-weight polar compounds, such as LD, are generally difficult to separate by using reversed-phase liquid chromatography (RP-LC) [10]. Generally, it is required to work below the pKa of the compound where it will be completely protonated, or to use an ion pair reagent to increase retention time. Chromatographic conditions as regards LC column and mobile-phase composition are also fundamental to obtain reliable results. Mostly, C₁₈ stationary phases have been used due to the highly polar structure of the analyte [10,11,13,23]. Acetate/phosphate buffers at acidic pH values (<3) have also been used, although some papers report the use of acetate/phosphate buffers at pH of 4.00, 4.55, 4.66, or 7.00 [10,19,20,23,24,37]. It should be pointed out that, under highly acidic conditions, both analyte and residual silanol groups on the silica column packing support are fully protonated, so they cannot interact electrostatically, avoiding tailing, peaks broadening, and poor retention reproducibility [37]. However, the use of a mobile phase with a certain percentage of organic phase should be considered to prevent the dewetting problem of the C₁₈ stationary phase, and, as a consequence, to limit the lowering of its retention capacity [38,39]. For these reasons, an optimization of chromatographic conditions is necessary.

As no systematic LC-UV method validation has been reported in the literature to analyze LD occurring in *Vicia faba* L. broad beans, with just a few quality parameters of the chromatographic method being ascertained [16], it is crucial to validate a reliable LC-UV method for LD quantification in this matrix.

In this work, a validated LC-UV method for LD analysis according to EURACHEM guidelines has been proposed, alongside the study of its stability in different acidic solutions and the systematic optimization of chromatographic conditions as regards both chromatographic column and mobile phase. Then, the validated method was tested to evaluate the LD contents in seven *Vicia faba* L. broad bean samples, differently stored (fresh, sun-dried for 10 and 30 days, freeze-dried, frozen for 10 and 30 days, and commercial long-life frozen), to find the best storage conditions to limit LD degradation.

2. Results and Discussion

2.1. Aqueous Stability Study of LD

Several studies highlighted LD instability in solution and plant matrices [14,26–32]. Based on its chemical structure, LD has three ionizable groups (Figure 1C). When the pH is between 2.3 and 8.11, LD takes on a zwitterionic structure, which is involved in the intermolecular bond between the protonated amino group and the deprotonated carboxylic group, thus leading to aggregated structures, responsible for the lower LD solubility and stability in neutral environments [10,11,32]. Recent studies have also shown that even oxygen tension affects LD stability. Under normoxic conditions, the analyte is prone to auto-oxidation by releasing protons and reactive oxygen species (ROS) as intermediates [33,34]. In acidic conditions, protons supplied by solvents would shift the auto-oxidation reaction equilibrium towards the reagents and avoid the formation of intermolecular bonding networks [30,32]. Instead, alkaline pH values in plants were shown to increase the enzymatic activity of phenol oxidase (PO). By going from pH 3.5 to pH 4.5, PO activity rises from 60% to 100% [35], thus encouraging the employment

of acidic environments when performing the determination of LD. Therefore, LD acidic structure requires working at a suitable mobile-phase pH value to avoid a significant conversion in the corresponding ionized structures [36].

To assess the aqueous stability and to identify the best extraction solvent, the performance of different standard acidic solutions of LD at 50 mg/L was evaluated in terms of reproducibility of chromatographic peak area. In Figure 2, the stability histogram of LD peak area is reported as mean values over 3 months with the corresponding standard deviations. Since the LD solution in ultrapure H₂O presented the lowest mean peak area and the highest standard deviation because of the area decreasing over time, it was ascertained as the least stable compared to the other acidic solutions. Furthermore, after two weeks, the solution acquired a dark color due to the formation of melanin [29]: this result confirmed the LD degradation and its chemical instability in H₂O, as already reported for LD solutions with alkaline pH or close to neutrality [10,11,29,32]. Instead, for standard LD solutions at acidic pH, the chromatographic peak area values remained stable over 3 months, with %RSD ranging from 0.99% to 4.30%. The best reproducibility in chromatographic peak areas was obtained with standard solutions in HCl 1 M (0.99% RSD) and acetic acid 5% *v/v* (1.17% RSD). However, in HCl 1 M, an additional chromatographic peak was observed rising over time, probably due to hydrolysis of LD. On the other hand, LD in acetic acid at 5% *v/v* showed a UV-absorption spectrum completely different from the characteristic profile of LD, reported in Figure 1A. This could be related to a possible analyte acetylation due to the presence of acetic acid at a high concentration. Based on these results, HCl 0.1 M was selected to prepare LD standard solutions as an appreciable signal intensity, with a good reproducibility (4.30% RSD) of the chromatographic peak areas was obtained [9].

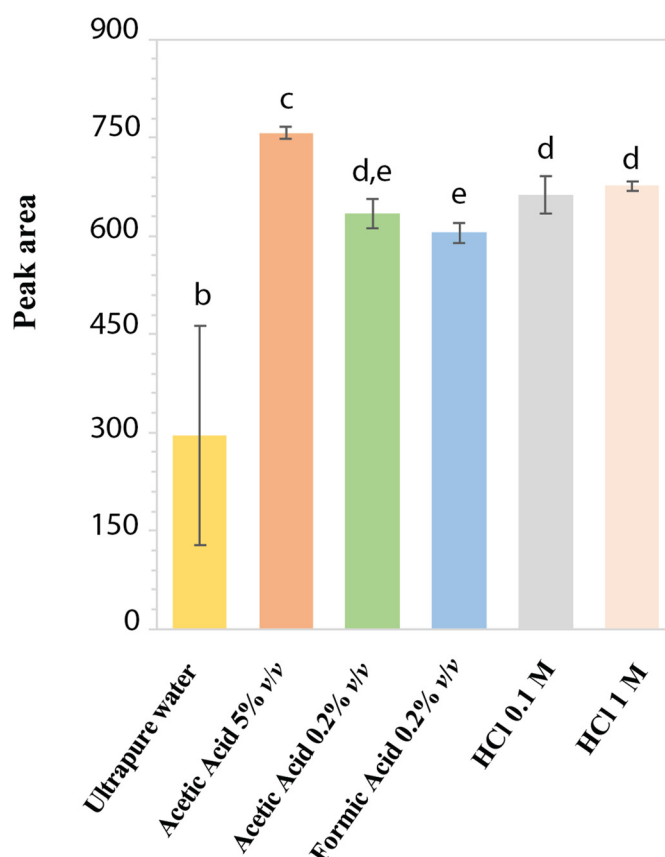


Figure 2. Stability histogram obtained by monitoring peak areas of LD standard solutions at 50 mg/L in different acidic media. Each bar represents the means \pm standard deviation of the results obtained weekly for 3 consecutive months. Values marked by the same letter are not significantly different ($p < 0.05$).

2.2. Chromatographic Performances

In the present work, a careful investigation of the LD separative chromatographic conditions has been carried out to develop a suitable method for analyzing *Vicia faba* L. extracted samples.

2.2.1. Choice of the Chromatographic Column

Starting from the chromatographic method proposed by Polanowska et al. [11], the performances of four different reverse-phase chromatographic columns (Agilent ZORBAX Eclipse XDB, Kinetex C₁₈ column, 100 × 4.6 mm, 2.6 μm, Discovery C₁₈ column, 150 × 2.1 mm, 5 μm, Discovery C₁₈ column, 250 × 4.6 mm, 5 μm) have been tested (for columns characteristics see Section 3). Owing to its high and strong retention towards polar compounds, the porous graphitic carbon (PGC) analytical column is not the best choice for trapping very polar compounds at highly aqueous conditions and, for this reason, it was not considered in this study [40]. As reported in Figure 3, LD retention times and peak shapes changed according to the analytical chromatographic column used. The Agilent ZORBAX Eclipse XDB column was successfully used by Long et al. [36] for the separation of acids, bases, and other highly polar analytes in reversed-phase liquid chromatography. However, when used for LD separation, the HPLC-UV chromatographic profile showed a broad and asymmetric chromatographic peak; hence, the column is not suitable for the analysis (Figure 3D). Kinetex C₁₈ column, 100 × 4.6 mm, 2.6 μm particle size, and Discovery C₁₈ column, 150 × 2.1 mm, 5 μm particle size showed the highest intensity of chromatographic peaks but poor retention of LD analytes, with retention times lower than 2 min, too close to the solvent front (Figure 3B,C). Discovery C₁₈ column, 250 × 4.6 mm, 5 μm particle size, instead showed an LD symmetrical peak eluted at 4.8 min. (Figure 3A) [10]. Although chromatograms in plots A and D were obtained with two columns with the same length, internal diameter (ID), and particle sizes, peaks show different retention time. This could be related to the different chemical and physical properties of the stationary phase, such as the type and surface area. In fact, the surface area accessible in a column can be considered as a key factor in influencing the retention of the analyte on different columns with the same type of stationary phase. The higher surface area of the Discovery C₁₈ provides a greater number of binding sites compared to the Eclipse XDB (see Section 3), increasing the retention of the analyte. Based on these results, Discovery C₁₈ column, 250 × 4.6 mm, 5 μm particle size was considered the most suitable for LD separation.

2.2.2. Optimization of the Mobile-Phase Composition

After choosing the most suitable stationary phase for LD separation, the mobile phase's optimization tests were carried out on the sample extracts of *Vicia faba* L. broad beans to evaluate potential interferences. Four different mobile phases were tested, as reported in Figure 4: 99% of acetic acid 0.2% *v/v* containing 1% of methanol (Figure 4A); 97% of acetic acid 0.2% *v/v* containing 3% of methanol (Figure 4B); 95% of acetic acid 0.2% *v/v* containing 5% of methanol (Figure 4C); 99% of formic acid 0.2% *v/v* containing 1% of methanol (Figure 4D). A percentage of methanolic organic phase not higher than 5% was used to limit the collapse of the stationary phase. By comparing plots A, B, and C, it is possible to observe a clear improvement in terms of resolution of the LD chromatographic peak, due to an increase in percentage of the aqueous phase, containing 0.2% acetic acid, from 95% (Figure 4C) to 99% (Figure 4A). A similar trend was observed for 0.2% *v/v* formic acid as the aqueous phase. Having set the aqueous-phase percentage of 99%, the performances of the two acids, formic and acetic, were compared (Figure 4A,D). In both cases, a well resolved peak was observed for LD (see insets) even if a chromatographic separation of the most abundant interference compounds is achieved only using formic acid (Figure 4D). Furthermore, the employment of formic acid ensured a longer retention time for LD (6.5 min) compared to acetic acid (5.2 min). Formic acid is known to be an ion-pairing reagent, whereas acetic acid is not. The authors of [36] state that ionic interactions between

the formate group ($-\text{COO}^-$) and basic group ($-\text{NH}_3^+$) of LD occur and are responsible for the increase in retention time, improving the selectivity of chromatographic separation [37].

After choosing 99% formic acid 0.2% *v/v*/1% methanol as the mobile phase, a new set of chromatographic runs of *Vicia faba* L. extracts were carried out on the Discovery C₁₈ column, in order to compare the selected mobile phase with the 100% phosphate buffer 125 mM (pH 2.5) [41]. In fact, a buffered mobile phase is recommended in the literature to guarantee a stable pH system value for good peak shape and retention time reproducibility.

The use of phosphate buffer as the mobile phase improved the chromatographic separation efficiency but, over time, caused blockages to the pump and pressure drops due to the precipitation of phosphate salts at the LC valves, requiring additional cleaning of the system to ensure reproducibility and repeatability. Furthermore, considering the higher compatibility of formic acid with most powerful detection techniques such as mass spectrometry, the use of 99% of formic acid 0.2% *v/v* containing 1% of methanol is the most suitable choice as the mobile phase.

In conclusion, the optimal chromatographic conditions for LD separation in plant matrices of *Vicia faba* L. can be achieved by using the Discovery C₁₈ column, 250 × 4.6 mm, 5 μm particle size as a stationary phase and a mobile phase composed of 99% formic acid 0.2% *v/v* containing 1% methanol, under isocratic conditions with a flow of 1 mL/min.

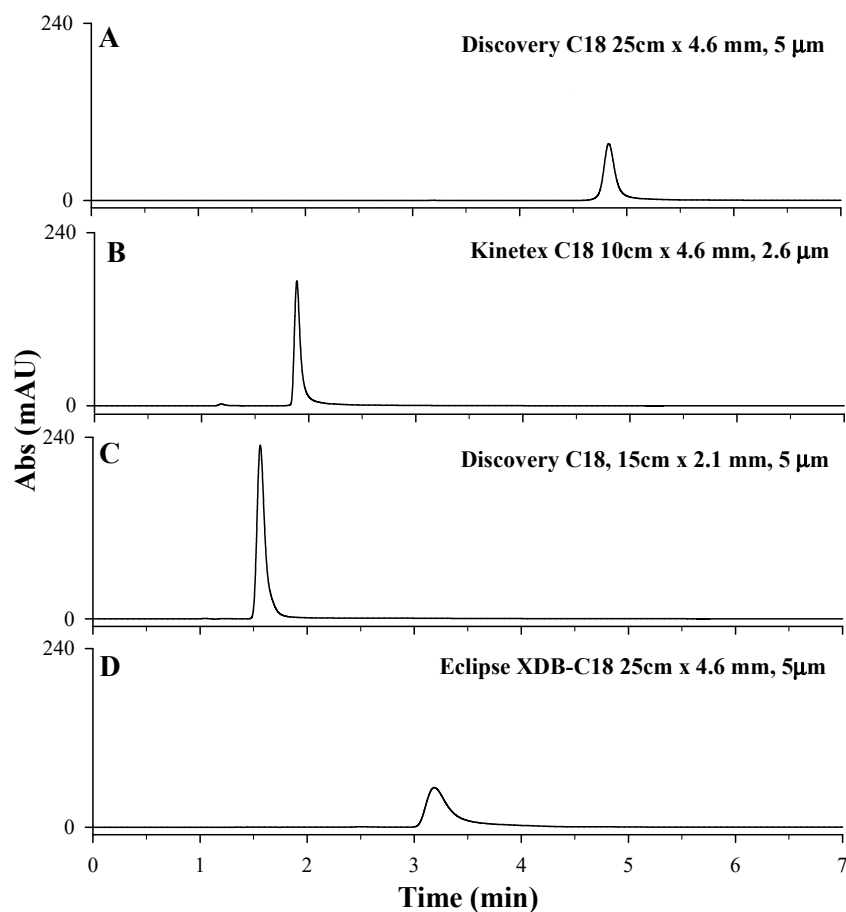


Figure 3. HPLC-UV chromatographic profiles obtained during the optimization of stationary phase: (A) Discovery C₁₈ column, 250 × 4.6 mm, 5 μm; (B) Kinetex C₁₈ column, 100 × 4.6 mm, 2.6 μm particle size; (C) Discovery C₁₈ column, 150 × 2.1 mm, 5 μm; (D) Agilent ZORBAX Eclipse XDB C₁₈ column, 250 × 4.6 mm, 5 μm. An LD standard solution at 50 mg/L solubilized in HCl 0.1 M, 97% acetic acid 0.2% *v/v*, and 3% methanol as mobile phase, under isocratic conditions depending on the tested C₁₈ column (1 mL/min for Discovery C₁₈ column, 0.8 mL/min for Kinetex C₁₈ column and Agilent ZORBAX Eclipse XDB, 0.5 mL/min for Discovery Supelco C₁₈ column.), injection volume of 20 μL and λ_{max} set of 280 nm, were used.

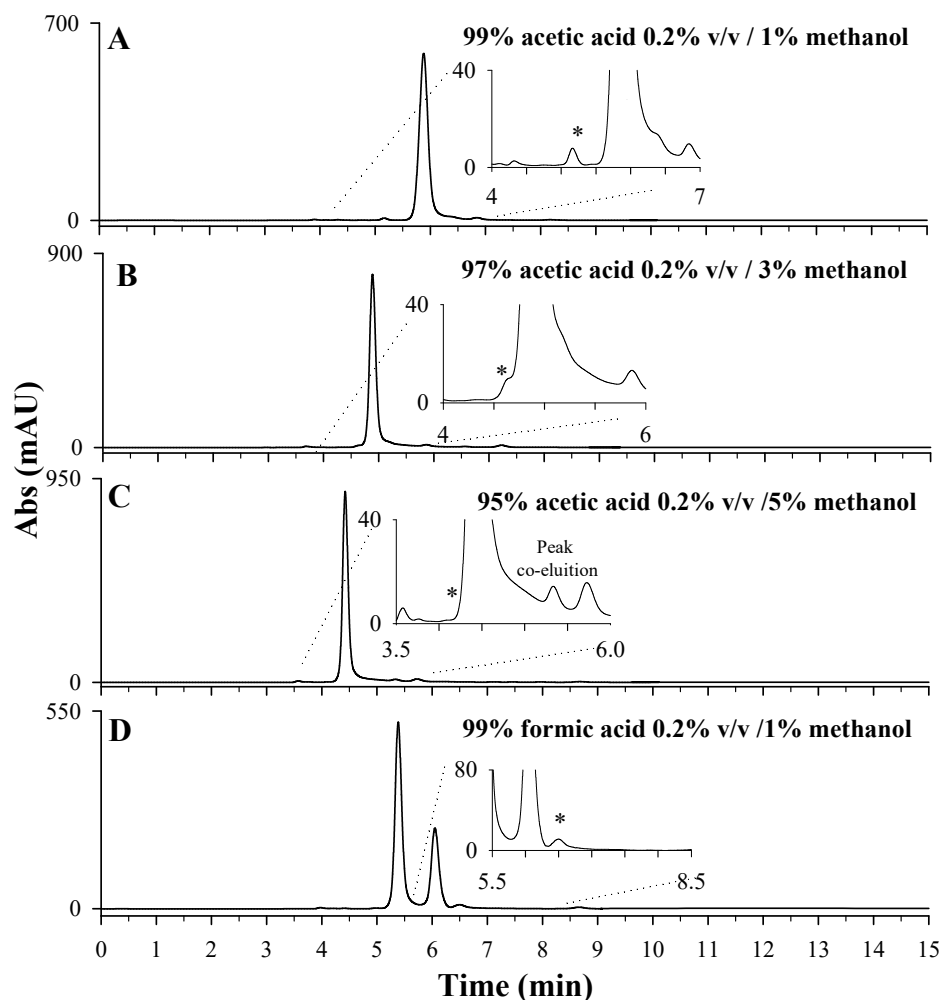


Figure 4. HPLC-UV chromatographic profiles obtained during the optimization of mobile-phase composition: 99% acetic acid 0.2% *v/v* containing 1% methanol (pH 3.04) (A); 97% acetic acid 0.2% *v/v* containing 3% methanol (pH 3.13) (B); 95% acetic acid 0.2% *v/v* containing 5% methanol (pH 3.13) (C); 99% formic acid 0.2% *v/v* containing 1% methanol (pH 2.61) (D). The LD peak is indicated with *. A 10-day dried extract of *Vicia faba* L. sample, diluted 1:10 in HCl 0.1 M, Discovery C₁₈ column, 250 × 4.6 mm, 5 μm, under isocratic conditions (flow rate 0.1 mL/min), injection volume of 20 μL and λ_{max} set of 280 nm, were used.

2.3. Method Validation

The performances of the analytic method were evaluated in terms of the estimation of linearity, LOD (limit of detection), LOQ (limit of quantification), accuracy, precision, matrix effect, and measurement uncertainties, according to European Action in Chemistry guidelines [42,43]. All these parameters are reported in Table 1.

The proposed method showed significant accuracy, precision, and linearity in the concentration range 0.5–50 mg/L. This range is much lower in concentration than that reported in the literature for *Vicia faba* L. matrix by Vora et al. [16], which validated a linear range 100–700 mg/L by using the same detector.

The calculated LOD and LOQ values of 0.0414 mg/L and 0.0452 mg/L, respectively, were lower than those of the only validated method by LC-UV reported in the literature for *Vicia faba* L. [16], highlighting the improved suitability of the proposed method for determination in samples with low LD content.

Table 1. Calibration curves, limit of detection and limit of quantification, precision, recovery, uncertainties, resolution, and tailing factor for LD determination by using LC-UV method.

Calibration Curve		Precision					Chromatographic Parameters		
Linear Range (<i>t</i> calc.) ^a	Linear Equation ^b , <i>R</i> ²	LoD (mg/L) LoQ (mg/L)	Level (mg/L)	Rep. RDS% (<i>r</i> calc.) ^c	Int. Precision RDS% (<i>r</i> calc.) ^d	Recovery, <i>R</i> _m ± <i>u</i> (<i>R</i> _m)	<i>U</i> (mg/L)	<i>Rs</i> ^e	<i>T</i> ^e
0.5–50 mg/L (99.98)	$y = (13.99 \pm 0.15)x + (6.35 \pm 3.52)$ <i>R</i> ² = 0.999	0.0414 0.0452	0.5	1.41 (0.36)	6.87 (1.44)	1.01 ± 0.02	0.24	1.64 ± 0.03	1.14 ± 0.02
			15	0.16 (1.31)	2.57 (17.80)	1.171 ± 0.002	0.93	1.65 ± 0.02	1.13 ± 0.01
			50	0.11 (2.73)	2.20 (48.38)	1.033 ± 0.004	2.93	1.67 ± 0.03	1.13 ± 0.01

^a Calculated *t* value was compared to tabulated value $t_{0.01,4} = 4.60$ (*k* = 6). ^b Calibration fitting: $y = x(m \pm s_m) + q \pm s_q$. ^c The repeatability was estimated for six replicates (*n* = 6) of three levels (*k* = 3) over the linear range in the same day (*p* = 1) and *r* was calculated according to tabulated value $t_{0.05,5} = 2.57$. ^d The intermediate precision was calculated within 3 days (*p* = 3) for the ten replicates (*n* = 10) of three levels (*k* = 3) over the linear range and *r* was calculated according to tabulated value $t_{0.05,5} = 2.26$. ^e Chromatographic parameter were estimated as mean values ± SD (standard deviations).

As regards the matrix effect (ME), a value of 100% means that there is not any kind of ME, as obtained in the proposed work. Therefore, it is possible to assess that the presence of matrix components does not interfere with the analysis of LD over the validated range.

The uncertainty measurements were expressed as expanded uncertainty (*U*, mg/L) for a normal distribution at a 95% confidence level [43,44], and the obtained results are reported in Table 1.

Finally, the results of tailing factor (*T*) and resolution (*Rs*) of the method at the three concentration levels, reported in Table 1, met the requirements for a good chromatographic method, showing well resolved peaks (*R* > 1.5) and no back tailing [45]

2.4. Quantitative Analysis of LD in Differently Stored Samples of *Vicia faba* L.

The proposed LC-UV method was successfully applied for the quantitative determination of LD occurring in local *Vicia faba* L. broad beans. Extracts from fresh broad bean sample were firstly analyzed. Then, the same sample was subjected to different storage treatments: sun-drying, freezing, and freeze-drying. Drying and freezing times were also varied (10 and 30 days). The aim was to suggest the best conditions able to preserve the LD content found in fresh samples. Table 2 shows the LD content in mg/g dry weight (dw) occurring in fresh sample, 10-day sun-dried sample, 30-day sun-dried sample, freeze-dried sample, 10-day frozen sample, 30-day frozen sample, and commercial long-life frozen sample.

Table 2. LD quantification in seven *Vicia faba* L. broad beans, stored by different processes: fresh sample, 10-day sun-dried sample, 30-day sun-dried sample, freeze-dried sample, 10-day frozen sample, 30-day frozen sample, and commercial long-life frozen sample. LD content is expressed as (mg/g dw) ± *U*(mg/g). Values marked by the same letter are not significantly different (*p* < 0.05).

Conservation Type	LD Concentration (mg/g dw)
<i>Vicia faba</i> L. fresh samples	1.21 ± 0.17 (a,b)
<i>Vicia faba</i> L. dried in the sun for 10 days	1.26 ± 0.15 (c,b)
<i>Vicia faba</i> L. dried in the sun for 30 days	0.81 ± 0.11 (f,g)
<i>Vicia faba</i> L. freeze-dried	0.76 ± 0.11 (h,g)
<i>Vicia faba</i> L. frozen for 10 days	1.03 ± 0.14 (d)
<i>Vicia faba</i> L. frozen for 30 days	0.51 ± 0.08 (e)
<i>Vicia faba</i> L. commercial long-life frozen	<LOQ

The most abundant LD concentration was detected for 10-day sun-dried sample (1.26 ± 0.15 mg/g dw), which was not significantly different from the content occurring in the fresh sample (1.21 ± 0.17 mg/g dw). Interestingly, the LD content decreased by prolonging sun-drying up to 30 days. Freezing proved to be a less effective conservation method since after 10 days, LD content was already reduced to 1.03 ± 0.14 mg/g dw and after 30 days, it further decreased. For the extreme situation of indefinitely prolonged freezing time, as the commercial long-life frozen sample, LD content decreases so much as to become undetectable using the proposed HPLC-UV method. The freeze-drying storage preserved the LD content better than the 30-day freezing treatment. Furthermore, for samples with a short storage time (10 days), a difference between the freezing and drying treatments was observed. Compared to freezing storage, it seems that the conservation of broad beans by sun-drying allows for better preservation of the analyte, in agreement with the literature data [46,47]. Some papers highlight that sudden changes in temperature cause inhibition of the plant enzymatic activity of cytochrome P450, responsible for the synthesis of LD. Additionally, LD instability under strong thermal processes was largely demonstrated (e.g., freeze-drying, freezing, cooking, and high-temperature heating) [11,23,31,48].

Therefore, this study confirmed the convenience of using short-time sun-dried samples, which guarantee high and reproducible LD contents.

3. Materials and Methods

3.1. Chemicals

Methanol ($\geq 99.8\%$) was purchased from Honeywell (Seelze, Germany). Analytical standard ($\geq 98\%$) of 3,4-Dihydroxy-L-phenylalanine (LD) was purchased from Sigma-Aldrich (Milano, Italy). Formic acid was purchased from Fluka (Buchs, Switzerland). Potassium dihydrogen phosphate ($\geq 98\%$), acetic acid ($\geq 96\%$) were acquired from Carlo Erba (Rodano, Italy). Hydrochloric acid 37% (GR for analysis) was purchased from Merck KGaA (Darmstadt, Germany). Ultrapure water was produced using a Milli-Q RG system from Millipore (Bedford, MA, USA).

3.2. LD Stability Study

Stock solutions of LD were prepared at 1000 mg/L, in different acidic solutions: acetic acid 0.2% *v/v* (pH 3.29), formic acid 0.2% *v/v* (pH 2.62), acetic acid 5% *v/v* (pH 2.40), HCl 1 mol/L (pH 0), HCl 0.1 mol/L (pH 1), and ultrapure H₂O (pH 5.37). LD working standard solutions at 50 mg/L were prepared by dilution from stock solutions and injected weekly by using Discovery C₁₈ column, 250 × 4.6 mm, 5 μm particle size and the chromatographic conditions proposed by Polanowska et al. [11]. This study was performed for 3 months to monitor the analyte stability in the aqueous solutions over a long time. All solutions were stored at 4 °C in the dark to minimize thermal and photolytic degradation [32]. Student's *t*-test (SPSS 19.0 for Windows; IBM SPSS Statistics, Armonk, NY, USA) was used to assess the presence of significant differences ($p < 0.05$) among the standard solution.

3.3. Analytical Method Validation

To optimize the method for the determination of LD by LC-UV system, the following parameters were assessed: LC performance, i.e., C₁₈ stationary phases and mobile phases, and validation parameters, i.e., linearity, limit of detection (LOD), limit of quantification (LOQ), precision, accuracy, matrix effects, and uncertainties, according to European Action in Chemistry (EURACHEM) guidelines [35].

3.3.1. LC Performance

Experiments were performed by using an Agilent 1200 Series Gradient HPLC System (Agilent Technologies, Santa Clara, CA, USA) equipped with a quaternary gradient pump unit, a diode array detector (DAD, 190–950 nm), and a standard autosampler (0.1 μL–100 μL) set to inject 20 μL. For all samples, to improve method selectivity, chromatograms at $\lambda = 280$ nm, combined with the absorbance spectrum (190–400 nm) were

acquired and purity of LD peaks was checked. All the experiments were carried out at room temperature (25 °C).

Four different C₁₈ analytical columns (Table 3) were used to optimize the best chromatographic separation: Discovery C₁₈ column, 250 × 4.6 mm, 5 µm particle size; Kinetex C₁₈ column, 100 × 4.6 mm, 2.6 µm particle size; Discovery Supelco C₁₈ column, 150 × 2.1 mm, 5 µm particle size; ZORBAX Eclipse XDB-C₁₈, 150 × 4.6 mm, 5 µm particle size. For the stationary-phase optimization study, a standard LD solution at 50 mg/L in 0.1 M HCl was injected, and chromatographic runs were carried out by using the mobile phase proposed by Polanowska et al. [11]: 97% of acetic acid at 0.2% *v/v* as aqueous phase containing 3% of methanol as organic phase, under isocratic conditions at 1 mL/min for Discovery C₁₈ column, 0.8 mL/min for Kinetex C₁₈ column and Agilent ZORBAX Eclipse XDB, 0.5 mL/min for Discovery Supelco C₁₈ column.

Table 3. Characteristics of columns tested in this work.

Column	Column Length (cm)	Column ID (mm)	Particle Size (µm)	Pore Size (Å)	Surface Area (m ² /g)	Carbon Content (%)	pH Range	Matrix Functional Group	Supplier
Discovery® C ₁₈ HPLC Column	15 cm	2.1 mm	5 µm	180 Å	300 m ² /g	12%	2–8	C ₁₈ (octadecyl) phase endcapping	Supelco
Discovery® C ₁₈ HPLC Column	25 cm	4.6 mm	5 µm	180 Å	300 m ² /g	12%	2–8	C ₁₈ (octadecyl) phase endcapping	Supelco
Kinetex Core-Shell Column	10 cm	4.6 mm	2.6 µm	100 Å	200 m ² /g	12%	1.5–10	C ₁₈ with TMS endcapping	Phenomenex
Eclipse XDB-C ₁₈ Column	25 cm	4.6 mm	5 µm	80 Å	180 m ² /g	10%	2–9	dimethyl-n-octadecylsilanes double endcapping	Agilent

Four different mobile phases were tested on the chosen column: 99% acetic acid 0.2% *v/v* (aqueous phase) containing 1% methanol (organic phase); 97% acetic acid 0.2% *v/v* (aqueous phase) containing 3% methanol (organic phase); 95% acetic acid 0.2% *v/v* (aqueous phase) containing 5% methanol (organic phase); 99% formic acid 0.2% *v/v* (aqueous phase) containing 1% methanol (organic phase). A 100% aqueous phase A consisting of a KH₂PO₄ 125 mM buffer solution (adjusted to pH 2.5 with concentrated H₃PO₄) was also tried. For mobile-phase optimization, 10-day sun-dried extract of *Vicia faba* L. sample, diluted 1:10 in HCl 0.1 M, Discovery C₁₈ column, 250 × 4.6 mm, 5 µm, under isocratic conditions (flow rate 1 mL/min) was used.

All tests were performed in triplicate. Data acquisition and analyses were accomplished using the HPLC 1200 offline (Agilent Technologies, Santa Clara, CA, USA). The chromatographic raw data were imported, elaborated, and plotted by SigmaPlot 11.0 (Systat Software, Inc., London, UK).

3.3.2. Validation Parameters

The linearity was assessed by the least-squares method in a concentration range between 0.5–50 mg/L of LD working solutions in 0.1M HCl. The linearity parameter was estimated at six concentration levels ($k = 6$) and the analyses were performed in three independent replicates ($n = 3$). Additionally, a statistic *t*-test was performed in order to assess the significance of the correlation coefficient R^2 [43,44,49,50].

LOD and LOQ were evaluated by analyzing ten independent blank samples, calculating the mean blank response (x_b) and its standard deviation (s_b) as follows: $y_{LoD} = x_b + 3s_b$ and $y_{LoQ} = x_b + 10s_b$.

The precision of the proposed method was studied as “repeatability” and “intermediate precision”, expressed as percentage relative standard deviation (%RSD). The first parameter is the precision under the same operating conditions over a short time interval, i.e., the %RSD for six replicates ($n = 6$) of three levels ($k = 3$) over the linear range in the same day ($p = 1$). The second is the within-laboratories variations (different days, different analysts, different equipment, etc.) [51], i.e., the %RSD within several days ($p = 3$) for the ten replicates ($n = 10$) of three levels ($k = 3$) over the linear range. Furthermore, according to the EURACHEM guidelines, the repeatability limit and the intermediate repeatability limit were also calculated as follows: $r = \sqrt{2} \times t_{\text{crit}} \times s$, where s is the standard deviation obtained under repeatability ($n = 6$) and intermediate precision ($n = 10$), the factor $\sqrt{2}$ reflects the difference between the two measurements, and the t_{crit} value is chosen at a 95% confidence level using a two-tailed distribution and a number of degrees of freedom equal to $(n-1)$.

Since a certified reference material is not commercially available for the plant matrix under study, the accuracy, expressed as recovery, was evaluated by fortifying the real samples at least at three concentration levels ($k = 3$) over the linear range for three replicates ($n = 3$) at each level, over three days ($p = 3$). Since the long-term dried commercial broad bean sample had an LD quantity significantly lower than the LOD and LOQ values of the proposed method, it was used for recovery evaluation. The fortified LD concentration levels were: 0.5 mg/L (5 mg/Kg), 15 mg/L (150 mg/kg), and 50 mg/L (500 mg/kg). The fortified broad bean samples and the corresponding blank samples without fortification were analyzed to calculate the concentration of the analyte from the calibration curve. The difference between the analyte amount in spiked ($C_{\text{sample_spk}}$) and unspiked ($C_{\text{sample_unspk}}$) samples was divided by the amount of spike (C_{spk}), to estimate the recovery as follows [42,43,49]: $R_m = (C_{\text{sample_spk}} - C_{\text{sample_unspk}})/C_{\text{spk}}$. The recovery standard deviation ($U(R_m)$) was calculated by following this equation [44,52]:

$$U(R_m) = R_m \times \sqrt{\frac{\frac{s_{\text{sample_spk}}^2}{n} + s_{\text{sample_unspk}}^2}{(C_{\text{sample_spk}} - C_{\text{sample_unspk}})^2} \left(\frac{s_{\text{spk}}}{C_{\text{spk}}}\right)^2} \quad (1)$$

where $s_{\text{sample_spk}}$ and $s_{\text{sample_unspk}}$ are the standard deviations of LD occurring in spiked and unspiked samples, and s_{spk} is the spike uncertainty.

Matrix effects (ME) were assessed using the post-extraction additions, which involve the calibration curve preparation with real extracts. Therefore, the calibration curve of the real samples was compared to the one achieved for the same standards in HCl 0.1 mol/L solvent. If both curves were parallel and overlapped, compounds are not subjected to any matrix effects. The ME was estimated by dividing the slopes of the matrix-matched calibration curves prepared with real extracts (slope matrix) and the slopes of the calibration curves prepared with solvent (slope std): $ME(\%) = 100 \times (\text{slope}_{\text{matrix}}/\text{slope}_{\text{std}})$ [43].

Finally, the expanded uncertainty was estimated as a combination of different contributions by using the bottom-up approach [43,44,52], as follows:

$$u_c/C_0 = \sqrt{\left(\frac{u_{\text{prep}}}{C_0}\right)^2 + \left(\frac{u_{\text{cal}}}{C_0}\right)^2 + \left(\frac{u_{R_m}}{R_m}\right)^2 + \left(\frac{u_{\text{LoD}}}{\text{LoD}}\right)^2} \quad (2)$$

where u_c is the combined standard uncertainty (mg/L); C_0 is the concentration level (mg/L); R_m is the recovery (%); LOD is the limit of detection (mg/L); u_{prep} is the uncertainty related to concentration levels preparation (mg/L); u_{cal} is the uncertainty of calibration curves (mg/L); u_{R_m} is the recovery uncertainty; u_{LoD} is the LoD uncertainty. Finally, extended uncertainties U , for $n = 3$ replicates, was estimated by multiplying the compound uncertainty by a coverage factor corresponding to $k = 1.98$, for a confidence level of 95%.

3.4. *Vicia faba* L. Broad Beans and LD Extraction

Vicia faba L. broad beans were purchased from a local producer in Potenza (Basilicata, Italy) as fresh sample. *Vicia faba* L. broad beans were then divided in different aliquots for different storage treatments: sun-drying for 10 and 30 days, freezing for 10 and 30 days, freeze-drying. Extraction conditions proposed by Polanowska et al. [11] were optimized to allow LD extraction from the fresh sample, sun-dried samples (10 and 30 days), freeze-dried sample, frozen samples (10 and 30 days), and commercial long-life frozen sample. Briefly, ultrasonic assisted extraction (UAE) was applied by using an extraction ratio of 1:10 weight/dry volume and HCl 0.1 mol/L as extracting solution; a sonication time of 20 min in an ice bath (4 °C) and a centrifugation for 10 min at 6000 × g was applied. This procedure was performed twice, and then supernatants were collected, filtered on PTFE 0.2 µm filters, and stored at 4 °C in the dark until the LC-UV analyses. The LD quantification on the various broad bean extracts was performed by the external standard method. A botanical sample is kept in the Science Department of the University of Basilicata. The genus and species of the plant have been unambiguously identified.

4. Conclusions

An LC-UV method has been successfully optimized and validated for L-Dopa separation and quantification in *Vicia faba* L. broad bean samples. A strongly acidic aqueous solution, consisting of HCl 0.1 M, proved to be the best extraction solvent to assure the stability of LD over 3 months. After testing different stationary and mobile phases, a Discovery C₁₈ column, 250 × 4.6 mm, 5 µm particle size as a stationary phase and a mobile phase consisting of 99% formic acid 0.2% v/v and 1% methanol (pH 2.61), under isocratic flow of 1 mL/min, were chosen for a reliable chromatographic separation. A rigorous LC-UV method validation, according to EURACHEM guidelines, reached LOD and LOQ values of 0.0414 and 0.0452 mg/L, respectively. High precision (less than 6.87% RSD) and accuracy (ranging between 1.01 and 1.03 of recovery) were obtained. No matrix effect was detected for the samples under study.

After validation, the proposed method was used for the LD quantitative analysis of differently stored *Vicia faba* L. broad bean samples, thus defining 10-day sun-drying as the best storage treatment able to preserve a high LD content in broad beans (1.26 ± 0.15 mg/g dw). The method described in this work was demonstrated to be robust and reliable for routine LD analyses in vegetable matrices, such as *Vicia faba* L. broad beans, which could be a potential functional food or an ingredient for food supplement preparation for PD patients.

Author Contributions: Conceptualization, F.L., R.C., G.B. and M.D.; methodology, C.T. and F.L.; validation, C.T., R.P. and G.B.; formal analysis, C.T., R.P., F.L. and R.C.; investigation, C.T., F.L., M.A.A. and A.D.C.; resources, L.S. and S.A.B.; data curation C.T., R.P. and M.A.A.; writing—original draft preparation C.T., A.D.C. and M.A.A.; writing—review and editing, F.L., R.C., G.B., A.G., M.D. and S.P.; supervision F.L., R.C. and A.D.C. All authors have read and agreed to the published version of the manuscript.

Funding: This research received no external funding.

Institutional Review Board Statement: Not applicable.

Informed Consent Statement: Not applicable.

Data Availability Statement: Not applicable.

Conflicts of Interest: The authors declare no conflict of interest.

Sample Availability: Samples of the compounds are available from the authors.

References

1. Ribeiro, R.P.; Gasparetto, J.C.; De Oliveira Vilhena, R.; De Francisco, T.M.G.; Martins, C.A.F.; Cardoso, M.A.; Pontarolo, R. Simultaneous determination of levodopa, carbidopa, entacapone, tolcapone, 3-O-methyldopa and dopamine in human plasma by an HPLC-MS/MS method. *Bioanalysis* **2015**, *7*, 207–220. [[CrossRef](#)] [[PubMed](#)]
2. Chen, X.; Wang, Y.; Wu, H.; Cheng, C.; Le, W. Research advances on L-DOPA-induced dyskinesia: From animal models to human disease. *Neurol. Sci.* **2020**, *41*, 2055–2065. [[CrossRef](#)] [[PubMed](#)]
3. Mortezaazadeh, T.; Seyedarabi, H.; Mahmoudian, B.; Islamian, J.P. Imaging modalities in differential diagnosis of Parkinson's disease: Opportunities and challenges. *Egypt. J. Radiol. Nucl. Med.* **2021**, *52*, 79. [[CrossRef](#)]
4. Balestrino, R.; Schapira, A.H.V. Parkinson disease. *Eur. J. Neurol.* **2020**, *27*, 27–42. [[CrossRef](#)] [[PubMed](#)]
5. Hall, M.F.E.; Church, F.C. Integrative Medicine and Health Therapy for Parkinson Disease. *Top. Geriatr. Rehabil.* **2020**, *36*, 176–186. [[CrossRef](#)]
6. Min, K.; Park, K.; Park, D.H.; Yoo, Y.J. Overview on the biotechnological production of l-DOPA. *Appl. Microbiol. Biotechnol.* **2015**, *99*, 575–584. [[CrossRef](#)] [[PubMed](#)]
7. Dhull, S.B.; Kidwai, M.K.; Noor, R.; Chawla, P.; Rose, P.K. A review of nutritional profile and processing of faba bean (*Vicia faba* L.). *Legum. Sci.* **2021**, *4*, e129. [[CrossRef](#)]
8. Benfica, J.; Morais, E.S.; Miranda, J.S.; Freire, M.G.; de Cássia Superbi de Sousa, R.; Coutinho, J.A.P. Aqueous solutions of organic acids as effective solvents for levodopa extraction from *Mucuna pruriens* seeds. *Sep. Purif. Technol.* **2021**, *274*, 119084. [[CrossRef](#)]
9. Apaydin, H.; Ertan, S.; Ozekmekçi, S. Broad bean (*Vicia faba*)—A natural source of L-dopa—Prolongs “on” periods in patients with Parkinson's disease who have “on-off” fluctuations. *Mov. Disord. Off. J. Mov. Disord. Soc.* **2000**, *15*, 164–166. [[CrossRef](#)]
10. Tesoro, C.; Lelario, F.; Ciriello, R.; Bianco, G.; Di Capua, A.; Acquavia, M.A. An Overview of Methods for L-Dopa Extraction and Analytical Determination in Plant Matrices. *Separations* **2022**, *9*, 224. [[CrossRef](#)]
11. Polanowska, K.; Lukasik, R.M.; Kuligowski, M. Development of a Sustainable, Simple, and Robust Method for Efficient l-DOPA Extraction. *Molecules* **2019**, *24*, 2325. [[CrossRef](#)] [[PubMed](#)]
12. Rathod, B.G.; Patel, N.M. Development of validated RP-HPLC method for the estimation of L-Dopa from *Mucuna pruriens*, its extracts and in Aphrodisiac formulation. *Int. J. Pharma Sci. Res.* **2014**, *5*, 508–513.
13. Renna, M.; De Cillis, F.; Leoni, B.; Acciardi, E.; Santamaria, P. From by-product to unconventional vegetable: Preliminary evaluation of fresh fava hulls highlights richness in L-DOPa and low content of anti-nutritional factor. *Foods* **2020**, *9*, 159. [[CrossRef](#)]
14. Siddhuraju, P.; Becker, K. Rapid reversed-phase high performance liquid chromatographic method for the quantification of L-Dopa (L-3,4-dihydroxyphenylalanine), non-methylated and methylated tetrahydroisoquinoline compounds from *Mucuna* beans. *Food Chem.* **2001**, *72*, 389–394. [[CrossRef](#)]
15. Singh, R.; Saini, P.; Mathur, S.; Singh, G.; Kumar, S. Application of high performance liquid chromatography to the determination and validation of levodopa in methanolic extract of *Mucuna utilis*. *Int. J. Green Pharm.* **2010**, *4*, 156–158. [[CrossRef](#)]
16. Vora, R.N.; Joshi, A.N.; Joshi, N.C. Comparison of L-Dopa Content in Two Varieties of Broad Beans (*Vicia faba*) By Different Extraction Techniques. *World J. Pharm. Med. Res.* **2017**, *3*, 271–274.
17. Yang, X.; Zhang, X.; Zhou, R. Determination of L-Dopa content and other significant nitrogenous compounds in the seeds of seven *Mucuna* and *Stizolobium* species in China. *Pharm. Biol.* **2001**, *39*, 312–316. [[CrossRef](#)]
18. Aware, C.; Patil, R.; Gaikwad, S.; Yadav, S.; Bapat, V.; Jadhav, J. Evaluation of L-dopa, proximate composition with in vitro anti-inflammatory and antioxidant activity of *Mucuna macrocarpa* beans: A future drug for Parkinson treatment. *Asian Pac. J. Trop. Biomed.* **2017**, *7*, 1097–1106. [[CrossRef](#)]
19. Baranowska, I.; Płonka, J. Simultaneous Determination of Biogenic Amines and Methylxanthines in Foodstuff—Sample Preparation with HPLC-DAD-FL Analysis. *Food Anal. Methods* **2015**, *8*, 963–972. [[CrossRef](#)]
20. Bulduk, İ.; Topal, N. Development and Validation of a Quantification Method for L-DOPA in Plants and Pharmaceutical Materials. *Hacettepe J. Biol. Chem.* **2020**, *49*, 1–10. [[CrossRef](#)]
21. Dhanani, T.; Singh, R.; Shah, S.; Kumari, P.; Kumar, S. Comparison of green extraction methods with conventional extraction method for extract yield, L-DOPA concentration and antioxidant activity of *Mucuna pruriens* seed. *Green Chem. Lett. Rev.* **2015**, *8*, 43–48. [[CrossRef](#)]
22. Duan, S.; Kwon, S.J.; Lim, Y.J.; Gil, C.S.; Jin, C.; Eom, S.H. L-3,4-dihydroxyphenylalanine accumulation in faba bean (*Vicia faba* L.) tissues during different growth stages. *Agronomy* **2021**, *11*, 502. [[CrossRef](#)]
23. Etemadi, F.; Hashemi, M.; Randhir, R.; Zand Vakili, O.; Ebadi, A. Accumulation of L-DOPA in various organs of faba bean and influence of drought, nitrogen stress, and processing methods on L-DOPA yield. *Crop J.* **2018**, *6*, 426–434. [[CrossRef](#)]
24. Goyoaga, C.; Burbano, C.; Cuadrado, C.; Varela, A.; Guillamón, E.; Pedrosa, M.M.; Muzquiz, M. Content and distribution of vicine, convicine and l-DOPA during germination and seedling growth of two *Vicia faba* L. varieties. *Eur. Food Res. Technol.* **2008**, *227*, 1537–1542. [[CrossRef](#)]
25. Pavón-Pérez, J.; Oviedo, C.A.; Elso-Freudenberg, M.; Henríquez-Aedo, K.; Aranda, M. LC-MS/MS Method For L-Dopa Quantification in Different Tissues of *Vicia faba*. *J. Chil. Chem. Soc.* **2019**, *64*, 4–6. [[CrossRef](#)]
26. Shetty, P.; Atallah, M.T.; Shetty, K. Effects of UV treatment on the proline-linked pentose phosphate pathway for phenolics and L-DOPA synthesis in dark germinated *Vicia faba*. *Process Biochem.* **2002**, *37*, 1285–1295. [[CrossRef](#)]

27. Neyra Recky, J.R.; Serrano, M.P.; Dántola, M.L.; Lorente, C. Oxidation of tyrosine: Antioxidant mechanism of L-DOPA disclosed. *Free Radic. Biol. Med.* **2021**, *165*, 360–367. [[CrossRef](#)]
28. Pulikkalpura, H.; Kurup, R.; Mathew, P.J.; Baby, S. Levodopa in *Mucuna pruriens* and its degradation. *Sci. Rep.* **2015**, *5*, 2–10. [[CrossRef](#)]
29. Omotani, H.; Yasuda, M.; Ishii, R.; Ikarashi, T.; Fukuuchi, T.; Yamaoka, N.; Mawatari, K.I.; Kaneko, K.; Nakagomi, K. Analysis of L-DOPA-derived melanin and a novel degradation product formed under alkaline conditions. *J. Pharm. Biomed. Anal.* **2016**, *125*, 22–26. [[CrossRef](#)]
30. Andrade, Á.L.; Cardoso, T.D.; Thomasi, S.S.; Alvarenga, M.E.; da Silva, M.A.N.; Magalhães, E.J.; Duarte, H.A.; de Almeida, K.J. A simple and efficient method for simultaneous quantification of levodopa and carbidopa based on controlled oxidation process. *Chem. Pap.* **2021**, *75*, 3091–3102. [[CrossRef](#)]
31. Gurumoorthi, P.; Janardhanan, K.; Myhrman, R.V. Effect of differential processing methods on L-Dopa and protein quality in velvet bean, an underutilized pulse. *LWT* **2008**, *41*, 588–596. [[CrossRef](#)]
32. Zhou, Y.Z.; Alany, R.G.; Chuang, V.; Wen, J. Studies of the rate constant of L-DOPA oxidation and decarboxylation by HPLC. *Chromatographia* **2012**, *75*, 597–606. [[CrossRef](#)]
33. Kostrzewa, R.M.; Kostrzewa, J.P.; Brus, R. Neuroprotective and neurotoxic roles of levodopa (L-DOPA) in neurodegenerative disorders relating to Parkinson’s disease. *Amino Acids* **2002**, *23*, 57–63. [[CrossRef](#)] [[PubMed](#)]
34. Hörmann, P.; Delcambre, S.; Hanke, J.; Geffers, R.; Leist, M.; Hiller, K. Impairment of neuronal mitochondrial function by L-DOPA in the absence of oxygen-dependent auto-oxidation and oxidative cell damage. *Cell Death Discov.* **2021**, *7*, 151. [[CrossRef](#)] [[PubMed](#)]
35. Tahvanainen, T.; Haraguchi, A. Effect of pH on phenol oxidase activity on decaying *Sphagnum* mosses. *Eur. J. Soil Biol.* **2013**, *54*, 41–47. [[CrossRef](#)]
36. Long, W.J.; Brooks, A.E.; Biazzo, W. Analysis of Polar Compounds Using 100% Aqueous Mobile Phases with Agilent ZORBAX Eclipse Plus Phenyl-Hexyl and Other ZORBAX Phenyl Columns. *Agil. Technol. Publ.* **2009**, 1–8.
37. Cai, B.; Li, J. Evaluation of trifluoroacetic acid as an ion-pair Analysis of Polar Compounds Using 100% Aqueous Mobile Phases with Agilent ZORBAX Eclipse Plus Phenyl-Hexyl and Other ZORBAX Phenyl Columns reagent in the separation of small ionizable molecules by reversed-phase liquid chromatography. *Anal. Chim. Acta* **1999**, *399*, 249–258. [[CrossRef](#)]
38. Bidlingmeyer, B.A.; Broske, A.D. The Role of Pore Size and Stationary Phase Composition in Preventing Aqueous-Induced Retention Time Loss in Reversed-Phase HPLC. *J. Chromatogr. Sci.* **2004**, *42*, 100–106. [[CrossRef](#)]
39. Buszewski, B.; Noga, S. Hydrophilic interaction liquid chromatography (HILIC)-a powerful separation technique. *Anal. Bioanal. Chem.* **2012**, *402*, 231–247. [[CrossRef](#)]
40. Thiébaud, D.; Vial, J.; Michel, M.; Hennion, M.C.; Greibrokk, T. Evaluation of reversed phase columns designed for polar compounds and porous graphitic carbon in “trapping” and separating neurotransmitters. *J. Chromatogr. A* **2006**, *1122*, 97–104. [[CrossRef](#)]
41. Arnetoli, M.; Montegrossi, G.; Buccianti, A.; Gonnelli, C. Determination of organic acids in plants of *Silene paradoxa* L. by HPLC. *J. Agric. Food Chem.* **2008**, *56*, 789–795. [[CrossRef](#)] [[PubMed](#)]
42. Magnusson, B.; Örnemark, U. *Eurachem Guide: The Fitness for Purpose of Analytical Methods—A Laboratory Guide to Method Validation and Related Topics*, 2nd ed.; Örnemark, U., Ed.; Eurachem: Gembloux, Belgium, 2014; ISBN 0-94948926-12-0.
43. Pascale, R.; Bianco, G.; Coviello, D.; Cristina Lafiosca, M.; Masi, S.; Mancini, I.M.; Bufo, S.A.; Scrano, L.; Caniani, D. Validation of a liquid chromatography coupled with tandem mass spectrometry method for the determination of drugs in wastewater using a three-phase solvent system. *J. Sep. Sci.* **2020**, *43*, 886–895. [[CrossRef](#)] [[PubMed](#)]
44. Pascale, R.; Bianco, G.; Calace, S.; Masi, S.; Mancini, I.M.; Mazzone, G.; Caniani, D. Method development and optimization for the determination of benzene, toluene, ethylbenzene and xylenes in water at trace levels by static headspace extraction coupled to gas chromatography–barrier ionization discharge detection. *J. Chromatogr. A* **2018**, *1548*, 10–18. [[CrossRef](#)] [[PubMed](#)]
45. Snyder, L.R.; Kirkland, J.J.; Glajchand, J.L. *Practical HPLC Method Development*, 2nd ed.; John Wiley & Sons: New York, NY, USA, 1997.
46. Saranya, G.; Jiby, M.V.; Jayakumar, K.S.; Pillai, P.P.; Jayabaskaran, C. L-DOPA synthesis in *Mucuna pruriens* (L.) DC. is regulated by polyphenol oxidase and not CYP 450/tyrosine hydroxylase: An analysis of metabolic pathway using biochemical and molecular markers. *Phytochemistry* **2020**, *178*, 112467. [[CrossRef](#)] [[PubMed](#)]
47. Van Beek, H.L.; Beyer, N.; Janssen, D.B.; Fraaije, M.W. Lyophilization conditions for the storage of monooxygenases. *J. Biotechnol.* **2015**, *203*, 41–44. [[CrossRef](#)]
48. Sharma, A.; Khamar, D.; Cullen, S.; Hayden, A.; Hughes, H. Innovative Drying Technologies for Biopharmaceuticals. *Int. J. Pharm.* **2021**, *609*, 121115. [[CrossRef](#)]
49. Coviello, D.; Pascale, R.; Ciriello, R.; Salvi, A.M.; Guerrieri, A.; Contursi, M.; Scrano, L.; Bufo, S.A.; Cataldi, T.R.I.; Bianco, G. Validation of an analytical method for nitrite and nitrate determination in meat foods for infants by ion chromatography with conductivity detection. *Foods* **2020**, *9*, 1238. [[CrossRef](#)]
50. Araujo, P. Key aspects of analytical method validation and linearity evaluation. *J. Chromatogr. B Anal. Technol. Biomed. Life Sci.* **2009**, *877*, 2224–2234. [[CrossRef](#)]
51. Guideline, ICH Harmonised tripartite. Validation of analytical procedures: Text and methodology Q2(R1). *Guidance* **2005**, *1*, 5.
52. Ellison, S.L.R.; Williams, A. (Eds.) *Eurachem/CITAC Guide: Quantifying Uncertainty in Analytical Measurement*, 3rd ed.; Eurachem/CITAC: Teddington, UK, 2012. [[CrossRef](#)]